Target Volume Definition in Radiation Oncology

Anca-Ligia Grosu
Carsten Nieder
Editors

Springer

Target Volume Definition in Radiation Oncology

Anca-Ligia Grosu • Carsten Nieder
Editors

Target Volume Definition in Radiation Oncology

Springer

Editors
Anca-Ligia Grosu
Department of Radiation Oncology
University Medical Center Freiburg
Freiburg
Germany

Carsten Nieder
Department of Oncology
Nordland Hospital
Bodo
Norway

ISBN 978-3-662-45933-1 ISBN 978-3-662-45934-8 (eBook)
DOI 10.1007/978-3-662-45934-8

Library of Congress Control Number: 2015938237

Springer Heidelberg New York Dordrecht London

Printed on acid-free paper

Springer-Verlag GmbH Berlin Heidelberg is part of Springer Science+Business Media (www.springer.com)

Preface

The history of radiation therapy for malignant diseases dates back throughout almost the complete twentieth century. Neither three-dimensional cross-sectional imaging, such as computed tomography or magnetic resonance imaging, nor functional imaging, such as positron emission tomography, was available during the first decades. This resulted in treatment planning approaches that most of today's radiation oncologists are completely unfamiliar with. One particular example highlighting the development in a highly radio-curable malignancy is Hodgkin's lymphoma. Compared to historical extended field radiotherapy based on bony landmarks defining the field borders, we have witnessed the introduction of involved field and involved node radiotherapy. Our ability to account for organ motion during treatment delivery has changed the way of administering radiation to the lung and mediastinum. Simultaneously, evolution of image-guided and high-precision application technology has outperformed clinician's ability to precisely define the clinical target volume (CTV) in a number of diseases. Practicing radiation oncologists have to make several important decisions during treatment planning and realization, one patient at a time. It all starts with staging, multi-disciplinary discussion and volume delineation, in case radiotherapy is indicated and recommended. It would be of limited or no value to precisely deliver the prescribed treatment to an incorrectly defined CTV.

The purpose of this book is to provide practicing radiation oncologists and therapists, as well as those in training, with a concise overview of the most important and up-to-date information pertaining to target volume definition. Several chapters, e.g., those dealing with lymphoma, sarcoma and spine/spinal cord malignancies, not only include common clinical scenarios but also present challenging cases and rare cancer types. The issue of interobserver variability is addressed, and when available, the reader is introduced to consensus guidelines.

We are most grateful for the enthusiasm and courtesy all chapter authors showed during preparation of this truly international volume and for the fruitful discussion with many colleagues. We also appreciate the excellent support from the publisher. We hope that the reader will find this book to be a useful summary of current knowledge. Only continued cooperative research will

provide a better basis for tolerable and efficacious treatment regimens, exploiting the promises put forward by the emerging concepts of personalized, ablative and adaptive radiation therapy.

Freiburg, Germany — Anca-Ligia Grosu
Bodo, Norway — Carsten Nieder

Contents

Brain Tumors

1

Anca-Ligia Grosu, Oliver Oehlke, and Carsten Nieder

Contents

A.-L. Grosu, MD (✉) • O. Oehlke, MD, PhD
Department of Radiation Oncology, University Medical Center Freiburg, Robert-Koch-Str. 3, Freiburg D-79106, Germany
e-mail: anca.grosu@uniklinik-freiburg.de

C. Nieder, MD
Department of Oncology and Palliative Medicine, Nordland Hospital, Bodo, Norway

Faculty of Health Sciences, Institute of Clinical Medicine, University of Tromso, Tromso, Norway

1.1 Brain Gliomas

1.1.1 Introduction

Radiation therapy, together with surgery and chemotherapy, plays a crucial role in the management of malignant brain gliomas. Considering the complex functional anatomy of the brain, in no other anatomical region, the exact delivery of the radiation dose and the protection of normal tissue have such a high impact like in the brain. Therefore, the exact target volume delineation plays an essential role in high-precision radiation therapy of brain lesions.

In glioblastoma (GBM) maximum safe surgical resection, conventionally fractionated postoperative radiation therapy over 6 weeks (60, 2 Gy/day) and chemotherapy with temozolomide (concomitant and post radiotherapy) represent the standard treatment approach (Stupp et al. 2005). Also in anaplastic (WHO grade III) astrocytomas (AA), oligodendrogliomas (AO) and oligoastrocytomas (AOA), radiation therapy plays an important role in the overall treatment strategy, together with chemotherapy with PCV (procarbazine, lomustine, vincristine) or temozolomide (Wick et al. 2009; Cairncross et al. 2013; van den Bent et al. 2013). In low-grade gliomas (WHO grade II), immediate radiation therapy has been shown to result in a progression-free survival benefit and an advantage in seizure control compared with the same treatment given on tumour progression. However, no overall survival benefit

A.-L. Grosu, C. Nieder (eds.), *Target Volume Definition in Radiation Oncology*,
DOI 10.1007/978-3-662-45934-8_1, © Springer-Verlag Berlin Heidelberg 2015

was demonstrated (Karim et al. 1996; Shaw et al. 2002, 2012; van den Bent et al. 2005).

In the current chapter we discuss the target volume delineation for radiation therapy of gliomas in adults. Therefore, we will focus our discussion on low-grade gliomas WHO grade II and high-grade gliomas WHO grades III and IV. For all these tumour entities, the pathological characteristics and the imaging modalities as computed tomography (CT), magnetic resonance imaging (MRI), positron emission tomography (PET) and single-photon emission computed tomography (SPECT) will be briefly described before the main principals of target volume delineation are individually discussed.

Table 1.1 Overview of WHO classification of glioma (Louis et al. 2007)

Grading	Entity
WHO I°	Pilocytic astrocytoma
	Subependymal giant cell astrocytoma
WHO II°	Diffuse astrocytoma
	Pleomorphic xanthoastrocytoma
	Oligodendroglioma
	Oligoastrocytoma
	Gemistocytic astrocytoma
WHO III°	Anaplastic astrocytoma
	Anaplastic oligodendroglioma
	Anaplastic oligoastrocytoma
	Gliomatosis cerebri
WHO IV°	Glioblastoma multiforme
	Gliosarcoma

1.1.2 Epidemiology

The incidence rate of newly diagnosed primary malignant brain tumours is estimated at 3.8 per 100,000 males and 3.1 per 100,000 females per year. This rate is higher in developed countries (males: 5.8 per 100,000; females: 4.4 per 100,000) than in less developed countries (males: 3.2 per 100,000; females: 2.8 per 100,000). About 70 % of these tumours are GBM, 10–15 % AA, 10 % AO and AOA and the rest are less common tumour entities like ependymomas and anaplastic gangliogliomas (Ferlay et al. 2010; Louis et al. 2007).

1.1.3 Pathology

Gliomas are neuroepithelial tumours and are further classified by the World Health Organization (WHO) according to the cell type they arise from, e.g. astrocytoma, oligodendroglioma and mixed oligoastrocytoma (Louis et al. 2007), Table 1.1. Tumour grading is assessed by histopathological features such as the presence of nuclear pleomorphism, increased mitotic activity and cellularity, endothelial cell proliferation and necrosis.

Interesting data on the biology of gliomas have been obtained by immunostaining of autopsy-derived human whole-brain sections of four patients with diffuse gliomas using a specific antibody detecting the R132H mutation of the gene encoding for isocitrate dehydrogenase 1 (IDH1) (Capper et al. 2009), illustrating that gliomas are not only diffusely infiltrating into central nervous tissue but are in fact diseases of the whole brain bearing tumour cells in macroscopically inconspicuous areas (Sahm et al. 2012).

The WHO classification of gliomas according to histological subtype and grade as predictor of malignant potential, response to treatment and survival is currently challenged by molecular findings that show a better prediction of the outcome than the histological grading alone (Tabatabai et al. 2010; Weller and Wick 2014).

Most prominently, epigenetic silencing of the DNA repair enzyme O6-methylguanine-DNA methyltransferase (MGMT) by promoter methylation in GBM cells predicts responsiveness to temozolomide chemotherapy (Esteller et al. 2000) and is an independent favourable prognostic factor irrespective of treatment (Hegi et al. 2005).

An integrated genomic analysis of GBM led to the discovery of recurrent mutations in the IDH1 gene associated with a significant increase in overall survival (Parsons et al. 2008). In a series of 382 patients with anaplastic astrocytoma (WHO III°) and GBM (WHO IV°), IDH1 mutation was the most prominent single prognostic factor followed by age, histological diagnosis and MGMT (Hartmann et al. 2010), whereas the prognostic value of IDH1 mutations in low-grade

astrocytomas is rather low compared with that in high-grade gliomas (Ahmadi et al. 2012).

Common genetic alterations in tumours with an oligodendroglial component are codeletions of 1p and 19q. Two large prospective randomised trials, RTOG 9402 and EORTC 26951, independently showed that loss of 1p/19q was associated with significantly longer progression-free and overall survival (Cairncross et al. 2013; van den Bent et al. 2013).

Considering the increased impact of molecular markers on the development of treatment strategies in gliomas, the introduction of molecular markers into the next WHO classification of tumours of the nervous system will be inevitable (Weller and Wick 2014).

Especially in unresectable gliomas with limited histological material available for neuropathologic examination, multimodal-imaging-guided stereotactic biopsy correlates significantly better with cell density and proliferation marker MIB-1 labelling than targets that were chosen for biopsy based on the highest amino acid uptake in [^{18}F] FET-PET or contrast enhancement on MRI (Gempt et al. 2014).

1.1.4 Imaging

1.1.4.1 Computed Tomography (CT)

CT information should be obtained from a contrast-enhanced, 1–2-mm, multi-slice CT, performed from the vertex to foramen magnum. Different CT windows (bones, orbit and soft tissue) should be used for the delineation of tumour and critical structures. CT could be an important additional investigation to MRI and PET for visualisation of blood/hemorrhagic tissue and soft tissue calcification or bone structures. Nowadays, target volume delineation for treatment of gliomas should no longer exclusively depend on CT imaging (Fiorentino et al. 2013). In rare cases where patients have an absolute or relative contraindication for MRI examination, e.g. all kinds of pacemakers, insulin or morphine pumps, recently implanted endoprostheses, neurostimulators, cochlear implants, granite splinters, etc., CT alone can be used for target volume delineation.

1.1.4.2 Magnetic Resonance Imaging (MRI)

Due to its outstanding contrast in soft tissue imaging and the availability of axial, sagittal and coronal 3D reconstructable datasets with a slice thickness in the range of 0.5–1.2 mm, pre- and postoperative MRI is the standard imaging modality in glioma target volume delineation and evaluation of treatment response. A standard set of MRI sequences available for glioma target volume delineation should include native and contrast-enhanced 3D-T1-weighted (e.g. MP-RAGE) sequences and thin-sliced 3D-T2-weighted sequences (e.g. fluid-attenuated inversion recovery, FLAIR, T2 SPACE).

Generally, low-grade gliomas WHO grade II are hyperintense on T2-weighted and FLAIR images and hypointense on native T1-weighted MRI. Characteristic for low-grade gliomas is the intact blood-brain barrier (BBB), and therefore no contrast enhancement is seen after intravenous application of gadolinium. However, both the T1-weighted images and the T2 sequences have considerable limitations in the precise visualisation of the gross tumour volume (GTV), especially in low-grade gliomas with diffuse infiltration. Neither on the T1- nor on the T2-weighted images precise differentiation between tumour infiltration, oedema, reactive gliosis and other treatment-related changes is possible.

High-grade gliomas WHO III and IV are characterised by contrast enhancement on T1-weighted MRI. Especially GBM shows areas of necrosis, compression of the surrounding normal tissue and sometimes midline deviation. Tumour-surrounding oedema cannot be differentiated from non-contrast enhancement tumour areas.

In summary, in low- and high-grade gliomas, conventional MRI shows a high sensitivity for the diagnosis of a brain tumour but a low specificity concerning the histology of the tumour tissue. Moreover, traditional MRI is unable to differentiate between tumour and oedema or treatment-related changes. Therefore, the traditional MRI alone does not offer the information necessary for accurate delineation of tumour margins in brain gliomas.

Advances in MRI can provide significant information about the biology of low- and high-grade gliomas and will be used in the future as bio-imaging/biomarkers for the development of improved treatment strategies. There are recent data showing that new MRI techniques are able to detect subtle changes in white matter organisation (diffusion tensor imaging), cellular proliferation (diffusion MRI and MR spectroscopy) or angiogenesis (perfusion MRI) (Price and Gillard 2011). Stadlbauer et al. (2011) used MR spectroscopy for the visualisation of the infiltration zone of gliomas. In 20 patients, they compared the proton-MRI spectroscopy data with the results of stereotactic biopsies and postulated that the method for automated segmentation of the lesion-related metabolic changes significantly improved tumour delineation in brain gliomas compared to traditional methods.

1.1.4.3 Positron Emission Tomography (PET)

Although MRI accurately depicts the anatomy of the brain, neither contrast enhancement in T1-weighted images nor hyperintensity in T2-weighted images is a specific surrogate for neoplastic lesions. Moreover, after intensive multimodality treatment of glioma, it has been realised that effects like pseudo-progression or pseudo-remission may occur, challenging the predominant role of MRI for visualisation of tumour tissue during follow-up (Brandsma et al. 2008).

Mitotically active glioma cells are characterised by increased metabolism (glycolysis, protein synthesis, DNA synthesis; Demetriades et al. 2014), and therefore, imaging of biological and molecular tumour characteristics by PET is an emerging approach to improve the visualisation of actual tumour extent and for radiotherapy treatment planning (Chen 2007; Weber et al. 2008; Grosu and Weber 2010; Götz et al. 2012).

The most widely used PET tracer in oncology is [^{18}F]fluorodeoxyglucose (FDG). In the context of malignant glioma, [^{18}F]FDG-PET was found to be of limited value for GTV delineation, due to the low contrast between healthy brain tissue and tumour (Gross et al. 1998). Amino acid PET has been shown to have a higher sensitivity and specificity, even in comparison to MRI (Grosu and Weber 2010).

Indeed, target volume delineation of malignant glioma can differ significantly between MRI and [^{11}C]methionine (MET)-PET (Grosu et al. 2005a). On the PET/MRI co-registered images, MET uptake on PET and gadolinium enhancement on T1-MRI were detected in all 39 patients (100 %). In 5 patients (13 %), MET uptake matched exactly with the gadolinium enhancement on T1-MRI. However, in 29 patients (74 %), MET uptake was also located outside the gadolinium enhancement on MRI, showing additional areas of tumour infiltration. Moreover, in 27 patients (69 %), gadolinium enhancement was also located outside the MET enhancement on PET, showing that gadolinium actually correlates with post-surgery BBB disturbances and not with tumour tissue. Evaluating the hyperintensity area on T2-MRI in comparison to MET uptake on PET, it was observed that the extension of MET uptake was different from the hyperintensity areas. MET uptake was located also outside of the hyperintensity area in 9 of 18 patients (50 %), suggesting tumour tissue, and in 100 %, the hyperintensity region on T2-weighted MRI extended beyond the MET enhancement area, suggesting post-surgery or tumour-related oedema. These findings could have a significant impact in the development of new recommendations for target volume delineation in gliomas, based on PET.

Lee et al. (2009) evaluated the association between MET uptake on PET and the site of failure after radiochemotherapy of GBM. They found that 19/26 patients had a significant (>1 cm^3) volume delineated by PET (GTV-PET). Five of 19 patients had PET-GTV that was not completely included within the high-dose area, and all the 5 showed noncentral failures (not located in high-dose area). In the group of patients with adequately covered PET-GTV (14/19), only 2 developed a noncentral treatment failure. The authors concluded that inadequate PET-GTV coverage was associated with increased risk of noncentral failure ($p < 0.01$).

The short half-life of [^{11}C]MET, however, requires the presence of an on-site cyclotron. A tracer with a much longer half-life is [^{18}F] fluoroethyl-l-tyrosine (FET), which has later been shown to equally detect biologically active tumour compared to [^{11}C]MET-PET acquired on the same day (Grosu et al. 2011). The impact of

PET-based radiation treatment planning on the outcome of patients with recurrent high-grade gliomas treated with fractionated stereotactic radiotherapy was evaluated in a prospective single-institution trial (Grosu et al. 2005b). The median overall survival was 5 months when treatment planning was based on MRI/CT compared with 9 months when target volume was delineated on amino acid PET and MRI/CT ($p = 0.03$). These data suggest that amino acid PET could have a significant impact on patient outcome. The potential clinical benefit of [^{18}F]FET-PET-based target volume delineation compared to MRI for re-irradiation of recurrent GBM is currently under investigation in a prospective multicentric phase II randomised trial (GLIAA NOA10/ARO 2013-01).

1.1.5 Target Volume Delineation and Radiation Treatment Planning in Gliomas

1.1.5.1 Low-Grade Gliomas (WHO II)

Gross tumour volume (GTV) delineation in low-grade gliomas (oligodendrogliomas, oligoastrocytomas and astrocytomas WHO grade II) is based generally on T2-weighted and FLAIR MRI images (Table 1.2, Shaw et al. 2012; Fairchild et al. 2012; Musat et al. 2010), considering that an important characteristic of these tumours is the absence of contrast enhancement on T1-weighted MRIs. However, it is well known that the sensitivity of T2 and FLAIR MRI for tumour tissue is very high, but the specificity is relatively low. Thus, tumour tissue cannot be differentiated from surrounding oedema or treatment-related changes (e.g. tissue injury after surgery). Therefore, the problem remains that in non-operated low-grade gliomas, the GTV delineated based on T2-weighted and/or FLAIR MRI could encompass not only tumour tissue but also oedematous normal brain tissue. Additionally, in operated patients, the GTV could include close to residual tumour non-tumoural tissue with hyperintense signal on T2 and FLAIR, e.g. post-surgery gliosis and oedema. After complete tumour resection, the concept of GTV encompassing the resection cavity – as used generally in different trials and publications – is not in line with the ICRU Criteria for GTV definition: the resection cavity should be included in the clinical target volume (CTV) and not in the GTV definition.

The CTV encompasses the possible microscopic tumour infiltration, including the resection cavity (in operated patients) and the surrounding normal appearing tissue in an area of 5–15 mm, excluding anatomical borders like the falx, skull, liquor areas, etc. (Fairchild et al. 2012). In our institution, we make the distinction between well-delineated low-grade gliomas, in which the margins from GTV to CTV are ca. 5 mm, and diffuse infiltrative low-grade gliomas, in which the distance from GTV to CTV should be larger (ca. 10–15 mm), considering anatomical borders (Fig. 1.1).

Table 1.2 EORTC and RTOG randomised phase III multicentric studies evaluating the impact of radiotherapy and chemotherapy in low-grade gliomas (WHO II): GTV, CTV and PTV definition

Trial	Irradiation dose	GTV	CTV	PTV	References
EORTC 22033-26033/CE5	50.4/1.8 Gy (28 fx)	Region of high signal intensity on T2 or FLAIR MRI corresponding to the hypodense area on CT, including any areas of CT enhancement, or surgical cavity + any residual tumour	GTV + 1–1.5 cm	CTV + 5–7 mm	Fairchild et al. (2012) Musat et al. (2010)
RTOG 9802	54/1.8 Gy (30 fx)	T2 or FLAIR MRI-defined tumour volume	Not defined s. PTV	GTV + ca. 1 cm[a]	Shaw et al. (2012)

[a]The treatment fields included the T2 or FLAIR MRI-defined tumour volume plus a 2-cm margin to block edge, resulting in an approximate 1-cm dosimetric margin

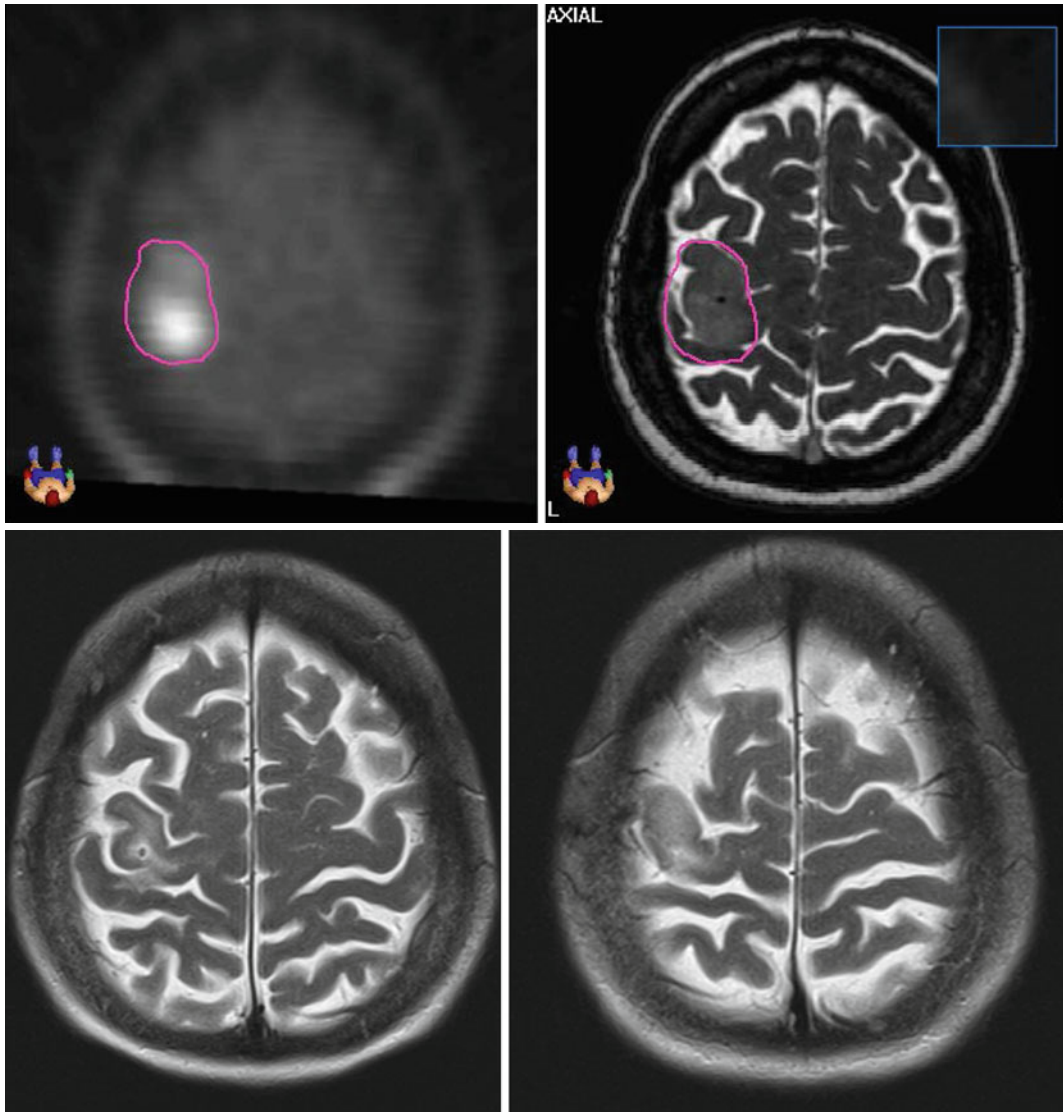

Fig. 1.1 Astrocytoma WHO grade II in a 54-year-old female patient with seizures treated with stereotactic fractionated radiotherapy (2002; total dose 54, 1.8 Gy per fraction). The GTV was delineated based on the MET-PET/T2-MRI image fusion (*upper pictures*). Due to the non-infiltrative pattern of tumour growth, the CTV was defined as 3-mm margin from GTV. The PTV was CTV plus 2 mm. The pictures below show the T2-MRI 10 years after treatment (2012), showing partial tumour remission. The patient showed also complete remission of the neurological symptoms (Department of Radiation Oncology, Technical University of Munich, Germany)

We generally recommend the co-registration of pre- and post-surgery MRI/CT images. The pre-surgery GTV can contribute significant information about the possible microscopic tumour infiltration (CTV). However, in this case, the possible changes of the brain anatomy after surgery should be taken in consideration.

The planning target volume (PTV) should be defined considering the precision of patient positioning in each institution. In low-grade gliomas, high-precision radiation therapy is mandatory. Stereotactic techniques and/or image-guided radiotherapy is needed to reduce the distance between CTV and PTV to 1–3 mm.

Summarising, the target volume delineation for high-precision radiation therapy in low-grade gliomas is based on T2-weighted and FLAIR MRI. Because of the relatively low specificity of

these MRI sequences for tumour tissue, new imaging methods for a higher precision in GTV delineation are needed.

For radiation treatment planning, intensity-modulated radiotherapy combined with stereotactic radiotherapy and/or image-guided radiotherapy should be considered. Multiple fields including vertex fields or combined dynamic arcs should be used to achieve a high conformity index. However, the dose to the thyroid gland, spinal cord and total body should be minimised (Fairchild et al. 2012). The total dose recommended in low-grade gliomas ranges between 50.4 and 54 Gy (Fairchild et al. 2012; Shaw et al. 2012) in 1.8 Gy/day, 5 days/week.

The results of the RTOG (Shaw et al. 2002) and EORTC (Karim et al. 1996; van den Bent et al. 2005) studies, in which the target volume was delineated based on the hypodense area on CT, showed 52–55 % progression-free survival 5 years after radiation therapy. The local recurrence was located in the irradiation field in more than 90 % of patients. The real impact of MRI in comparison to CT for target delineation on the clinical outcome was not evaluated systematically – this could be an interesting question for the more recent RTOG and EORTC trials (Whitfield et al. 2014).

1.1.5.2 High-Grade Gliomas WHO III

Describing target volume delineation for WHO grade III gliomas, Whitfield et al. (2014) mentioned two radiological patterns of such tumours:

1. WHO grade III gliomas that have the radiological characteristics of GBM. These might best be treated based on T1-MRI with gadolinium (see Sect. 5.3).
2. WHO grade III gliomas with low or lack of contrast enhancement on T1-MRI. In these tumours, the GTV should encompass the Gd-T1-MRI plus the hyperintensity area on T2/FLAIR. The CTV should include the GTV plus 1.0–1.5 cm.

Even though, as the authors comment, there is no hard evidence for this strategy, it is well supported by clinical experience. In aggressive high-grade gliomas (group 1), like in GBM, recurrences occurred in more than 90 % in the contrast enhancement area. In a significant number of patients, hyperintensity on T2 is due to oedema, and oedema is a consequence of tumour compression and not of macroscopic tumour invasion (s. amino acid PET data, Sect. 4.3). Therefore, T1-MRI and not T2/FLAIR should be used for GTV delineation. On the other side, in WHO grade III gliomas arising from previous low-grade gliomas (group 2), the regional malignant transformation in small islands is a frequent pathological characteristic. Moreover, oedema due to tumour compression is smaller or absent. Therefore, the T2/FLAIR sequences should be included in target volume delineation because changes in T2/FLAIR are related to tumour invasion. This concept was generally followed also by the EORTC and RTOG clinical trials, like what is presented in Table 1.3.

In our opinion, we have to keep in mind that, fortunately, the prognosis in a significant number of these patients might be favourable. Therefore, we have to put a lot of effort in sparing normal brain tissue to avoid late side effects after radiotherapy. We recommend using additional information from amino acid PET (if available; Fig. 1.2) and pre-surgery MRI/CT for GTV and CTV delineation. Anatomical borders should also be considered. Stereotactic fixation and image-guided radiotherapy could help to reduce the distance from CTV to PTV to 1–2 mm.

The total dose should be 59.4 Gy in 1.8 Gy/day, 5×/week. The delivery of a lower dose (45–50.4 Gy) to a larger PTV (based on T2-MRI/FLAIR) and a higher dose to the boost region (based on GdT1-MRI) is in many cases a good concept, sparing more normal brain tissue (Table 1.3).

1.1.5.3 High-Grade Gliomas WHO IV: Glioblastoma Multiforme

In GBM (WHO IV°), a GTV to CTV margin of even 2 cm is the standard (Hochberg and Pruitt 1980; Wallner et al. 1989). It should be noted that despite the local treatment approach, diffuse glioma represents a systemic brain disease upon diagnosis (Sahm et al. 2012). This fact might explain the limited, if any, role of dose escalation beyond 60 Gy, which was demon-

Table 1.3 EORTC and RTOG randomised phase III multicentric studies evaluating the impact of radiotherapy and chemotherapy in high-grade gliomas (WHO III): GTV, CTV and PTV definition

Trial	Histology	Irradiation dose	GTV	CTV	PTV	References
RTOG 9402	WHO III° AOA, AO	After complete resection: 50.4/1.8 Gy + boost 9 Gy/1.8 Gy	Surgical cavity and T2 abnormality	Not defined (considered in PTV)	GTV + 2 cm, boost: GTV +1 cm	Cairncross et al. (2013)
		After biopsy/incomplete resection: 50.4/1.8 Gy+boost 9/1.8 Gy	Contrast enhancement on T1 and T2 abnormality	Not defined (considered in PTV)	GTV +2 cm, boost: T1 abnormality+1 cm	
EORTC 26951	WHO III° AOA, AO	PTV-1: 45/1.8 Gy PTV-2: 14.4/1.8 Gy	Low-density area on preoperative CT and/or the hyperintensity area on preoperative T2-MRI	Not defined (considered in PTV)	PTV-1: GTV + 2.5 cm PTV-2: GTV + 1.5 cm	van den Bent et al. (2013)
CATNON EORTC 26053/22054	WHO III° glioma	59.4/1.8 Gy	Surgical cavity + contrast-enhancing T1 abnormality + T2/FLAIR abnormality	GTV + 1.5–2 cm	CTV + 5–7 mm	EORTC protocol 26053/22054
NOA 4	WHO III° AA, AOA, AO	59.4–60/1.8 Gy	Preoperative MRI/CT	Not defined (considered in PTV)	GTV + 2 cm	Wick et al. (2009)

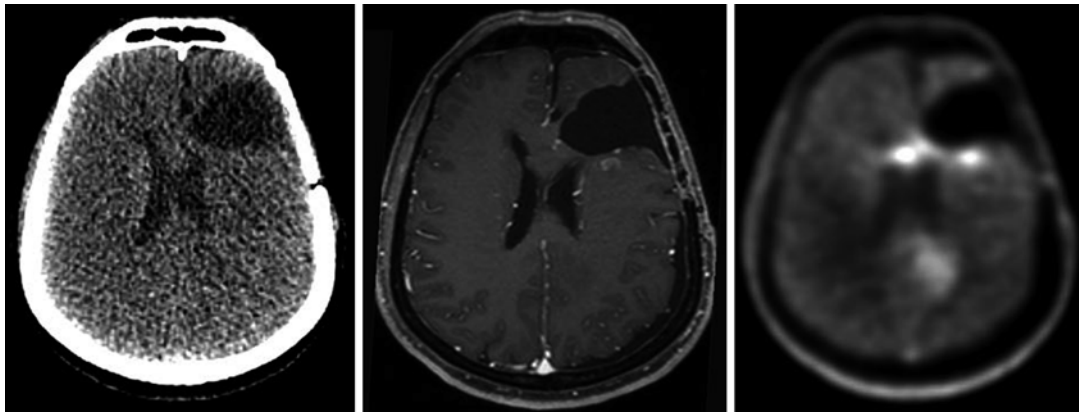

Fig. 1.2 CT, GdT1-MRI and FET-PET in a patient with high-grade astrocytoma (WHO III) after surgery. The FET-PET images offer additional information concerning residual tumour location

strated in numerous studies. However, the impact of dose escalation might become clinically apparent if clear definition of a biologically relevant subvolume or molecular disease feature allows for targeted dose escalation to the right volume in the right patient (Nieder and Mehta 2011).

In GBM, T2/FLAIR sequences often show oedema surrounding the tumour, suspicious of subclinical tumour cell infiltration. However, for GBM it has been shown that inclusion of this oedema in the GTV leads to significantly larger irradiation volumes and doses to the whole brain compared to a standard GTV to CTV margin of 2 cm without inclusion of oedema, but does not alter the central pattern of failure (Chang et al. 2007). Therefore, GdT1-MRI sequences should be the basis for GTV delineation in GBM (Fig. 1.3). Excluding peritumoural oedema may permit a significant reduction of irradiated brain volume, but safety, efficacy and reduction in treatment-related neurotoxicity have not been demonstrated in prospective, randomised trials yet (Minniti et al. 2010). Different strategies for target volume delineation in GBM are presented in Table 1.4.

Like in other gliomas, amino acid PET and pre-surgery MRI/CT should be co-registered with the planning imaging and considered in the GTV and CTV delineation.

Generally, GBMs are treated with a total dose of 60, 2 Gy/day, 5×/week. Recent studies show that in elderly patients hypofractionation could reduce the treatment time without significant side effects (Fariselli et al. 2013; Minniti et al. 2013; Tanaka et al. 2013).

1.1.5.4 Recurrent Gliomas

Summarising the data from the literature about re-irradiation in high-grade gliomas, we found a significant number of studies (14 included in a previous review) evaluating 300 patients with GBM. Six months progression-free survival was 28–39 %, 1-year survival was 18–48 % without additional chemotherapy (two studies: topotecan and CCNU), and the median value for 1-year survival rate was 26 % (Nieder et al. 2008). These are encouraging results considering the relatively low rate of serious side effects if the total re-irradiation dose remains lower than 30–40 Gy in 2–5 Gy/fraction (Mayer and Sminia 2008). However, systematic randomised trials are needed to fully elucidate the role of re-irradiation. Ryu et al. (2014) recently reported class III evidence confirming that re-irradiation can be safely given for progressive GBM. Generally, the GTV encompasses the contrast enhancement on GdT1-MRI with a small margin of 3–5 mm to CTV. Re-irradiation should be performed using high-precision radiation therapy (stereotactic radiotherapy, image-guided radiotherapy). Therefore, the typical distance from CTV to PTV is small, e.g. 1–3 mm (see also Sect. 4.3) (Grosu et al. 2005b).

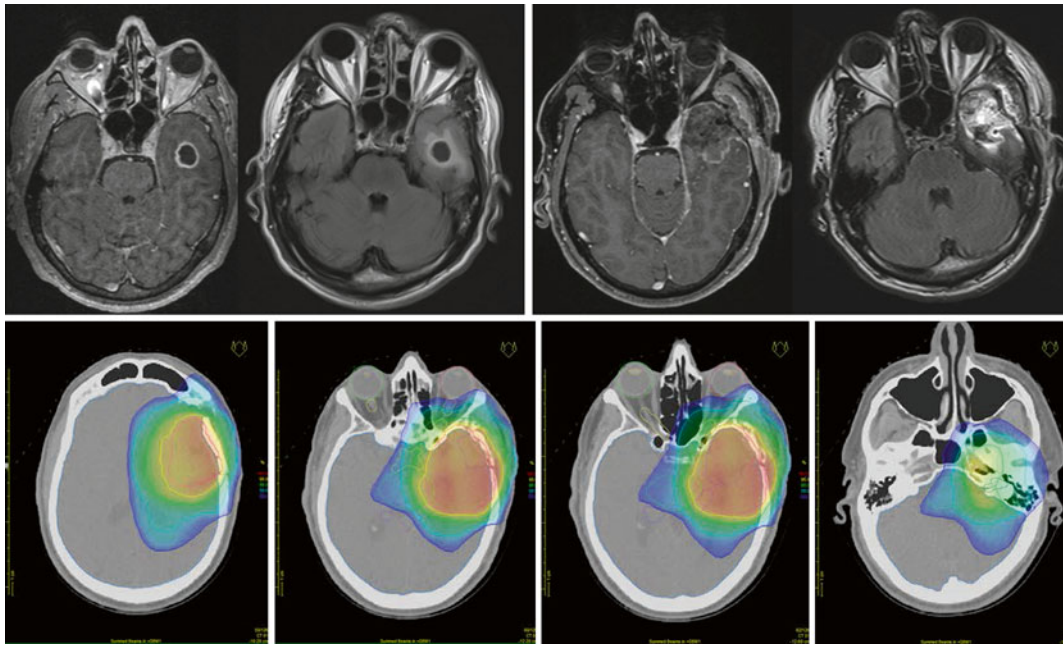

Fig. 1.3 A 49-year-old male patient with GBM. From *left to right*: Preoperative contrast-enhanced T1 and FLAIR MRI and postoperative contrast-enhanced T1 and FLAIR MRI sequences. Corresponding radiotherapy treatment plan: *yellow* 95 % isodose, *green* 80 % isodose, *light blue* 50 % isodose and *dark blue* 30 % isodose

Table 1.4 EORTC and RTOG randomised phase III multicentric studies evaluating the impact of radiotherapy and chemotherapy in glioblastoma (GBM, WHO IV): GTV, CTV and PTV definition

Trial	Irradiation dose	GTV	CTV	PTV	References
EORTC 22981/26981/ NCIC CE3, BO21990	60/2 Gy	Surgical cavity + contrast-enhancing T1 abnormality	GTV + 2–3 cm	Not defined	Stupp et al. (2005) Chinot et al. (2014)
RTOG 0825	PTV1: 46/2 Gy PTV2: 14/2 Gy	GTV1: surgical cavity + T1 contrast-enhancing abnormality + T2/ FLAIR abnormality GTV2: surgical cavity + T1 contrast-enhancing abnormality	CTV1: GTV1 + 2–2.5 cm CTV2: GTV2 + 2 cm	PTV1: CTV1 + 3–5 mm PTV2: CTV2 + 3–5 mm	Gilbert (2014)

1.1.5.5 Organs at Risk

The organs at risk that should also be delineated include the eyes, lenses, optic nerves, optic chiasm, inner ears, brainstem, pituitary gland and hypothalamus. Additionally, the volume of the whole brain should be contoured to be able to evaluate the mean brain dose. Many centres also delineate the hippocampi to estimate the risk of neurocognitive decline and to be able to spare these structures as much as possible by using IMRT, if applicable (Table 1.5).

1.2 Brain Metastases

1.2.1 Epidemiology

Brain metastases are by far the most common neoplasms in the adult brain and approximately 20–30 % of all patients with metastatic cancer develop brain metastases during the history of their disease (Posner and Chernik 1978).

Table 1.5 Tolerance doses for intracranial organs

Organ	Volume	Volume max	Max point dose	Clinical endpoint/toxicity ≥grade 3	References
Brain	1/3	TD5/5: 60 Gy TD50/5: 75 Gy	n.a.	Necrosis infarction	Emami et al. (1991)
	2/3	TD5/5: 50 Gy TD50/5: 65 Gy	n.a.	Necrosis infarction	
	3/3	TD5/5: 45 Gy TD50/5: 60 Gy	n.a.	Necrosis infarction	
	1/3	TD5/5: 72 Gy	n.a.	Necrosis infarction	Lawrence et al. (2010)
Optic nerves and chiasm	1/3	TD5/5: 50 Gy TD50/5: 65 Gy	n.a.	Visual impairment	Emami et al. (1991)
	2/3	TD5/5: 50 Gy TD50/5: 65 Gy	n.a.	Visual impairment	
	3/3	TD5/5: 50 Gy TD50/5: 65 Gy	n.a.	Visual impairment	
	n.a.	n.a.	55 Gy	Visual impairment	Mayo et al. (2010)
Brainstem	n.a.	n.a.	≤54 Gy	Neuropathy	Daly et al. (2007)
	<1 ml	55 Gy	n.a.	Neuropathy	Schoenfeld et al. (2008)
	1/3	TD5/5: 60 Gy TD50/5: 75 Gy	n.a.	Neuropathy	Emami et al. (1991)
	2/3	TD5/5: 53 Gy TD50/5: 70 Gy	n.a.	Neuropathy	
	3/3	TD5/5: 50 Gy TD50/5: 65 Gy	n.a.	Neuropathy	
Retinae	1/3	TD5/5: 45 Gy TD50/5: 65 Gy	n.a.	Blindness	Emami et al. (1991)
	2/3	TD5/5: 45 Gy TD50/5: 65 Gy	n.a.	Blindness	
	3/3	TD5/5: 45 Gy TD50/5: 65 Gy	n.a.	Blindness	
Lenses	1/3	TD5/5: 10 Gy TD50/5: 18 Gy	n.a.	Cataract	Emami et al. (1991)
	2/3	TD5/5: 10 Gy TD50/5: 18 Gy	n.a.	Cataract	
	3/3	TD5/5: 10 Gy TD50/5: 18 Gy	n.a.	Cataract	

TD5/5: tolerance dose of 5% risk to develop ≥ grade 3 toxicity within 5 years
TD50/5: tolerance dose of 50% risk to develop ≥ grade 3 toxicity within 5 years

1.2.2 Pathology

At autopsy, parenchymal metastases are typically well-circumscribed nodules (in sharp contrast to the diffusely infiltrating gliomas) of various sizes which, depending on their histological site of origin, can be solid to partially cystic structures filled with hemorrhagic fluid, mucinous material or necrotic debris (Barajas and Cha 2012).

The development of brain metastases requires distinct molecular interactions between the cancer cell and the cerebral microenvironment (Langley and Fidler 2013; Martinez et al. 2013). Since the brain is not equipped with lymphatic vessels, tumour cells can only access the brain via the blood stream and subsequent conquering of the blood-brain barrier (BBB), mainly built by vascular endothelium, pericytes and astroglial end-feet processes (Armulik et al. 2010). There is evidence from animal models that the invasion of the BBB requires interaction of the metastatic cell with all of the mentioned cell types (Kienast et al. 2010).

Furthermore, once a tumour cell has managed to circumvent the BBB, the cerebral microenvironment may provide a chemoprotective niche, exemplified by the well-known fact that patients respond to a systemic treatment (chemotherapy, antihormonal therapy, tyrosine-kinase inhibitors, etc.) in all tumour sites except the brain or develop new brain metastases while the systemic disease is not progressing under therapy (Palmieri et al. 2007). On the one hand, it is straightforward to hypothesise that the BBB also hinders drugs to penetrate into the CNS so that an effective serum level of chemotherapy does not necessarily lead to therapeutic levels in the brain. On the other hand, preclinical data indicate astrocyte-induced upregulation of survival genes in the tumour cells associated with drug resistance, increased survival and decreased apoptosis (Régina et al. 2001).

A somehow related, but yet distinct, survival strategy of a metastatic tumour cell is called dormancy, a state in which a cancer cell is unable to proliferate but still able to resist apoptosis (Bragado et al. 2012). The mechanisms of dormancy are not understood yet. Several mechanisms are discussed: a signal from the tissue the cancer originated from could inhibit proliferation but not induce apoptosis (Kim et al. 2009), a missing signal for proliferation from the host tissue (Horak et al. 2008), or the host microenvironment inducing epigenetic changes that induce quiescence (Husemann et al. 2008) are the predominant hypothesis.

From the clinical perspective, indirect hints on the biology of individual metastases were derived from a study correlating contrast enhancement of brain metastases on T1 magnetic resonance (MR) images with the freedom from progression (FFP) probability after radiosurgery (Goodman et al. 2001), with the highest FFP probability in homogeneously enhancing lesions and the lowest FFP probability in ring-enhancing brain metastases. Non-contrast-enhancing areas within a single brain metastasis indicate the presence of poorly perfused subregions that may contain hypoxic, and therefore more radioresistant, tumour cells. Data from the pre-MRI era already suggested that homogeneously enhancing lesions responded better to whole-brain radiotherapy (WBRT) than ring-enhancing lesions with central necrosis and that extent of necrosis added additional information to lesion volume when predicting the likelihood of complete remission (Nieder et al. 1997).

1.2.3 Imaging

1.2.3.1 Computed Tomography (CT)

For high-precision radiation therapy, CT for radiation treatment planning should be performed in 1 to (max.) 2 mm slices, without gap, with i.v. contrast. The CT should be co-registered with the MRI. The accuracy of the image registration should be evaluated based on anatomical markers slide by slide.

In patients with multiple brain metastases not eligible for a local treatment approach and/or in a reduced performance status, a contrast-enhanced diagnostic CT scan alone can be sufficient for diagnosis and referral for 2D-planned WBRT. For screening purposes in neurologically asymptomatic patients, retrospective data in stage III non-small cell lung cancer (NSCLC) patients indicate no additive value of cranial MRI to contrast-enhanced diagnostic CT together with [^{18}F]FDG-PET (Hendriks et al. 2013). However, because of the high sensitivity and specificity, MRI is still considered the gold standard for the diagnosis of brain metastases (s. below). In the context of radiotherapy treatment planning, especially when high-precision stereotactic radiosurgery (SRS) or stereotactic fractionated radiotherapy (SFRT) is the treatment of choice, treatment planning should not depend on cranial CT imaging alone.

1.2.3.2 Magnetic Resonance Imaging (MRI)

Contrast-enhanced T1-weighted MRI sequences (axial, sagittal and coronal axes) are the gold standard for diagnosis and radiation treatment planning of brain metastases, and sequences should include native and contrast-enhanced T1 sequences, as well as T2-weighted and FLAIR sequences (Barajas and Cha 2012; Anzalone et al. 2013). Ohana et al. (2014) evaluated if standard one single contrast-enhanced T1-weighted 3D gradient-echo MRI is sufficient for cerebral staging of lung cancer and concluded that, if positive, the investigation can be completed with a T2* sequence for hemorrhagic assessment.

In contrast to glioma, most brain metastases grow expansively rather than diffusely infiltrating the surrounding tissue and take up contrast due to the fact that they reach the brain via the blood stream and can settle down in the CNS via disruption of the BBB. Minimal slice thicknesses for MRI as well as for planning CT scans should be ≤2 mm.

The role of functional MRI for radiation treatment planning in brain metastases is intensively discussed in the literature.

Integration of functional MRI (fMRI) and white matter tractography in target volume definition and treatment planning may be helpful to identify and protect eloquent areas in the brain (Pantelis et al. 2010).

Novel developments, such as 3 T diffusion-weighted MRI (DWI, Chiang et al. 2004), diffusion tensor imaging (DTI, Lu et al. 2003) or delayed contrast extravasation MRI (Zach et al. 2012), may in the future further improve discrimination between tumour and surrounding normal tissue and therefore serve even more precise definition of GTV and target volumes with regard to radiotherapy treatment planning (Lee et al. 2013; Galldiks et al. 2012).

Jakubovic et al. (2014) observed that MRI-based tumour perfusion parameters are biomarkers predicting the response of brain metastases after radiation treatment: a lower K2trans in responders relative to non-responders at 1 week post-irradiation was predictive for tumour response and progressive disease showed a low relative cerebral blood volume (rCBV) at 1 month relative to non-progression. They concluded that further study is required to determine whether these biomarkers can serve as clinically useful surrogates to guide treatment decisions.

A Japanese group (Ohtakara and Hoshi 2014) evaluated the potential geometrical change and/or displacement of the target relative to the cranium during stereotactic fractionated radiotherapy (SFRT) for brain metastases. They reported that target deformity and/or deviation can unexpectedly occur even during relatively short-course SFRT, inevitably leading to a gradual discrepancy between the planned and actually delivered doses to the tumour and surrounding tissue. Therefore, this factor should also be considered in addition to the immobilisation accuracy, as image guidance with bony anatomy alignment does not necessarily guarantee accurate target localisation until completion of SFRT. This interesting observation should be evaluated in larger studies, in the broader context of adaptive radiation therapy (ART).

1.2.3.3 Positron Emission Tomography (PET)

Due to the low spatial resolution of PET, neither FDG, nor MET, nor FET is currently in use for high-precision treatment planning. Nevertheless, [^{18}F]FDG-PET, [^{9}C]MET-PET or [^{18}F]FET-PET examinations can be extremely valuable tools to distinguish between a recurrent lesion after treatment and radiation necrosis (Ericson et al. 1996; Grosu et al. 2011; Galldiks et al. 2012).

1.2.4 Target Volume Delineation in Brain Metastases

1.2.4.1 Target Volume Delineation in Whole-Brain Radiotherapy (WBRT)

The life expectancy of patients with multiple brain metastases receiving best supportive care (BSC) with symptom-relieving administration of corticoids is very limited (Nieder et al. 2013). For decades, WBRT was the standard of care for the vast majority of patients diagnosed with brain metastases, prolonging the survival time by 3–6 months (Tsao et al. 2012). For patients with multiple brain metastases (>4) and/or meningiosis carcinomatosa, WBRT is still the treatment of choice.

Conventional WBRT is usually planned using the treatment simulator, and dose is applied via two opposing beams encompassing the osseous boundaries of the brain including the first cervical vertebra to ensure safe and proper dose delivery (Fig. 1.4).

Standard treatment regimen is 30-35-40 Gy in 3–2.5-2 Gy per fraction. Prophylactic cranial irradiation (PCI) for prevention of brain metastases from small cell cancers, most prominently small cell lung cancer (SCLC), is often applied in 2 Gy per fraction to a total dose of 30 or 2.5 Gy per fraction to a total dose of 25 Gy.

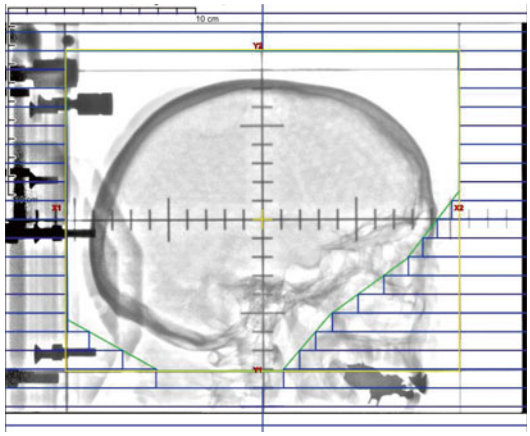

Fig. 1.4 Simulator-based conventional WBRT treatment set-up

1.2.4.2 Target Volume Delineation in Hippocampal-Avoiding Whole-Brain Radiotherapy (HA-WBRT)

In contrast to conventional 2D-planned WBRT, hippocampal-avoiding whole-brain radiotherapy (HA-WBRT) is a novel technique using either linear accelerator-based IMRT/IMAT or helical tomotherapy (Gondi et al. 2010a; Prokic et al. 2013) to prevent the treatment-related side effect of neurocognitive deterioration.

The human brain structure that is most critically involved in episodic memory processing is the hippocampus (Milner et al. 1998; Dickerson and Eichenbaum 2010). Damage to the hippocampi can lead to profound amnestic syndromes (Scoville and Milner 1957). Recently, it has been demonstrated that a reduction of adult neurogenesis within the hippocampus leads to hippocampal dysfunction (Shors et al. 2001; Deng et al. 2010; Small et al. 2011). Irradiation blocks adult neurogenesis in the subgranular zone of the hippocampus, as has been shown in rodents (Monje et al. 2002). Furthermore, cranial irradiation has been shown to compromise the cellular and subcellular architecture of the hippocampal formation in mice with regard to dendritic branching, number and density of dendritic spines as well as abundance of pre- and postsynaptic markers (Parihar and Limoli 2013). Episodic memory deficits after WBRT have therefore been concluded to be associated with hippocampal damage (Dietrich et al. 2008), and this damage might be prevented by hippocampal-avoidance WBRT, which in turn is hypothesised to attenuate cognitive decline after HA-WBRT as measured by standardised neuropsychological testing.

Indeed, clinical data strongly support this hypothesis. In a prospective randomised trial investigating neurocognition in patients after SRS versus SRS plus WBRT, patients treated with SRS plus WBRT were at a greater risk of a significant decline in learning and memory function by 4 months after treatment compared with the group that received SRS alone (Chang et al. 2009). In 18 adult patients receiving SFRT for benign or low-grade intracranial tumours, an EQD2 > 7.3 Gy to 40 % of the bilateral hippocampi was associated with long-term impairment in neurocognitive function tests (Gondi et al. 2012). Preliminary results of the RTOG 0933 phase II trial showed that conformal avoidance of the hippocampus during WBRT is indeed associated with a significant memory preservation at 4 and 6 months of follow-up (Gondi et al. 2014).

In preparation of RTOG 0933 a safety profile to estimate the risk of developing new metastases within 5 mm of the hippocampus has been established, showing that there is a baseline risk for metastases in this region of 8.6 % (Gondi et al. 2010b). Additionally, HA-WBRT was tested for bearing the risk of undertreatment. For SCLC, it bears a minimally elevated risk of failure compared to standard WBRT. In NSCLC, HA-WBRT is most likely not associated with a clinically relevant increase in risk of failure (Harth et al. 2013). Taken together, these data predict that HA-WBRT is safe for clinical testing in patients with brain metastases.

In order to further improve local control, protocols employing a simultaneous integrated boost on macroscopic metastases in addition to hippocampal avoidance are emerging. First results indicate that these concepts are feasible, safe and associated with similar survival times and toxicities compared to conventional SRS/SFRT +/– WBRT (Prokic et al. 2013; Awad et al. 2013; Oehlke et al. 2015).

To date, several contouring atlases exist to standardise hippocampal delineation on contrast-

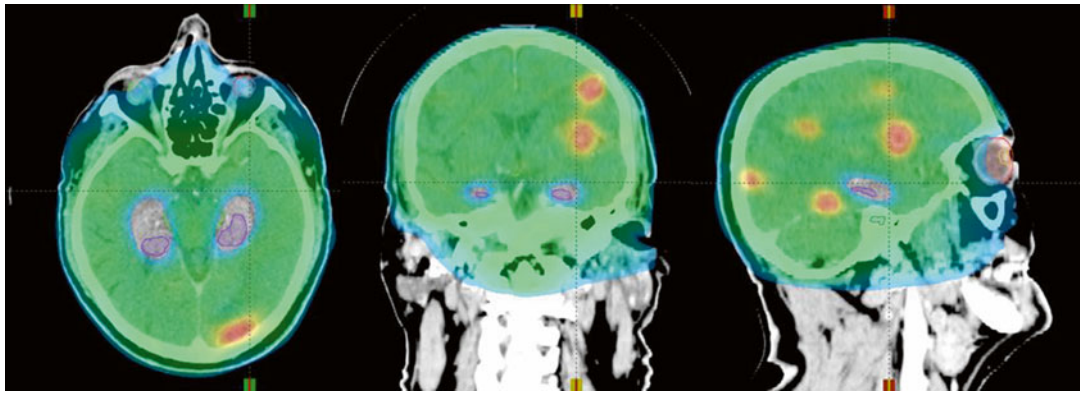

Fig. 1.5 Example of hippocampal-avoiding whole-brain radiotherapy (*HA-WBRT*) and additional simultaneous integrated boost (*SIB*) on multiple brain metastases in a patient with disseminated NSCLC (Courtesy of O. Oehlke and A.-L. Grosu, University Medical Center Freiburg, Germany)

enhanced T1-weighted MRI in the context of clinical trials (Chera et al. 2009; Gondi et al. 2009). The whole-brain contour is usually delineated as the inner boundary of the osseous skull from the vertex to approximately 0.5 cm caudal to the foramen magnum. For creation of a PTV, this volume is expanded by 3–5 mm depending on the accuracy achievable by the fixation system employed. The OAR that should be delineated includes eyes, lenses, lacrimal glands, optic nerves, optic chiasm, inner ears and brainstem (Fig. 1.5).

1.2.4.3 Target Volume Delineation for Stereotactic Radiosurgery (SRS) and Stereotactic Fractionated Radiotherapy (SFRT)

The standard treatment for patients in a good performance status with a limited number of brain metastases, usually 1–3, from solid tumours is stereotactic radiosurgery (SRS; Kocher et al. 2011; Nieder et al. 2014). Addition of WBRT improves intracranial relapse-free time, but negatively impacts health-related quality of life (HRQoL, see above) and is not associated with an improvement in overall survival (Chang et al. 2009; Kocher et al. 2011; Soffietti et al. 2013). Consequently, observation with close monitoring with MRI after a local treatment approach became a feasible concept that is neither detrimental for HRQoL nor significantly compromising overall survival (Kocher et al. 2014).

In general, SRS should be considered in patients with either a single lesion up to 3.5 cm in diameter or up to four lesions with a maximum diameter of 2.5 cm each, especially including metastases not suitable for a surgical approach, located in the brainstem and without mass effect (Kocher et al. 2014).

SRS is also an established treatment option for patients previously irradiated with WBRT. The RTOG performed a prospective phase I clinical trial of SRS in recurrent, previously irradiated primary brain tumours and brain metastases. RTOG study 90-05 was a dose escalation trial, which included 100 patients with brain metastases and 56 with primary brain tumours. The brain metastases patients were included after prior WBRT to a median dose of 30 Gy (Shaw et al. 1996, 2000). SRS could be administered with a linear accelerator or Gamma Knife. Eligible patients had received first-line radiotherapy at least 3 months prior to study entry, and in the study, the actual median interval was 17 months. Seventy-eight percent had single lesions. Dose was determined by the maximum diameter of the tumour. Initial doses were 18 Gy for lesions ≤20 mm, 15 Gy for lesions measuring 21–30 mm and 12 Gy for lesions measuring 31–40 mm. Dose was prescribed to the 50–90 % isodose line, which was to encompass the entire enhancing tar-

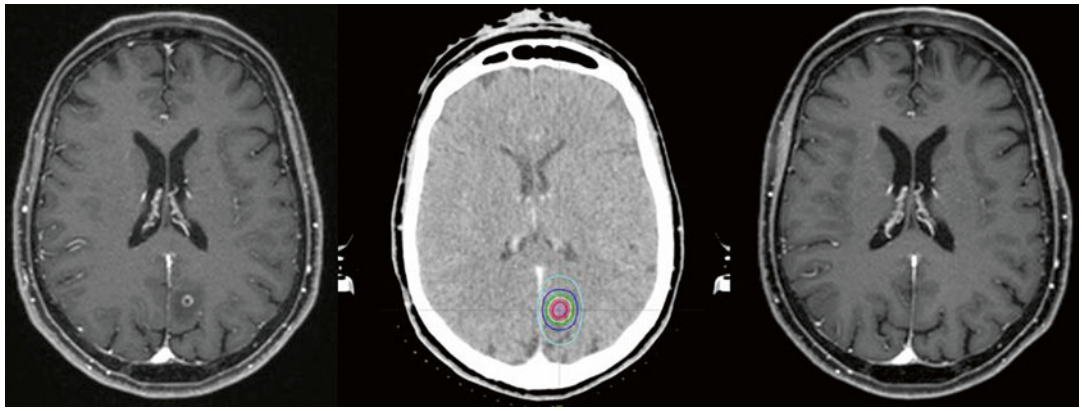

Fig. 1.6 Contrast-enhanced T1-weighted MR images from a patient with a solitary brain metastasis from NSCLC pre- (*left*) and 3 months post-SRS (*right*) showing complete remission of the treated lesion. The corresponding dose distribution is shown in the *middle*

get volume. The dose was escalated in 3 Gy increments providing there was not an excess of unacceptable toxicity. The trial eventually defined the maximum acutely tolerable SRS dose in this setting, except for lesions ≤20 mm where the dose was not escalated beyond 24 Gy because of investigators' reluctance. While small lesions ≤20 mm can be treated with up to 24 Gy to the margin of the lesion, those that measure between 21 and 30 mm might receive 18 Gy and those that measure between 31 and 40 mm 15 Gy. Long-term toxicity data for brain metastases patients are available only from the initial publication (Shaw et al. 1996). They are based on 64 patients. Four patients developed radionecrosis requiring operation 5–14 months after SRS. From the final report, (Shaw et al. 2000), combined radionecrosis data on patients with brain metastases and primary brain tumours are available. The actuarial incidence was 8 and 11 % at 12 and 24 months, respectively. Due to the fact that a high dose (usually 15–25 Gy on the tumour-surrounding isodose) is delivered in a single fraction with a steep dose gradient towards the surrounding normal tissue (Fig. 1.6), the GTV encompasses only the contrast-enhanced lesion in T1-weighted MRI sequences. In some centres the GTV then equals the PTV, reflecting the fact that, in contrast to primary CNS tumours, brain metastases rather grow expansively than diffusely infiltrating the surrounding tissue. Especially by using invasive fixation methods (e.g. a stereotactic head frame), a GTV to PTV margin can be omitted. In times of IGRT, a rigid head frame is more and more replaced by thermoplastic masks combined with non-invasive patient positioning systems built in the linear accelerator (LINAC) or CyberKnife technology. Nevertheless, it has been shown that brain metastases especially from SCLC and melanoma show an infiltration beyond the contrast-enhancing lesion visible in T1-weighted MRI (Baumert et al. 2006) and therefore often a 1 mm margin is added from GTV to PTV which has been shown to increase local control (Noel et al. 2003). Increasing the GTV to PTV margin to 2 mm, no further increase in local control was observed, but significantly more side effects occurred (Nataf et al. 2008).

For the treatment of brain metastases that are too large for SRS, a fractionated regime (SFRT) is often preferred. Delineation of the GTV equals the approach employed for SRS, but the GTV to PTV margin may be increased to up to 3 mm in total.

1.2.4.4 Organs of Risk (OAR) Delineation and Tolerance Dose of OAR

The OAR that should be delineated includes whole brain, eyes, lenses, retina, lacrimal glands, optic nerves, optic chiasm, inner ears (cochlea), pituitary gland, hypothalamus, hippocampi and brainstem.

Since the use of hypofractionation bears the risk of serious treatment-related late side effects

Table 1.6 Tolerance doses for intracranial organs

Organ	No. of fractions	Volume	Volume max	Max point dose	Clinical endpoint/toxicity ≥ grade 3	Reference
Brain	1	<10 ml	10 Gy	n.a.	Necrosis/infarction	Lawrence et al. (2010)
	1	<5 ml	12 Gy	n.a.	Necrosis/infarction	
Brainstem	1	<1 ml	10 Gy	15 Gy	Neuropathy	Timmerman (2008)
	3	<1 ml	18 Gy	23 Gy	Neuropathy	
	4	<1 ml	24 Gy	28 Gy	Neuropathy	
	5	<1 ml	26 Gy	31 Gy	Neuropathy	
Optic/cranial nerves	1	<0.2 ml	8 Gy	10 Gy	Neuritis	Timmerman (2008)
	3	<0.2 ml	15 Gy	19.5 Gy	Neuritis	
	4	<0.2 ml	18 Gy	22.8 Gy	Neuritis	
	5	<0.2 ml	20 Gy	25 Gy	Neuritis	
Chiasm	1	<0.2 ml	8 Gy	10 Gy	Neuritis	Timmerman (2008)
	3	<0.2 ml	15 Gy	19.5 Gy	Neuritis	
	4	<0.2 ml	18 Gy	22.8 Gy	Neuritis	
	5	<0.2 ml	20 Gy	25 Gy	Neuritis	
Cochlea	1	n.a.	n.a.	12 Gy	Hearing loss	Timmerman (2008)
	3	n.a.	n.a.	20 Gy	Hearing loss	
	4	n.a.	n.a.	25 Gy	Hearing loss	
	5	n.a.	n.a.	27.5 Gy	Hearing loss	

and availability of prospective data concerning dose tolerance of different (not only intracranial) organs is still limited, commonly accepted normal tissue dose constraints are often invalidated but empirically found to be safe in clinical routine (Timmerman 2008). Collecting and reporting dosimetric data of patients treated with SRS or SFRT is therefore an important basis of further relating dose to toxicity and clinical outcome. Due to the fact that nervous tissue is regarded as a serial organ, the maximum point dose and maximum dose to a small volume of OARs is of special importance. An overview of widely accepted normal tissue dose constraints in brain SRS and SFRT is given in Table 1.6.

References

Ahmadi R, Stockhammer F, Becker N et al (2012) No prognostic value of IDH1 mutations in a series of 100 WHO grade II astrocytomas. J Neurooncol 109: 15–22

Anzalone N, Essig M, Lee SK et al (2013) Optimizing contrast-enhanced magnetic resonance imaging characterization of brain metastases: relevance to stereotactic radiosurgery. Neurosurgery 72:691–701

Armulik A, Genove G, Mae M et al (2010) Pericytes regulate the blood-brain barrier. Nature 468:557–561

Awad R, Fogarty G, Hong A et al (2013) Hippocampal avoidance with volumetric modulated arc therapy in melanoma brain metastases – the first Australian experience. Radiat Oncol 8:62

Barajas RF, Cha S (2012) Imaging diagnosis of brain metastasis. Prog Neurol Surg 25:55–73

Baumert BG, Rutten I, Dehing-Oberije C et al (2006) A pathology-based substrate for target definition in radiosurgery of brain metastases. Int J Radiat Oncol Biol Phys 66:187–194

Bragado P, Sosa MS, Keely P et al (2012) Microenvironments dictating tumor cell dormancy. Recent Results Res Cancer 195:25–39

Brandsma D, Stalpers L, Taal W et al (2008) Clinical features, mechanisms, and management of pseudoprogression in malignant gliomas. Lancet Oncol 9:453–461

Cairncross G, Wang M, Shaw E et al (2013) Phase III trial of chemoradiotherapy for anaplastic oligodendroglioma: long-term results of RTOG 9402. J Clin Oncol 31:337–343

Capper D, Zentgraf H, Balss J et al (2009) Monoclonal antibody specific for IDH1 R132H mutation. Acta Neuropathol 118:599–601

Chang EL, Akyurek S, Avalos T et al (2007) Evaluation of peritumoral edema in the delineation of radiotherapy clinical target volumes for glioblastoma. Int J Radiat Oncol Biol Phys 68:144–150

Chang EL, Wefel JS, Hess KR et al (2009) Neurocognition in patients with brain metastases treated with radiosurgery or radiosurgery plus whole-brain irradiation: a randomised controlled trial. Lancet Oncol 10:1037–1044

Chen W (2007) Clinical applications of PET in brain tumors. J Nucl Med 48:1468–1481

Chera BS, Amdur RJ, Patel P et al (2009) A radiation oncologist's guide to contouring the hippocampus. Am J Clin Oncol 32:20–22

Chiang IC, Kuo YT, Lu CY et al (2004) Distinction between high-grade gliomas and solitary metastases using peritumoral 3-T magnetic resonance spectroscopy, diffusion, and perfusion imagings. Neuroradiology 46:619e27

Chinot OL, Wick W, Mason W et al (2014) Bevacizumab plus radiotherapy-temozolomide for newly diagnosed glioblastoma. N Engl J Med 370:709–722

Daly ME, Chen AM, Bucci MK et al (2007) Intensity-modulated radiation therapy for malignancies of the nasal cavity and paranasal sinuses. Int J Radiat Oncol Biol Phys 67:151–157

Demetriades AK, Almeida AC, Bhangoo RS et al (2014) Applications of positron emission tomography in neuro-oncology: a clinical approach. Surgeon 12(3):148–157

Deng W, Aimone JB, Gage FH (2010) New neurons and new memories: how does adult hippocampal neurogenesis affect learning and memory? Nat Rev Neurosci 11:339–350

Dickerson BC, Eichenbaum H (2010) The episodic memory system: neurocircuitry and disorders. Neuropsychopharmacology 35:86–104

Dietrich J, Monje M, Wefel J et al (2008) Clinical patterns and biological correlates of cognitive dysfunction associated with cancer therapy. Oncologist 13:1285–1295

Emami B, Lyman J, Brown A et al (1991) Tolerance of normal tissue to therapeutic irradiation. Int J Radiat Oncol Biol Phys 21:109–122

EORTC protocol 26053-22054. (2007) Phase III trial on concurrent and adjuvant temozolomide chemotherapy in non-1p/19q deleted anaplastic glioma. The CATNON intergroup trial. http://www.eortc.be/protoc/Details.asp?Protocol=26053

Ericson K, Kihlström L, Mogard J et al (1996) Positron emission tomography using 18 F-fluorodeoxyglucose in patients with stereotactically irradiated brain metastases. Stereotact Funct Neurosurg 66(Suppl 1):214–224

Esteller M, Garcia-Foncillas J, Andion E et al (2000) Inactivation of the DNA-repair gene MGMT and the clinical response of gliomas to alkylating agents. N Engl J Med 343:1350–1354, Erratum in: N Engl J Med 343:1740

Fairchild A, Weber DC, Bar-Deroma R et al (2012) Quality assurance in the EORTC 22033–26033/CE5 phase III randomized trial for low grade glioma: the digital individual case review. Radiother Oncol 103:287–292

Fariselli L, Pinzi V, Milanesi I et al (2013) Short-course radiotherapy in elderly patients with glioblastoma: feasibility and efficacy of results from a single centre. Strahlenther Onkol 189:456–461

Ferlay J, Shin HR, Bray F et al (2010) Estimates of worldwide burden of cancer in 2008: GLOBOCAN 2008. Int J Cancer 127:2893–2917

Fiorentino A, Caivano R, Pedicini P et al (2013) Clinical target volume definition for glioblastoma radiotherapy planning: magnetic resonance imaging and computed tomography. Clin Transl Oncol 15:754–758

Galldiks N, Stoffels G, Filss CP et al (2012) Role of O-(2-(18)F-fluoroethyl)-L-tyrosine PET for differentiation of local recurrent brain metastasis from radiation necrosis. J Nucl Med 53:1367–1374

Gempt J, Soehngen E, Förster S et al (2014) Multimodal imaging in cerebral gliomas and its neuropathological correlation. Eur J Radiol 83:829–834

Gilbert MR, Dignam JJ, Armstrong TS et al (2014) A randomized trial of bevacizumab for newly diagnosed glioblastoma. N Engl J Med 370:699–708

Gondi V, Tomé W, Rowley H, Mehta M (2009) Hippocampal contouring: a contouring atlas for RTOG 0933. http://www.rtog.org/CoreLab/ContouringAtlases/HippocampalSparing.aspx

Gondi V, Tolakanahalli R, Mehta MP et al (2010a) Hippocampal-sparing whole-brain radiotherapy: a "how-to" technique using helical tomotherapy and linear accelerator-based intensity-modulated radiotherapy. Int J Radiat Oncol Biol Phys 78:1244–1252

Gondi V, Tome WA, Marsh J et al (2010b) Estimated risk of perihippocampal disease progression after hippocampal avoidance during whole-brain radiotherapy: safety profile for RTOG 0933. Radiother Oncol 95(3):327–331

Gondi V, Hermann BP, Mehta MP, Tomé WA (2012) Hippocampal dosimetry predicts neurocognitive function impairment after fractionated stereotactic radiotherapy for benign or low-grade adult brain tumors. Int J Radiat Oncol Biol Phys 83:e487–e493

Gondi V, Pugh SL, Tome WA et al (2014) Preservation of memory with conformal avoidance of the hippocampal neural stem-cell compartment during whole-brain radiotherapy for brain metastases (RTOG 0933): a phase II multi-institutional trial. J Clin Oncol 32:3810–3816

Goodman KA, Sneed PK, McDermott MW et al (2001) Relationship between pattern of enhancement and local control of brain metastases after radiosurgery. Int J Radiat Oncol Biol Phys 50:139–146

Götz L, Spehl TS, Weber WA et al (2012) PET and SPECT for radiation treatment planning. Q J Nucl Med Mol Imaging 56(2):163–172

Gross MW, Weber WA, Feldmann HJ et al (1998) The value of F-18-fluorodeoxyglucose PET for the 3-D radiation treatment planning of malignant gliomas. Int J Radiat Oncol Biol Phys 41:989–995

Grosu AL, Weber WA (2010) PET for radiation treatment planning of brain tumours. Radiother Oncol 96:325–327

Grosu AL, Weber WA, Riedel E et al (2005a) L-(methyl-11C) methionine positron emission tomography for

target delineation in resected high-grade gliomas before radiotherapy. Int J Radiat Oncol Biol Phys 63:64–74

Grosu AL, Weber WA, Franz M et al (2005b) Reirradiation of recurrent high grade gliomas using amino acid PET (SPECT)/CT/MRI image fusion to determine gross tumor volume for stereotactic fractionated radiotherapy. Int J Radiat Oncol Biol Phys 63:511–519

Grosu AL, Astner ST, Riedel E et al (2011) An interindividual comparison of O-(2-[18F]fluoroethyl)-L-tyrosine (FET)- and L-[methyl-11C]methionine (MET)-PET in patients with brain gliomas and metastases. Int J Radiat Oncol Biol Phys 81:1049–1058

Harth S, Abo-Madyan Y, Zheng L et al (2013) Estimation of intracranial failure risk following hippocampal-sparing whole brain radiotherapy. Radiother Oncol 109:152–158

Hartmann C, Hentschel B, Wick W et al (2010) Patients with IDH1 wild type anaplastic astrocytomas exhibit worse prognosis than IDH1-mutated glioblastomas, and IDH1 mutation status accounts for the unfavorable prognostic effect of higher age: implications for classification of gliomas. Acta Neuropathol 120:707–718

Hegi ME, Diserens AC, Gorlia T et al (2005) MGMT gene silencing and benefit from temozolomide in glioblastoma. N Engl J Med 352:997–1003

Hendriks LE, Bootsma GP, de Ruysscher DK et al (2013) Screening for brain metastases in patients with stage III non-small cell lung cancer: is there additive value of magnetic resonance imaging above a contrast-enhanced computed tomography of the brain? Lung Cancer 80:293–297

Hochberg FH, Pruitt A (1980) Assumptions in the radiotherapy of glioblastoma. Neurology 30:907–911

Horak CE, Lee JH, Marshall JC et al (2008) The role of metastasis suppressor genes in metastatic dormancy. APMIS 116:586–601

Husemann Y, Geigl JB, Schubert F et al (2008) Systemic spread is an early step in breast cancer. Cancer Cell 13:58–68

Jakubovic R, Sahgal A, Soliman H et al (2014) Magnetic resonance imaging-based tumour perfusion parameters are biomarkers predicting response after radiation to brain metastases. Clin Oncol 26(11):704–712

Karim AB, Maat B, Hatlevoll R et al (1996) A randomized trial on dose-response in radiation therapy of low-grade cerebral glioma: European Organization for Research and Treatment of Cancer (EORTC) Study 22844. Int J Radiat Oncol Biol Phys 36(3): 549–556

Kienast Y, von Baumgarten L, Fuhrmann M et al (2010) Real-time imaging reveals the single steps of brain metastasis formation. Nat Med 16:116–122

Kim MY, Oskarsson T, Acharyya S et al (2009) Tumor self-seeding by circulating cancer cells. Cell 139:1315–1326

Kocher M, Soffietti R, Abacioglu U et al (2011) Adjuvant whole-brain radiotherapy versus observation after radiosurgery or surgical resection of one to three cerebral metastases: results of the EORTC 22952–26001 study. J Clin Oncol 29:134–141

Kocher M, Wittig A, Piroth MD et al (2014) Stereotactic radiosurgery for treatment of brain metastases. A report of the DEGRO Working Group on Stereotactic Radiotherapy. Strahlenther Onkol 190:521–532

Langley RR, Fidler IJ (2013) The biology of brain metastasis. Clin Chem 59:180–189

Lawrence YR, Li XA, el Naqa I et al (2010) Radiation dose–volume effects in the brain. Int J Radiat Oncol Biol Phys 76:S20–S27

Lee IH, Piert M, Gomez-Hassan D et al (2009) Association of 11C-methionine PET uptake with site of failure after concurrent temozolomide and radiation for primary glioblastoma multiforme. Int J Radiat Oncol Biol Phys 73:479–485

Lee EJ, Ahn KJ, Lee EK et al (2013) Potential role of advanced MRI techniques for the peritumoural region in differentiating glioblastoma multiforme and solitary metastatic lesions. Clin Radiol 68:e689–e697

Louis DN, Ohgaki H, Wiestler OD et al (2007) The 2007 WHO classification of tumours of the central nervous system. Acta Neuropathol 114:97–109

Lu S, Ahn D, Johnson G et al (2003) Peritumoral diffusion tensor imaging of high-grade gliomas and metastatic brain tumors. AJNR Am J Neuroradiol 24:937e41

Martinez N, Boire A, DeAngelis LM (2013) Molecular interactions in the development of brain metastases. Int J Mol Sci 14:17157–17167

Mayer R, Sminia P (2008) Reirradiation tolerance of the human brain. Int J Radiat Oncol Biol Phys 70:1350–1360

Mayo C, Martel MK, Marks LB et al (2010) Radiation dose-volume effects of optic nerves and chiasm. Int J Radiat Oncol Biol Phys 76:S28–S35

Milner B, Squire LR, Kandel ER (1998) Cognitive neuroscience and the study of memory. Neuron 20: 445–468

Minniti G, Amelio D, Amichetti M et al (2010) Patterns of failure and comparison of different target volume delineations in patients with glioblastoma treated with conformal radiotherapy plus concomitant and adjuvant temozolomide. Radiother Oncol 97:377–381

Minniti G, Scaringi C, Baldoni A et al (2013) Health-related quality of life in elderly patients with newly diagnosed glioblastoma treated with short-course radiation therapy plus concomitant and adjuvant temozolomide. Int J Radiat Oncol Biol Phys 86: 285–291

Monje ML, Mizumatsu S, Fike JR et al (2002) Irradiation induces neural precursor-cell dysfunction. Nat Med 8:955–962

Musat E, Roelofs E, Bar-Deroma R et al (2010) Dummy run and conformity indices in the ongoing EORTC low-grade glioma trial 22033-26033: first evaluation of quality of radiotherapy planning. Radiother Oncol 95:218–224

Nataf F, Schlienger M, Liu Z et al (2008) Radiosurgery with or without a 2-mm margin for 93 single brain metastases. Int J Radiat Oncol Biol Phys 70:766–772

Nieder C, Mehta MP (2011) Advances in translational research provide a rationale for clinical re-evaluation of high-dose radiotherapy for glioblastoma. Med Hypotheses 76:410–413

Nieder C, Berberich W, Schnabel K (1997) Tumor-related prognostic factors for remission of brain metastases after radiotherapy. Int J Radiat Oncol Biol Phys 39:25–30

Nieder C, Astner ST, Mehta MP et al (2008) Improvement, clinical course, and quality of life after palliative radiotherapy for recurrent glioblastoma. Am J Clin Oncol 31:300–305

Nieder C, Norum J, Dalhaug A et al (2013) Radiotherapy versus best supportive care in patients with brain metastases and adverse prognostic factors. Clin Exp Metastasis 30:723–729

Nieder C, Grosu AL, Gaspar LE (2014) Stereotactic radiosurgery (SRS) for brain metastases: a systematic review. Radiat Oncol 9:155

Noel G, Simon JM, Valery CA et al (2003) Radiosurgery for brain metastasis: impact of CTV on local control. Radiother Oncol 68:15–21

Oehlke O, Wucherpfennig D, Fels F et al (2015) Whole brain irradiation with hippocampal sparing and dose escalation on multiple brain metastases : Local tumour control and survival. Strahlenther Onkol. [Epub ahead of print]

Ohana M, Jeung MY, Bazille G, Roy C (2014) Cerebral staging of lung cancer: is one single contrast-enhanced T1-weighted three-dimensional gradient-echo sequence sufficient? Neuroradiology 56:621–627

Ohtakara K, Hoshi H (2014) Target volume geometric change and/or deviation from the cranium during fractionated stereotactic radiotherapy for brain metastases: potential pitfalls in image guidance based on bony anatomy alignment. J Med Imaging Radiat Oncol 58(6):729–736

Palmieri D, Chambers AF, Felding-Habermann B et al (2007) The biology of metastasis to a sanctuary site. Clin Cancer Res 13:1656–1662

Pantelis E, Papadakis N, Verigos K et al (2010) Integration of functional MRI and white matter tractography in stereotactic radiosurgery clinical practice. Int J Radiat Oncol Biol Phys 78:257–267

Parihar VK, Limoli CL (2013) Cranial irradiation compromises neuronal architecture in the hippocampus. Proc Natl Acad Sci U S A 110:12822–12827

Parsons DW, Jones S, Zhang X et al (2008) An integrated genomic analysis of human glioblastoma multiforme. Science 321:1807–1812

Posner JB, Chernik NL (1978) Intracranial metastases from systemic cancer. Adv Neurol 19:579–592

Price SJ, Gillard JH (2011) Imaging biomarkers of brain tumour margin and tumour invasion. Br J Radiol 84:S159–S167

Prokic V, Wiedenmann N, Fels F et al (2013) Whole brain irradiation with hippocampal sparing and dose escalation on multiple brain metastases: a planning study on treatment concepts. Int J Radiat Oncol Biol Phys 85:264–270

Régina A, Demeule M, Laplante A et al (2001) Multidrug resistance in brain tumors: roles of the blood-brain barrier. Cancer Metastasis Rev 20:13–25

Ryu S, Buatti JM, Morris A, et al; AANS/CNS Joint Guidelines Committee (2014) The role of radiotherapy in the management of progressive glioblastoma: a systematic review and evidence-based clinical practice guideline. J Neurooncol 118:489–499

Sahm F, Capper D, Jeibmann A et al (2012) Addressing diffuse glioma as a systemic brain disease with single-cell analysis. Arch Neurol 69:523–526

Schoenfeld GO, Amdur RJ, Morris CG et al (2008) Patterns of failure and toxicity after intensity-modulated radiotherapy for head and neck cancer. Int J Radiat Oncol Biol Phys 71:377–385

Scoville WB, Milner B (1957) Loss of recent memory after bilateral hippocampal lesions. J Neurol Neurosurg Psychiatry 20:11–21

Shaw E, Scott C, Souhami L et al (1996) Radiosurgery for the treatment of previously irradiated recurrent primary brain tumors and brain metastases: initial report of RTOG protocol 90–05. Int J Radiat Oncol Biol Phys 34:647–654

Shaw E, Scott C, Souhami L et al (2000) Single dose radiosurgical treatment of recurrent previously irradiated primary brain tumors and brain metastases: final report of RTOG protocol 90–05. Int J Radiat Oncol Biol Phys 47:291–298

Shaw E, Arusell R, Scheithauer B et al (2002) Prospective randomized trial of low- versus high-dose radiation therapy in adults with supratentorial low-grade glioma: initial report of a North Central Cancer Treatment Group/Radiation Therapy Oncology Group/Eastern Cooperative Oncology Group study. J Clin Oncol 20:2267–2276

Shaw EG, Wang M, Coons SW et al (2012) Randomized trial of radiation therapy plus procarbazine, lomustine, and vincristine chemotherapy for supratentorial adult low-grade glioma: initial results of RTOG. J Clin Oncol 30:3065–3070

Shors TJ, Miesegaes G, Beylin A et al (2001) Neurogenesis in the adult is involved in the formation of trace memories. Nature 410:372–376

Small SA, Schobel SA, Buxton RB et al (2011) A pathophysiological framework of hippocampal dysfunction in ageing and disease. Nat Rev Neurosci 12:585–601

Soffietti R, Kocher M, Abacioglu UM et al (2013) A European Organisation for Research and Treatment of Cancer phase III trial of adjuvant whole-brain radiotherapy versus observation in patients with one to three brain metastases from solid tumors after surgical resection or radiosurgery: quality-of-life results. J Clin Oncol 31:65–72

Stadlbauer A, Buchfelder M, Doelken MT et al (2011) Magnetic resonance spectroscopic imaging for visualization of the infiltration zone of glioma. Cent Eur Neurosurg 72:63–69

Stupp R, Mason WP, van den Bent MJ et al (2005) Radiotherapy plus concomitant and adjuvant temozolomide for glioblastoma. N Engl J Med 352:987–996

Tabatabai G, Stupp R, van den Bent MJ et al (2010) Molecular diagnostics of gliomas: the clinical perspective. Acta Neuropathol 120:585–592

Tanaka S, Meyer FB, Buckner JC et al (2013) Presentation, management, and outcome of newly diagnosed glioblastoma in elderly patients. J Neurosurg 118:786–798

Timmerman RD (2008) An overview of hypofractionation and introduction to this issue of seminars in radiation oncology. Semin Radiat Oncol 18:215–222

Tsao MN, Rades D, Wirth A et al (2012) Radiotherapeutic and surgical management for newly diagnosed brain metastasis(es): an American Society for Radiation Oncology evidence-based guideline. Pract Radiat Oncol 2:210–225

van den Bent MJ, Afra D, de Witte O et al (2005) Long-term efficacy of early versus delayed radiotherapy for low-grade astrocytoma and oligodendroglioma in adults: the EORTC 22845 randomised trial. Lancet 366:985–990

van den Bent MJ, Brandes AA, Taphoorn MJ et al (2013) Adjuvant procarbazine, lomustine, and vincristine chemotherapy in newly diagnosed anaplastic oligodendroglioma: long-term follow-up of EORTC brain tumor group study 26951. J Clin Oncol 31:344–350

Wallner KE, Galicich JH, Krol G et al (1989) Patterns of failure following treatment for glioblastoma multiforme and anaplastic astrocytoma. Int J Radiat Oncol Biol Phys 16:1405–1409

Weber WA, Grosu AL, Czernin J (2008) Technology Insight: advances in molecular imaging and an appraisal of PET/CT scanning. Nat Clin Pract Oncol 5:160–170

Weller M, Wick W (2014) Improving outcome in newly diagnosed malignant glioma. Nat Rev Neurol 10:68–70

Whitfield GA, Kennedy SR, Djoukhadar IK et al (2014) Imaging and target volume delineation in glioma. Clin Oncol 26:364–376

Wick W, Hartmann C, Engel C et al (2009) NOA-04 Randomized phase III trial of sequential radiochemotherapy of anaplastic glioma with procarbazine, lomustine, and vincristine or temozolomide. J Clin Oncol 27:5874–5880

Zach L, Guez D, Last D et al (2012) Delayed contrast extravasation MRI for depicting tumor and non-tumoral tissues in primary and metastatic brain tumors. PLoS One 7:e52008

Base of the Skull and Orbit Tumors

2

Sabrina T. Astner, Tobias Boeckh-Behrens,
and Claire Delbridge

Contents

S.T. Astner (✉)
Klinik und Poliklinik für Strahlentherapie und Radiologische Onkologie, Klinikum rechts der Isar, Technische Universität München, Ismaninger Str. 22, Munich 81675, Germany
e-mail: sabrina.astner@gmx.de

T. Boeckh-Behrens
Abteilung für diagnostische und interventionelle Neuroradiologie, Klinikum rechts der Isar, Technische Universität München, Neuro-Kopf-Zentrum, Ismaninger Str. 22, Munich 81675, Germany

C. Delbridge
Institut für Allgemeine Pathologie und Pathologische Anatomie, der Technischen Universität München, Trogerstr. 18, Munich 81675, Germany

2.1 Characteristics of Skull Base Imaging

Imaging of the skull base is a challenge, technically as well as in terms of interpretation. The close proximity of the structures demands sound knowledge of anatomy on one hand and high-resolution and high-contrast imaging techniques on the other. The direct vicinity of structurally different tissue types such as compact bone, air within the paranasal sinuses/nasopharynx/middle ear, soft tissue structures such as the brainstem/cranial nerves/mucosa/pituitary gland and liquor-containing cavities might often result in the formation of artefacts and demand examination protocols adjusted to the special needs of the clinical question. For this reason skull base processes are routinely examined by both computed tomography (CT) and magnetic resonance imaging (MRI).

CT

In skull base imaging CT is indispensable for evaluation of the osseous structures. It is important for anatomical correlation as well as for the assessment of pathological alterations like erosion or destruction of the bone and dilatation of the foramina, recognition of calcifications, etc. Ideally very high-resolution spiral CT imaging using slices lower than 1 mm (0.6–1 mm) and a 1,024 × 1,024 matrix are acquired. From this 3D dataset multiplanar reconstructions can be performed.

Contrast-enhanced CT has a lower impact in routine skull base imaging but can be used in

A.-L. Grosu, C. Nieder (eds.), *Target Volume Definition in Radiation Oncology*,
DOI 10.1007/978-3-662-45934-8_2, © Springer-Verlag Berlin Heidelberg 2015

patients which are not suitable for MRI or in cases where CT angiography to visualise vascular structures is expected to provide additional information.

MRI

MRI is characterised by excellent soft tissue contrast and high resolution. High-power-field magnets, progress in coil technology and design of sequences allow the acquisition of high resolution (1–1.2 mm slice thickness) 3D datasets of the whole brain within a reasonable examination time. Those datasets can be reconstructed into any orientations and slice thicknesses, depending on the clinical question and the anatomical region. Basic sequences are, for example, a native and contrast-enhanced 3D T1 sequence (e.g. spoiled fast gradient echo sequences as MP-RAGE, 3D-SPGR, VIBE) together with a thin-sliced (2 or 3 mm) T2 sequence in one or better two planes. Those sequences are usually sufficient for diagnostic purposes and can be used for radiotherapy treatment planning. The native T1 sequence is important for the judgement of intraosseous processes, which can be diagnosed by abolishment of the typical signal of the fatty bone marrow. Therefore fat saturation is counterproductive in the native T1 images. After application of contrast media, fat saturation can be helpful to enhance the contrast between nonfatty and fatty structures (e.g. in the orbita). Dependent on the pathology several MRI sequences can be complementary to ensure the diagnosis or to get a more exact anatomical or functional image. Examples are heavy T2-weighted 3D sequences for the imaging of cranial nerves (e.g. CISS, FIESTA), diffusion-weighted images, including diffusion tensor imaging (DTI) if necessary, MR angiography techniques (TOF, CE-MRA, time-resolved 4D MRA), fat saturation or the like. Generally, for the detection of all intraorbital infectious or tumoral diseases, thin T1-weighted sequences after application of contrast media and T2 sequences, both with fatty saturation, are most suitable. The saturation of the orbital fat leads to optimal contrast between the pathological process and the lucid signal of the contrast media in T1 and the accompanying edema with high T2 signal. In case of a process that reaches to the bony orbit, additional CT bone imaging is helpful.

2.2 Anatomy

2.2.1 Base of the Skull

The skull base is built from five bones: the paired temporal and frontal bones (the latter are fused in the axis) and the unpaired ethmoidal, sphenoidal and occipital bones. These osseous structures form the anterior, middle and posterior cranial fossa in which important structures and conjunctions with the extracranial area are installed.

The anterior cranial fossa is confined by the calvarium in the front and the edge of the small sphenoid bone in the rear. Olfactory fibres as well as ethmoidal vessels are crossing through the cribriform plate of the ethmoidal bone.

The middle cranial fossa is confined by the edge of the large sphenoid bone and the sphenoidal plane in the front, in the rear by the edge of the petrous portion of the temporal bone and the posterior clinoid process as well as the dorsum sellae of the sphenoidal bone. Laterally the middle cranial fossa extends to the border of the temporal bones. The region contains a number of anatomically and functionally important structures like the pituitary gland or the Meckel's cave and crucial connections to the extracranial area like the optical canal; the superior and inferior orbital fissure; the foramina rotundum, ovale, spinosum and lacerum; as well as the carotid channel.

The posterior cranial fossa is confined by the clivus and the posterior clinoid process, in the front, frontolaterally by the edge of the temporal bones, dorsolaterally and in the back by the occipital bone and caudally by the foramen magnum. Important structures are the cerebellopontine angle and the caudal cranial nerves which pass through the corresponding foramina (meatus acusticus internus, foramen jugulare, canalis hypoglossi and foramen magnum).

In Table 2.1 different tumour types arising close to the most important anatomical structures

Table 2.1 Tumours of the base of the skulls and their exact anatomical localisation

Anatomical structure	Localisation	Diagnosis
Anterior cranial fossa		
Dura, olfactory fibres/olfactory stem cells	Cribriform plate	Meningioma of the olfactory groove, esthesioneuroblastoma
Dura	Sphenoidal plane/clinoid process, sphenoid wing, orbital roof	Meningioma
Bony orbital roof	Frontal bone	Fibrous dysplasia
Middle cranial fossa		
Dura	Dorsum sellae, clivus, sphenoid wing	Meningioma
Optic nerve, optic sheath, meninges	Optic canal	Meningioma, optic glioma, sarcoidosis, Tolosa-Hunt syndrome
Trigeminal ganglion	Meckel's cave	Neuroma
Oculomotor nerve, trochlear, ophthalmic, abducens nerve	Superior orbital fissure	Neuroma (rare)
Maxillary nerve	Foramen rotundum	Neuroma, metastasis
Mandibular nerve	Foramen ovale	Neuroma, metastasis
Pituitary gland	Sella turcica	Adenoma, metastasis, craniopharyngioma
Posterior cranial fossa		
Bones and epithelium of petrous bone	Petrous apex, middle ear	Cholesterol granuloma, cholesteatoma
Dura	Clivus, posterior part of petrous bone, occipital bone	Meningioma
Vestibulocochlear nerve, facial nerve	Internal acoustic canal, cerebellopontine angle	Neuroma (acoustic, facial nerve neuroma)
Glossopharyngeal, vagal and accessory nerves, glomus jugulare	Jugular foramen	Neuroma, paraganglioma
Hypoglossal nerve	Hypoglossal canal	Neuroma
Bony clivus	Clivus	Chordoma, metastasis, chondroid tumour

and the connections to the base of the skulls are summarised (Fig. 2.1).

2.2.2 Orbit

The orbit is formed from seven different bones, the frontal, sphenoidal, zygomatic, palatine, ethmoidal, lacrimal and maxillary bones. The intraorbital soft tissue containing the orbit bulb, ocular muscles, the lacrimal apparatus, fascia, nerves, the ciliary ganglion, vessels and the orbital fat is protected within this cavity.

Considering the differential pathological processes, which can occur within the orbit, the separation into an extra- and intraconal space is useful.

The extraconal space is confined by the periost of the bony orbit to the outside. The periost fades out medially posterior of the saccus lacrimalis into the orbital septum and laterally into the fibres of the musculus orbicularis oculi. The boarders to the inner are the rectus muscles and their intramuscular septum. Within this boarder the intraconal space contains six eye muscles (four rectus muscles, M. obliquus superior and inferior, M. levator palpebrae) and the separate structures bulbus and optical nerve. Table 2.2 summarises the most important intraorbital pathologies and their position within the compartments.

2.3 Target Volume Definition by Pathology

Because of the complementary nature of CT and MRI, both modalities are performed for treatment planning of skull base tumours. Sequences which are most appropriate for planning purposes

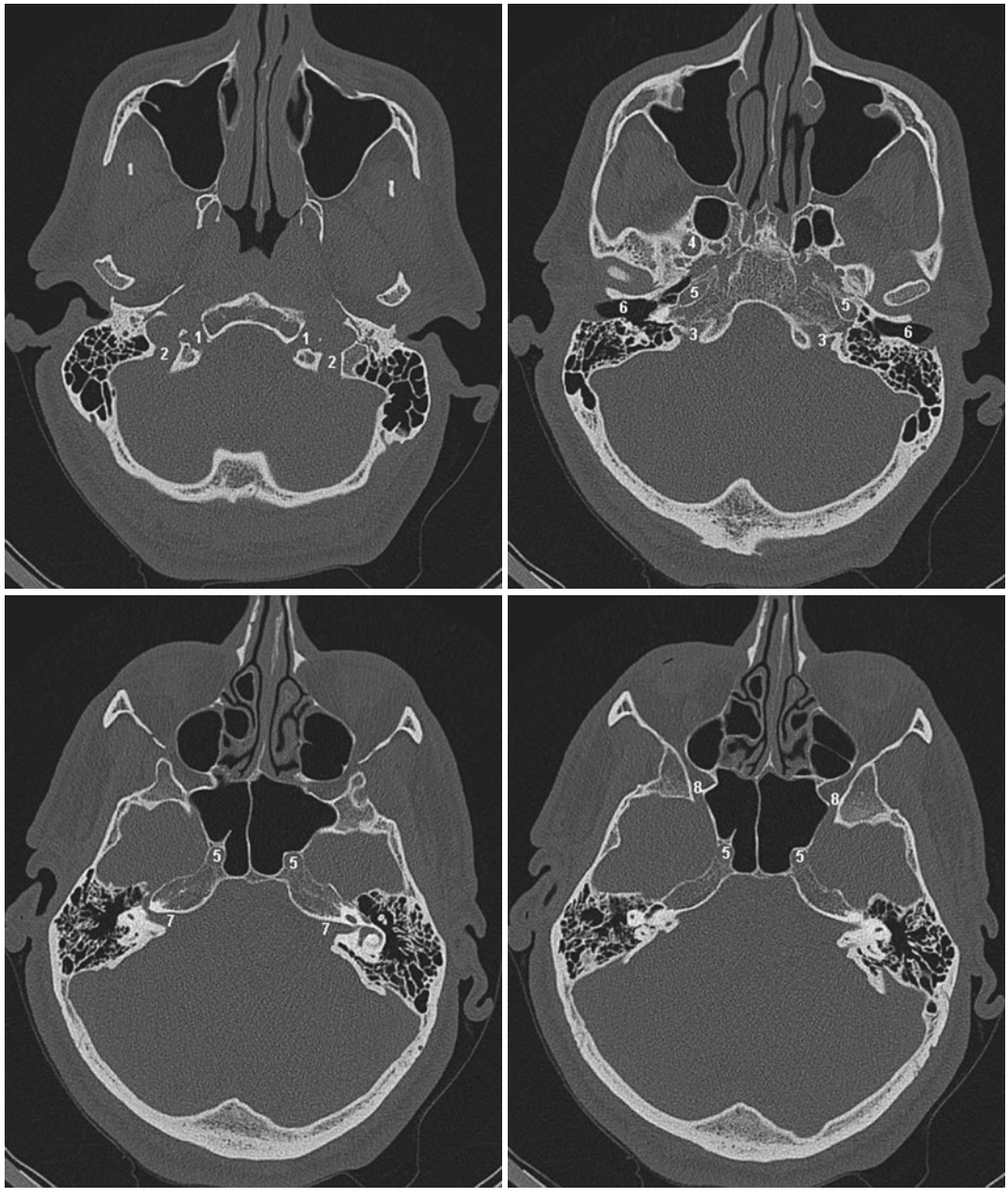

Fig. 2.1 Four axial slides of the skull base ascending from inferior (*upper left*) to superior (*lower right*) showing the most important foramina and their contents: *1* Canalis hypoglossi, *N. hypoglossus (cranial nerve XII). 2* Foramen jugulare (lower and posterior part), *sinus sigmoideus. 3* Foramen jugulare (upper and anterior part), *sinus petrosus inferior, N. glossopharyngeus, N. vagus and N. accessorius (cranial nerves IX, X and XI). 4* Foramen ovale, *N. mandibularis (cranial nerve* V_3*). 5* Canalis caroticus, *internal carotid artery. 6* Meatus acusticus externus. *7* Meatus acusticus internus, *N. facialis and N. vestibulocochlearis (cranial nerves VII and VIII). 8* Foramen rotundum, *N. maxillaris (cranial nerve* V_2*)*

Table 2.2 Tumours of the orbit and their exact anatomical localisation

Anatomical structure	Localisation	Pathology
Extraconal space		
Surrounding bony structures, periost	Bony orbital borders	Primary bone or chondroid neoplasias, metastasis, infiltration of sinonasal tumours
Fat/conjunctive tissue	Extraconal tissue	Lymphoma, lipoma, lymphangioma, capillary haemangioma, dermoid/epidermoid, rhabdomyosarcoma
Tear system	Lacrimal gland	Lymphoma, epithelial tumours, sarcoidosis, pseudotumour
Intraconal space		
Muscle tissue, mesenchymal tissue	Extraocular muscles	Lymphoma, metastasis, myositis/ pseudotumour, rhabdomyosarcoma
Fat/conjunctive tissue	Intraconal fat	Cavernous haemangioma, lymphangioma, lymphoma, rhabdomyosarcoma
Optic nerve		
Neural tissue, glial cells	Entire route of optic nerve	Optic glioma, neuritis, sarcoidosis, schwannoma
Dura	Optic sheath	Meningioma, lymphoma
Ocular bulb		
Retina	Retina, posterior lining of the bulb	Retinoblastoma
Choroidea, ciliary body	Choroidea, ciliary body	Melanoma, metastasis

will be described for each tumour entity. Sometimes a positron emission tomography (PET) scan can be helpful but is not mandatory. To improve the result of image fusion, contrast media in the planning CT is helpful and should be injected if not contraindicated. As in many cases the tumour will not be recognised on CT, but only on MRI; thorough image fusion is essential for exact gross tumour volume (GTV) definition in the fused dataset. Therefore automatic coregistration of the datasets needs to be reviewed carefully and if necessary adapted manually.

2.3.1 Skull Base Meningioma

The World Health Organization (WHO) separates meningiomas into three groups: WHO °I–III.

In general brain tumours are graded according to their prognosis, taking into account proliferation, mitotic activity, growth pattern and evidence of necrosis. As growth characteristics are different, target volume delineation will be described separately for WHO °I, WHO °II and WHO °III (Table 2.3).

Table 2.3 Characteristics of meningiomas by WHO grade

	WHO °I	WHO °II	WHO °III
Risk of recurrence	Very low	Low	High
Aggressive behaviour	Very low	Low	High

WHO °I and WHO °II

Benign meningioma (WHO° I) can be classified into many histological subtypes; the most common are the meningothelial, the fibrous or the mixture of both these types, the transitional meningioma. These subtypes vary in their growth pattern (Table 2.4).

The meningothelial meningioma forms lobules of mostly uniform tumour cells that show oval nuclei, often with a central clearing.

The fibrous meningioma shows parallel fascicles of spindle cells that are accompanied by thin layers of collagenous tissue.

In the transitional (mixed) subtype, both of the above-described growth patterns can be seen, with the addition of tight whorl formations and frequent psammoma bodies.

All three described subtypes, as well as all other grade I meningiomas, show a low mitotic

Table 2.4 Meningioma with low recurrence rate and risk for aggressive growth (WHO Classification 2007)

WHO °I	WHO °II
Transitional meningioma	Atypical meningioma
Meningothelial meningioma	Clear cell meningioma
Fibrous meningioma	Chordoid meningioma
Psammomatous meningioma	
Angiomatous meningioma	
Microcystic meningioma	
Lymphoplasmacyte-rich meningioma	
Metaplastic meningioma	

activity of less than four mitoses in ten high-power fields (at a 40× magnification).

The atypical meningioma (WHO °II) presents a much more sheetlike growth and increased cellularity in comparison to grade I tumours. Often cellular atypia with enlarged nuclei, as well as areas of necrosis, can be found. The WHO grading requires four or more mitoses in ten high-power fields for this type. The recurrence rate for the more aggressive °II tumours after surgical resection is approximately ten times as high compared to °I.

For primary radiotherapy (after biopsy) of °I and °II meningiomas, there is no difference regarding the delineation of the target volume.

To define the GTV, thin-sliced 3D T1-weighted images (e.g. MP-RAGE, FSPGR, VIBE) acquired after injection of contrast medium are necessary and in most cases sufficient because of the typically strong enhancement and mostly quite sharp margins. Delineation of intraosseous tumour parts can be more challenging as the contrast enhancement can be very restrained or missing. In these cases of bony infiltration, the bone windowing of the CT is needed (Fig. 2.2).

In regions where tumour cannot be easily separated from normal structures (e.g. within the cavernous sinus, in previously operated regions), a thin (2 or 3 mm) T2 sequence can be useful. Also PET using somatostatin receptor tracer or amino acid tracer can be performed, if available (Milker-Zabel et al. 2006; Astner et al. 2008; Combs et al. 2013) (Fig. 2.3).

Several groups were able to show that PET is useful for contouring of skull base meningiomas. Based on our own work, it can be assumed that ^{11}C-methionine (MET) can be substituted by ^{18}F-fluor-ethyl-tyrosine (FET), which is easier to handle because of its longer half-life (Grosu et al. 2011). Amino acid tracers like MET or FEt allow for an image fusion based on intrinsic structures. This allows for image fusion without external marker. Other tracers like somatostatin-affine tracers show a high specificity; therefore, background activity is low and image fusion is difficult without external marker. Development of combined PET-MRI machines allows the use of SSTR tracer without the addition of external marker.

For the GTV all the visible (T1 + contrast, eventually CT for bony infiltration) tumour is contoured. Because of potential microscopic spread along the meninges, additional 3–5 mm is added at meningeal extensions resulting in the CTV. The tumour border without contact to the meninges (e.g. the border to the brain) does not need any margin for the CTV.

For recurrence after complete resection or radiotherapy after incomplete resection, tumour extension before surgery must be considered. Ideally the preoperative MRI is coregistered with the planning CT. If radiotherapy is performed after incomplete resection, all preoperative contact areas of the tumour with the skull base must be included in the CTV. In radiotherapy of recurrence after complete resection (Simpson °I), GTV and CTV are defined as in primary radiotherapy.

A radiation technique should be chosen, which requires a maximal setup margin of 3 mm (stereotactic fractionated radiotherapy, image-guided radiotherapy).

WHO °III

The anaplastic meningioma (°III) is the most malignant form of meningiomas. In comparison to the atypical meningioma (°II), the mitotic activity is increased to 20 or more mitoses in ten high-power fields. In most cases the typical histological architecture is no longer apparent, resulting in a growth pattern that can resemble melanoma, carcinoma or high-grade sarcoma (Table 2.5).

Guidelines for target volume delineation of atypical and malignant meningioma are rare. The NCCN suggests adding a 2–3 cm margin to the

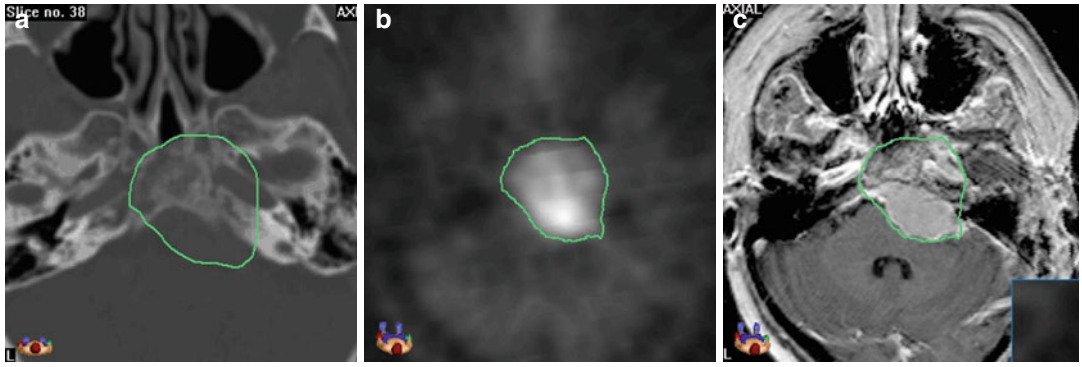

Fig. 2.2 CT and MRI T1 + contrast (**a**, **c**) of a meningioma (*encircled in green*) infiltrating the clivus, which is confirmed by amino acid PET (**b**)

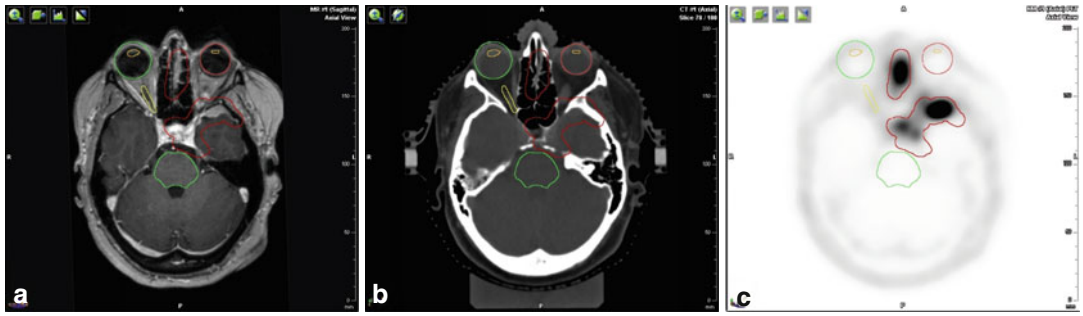

Fig. 2.3 PTV (*red*) of a meningioma infiltrating the cavernous sinus on the left side; (**a**) T1W MRI with contrast, (**b**) CT scan and (**c**) DOTATOC-PET

Table 2.5 Meningioma with higher risk of recurrence and/or aggressive behaviour (WHO Classification 2007)

WHO °III
Anaplastic meningioma
Papillary meningioma
Rhabdoid meningioma

tumour bed and/or the macroscopic tumour. A more detailed description can be found in the EORTC trial for atypical and malignant meningioma (Coskun et al. 2013). Within this study the GTV is defined as the visible tumour including thickened dural trails and hyperostotic bone regions. The PTVs are generated according to the resulting Simpson Grade after surgery (Simpson 1957). For areas with Simpson Grade 1–3 resection without residual tumour left in the postoperative imaging, GTV is defined according to preoperative imaging and pathology report, adding 10 mm margin accounting for microscopic spread. This CTV receives 60 Gy. In areas with Simpson Grade 4–5 resection where a GTV can be defined, 5 mm are added to result in a CTV that receives 70 Gy.

The PTV is defined as CTV plus a margin depending on the institutional protocols and treatment technique. An example for contouring is given in Fig. 2.4.

2.3.2 Optic Meningioma

As described in Sect. 2.2.2, contrast-enhanced T1 sequences with fatty saturation are suited best for imaging of tumours within the orbit. Optic nerve sheath meningiomas are usually seen as a contrast-enhancing line encompassing the optic nerve. In some cases a solid mass can be seen close to the optic chiasm. For the GTV the whole optic nerve(s) and/or chiasm where contrast enhance-

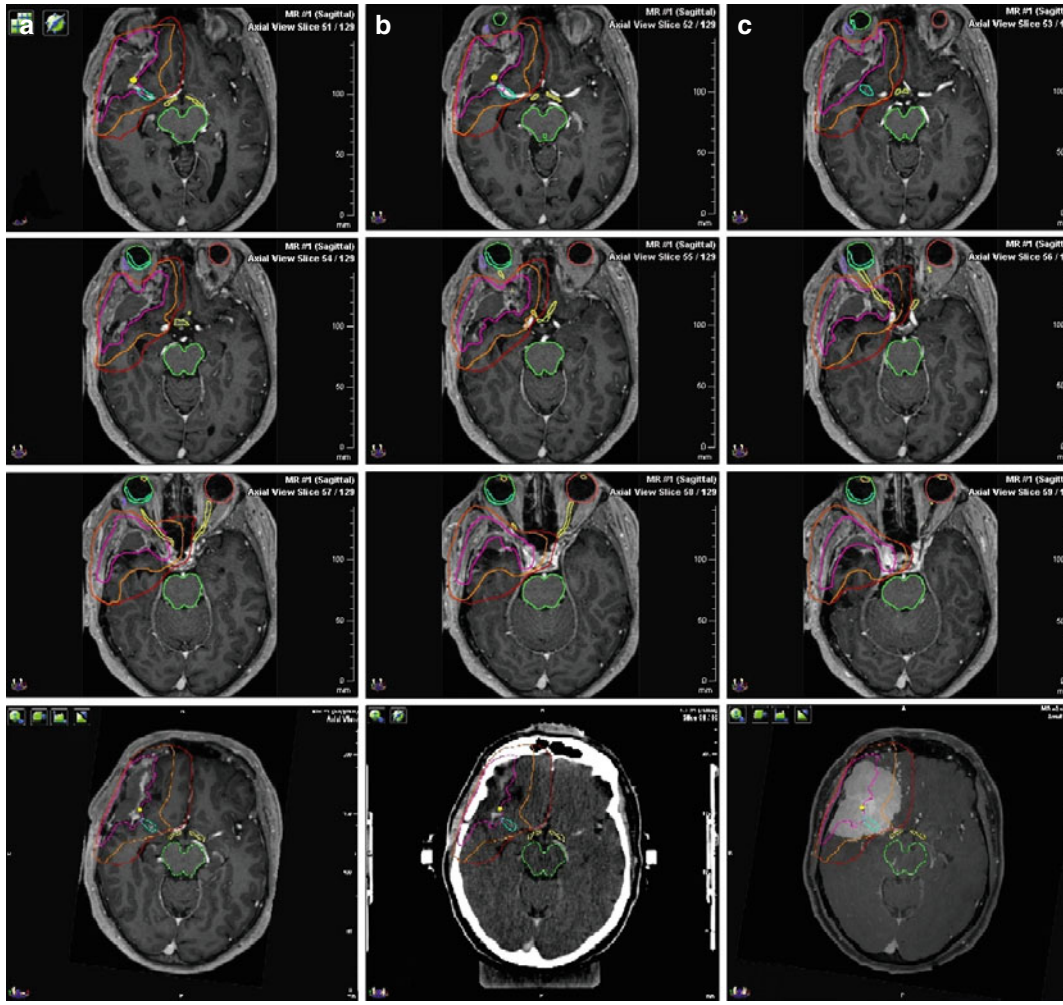

Fig. 2.4 Radiotherapy for atypical meningioma after surgery. (**a**) Contrast-enhanced T1W MRI after surgery. (**b**) Contrast-enhanced CT scan. (**c**) Contrast-enhanced T1W MRI before surgery. *Purple* GTV, *orange* CTV, *red* PTV

ment of the nerve sheath can be seen is contoured. In the mediolateral extension no additional margin is needed for the CTV, but along the length of the optic nerve and chiasm, a margin of 5 mm is suggested. Some authors suggest inclusion of the whole optic nerve for the GTV due to the difficulty to separate the tumour itself from the rest of the nerve in many cases (Jeremic et al. 2008).

In order to create the PTV, the CTV is expanded by 2–3 mm depending on the precision of the equipment. Depending on tumour location (close or distant from the optic channel), additional margins for movement of the optic nerve within the orbit should be added, resulting in final margins between 3 and 5 mm (Fig. 2.5).

2.3.3 Neurinoma

Neurinomas (or schwannomas) are graded as WHO °I tumours that derive from Schwann cells, the principal glial cells of the peripheral nervous system. Most neurinomas are well-differentiated tumours that most commonly arise from peripheral sensory nerves. The majority are located in the cerebellopontine angle with a strong predilection for the vestibular branch of the vestibulocochlear nerve (cranial nerve VIII).

Histologically neurinomas show two main histological patterns, the so-called Antoni A and the regressive Antoni B areas.

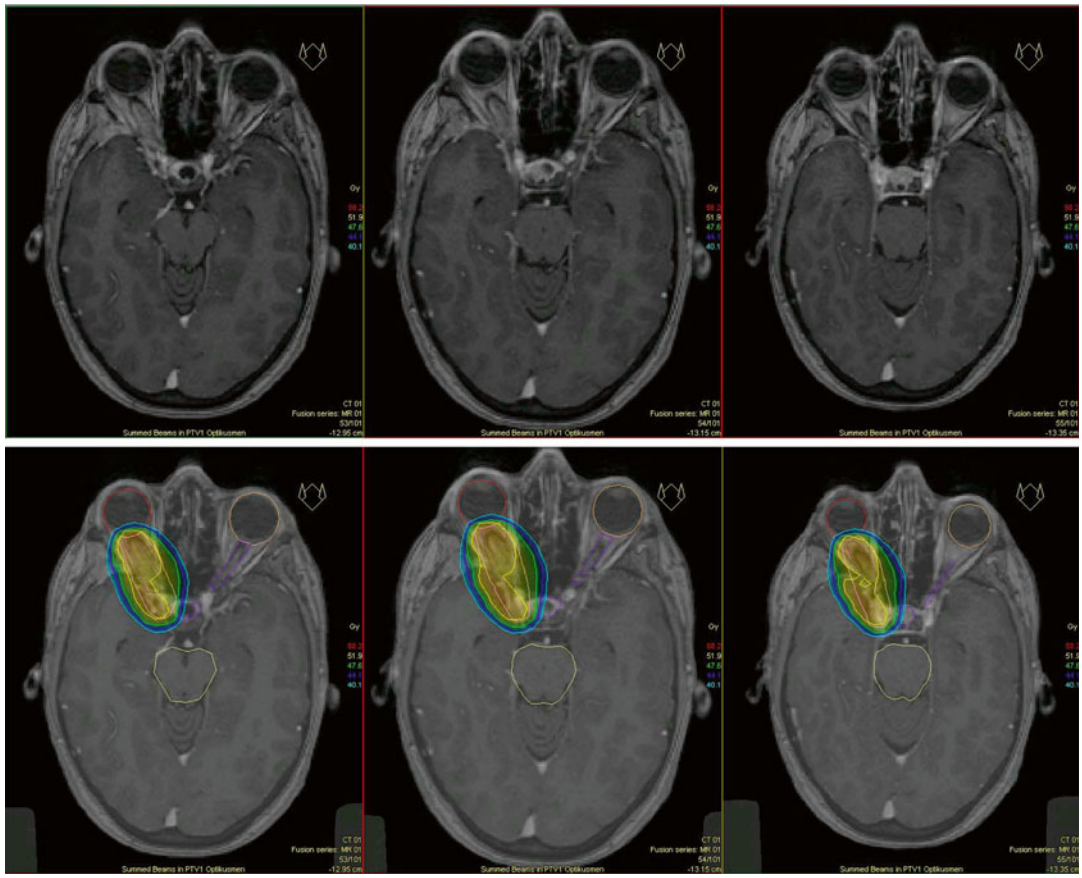

Fig. 2.5 Optic nerve sheath meningioma of the right optic nerve. *Upper*: MRI, *Down*: Radiation treatment planning

The Antoni A pattern is characterised by densely packed areas of spindle-shaped cells with pericellular reticulin, resulting in compact fascicles, one arranged parallel to the next. This pattern shows resemblance to a draft of fish.

The regressive Antoni B areas are much less cellular with smaller, hyperchromatic nuclei and loosely arranged pericellular myxoid stroma and occasional scattered lipidisation.

Tumour vessels can be hyalinised, with consequential wall thickening and possible haemorrhage.

For target volume definition, a CT in bone windowing and thin-sliced MRI T1 scan after contrast enhancement are used. To get optimal coregistration of CT and MRI, scanning the tumour region is not sufficient. Rather the whole brain needs to be scanned in the thin-sliced MRI. The GTV consists of the contrast-enhancing tumour within the internal acoustic meatus and the extrameatal portion. The resulting GTV contoured in the MRI must be within the bony internal auditory canal in the CT. For radiosurgery GTV is equivalent to PTV. For (stereotactic) fractionated treatment a setup margin of 1–2 mm according to institutional standard is used to create the PTV (Kopp et al. 2011). An example is shown in Fig. 2.6.

2.3.4 Pituitary Adenoma

These adenomas are common benign tumours that arise from gland cells of the anterior pituitary lobe. Clinically and anatomically they are mostly distinguished according to their size:

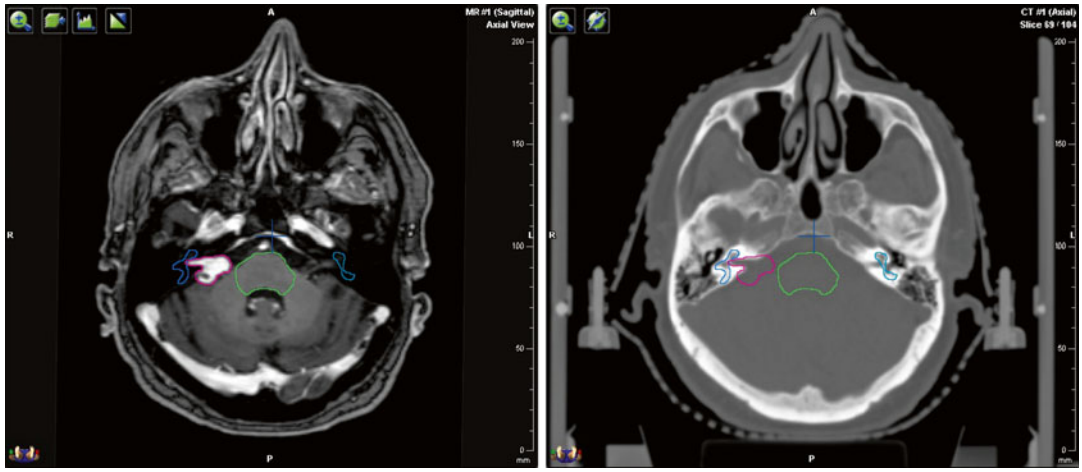

Fig. 2.6 MRI and CT of a patient treated for vestibularis schwannoma by radiosurgery. PTV in *pink*. For fractionated stereotactic treatment, we would use a setup margin of 2 mm

Microadenoma <1 cm
Macroadenoma ≥1 cm

Most commonly pituitary adenomas are classified according to their hormonal expression in immunohistochemical staining (see Table 2.6). Further subtypes are determined according to their ultrastructural differences in electron microscopy.

Imaging and target volume definition are different for pituitary micro- or macroadenoma. For radiosurgery of microadenoma adequate imaging is of high priority. The pituitary gland is intensively vascularised, which leads to very rapid and strong contrast enhancement. The adenoma tissue shows mostly less and more slow contrast enhancement. Therefore the adenoma is demarcated as a hypointense lesion in thin (2 mm)-sliced, ideally coronal- or sagittal-sliced T1-weighted sequences after contrast enhancement. In some cases the enhancement is cleared after a few minutes, and the adenoma is not anymore demarcated. In such cases (ca.10–20 %) a dynamic examination with fast T1-weighted turbo spin-echo sequences has to be done, which can show the delayed flow of the contrast media within the adenoma tissue. Temporal resolution should be at least 20–30 s. Thin T2 sequences, coronal or sagittal can be helpful, although hereby the adenoma tissue shows a range of signal changes from hypointense in case of hemorrhagic parts to hyperintense in cases of cystic degenerations. The visible tumour is contoured for the GTV. As usual in radiosurgery, no margin is added to create the PTV.

Table 2.6 Classification of pituitary adenomas

Subtype of functioning adenoma	Nonfunctioning adenomas
ACTH family	
Densely or sparsely granulated corticotroph adenomas	Silent corticotroph adenomas (type I or II)
Crooke cell adenomas	
GH-PRL-TSH family	
Adenomas causing GH excess (further subtypes)	Silent somatotroph adenomas
Adenomas causing PRL excess (further subtypes)	Silent lactotroph adenomas
Adenomas causing TSH excess (further subtypes)	Silent thyrotroph adenomas
Gonadotropin family	
Adenomas causing gonadotropin excess	Silent gonadotroph adenomas
Gonadotroph adenomas	
Unclassified adenomas	
Unusual plurihormonal adenomas	Null cell adenomas, oncocytomas

Clinicopathologic Classification of Pituitary Adenomas (p. 63), Asa (2011)

Radiotherapy of macroadenoma is usually indicated in patients who have undergone surgery (Kopp et al. 2013). Macroadenomas typically show strong enhancement after application of contrast

media. Differentiation between postoperative scar tissue, remaining pituitary tissue or cavernous sinus is very difficult because of similar contrast behaviour and it is not always possible. 3D T1 sequences after contrast application and thin T2 sequences, eventually also strongly T2-weighted 3D sequences (e.g. CISS), can be helpful.

For delineation of the CTV, preoperative imaging has to be considered. In case of partial resection of the adenoma, it is not necessary to include the complete pre-op tumour volume that extended to the brain, but otherwise all areas of contact are included into the CTV (see Fig. 2.7). Setup margin is used according to the institutional protocol.

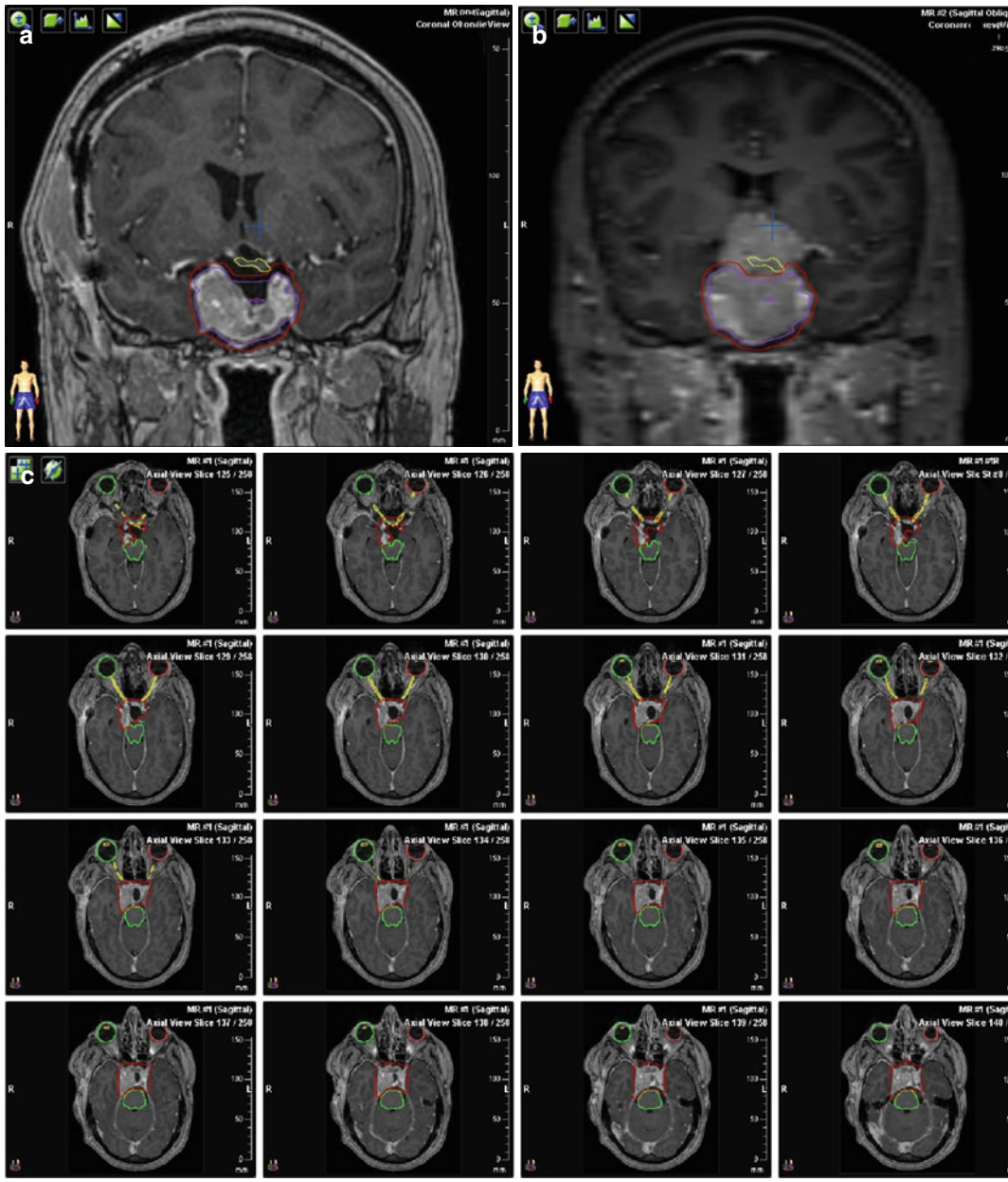

Fig. 2.7 Macroadenoma of the pituitary gland, T1 + Gd (**a**) coronal view after surgery, (**b**) coronal view before surgery and (**c**) axial slices; *purple* GTV, *red* PTV

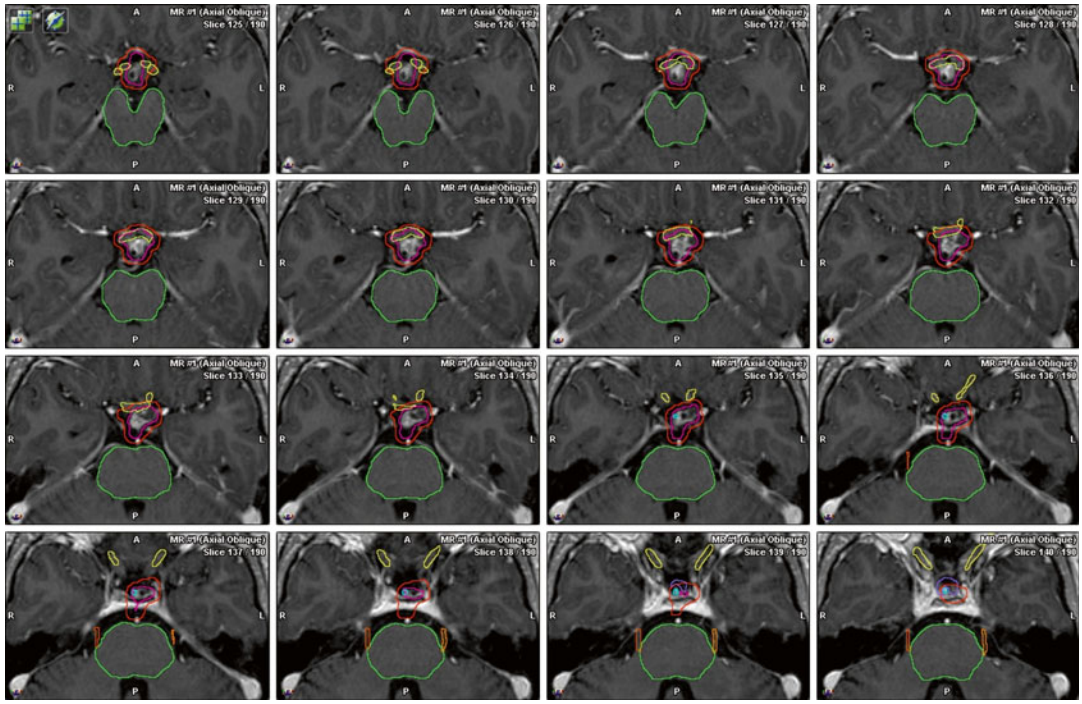

Fig. 2.8 Postoperative recurrence of a craniopharyngioma with typical cystic structure. The GTV (*pink*) consists of macroscopic tumour. For the PTV (*red*) a 2 mm safety margin was added

2.3.5 Craniopharyngioma

Craniopharyngioma arises from epithelium of Rathke's pouch, which is a pituitary gland embryonic tissue. It is a benign, slow growing tumour that can show a cystic histoarchitecture, as well as calcium deposits, which are typically found in the most common subtype, the adamantinomatous craniopharyngioma. The second histological subtype is the papillary craniopharyngioma, which shows a more solid growth pattern with stratified squamous epithelium and papillary epithelial cords.

Craniopharyngiomas typically appear as partly cystic tumours with larger calcified areas. Therefore optimal imaging includes thin-sliced (better 3D) T1 sequences with and without contrast for delineating the solid parts and a T2 sequence for the cystic areas. In addition, CT imaging is helpful for the visualisation of the calcifications.

In target volume delineation of craniopharyngiomas, the most challenging task is to enclose all the cystic parts of the tumour. As in the other benign tumours, the GTV consists of the complete contrast-enhancing tumour. Usually indication for radiotherapy is postoperative recurrence, often after repeated surgery (Combs et al. 2007). Therefore, for the definition of the CTV, the preoperative images should be considered. To create the PTV from CTV, a margin of 2–3 mm, depending on the technique, is added. For an example, see Fig. 2.8.

2.3.6 Glomus Tumours

Paraganglioma, of the glomus jugulare and tympanicum, mainly spread to the petrous part of the temporal bone. Arising from the jugular bulb, 20 % spread to the cranial cavity.

These tumours are highly vascularised and show a distinct pattern of "Zellballen", round nests of epithelioid main cells and marginal sustentacular cells. These cell clusters are surrounded by a vascular stroma.

For the exact imaging of paragangliomas of the skull base (glomus jugulare and tympanicum), a 3D time-of-flight (TOF) angiography in MRI after

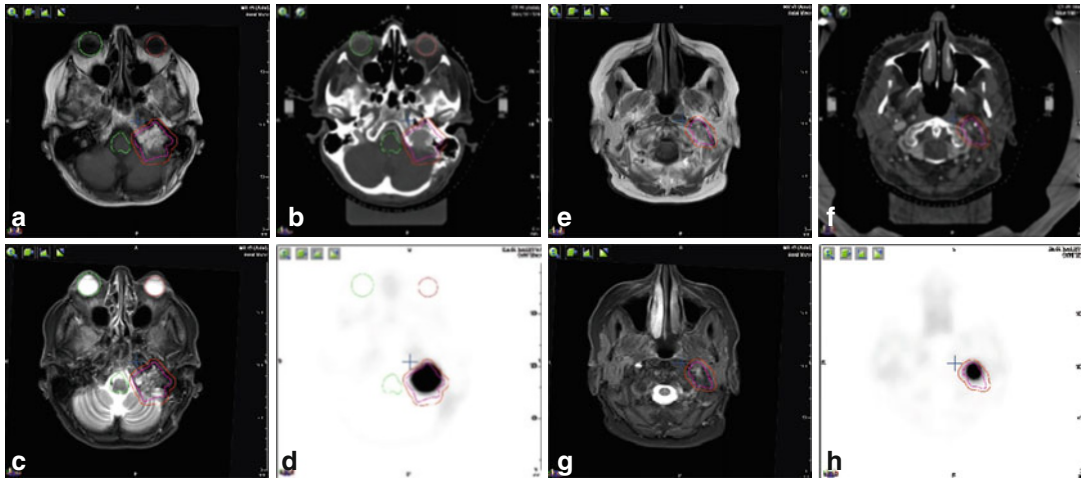

Fig. 2.9 Axial slices of T-weighted MRI, CT, T2-weighted MRI and PET of a glomus jugulare tumour through the upper region (**a**–**d**) and the lower portion of the tumour (**e**–**h**). GTV is *encircled* in *pink*, PTV in *orange*. Contouring was performed for a treatment by stereotactic fractionated radiotherapy

application of contrast media is suited best to determine the exact extension as well as to image the accompanying vessels. Using this technique contrast enhancement as well as vascularisation can be ideally depicted. In addition a thin-sliced CT in bone windowing is indicated for the evaluation of osseous erosions or widening of foramina. For imaging of glomus tumours at the bifurcation of the carotid artery, a 3D T1 sequence after contrast enhancement is sufficient, alternatively a 3D TOF angiography after contrast application. As glomus tumours are positive for somatostatin receptors (SSR), they can easily be detected by SSR-PET such as DOTATOC-PET or DOTATATE-PET. In our experience it is often useful for definition of the lower boarder or in cases of radiotherapy after surgery (Astner et al. 2008). A CTV is not defined. Adding the necessary margin for setup errors, which depends on the irradiation technique, results in the PTV. Figure 2.9 shows an example for contouring of a glomus jugulare tumour.

2.3.7 Clivus Chordomas/ Chondrosarcomas

Clivus chordoma is a rare tumour of notochordal differentiation. Apart from the skull base, it is also found along the neuraxis in the vertebral bodies and the sacrococcygeal bone, where it often grows infiltratively and destructively.

Histologically clivus chordomas show a lobulated architecture with large vacuolated cells, which grow in chords, embedded in a myxoid matrix.

Chondrosarcoma involving the base of the skull is rare, in comparison to other skeletal sites.

It is usually a tumour of older patients, with a peak incidence between the fifth and the seventh decade of life.

The tumour consists of lobules of cartilage with possible areas of calcification. Depending on high cellularity, pleomorphism and mitotic activity of the tumour cells, a grade (G) 1–3 is determined.

In addition to the regular imaging sequences such as 3D T1 postcontrast with fat saturation and 3D bone CT, a thin T2-weighted image is often helpful for the exact determination of the tumour borders in chordomas or chondrosarcomas of the clivus. As the chondroid matrix of those tumours shows a strong T2 signal, this gives a good contrast compared to the surrounding tissue. Contrast enhancement is often heterogeneous and not very strong.

The CTV includes the macroscopic tumour volume as well as any suspected microscopic disease, based on imaging findings, pathology reports and surgery reports, also taking into account the tolerance doses of surrounding normal tissues. For chordomas, the entire clivus and the prevertebral

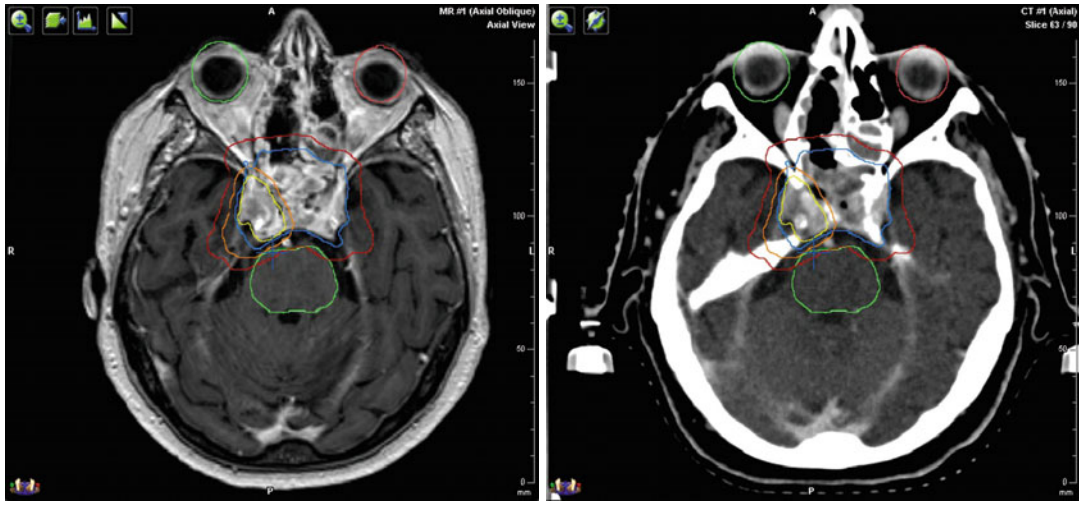

Fig. 2.10 MRI and CT in a patient with chordoma after surgery. Postoperative remaining macroscopic tumour is contoured in *yellow* and the tumour region in *blue*. The resulting PTV is shown in *red* and the resulting PTV for the boost in *orange*. Contouring was performed for stereotactic fractionated treatment

musculature reaching down to the basis of the second cervical vertebra are included (Nikoghosyan et al. 2010). The surgical pathway is not included into the CTV, as this may lead to unacceptable toxicity to normal tissue. For the boost the GTV (entire residual tumour) plus a setup margin results in the PTV. Figure 2.10 shows an example.

2.3.8 Metastases of the Skull Base

Skull base metastases can originate from intracranial structures such as the meninges or from extracranial bony tissue. In case of meningeal involvement, irradiation of the whole brain is indicated. Therapy can be followed by a boost to the macroscopic tumour. In case of bone metastases, the GTV has to be defined on CT (bone windowing) and MRI. Frequently, skull base metastases can be very well seen in native 3D T1-sequence without fat saturation as hypointense processes, as the normal bone marrow is substituted by tumour cells. For intracranial metastases the MRI (T1 + contrast) is sufficient. The GTV (see Fig. 2.11) has to be expanded by the necessary setup error, which depends on the irradiation technique (e.g. 1 cm).

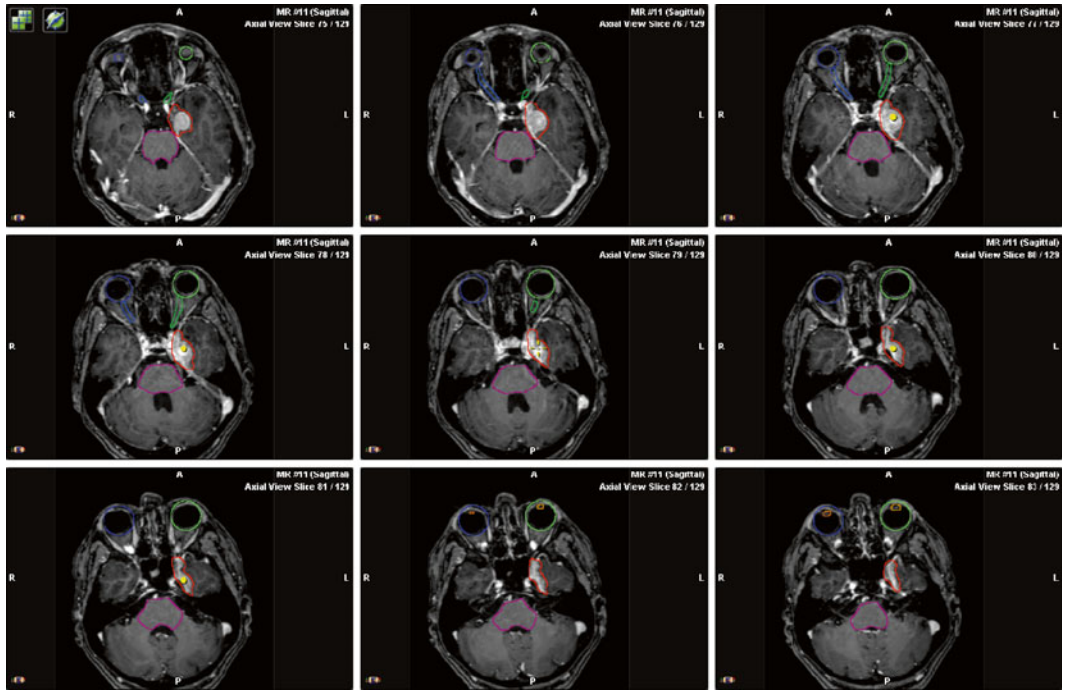

Fig. 2.11 Metastasis at the base of the skulls in a patient with breast cancer. GTV in *red*

References

Asa S (2011) Tumors of the pituitary gland. AFIP atlas of tumor pathology. Fourth series. Fascicle 15. Lyon, ARP Press

Astner ST, Dobrei-Ciuchendea M, Essler M, Bundschuh RA, Sai H, Schwaiger M, Molls M, Weber WA, Grosu AL (2008) Effect of 11C-methionine-positron emission tomography on gross tumor volume delineation in stereotactic radiotherapy of skull base meningiomas. Int J Radiat Oncol Biol Phys 72(4):1161–1167

Combs SE, Thilmann C, Huber PE, Hoess A, Debus J, Schulz-Ertner D (2007) Achievement of long-term local control in patients with craniopharyngiomas using high precision stereotactic radiotherapy. Cancer 109(11):2308–2314

Combs SE, Welzel T, Habermehl D, Rieken S, Dittmar JO, Kessel K, Jäkel O, Haberkorn U, Debus J (2013) Prospective evaluation of early treatment outcome in patients with meningiomas treated with particle therapy based on target volume definition with MRI and 68Ga-DOTATOC-PET. Acta Oncol 52(3):514–520

Coskun M, Straube W, Hurkmans CW, Melidis C, de Haan PF, Villà S, Collette S, Weber DC (2013) Quality assurance of radiotherapy in the ongoing EORTC 22042–26042 trial for atypical and malignant meningioma: results from the dummy runs and prospective individual case Reviews. Radiat Oncol 8:23. doi:10.1186/1748-717X-8-23

Grosu AL, Astner ST, Riedel E, Nieder C, Wiedenmann N, Heinemann F, Schwaiger M, Molls M, Wester HJ, Weber WA (2011) An interindividual comparison of O-(2-[18F]fluoroethyl)-L-tyrosine (FET)- and L-[methyl-11C]methionine (MET)-PET in patients with brain gliomas and metastases. Int J Radiat Oncol Biol Phys 81(4):1049–1058

Jeremic B, Werner Wasik M, Villa S, Paulsen F, Bednarz G, Linero D, Buchgeister M (2008) Stereotactic radiation therapy. In: Jeremic B, Pitz S (eds) Primary optic nerve sheath meningioma. Springer, Berlin, pp 104–127

Kopp C, Fauser C, Müller A, Astner ST, Jacob V, Lumenta C, Meyer B, Tonn JC, Molls M, Grosu AL (2011) Stereotactic fractionated radiotherapy and LINAC radiosurgery in the treatment of vestibular schwannoma-report about both stereotactic methods from a single institution. Int J Radiat Oncol Biol Phys 80(5):1485–1491

Kopp C, Theodorou M, Poullos N, Astner ST, Geinitz H, Stalla GK, Meyer B, Molls M, Nieder C, Grosu AL (2013) Fractionated stereotactic radiotherapy in the treatment of pituitary adenomas. Strahlenther Onkol 189(11):932–937

Milker-Zabel S, Zabel-du Bois A, Henze M, Huber P, Schulz-Ertner D, Hoess A, Haberkorn U, Debus J

(2006) Improved target volume definition for fractionated stereotactic radiotherapy in patients with intracranial meningiomas by correlation of CT, MRI, and [68Ga]-DOTATOC-PET. Int J Radiat Oncol Biol Phys 65(1):222–227

Nikoghosyan AV, Rauch G, Münter MW, Jensen AD, Combs SE, Kieser M, Debus J (2010) Randomised trial of proton vs. carbon ion radiation therapy in patients with low and intermediate grade chondrosarcoma of the skull base, clinical phase III study. BMC Cancer 10:606

Simpson D (1957) The recurrence of intracranial meningiomas after surgical treatment. J Neurol Neurosurg Psychiatry 20:22–39

WHO Classification of Tumours of the Central Nervous System (2007) (Cavenee, Louis, Ohgaki & Wiestler) Lyon, IARC Press. ISBN 9283224302

Spinal Cord Tumors

3

Arjun Sahgal, Louis Lao, Eugene Yu, C. Shun Wong, David A. Larson, Normand J. Laperriere, and Jason Karamchandani

Contents

A. Sahgal, MD (✉)
Department of Radiation Oncology, Sunnybrook Health Sciences Centre and Princess Margaret Cancer Centre, University of Toronto, 2075 Bayview Avenue, Toronto, ON M4N 3M5, Canada
e-mail: Arjun.Sahgal@sunnybrook.ca

L. Lao, MBChB • N.J. Laperriere, MD
Department of Radiation Oncology, Princess Margaret Hospital, University of Toronto, Toronto, ON Canada

E. Yu, MD
Department of Radiology, University Health Network, University of Toronto, Toronto, ON Canada

C.S. Wong, MD
Department of Radiation Oncology, Sunnybrook Health Sciences Center, University of Toronto, Toronto, ON Canada

D.A. Larson MD, PhD
Department of Radiation Oncology, University of California San Francisco, San Francisco, CA, USA

J. Karamchandani, MD
Department of Anatomic Pathology, St. Michaels Hospital, University of Toronto, Toronto, ON Canada

3.1 Introduction

The spinal cord is an organ that can be affected by tumors which arise from within it, disseminate to it, or impinge upon it. There are 850–1,700 new cases of spinal cord tumors diagnosed each year in the United States, and these tumors are 10–15 times less common than primary brain tumors (Traul et al. 2007; Sansur et al. 2007). Spinal cord tumors can be classified as intramedullary, intradural and extramedullary, and extradural (Traul et al. 2007; Sansur et al. 2007). The focus of this chapter is on radiation treatment planning for spinal cord tumors. Radiation is one of the main treatments of spinal cord tumors due to the rarity of achieving a gross-total tumor resection, and for operable tumors, the morbidity can be significant such that a biopsy alone is typical, with definitive radiation to follow.

A.-L. Grosu, C. Nieder (eds.), *Target Volume Definition in Radiation Oncology*,
DOI 10.1007/978-3-662-45934-8_3, © Springer-Verlag Berlin Heidelberg 2015

In comparison to the rarity of spinal cord tumors, the spinal cord is one of the most important organs at risk (OAR) to be respected in radiation planning. The consequence of overdosing the spinal cord is radiation myelopathy which can leave a patient paralyzed and incontinent (Sahgal et al. 2008a). This toxicity has been largely regarded as associated with crude radiotherapy techniques and lack of sophisticated computer technology that can model radiation dose accurately. With technologic advances we now rarely observe this toxicity; however, this devastating side effect is reemerging with the advent of delivering high-dose hypofractionated radiation [stereotactic body radiotherapy (SBRT)] adjacent to and even within the spinal cord (Sahgal et al. 2008b, 2011a). This chapter will also summarize the current knowledge of spinal dose limits for conventional and SBRT to guide safe practice.

3.2 Anatomy

The spinal cord is an extension beyond the brain. It is protected by the spinal column and extends from the level of the foramen magnum to approximately the first to second lumbar vertebrae (L1–L2). The spinal cord is bathed in cerebrospinal fluid (CSF) and enclosed by the meninges, consisting of the dura, arachnoid, and pia (which are separated by the subdural and subarachnoid spaces). The spinal cord contains 31 segments, and each segment provides the attachment of the rootlets for a dorsal and ventral root that traverse the dura and unite close to their intervertebral foramina to form spinal nerves. The cord gradually tapers craniocaudally except at the level of two enlargements. The cervical enlargement (C3–T2) is the source of large spinal nerves forming the brachial plexus that innervates the upper limbs, and the corresponding nerves from the lumbar enlargement (L1-S3) form the lumbosacral plexus that innervates the lower limbs (Gray 1918; Moore and Dalley 1999). Nerve roots of the lumbar and sacral segments of the cord form a bundle of roots (known as the cauda equina) as they descend to their respective intervertebral foramina (Gray 1918; Moore and Dalley 1999).

The basic structural organization of the spinal cord consists of central butterfly-shaped gray matter and outer white matter. Ascending tracts of sensory fibers and descending motor tracts are the main components of the white matter. Gray matter contains the neuronal cell bodies, including those of the large motor and sensory neurons. The anterior spinal artery and the paired posterior spinal arteries run longitudinally throughout the length of the cord to provide its blood supply. In addition, there are segmental arteries which enter the vertebral canal through the intervertebral foramina that supplement the blood supply to the cord. For specific details regarding anatomy, the reader is directed to neuroanatomy textbooks.

3.3 Cell Type and Function

The major cell types in the spinal cord consist of neurons, glial cells, hematopoietic cells, and vascular endothelial cells. Neurons are the nerve cells responsible for excitation and nerve impulse conduction, whereas the glial cells are the interstitial cells that have important ancillary functions. Glial cells include oligodendrocytes, astrocytes, and ependymal cells. Oligodendrocytes are responsible for myelination of axons in the CNS. Myelin sheaths are formed by the wrapping of oligodendrocyte cytoplasmic processes around the axon and are interrupted by the nodes of Ranvier which serve to enhance propagation of action potentials. Myelination thus allows for the propagation of nerve impulses or action potentials. One oligodendrocyte can myelinate several adjacent axons via its cytoplasmic processes. In contrast, each Schwann cell myelinates one segment of an axon within a peripheral nerve/spinal nerve root. Astrocytes are irregularly shaped glial cells with a large number of branched processes. Many of these processes end in terminal expansions upon the basement membrane of capillaries known as

perivascular feet. Astrocytes participate in the transmission of neuronal signals as well as in the formation and maintenance of the blood–spinal cord barrier (BSCB). Ependymal cells are ciliated cells which facilitate the circulation of CSF and line the central canal. Microglial cells are bone-marrow-derived histiocytes resident to the central nervous system that, upon activation in response to injury, have phagocytic properties.

Endothelial cells in the spinal cord form the BSCB that severely restricts the passage of most proteins, hydrophilic molecules, and ions in the circulation into the spinal cord. The unusual impermeability of CNS capillaries is attributed to tight junctions between endothelial cells and very limited endothelial vesicular transport. In addition to the specialized endothelium of the spinal cord, other important components of BSCB include the basement membrane, astrocytes, and pericytes in immediate proximity. It is now recognized that neural progenitors and neural stem cells persist in the adult central nervous system. Although these cells are generally believed to reside in certain areas of the brain, neural stem cells/progenitors can be isolated from the adult spinal cord (Weiss et al. 1996).

3.4 Spine Imaging

Magnetic resonance imaging (MRI) is the preferred modality for imaging the spinal cord. MRI has a very high sensitivity and specificity with respect to evaluating the spinal cord parenchyma, CSF, and adjacent epidural and paraspinal soft tissues for tumor involvement. Routine imaging sequences include sagittal T1-weighted spine echo (SE) and T2-weighted fast spin echo (FSE) series. These sagittal series allow for assessment of the vertebrae, intervertebral discs, neuroforamina, spinal cord, cauda equina, as well as the CSF space. Abnormal spinal curvature or vertebral compression deformity is well depicted on such series. Routine axial imaging is also performed, usually through affected level(s) of interest. Depending upon institutional preferences, axial imaging can be performed with either axial T1- or axial T2-weighted sequences. These allow for an acute assessment of spinal canal compromise as well as visualization of the pedicles, transverse processes, lamina, and spinous processes. Tumor involving the vertebral bodies is usually depicted as intermediate or hypointense signal on T1-weighted imaging. This is easily visible against the normal hyperintense signal within the fatty marrow of the vertebra. Tumor on T2-weighted images is usually mildly hyperintense and is somewhat less conspicuous against the native marrow space (Fig. 3.1). Densely sclerotic tumor foci will often show very low T1 and T2 signal.

Gadolinium enhancement is usually reserved for the assessment of primary spinal cord tumors and leptomeningeal tumor. The normal spinal cord demonstrates uniform intermediate or isointense T1 and hypointense T2 signal (Fig. 3.2). Normally, there is minimal, if any, pial enhancement on the surface of the cord (Fig. 3.2). Primary or secondary parenchymal cord tumor will enhance following contrast administration, and examples are shown in Fig. 3.3. Associated peritumoral edema and cord expansion may also be evident. Leptomeningeal disease will manifest as linear or nodular foci of enhancement along the surface of the cord. Severe leptomeningeal disease can give a classic "frosting-like" appearance along the cord surface and show marked nodularity in the cauda equina (Fig. 3.4).

Gadolinium enhancement should be performed with fat saturation techniques which act to decrease the signal of native fat within the marrow spaces. This is of particular importance when evaluating for the presence of vertebral metastases. The use of gadolinium contrast without such suppression techniques will raise the signal of vertebral body metastases on T1-weighted sequences. Such lesions can potentially enhance to such a degree as to be isointense with non-suppressed bright marrow signal and thus be "masked" (Fig. 3.5). Some institutions will also employ methods to suppress marrow signal on

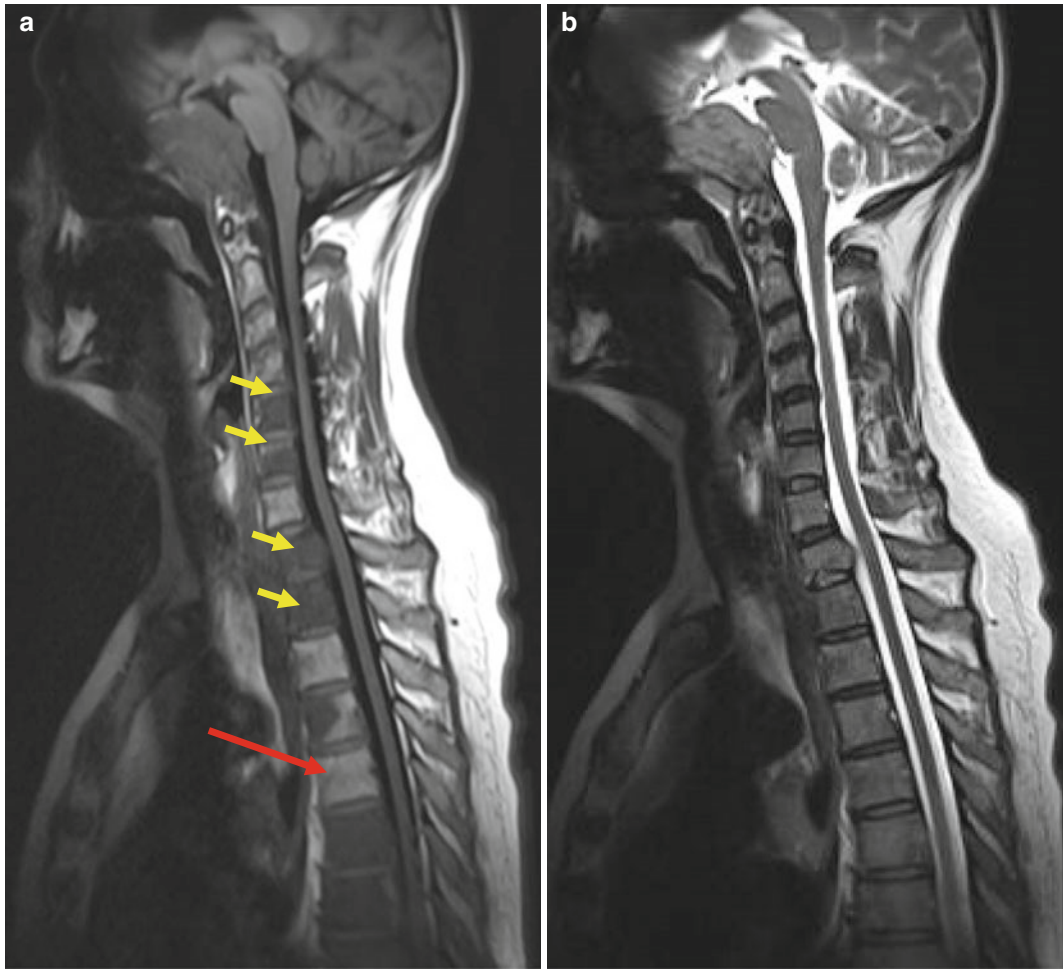

Fig. 3.1 Sagittal T1-weighted (**a**) and T2-weighted images (**b**) through the cervical and upper thoracic spine. Normal marrow shows high signal on T1 imaging (*red arrow*) reflecting the presence of yellow fatty marrow. Note the presence of multiple foci of intermediate signal within the vertebral bodies (*short arrows* in **a**) representing metastatic disease. Also note the difference in conspicuity of the metastatic foci when compared with the T2 image (**b**)

T2-weighted acquisitions. This can be performed via use of a chemical fat saturation technique or via short inversion time inversion recovery (STIR) technique. These sequences have a high degree of sensitivity for the visualization of edema, inflammation, and tumor and will increase the conspicuity of vertebral lesions. We also routinely employ a coronal T1-weighted series through the sacrum. This gives a good overview of the sacral bone and the neuroforamina.

Computed tomography (CT) still plays an important role in imaging the spine, primarily in evaluating bone. In particular, the nature of tumor being lytic, blastic, or mixed is based on CT and not MRI characteristics. Furthermore, for the spine surgeon planning to perform a reconstructive spine surgery with instrumentation, a spine CT is typically required to evaluate the bony quality above and below the affected levels in order to confidently determine the best levels at which to apply instrumentation. Lastly, for patients who have contraindications to MRI, a CT myelogram may be performed to adequately visualize the relationship between tumor, CSF, and the spinal cord/cauda equina. This procedure has become more frequently used with the advent of spine SBRT, as the precise delineation of the spinal cord and thecal sac helps to ensure safe practice.

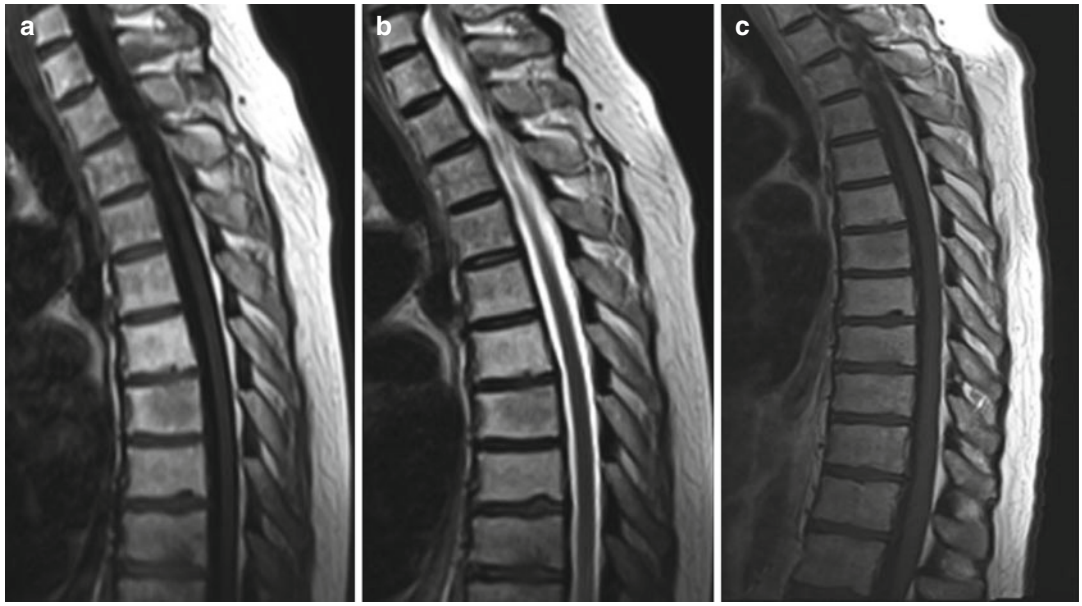

Fig. 3.2 Sagittal T1 (**a**), T2 (**b**), and post-contrast T1 (**c**) images showing the normal appearance of the spinal cord. T1 imaging shows a uniform isointense signal of the cord. Minimal if any pial enhancement is seen. T2 imaging shows the cord to be of uniform hypointensity

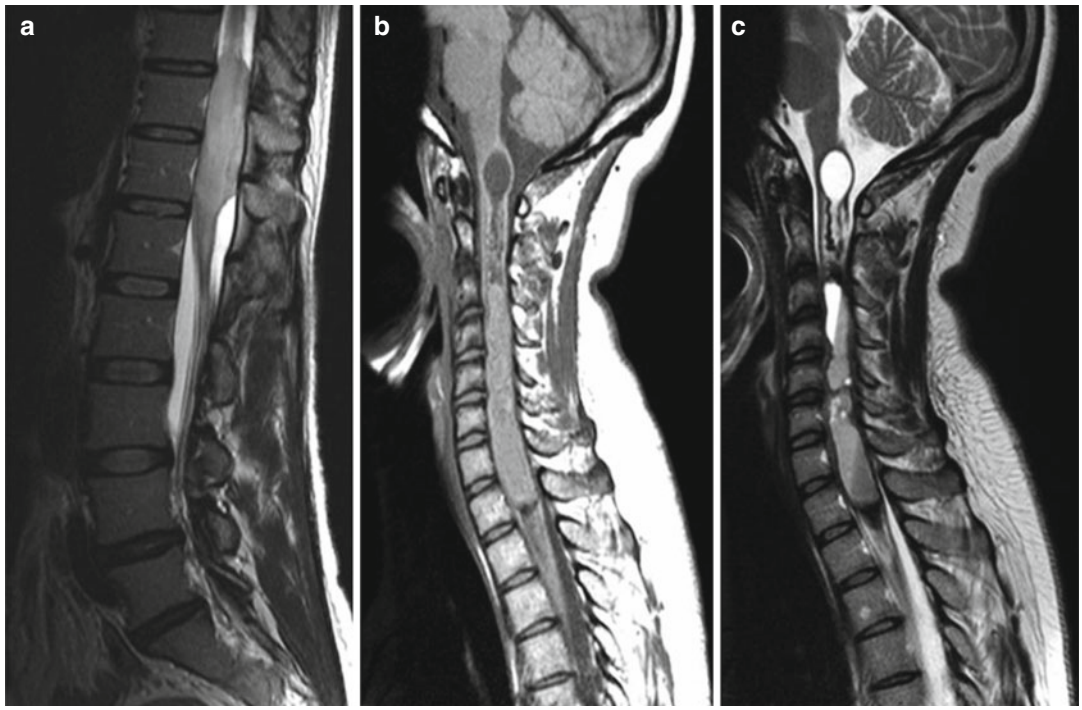

Fig. 3.3 Sagittal T2 image (**a**) showing an expansile anaplastic astrocytoma involving the distal cord. Hyperintense signal extending into the conus is compatible with peritumoral edema. Sagittal gadolinium-enhanced T1 (**b**) and T2 images (**c**) of an ependymoma involving the cervical cord. This mass is quite complex with areas of cystic change with internal fluid–fluid levels. Also note the presence of dark signal "cap" along the inferior margin (**b**, **c**) of the lesion representing chronic blood product

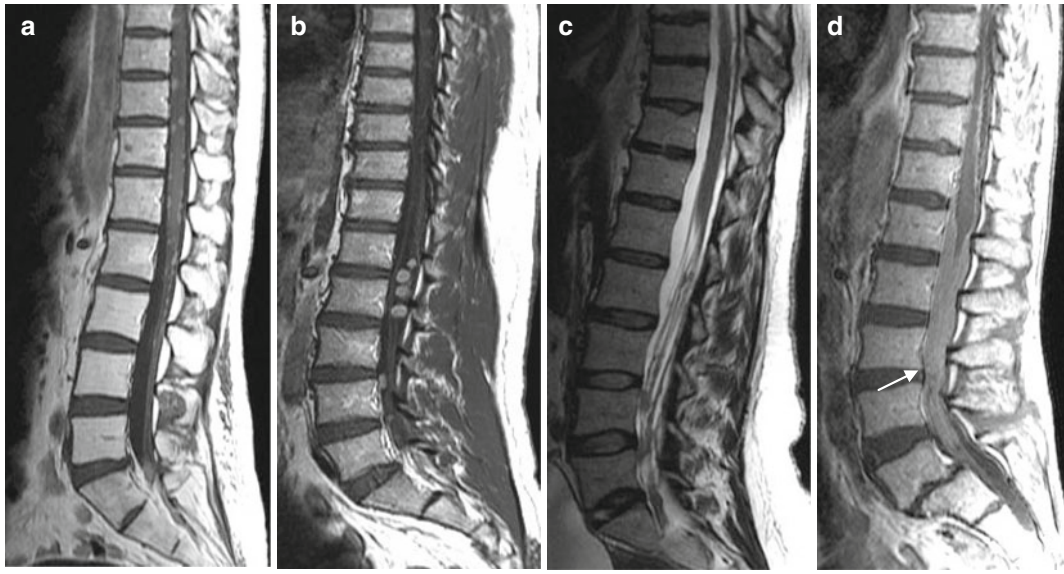

Fig. 3.4 Leptomeningeal spinal metastases. Sagittal enhanced T1 images (**a**, **b**) showing pial "drop metastases" manifesting as enhancing foci studding the surface of the cord and cauda (**a** – lung carcinoma) and as larger more discrete enhancing nodules along the cauda equina (**b** – endolymphatic sac tumor). Sagittal T2 image (**c**) in a patient with breast carcinoma also shows nodularity along the cauda equina. Sagittal enhanced T1 image (**d**) shows very marked diffuse plaque-like enhancing tumor infiltrating the cauda equina (*arrows*) in a patient with sinonasal carcinoma

3.5 Case-Based Discussion of Common Spinal Cord Tumors

IMST of all three glial lines can occur in the spinal cord. Table 3.1 details the more common IMST tumor types. A full description of all tumor types is beyond the scope of this chapter as the focus is on treatment planning. The following is a brief description of the more common types that a radiation oncologist should be aware of and difficult cases will be presented with treatment planning details. Although the focus is on IMST, additional spinal tumors will be presented to provide a comprehensive case discussion. In the discussion of radiotherapy planning that follows, GTV refers to the gross tumor volume as tumor evident on imaging (note this can also include the postoperative bed in selected circumstances), CTV refers to the clinical target volume which is a margin applied to encompass potential microscopic disease that should be included in the high-dose volume to achieve the intent of therapy and this margin respects anatomic boundaries to tumor invasion, and PTV refers to the planning target volume which is a geometric margin that is applied to account for uncertainties in delivery, planning, dose calculation, etc. A complete description of these definitions can be found in the ICRU 50 report (ICRU 1993). In addition, the approaches described with respect to dose selection and volume contouring are those currently in practice at the University of Toronto and subject to change. At this time there is a lack of data and consensus as to optimal margins, and the reader should be aware of the limitations in the literature.

3.5.1 Ependymoma

Ependymomas are characterized by perivascular pseudorosettes and are the most common gliomas of the spinal cord. Classical ependymomas are considered either World Health Organization (WHO) grade II or WHO grade III (anaplastic) tumors, though the latter occur less frequently in the spinal cord. Unlike their astrocytic and oligodendroglial counterparts, ependymomas

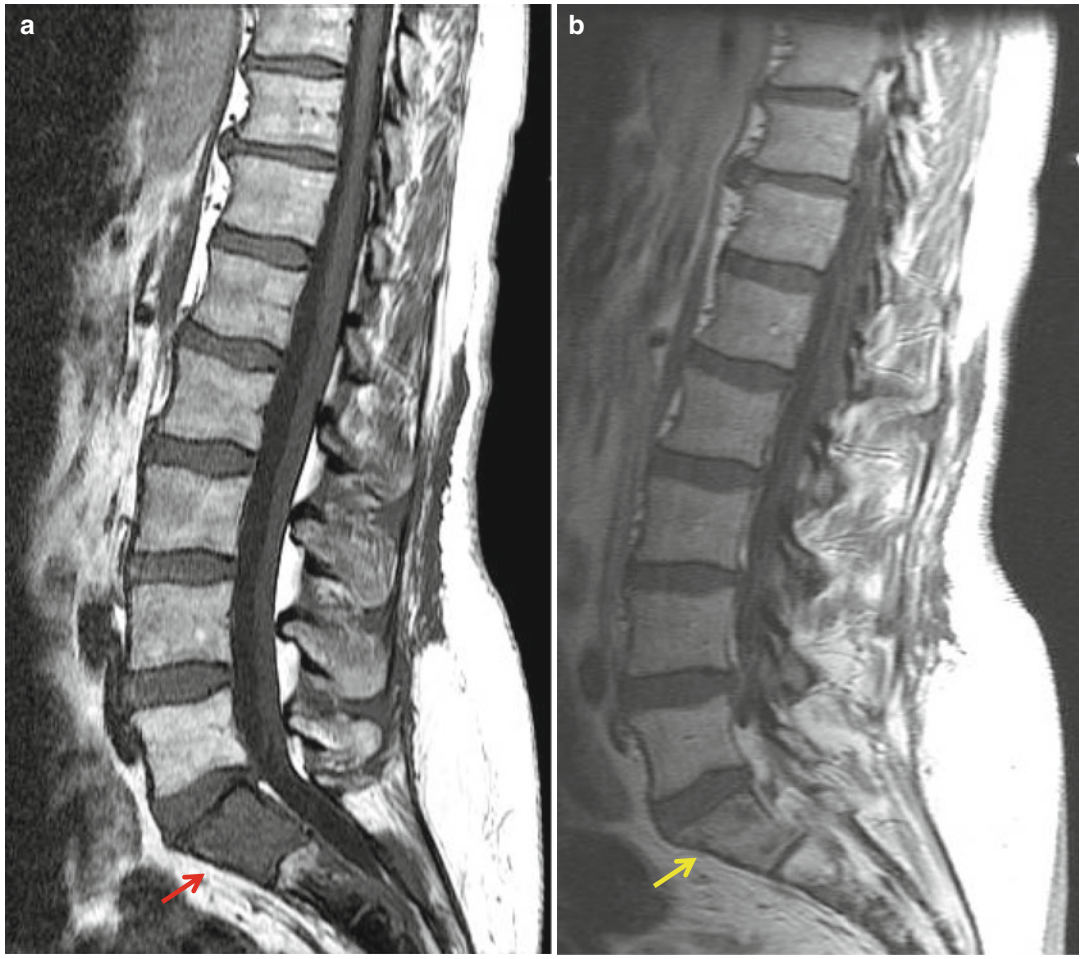

Fig. 3.5 Sagittal T1-weighted images without (**a**) and with gadolinium (**b**) enhancement. The metastasis within the S1 segment of the sacrum is seen as an area of intermediate signal and is easily visible (*red arrow*) on the unenhanced image. Following contrast, the tumor enhances and becomes nearly isointense with the native marrow signal and is more difficult to discern (*yellow arrow*)

frequently have a pushing border and are more amenable to surgical resection (Chamberlain and Tredway 2011). Ependymoma is the most common glioma diagnosed in the setting of neurofibromatosis type 2, and the vast majority of these tumors occur in the spinal cord (Louis et al. 2007). Myxopapillary ependymomas (Fig. 3.6) generally occur in the region of the cauda equina and conus medullaris. These tumors are currently considered WHO grade I neoplasms, but recurrence is not uncommon, particularly in the pediatric population (Bagley et al. 2009). Classical ependymoma also have distinct gene expression profiles as compared to myxopapillary ependymoma (Barton et al. 2010). With respect to workup, MRI brain is recommended, and for anaplastic tumors, a 14-day postoperative lumbar puncture is recommended to rule out CSF spread.

For WHO grade I/II spinal ependymomas without evidence of CSF dissemination, observation is an option following a gross-total resection (GTR). If a GTR is not achieved, or if the tumor is anaplastic, localized radiation is recommended to a dose of 54 Gy in 30 fractions. If CSF dissemination is evident, then craniospinal radiation is recommended to a dose of 36 Gy in 20 fractions (39.6 Gy in 22 fractions if macroscopic CSF disease spread) followed by a boost

Table 3.1 Summary of common primary intramedullary tumors

Primary intramedullary tumors	
Neuroepithelial tumors	*Other primary tumors*
Glial	Hemangioblastoma
Pilocytic astrocytoma	Paraganglioma
Astrocytoma, diffuse/anaplastic	Lipoma
Glioblastoma	Lymphoma
Oligodendroglioma	*Vascular malformations*
Ependymoma	Arteriovenous malformation
Mixed neuronal–glial	Capillary hemangioma
Ganglioglioma	Cavernous hemangioma
	Nerve sheath tumors
	Schwannoma
	Neurofibroma
	Malignant peripheral nerve sheath tumor
	Synovial sarcoma

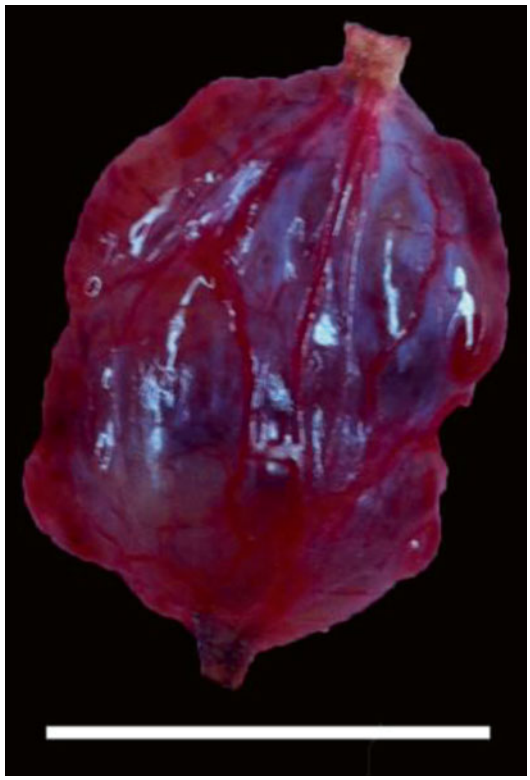

Fig. 3.6 Myxopapillary ependymoma demonstrating well-defined non-infiltrating border with associated nerve seen at the superior and inferior specimen margins. Scale bar = 1 cm

to the primary site and all disseminated gross disease to a total of 54 Gy (or 59.4 Gy if the tumor involves the brain).

3.5.1.1 MR Imaging Characteristics

Ependymomas arising within the spinal cord parenchyma are most likely of the cellular subtype. These lesions are usually well delineated and have hypointense T1 and hyperintense T2 signal. Tumors will typically show avid enhancement with gadolinium. Depending upon the size of the tumor, focal spinal cord expansion may be evident. Intra-tumoral cystic change can be present. Acute to subacute hemorrhage can also arise which will give rise to regions of high T1 and variable T2 signal. Chronic blood product in the form of hemosiderin will give rise to a characteristic low T1 and T2 signal "cap" or peripheral rim along the edge of the mass. Gradient echo or susceptibility weighted imaging will also highlight areas of hemorrhage as regions of very low signal. Surrounding high T2 signal edema will be seen surrounding the periphery of the lesion.

The myxopapillary subtype is characteristically located within the distal conus or cauda equina and manifests as a heterogeneously enhancing, often cystic and hemorrhagic mass. Expansion of the spinal canal and remodeling and scalloping of the posterior aspect of the adjacent vertebral bodies may be seen. These tumors show low T1 and bright T2 signal. Areas of high T1 signal may reflect the presence of hemorrhage or possibly mucin content. The presence of CSF dissemination will manifest as enhancing areas of thickening and/or nodularity along the surface of the spinal cord.

3.5.1.2 Radiotherapy Volume Delineation

GTV should encompass the T1 post-gadolinium abnormality, the postsurgical tumor bed, and the T2 FLAIR abnormality (not including non-enhancing syrinx). The CTV includes a margin of 1.5–2 cm superiorly and inferiorly and the entire canal radially along the length of the CTV. A margin of 0.3–0.5 cm is applied as PTV (this margin is based on the patient immobilized in a suitable device and daily cone-beam CT image guidance).

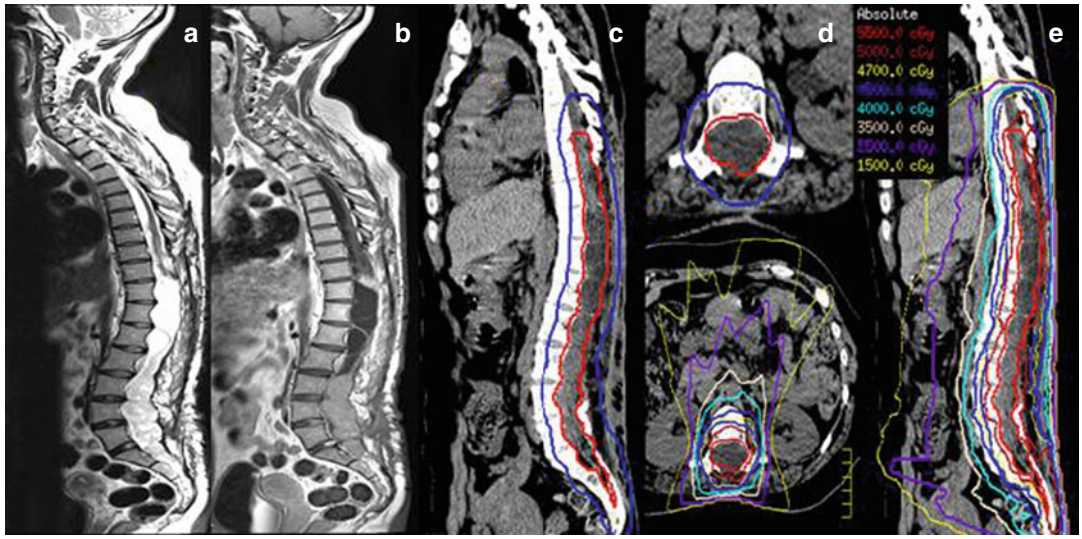

Fig. 3.7 An example of a myxopapillary ependymoma treated with 54 Gy in 30 fractions with IMRT. The pre-radiation T2 FLAIR and T1 post-gadolinium sagittal MR images are shown on Panels (**a**, **b**). The treatment planning volumes shown in Panel (**c**) with the CTV in *red* and PTV in blue (for clarity the GTV contour omitted), Panel (**d**) illustrates an axial image showing the CTV and PTV and below a representation of the isodose distribution, and Panel (**e**) illustrates the sagittal view of the treatment plan with representative isodose lines

3.5.1.3 Case

Although most myxopapillary ependymomas can be completely resected and no further intervention with radiotherapy is required, in select cases up-front radiotherapy is delivered. We present a case of a 34-year-old woman who presented with progressive bilateral leg weakness and sensory findings (paresthesia) who ultimately progressed to develop a neurogenic bladder. The patient had an MRI spine with contrast and was found to have an extensive intramedullary mass. In Fig. 3.7, the T2 FLAIR and T1 post-gadolinium sagittal images are shown depicting an enhancing cystic and solid tumor extending cranially from T10 to S2 caudally, and axially the tumor involved the entire canal. The patient then underwent a subtotal resection and the pathology confirmed the diagnosis of myxopapillary ependymoma. As a complete resection was not possible, the patient was treated adjuvantly with radiotherapy. We prescribed 54 Gy in 30 fractions and delivered treatment using intensity modulated radiotherapy (IMRT) using a 12 coplanar beam technique. When the tumor is also inherently the organ at risk (OAR), our practice is to prescribe to a point maximum (in this case 54 Gy) and aim to achieve at least >95 % coverage of the CTV and >90 % of PTV. This practice ensures no hot spot in the treatment plan and hence within the OAR.

The GTV was the T1 post-contrast enhancing disease and included the T2 FLAIR signal change, and a 1.5 cm margin beyond the GTV cranially and caudally was applied (respecting anatomic barriers) as CTV. However, in this case the inferior aspect of the CTV was extended to encompass the spinal canal to its inferior aspect which was ~S5 (red contour, Fig. 3.7). For more limited target lengths, a 0.3–0.5 cm PTV margin is applied; however, in this case due to the uncertainties at the extremes of the target with respect to patient motion and setup uncertainties, a 1 cm PTV was applied (blue contour, Fig. 3.7). Representative axial and sagittal images of the dose distribution are also shown, and the conformal nature of the higher isodose lines is apparent with the lower doses (e.g., the 2,500 cGy isodose line) spilling due to the nature of IMRT delivery.

3.5.1.4 Selected Evidence

The Cleveland Clinic group recently reported on 37 patients with spinal myxopapillary ependymoma (Chao et al. 2011). Of the 37 patients, 9

were treated with a planned up-front postoperative adjuvant radiation, 5 of which had a gross tumor resection (GTR), and 32 patients were observed postoperatively (20 of whom had a GTR). They observed a mean survival time of 12.2 years and a median time to recurrence of 7.7 years (16/37 had relapsed). The use of up-front radiation did not yield any significant differences in overall survival (OS) or relapse-free survival (RFS). Importantly, they observed that for those who relapsed and were treated with radiation at that time, the median RFS was significantly prolonged at 9.6 years as opposed to 1.1 years in those who did not receive radiation ($p = 0.0093$). The reader is cautioned to recognize that there are other data that have reported benefits with respect to RFS with up-front radiation and overall there is much controversy as to the optimal management with respect to the timing of radiation.

The Princess Margaret Hospital (Toronto, Canada) experience has been reported. The series consisted of 59 patients and all patients were treated with radiotherapy. Overall survival at 5 and 10 years was 83 and 75 %, respectively. They observed that grade correlated with survival with 5-year cause-specific survivals of 97 % vs. 75 % for well-differentiated tumors as compared to intermediate or poorly differentiated tumors. The median time to recurrence for the 11 local failures was 2 years (Waldron et al. 1993).

3.5.2 Astrocytoma

Astrocytomas of all WHO grades can occur in the spinal cord. Pilocytic astrocytomas are WHO grade I neoplasms with low proliferative activity featuring biphasic morphology and Rosenthal fiber formation. These typically occur in children and young adults and account for 12.5 % of spinal cord tumors in the pediatric population (Dolecek et al. 2012). Infiltrating astrocytomas of the CNS are graded on the basis of pleomorphism (diffuse astrocytoma – WHO grade II), mitotic activity (anaplastic astrocytoma – WHO grade III), and the presence of vascular proliferation and/or necrosis (glioblastoma – WHO grade IV). Similar to ependymoma, there is potential for complete resection of well-defined tumors such as pilocytic astrocytoma. For extensive tumors and/or more infiltrative tumors, subtotal resection or biopsy alone may be the only surgical result achievable, and these patients typically will require up-front radiation.

3.5.2.1 MR Imaging Characteristics

Spinal cord astrocytomas appear as expansile mass lesions most commonly located in the cervical or thoracic cord. They show low T1 and bright T2 signal. Hemorrhage and cystic change are less frequent compared with ependymoma. Tumor enhancement is variable and may range from no enhancement to fairly avid enhancement. Those lesions which do enhance are usually less avid when compared with ependymoma. Enhancement patterns can range from focal nodular, patchy, and diffuse, and astrocytomas are also usually more eccentrically located in the cord compared with ependymomas.

3.5.2.2 Radiotherapy Volume Delineation

For pilocytic astrocytoma, the GTV includes the residual enhancing disease and the surgical bed. A 0.5–1 cm margin cranially and caudally is applied as CTV that also encompasses the T2 FLAIR abnormality and radially the entire spinal canal along the CTV length. A 0.3–0.5 cm margin is applied for PTV. For higher-grade tumors, the GTV includes the residual enhancing disease, the surgical bed, and the T2 FLAIR abnormality. A CTV margin of 1 cm cranially and caudally is applied of grade II tumors and 1.5 cm for grade III and IV tumors and radially the entire spinal canal along the CTV length. A 0.5 cm margin is applied for PTV (this margin is based on the patient immobilized in a suitable device and cone-beam CT image guidance).

3.5.2.3 Pilocytic Astrocytoma Case

This 29-year-old female initially presented with neck pain and an episode of transient quadriparesis following a chiropractic neck manipulation. The preoperative and postoperative sagittal T1 post-gadolinium and T2 FLAIR MRI sequences

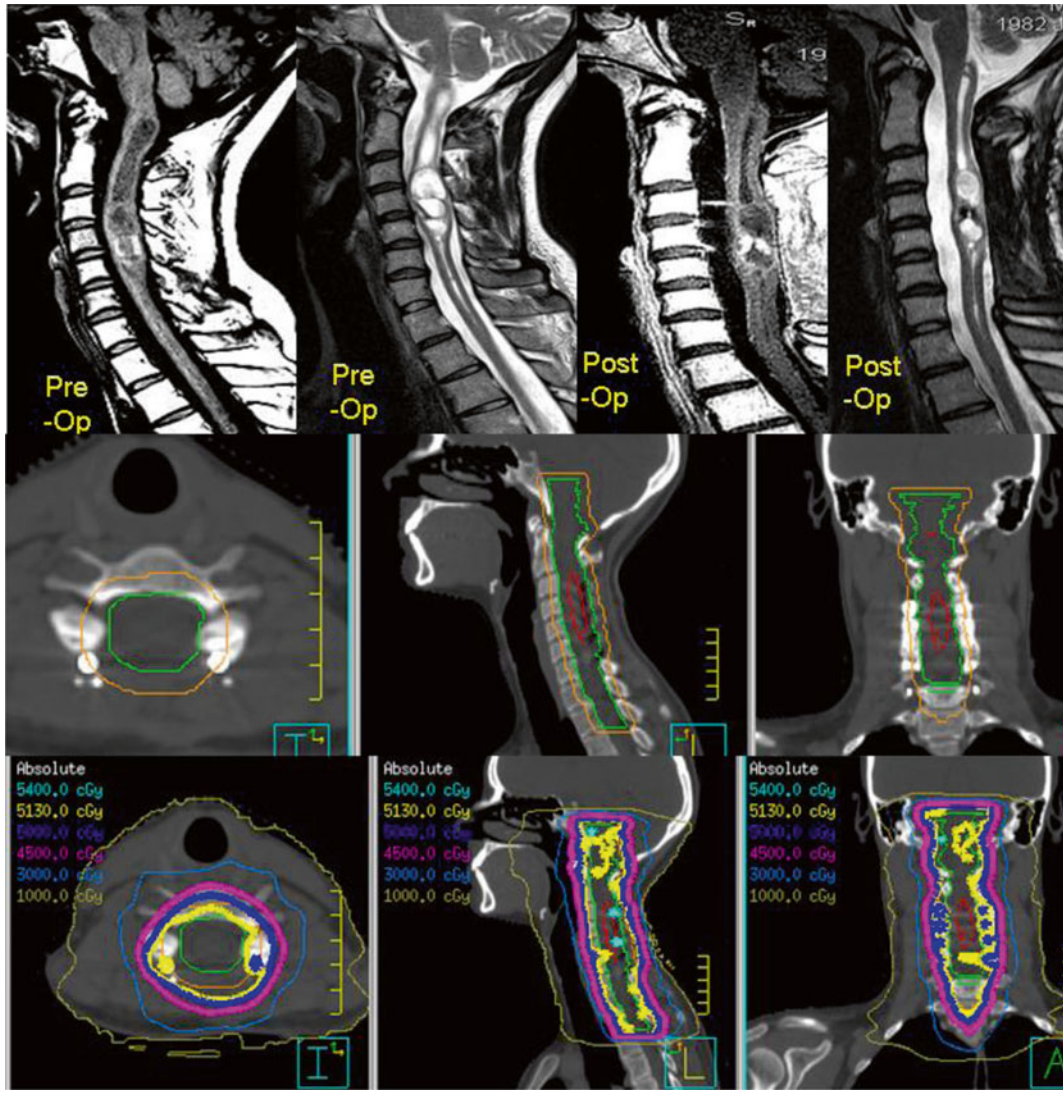

Fig. 3.8 A cervical pilocytic astrocytoma subtotally resected and treated with adjuvant radiation. The *top row* illustrates the preoperative and postoperative sagittal MR images. The *middle panel* illustrates the treatment planning volumes on the treatment planning CT with GTV in *red*, CTV in *green*, and PTV in *orange* and axial, sagittal, and coronal slices. The corresponding isodose distribution is shown in the *bottom row*, and this patient was treated with 54 Gy in 30 fractions

are shown in Fig. 3.8 and illustrate an enhancing mass that was cystic and solid in nature. The mass extended from C1 to T1. Following a subtotal resection, the patient was treated adjuvantly with 54 Gy in 30 fractions using IMRT and a nine-beam coplanar beam arrangement. We prescribed 54 Gy to a point maximum within the PTV and aimed to achieve at least >95 % coverage of the CTV and >90 % of the PTV.

The GTV was contoured as the T1 post-gadolinium residual disease and surgical bed. The CTV encompassed the GTV, the T2 FLAIR abnormality, and a 1 cm margin beyond the T2 FLAIR abnormality cranially (which extends into the brainstem) and caudally (respecting anatomic barriers). Radially, the entire spinal canal was included and at the level of the brainstem, the entire brainstem is taken axially along

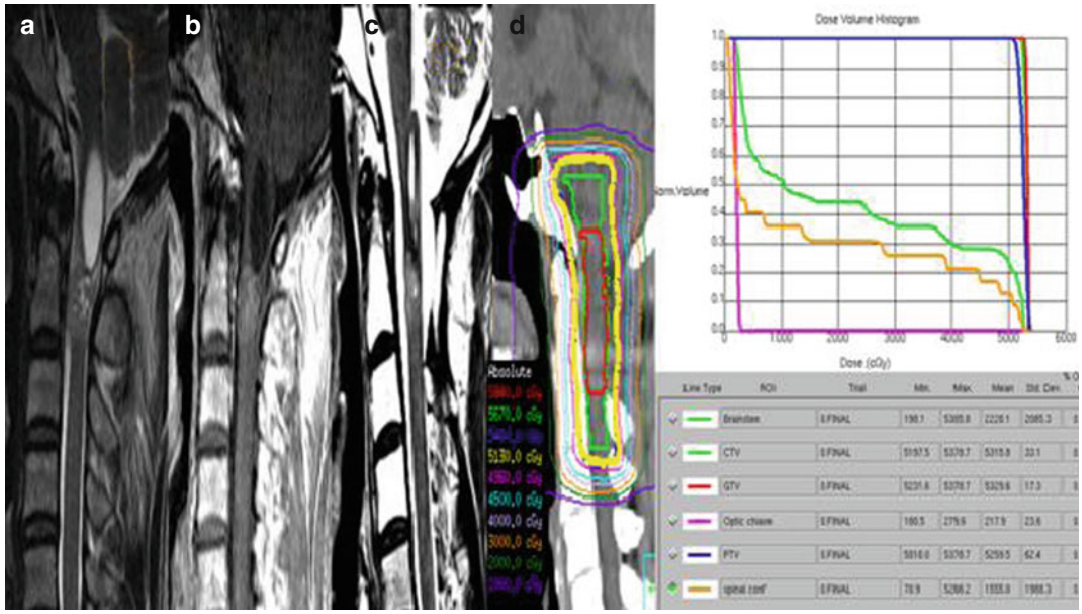

Fig. 3.9 A patient with a cervical spine diffuse grade II low-grade astrocytoma with preoperative T2 FLAIR and T1 post-gadolinium sagittal images on the left (Panels **a**, **b**), the post subtotal resection and cyst decompression sagittal T2 FLAIR image in Panel (**c**), and the treatment planning CT with representative isodose lines in Panel (**d**) with the corresponding DVH

the length of the CTV (respecting anatomic barriers). A 0.5 cm margin was then applied as PTV. The middle panel of Fig. 3.8 shows the contoured volumes with GTV in red, CTV in green, and PTV in orange. Representations of the dose distribution are also shown in the bottom panel of Fig. 3.8.

3.5.2.4 Selected Evidence

A recent study by Ishkanian et al. reviewed the Princess Margaret Hospital (Toronto, Canada) adult pilocytic astrocytoma experience (Ishkanian et al. 2011). The focus was on analyzing the role of up-front radiation as opposed to observation. In that series, 4 out of 30 tumors were located within the spinal cord. The study concluded that the timing of radiation did not impact OS. However, progression-free survival (PFS) was significantly extended with up-front radiation. At 10 years, the PFS rate was 17 % in the observation cohort as compared to 60 % in those radiated up front.

3.5.2.5 Low-Grade Glioma Case

This 45-year-old female presented with headache, blurred vision, and paresthesia over her left side. MRI was performed and shown in Fig. 3.9. Essentially a mass spanning the C2 vertebrae was observed clearly on T2 FLAIR imaging and faintly enhancing on T1 post-gadolinium. An associated cyst was also evident on the T2 FLAIR MRI extending to the level of the clivus. The patient underwent a cyst decompression and subtotal resection, and the postoperative T2 FLAIR imaging is shown in Fig. 3.9. The pathology confirmed a grade II diffuse low-grade astrocytoma. The patient was treated with 54 Gy in 30 fractions prescribed to a point maximum in the PTV. A five-beam coplanar IMRT technique was used, and the sagittal dose distribution is shown in Fig. 3.9. The GTV included the T2 FLAIR abnormality, T1 post-gadolinium abnormality, and surgical bed as shown as the red contour; the CTV consisted of a 1.5 cm cranial–caudal extension beyond the GTV and radially to encompass

the entire canal (respecting anatomic barriers) and a margin of 0.5 cm applied as PTV. The DVH is also shown in Fig. 3.9.

3.5.2.6 Selected Evidence

Outcomes from 52 patients with non-ependymoma spinal cord glioma treated with radiation were reported from the Princess Margaret Hospital (Toronto, Canada) (Rodrigues et al. 2000). Of the 52 cases, 37 (71 %) were low grade (no malignant features) and 15 (29 %) were intermediate (malignant features without frank anaplasia)/high grade (frank anaplasia). Biopsy alone was performed in 52 %, subtotal resection in 38 %, and a gross-total resection in 10 % of cases. The 5-year cause-specific survival and PFS were 73 and 64 % for low-grade tumors and 30 and 20 % for high-grade tumors, respectively.

3.5.3 Extramedullary Intradural Spinal Tumors

3.5.3.1 Meningioma

Meningioma is the most common primary tumor of the CNS and spinal cord, accounting for 46 % of all intradural spinal neoplasms. The incidence of meningioma increases linearly with patient age. Meningiomas are also the most common radiation-induced tumor of the central nervous system. Spinal meningiomas are most commonly classified as WHO grade I tumors, but these can also be more aggressive and categorized as atypical (WHO grade II) or anaplastic (WHO grade III). Grading is based on the histological patterns, as well as assessment of parenchymal invasion and mitotic activity. The majority of spinal meningiomas are solitary; however, multiple tumors may occur and most frequently in the setting of neurofibromatosis type 2. The psammomatous variant of meningioma (WHO grade I), characterized by innumerable calcifications, occurs most commonly in the dura of the thoracic cord.

The primary therapeutic modalities are surgery and radiation. The aim of surgery is to attempt a GTR. For grade I tumors if a subtotal resection or biopsy is performed, then observation and up-front radiation are potential options. In certain cases in which histological confirmation is not possible and if the imaging is consistent with meningioma, then again observation and up-front adjuvant radiation are the options. For grade II tumors, postsurgical management options include observation or up-front radiation if a GTR has been achieved; otherwise, up-front radiation is typically performed as the risk of recurrence/progression is significant. For grade III tumors, adjuvant radiation is recommended regardless of the degree of resection to optimize local control.

3.5.3.2 MR Imaging Characteristics

Meningiomas are characteristically intradural, extramedullary lesions. They typically show isointense (to spinal cord) T1 and T2 signal and will avidly enhance. The presence of calcification may give rise to low regions of T1 and T2 signal. An enhancing "dural tail" that trails and tapers off as it extends away from the mass may be seen and reflects dural reaction. Rarely, cystic change or fatty degeneration may arise, the latter giving rise to regions of bright T1 signal that will become dark on fat saturation sequences. Due to their intradural location, meningiomas may cause significant mass effect on the spinal cord which may show deformity as well as regions of high T2 signal due to parenchymal edema.

3.5.3.3 Radiotherapy Volume Delineation

For grade I tumors treated with fractionated radiotherapy, typical doses range from 45 Gy in 25 fractions to 54 Gy in 30 fractions. The GTV is the enhancing disease based on the T1 post-gadolinium MRI, and the T2 FLAIR imaging can assist in delineating disease. The inclusion of the dural tail is controversial; however, if toxicity is not significantly increased as a result of its inclusion, then it is typically taken in the volume. A CTV ranging from 0 to 0.5 cm may be applied and depends on the clinical situation. For grade II and III tumors, the surgical bed is included in the GTV contour, and a CTV ranging from 0.5 to 1 cm that respects anatomic barriers to tumor

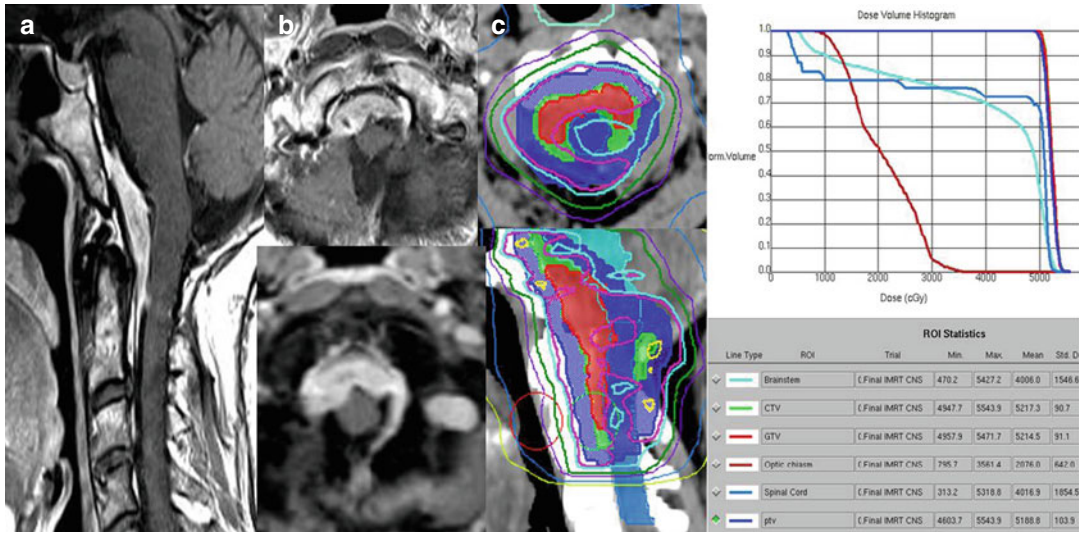

Fig. 3.10 A patient with a cervical spine intradural extramedullary meningioma with the postoperative T1 post-gadolinium sagittal image shown in Panel (**a**), the axial T1 post-gadolinium images at two separate levels shown on Panel (**b**), and the treatment planning CT with GTV in *red color* wash, CTV in *green color* wash, and PTV in *blue color* wash on both an axial and sagittal slice, with the corresponding DVH shown in Panel (**c**)

spread is applied. Of note, the CTV margin should account for contiguous spread into the adjacent brain tissue, unlike grade I tumors, due to the potential for brain invasion. Using a standard thermoplastic mask and image guidance, a 0.3 cm PTV margin may be applied; otherwise, 0.5 cm is recommended. The dose used at the University of Toronto is currently 60 Gy in 30 fractions for atypical and malignant meningioma tumors of the brain, and for the spine, typically the dose is restricted to 54 Gy; however, with modern IMRT treatment planning, there may be potential to boost the GTV to 60 Gy while sparing the spinal cord to 54 Gy.

With respect to spine SBRT, there is emerging evidence to apply single fraction (or few fractions of high-dose-per-fraction radiation) to these tumors despite the location within the spinal canal (Sahgal et al. 2007; Bhatnagar et al. 2005). The issue is the spinal cord tolerance and the lack of literature as to long-term safety following exposure to high-dose-per-fraction radiation, which is less of an issue as compared to the patient with metastatic disease where the technique has been rapidly adopted in North America. Therefore, at this time use of spine SBRT for benign tumors is considered experimental and very few centers have been developing this technique for this indication. Spine SBRT will be discussed in greater detail in the metastases section.

3.5.3.4 Case

This 50-year-old female presented with right arm numbness prompting an MRI which showed an enhancing mass consistent with an intradural meningioma at the level of the foramen magnum. A subtotal resection was performed followed by postoperative radiation given that a GTR was not achievable and a decision was made to maximize local control. The postoperative MRI is shown in Fig. 3.10. This WHO grade I meningioma extends from the lower clivus to the level of C2, and there was encasement of both vertebral arteries and the basilar artery with compression of the medulla oblongata.

The patient was treated with 54 Gy in 30 fractions, again restricting the dose within the PTV to a maximum of 54 Gy. The GTV was defined as the contrast enhancing residual mass (red contour, Fig. 3.10). In this case we also took all visible dural tail in the GTV. A 0.5 cm radial margin was then applied while respecting anatomic

barriers (e.g., bone, spinal cord) as CTV, and we allowed a more generous superior and inferior CTV extension of approximately 1 cm as there is essentially no barrier to spread, and our aim was to minimize any chance of further surgery given the morbidity of operating in this location (green contour, Fig. 3.10). For PTV, we added a 0.5 cm geometric expansion (blue contour, Fig. 3.10).

3.5.3.5 Selected Evidence

A large series of spinal meningiomas was recently reported from Japan with long-term follow-up (mean postoperative follow-up 12.1 years) (Nakamura et al. 2012). Sixty-eight patients underwent resection with 43 being a Simpson grade 1 (complete resection including underlying bone and associated dura), 19 a Simpson grade 2 (complete removal with coagulation of dural attachment), and 6 a Simpson grade 3/4 (complete removal without coagulation of dural/subtotal resection). They observed no tumor recurring for those achieving a Simpson grade 1 resection, 6/19 (32 %) recurring in the Simpson grade 2 group, and 6/6 (100 %) recurring in the Simpson grade 3/4 group. Although the time to progression was within 5 years for all patients in the Simpson grade 3 group, the mean (± standard deviation) time to progression was 12.2 (± 5.2) years in the Simpson grade 2 group. These data highlight the role of observation in patients having had a gross complete resection (Simpson grade 1) and radiation in patients subtotally resected (Simpson Grade 3/4). The use of up-front radiation in the Simpson grade 2 group is controversial. This study, and one from the Mayo Clinic (Cohen-Gadol et al. 2003), identified younger patients (age <50 years) as having a greater risk of tumor recurrence as compared to older patients and may influence the decision to offer up-front adjuvant radiation in the Simpson 2 cohort.

3.5.4 Vertebral and Intramedullary Spinal Metastases

Vertebral body metastases are a frequent complication of advanced cancer occurring in up to 40 % of all cancer patients (Sahgal et al. 2011a, 2008b; Masucci et al. 2011). For patients who do not require an urgent operation, i.e., mechanically stable and/or no spinal cord compression, radiation has been the preferred treatment. This is due to the ability of radiation to palliate the pain and treat the tumor to reduce the risk of progression. With respect to the optimal dose-fractionation scheme, there have been several randomized trials and meta-analyses dedicated to this question (Chow et al. 2007). The primary endpoint of these studies has been short-term pain control and has concluded equivalence with the caveat that treatment with a single fraction of 8 Gy results in greater re-treatment rates as compared to fractionated courses like 20 Gy in 5 fractions or 30 Gy in 10 fractions (Chow et al. 2007). The radiotherapy technique has been rather simple with at least one healthy vertebrae above and below included in the radiation field and either an anterior–posterior parallel-opposed beam arrangement or a direct posterior field prescribed to a depth.

Following conventional radiation, pain outcomes have been relatively consistent in the randomized trials with ~60 % of patients achieving a partial response and 0–20 % a complete response (Chow et al. 2007; Howell et al. 2013; Foro Arnalot et al. 2008; Nguyen et al. 2011). With respect to local control, there is a lack of literature documenting imaging-based tumor control rates until recently. Mizumoto et al. reported on 603 patients with spinal metastases following conventional radiation and found that patients with bulky tumors had inferior local control rates (Mizumoto et al. 2011). At 1 year, the local control rate was 46 % in those with "mass"-type tumors and 86 % in those with "non-mass"-type tumors. These data suggest that there is significant room for improvement in both complete pain response rates and local control; however, progress has only recently been made with the advent of SBRT. The Canadian Association of Radiation Oncology (CARO) recently defined SBRT as the precise delivery of highly conformal and image-guided hypofractionated external beam radiotherapy, delivered in a single or few fraction(s), to an extracranial body target with doses at least biologically equivalent to a radical course when given over a conventionally fractionated (1.8–3.0 Gy/fraction) schedule

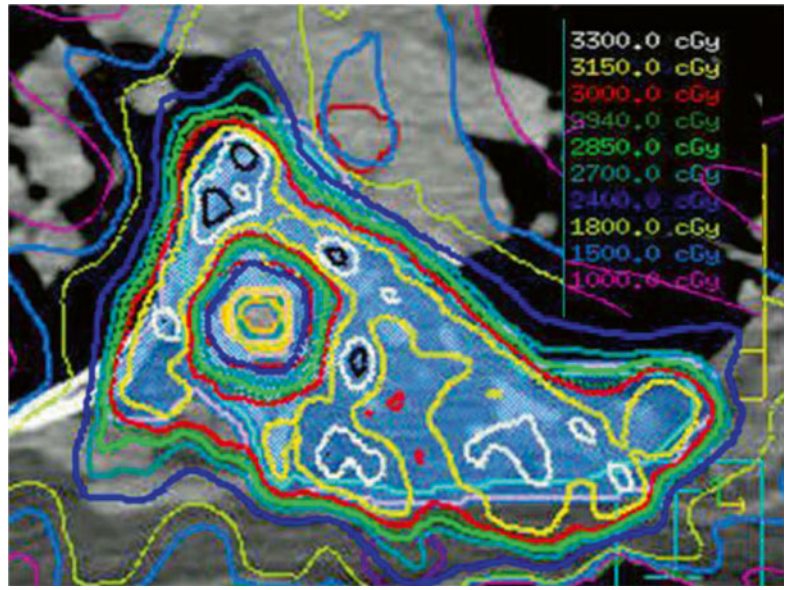

Fig. 3.11 A patient with a lung cancer metastasis involving T9 and significant paraspinal disease extension treated with 30 Gy in 4 fractions. The conformality of the isodose lines is clearly evident with sparing of the central spinal cord and representative isodose lines shown

(Sahgal et al. 2012a). With respect to metastatic disease, this definition reflects the paradigm shift in treatment philosophy such that "locally curative doses" as opposed to "locally palliative doses" are delivered. The current spine SBRT literature suggests complete pain relief rates of ~50 % and local control rates that range from 70 to 100 % (Sahgal et al. 2011a; Nguyen et al. 2011; Wang et al. 2012). A randomized trial is underway comparing 8 Gy in 1 fraction delivered conventionally to 16–18 Gy delivered as SBRT, and the primary endpoint is pain relief (RTOG 0631). There are several reviews that detail the current state of the literature with respect to the application of spine SBRT to metastases that are radiation naive, previously radiated and progressed requiring salvage, and in the postoperative patient (Sahgal et al. 2011a; Masucci et al. 2011). The field is growing rapidly, and Fig. 3.11 illustrates a typical spine SBRT distribution.

With respect to intramedullary metastases, these tumors are exceedingly rare (less than 5 % of all spinal metastases) and typically these patients are irradiated (Sung et al. 2013). There is potential for surgical excision; however, surgery tends to be high risk with respect to complications. A recent analysis of eight cases within a single institution over a 20-year history, and a review of the literature totaling 293 cases, was reported by Sung et al. (2013) They observed that the most common primary cancers resulting in intramedullary metastases were lung and breast cancers, most patients presented with neurologic deficits (weakness in 88 %) and pain, and the median survival was on the order of 4 months.

Some groups have been applying spine SBRT to these tumors with the aim to optimize local control; however, the issue is spinal cord tolerance and the balance of treating the lesion effectively while not overdosing the normal spinal cord tissue. One of the largest series is from Stanford who recently reported on nine patients with 11 intramedullary metastases (Veeravagu et al. 2012). The median survival was 4 months and 4 days (1.1–13 months) and the total dose varied from 14 to 27 Gy delivered over 1–5 fractions. With such a small number of patients, limited follow-up and poor survival conclusions cannot be drawn. Although they reported no complications despite these potentially prohibitive doses within the spinal cord, separate reports from this group have reported radiation myelopathy (Daly et al. 2011a, b). A detailed discussion on spinal cord tolerance and radiation myelopathy is the focus of the subsequent sections.

3.6 Radiation Myelopathy and Spinal Cord Tolerance

Permanent myelopathy is one of the most devastating late complications of radiotherapy. Signs and symptoms can manifest in various combinations of motor and sensory deficits depending on the anatomic level of cord injury. Initial signs and symptoms may be nonspecific and often include a diminished sense of proprioception and/or temperature sensation, minor motor weakness, and clumsiness. Changes in gait, incontinence, Brown-Sequard syndrome, hyperreflexia, plegia, paresis, spasticity, and the Babinski sign are examples of more characteristic symptoms and signs that develop as the injury progresses (Sahgal et al. 2011b). Radiation myelopathy is a diagnosis of exclusion and based on neurological symptoms and signs of myelopathy that are consistent with the segment of cord irradiated and a consistent clinical course. Evidence of neoplastic disease involving the spinal cord or central nervous system must be excluded.

The diagnosis of radiation myelopathy is typically supplemented by certain signal changes within the cord on MRI. Typically within the irradiated segment, low or normal signal intensity on T1-weighted images, high signals on T2-weighted images, and focal to diffuse contrast enhancement in the irradiated segment of the cord indicating necrosis are observed (Wang et al. 1995; Alfonso et al. 1997). Histopathologic descriptions of human myelopathy cases have described lesions that involved only white matter parenchyma with minor vascular changes, lesions that were mainly vascular, and lesions that demonstrated both white matter and vascular damage (Schultheiss et al. 1988).

3.6.1 Human Clinical Data for Radiation Myelopathy and Guidelines for Safe Practice

Much of what is known about human spinal cord tolerance is based on myelopathy data following conventionally fractionated radiotherapy and techniques. Here, conventional fractionation refers to fraction sizes ≤5 Gy. Due to the heterogeneity in the dose-fractionation schemes, total doses are equated using the linear quadratic (LQ) model. The biologically effective dose (BED) is based on the LQ model and calculated according to the formula, $BED = nd(1 + d/\alpha/\beta)$, where d is the dose per fraction, n is the number of fractions, and α/β is a value describing the fractionation radiosensitivity of the tissue (Sahgal et al. 2012b, 2010, 2013). The BED can then be simplified to an equivalent total dose delivered in 2 Gy per day fraction sizes using the EQD2 derivation (Bentzen et al. 2012). An α/β of 2 Gy is widely used for neural tissue in clinical practice. When equated to 2 Gy fraction sizes and using an α/β of 2 Gy, the EQD2 is simply calculated by dividing the BED by 2. This calculation has also been described as a normalized BED (nBED) (Sahgal et al. 2010, 2012b, 2013).

The LQ model provides a satisfactory description of the dose-fractionation response of the cord when the dose per fraction is under ~14 Gy (Brenner 2008); however, its use in higher-dose-per-fraction radiation >15 Gy has been questioned (Park et al. 2008). At the present time, it represents the most accepted model in clinical use and the advantage of the BED calculation is the lack of assumptions in its derivation. In the following sections all BED values will be based on an α/β of 2.

3.6.1.1 Spinal Cord Tolerance After Conventional Radiation (≤5 Gy/Fraction) in Radiation-Naive Patients

A 5 % risk of myelopathy at 5 years posttreatment with 50 Gy in 25 fractions was largely based on expert opinions as summarized by Emami et al. (1991). When the different dose-fractionation schemes that have caused myelopathy are calculated, Sahgal, Wong, and van der Kogel observed that if the EQD2 is under 50 $Gy_{2/2}$, the risk of myelopathy is negligible (Sahgal et al. 2011b). Within a range of 50–60 $Gy_{2/2}$, there might be a small risk of radiation myelopathy (Sahgal et al. 2011b). Therefore, an EQD2 up to 60 $Gy_{2/2}$ (BED = 120 Gy_2) given conventional fractionation delivered with 1.8–2.0 Gy/day fraction sizes using

modern CT-based planning is acceptable depending on the clinical context (Sahgal et al. 2011b). Importantly, their work does not apply to altered fractionation schemes (hyperfractionated or accelerated delivery) as the radiobiology is completely distinct.

3.6.1.2 Re-irradiation Spinal Cord Tolerance Following Prior Conventional Radiation (<5 Gy/Fraction)

Compared to a single course of radiation, there is even less data with respect to re-treatment tolerance of the human spinal cord (Sahgal et al. 2011b). The report by Wong et al. represents the largest series describing re-irradiation myelopathy with conventionally fractionated radiotherapy (Wong et al. 1994). The total BED of the spinal cord in the 11 cases ranged from 129 to 170 Gy_2 (EQD2 ranging from 64 to 85 $Gy_{2/2}$). Therefore, one could propose a cumulative BED up to 120 Gy_2 as safe, and this fits well considering in the unirradiated patient that 60 $Gy_{2/2}$ represents a dose resulting in a small risk of radiation myelopathy (Sahgal et al. 2011b; Schultheiss et al. 1995).

The analysis of re-treatment cord tolerance is more complex than just the total EQD2, as each course of radiation has its own risk of myelopathy. We still do not know how to model the degree of repair following radiation to the spinal cord, as it is assumed that some proportion of the dose is remembered by the tissue and this impacts the subsequent dose deliverable. Nieder et al. made a major contribution to the literature in this regard and our understanding of re-treatment cord tolerance in their report (Nieder et al. 2005). They reanalyzed the Wong cases and reviewed the published literature to gain control cases. They were able to suggest that a cumulative BED of 135.5 Gy_2 or less could be safe if neither course of radiation exceeds a BED of 98 Gy_2 and the time interval between courses is no shorter than 6 months (Nieder et al. 2005). One has to note that the actual dosimetry of these controls was not reviewed and verified.

3.6.1.3 Spinal Cord Tolerance After Hypofractionated Radiation (≥5 Gy/Fraction) with No Prior Radiation

Sahgal et al. recently reported a detailed dosimetric analysis of nine cases of radiation myelopathy following spine SBRT in radiation-naive patients. These data are unique in that all DVH data were centrally reviewed and all treatments delivered using a unit that delivers the radiation with the extreme precision mandated for SBRT. These cases were compared to 66 controls as a multi-institutional collaboration (Sahgal et al. 2013). All DVH data were reviewed for each case and dose to the thecal sac analyzed. They observed that the most significant predictor of radiation myelopathy was the point maximum dose to the thecal sac. Based on a logistic regression model, they were able to derive probabilities of radiation myelopathy specific to spine SBRT. The data suggested that an EQD2 up to 45 $Gy_{2/2}$ maintains the risk to ≤5 %. This translates practically to 12.4 Gy in a single fraction, 17 Gy in 2 fractions, 20 Gy in 3 fractions, 23 Gy in four fractions, and 25 Gy in 5 fractions again to the thecal sac point maximum volume.

3.6.1.4 Spinal Cord Tolerance After Hypofractionated Radiation (≥5 Gy/Fraction) with Prior Radiation and Recommendations for Re-treatment

Re-treatment with high-dose-per-fraction radiation using SBRT is an emerging practice that is likely to become standard, as it allows the delivery of a second radical course of radiation to the tumor while sparing the spinal cord (Masucci et al. 2011; Sahgal et al. 2009). Sahgal et al. reported a detailed dosimetric analysis on five cases of re-irradiation myelopathy, and the cumulative EQD2 ranged from 72 to 153 $Gy_{2/2}$ (Sahgal et al. 2012b). By comparing the DVH data to a group of controls from the University of California San Francisco, they were able to generate the following guidelines for safe practice:

(1) the cumulative thecal sac point maximum EQD2 should not exceed 70 $Gy_{2/2}$, (2) the SBRT re-irradiation thecal sac point maximum EQD2 should not exceed 25 $Gy_{2/2}$, (3) the ratio of the SBRT thecal sac point maximum dose to the total EQD2 should not exceed 0.5, and (4) a minimum time interval of 5 months between courses.

Conclusion

Spinal cord tumors are rare and their management represents a major challenge for spine surgeons, neurosurgeons, and radiation oncologists. The management decisions are largely based on clinical experience, and the few published data consist mainly of single institution retrospective reviews. Therefore, tumor board discussions are of great importance with all disciplines participating in the care of these patients engaged. This chapter provides the basics as to spinal cord anatomy, spinal cord histology, management of the more common tumors, and spinal cord tolerance. Although high-dose radiation using SBRT is rapidly emerging in clinical practice, its role is predominantly in the management of vertebral metastases and not primary spinal cord tumors.

References

Alfonso ER, De Gregorio MA, Mateo P, Esco R, Bascon N, Morales F et al (1997) Radiation myelopathy in over-irradiated patients: MR imaging findings. Eur Radiol 7(3):400–404

Bagley CA, Wilson S, Kothbauer KF, Bookland MJ, Epstein F, Jallo GI (2009) Long term outcomes following surgical resection of myxopapillary ependymomas. Neurosurg Rev 32(3):321–334; discussion 34. Epub 2009/02/18

Barton VN, Donson AM, Kleinschmidt-DeMasters BK, Birks DK, Handler MH, Foreman NK (2010) Unique molecular characteristics of pediatric myxopapillary ependymoma. Brain Pathol 20(3):560–570. Epub 2009/10/02

Bentzen SM, Dörr W, Gahbauer R, Howell RW, Joiner MC, Jones B et al (2012) Bioeffect modeling and equieffective dose concepts in radiation oncology – terminology, quantities and units. Radiother Oncol 105(2):266–268. Epub 2012/11/20

Bhatnagar AK, Gerszten PC, Ozhasaglu C, Vogel WJ, Kalnicki S, Welch WC et al (2005) CyberKnife frameless radiosurgery for the treatment of extracranial benign tumors. Technol Cancer Res Treat 4(5):571–576

Brenner DJ (2008) The linear-quadratic model is an appropriate methodology for determining isoeffective doses at large doses per fraction. Semin Radiat Oncol 18(4):234–239

Chamberlain MC, Tredway TL (2011) Adult primary intradural spinal cord tumors: a review. Curr Neurol Neurosci Rep 11(3):320–328. Epub 2011/02/18

Chao ST, Kobayashi T, Benzel E, Reddy CA, Stevens GH, Prayson RA et al (2011) The role of adjuvant radiation therapy in the treatment of spinal myxopapillary ependymomas. J Neurosurg Spine 14(1):59–64. Epub 2010/12/15

Chow E, Harris K, Fan G, Tsao M, Sze WM (2007) Palliative radiotherapy trials for bone metastases: a systematic review. J Clin Oncol 25(11):1423–1436

Cohen-Gadol AA, Zikel OM, Koch CA, Scheithauer BW, Krauss WE (2003) Spinal meningiomas in patients younger than 50 years of age: a 21-year experience. J Neurosurg 98(3 Suppl):258–263. Epub 2003/04/15

Daly ME, Choi CY, Gibbs IC, Adler JR Jr, Chang SD, Lieberson RE et al (2011a) Tolerance of the spinal cord to stereotactic radiosurgery: insights from hemangioblastomas. Int J Radiat Oncol Biol Phys 80(1):213–220. Epub 2011/04/13

Daly ME, Luxton G, Choi CY, Gibbs IC, Chang SD, Adler JR et al (2011b) Normal tissue complication probability estimation by the Lyman-Kutcher-Burman method does not accurately predict spinal cord tolerance to stereotactic radiosurgery. Int J Radiat Oncol Biol Phys 82(5):2025–2032. Epub 2011/05/03

Dolecek TA, Propp JM, Stroup NE, Kruchko C (2012) CBTRUS statistical report: primary brain and central nervous system tumors diagnosed in the United States in 2005–2009. Neuro Oncol 14(Suppl 5):v1–v49. Epub 2012/11/01

Emami B, Lyman J, Brown A, Coia L, Goitein M, Munzenrider JE et al (1991) Tolerance of normal tissue to therapeutic irradiation. Int J Radiat Oncol Biol Phys 21(1):109–122

Foro Arnalot P, Fontanals AV, Galceran JC, Lynd F, Latiesas XS, de Dios NR et al (2008) Randomized clinical trial with two palliative radiotherapy regimens in painful bone metastases: 30 Gy in 10 fractions compared with 8 Gy in single fraction. Radiother Oncol 89(2):150–155

Gray H (1918/2000) In: Lewis WH (ed) Anatomy of the human body. Central nervous system. Lea & Febiger, Philadelphia, 1396 p

Howell DD, James JL, Hartsell WF, Suntharalingam M, Machtay M, Suh JH et al (2013) Single-fraction radiotherapy versus multifraction radiotherapy for palliation of painful vertebral bone metastases-equivalent efficacy, less toxicity, more convenient: a subset

analysis of Radiation Therapy Oncology Group trial 97-14. Cancer 119:888–896
ICRU (1993) Report 50. Prescribing, recording, reporting photon beam therapy. ICRU, Bethesda
Ishkanian A, Laperriere NJ, Xu W, Millar BA, Payne D, Mason W et al (2011) Upfront observation versus radiation for adult pilocytic astrocytoma. Cancer 117(17):4070–4079
Louis DN, Ohgaki H, Wiestler OD, Cavenee WK, Burger PC, Jouvet A et al (2007) The 2007 WHO classification of tumours of the central nervous system. Acta Neuropathol 114(2):97–109. Epub 2007/07/10
Masucci GL, Yu E, Ma L, Chang EL, Letourneau D, Lo S et al (2011) Stereotactic body radiotherapy is an effective treatment in reirradiating spinal metastases: current status and practical considerations for safe practice. Expert Rev Anticancer Ther 11(12):1923–1933. Epub 2011/11/26
Mizumoto M, Harada H, Asakura H, Hashimoto T, Furutani K, Hashii H et al (2011) Radiotherapy for patients with metastases to the spinal column: a review of 603 patients at Shizuoka Cancer Center Hospital. Int J Radiat Oncol Biol Phys 79(1):208–213
Moore K, Dalley A (1999) Clinically oriented anatomy, 4th edn. Williams and Wilkins, Philadelphia, 1164 p
Nakamura M, Tsuji O, Fujiyoshi K, Hosogane N, Watanabe K, Tsuji T et al (2012) Long-term surgical outcomes of spinal meningiomas. Spine (Phila Pa 1976) 37(10):E617–E623. Epub 2011/12/08
Nguyen J, Chow E, Zeng L, Zhang L, Culleton S, Holden L et al (2011) Palliative response and functional interference outcomes using the Brief Pain Inventory for spinal bony metastases treated with conventional radiotherapy. Clin Oncol (R Coll Radiol) 23(7):485–491
Nieder C, Grosu AL, Andratschke NH, Molls M (2005) Proposal of human spinal cord reirradiation dose based on collection of data from 40 patients. Int J Radiat Oncol Biol Phys 61(3):851–855
Park C, Papiez L, Zhang S, Story M, Timmerman RD (2008) Universal survival curve and single fraction equivalent dose: useful tools in understanding potency of ablative radiotherapy. Int J Radiat Oncol Biol Phys 70(3):847–852
Rodrigues GB, Waldron JN, Wong CS, Laperriere NJ (2000) A retrospective analysis of 52 cases of spinal cord glioma managed with radiation therapy. Int J Radiat Oncol Biol Phys 48(3):837–842. Epub 2000/10/06
Sahgal A, Chou D, Ames C, Ma L, Lamborn K, Huang K et al (2007) Image-guided robotic stereotactic body radiotherapy for benign spinal tumors: the university of california san francisco preliminary experience. Technol Cancer Res Treat 6(6):595–604
Sahgal A, Van der Kogel AJ, Wong CS (2008a) Spinal cord radiobiology. In: Ryu S, Gerszten P (eds) Spine radiosurgery. Thieme Medical Publishers Inc, New York
Sahgal A, Larson DA, Chang EL (2008b) Stereotactic body radiosurgery for spinal metastases: a critical review. Int J Radiat Oncol Biol Phys 71(3):652–665
Sahgal A, Ames C, Chou D, Ma L, Huang K, Xu W et al (2009) Stereotactic body radiotherapy is effective salvage therapy for patients with prior radiation of spinal metastases. Int J Radiat Oncol Biol Phys 74(3):723–731
Sahgal A, Ma L, Gibbs I, Gerszten PC, Ryu S, Soltys S et al (2010) Spinal cord tolerance for stereotactic body radiotherapy. Int J Radiat Oncol Biol Phys 77(2):548–553
Sahgal A, Bilsky M, Chang EL, Ma L, Yamada Y, Rhines LD et al (2011a) Stereotactic body radiotherapy for spinal metastases: current status, with a focus on its application in the postoperative patient. J Neurosurg Spine 14(2):151–166
Sahgal A, Wong CS, Van der Kogel AJ (2011b) Spinal cord. In: Shrieve D, Loeffler JS (eds) Human radiation injury. Lippincott Williams & Wilkins, Philadelphia, pp 225–235
Sahgal A, Roberge D, Schellenberg D, Purdie TG, Swaminath A, Pantarotto J et al (2012a) The Canadian Association of Radiation Oncology scope of practice guidelines for lung, liver and spine stereotactic body radiotherapy. Clin Oncol (R Coll Radiol) 24(9):629–639. Epub 2012/05/29
Sahgal A, Ma L, Weinberg V, Gibbs IC, Chao S, Chang UK et al (2012b) Reirradiation human spinal cord tolerance for stereotactic body radiotherapy. Int J Radiat Oncol Biol Phys 82(1):107–116
Sahgal A, Weinberg V, Ma L, Chang E, Chao S, Muacevic A et al (2013) Probabilities of radiation myelopathy specific to stereotactic body radiation therapy to guide safe practice. Int J Radiat Oncol Biol Phys 85:341–347
Sansur CA, Pouratian N, Dumont AS, Schiff D, Shaffrey CI, Shaffrey ME (2007) Part II: spinal-cord neoplasms–primary tumours of the bony spine and adjacent soft tissues. Lancet Oncol 8(2):137–147. Epub 2007/02/03
Schultheiss TE, Stephens LC, Maor MH (1988) Analysis of the histopathology of radiation myelopathy. Int J Radiat Oncol Biol Phys 14(1):27–32
Schultheiss TE, Kun LE, Ang KK, Stephens LC (1995) Radiation response of the central nervous system. Int J Radiat Oncol Biol Phys 31(5):1093–1112
Sung WS, Sung MJ, Chan JH, Manion B, Song J, Dubey A et al (2013) Intramedullary spinal cord metastases: a 20-year institutional experience with a comprehensive literature review. World Neurosurg 79:576–584
Traul DE, Shaffrey ME, Schiff D (2007) Part I: spinal-cord neoplasms-intradural neoplasms. Lancet Oncol 8(1):35–45. Epub 2007/01/02
Veeravagu A, Lieberson RE, Mener A, Chen YR, Soltys SG, Gibbs IC et al (2012) CyberKnife stereotactic radiosurgery for the treatment of intramedullary spinal cord metastases. J Clin Neurosci 19(9):1273–1277. Epub 2012/07/07
Waldron JN, Laperriere NJ, Jaakkimainen L, Simpson WJ, Payne D, Milosevic M et al (1993) Spinal cord ependymomas: a retrospective analysis of 59 cases. Int

J Radiat Oncol Biol Phys 27(2):223–229. Epub 1993/09/30

Wang PY, Shen WC, Jan JS (1995) Serial MRI changes in radiation myelopathy. Neuroradiology 37(5):374–377

Wang XS, Rhines LD, Shiu AS, Yang JN, Selek U, Gning I et al (2012) Stereotactic body radiation therapy for management of spinal metastases in patients without spinal cord compression: a phase 1-2 trial. Lancet Oncol 13(4):395–402. Epub 2012/01/31

Weiss S, Dunne C, Hewson J, Wohl C, Wheatley M, Peterson AC et al (1996) Multipotent CNS stem cells are present in the adult mammalian spinal cord and ventricular neuroaxis. J Neurosci 16(23): 7599–7609

Wong CS, Van Dyk J, Milosevic M, Laperriere NJ (1994) Radiation myelopathy following single courses of radiotherapy and retreatment. Int J Radiat Oncol Biol Phys 30(3):575–581

Head and Neck Cancer

4

Jeffrey M. Vainshtein and Avraham Eisbruch

Contents

J.M. Vainshtein, MD (✉)
Department of Radiation Oncology, Winship Cancer Institute of Emory University Atlanta, GA, USA
e-mail: Jeffrey.Vainshtein@emory.edu

A. Eisbruch, MD
Department of Radiation Oncology, University of Michigan Health System, Ann Arbor, MI, USA
e-mail: eisbruch@umich.edu

Abbreviations

CN	Cranial nerve
CT	Computed tomography
CTV	Clinical target volume
FDG	18-Fluorodeoxyglucose
Fmiso	Fluoromisonidazole
GTV	Gross tumor volume
HNC	Head and neck cancer
IMRT	Intensity-modulated radiation therapy
MRI	Magnetic resonance imaging
OAR	Organ at risk
PET	Positron emission tomography
PTV	Planning target volume
RP	Retropharyngeal
RT	Radiotherapy

4.1 Introduction

The ability of intensity-modulated radiotherapy (IMRT) to deliver highly conformal radiation doses to the treatment targets while limiting the dose to non-target tissues and organs at risk (OARs) has allowed for significant improvements in the therapeutic index of head and neck radiotherapy (RT) in recent years (Dirix and Nuyts 2010; Feng and Eisbruch 2007; Wu et al. 2000; Vergeer et al. 2009). Sparing portions of the parotid and submandibular glands, oral cavity, mandible, and pharyngeal constrictors musculature with IMRT have produced significant

A.-L. Grosu, C. Nieder (eds.), *Target Volume Definition in Radiation Oncology*,
DOI 10.1007/978-3-662-45934-8_4, © Springer-Verlag Berlin Heidelberg 2015

improvements in patients' quality of life that were previously unachievable with conventional or 3D conformal radiotherapy (Eisbruch et al. 2001, 2004b; Lin et al. 2003). Achieving the ideal balance between target coverage and OAR avoidance requires both proper identification of the targets and structures at hand as well as careful consideration of dosimetric compromises between them in order to optimize treatment outcomes for the patient. Inadequate target volume delineation poses the risk of marginal tumor recurrences in both the primary site and regional lymphatics, while failure to appropriately reduce dose to avoidable normal structures can result in undue treatment toxicity and a detrimental impact on patient quality of life. This decision balance is of particular importance in radiotherapy for head and neck cancer (HNC), in which interobserver differences in target selection and definition, rather than deficiencies in physical target dose coverage or dose uncertainties due to setup errors, are a common source of variability in treatment delivery (Hong et al. 2012). A detailed understanding of the natural history and patterns of spread of head and neck cancer, as well as of the data from clinical studies of IMRT treatment outcomes, can address many of the risk/benefit issues. In this chapter, we review target delineation for the gross tumor volumes (GTVs) and clinical target volumes (CTVs), as well as identification and avoidance of critical OARs that often lie within or adjacent to target volumes, for the purposes of IMRT planning for HNC.

4.2 Treatment of the Primary Tumor

4.2.1 Delineating the Primary Gross Tumor Volume

As the GTV defines the known gross tumor which must be eradicated in order for cure, accurate GTV delineation and dose delivery to the corresponding planning target volume (PTV) are the highest priority step in IMRT planning for HNC. This is doubly important when one considers the implications of a significant overestimation of the GTV by adjacent areas of inflammation or imaging artifacts, which results in inclusion of uninvolved normal tissue within the highest dose target. Imaging studies and physical examination form the basis for the definition of the primary tumor GTV. Contrast-enhanced computer tomography (CT) provides the greatest imaging accuracy for most head and neck tumors. However, for GTVs near the base of the skull, magnetic resonance imaging (MRI) is superior to CT for detection of tumor involvement of the parapharyngeal and retropharyngeal spaces, skull base foramina, cranial nerves, and bone marrow (i.e., of the clivus) in cases of nasopharyngeal carcinoma, neoplasms of the paranasal sinuses, and esthesioneuroblastoma (Abdel Khalek Abdel Razek and King 2012; Lloyd et al. 2000; Ng et al. 1997; Som 1997). MRI with fat-saturated, contrast-enhanced T1-weighted images also provides superior sensitivity for detection of perineural spread to the skull base in cases of locally advanced cutaneous squamous cell carcinoma and malignant salivary gland tumors, such as adenoid cystic carcinoma or high-grade acinic cell carcinoma (Gandhi et al. 2011; Hanna et al. 2007; Nemzek et al. 1998). The improved detection of tumor extension by MRI in these settings has been shown to improve interobserver variability in GTV definition, which may thereby minimize tumor underdosing and reduce the risk of marginal recurrence (Chung et al. 2004; Hsu et al. 2004; Som 1997; Emami et al. 2003).

The use of 18-fluorodeoxyglucose (FDG) positron emission tomography (PET) for GTV definition has been extensively investigated in recent years (Ahn and Garg 2008; Zaidi et al. 2009). A number of studies have reported that the use of PET in addition to CT in target delineation results in smaller GTVs, reduces interobserver variability in GTV definition, and produces GTVs that correlate more closely with pathological findings (Ashamalla et al. 2007; Daisne et al. 2004; Geets et al. 2006; Guido et al. 2009; Murakami et al. 2008). Others, however, have shown contrary findings, such as larger GTVs when based upon PET imaging, and worse interobserver correlation between PET-based GTVs compared to those from CT and underestimation of the

mucosal tumor extension by PET when compared with a surgical pathology gold standard (Burri et al. 2008; Daisne et al. 2004; Riegel et al. 2006; Paulino et al. 2005). While some of these conflicting findings may be attributed to the impact of variable standardized update value threshold levels on tumor definition, the larger glaring deficiency in many studies is the lack of physical examination information to aid the observer in defining mucosal tumor extension (Burri et al. 2008; Daisne et al. 2004; Greco et al. 2008; Thiagarajan et al. 2012). Daisne et al., for example, demonstrated that while GTVs delineated with PET were smaller than those delineated with CT or MRI, the GTVs from all three imaging modalities are significantly overestimated than the actual pathological tumor size in nine larynx cancer patients who underwent total laryngectomy (Daisne et al. 2004). More importantly, despite the overestimation of the total tumor volume, each imaging modality actually underestimated superficial mucosal disease extension into the contralateral larynx, subglottis, and extralaryngeal tissues, with 10, 9, and 13 % of gross tumor identified in the pathological specimen not included in the GTVs delineated from CT, MRI, and PET, respectively. Similar findings on the failure of CT, MRI, and PET to adequately identify superficial mucosal extension in oropharyngeal cancer were demonstrated by investigators from Memorial Sloan Kettering Cancer Center (Thiagarajan et al. 2012). GTVs delineated from PET/CT versus the combination of MRI and CT showed poor correlation to one another and to reference GTVs defined by the treating physician with knowledge of both the physical exam and all of the imaging studies. As in the study by Daisne, mucosal disease was often underestimated in GTVs delineated based solely upon imaging study findings, highlighting the limits in spatial resolution of current imaging modalities underscoring the indispensable and essential role of clinical examination for accurate target definition in HNC.

The subsites of the oropharynx provide instructive examples of some of the advantages of physical examination over imaging in most accurately delineating the extent of tumor involvement. In the base of tongue cancer, mucosal extension can easily be appreciated by palpation, whereas uncertainties on CT and nonspecific, physiologic FDG-PET uptake in the non-involved base of the tongue may hamper the extent to which these imaging studies can supply the information necessary for accurate tumor delineation in treatment planning. Similarly, in locally advanced tonsillar cancer, the presence and extent of palate involvement, whether to the lateral palate or more extensively toward the midline, is more accurately assessed by careful visual inspection and manual palpation than by any imaging modality. Palpation of the glossotonsillar sulcus can similarly reveal tonsillar tumor extension into the lateral base of the tongue more readily than imaging studies. Determining such tumor extension into adjacent at-risk subsites within the oropharynx is crucial to avoiding both GTV overestimation, which may produce excess treatment-related toxicity due to delivery of unnecessary dose to the oral cavity, and underestimation, which increases the risk for local treatment failure. Thus, incorporation of information gleaned from the physical examination in addition to that from imaging studies, whether contrast-enhanced CT, PET/CT, or MRI, is likely to provide the most consistent and accurate GTV definition in clinical practice.

In addition to the lack of spatial resolution that limits the ability of PET/CT to detect superficial tumor extension which may be readily appreciable on physical exam, the mismatch between PET-delineated GTVs and the true extent of the tumor is also affected by the specific methods used for PET image reconstruction algorithm, display windowing, image segmentation, and choice of SUV threshold levels for differentiating tumor from normal tissues (Burri et al. 2008; Ford et al. 2006; Greco et al. 2008; Schinagl et al. 2007). These limitations notwithstanding investigators have validated objective, reproducible, user-independent methods for automatic segmentation of PET images, which may be preferable to subjective techniques in order to standardize functional target volume definition (Daisne et al. 2004; Geets et al. 2007a; Lee 2010). Even with optimized PET segmentation methods, however,

the best approach by which to integrate functional and anatomic imaging remains an area of ongoing debate. At the University of Michigan, we favor a strategy that combines the anatomic findings from clinical examination, CT, and MRI with the PET-defined tumor to yield a composite GTV. While this approach may result in larger GTVs than one that uses FDG-PET automatic segmentation alone to define the GTV, it likely reduces the risk of marginal misses, as supported by studies demonstrating that local recurrences outside the PET-defined GTV but within the CT-defined GTV do infrequently occur (Madani et al. 2007; Soto et al. 2008). Furthermore, whether the use of smaller PET-defined GTVs will translate into reduced toxicity remains highly uncertain, given that the dosimetric differences between such treatment plans are likely to be small after considering the significant impact of prophylactic nodal target irradiation on doses received by non-target OARs such as the salivary glands and pharyngeal constrictors (Geets et al. 2007b; Gregoire et al. 2012). Irrespective of whether FDG-PET is used to define the GTV, incorporation of physical exam findings into imaging-based GTV definition is an essential step in determining the final composite GTV. By expanding the GTV by a small margin, typically 0.5 cm, one will ensure that a very high concentration of tumor cells will receive the full prescribed dose aimed at the gross disease.

The use of IMRT instead of 3D conformal RT has the potential for delivery of nonuniform doses to the GTVs (Boyer et al. 1997). With careful treatment planning and quality assurance, GTV inhomogeneities can be manipulated to deliberately deliver higher "boost" doses to subvolumes of the gross tumor in an effort to improve tumor control, while achieving steeper dose gradients outside the tumor to more effectively spare neighboring tissue (Vineberg et al. 2002). Tome and Fowler postulated that tumor control probability could be significantly improved if a boost could be delivered to a substantial portion of the GTV (60–80 %) with a boost dose ratio of 1.2:1.3 (Tome and Fowler 2000). It must be emphasized that the tolerability of dose escalation in HNC hinges on selective escalation of dose to only a portion of the GTV, as demonstrated by investigators at the Medical College of Virginia who determined the maximum tolerable dose to the entire GTV to be 70.8 Gray (Gy) in 30 fractions, due to severe acute mucosal toxicity encountered at the next dose level of 73.8 Gy (Lauve et al. 2004). The therapeutic ratio of a partial tumor boost may be even further maximized if radioresistant sub-volumes of the GTV at highest risk of recurrence can be identified and focally targeted. "Dose painting," as this approach has been termed, has thus far been investigated most extensively in HNC cancer, using FDG-PET or hypoxia imaging to identify suspected radioresistant sub-volumes for focal boosting (Ling et al. 2000). One phase I dose escalation study at Ghent University Hospital which boosted FDG-PET active sub-volumes of the anatomic CT-based GTV found that 44 % of locoregional relapses occurred within the boosted sub-volume, attesting to both the validity of the underlying hypothesis that these tumor sub-volumes are indeed radioresistant and the limitations of additional RT to overcome this resistance (Madani et al. 2007). The choice of SUV threshold to guide selection of sub-volumes for boosting remains an area of ongoing investigation and has been addressed by some groups using a "dose painting by numbers" IMRT approach, which uses inverse planning to deliver RT doses proportional to the voxel SUV intensity within metabolically active tumor (Bentzen 2005; Geets et al. 2007b). This strategy has also been employed in an adaptive manner by the Ghent group to deliver higher RT doses to presumed radioresistant regions of tumor that remained metabolically active on FDG-PET after part of the treatment course has been delivered (Duprez et al. 2011). Preliminary results demonstrating feasibility and acceptable toxicity at the lower dose level of 80.9 Gy in 32 fractions. At the higher dose level of 85.9 Gy, however, 36 % of patients experienced late mucosal ulceration, highlighting the need for careful sparing of uninvolved mucosa in any dose escalation effort in HNC (Madani et al. 2011).

Similar to FDG-PET, hypoxia imaging has been proposed as a method to identify radioresistant tumor sub-volumes that may serve as rationale

targets for dose escalation (Hendrickson et al. 2011; Rajendran et al. 2006; Rischin et al. 2006) While fluorine-18-labeled fluoromisonidazole (Fmiso) PET has been the most commonly used hypoxia imaging modality in studies that have demonstrated correlations between tumor hypoxia and prognosis, the lack of temporal and spatial stability of Fmiso-PET both prior to and during therapy poses a major obstacle to the use of hypoxia imaging use for identification of tumor sub-volumes for boosting with IMRT (Lin et al. 2008; Nehmeh et al. 2008; Thorwarth et al. 2007). Tumor hypoperfusion, on the other hand, is a surrogate measure of hypoxia that is both temporally and spatially stable on dynamic contrast-enhanced CT and MRI and has been shown to correlate with treatment outcome (Cao et al. 2008; Chawla et al. 2011; Shukla-Dave et al. 2012). Importantly, persistent hypoperfusion with tumor sub-volumes after initiation of chemoradiation appears to predict the sites of local failure, suggesting these sub-volumes as feasible targets for adaptive dose escalation during therapy (Cao et al. 2008; Wang et al. 2012a). Efforts are underway to determine whether adaptively boosting hypoperfused sub-volumes can yield an important breakthrough in overcoming tumor radioresistance in HNC.

4.2.2 Delineating the Clinical Target Volume Around the Primary GTV

Defining the primary tumor CTV for subclinical target doses coverage is an area that has been largely unexplored in the literature. Proposed general guidelines for major head and neck sites emphasize that the primary tumor CTV should encompass those tissues at risk for harboring microscopic disease, as determined by the common pathways of spread of primary tumor into and along the surrounding anatomic compartments (Eisbruch et al. 2002). Lesions of the tonsillar fossa, for example, may spread anteriorly to involve the glossotonsillar sulcus and base of the tongue; superiorly to the soft palate, nasopharynx, and base of the skull; laterally through the pharyngeal constrictor to invade the parapharyngeal space; inferiorly to the lateral pharyngeal wall and supraglottic larynx; and posteriorly to the posterior pharyngeal wall. While clearly not all of these at-risk sites need to be included in the primary CTV for every early tonsil carcinoma, detailed attention to involvement of points of access to adjacent anatomical sites by the primary tumor on clinical examination and imaging is crucial to determining adequate CTV coverage in order to prevent marginal recurrence. Additionally, measures of tumor aggressiveness such as size, stage, differentiation, and morphology (ulcerative or exophytic, infiltrative or pushing front) are used to determine how much tissue beyond the GTV is appropriate for inclusion in the CTV. The attention to these details is particularly important when using IMRT, in which steep dose gradients created greater susceptibility to marginal misses when using 3D conformal radiotherapy. Additionally, knowledge of the barriers to spread of tumor, such as the vertebral bodies, mandibular cortex, and muscular fascia, and avoiding inclusion of tissues beyond these barriers in the primary CTV is essential in order to limit excess toxicity from treatment of those tissues at risk for microscopic tumor involvement.

Guidelines for delineating the primary tumor CTV as previously detailed for specific sites are summarized below (Eisbruch et al. 2002). The CTV for tumors involving more than one primary site or subsite should include the structures at risk for each involved site.

4.2.2.1 Oral Cavity

- *Floor of the Mouth*: The laterality of the primary tumor determines the extent of CTV across midline. However, the bilateral genioglossus and geniohyoid muscles should be included in all cases, whereas the sublingual and submandibular glands should be included ipsilaterally for well-lateralized tumors and bilaterally for midline tumors. The adjacent alveolar ridge, mandible, and root of the tongue should additionally be included.
- *Oral Tongue*: Generous portion of the intrinsic and extrinsic muscles of the oral tongue, base of the tongue, floor of the mouth, ipsilateral

glossotonsillar sulcus, and ipsilateral anterior tonsillar pillar should be included in the CTV.
- *Buccal Mucosa*: A generous CTV should be delineated due to the lack of anatomical barriers to submucosal tumor spread, extending to include the maxillary gingival-buccal sulcus and infratemporal fossa superiorly, the mandibular gingival-buccal sulcus and submandibular gland inferiorly, immediately lateral to the labial commissure anteriorly, and the retromolar trigone posteriorly.

4.2.2.2 Oropharynx

- *Tonsillar Cancer*: The adjacent buccal mucosa laterally, soft palate medially, and glossotonsillar sulcus/base of the tongue anteriorly are included in the CTV in all cases. For advanced cases, the CTV should also include the ipsilateral parapharyngeal space, pterygoid musculature, and inferior portion of the nasopharynx. In cases of posterior tonsillar pillar involvement, the pharyngoepiglottic fold and adjacent portions of the posterior pharyngeal wall are included.
- *Base of the Tongue*: The CTV should include the entire base of the tongue, vallecula, and significant portions of the adjacent oral tongue (at least 2 cm beyond the GTV). In cases of involvement of the vallecula, the suprahyoid epiglottic larynx and pre-epiglottic fat space should additionally be included.
- *Soft Palate*: The entire soft palate, adjacent superior tonsillar pillars and fossas, and the pterygopalatine fossa should be included in the CTV. For advanced primary tumors, the CTV should additionally include the adjacent nasopharynx and pterygoid musculature. For advanced cases, a skull base protocol MRI including fat-saturated contrast-enhanced T1-weighted sequences should be obtained to evaluate for involvement of the pterygopalatine fossa and skull base foramina. If the pterygopalatine fossa is involved, both the skull base and ipsilateral sphenoid sinus should be included in the CTV. For minor salivary gland cancers of the soft palate with perineural invasion (i.e., adenoid cystic carcinoma, high-grade acinic cell carcinoma), the CTV should include the course of the greater palatine nerve and more proximal maxillary branch of the trigeminal nerve (V2) to the Gasserian (aka trigeminal, semilunar) ganglion in Meckel's cave within the cavernous sinus.
- *Pharyngeal Wall*: The lymphatic channels within the submucosa of the pharyngeal wall provide a conduit for longitudinal spread and skip lesions. The CTV therefore should include the posterior pharyngeal wall extending superiorly through the nasopharynx and inferiorly through the hypopharynx, as well as the parapharyngeal space laterally.

4.2.2.3 Larynx

The CTV for advanced cancers of the supraglottic, glottic, and subglottic larynx should include the entire larynx (including all three of these subsites), the vallecula, pre-epiglottic space, paraglottic spaces, entire thyroid cartilage, and pyriform sinus. For the paraglottic space and pyriform sinus, the decision to include the structure ipsilaterally or bilaterally is based upon laterality and extension of the primary tumor.

4.2.2.4 Hypopharynx

As in the posterior pharyngeal wall in the oropharynx, longitudinal submucosal spread and skip lesions are common, thus necessitating generous extension of the CTV to include the pharyngeal wall and parapharyngeal space superiorly through the nasopharynx and inferiorly to 2 cm below the cricoid cartilage. For pyriform sinus and lateral pharyngeal wall cancers, the ipsilateral hemilarynx is additionally included in the CTV. The ipsilateral lobe of the thyroid lobe is also included in the CTV for pyriform sinus cancers with involvement of the apex or lateral extension.

4.2.2.5 Paranasal Sinuses

The CTV is dependent on the involved sinus and tumor extent, which is best characterized on MRI. For maxillary sinus tumors, the CTV includes portions of the ipsilateral palate, alveolar ridge, nasal cavity, nasopharynx, and medial orbit. For ethmoid sinus cancers, the medial orbit, cribriform plate, and a rim of frontal lobe are

included. The CTV for both ethmoid and maxillary sinus cancers also includes the pterygopalatine fossa and infratemporal fossa, which are frequently at risk for subclinical disease. Superior lesions require extension of the CTV to include the sphenoid sinus and foramen rotundum to cover potential involvement of V2. If MRI suggests V2 involvement, the CTV should be extended to include Meckel's cave within the cavernous sinus. Lesions of the upper nasal cavity also require inclusion of the cribriform plate and a rim of the frontal lobe in the CTV. For cases with intracranial extension, the anterior cranial fossa is also included.

4.2.2.6 Nasopharynx

The CTV should encompass the base of the skull, pterygoid plates, pterygopalatine fossa, and superior parapharyngeal space extending laterally to include the pterygoid muscles and deep lobe of the parotid gland. The pterygoid muscles can be excluded only in very small primary tumors. Specific skull base structures that should be included superiorly include the foramen ovale, foramen spinosum, carotid canal, sphenoid sinus, and cavernous sinus. Inferiorly, the CTV should include the parapharyngeal space to approximately the level of the mid-tonsil. The retropharyngeal space is outlined as a part of the nodal CTV to cover the retropharyngeal lymph nodes to the level of the hyoid bone, as discussed below. Anteriorly, the CTV includes the posterior third of the maxillary sinuses, the posterior ethmoid sinuses, and the posterior third of the nasal cavity. Posteriorly the clivus should be included, as subclinical involvement is common. MRI is mandatory for the assessment of the skull base and parapharyngeal tumor extension. If the base of the skull involvement is evident, then the hypophysis, optic nerves, and chiasm may be included in the CTV, with dose to these structures limited to 45–55 Gy (at daily fraction size <2 Gy).

4.2.2.7 Major Salivary Glands

For patients with malignant tumors of the parotid and submandibular glands with a propensity for perineural involvement, such as adenoid cystic carcinoma, high-grade acinic cell carcinoma, carcinoma ex-pleomorphic adenoma, and salivary duct carcinoma, fat-saturated contrast-enhanced T1-weighted MRI is essential to establish whether radiographic perineural spread is present prior to definitive therapy. Sensory or motor disturbances in the distribution of the cranial nerve (CN) at risk are additionally highly suggestive of clinical perineural spread, which should prompt inclusion of appropriate CN coverage irrespective of MRI findings. For cancers of the submandibular gland, the mandibular branch of the trigeminal nerve (V3), marginal mandibular branch of the facial nerve (CN VII), and hypoglossal nerve (CN XII) may all be at risk, and evidence of involvement of these nerves necessitates inclusion of the course of each nerve in the CTV to the skull base at the foramen ovale, stylomastoid foramen, or hypoglossal canal, respectively. If the named nerve is grossly involved, the CTV should include the course of the nerve all the way to its ganglion (Garden et al. 1994). For tumors of the parotid gland with a propensity for perineural invasion, the facial nerve is at risk, and thus the CTV should cover the path of the nerve to the stylomastoid foramen superiorly. If CN VII is grossly involved, the CTV should additionally include the portion of the nerve traversing the mastoid air cells posterior to the external acoustic meatus, the cochlea, and the internal auditory meatus. Although salivary gland tumors are managed with surgical resection as the primary therapeutic modality where possible, these guidelines also apply to CTV delineation in the postoperative setting for patients with tumors that are high grade, T3 or T4, recurrent, resected incompletely or with close margins, have perineural or gross nerve invasion, or have lymph node metastases (Chen et al. 2007a, c; Terhaard et al. 2005).

4.3 Treatment of the Neck

4.3.1 Delineating the Gross Tumor Volumes in the Neck

Understanding the regional lymphatics at risk in the neck depends on an accurate evaluation of disease involvement of both the primary site and

the regional lymphatics. As described in the detail above, the extent of the primary GTV should precisely be defined by a combination of physical examination (including visual inspection, manual palpation, and indirect mirror and fiberoptic exam), the surgeon's report of direct endoscopy under anesthesia, and the relevant imaging studies, including contrast-enhanced CT and, where appropriate, FDG-PET and/or MRI. While MRI is not typically necessary to assist in definition of primary tumors in the oropharynx, larynx, and hypopharynx, it is an essential adjunct to CT in tumors near the skull base such as paranasal sinus and nasopharynx cancers, for which MRI is superior for identifying tumor extension into the parapharyngeal and retropharyngeal spaces, skull base foramina, cranial nerves, and bone marrow (i.e., of the clivus) (Abdel Khalek Abdel Razek and King 2012; Ng et al. 1997; Som 1997). While PET/CT may aid in primary tumor target definition when added to CT and MRI, as previously discussed, this modality is of particular benefit in detecting regional lymph node involvement in non-enlarged or borderline-enlarged lymph nodes (Schechter et al. 2001). The impact of this nodal upstaging compared to CT is significant, as the node thought previously to be uninvolved will now receive gross tumor dose rather than a subclinical dose, while the dose to the next echelon lymphatic drainage levels will be accordingly increased from a low-risk to a high-risk subclinical dose. In more extreme cases, lymphatic levels that may not have been deemed to be at risk for subclinical disease based on CT findings would be included as a low-risk CTV if nodal involvement is detected on PET/CT (i.e., inclusion of level VI in the case of level IV involvement). Additionally, PET/CT may be useful in the detection of the primary site in cases of head and neck carcinoma of unknown primary, as well as for diagnosing distant metastatic disease, with significant resultant changes in the treatment plan (Chen et al. 2012).

Based on the experience of imaging sciences and radiation oncology practice, our institution has developed some broad policies regarding the definition of the lymph node GTVs. PET/CT is utilized as an adjunctive study to contrast-enhanced CT simulation scan, and lymph nodes are included in the GTV if they have any of the radiologic criteria shown in Table 4.1. For nodal disease with radiographic extracapsular extension in the muscle, an additional margin of at least 1 cm into the involved muscle should be added to the GTV to account for gross disease that may be poorly visualized radiographically.

Table 4.1 Lymph nodes are included in the GTV if they meet any of the radiologic criteria

1. Diameter >1 cm (or in the case of the jugulodigastric nodes, >1.5 cm)
2. Smaller than 1 cm with spherical rather than ellipsoidal (or "kidney-bean") shape
3. Contain inhomogeneities suggestive of necrotic centers
4. Cluster of three or more borderline nodes (Castelijns and van den Brekel 2002; van den Brekel et al. 1996)
5. FDG-PET positive

4.3.2 Defining the Nodal Levels at Risk in the Neck

Much as the CTV surrounding the primary tumor encompasses tissue deemed to be at risk for microscopic tumor extension, the CTVs in the neck consist of the lymph node levels containing nodes not meeting radiologic criteria for gross involvement that are nonetheless at risk for microscopic involvement. The bulk of modern knowledge on the pattern of lymphatic drainage from each head and neck site is based upon the classic anatomical work by Rouvière, the descriptive report by Lindberg on the prevalence and distribution of clinical neck metastases at presentation, and reports on the incidence and distribution of microscopic pathological lymph node involvement at elective neck dissection by Byers et al., Candela et al., and others (Mukherji et al. 2001; Rouvière 1938; Candela et al. 1990; Lindberg 1972; Byers et al. 1988). Taken together, this body of literature demonstrates that squamous cell carcinomas of the upper aerodigestive tract tend to metastasize to the neck in predictable patterns, with the distribution and likelihood of involvement governed by the

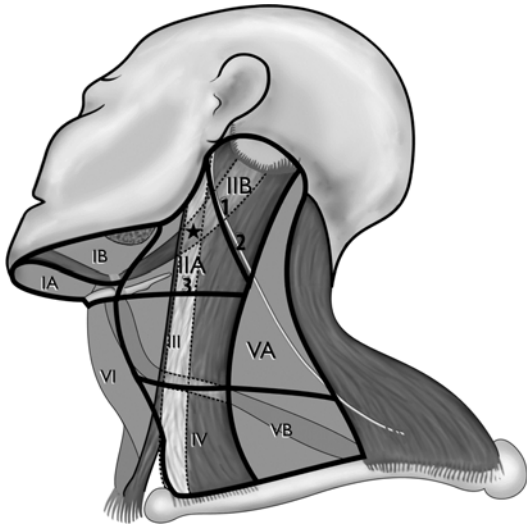

Fig. 4.1 Neck node levels. *1* Posterior belly of the digastric muscle; *2* accessory nerve; *3* jugular vein; *asterisk* jugulodigastric nodes: where jugular vein bisects the posterior belly of the digastric muscle (just below the transverse process of C1)

density and drainage of the lymphatics at each mucosal site, and with increasing risk at each nodal level if the adjoining proximal level is involved.

An anatomical reference standard for classifying neck lymph node regions was devised by surgeons from the Memorial Sloan Kettering Hospital and revised by Robbins et al. and Robbins (Robbins 1998; Robbins et al. 1991; Shah et al. 1981) (Fig. 4.1). This classification defined six neck levels with three sublevel divisions, each with discrete anatomical boundaries that can be readily identified during neck dissection to facilitate standardized reporting of the locations of nodal involvement and the extent of surgical therapy in the neck. A corresponding nodal level classification system based upon landmarks readily identifiable on axial imaging was subsequently proposed by Som et al. (1999). The application of this classification system toward CTV delineation in the neck has been extensively described and has been integrated into multinational cooperative group consensus panel guidelines, summarized in Table 4.2 (Gregoire et al. 2000; Gregoire and Levendag; Nowak et al. 1999; Wijers et al. 1999) and available online at http://www.rtog.org/corelab/contouringatlases/hn.aspx. Gregoire et al. recently published an extensive review of the literature on the risk of metastases to each neck level, with accompanying elective nodal coverage recommendations by primary tumor site (Gregoire et al. 2000). Eisbruch et al. have similarly proposed more detailed guidelines for target selection in the neck (Eisbruch et al. 2002). These publications and the DAHANCA, EORTC, GORTEC, NCIC, and RTOG consensus panel contouring guidelines and atlas are highly recommended for the reader before embarking upon three-dimensional conformal radiation therapy or IMRT for the treatment of head and neck cancer.

In determining whether to include a specific nodal level in the CTV, we typically consider that a 10 % or higher risk of metastatic involvement warrants elective treatment, whereas a less than 10 % risk of microscopic involvement may be inadequate to justify the risk of complications from prophylactic RT. The factors that dictate this risk for each nodal level vary from case to case and depend on primary tumor site, tumor stage, tumor size, thickness or depth of invasion (i.e., 3 mm or more is associated with a high metastatic risk for oral cavity tumors), tumor grade/differentiation, keratinization status, lymphatic vessel invasion in the tumor specimen, and the presence, distribution, and extent of nodal involvement (Eisbruch et al. 2002). For tumors of the major or minor salivary glands, high-grade or large tumors harbor a significant risk of subclinical nodal involvement warranting prophylactic ipsilateral nodal coverage (or bilateral coverage for soft palate tumors), with the notable exception of adenoid cystic carcinoma and acinic cell carcinoma, which infrequently spread to lymph nodes (Armstrong et al. 1992; Chen et al. 2007b).

4.3.3 Specific Clinical Target Volumes in the Neck

In selecting the CTVs for head and neck cancer IMRT, the following nodal levels should be included where appropriate, as described. While these general concepts are broadly useful, specific

Table 4.2 Radiographic anatomical boundaries for lymph node levels in the clinically node negative and surgically unviolated neck

	Cranial	Caudal	Anterior	Posterior	Lateral	Medial
IA *Submental nodes*	Geniohyoid and mylohyoid muscles	Central body of the hyoid bone	Symphysis menti and platysma muscle	Body of the hyoid bone	Medial aspect of the anterior belly of the digastric muscle	N/A (midline nodal region)
IB *Submandibular nodes*	Mylohyoid muscle and cranial aspect of submandibular gland	Central body of the hyoid bone	Symphysis menti and platysma muscle	Posterior aspect of the submandibular gland	Medial aspect of the mandible, platysma muscle, or skin	Lateral aspect of the anterior belly of the digastric muscle
IIA *Upper jugular nodes (anterior)*	Caudal aspect of lateral process of C1[a]	Caudal aspect of the body of the hyoid bone	Posterior aspect of the submandibular gland; anterior aspect of the ICA; posterior aspect of the posterior belly of the digastric muscle	Posterior border of the IJV	Medial aspect of the SCM	Medial aspect of the ICA; paraspinal muscles (levator scapulae and scalenes)
IIB *Upper jugular nodes (posterior)*	Caudal aspect of lateral process of C1[a]	Caudal aspect of the body of the hyoid bone	Posterior border of the IJV	Posterior border of the SCM	Medial aspect of the SCM	Medial aspect of the ICA; paraspinal muscles (levator scapulae and scalenes)
III *Middle jugular nodes*	Caudal aspect of the body of the hyoid bone	Caudal aspect of the cricoid cartilage	Posterolateral aspect of the sternohyoid muscles and anterior aspect of the SCM	Posterior aspect of the SCM	Medial aspect of the SCM	Medial aspect of the internal/common carotid artery; paraspinal muscles (scalenes)
IV *Lower jugular nodes*	Caudal aspect of the cricoid cartilage	2 cm cranial to the sternoclavicular joint	Anteromedial aspect of the SCM	Posterior aspect of the SCM	Medial aspect of the SCM	Medial aspect of the common carotid artery; paraspinal muscles (scalenes)

VA *Posterior triangle (upper)*	Skull base	Caudal aspect of the cricoid cartilage	Posterior aspect of the SCM	Anterior border of the trapezius muscle	Platysma muscle and skin	Paraspinal muscles (levator scapulae, scalenes, splenius capitis)
VB *Posterior triangle/spinal accessory nodes (lower)*	Caudal aspect of the cricoid cartilage	Transverse cervical vessels	Posterior aspect of the SCM	Anterior border of the trapezius muscle	Platysma muscle and skin	Paraspinal muscles (levator scapulae, scalenes, splenius capitis)
VI *Pretracheal and paratracheal nodes*	Caudal aspect of body of the thyroid cartilage (pretracheal nodes) or cricoid cartilage (pretracheal nodes)	Sternal manubrium	Skin and platysma muscle	Posterior aspect of the trachea; anterior aspect of cricoid cartilage	Medial aspect of the internal/common carotid artery	N/A (midline nodal region)
VII *Upper mediastinal nodes*	Sternal manubrium	Innominate vein	Posterior aspect of the sternal manubrium	Tracheoesophageal groove	Lateral aspect of the common carotid artery	N/A (midline nodal region)
RP *Retropharyngeal nodes*	Base of the skull	Caudal aspect of the C2 vertebral body	Fascia underlying the pharyngeal mucosa	Prevertebral muscles (longus colli, longus capitis)	Medial aspect of the internal carotid artery	Midline[b]

Adapted from Gregoire et al. (2000), Gregoire and Levendag (RTOG Atlas), and Som et al. (1999)
ICA internal carotid artery, *IJV* internal jugular vein, *N/A* not applicable, *SCM* sternocleidomastoid muscle
[a]If ipsilateral level II is involved, then the cranial border is the skull base at the retrostyloid space
[b]In elective treatment of the retropharyngeal nodes, only the lateral RP nodes are included in the CTV

approaches for individual tumor sites have been previously described elsewhere in detail (Eisbruch et al. 2002; Million 1994).

4.3.3.1 Level II Nodes

Level II is the most frequent nodal metastatic site for tumors in all mucosal sites. This level can be subdivided into the internal jugular (IIA) and spinal accessory (IIB) subdivisions. In the surgical classification system, the spinal accessory nerve serves as the division between these levels, with level IIA lying anteriorly and IIB posteriorly (Fig. 4.1) (Robbins 1998). Due to the difficulty in discerning the division between these levels on axial imaging, however, the adapted radiographic classification instead defined these nodes relative to the posterior border of the internal jugular vein, which can be readily visualized on a simulation CT scan (Som et al. 1999). By this widely adopted system, level IIA includes those nodes located anteriorly, laterally, or medially to the internal jugular vein as well as those located posteriorly without a fat plane separating them from the jugular vein; level IIB nodes lie posterior to jugular vein with an intervening fat plane, thus approximating a location posterior to the spinal accessory nerve. The important specific nodal stations within level II include the subdigastric (jugulodigastric) node, which is located within level IIA immediately inferior to the crossing of the posterior belly of the digastric muscle past the internal jugular vein, and the more cranially located "junctional" node, aptly named for its location within level IIB at the superior junction of the jugular nodal chain (level II) and spinal accessory nodal chain (level V) (Rouvière 1938). The subdigastric node is the most commonly involved node for both ipsilateral and contralateral nodal metastases from primary tumors of the oropharynx, supraglottic larynx, and hypopharynx, while the more cephalad junctional node is the first echelon node for the nasopharynx and parotid gland, which is commonly involved in cases of nasopharyngeal cancer and is at risk in the case of coexistent metastases to levels II, III, or VA (Million 1994). Therefore, the ipsilateral subdigastric node and level IIA below the transverse process of C1 should be included in the CTV for all N0 patients with cancers arising in most head and neck mucosal sites receiving definitive radiotherapy (with or without chemotherapy), with the notable exception of early stage, node-negative squamous cell carcinomas of the glottic larynx (i.e., T1–2N0). Ipsilateral level IIA superior to the C1 transverse process and level IIB, meanwhile, are included in the CTV in all patients with nasopharynx primary cancers, irrespective of nodal involvement, and in those patients with other primary sites with nodal metastases in the ipsilateral level II. Contralateral level IIA below the C1 transverse process should be included in the elective CTV in all cases of mucosal squamous cell carcinomas originating in sites with bilateral lymphatic drainage (i.e., base of the tongue, soft palate, nasopharynx, supraglottic larynx, hypopharynx) or in any case of N2a or greater nodal involvement with any primary mucosal tumor site (Fig. 4.2). In contrast, contralateral level IIA superior to the C1 transverse process and level IIB can be safely excluded from the CTV in non-nasopharyngeal cancer patients without involvement of the adjacent level II, thus allowing for sparing of the majority of the contralateral parotid gland and a significant preservation of salivary function (Eisbruch et al. 2001; Beetz et al. 2012) (Fig. 4.3).

4.3.3.2 Level III

Level III is included in the CTV when there is a risk of subclinical disease or if level II on the same side of the neck is grossly involved. Designation of level III as a high-risk or low-risk CTV is dependent on whether lymph nodes in this level are grossly involved (as described below).

4.3.3.3 Level IB Nodes

Level IB is treated in all cases with a significant clinical involvement of ipsilateral level II (e.g., oropharyngeal cancer with nodal involvement of level II of >N1) and in primary tumors that drain directly to level IB (i.e., oral tongue, floor of the mouth, anterior tonsillar pillar, retromolar trigone, buccal mucosa), irrespective of clinical nodal involvement (Figs. 4.3 and 4.4). Level IB should additionally be included for oropharyngeal cancers of the tonsil or base of the tongue with a

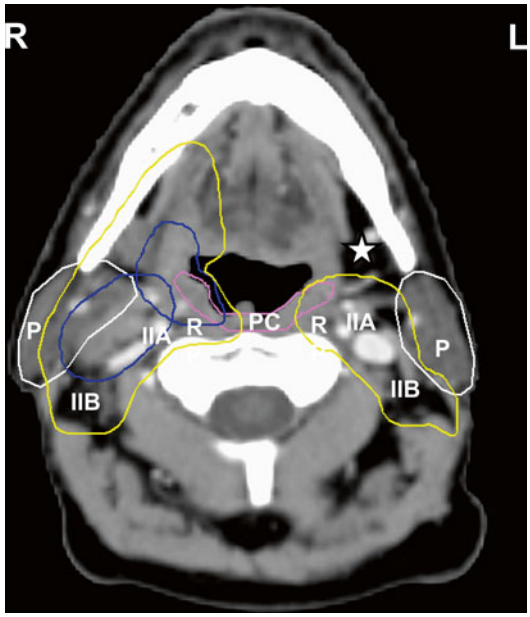

Fig. 4.2 Axial contrast-enhanced CT image of a patient with a right tonsillar T1 N2a M0 squamous cell carcinoma with involvement of the ipsilateral subdigastric node (level *IIA*). The PTV surrounding the gross primary and nodal disease is displayed in *blue*. At this level below the transverse process of C1, the bilateral level *IIA* and *IIB* (II) and the RP nodes are included in the subclinical PTV bilaterally (*yellow*). As demonstrated, right level IB located ipsilateral to the involved node and primary tumor is included in the subclinical PTV (*yellow*), while the contralateral left level IB is excluded (*white asterisk*). Important organs at risk contoured at this level include the tail of the parotid glands (*P*, white contour) and superior pharyngeal constrictor muscle (*PC*, *violet*)

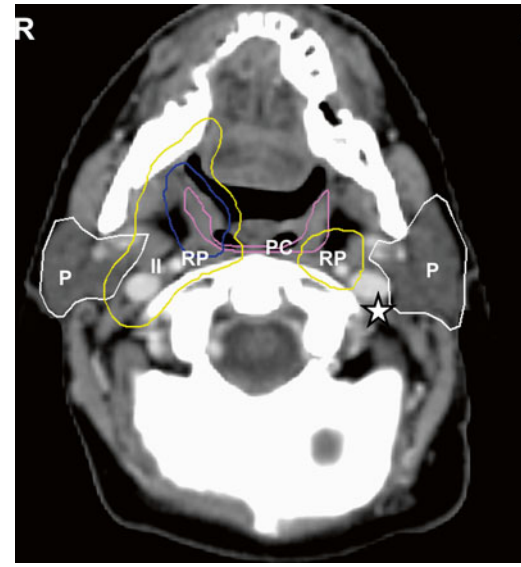

Fig. 4.3 Axial CT image C1 in the same patient as Fig. 4.2 (right tonsillar T1 N2a M0 squamous cell carcinoma). The primary tumor PTV in displayed in *blue*. At this axial level near the base of the skull *superior* to the transverse process of C1, left level *II* (*star*) in the uninvolved contralateral neck is excluded, while right level II (*II*) and the bilateral RP nodes (*RP*) are included in the subclinical PTV (*yellow*). The parotid glands (*P*, *white contour*) and superior pharyngeal constrictor muscle (*PC*, *violet*) are among the important structures to delineate for avoidance

significant anterior extension to the anterior tonsillar pillar or oral tongue, respectively. For well-lateralized primary tumors (i.e., buccal mucosa, retromolar trigone), only the ipsilateral side can be treated, whereas more midline tumors (i.e., floor of the mouth) or those with bilateral lymphatic drainage (i.e., oral tongue for both level IB) require bilateral coverage. Exclusion of level IB from the CTV in cases lacking the above risk factors facilitates partial sparing of the submandibular gland, preserving non-stimulated, mucin-rich submandibular salivary flow and thereby reducing xerostomia (Eisbruch et al. 2001; Little et al. 2012; Murdoch-Kinch et al. 2008).

4.3.3.4 Level IV Nodes

Level IV is treated in all cases of either ipsilateral level II or III involvement and in primary sites that drain directly to level IV, regardless of additional nodal involvement (i.e., tip of the oral tongue, supraglottic larynx, hypopharynx). As is the case for level IB above, midline tumors and those with bilateral lymphatic drainage (i.e., oral tongue, posterior pharyngeal wall) require bilateral level IV coverage.

4.3.3.5 Level V Nodes

Inclusion of level V in the CTV is advised in all cases of a significant (>N1) involvement of levels II–IV on the same side of the neck (Fig. 4.4) as well as in primary tumors of the nasopharynx, which drains directly to level V.

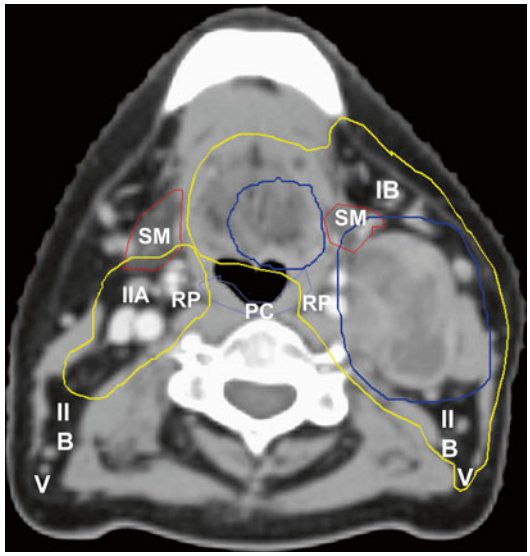

Fig. 4.4 Axial CT image of a patient with a left base of the tongue T1 N2a squamous cell carcinoma. PTVs for the primary tumor and involved left level II node are displayed in *blue*. Level *IB* and *V* on the ipsilateral left side are included in the elective PTV (*yellow*), whereas the contralateral right-sided elective PTV excludes level *IB*, posterior *IIB*, and *V*. The bilateral RP nodes (*RP*) are additionally included bilaterally. The superior pharyngeal constrictor muscles (*PC*, *violet*) and submandibular glands (*SM*, *brown*) are notable OARs at this level

4.3.3.6 Retropharyngeal Nodes

The risk of RP involvement relates strongly to the primary tumor site and to the extent of jugular chain nodal involvement (McLaughlin et al. 1995). As such, the lateral retropharyngeal (RP) nodes are treated *bilaterally* in all cases of nasopharyngeal cancer, tumors that involve the posterior pharyngeal wall, and oropharyngeal and hypopharyngeal cancers with clinical involvement of levels II–IV (Figs. 4.2 and 4.3). At present, our policy is to limit the coverage of the lateral RP nodes to the ipsilateral side only in cases of early lateralized oropharyngeal tumors with N0 or small-volume N1 disease. Recent preliminary evidence, however, suggests that the contralateral RP nodes may be safely excluded from the CTV in oropharyngeal cancers without contralateral jugular chain involvement, which if supported by more mature and conclusive evidence will provide a strong rationale for limiting treatment to only the ipsilateral RP nodes in this circumstance as well (Spencer et al. 2012). The medial RP nodes are included only in tumors that involve the posterior pharyngeal wall.

4.3.3.7 Level VI Nodes

Level VI nodes are treated in all cases with clinical involvement of level IV nodes, in cases of hypopharynx cancer where the apex of the pyriform sinus is involved, laryngeal cancers extending to the subglottic larynx, and in all cases of thyroid cancer for which RT is indicated.

4.3.3.8 Level VII Nodes

Level VII nodes are treated in all cases of gross level VI nodal involvement.

4.3.4 Special Considerations for Target Delineation

A number of aforementioned anatomical and surgical studies form the fundamental basis for elective nodal CTV coverage in squamous cell carcinoma of the head and neck (Byers et al. 1988; Candela et al. 1990; Lindberg 1972; Rouvière 1938). Further rationale for these CTV definition guidelines when using IMRT is provided by patterns of failure studies from the University of Michigan and other institutions (Chen et al. 2010, 2011; Dawson et al. 2000; Eisbruch et al. 2004a). One series of 133 patients from our institution with non-nasopharyngeal HNC treated with either definitive or postoperative IMRT with sparing of the parotid glands evaluated the site of failure in each of 21 patients with locoregional failure (Dawson et al. 2000; Eisbruch et al. 2004a). All patients in this study, even those who were clinically node negative, received bilateral neck irradiation due to a high risk of subclinical bilateral neck disease. The superior borders of the CTV in most patients was the skull base for the ipsilateral neck, the level of the posterior belly of the digastric muscle crossing the internal jugular vein for the contralateral neck, and the top of the C1 vertebral body for the RP nodes, in accordance with Rouvière's description of the location of the lateral RP nodes (Figs. 4.2 and 4.3) (Rouvière 1938). At a median

follow-up period of 32 months, 21 of the 133 patients (16 %) had locoregional recurrences; 17 occurred infield, whereas four were marginal. The findings from this study and other institutions underscore the following particular concerns with the use of IMRT for head and neck cancer.

4.3.4.1 Retropharyngeal Nodes

Two of the four marginal recurrences in our institutional series occurred near the base of the skull at the site of the lateral RP nodes (Eisbruch et al. 2004a). Both occurred in patients with oropharyngeal cancer (one tonsillar and one base of the tongue) who presented with N0 necks, in whom the RP nodes had been included within the CTV with a cranial most extent to the top of C1. However, the epicenter of the recurrence volume of the two marginal RP recurrences lays cranial to the top of C1, one ipsilateral to the primary tumor and the other contralateral and extensive. Given this unexpected pattern of failure, and the scant details in the literature regarding the pattern of metastases to the RP nodes in non-nasopharyngeal cancers, our institutional policy was modified to include the lateral RP nodes bilaterally with a cranial extent to the skull base in all cases of locally advanced oropharyngeal cancer, irrespective of extent of neck node involvement (Figs. 4.2 and 4.3) (King et al. 2000; McLaughlin et al. 1995). This practice is consistent with the recent cooperative group consensus guidelines for CTV delineation and is supported by surgical series of RP node involvement, other institutional case reports of marginal RP failures near the skull base, and RT series demonstrating an absence of RP nodal failures following IMRT using elective CTVs extending to the skull base (Chen et al. 2011; Chung et al. 2011; Coskun et al. 2011; Eisbruch et al. 2004a; Gregoire and Levendag; Hasegawa and Matsuura 1994). One recent preliminary report, however, suggested that in selected cases of ipsilateral-only nodal involvement, treatment of the contralateral RP nodes can be avoided without an increased risk of marginal or out-of-field failure (Spencer et al. 2012). If supported by more mature and conclusive evidence, exclusion of the contralateral RP nodes in cases of locally advanced oropharynx cancer without contralateral nodal involvement will be incorporated into our future treatment policies and recommendations.

4.3.4.2 Lymph Nodes at Risk Due to Aberrant Lymphatic Drainage from Extensive Neck Disease

The third marginal recurrence in our institutional series was in a patient with oral tongue cancer who had bulky low neck nodal involvement (Eisbruch et al. 2004a). Despite achieving a complete response after RT, the patient subsequently recurred in level VI, highlighting the potential for involvement retrograde lymphatic flow and unpredictable patterns of nodal metastasis in patients with bulky nodes (Fisch 1968). Rouvière described lymphatic drainage channels to the pretracheal/prelaryngeal nodes (level VI) from the jugular nodes (levels III–IV) which provide a conduit for distal lymphatic drainage in cases of extensive nodal involvement (Rouvière 1938). These connections, in tandem with flow obstruction at level IV, explain this marginal recurrence at level VI. As such, level VI nodes should be treated in all cases with clinical involvement of level IV nodes.

A recent review of our institutional experience between 2003 and 2011 revealed six cases of patients with primary cancers of the oropharynx and nasopharynx who presented with pathologically confirmed parotidean metastases (unpublished data). All of these patients had locally advanced stage N2c or N3 disease, with diffuse multilevel and bulky involvement of ipsilateral level II. Based on these findings, we have changed out institutional practice to include elective coverage of the ipsilateral parotidean nodes in all cases of extensive involvement of the level II lymph nodes.

4.3.4.3 Prior Surgery

The fourth marginal recurrence in our institutional patterns of failure series was observed in a patient who had a history of prior neck dissection more than 1 year prior to recurrence of an oral cavity cancer (Eisbruch et al. 2004a). He

was treated with local excision of the primary site recurrence followed by postoperative IMRT and experienced subsequent recurrence in the subcutaneous tissues of contralateral level I – an unpredictable location given the site of his primary tumor. As in patients with extensive nodal involvement, those patients with a history of neck surgery more than 1 year prior to tumor recurrence may experience unpredictable lymphatic drainage, in this case due to collateral lymphatics which fully develop 1 or more years after surgery (Fisch 1968; Rouvière 1938). These collaterals commonly develop in the submental and submandibular areas, including within the subdermal tissues, thus leading to unpredictable patterns of recurrence. As such, the use of IMRT in patients who have had major neck surgery more than 1 year prior to tumor diagnosis should be approached with caution due to the uncertainty regarding their targets.

4.3.4.4 Selection of Split-Neck Versus Whole-Neck IMRT for Supraclavicular Treatment

Chao et al. reported the outcomes of 126 HNC patients treated at Washington University in St. Louis using IMRT for the upper neck only to spare the parotid glands with a matched anterior low neck field (Chao et al. 2003). Twenty-eight percent of recurrences in this series (five patients) occurred in the supraclavicular area, underscoring the importance of avoiding underdosing of low neck nodal levels in patients in whom these regions are at high risk, such as those with clinical nodal involvement in levels III or IV or with bulky nodal involvement of level II. In cases where the lower neck is at low risk, a split-neck technique with a larynx block does confer certain potential benefits over a comprehensive IMRT plan, such as reduced dose to the glottic larynx, reduced labor-intensiveness of target delineation, short treatment time, less monitor unit delivery, and less daily setup deviation in the low neck (Eisbruch and Gregoire 2009). These benefits, however, may come at the cost of reduced dose certainty to targets in the low neck targets and particularly at the IMRT field and low neck field junction, potentially resulting in over- or underdosing in these regions. Additionally, we have found that in cases where the low neck is at low risk, a comprehensive IMRT plan which prioritizes avoidance of the glottic larynx, inferior pharyngeal constrictor, and upper esophagus can consistently reduce the mean dose to these structures to 20–30 Gy over 35 fractions, which is comparable to the dose received when using a split-neck technique. In cases where the low neck is a high risk, a comprehensive IMRT plan may result in higher doses to these avoidance structures, but with the benefit of more accurate coverage of at-risk targets in the low neck, reduced risk of underdosing at the split-neck field junction, and the ability to partially spare OARs such as the larynx, cricopharyngeus, esophagus, and brachial plexus while delivering high doses to gross disease in the low neck (i.e., level IV). Therefore, at our institution, we employ the use of a single comprehensive IMRT plan rather than a matched anterior low neck field for treatment of the low neck and strongly recommend this approach in cases where the low neck targets are grossly involved or at high risk of subclinical metastases.

4.3.4.5 Preservation of the Swallowing Structures

Dysfunction of the swallowing structures is a common cause of severe acute and late toxicity after head and neck radiotherapy and is perhaps the strongest determinant of long-term quality of life in HNC survivors (Hunter et al. 2013; Langendijk et al. 2008; Machtay et al. 2008; Terrell et al. 2004). Radiotherapy dose to the swallowing structures, specifically the pharyngeal constrictor (PC) muscles, has been implicated as a primary treatment-related predictor of swallowing dysfunction after chemoradiotherapy (Eisbruch et al. 2011; Feng et al. 2007; Popovtzer et al. 2009). Therefore, avoidance of dose to the PCs should be attempted where possible, although this goal must be balanced against the need for adequate coverage of the RP nodes, due to their frequent involvement in cancers of the nasopharynx, oropharynx, and hypopharynx (Chung et al. 2011; Coskun et al. 2011; Eisbruch et al. 2004a; Hasegawa and Matsuura 1994; King et al. 2000). The RP nodes consist of lateral and medial groups, with the medial RPs located near midline close to the center of the PCs. As

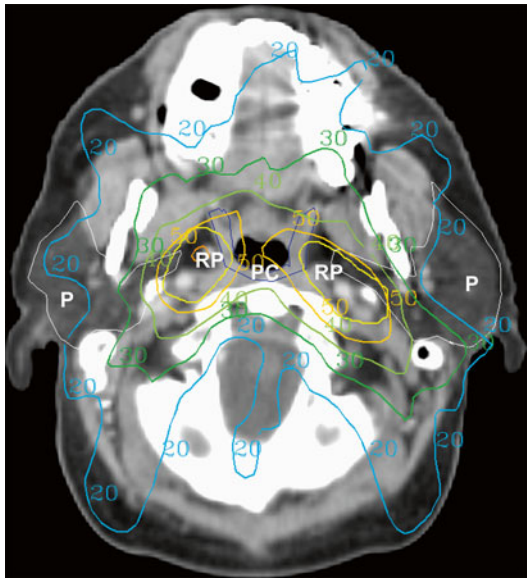

Fig. 4.5 Example of an intensity-modulated radiotherapy plan for a patient with a left base of the tongue T1 N2a squamous cell carcinoma. Dose distributions (displayed in Gy) are labeled. Note the avoidance of high dose to the medial pharyngeal constrictor muscles (*PC*, *blue contour*) while treating the lateral retropharyngeal (*RP*) node planning target volumes (*yellow contour*). The bilateral parotid glands (*P*, white contour) are also largely spared

metastatic involvement of the medial RP nodes is rare in HNC (with the exception of tumors that invade the posterior pharyngeal wall), it has been postulated that these nodes may be excluded from the CTV such that high dose to adjacent PCs can be avoided. This hypothesis was tested at the University of Michigan in a prospective study of 73 patients with locally advanced (stages III–IV) oropharynx cancer designed to assess the clinical and functional results of chemoradiotherapy using IMRT to spare the important swallowing structures (Feng et al. 2010). IMRT planning was performed with the intent of sparing non-involved parts of the swallowing structures, namely, the pharyngeal constrictors, glottic larynx, supraglottic larynx, and esophagus as well as the oral cavity and major salivary glands (Fig. 4.5). At a median follow-up of 36 months, 3-year disease-free and locoregional recurrence-free survival was 88 and 96 %, respectively. At 1 year after completion of therapy, observer-rated dysphagia was absent or minimal (scores 0–1) in all except four patients: one who was feeding-tube dependent and three who required soft diet. These outcomes clearly indicate that IMRT aimed at reducing dose to the swallowing structures in oropharynx cancer can safely minimize dysphagia while maintaining high rates of locoregional tumor control.

Table 4.3 Additional recommendations for target delineation based on recent studies

The lateral RP nodes should be treated *bilaterally* in all cases of nasopharyngeal cancer, cancers involving the posterior pharyngeal wall, and most cases of locally advanced oropharyngeal cancer
Treatment limited to the ipsilateral RP nodes in oropharyngeal cancer is at present recommended only in cases of small, well-lateralized oropharyngeal tumors with N0 or small-volume N1 disease. In the future, however, this recommendation may be extended to also include those cancers without contralateral nodal involvement (i.e., N0–N2b), pending validation of recently reported evidence suggesting that this practice may not increase the risk of marginal or out-of-field locoregional failures (Spencer et al. 2012)
The superior extent of the CTV for the lateral RP nodes should extend cranially beyond C1 to the skull base
The medial RP nodes are not included in the CTV unless the posterior pharyngeal wall is involved; thus, the medial parts of the pharyngeal constrictors can be spared from effects of high radiotherapy doses
In patients who have had major neck surgery more than 1 year prior to treatment, IMRT should be used with extreme caution due to the uncertainty regarding their targets
When the low neck is at high risk, such as in patients with significant upper neck nodal involvement, particular attention must be paid to the low neck targets to ensure appropriate dose delivery. This is of paramount importance when using a low anterior photon field matched to an upper neck IMRT plan

4.3.4.6 Summary

In summary, these analyses suggest the additional recommendations shown in Table 4.3 for target volume delineation in IMRT and augment those already understood.

4.4 The Postoperative Case: Defining the Clinical Target Volumes

In surgically treated head and neck squamous cell carcinoma with pathological risk factors in either the primary or regional sites of involvement

to warrant adjuvant radiotherapy (either with or without concurrent chemotherapy), the surgical specimen provides valuable information that should be helpful in determining the neck levels at risk. Resection of the primary site, neck dissection, and surgical reconstruction disrupts some of the anatomical landmarks used to define the borders between the levels. The surgical bed, however, remains apparent on CT and should be encompassed entirely within the CTV. As it is often impossible to distinguish between the primary tumor resection site and the adjacent neck dissection bed, they are encompassed within a unified CTV. Sites of positive margins or extracapsular extension are delineated generously as a higher-risk CTV which should receive a higher radiotherapy dose (as described below). Additionally, irrespective of whether they were included in the neck dissection, nodal levels deemed at risk based upon the primary site location or extent of neck involvement (i.e., level VI in cases of pathological level IV involvement) should be included in the CTV (see Sect. 4.3.2). For malignant salivary gland tumors which are primarily managed surgically, those with tumors that are high grade, T3 or T4, recurrent, resected incompletely or with close margins, have perineural or gross nerve invasion, or have lymph node metastases should receive adjuvant RT (Chen et al. 2007a, c; Terhaard et al. 2005). CTV delineation guidelines for the primary site and neck are as detailed above (see Sects. 4.2.2, 4.3.2, and 4.3.3, respectively).

Recent surgical series of transoral robotic surgery (TORS) and transoral laser microsurgery (TLM) for oropharynx cancer with favorable outcomes after surgery alone, even in stage III and IV disease, have proposed that postoperative radiotherapy can be safely omitted in cases with traditional indications for adjuvant RT after TORS or TLM (Grant et al. 2009; Weinstein et al. 2012). These studies, however, are limited by their small patient numbers, patient selection biases, lack of matched comparator groups of patients who received RT, and in the case of the TLM studies, their retrospective nature. Until omission of RT in such patients is supported by higher-level evidence, the use of postoperative RT to both the primary site and neck for those with appropriate indications should remain the standard of care.

4.5 Target Doses and Treatment Techniques

4.5.1 Doses

At our institution, our current treatment policy is to deliver 70 Gy to the GTV in 35 fractions (2.0 Gy per fraction). The high-risk CTV, which is around the GTV and the first echelon nodes, receives 59–63 Gy (at 1.7–1.8 Gy per fraction, biologically equivalent to 54–60 Gy at 2.0 Gy per fraction). The lower-risk areas receive 56–59 Gy (1.6–1.7 Gy per fraction, biologically equivalent to approximately 49–54 Gy at 2.0 Gy per fraction). These specifications are very similar to the policies at UCSF, Washington University in St. Louis, University of Iowa, and MSKCC (Chao et al. 2003; Lee et al. 2003; Setton et al. 2012; Yao et al. 2005). Concurrent chemotherapy for patients with locally advanced (stages III–IV) disease is strongly recommended for fit patients based upon level I evidence (Denis et al. 2004; Forastiere et al. 2003; Pignon et al. 2009). For patients receiving concurrent RT, we favor the use of the standard fractionation scheme above rather than accelerated radiotherapy, which has failed to show a benefit in terms of locoregional control or survival in phase III studies (Ang et al. 2010; Bourhis et al. 2012). In patients with locally advanced disease who do not receive concurrent chemotherapy, due typically to comorbid illness or other contraindication, accelerated or hyperfractionated radiotherapy is recommended, on the basis of multiple randomized trials demonstrating improvement in locoregional control and a meta-analysis demonstrating an improvement in overall survival compared with conventional radiotherapy (Bourhis et al. 2006; Fu et al. 2000; Horiot et al. 1992; Overgaard et al. 2003). Our institutional preference in this situation has been to use the DAHANCA regimen of 6 fractions per week (with the sixth fraction given either on Saturday or as a second fraction 1 day

per week given at least 6 h apart) to deliver our standard fractionation scheme above while accelerating the course of therapy by 1 week (Overgaard et al. 2003).

For postoperative radiotherapy delivered, our institutional policy is to define standard-risk and low-risk CTV. The standard-risk CTV includes the primary tumor surgical bed, involved nodal levels, and first echelon nodal levels and receives 60 Gy in 30 fractions (at 2.0 Gy per fraction). The low-risk CTV, consisting of second echelon nodal levels, receives 54 Gy in 30 fractions (at 1.8 Gy per fraction). In the case of positive margins or extracapsular extension (ECE), chemotherapy should be administered concurrent with RT (Bernier et al. 2005). In this setting, we define an additional high-risk CTV at the sites of positive margin and/or ECE, which receives 66 Gy in 33 fractions (2 Gy per fraction), while the standard-risk CTV and low-risk CTV, as defined above, receive 60 and 54 Gy in 33 fractions (at 1.82 and 1.64 Gy per fraction, respectively). In patients with small-volume high-risk CTVs (for positive margins or ECE) receiving concurrent chemotherapy, the treatment course can be delivered over 30 fractions, such that the high-risk, standard-risk, and low-risk CTVs receive 2.2, 2.0, and 1.8 Gy per fraction. When delivered to larger volumes with concurrent chemotherapy, however, hypofractionation may significantly increase the toxicity of therapy, and as such is discouraged. For residual gross disease, definitive radiotherapy doses of 70 Gy should be prescribed to the residual GTV.

4.5.2 Sparing the Organs at Risk

Evidence accumulated over the past 10 years has demonstrated that sparing of a number of organs in the head and neck with highly conformal RT can translate into significant reductions in both acute and late toxicity and tangible improvements in quality of life. Clear dose-response relationships have been demonstrated between xerostomia and dose to the parotid glands, submandibular glands, and oral cavity; mucositis and dose to the oral cavity mucosa; dysphagia and dose to the pharyngeal constrictors; and osteoradionecrosis and dose to the mandible (Bentzen et al. 2001; Beumer et al. 1984; Eisbruch et al. 2001, 1999; Lee et al. 2009; Little et al. 2012; Murdoch-Kinch et al. 2008; Narayan et al. 2008; Spanos et al. 1976; Tsai et al. 2013). Subsequent efforts to reduce the dose to a number of these structures, including the parotid glands, pharyngeal constrictors, mandible, and uninvolved oral cavity, have produced clinically meaningful improvements in organ-specific toxicities and quality of life (Ben-David et al. 2007; Eisbruch et al. 2001; Feng et al. 2010; Kam et al. 2007; Nguyen et al. 2012; Nutting et al. 2011; Studer et al. 2006; Wang et al. 2012b). Treatment-related toxicity may potentially be further reduced by sparing other normal tissues, including the skin, pharyngeal mucosa, neck musculature, and nonspecific normal head and neck tissue, irradiation of which is associated with an increased risk of second malignancy (Lee et al. 2002; Sanguineti et al. 2006). Attention to sparing of the non-involved glottic larynx, additionally, is likely to not only preserve voice quality but also reduce the risk of long-term aspiration and dysphagia, which may result from delivery of IMRT without inclusion of the larynx and midline swallowing structures in the planning cost function (Caudell et al. 2010; Caglar et al. 2008; Eisbruch et al. 2004b; Feng et al. 2007; Jensen et al. 2007). However, one must bear in mind that the selection of OARs and extent to which each should be spared must be carefully balanced against coverage of the GTVs and CTVs, as failure to achieve locoregional control due to inadequate target coverage is certain to negate any potential quality of life derived from sparing of OARs. This decision is individual for each case and requires consideration of the dose-response relationships of the OARs and targets involved, as tradeoffs between these structures, as well as between competing OARs, are inevitable. For instance, while sparing the contralateral submandibular gland is feasible when the adjacent level IB is not included in the CTV, this may only be achievable at the cost of increased dose to the parotid gland and swallowing structures (Murdoch-Kinch et al. 2008). The clinical implications of such tradeoffs must be considered within the context of

Table 4.4 Head and neck IMRT dose constraint goals for non-involved normal structures at the University of Michigan

Organ	Dose parameter[a]	Goal (Gy)
Spinal cord	Maximum	≤45
Spinal cord +0.5 cm	Maximum	≤50
Brainstem +0.3 cm	Maximum	≤54
Optic chiasm +0.3 cm	Maximum	≤50
Optic nerve	Maximum	≤50
Parotid gland	Mean	≤24
Submandibular glands	Mean	≤30
Oral cavity	Mean	≤30
Glottic larynx	Mean	≤20
Superior and middle pharyngeal constrictors	Mean	≤50
Inferior pharyngeal constrictors	Mean	≤20
Esophagus	Mean	≤20
Mandible	Maximum	≤70
Lips	Mean	≤30
Eyes	Maximum	≤40
Brachial plexus	Maximum	≤60
Cochlea	Maximum	≤40

[a]Maximum dose constraints pertain to 1 % of the volume of the normal tissue structure

the dose-response relationships for each involved OAR in order to achieve the optimal balance between these competing goals.

An additional consideration in defining and prioritizing avoidance structures when using IMRT is the steep dose fall-off that occurs at the interface between targets and OARs. This is most evident in the oral cavity, where the distinction between CTV and the mucosa to be spared may be arbitrary, and in the pharyngeal constrictor muscles, which lie between the CTVs in the bilateral necks and adjacent to most of primary sites in the head and neck. Selecting a greater number of avoidance structures results in steeper dose gradients around the CTVs, which may increase the risk of marginal recurrences if CTVs are not conservatively (i.e., generously) defined.

Recommendations for IMRT dose constraint goals for normal tissue structures based on our current institutional policies are included in Table 4.4 (Eisbruch et al. 2001, 2004b, 2011; Little et al. 2012; Murdoch-Kinch et al. 2008).

4.5.3 IMRT Planning

For IMRT planning, uniform 3–5 mm expansions around each GTV and CTV are used to generate planning target volumes (PTVs) for each target, depending on the reproducibility of patient setup at the treating center. At the University of Michigan, IMRT optimization is performed using minimum and maximum target coverage goals of 99 and 107 % of prescription dose, respectively, for the PTV surrounding the GTVs. For the PTVs surrounding the subclinical CTVs, target coverage goals are ±5 % of the prescribed dose.

With a greater number of beam angles, higher treatment conformality may be achieved, although at the cost of additional time required for the planning and delivery of each field, which reduces the overall efficiency of the clinic. To this end, one must assess to what degree of additionally conformality in planning provides a clinically significant benefit for the patient. At our institution, we have found that nine equidistant fields are sufficient for most head and neck IMRT courses. In a complex case, such as a locally advanced sinonasal tumor with nodal involvement and extension into the skull base, in which both the extensive gross disease and nodal targets must be covered while limiting dose to the adjacent optic structures and brain, the use of 11 or more equidistant fields may provide a somewhat more conformal plan and yield better treatment outcomes. Beyond this, a greater number of delivery angles, and the technologies that enable their use, seem unlikely to provide additional benefit, such that their value would need to be demonstrated in clinical evaluations.

4.5.4 Adaptive Replanning

As is not infrequent due to weight loss or tumor shrinkage during head and neck RT, a patient's contour may change such that their thermoplastic mask may no longer fit. In this circumstance, re-simulation is necessary to confirm the reproducibility of the original simulation position, typically using co-registration of the new simulation CT scan with the original treatment

plan to confirm adequate target coverage and OAR avoidance. A number of small studies have examined the dosimetric impact of anatomy changes during RT on the delivery of planned dose to the OARs and target volumes (Castadot et al. 2011; Cheng et al. 2012; Lee et al. 2008; Loo et al. 2011; Wu et al. 2009; Hansen et al. 2006; Ho et al. 2012; O'Daniel et al. 2007). For OARs, most studies demonstrate that during RT, the volume of parotid glands decreases and their position is medially displaced, resulting in an increase in delivered dose to the parotids compared to the planned dose. Both the medial displacement of the parotids and increased parotid doses appear to be highly correlated with weight loss during RT (Barker et al. 2004; Lee et al. 2008; Castadot et al. 2011). Although increase in mean parotid dose in these studies is on average less than 5 %, delivered mean parotid doses of up to 40 % or greater above planned dose occurred not infrequently in individual patients. A number of these studies also assessed delivered dose to more critical avoidance structures such as the spinal cord and brainstem, with no clear consensus among studies as to whether delivered dose differed from intended dose (Cheng et al. 2012; Hansen et al. 2006; Ho et al. 2012; Wu et al. 2009; Castadot et al. 2011; Loo et al. 2011). In the studies that did demonstrate differences between planned and delivered doses, however, those differences did appear clinically significant, with maximum doses up to 15.4 and 8.1 Gy over the planned dose delivered to the spinal cord and brainstem in one study and delivered dose to each of these structures exceeding accepted tolerance doses in 11 and 16 % of patients in another study, respectively (Cheng et al. 2012; Hansen et al. 2006). For target volumes, delivered dose and target coverage differed minimally from the planned dose in most studies, even despite frequent tumor shrinkage during RT (Castadot et al. 2011; Cheng et al. 2012; Hansen et al. 2006; Loo et al. 2011; O'Daniel et al. 2007; Wu et al. 2009). Unsurprisingly, for both the OARs and targets, while adaptive replanning statistically improved dose distribution and conformality compared of the original plans, the magnitude of the improvements in dose delivered by the adaptive plans was rarely clinically significant (Castadot et al. 2011; Hansen et al. 2006; O'Daniel et al. 2007). Taken together, these results suggest that while most patients do not experience anatomical changes with a clinically meaningful impact on dose delivered to either the OARs or target volumes, a selected minority of patients with larger anatomical changes may potentially benefit from adaptive replanning.

Given the labor-intensive nature of assessing for dosimetric changes and adaptive replanning, the optimal strategy for incorporating this process into routine clinical practice remains to be determined. Methodologies for replanning can vary widely, ranging from "simple adaptation to changing geometry" to significantly more complex adaptation to both geometry and delivered dose (Wu et al. 2009). However, the routine use of even "simple" adaptation techniques requires significant clinical resources on the part of the physician, dosimetrists, and physicists. Schwartz et al. recently reported early results from the first prospective clinical study of adaptive IMRT in 24 patients with locally advanced oropharynx cancer (Schwartz et al. 2012). Using an automated process of deformable image registration and automatic segmentation, baseline treatment plans were mapped onto daily on-treatment CT scans and reviewed for significant anatomical changes. Adaptive replanning was performed when necessary to correct for inadequate target coverage or insufficient sparing of OARs. All 24 patients required at least one replan due to protocol specified changes in CTV or normal tissue coverage, while eight patients required an additional second replan later in the treatment course. Compared to the original plan, a single replan improved delivered mean doses to the ipsilateral and contralateral parotid glands by 0.6 Gy (2.8 %) and 1.3 Gy (3.9 %), respectively, while also reducing the body volume receiving greater than 60, 40, and 20 Gy by 31, 36, and 13 cc, respectively. Acute toxicity was comparable to previous reports with standard IMRT, while late toxicity, particularly with respect to dysphagia and aspiration, appears quite favorable in this preliminary report (Feng et al. 2010). Whether these outcomes can be attributed to the relatively small dosimetric

improvements achieved by adaptive RT, rather than to other factors such as favorable patient selection, cannot be addressed by this study, and will require definitive assessment and validation in a randomized trial of adaptive versus standard IMRT. Nonetheless, the relatively automated and streamlined system described by Schwartz et al. represents a promising approach by which adaptive IMRT may be integrated into routine clinical practice in the future.

At present, outside of the context of a clinical trial, we recommend that head and neck IMRT continue to be planned and delivered based upon the original pretreatment CT simulation, without routine adaptive replanning during the treatment course. However, if the original treatment position cannot be reproduced or large changes in external patient contour occur (such as due to a significant regression of bulky neck disease), we recommend repeat CT simulation and co-registration of the new CT with the original treatment plan, with physician assessment of adequacy of target coverage. If unacceptable deviations in either target coverage or sparing of critical organs are found, then replanning should be performed to ensure acceptable treatment plan delivery. However, this should not be anticipated or planned in the setting of primary tumor regression alone, in which circumstance we recommend that the entirety of the original GTV receive the originally intended full prescription dose, irrespective of radiographic or clinically visible regression of gross tumor. Further investigations may determine whether adaptive planning to either boost nonresponding tumor or de-escalate the dose to rapidly responding tumor may improve the efficacy or toxicity of head and neck radiotherapy.

4.5.5 Radiotherapy After Induction Chemotherapy

In patients who receive induction chemotherapy prior to radiotherapy, a frequent concern that arises is whether to reduce the CTV or PTV in areas of significant tumor regression. Although such an approach has been employed successfully in other disease sites and certainly warrants further investigation in head and neck cancer, at present its use is not recommended in head and neck radiotherapy (Salama et al. 2009). Our policy is to use the same PTV and CTV that would be indicated before induction chemotherapy, unless there was a change in the involved compartment as tumor shrank, with the same doses based only on the clinical indications for each particular tumor. As recent data from randomized studies failed to show clear benefit for induction chemotherapy, its use is likely to decline in the future (Cohen et al. 2012; Haddad et al. 2012).

Conclusion

The use IMRT for the treatment of head and neck cancer requires accurate target delineation and treatment planning in order to achieve optimized patient outcomes. Incorporation of physical examination and imaging studies with knowledge of the natural history and patterns of spread for tumors of each anatomical site and histological type is essential for accurate definition of the gross and at-risk subclinical target volumes and avoidance of marginal or out-of-field locoregional recurrences. Identification of normal tissue structures that are not at risk, and can therefore be safely spared without compromising locoregional control, is additionally further central to reducing the toxicity of head and neck radiotherapy. Adaptive dose escalation to tumor sub-volumes at highest risk of treatment failure has the potential to improve the efficacy of head and neck radiotherapy and impact the paradigm by which functional imaging is incorporated into target delineation in the future.

References

Abdel Khalek Abdel Razek A, King A (2012) MRI and CT of nasopharyngeal carcinoma. AJR Am J Roentgenol 198(1):11–18

Ahn PH, Garg MK (2008) Positron emission tomography/computed tomography for target delineation in head and neck cancers. Semin Nucl Med 38(2):141–148

Ang KK, Harris J, Wheeler R, Weber R, Rosenthal DI, Nguyen-Tan PF, Westra WH, Chung CH, Jordan RC, Lu C, Kim H, Axelrod R, Silverman CC, Redmond

KP, Gillison ML (2010) Human papillomavirus and survival of patients with oropharyngeal cancer. N Engl J Med 363(1):24–35

Armstrong JG, Harrison LB, Thaler HT, Friedlander-Klar H, Fass DE, Zelefsky MJ, Shah JP, Strong EW, Spiro RH (1992) The indications for elective treatment of the neck in cancer of the major salivary glands. Cancer 69(3):615–619

Ashamalla H, Guirgius A, Bieniek E, Rafla S, Evola A, Goswami G, Oldroyd R, Mokhtar B, Parikh K (2007) The impact of positron emission tomography/computed tomography in edge delineation of gross tumor volume for head and neck cancers. Int J Radiat Oncol Biol Phys 68(2):388–395

Barker JL Jr, Garden AS, Ang KK, O'Daniel JC, Wang H, Court LE, Morrison WH, Rosenthal DI, Chao KS, Tucker SL, Mohan R, Dong L (2004) Quantification of volumetric and geometric changes occurring during fractionated radiotherapy for head-and-neck cancer using an integrated CT/linear accelerator system. Int J Radiat Oncol Biol Phys 59(4):960–970

Beetz I, Schilstra C, van der Schaaf A, van den Heuvel ER, Doornaert P, van Luijk P, Vissink A, van der Laan BF, Leemans CR, Bijl HP, Christianen ME, Steenbakkers RJ, Langendijk JA (2012) NTCP models for patient-rated xerostomia and sticky saliva after treatment with intensity modulated radiotherapy for head and neck cancer: the role of dosimetric and clinical factors. Radiother Oncol 105(1):101–106

Ben-David MA, Diamante M, Radawski JD, Vineberg KA, Stroup C, Murdoch-Kinch CA, Zwetchkenbaum SR, Eisbruch A (2007) Lack of osteoradionecrosis of the mandible after intensity-modulated radiotherapy for head and neck cancer: likely contributions of both dental care and improved dose distributions. Int J Radiat Oncol Biol Phys 68(2):396–402

Bentzen SM (2005) Theragnostic imaging for radiation oncology: dose-painting by numbers. Lancet Oncol 6(2):112–117

Bentzen SM, Saunders MI, Dische S, Bond SJ (2001) Radiotherapy-related early morbidity in head and neck cancer: quantitative clinical radiobiology as deduced from the CHART trial. Radiother Oncol 60(2):123–135

Bernier J, Cooper JS, Pajak TF, van Glabbeke M, Bourhis J, Forastiere A, Ozsahin EM, Jacobs JR, Jassem J, Ang KK, Lefebvre JL (2005) Defining risk levels in locally advanced head and neck cancers: a comparative analysis of concurrent postoperative radiation plus chemotherapy trials of the EORTC (#22931) and RTOG (# 9501). Head Neck 27(10):843–850

Beumer J, Harrison R, Sanders B, Kurrasch M (1984) Osteoradionecrosis: predisposing factors and outcomes of therapy. Head Neck Surg 6(4):819–827

Bourhis J, Overgaard J, Audry H, Ang KK, Saunders M, Bernier J, Horiot JC, Le Maitre A, Pajak TF, Poulsen MG, O'Sullivan B, Dobrowsky W, Hliniak A, Skladowski K, Hay JH, Pinto LH, Fallai C, Fu KK, Sylvester R, Pignon JP (2006) Hyperfractionated or accelerated radiotherapy in head and neck cancer: a meta-analysis. Lancet 368(9538):843–854

Bourhis J, Sire C, Graff P, Gregoire V, Maingon P, Calais G, Gery B, Martin L, Alfonsi M, Desprez P, Pignon T, Bardet E, Rives M, Geoffrois L, Daly-Schveitzer N, Sen S, Tuchais C, Dupuis O, Guerif S, Lapeyre M, Favrel V, Hamoir M, Lusinchi A, Temam S, Pinna A, Tao YG, Blanchard P, Auperin A (2012) Concomitant chemoradiotherapy versus acceleration of radiotherapy with or without concomitant chemotherapy in locally advanced head and neck carcinoma (GORTEC 99–02): an open-label phase 3 randomised trial. Lancet Oncol 13(2):145–153

Boyer AL, Geis P, Grant W, Carol M (1997) Modulated beam conformal therapy for head and neck tumors. Int J Radiat Oncol Biol Phys 39(1):227–236

Burri RJ, Rangaswamy B, Kostakoglu L, Hoch B, Genden EM, Som PM, Kao J (2008) Correlation of positron emission tomography standard uptake value and pathologic specimen size in cancer of the head and neck. Int J Radiat Oncol Biol Phys 71(3):682–688

Byers RM, Wolf PF, Ballantyne AJ (1988) Rationale for elective modified neck dissection. Head Neck Surg 10(3):160–167

Caglar HB, Tishler RB, Othus M, Burke E, Li Y, Goguen L, Wirth LJ, Haddad RI, Norris CM, Court LE, Aninno DJ, Posner MR, Allen AM (2008) Dose to larynx predicts for swallowing complications after intensity-modulated radiotherapy. Int J Radiat Oncol Biol Phys 72(4):1110–1118

Candela FC, Shah J, Jaques DP, Shah JP (1990) Patterns of cervical node metastases from squamous carcinoma of the larynx. Arch Otolaryngol Head Neck Surg 116(4):432–435

Cao Y, Popovtzer A, Li D, Chepeha DB, Moyer JS, Prince ME, Worden F, Teknos T, Bradford C, Mukherji SK, Eisbruch A (2008) Early prediction of outcome in advanced head-and-neck cancer based on tumor blood volume alterations during therapy: a prospective study. Int J Radiat Oncol Biol Phys 72(5):1287–1290

Castadot P, Geets X, Lee JA, Gregoire V (2011) Adaptive functional image-guided IMRT in pharyngo-laryngeal squamous cell carcinoma: is the gain in dose distribution worth the effort? Radiother Oncol 101(3):343–350

Castelijns JA, van den Brekel MW (2002) Imaging of lymphadenopathy in the neck. Eur Radiol 12(4): 727–738

Caudell JJ, Schaner PE, Desmond RA, Meredith RF, Spencer SA, Bonner JA (2010) Dosimetric factors associated with long-term dysphagia after definitive radiotherapy for squamous cell carcinoma of the head and neck. Int J Radiat Oncol Biol Phys 76(2):403–409

Chao KS, Ozyigit G, Tran BN, Cengiz M, Dempsey JF, Low DA (2003) Patterns of failure in patients receiving definitive and postoperative IMRT for head-and-neck cancer. Int J Radiat Oncol Biol Phys 55(2):312–321

Chawla S, Kim S, Loevner LA, Hwang WT, Weinstein G, Chalian A, Quon H, Poptani H (2011) Prediction of disease-free survival in patients with squamous cell carcinomas of the head and neck using dynamic contrast-enhanced MR imaging. AJNR Am J Neuroradiol 32(4):778–784

Chen AM, Garcia J, Bucci MK, Quivey JM, Eisele DW (2007a) The role of postoperative radiation therapy in carcinoma ex pleomorphic adenoma of the parotid gland. Int J Radiat Oncol Biol Phys 67(1):138–143

Chen AM, Garcia J, Lee NY, Bucci MK, Eisele DW (2007b) Patterns of nodal relapse after surgery and postoperative radiation therapy for carcinomas of the major and minor salivary glands: what is the role of elective neck irradiation? Int J Radiat Oncol Biol Phys 67(4):988–994

Chen AM, Granchi PJ, Garcia J, Bucci MK, Fu KK, Eisele DW (2007c) Local-regional recurrence after surgery without postoperative irradiation for carcinomas of the major salivary glands: implications for adjuvant therapy. Int J Radiat Oncol Biol Phys 67(4):982–987

Chen AM, Farwell DG, Luu Q, Chen LM, Vijayakumar S, Purdy JA (2010) Misses and near-misses after postoperative radiation therapy for head and neck cancer: comparison of IMRT and non-IMRT techniques in the CT-simulation era. Head Neck 32(11):1452–1459

Chen AM, Farwell DG, Luu Q, Chen LM, Vijayakumar S, Purdy JA (2011) Marginal misses after postoperative intensity-modulated radiotherapy for head and neck cancer. Int J Radiat Oncol Biol Phys 80(5): 1423–1429

Chen YH, Yang XM, Li SS, Wang YH, He JJ, Yang YD, Wang S, Liu JJ, Zhang XL (2012) Value of fused positron emission tomography CT in detecting primaries in patients with primary unknown cervical lymph node metastasis. J Med Imaging Radiat Oncol 56(1):66–74

Cheng HC, Wu VW, Ngan RK, Tang KW, Chan CC, Wong KH, Au SK, Kwong DL (2012) A prospective study on volumetric and dosimetric changes during intensity-modulated radiotherapy for nasopharyngeal carcinoma patients. Radiother Oncol 104(3):317–323

Chung NN, Ting LL, Hsu WC, Lui LT, Wang PM (2004) Impact of magnetic resonance imaging versus CT on nasopharyngeal carcinoma: primary tumor target delineation for radiotherapy. Head Neck 26(3): 241–246

Chung EJ, Oh JI, Choi KY, Lee DJ, Park IS, Kim JH, Rho YS (2011) Pattern of cervical lymph node metastasis in tonsil cancer: predictive factor analysis of contralateral and retropharyngeal lymph node metastasis. Oral Oncol 47(8):758–762

Cohen EEW, Karrison T, Kocherginsky M, Huang CH, Agulnik M, Mittal BB, Yunus F, Samant S, Brockstein B, Raez LE, Mehra R, Kumar P, Ondrey FG, Seiwert TY, Villaflor VM, Haraf DJ, Vokes EE (2012) DeCIDE: a phase III randomized trial of docetaxel (D), cisplatin (P), 5-fluorouracil (F) (TPF) induction chemotherapy (IC) in patients with N2/N3 locally advanced squamous cell carcinoma of the head and neck (SCCHN). J Clin Oncol 30(Suppl):abstr 5500

Coskun HH, Ferlito A, Medina JE, Robbins KT, Rodrigo JP, Strojan P, Suarez C, Takes RP, Woolgar JA, Shaha AR, de Bree R, Rinaldo A, Silver CE (2011) Retropharyngeal lymph node metastases in head and neck malignancies. Head Neck 33(10):1520–1529

Daisne JF, Duprez T, Weynand B, Lonneux M, Hamoir M, Reychler H, Gregoire V (2004) Tumor volume in pharyngolaryngeal squamous cell carcinoma: comparison at CT, MR imaging, and FDG PET and validation with surgical specimen. Radiology 233(1):93–100

Dawson LA, Anzai Y, Marsh L, Martel MK, Paulino A, Ship JA, Eisbruch A (2000) Patterns of local-regional recurrence following parotid-sparing conformal and segmental intensity-modulated radiotherapy for head and neck cancer. Int J Radiat Oncol Biol Phys 46(5): 1117–1126

Denis F, Garaud P, Bardet E, Alfonsi M, Sire C, Germain T, Bergerot P, Rhein B, Tortochaux J, Calais G (2004) Final results of the 94–01 French Head and Neck Oncology and Radiotherapy Group randomized trial comparing radiotherapy alone with concomitant radiochemotherapy in advanced-stage oropharynx carcinoma. J Clin Oncol 22(1):69–76

Dirix P, Nuyts S (2010) Value of intensity-modulated radiotherapy in Stage IV head-and-neck squamous cell carcinoma. Int J Radiat Oncol Biol Phys 78(5): 1373–1380

Duprez F, De Neve W, De Gersem W, Coghe M, Madani I (2011) Adaptive dose painting by numbers for head-and-neck cancer. Int J Radiat Oncol Biol Phys 80(4): 1045–1055

Eisbruch A, Gregoire V (2009) Balancing risk and reward in target delineation for highly conformal radiotherapy in head and neck cancer. Semin Radiat Oncol 19(1):43–52

Eisbruch A, Ten Haken RK, Kim HM, Marsh LH, Ship JA (1999) Dose, volume, and function relationships in parotid salivary glands following conformal and intensity-modulated irradiation of head and neck cancer. Int J Radiat Oncol Biol Phys 45(3):577–587

Eisbruch A, Kim HM, Terrell JE, Marsh LH, Dawson LA, Ship JA (2001) Xerostomia and its predictors following parotid-sparing irradiation of head-and-neck cancer. Int J Radiat Oncol Biol Phys 50(3):695–704

Eisbruch A, Foote RL, O'Sullivan B, Beitler JJ, Vikram B (2002) Intensity-modulated radiation therapy for head and neck cancer: emphasis on the selection and delineation of the targets. Semin Radiat Oncol 12(3): 238–249

Eisbruch A, Marsh LH, Dawson LA, Bradford CR, Teknos TN, Chepeha DB, Worden FP, Urba S, Lin A, Schipper MJ, Wolf GT (2004a) Recurrences near base of skull after IMRT for head-and-neck cancer: implications for target delineation in high neck and for parotid gland sparing. Int J Radiat Oncol Biol Phys 59(1):28–42

Eisbruch A, Schwartz M, Rasch C, Vineberg K, Damen E, Van As CJ, Marsh R, Pameijer FA, Balm AJ (2004b) Dysphagia and aspiration after chemoradiotherapy for head-and-neck cancer: which anatomic structures are affected and can they be spared by IMRT? Int J Radiat Oncol Biol Phys 60(5):1425–1439

Eisbruch A, Kim HM, Feng FY, Lyden TH, Haxer MJ, Feng M, Worden FP, Bradford CR, Prince ME, Moyer JS, Wolf GT, Chepeha DB, Ten Haken RK (2011)

Chemo-IMRT of oropharyngeal cancer aiming to reduce dysphagia: swallowing organs late complication probabilities and dosimetric correlates. Int J Radiat Oncol Biol Phys 81(3):e93–e99

Emami B, Sethi A, Petruzzelli GJ (2003) Influence of MRI on target volume delineation and IMRT planning in nasopharyngeal carcinoma. Int J Radiat Oncol Biol Phys 57(2):481–488

Feng M, Eisbruch A (2007) Future issues in highly conformal radiotherapy for head and neck cancer. J Clin Oncol 25(8):1009–1013

Feng FY, Kim HM, Lyden TH, Haxer MJ, Feng M, Worden FP, Chepeha DB, Eisbruch A (2007) Intensity-modulated radiotherapy of head and neck cancer aiming to reduce dysphagia: early dose-effect relationships for the swallowing structures. Int J Radiat Oncol Biol Phys 68(5):1289–1298

Feng FY, Kim HM, Lyden TH, Haxer MJ, Worden FP, Feng M, Moyer JS, Prince ME, Carey TE, Wolf GT, Bradford CR, Chepeha DB, Eisbruch A (2010) Intensity-modulated chemoradiotherapy aiming to reduce dysphagia in patients with oropharyngeal cancer: clinical and functional results. J Clin Oncol 28(16):2732–2738

Fisch U (1968) Lymphography of the cervical lymphatic system. Saunders, Philadelphia

Forastiere AA, Goepfert H, Maor M, Pajak TF, Weber R, Morrison W, Glisson B, Trotti A, Ridge JA, Chao C, Peters G, Lee DJ, Leaf A, Ensley J, Cooper J (2003) Concurrent chemotherapy and radiotherapy for organ preservation in advanced laryngeal cancer. N Engl J Med 349(22):2091–2098

Ford EC, Kinahan PE, Hanlon L, Alessio A, Rajendran J, Schwartz DL, Phillips M (2006) Tumor delineation using PET in head and neck cancers: threshold contouring and lesion volumes. Med Phys 33(11):4280–4288

Fu KK, Pajak TF, Trotti A, Jones CU, Spencer SA, Phillips TL, Garden AS, Ridge JA, Cooper JS, Ang KK (2000) A Radiation Therapy Oncology Group (RTOG) phase III randomized study to compare hyperfractionation and two variants of accelerated fractionation to standard fractionation radiotherapy for head and neck squamous cell carcinomas: first report of RTOG 9003. Int J Radiat Oncol Biol Phys 48(1):7–16

Gandhi MR, Panizza B, Kennedy D (2011) Detecting and defining the anatomic extent of large nerve perineural spread of malignancy: comparing "targeted" MRI with the histologic findings following surgery. Head Neck 33(4):469–475

Garden AS, Weber RS, Ang KK, Morrison WH, Matre J, Peters LJ (1994) Postoperative radiation therapy for malignant tumors of minor salivary glands. Outcome and patterns of failure. Cancer 73(10):2563–2569

Geets X, Daisne JF, Tomsej M, Duprez T, Lonneux M, Gregoire V (2006) Impact of the type of imaging modality on target volumes delineation and dose distribution in pharyngo-laryngeal squamous cell carcinoma: comparison between pre- and per-treatment studies. Radiother Oncol 78(3):291–297

Geets X, Lee JA, Bol A, Lonneux M, Gregoire V (2007a) A gradient-based method for segmenting FDG-PET images: methodology and validation. Eur J Nucl Med Mol Imaging 34(9):1427–1438

Geets X, Tomsej M, Lee JA, Duprez T, Coche E, Cosnard G, Lonneux M, Gregoire V (2007b) Adaptive biological image-guided IMRT with anatomic and functional imaging in pharyngo-laryngeal tumors: impact on target volume delineation and dose distribution using helical tomotherapy. Radiother Oncol 85(1):105–115

Grant DG, Hinni ML, Salassa JR, Perry WC, Hayden RE, Casler JD (2009) Oropharyngeal cancer: a case for single modality treatment with transoral laser microsurgery. Arch Otolaryngol Head Neck Surg 135(12):1225–1230

Greco C, Nehmeh SA, Schoder H, Gonen M, Raphael B, Stambuk HE, Humm JL, Larson SM, Lee NY (2008) Evaluation of different methods of 18F-FDG-PET target volume delineation in the radiotherapy of head and neck cancer. Am J Clin Oncol 31(5):439–445

Gregoire V, Levendag P. DAHANCA, EORTC, GORTEC, NCIC and RTOG endorsed consensus guidelines for the delineation of the CTV in the N0 neck of patients with head & neck squamous cell carcinoma. http://www.rtog.org/CoreLab/ContouringAtlases/HN.aspx. Accessed 17 Dec 2012

Gregoire V, Coche E, Cosnard G, Hamoir M, Reychler H (2000) Selection and delineation of lymph node target volumes in head and neck conformal radiotherapy. Proposal for standardizing terminology and procedure based on the surgical experience. Radiother Oncol 56(2):135–150

Gregoire V, Jeraj R, Lee JA, O'Sullivan B (2012) Radiotherapy for head and neck tumours in 2012 and beyond: conformal, tailored, and adaptive? Lancet Oncol 13(7):e292–e300

Guido A, Fuccio L, Rombi B, Castellucci P, Cecconi A, Bunkheila F, Fuccio C, Spezi E, Angelini AL, Barbieri E (2009) Combined 18F-FDG-PET/CT imaging in radiotherapy target delineation for head-and-neck cancer. Int J Radiat Oncol Biol Phys 73(3):759–763

Haddad RI, Rabinowits G, Tishler RB, Adkins D, Khuri FJ, Clark J, Lorch JH, Limaye SA, Wirth LJ, O'Neill A, Riley S, Posner MR (2012) The PARADIGM trial: a phase III study comparing sequential therapy (ST) to concurrent chemoradiotherapy (CRT) in locally advanced head and neck cancer (LANHC). J Clin Oncol 30(Suppl):abstr 5501

Hanna E, Vural E, Prokopakis E, Carrau R, Snyderman C, Weissman J (2007) The sensitivity and specificity of high-resolution imaging in evaluating perineural spread of adenoid cystic carcinoma to the skull base. Arch Otolaryngol Head Neck Surg 133(6):541–545

Hansen EK, Bucci MK, Quivey JM, Weinberg V, Xia P (2006) Repeat CT imaging and replanning during the course of IMRT for head-and-neck cancer. Int J Radiat Oncol Biol Phys 64(2):355–362

Hasegawa Y, Matsuura H (1994) Retropharyngeal node dissection in cancer of the oropharynx and hypopharynx. Head Neck 16(2):173–180

Hendrickson K, Phillips M, Smith W, Peterson L, Krohn K, Rajendran J (2011) Hypoxia imaging with [F-18] FMISO-PET in head and neck cancer: potential for guiding intensity modulated radiation therapy in overcoming hypoxia-induced treatment resistance. Radiother Oncol 101(3):369–375

Ho KF, Marchant T, Moore C, Webster G, Rowbottom C, Penington H, Lee L, Yap B, Sykes A, Slevin N (2012) Monitoring dosimetric impact of weight loss with kilovoltage (kV) cone beam CT (CBCT) during parotid-sparing IMRT and concurrent chemotherapy. Int J Radiat Oncol Biol Phys 82(3):e375–e382

Hong TS, Tome WA, Harari PM (2012) Heterogeneity in head and neck IMRT target design and clinical practice. Radiother Oncol 103(1):92–98

Horiot JC, Le Fur R, N'Guyen T, Chenal C, Schraub S, Alfonsi S, Gardani G, Van Den Bogaert W, Danczak S, Bolla M et al (1992) Hyperfractionation versus conventional fractionation in oropharyngeal carcinoma: final analysis of a randomized trial of the EORTC cooperative group of radiotherapy. Radiother Oncol 25(4):231–241

Hsu IC, Lessard E, Weinberg V, Pouliot J (2004) Comparison of inverse planning simulated annealing and geometrical optimization for prostate high-dose-rate brachytherapy. Brachytherapy 3(3):147–152

Hunter KU, Schipper M, Feng FY, Lyden T, Haxer M, Murdoch-Kinch CA, Cornwall B, Lee CS, Chepeha DB, Eisbruch A (2013) Toxicities affecting quality of life after chemo-IMRT of oropharyngeal cancer: prospective study of patient-reported, observer-rated, and objective outcomes. Int J Radiat Oncol Biol Phys 85:935–940

Jensen K, Lambertsen K, Grau C (2007) Late swallowing dysfunction and dysphagia after radiotherapy for pharynx cancer: frequency, intensity and correlation with dose and volume parameters. Radiother Oncol 85(1):74–82

Kam MK, Leung SF, Zee B, Chau RM, Suen JJ, Mo F, Lai M, Ho R, Cheung KY, Yu BK, Chiu SK, Choi PH, Teo PM, Kwan WH, Chan AT (2007) Prospective randomized study of intensity-modulated radiotherapy on salivary gland function in early-stage nasopharyngeal carcinoma patients. J Clin Oncol 25(31):4873–4879

King AD, Ahuja AT, Leung SF, Lam WW, Teo P, Chan YL, Metreweli C (2000) Neck node metastases from nasopharyngeal carcinoma: MR imaging of patterns of disease. Head Neck 22(3):275–281

Langendijk JA, Doornaert P, Verdonck-de Leeuw IM, Leemans CR, Aaronson NK, Slotman BJ (2008) Impact of late treatment-related toxicity on quality of life among patients with head and neck cancer treated with radiotherapy. J Clin Oncol 26(22):3770–3776

Lauve A, Morris M, Schmidt-Ullrich R, Wu Q, Mohan R, Abayomi O, Buck D, Holdford D, Dawson K, Dinardo L, Reiter E (2004) Simultaneous integrated boost intensity-modulated radiotherapy for locally advanced head-and-neck squamous cell carcinomas: II–clinical results. Int J Radiat Oncol Biol Phys 60(2):374–387

Lee JA (2010) Segmentation of positron emission tomography images: some recommendations for target delineation in radiation oncology. Radiother Oncol 96(3): 302–307

Lee N, Chuang C, Quivey JM, Phillips TL, Akazawa P, Verhey LJ, Xia P (2002) Skin toxicity due to intensity-modulated radiotherapy for head-and-neck carcinoma. Int J Radiat Oncol Biol Phys 53(3):630–637

Lee N, Xia P, Fischbein NJ, Akazawa P, Akazawa C, Quivey JM (2003) Intensity-modulated radiation therapy for head-and-neck cancer: the UCSF experience focusing on target volume delineation. Int J Radiat Oncol Biol Phys 57(1):49–60

Lee C, Langen KM, Lu W, Haimerl J, Schnarr E, Ruchala KJ, Olivera GH, Meeks SL, Kupelian PA, Shellenberger TD, Manon RR (2008) Assessment of parotid gland dose changes during head and neck cancer radiotherapy using daily megavoltage computed tomography and deformable image registration. Int J Radiat Oncol Biol Phys 71(5):1563–1571

Lee IJ, Koom WS, Lee CG, Kim YB, Yoo SW, Keum KC, Kim GE, Choi EC, Cha IH (2009) Risk factors and dose-effect relationship for mandibular osteoradionecrosis in oral and oropharyngeal cancer patients. Int J Radiat Oncol Biol Phys 75(4):1084–1091

Lin A, Kim HM, Terrell JE, Dawson LA, Ship JA, Eisbruch A (2003) Quality of life after parotid-sparing IMRT for head-and-neck cancer: a prospective longitudinal study. Int J Radiat Oncol Biol Phys 57(1): 61–70

Lin Z, Mechalakos J, Nehmeh S, Schoder H, Lee N, Humm J, Ling CC (2008) The influence of changes in tumor hypoxia on dose-painting treatment plans based on 18F-FMISO positron emission tomography. Int J Radiat Oncol Biol Phys 70(4):1219–1228

Lindberg R (1972) Distribution of cervical lymph node metastases from squamous cell carcinoma of the upper respiratory and digestive tracts. Cancer 29(6): 1446–1449

Ling CC, Humm J, Larson S, Amols H, Fuks Z, Leibel S, Koutcher JA (2000) Towards multidimensional radiotherapy (MD-CRT): biological imaging and biological conformality. Int J Radiat Oncol Biol Phys 47(3): 551–560

Little M, Schipper M, Feng FY, Vineberg K, Cornwall C, Murdoch-Kinch CA, Eisbruch A (2012) Reducing xerostomia after chemo-IMRT for head-and-neck cancer: beyond sparing the parotid glands. Int J Radiat Oncol Biol Phys 83(3):1007–1014

Lloyd G, Lund VJ, Howard D, Savy L (2000) Optimum imaging for sinonasal malignancy. J Laryngol Otol 114(7):557–562

Loo H, Fairfoul J, Chakrabarti A, Dean JC, Benson RJ, Jefferies SJ, Burnet NG (2011) Tumour shrinkage and contour change during radiotherapy increase the dose to organs at risk but not the target volumes for head and neck cancer patients treated on the TomoTherapy HiArt system. Clin Oncol (R Coll Radiol) 23(1):40–47

Machtay M, Moughan J, Trotti A, Garden AS, Weber RS, Cooper JS, Forastiere A, Ang KK (2008) Factors associated with severe late toxicity after concurrent chemoradiation for locally advanced head and neck cancer: an RTOG analysis. J Clin Oncol 26(21): 3582–3589

Madani I, Duthoy W, Derie C, De Gersem W, Boterberg T, Saerens M, Jacobs F, Gregoire V, Lonneux M, Vakaet L, Vanderstraeten B, Bauters W, Bonte K, Thierens H, De Neve W (2007) Positron emission tomography-guided, focal-dose escalation using intensity-modulated radiotherapy for head and neck cancer. Int J Radiat Oncol Biol Phys 68(1):126–135

Madani I, Duprez F, Boterberg T, Van de Wiele C, Bonte K, Deron P, De Gersem W, Coghe M, De Neve W (2011) Maximum tolerated dose in a phase I trial on adaptive dose painting by numbers for head and neck cancer. Radiother Oncol 101(3):351–355

McLaughlin MP, Mendenhall WM, Mancuso AA, Parsons JT, McCarty PJ, Cassisi NJ, Stringer SP, Tart RP, Mukherji SK, Million RR (1995) Retropharyngeal adenopathy as a predictor of outcome in squamous cell carcinoma of the head and neck. Head Neck 17(3): 190–198

Million R (1994) Management of head and neck cancer: a multidisciplinary approach, 2nd edn. Lippincott, Philadelphia

Mukherji SK, Armao D, Joshi VM (2001) Cervical nodal metastases in squamous cell carcinoma of the head and neck: what to expect. Head Neck 23(11):995–1005

Murakami R, Uozumi H, Hirai T, Nishimura R, Katsuragawa S, Shiraishi S, Toya R, Tashiro K, Kawanaka K, Oya N, Tomiguchi S, Yamashita Y (2008) Impact of FDG-PET/CT fused imaging on tumor volume assessment of head-and-neck squamous cell carcinoma: intermethod and interobserver variations. Acta Radiol 49(6):693–699

Murdoch-Kinch CA, Kim HM, Vineberg KA, Ship JA, Eisbruch A (2008) Dose-effect relationships for the submandibular salivary glands and implications for their sparing by intensity modulated radiotherapy. Int J Radiat Oncol Biol Phys 72(2):373–382

Narayan S, Lehmann J, Coleman MA, Vaughan A, Yang CC, Enepekides D, Farwell G, Purdy JA, Laredo G, Nolan K, Pearson FS, Vijayakumar S (2008) Prospective evaluation to establish a dose response for clinical oral mucositis in patients undergoing head-and-neck conformal radiotherapy. Int J Radiat Oncol Biol Phys 72(3):756–762

Nehmeh SA, Lee NY, Schroder H, Squire O, Zanzonico PB, Erdi YE, Greco C, Mageras G, Pham HS, Larson SM, Ling CC, Humm JL (2008) Reproducibility of intratumor distribution of (18)F-fluoromisonidazole in head and neck cancer. Int J Radiat Oncol Biol Phys 70(1):235–242

Nemzek WR, Hecht S, Gandour-Edwards R, Donald P, McKennan K (1998) Perineural spread of head and neck tumors: how accurate is MR imaging? AJNR Am J Neuroradiol 19(4):701–706

Ng SH, Chang TC, Ko SF, Yen PS, Wan YL, Tang LM, Tsai MH (1997) Nasopharyngeal carcinoma: MRI and CT assessment. Neuroradiology 39(10):741–746

Nguyen NP, Vock J, Chi A, Ewell L, Vos P, Mills M, Khan R, Almeida F, Davis R, Betz M, Jang S, Gelumbauskas S, Vo RP, Vinh-Hung V (2012) Effectiveness of intensity-modulated and image-guided radiotherapy to spare the mandible from excessive radiation. Oral Oncol 48(7):653–657

Nowak PJ, Wijers OB, Lagerwaard FJ, Levendag PC (1999) A three-dimensional CT-based target definition for elective irradiation of the neck. Int J Radiat Oncol Biol Phys 45(1):33–39

Nutting CM, Morden JP, Harrington KJ, Urbano TG, Bhide SA, Clark C, Miles EA, Miah AB, Newbold K, Tanay M, Adab F, Jefferies SJ, Scrase C, Yap BK, A'Hern RP, Sydenham MA, Emson M, Hall E (2011) Parotid-sparing intensity modulated versus conventional radiotherapy in head and neck cancer (PARSPORT): a phase 3 multicentre randomised controlled trial. Lancet Oncol 12(2):127–136

O'Daniel JC, Garden AS, Schwartz DL, Wang H, Ang KK, Ahamad A, Rosenthal DI, Morrison WH, Asper JA, Zhang L, Tung SM, Mohan R, Dong L (2007) Parotid gland dose in intensity-modulated radiotherapy for head and neck cancer: is what you plan what you get? Int J Radiat Oncol Biol Phys 69(4): 1290–1296

Overgaard J, Hansen HS, Specht L, Overgaard M, Grau C, Andersen E, Bentzen J, Bastholt L, Hansen O, Johansen J, Andersen L, Evensen JF (2003) Five compared with six fractions per week of conventional radiotherapy of squamous-cell carcinoma of head and neck: DAHANCA 6 and 7 randomised controlled trial. Lancet 362(9388):933–940

Paulino AC, Koshy M, Howell R, Schuster D, Davis LW (2005) Comparison of CT- and FDG-PET-defined gross tumor volume in intensity-modulated radiotherapy for head-and-neck cancer. Int J Radiat Oncol Biol Phys 61(5):1385–1392

Pignon JP, le Maitre A, Maillard E, Bourhis J (2009) Meta-analysis of chemotherapy in head and neck cancer (MACH-NC): an update on 93 randomised trials and 17,346 patients. Radiother Oncol 92(1):4–14

Popovtzer A, Cao Y, Feng FY, Eisbruch A (2009) Anatomical changes in the pharyngeal constrictors after chemo-irradiation of head and neck cancer and their dose-effect relationships: MRI-based study. Radiother Oncol 93(3):510–515

Rajendran JG, Schwartz DL, O'Sullivan J, Peterson LM, Ng P, Scharnhorst J, Grierson JR, Krohn KA (2006) Tumor hypoxia imaging with [F-18] fluoromisonidazole positron emission tomography in head and neck cancer. Clin Cancer Res 12(18):5435–5441

Riegel AC, Berson AM, Destian S, Ng T, Tena LB, Mitnick RJ, Wong PS (2006) Variability of gross tumor volume delineation in head-and-neck cancer using CT and PET/CT fusion. Int J Radiat Oncol Biol Phys 65(3):726–732

Rischin D, Hicks RJ, Fisher R, Binns D, Corry J, Porceddu S, Peters LJ (2006) Prognostic significance of [18F]-misonidazole positron emission tomography-detected tumor hypoxia in patients with advanced head and neck cancer randomly assigned to chemoradiation with or without tirapazamine: a substudy of Trans-Tasman Radiation Oncology Group Study 98.02. J Clin Oncol 24(13):2098–2104

Robbins KT (1998) Classification of neck dissection: current concepts and future considerations. Otolaryngol Clin North Am 31(4):639–655

Robbins KT, Medina JE, Wolfe GT, Levine PA, Sessions RB, Pruet CW (1991) Standardizing neck dissection terminology. Official report of the Academy's Committee for Head and Neck Surgery and Oncology. Arch Otolaryngol Head Neck Surg 117(6):601–605

Rouvière H (1938) Lymphatic system of the head and neck (trans: Tobias M). Edward Brothers, Ann Arbor

Salama JK, Haddad RI, Kies MS, Busse PM, Dong L, Brizel DM, Eisbruch A, Tishler RB, Trotti AM, Garden AS (2009) Clinical practice guidance for radiotherapy planning after induction chemotherapy in locoregionally advanced head-and-neck cancer. Int J Radiat Oncol Biol Phys 75(3):725–733

Sanguineti G, Endres EJ, Gunn BG, Parker B (2006) Is there a "mucosa-sparing" benefit of IMRT for head-and-neck cancer? Int J Radiat Oncol Biol Phys 66(3):931–938

Schechter NR, Gillenwater AM, Byers RM, Garden AS, Morrison WH, Nguyen LN, Podoloff DA, Ang KK (2001) Can positron emission tomography improve the quality of care for head-and-neck cancer patients? Int J Radiat Oncol Biol Phys 51(1):4–9

Schinagl DA, Vogel WV, Hoffmann AL, van Dalen JA, Oyen WJ, Kaanders JH (2007) Comparison of five segmentation tools for 18F-fluoro-deoxy-glucose-positron emission tomography-based target volume definition in head and neck cancer. Int J Radiat Oncol Biol Phys 69(4):1282–1289

Schwartz DL, Garden AS, Thomas J, Chen Y, Zhang Y, Lewin J, Chambers MS, Dong L (2012) Adaptive radiotherapy for head-and-neck cancer: initial clinical outcomes from a prospective trial. Int J Radiat Oncol Biol Phys 83(3):986–993

Setton J, Caria N, Romanyshyn J, Koutcher L, Wolden SL, Zelefsky MJ, Rowan N, Sherman EJ, Fury MG, Pfister DG, Wong RJ, Shah JP, Kraus DH, Shi W, Zhang Z, Schupak KD, Gelblum DY, Rao SD, Lee NY (2012) Intensity-modulated radiotherapy in the treatment of oropharyngeal cancer: an update of the Memorial Sloan-Kettering Cancer Center experience. Int J Radiat Oncol Biol Phys 82(1):291–298

Shah JP, Strong E, Spiro RH, Vikram B (1981) Surgical grand rounds. Neck dissection: current status and future possibilities. Clin Bull 11(1):25–33

Shukla-Dave A, Lee NY, Jansen JF, Thaler HT, Stambuk HE, Fury MG, Patel SG, Moreira AL, Sherman E, Karimi S, Wang Y, Kraus D, Shah JP, Pfister DG, Koutcher JA (2012) Dynamic contrast-enhanced magnetic resonance imaging as a predictor of outcome in head-and-neck squamous cell carcinoma patients with nodal metastases. Int J Radiat Oncol Biol Phys 82(5):1837–1844

Som PM (1997) The present controversy over the imaging method of choice for evaluating the soft tissues of the neck. AJNR Am J Neuroradiol 18(10):1869–1872

Som PM, Curtin HD, Mancuso AA (1999) An imaging-based classification for the cervical nodes designed as an adjunct to recent clinically based nodal classifications. Arch Otolaryngol Head Neck Surg 125(4): 388–396

Soto DE, Kessler ML, Piert M, Eisbruch A (2008) Correlation between pretreatment FDG-PET biological target volume and anatomical location of failure after radiation therapy for head and neck cancers. Radiother Oncol 89(1):13–18

Spanos WJ Jr, Shukovsky LJ, Fletcher GH (1976) Time, dose, and tumor volume relationships in irradiation of squamous cell carcinomas of the base of the tongue. Cancer 37(6):2591–2599

Spencer C, Gay H, Haughey B, Nussenbaum B, Adkins D, Wildes T, Lewis JS, Thorstad WL (2012) Limiting high level 2 and contralateral retropharyngeal lymph node (RPN) treatment in selected patients with head-and-neck squamous cell carcinoma (HNSCC). Int J Radiat Oncol Biol Phys 84(3):S22

Studer G, Studer SP, Zwahlen RA, Huguenin P, Gratz KW, Lutolf UM, Glanzmann C (2006) Osteoradionecrosis of the mandible: minimized risk profile following intensity-modulated radiation therapy (IMRT). Strahlenther Onkol 182(5):283–288

Terhaard CH, Lubsen H, Rasch CR, Levendag PC, Kaanders HH, Tjho-Heslinga RE, van Den Ende PL, Burlage F (2005) The role of radiotherapy in the treatment of malignant salivary gland tumors. Int J Radiat Oncol Biol Phys 61(1):103–111

Terrell JE, Ronis DL, Fowler KE, Bradford CR, Chepeha DB, Prince ME, Teknos TN, Wolf GT, Duffy SA (2004) Clinical predictors of quality of life in patients with head and neck cancer. Arch Otolaryngol Head Neck Surg 130(4):401–408

Thiagarajan A, Caria N, Schoder H, Iyer NG, Wolden S, Wong RJ, Sherman E, Fury MG, Lee N (2012) Target volume delineation in oropharyngeal cancer: impact of PET, MRI, and physical examination. Int J Radiat Oncol Biol Phys 83(1):220–227

Thorwarth D, Eschmann SM, Paulsen F, Alber M (2007) A model of reoxygenation dynamics of head-and-neck tumors based on serial 18F-fluoromisonidazole positron emission tomography investigations. Int J Radiat Oncol Biol Phys 68(2):515–521

Tome WA, Fowler JF (2000) Selective boosting of tumor subvolumes. Int J Radiat Oncol Biol Phys 48(2):593–599

Tsai CJ, Hofstede TM, Sturgis EM, Garden AS, Lindberg ME, Wei Q, Tucker SL, Dong L (2013) Osteoradionecrosis and radiation dose to the mandible in patients with oropharyngeal cancer. Int J Radiat Oncol Biol Phys 85:415–420

van den Brekel MW, Castelijns JA, Snow GB (1996) Imaging of cervical lymphadenopathy. Neuroimaging Clin N Am 6(2):417–434

Vergeer MR, Doornaert PA, Rietveld DH, Leemans CR, Slotman BJ, Langendijk JA (2009) Intensity-modulated radiotherapy reduces radiation-induced morbidity and improves health-related quality of life: results of a nonrandomized prospective study using a standardized follow-up program. Int J Radiat Oncol Biol Phys 74(1):1–8

Vineberg KA, Eisbruch A, Coselmon MM, McShan DL, Kessler ML, Fraass BA (2002) Is uniform target dose possible in IMRT plans in the head and neck? Int J Radiat Oncol Biol Phys 52(5):1159–1172

Wang P, Popovtzer A, Eisbruch A, Cao Y (2012a) An approach to identify, from DCE MRI, significant subvolumes of tumors related to outcomes in advanced head-and-neck cancer. Med Phys 39(8):5277–5285

Wang ZH, Zhang SZ, Zhang ZY, Zhang CP, Hu HS, Tu WY, Kirwan J, Mendenhall WM (2012b) Protecting the oral mucosa in patients with oral tongue squamous cell carcinoma treated postoperatively with intensity-modulated radiotherapy: a randomized study. Laryngoscope 122(2):291–298

Weinstein GS, Quon H, Newman HJ, Chalian JA, Malloy K, Lin A, Desai A, Livolsi VA, Montone KT, Cohen KR, O'Malley BW (2012) Transoral robotic surgery alone for oropharyngeal cancer: an analysis of local control. Arch Otolaryngol Head Neck Surg 138(7):628–634

Wijers OB, Levendag PC, Tan T, van Dieren EB, van Sornsen de Koste J, van der Est H, Senan S, Nowak PJ (1999) A simplified CT-based definition of the lymph node levels in the node negative neck. Radiother Oncol 52(1):35–42

Wu Q, Manning M, Schmidt-Ullrich R, Mohan R (2000) The potential for sparing of parotids and escalation of biologically effective dose with intensity-modulated radiation treatments of head and neck cancers: a treatment design study. Int J Radiat Oncol Biol Phys 46(1):195–205

Wu Q, Chi Y, Chen PY, Krauss DJ, Yan D, Martinez A (2009) Adaptive replanning strategies accounting for shrinkage in head and neck IMRT. Int J Radiat Oncol Biol Phys 75(3):924–932

Yao M, Dornfeld KJ, Buatti JM, Skwarchuk M, Tan H, Nguyen T, Wacha J, Bayouth JE, Funk GF, Smith RB, Graham SM, Chang K, Hoffman HT (2005) Intensity-modulated radiation treatment for head-and-neck squamous cell carcinoma–the University of Iowa experience. Int J Radiat Oncol Biol Phys 63(2): 410–421

Zaidi H, Vees H, Wissmeyer M (2009) Molecular PET/CT imaging-guided radiation therapy treatment planning. Acad Radiol 16(9):1108–1133

Lung Cancer

5

Ursula Nestle, Sonja Adebahr,
and Tanja Schimek-Jasch

Contents

U. Nestle (✉) • S. Adebahr • T. Schimek-Jasch
Department of Radiation Oncology,
Medical Center - University of Freiburg,
Freiburg, Germany
e-mail: ursula.nestle@uniklinik-freiburg.de

5.1 Introduction

Lung cancer is still the most frequent malignancy around the world, and radiotherapy together with surgery and systemic therapy is a key modality in the curative treatment of both non-small cell lung cancer (NSCLC) and small cell lung cancer (SCLC). Due to modern effective screening and staging methods, the selection of patients with curative treatment options has improved. In times of increasingly precise radiotherapy techniques, accurate target and normal tissue delineation belong to the tools which guarantee the maximum chance of long-term survival along with acceptable side effects. Systematic errors, introduced by incorrect delineation of GTV (gross tumour volume), CTV (clinical target volume), necessary margins and normal tissues, will significantly reduce the probability of local tumour control and normal tissue sparing.

During the last decade, radiotherapy techniques have significantly improved (Bentzen et al. 2008), including the development of intensity-modulated radiotherapy (IMRT) and image-guided radiotherapy (IGRT) with on-site imaging and treatment verification techniques (e.g. cone-beam CT and MV-CT, kV imaging), the incorporation of imaging such as 4D CT and positron emission tomography (PET-CT) and the use of more accurate dose calculation algorithms (e.g. type B algorithms, Monte Carlo methods). These techniques allow for increased accuracy of dose delivery (e.g. stereotactic body radiotherapy) and

A.-L. Grosu, C. Nieder (eds.), *Target Volume Definition in Radiation Oncology*,
DOI 10.1007/978-3-662-45934-8_5, © Springer-Verlag Berlin Heidelberg 2015

also for adaptive radiotherapy techniques based on morphologic and pathophysiologic changes. High cure rates can now be achieved with SBRT in patients with early disease, which is motivating towards further optimisation of other techniques to also improve the outcome of NSCLC patients with more advanced disease.

For locally advanced SCLC, concurrent radiochemotherapy has been adopted as standard (Auperin et al. 2010; Pijls-Johannesma et al. 2007). Using modern target volume and application concepts, the necessary doses, even if applied simultaneously with toxic chemotherapy, can be given far more often as compared to 10 years ago (Liao et al. 2010).

Overall, the three prerequisites for successful modern radiotherapy of lung cancer patients are:

1. Accurately delineated GTVs and clear CTV concepts
2. Delivery of sufficient radiation dose, as has convincingly been shown in SBRT (Guckenberger et al. 2013)
3. Cautious handling of normal tissues in the setting of high-dose hypofractionation

This chapter will highlight some aspects of practical importance for target volume and normal tissue delineation in the context of radiotherapy planning for lung cancer patients.

5.2 Anatomy

The challenge of radiotherapy in the chest is characterised by the necessity to deliver high doses of radiation to malignant sites, which are surrounded or neighboured by large volumes of rather radiosensitive but healthy lung parenchyma. Furthermore, the cooperation and communication between imaging specialist, surgeon and radiation oncologist in order to provide optimal care and avoid geographic miss of target volumes remains an interdisciplinary challenge.

5.2.1 Mediastinal Lymphatics

Lung tumours usually arise either in or near to the central bronchial system or in the peripheral lung tissue, all having their lymphatic drainage via the mediastinum. For staging, treatment decision and target volume delineation purposes, solid knowledge about the classification and diagnostic procedures of the mediastinum is essential.

Unfortunately, the lymphatic drainage of lung tumours through the mediastinum varies, and beyond individually different anatomical routes, it may be hampered by pre-existing comorbidities like COPD and former inflammatory disease, leading to variations in the drainage with skip lesions and unexpected contralateral spread. Therefore, meticulous mediastinal staging by imaging and invasive methods is mandatory before any curative intended treatment of a lung cancer patient.

Most of the mediastinal drainages ultimately reach the upper mediastinum and the right supraclavicular fossa, which means that the right-sided tumours usually drain via the right hilar and paratracheal nodes, whereas the left-sided tumours may soon drain via the contralateral side (LoCicero et al. 2005). The mediastinal staging may be done non-invasively by CT, FDG-PET or FDG-PET/CT, leading to a high sensitivity but relatively lower specificity in the diagnosis of lymph node metastases (see paragraph “imaging” below). Therefore, imaging findings suggestive for mediastinal lymph node metastases need to be confirmed by invasive staging if they are crucial for treatment decisions (e.g. pro/contra resection). For invasive staging, beyond the former gold standard mediastinoscopy, transbronchial fine-needle aspiration (FNA), endoscopic oesophageal ultrasound-guided FNA (EUS-FNA) and endobronchial ultrasound-guided FNA (EBUS-FNA) have been established (De Leyn et al. 2006) in recent years, with improving test sensitivity and specificity (Tofts et al. 2013). However, it should be clear that none of the invasive methods are able to investigate all nodal stations of the mediastinum and that all methods suffer from a certain observer bias related to biopsy success, which may reduce their sensitivity (Table 5.1) in comparison to literature data (Tofts et al. 2013). Furthermore, biopsies are usually only taken from treatment-relevant areas and not from all areas which could be reached by the respective method.

Table 5.1 Mediastinal lymph node stations and their accessibility for biopsy

AJCC/UICC lymph node classification by Mountain and Dresler			Laterality	Localisation (for detailed description, see Chapet et al. 2005)	Accessible by	
					EBUS-FNA	Mediastinoscopy
Superior mediastinal nodes	Highest mediastinal	1	R/L	Upper limit sternal notch, above brachiocephalic (left innominate) vein	Yes	Yes
	Upper paratracheal	2	R/L	Below lymph node station 1, above top of aortic arch. Located posteriorly the great vessels and anteriorly the trachea	Yes	Yes
	Prevascular/retrosternal	3A	Bilateral	Upper limit sternal notch, lower limit carina. Located posteriorly the sternum and anteriorly the great arteries	No	No
	Retrotracheal	3P	Bilateral	Upper and lower limit as for 3A. Located posteriorly of the trachea and until 1 cm ventral of vertebral bodies	No	No
	Lower paratracheal	4	R/L	Upper limit top of aortic arch, lower limit top of upper lobe bronchus	Yes	Yes
Aortic nodes	Subaortic (aortopulmonary window)	5	L	Lateral to aorta/ligamentum arteriosum/left pulmonary artery and proximal to first branch of pulmonary artery	No	No
	Para-aortic (ascending aorta or phrenic nerve)	6	Bilateral	Anterior and lateral to ascending aorta and aortic arch or the innominate artery	No	No
Inferior mediastinal nodes	Subcarinal	7	Bilateral	Caudal the tracheal carina, not associated with lower lobe bronchi or arteries	Yes (anterior)	Yes (anterior/ posterior)
	Paraoesophageal	8	Bilateral	Adjoining the oesophageal wall and bilateral the midline, excluding subcarinal nodes	No	No
	Pulmonary ligament	9		Within the pulmonary ligament	No	No
N1 nodes	Hilar	10	R, peribronchial; L, trachea-bronchial	Proximal lobar, distal to mediastinal pleural reflection and nodes adjacent to bronchus intermedius right	Yes	No
	Interlobular	11	R/L	Intrapulmonary, between the lobar bronchi	Yes	No
	Lobular	12	R/L	Adjacent to distal lobar bronchi	Yes	No
	Segmental	13	R/L	Adjacent to segmental bronchi	Yes	No
	Subsegmental	14	R/L	Adjacent to subsegmental bronchi	Yes	No

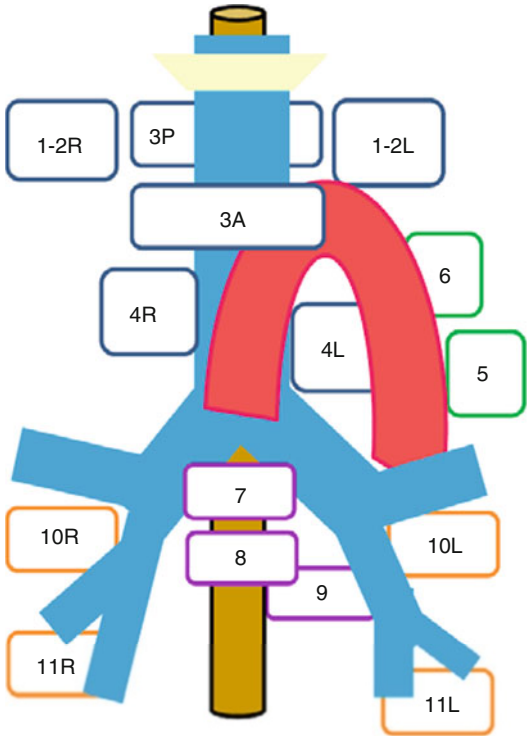

Fig. 5.1 Schematic illustration of the main Mountain-Dresler lymph node stations

Concerning the communication of biopsy findings, in comparison to imaging, postoperative staging and transfer into target volumes, the anatomical classification of nodal stations originally proposed by Mountain and Dresler (1997) is of great help. Its standardised use in a lung cancer treatment facility will improve patients' outcome, as it will help to avoid geographical miss. An overview of the Mountain-Dresler stations is displayed in Table 5.1 and Fig. 5.1. For radiotherapy treatment planning purposes, a very helpful interdisciplinary atlas has been provided by the University of Michigan (Chapet et al. 2005), describing detailed anatomical borders for all relevant nodal stations.

5.2.2 Normal Tissues

Normal tissues in the chest, including the healthy lungs, oesophagus, heart, brachial plexus and spinal cord, are often limiting the dose of radiotherapy. These dosimetric limits globally guide daily practice, but delineation itself is often not standardised between institutions. Some research groups like the EORTC and RTOG have therefore initiated standardisation of OAR delineation within their protocols. Evaluation of planning data has shown that the effect of varying OAR delineations on treatment planning can be significant and will influence treatment decisions and outcome both in clinical trials and daily routine practice (Collier et al. 2003). In this context, delineation atlases have been published, which provide guidelines for normal tissue contouring (Kong et al. 2011; Feng et al. 2011).

Standardised delineation is clearly linked to the use of guideline dose/volume restrictions for treatment plan optimisation and evaluation. Most reliable data hereon can be derived from the QUANTEC reviews (see below) and actual treatment protocols, as shown in Table 5.2 for conventional fractionated radiotherapy and in Table 5.3 for SBRT.

5.2.2.1 Lung

The lung is the largest and the most radiosensitive organ in the chest and thus it is frequently the dose-limiting organ. Numerous publications have addressed the importance of dosimetric and clinical parameters in the context of radiation-induced lung toxicity (RILD) (Marks et al. 2010). This disease appears in two phases with an acute phase within several weeks after treatment initiation, followed by an irreversible fibrosis which usually appears weeks to months after radiotherapy. Both may be life threatening and only symptomatic treatment is available. For the prediction of toxicity, clear dose-response and volume and fractionation effects have been shown, and multiple clinical factors like age, smoking habits and chemotherapy are known to influence the risk. However, the clinical factors do not adequately characterise patients at high risk for RILD (Dehing-Oberije et al. 2009), and therefore most groups use radiotherapy-derived parameters as surrogates, in order to adjust the radiotherapy plans. Among these, most commonly used are V20 (representing the relative lung volume receiving more than 20 Gy) and the mean lung dose (MLD). It should be noted that although

Table 5.2 Dose constraints for normal tissues in the chest as used for conventional radiotherapy (fraction dose 1.8–2.0 Gy) according to study protocols and literature reports

Lung		**Sources**
V20 Gy (for lungs minus GTV)	≤30–35 %	QUANTEC (Marks et al. 2010)
	≤35 %	PET-Plan[a]
V20 Gy (for lungs minus CTV)	≤37 %	RTOG 0617[a]
V20 Gy (for lungs minus PTV)	≤30 %	RTOG 0117[a]
	≤35 %	Convert[a]
	≤31 % after lobectomy	LungART[a]
	≤22 % after pneumectomy	
V20 Gy (combined lung volume)	<35 %	RTOG 0972/CALGB 36050[a]
Mean lung dose (MLD) (for lungs minus GTV)	≤20–23 Gy	QUANTEC (Marks et al. 2010)
	<20 Gy	PET-Plan,[a] PET-Boost[a]
Mean lung dose (MLD) (for lungs minus CTV)	≤20 Gy	RTOG 0617[a]
V5 Gy	≤65 %	Jo et al. (2014)
Oesophagus		**Sources**
Mean oesophageal dose (MED)	≤34 Gy	RTOG 0117[a]
		RTOG 0617[a]
		PET-Plan[a]
V35 Gy	<80 %	PET-Boost[a]
V55 Gy	≤30 %	RTOG 0117[a]
		PET-Plan[a]
Volume dose	>40–50 Gy: risk of acute oesophagitis	QUANTEC (Werner-Wasik et al. 2010)
Maximum dose (segment)	74 Gy	QUANTEC (Werner-Wasik et al. 2010)
Heart		**Sources**
Whole organ	≤40 Gy	RTOG 0117[a], RTOG 0617[a]
V25 Gy	<10 % (<1 % risk of cardiac mortality)	QUANTEC (Gagliardi et al. 2010)
V35 Gy	≤30 %	LungART[a]
V40 Gy	≤50 %	PET-Plan[a]
V45 Gy	<2/3 of heart	RTOG 0617[a]
V60 Gy	<1/3 of heart	
V50%	<33 Gy	Convert[a]
	≤50 % of total (PTV) dose	
Maximum dose	0.5 cc ≤76 Gy	PET-Boost[a]
Spinal cord		**Sources**
Maximum point dose (0.5 cc)	≤45 Gy	RTOG 0117[a]
		LungART[a]
	≤48 Gy	Convert[a]
		PET-Plan[a]
	≤50 Gy	RTOG 0972/CALGB 36050[a]
	≤50.5 Gy	RTOG 0617[a]
	≤51 Gy	PET-Boost[a]
Risk of myelopathy by dose (full-thickness cord including cord cross section)	50 Gy: 0.2 %	QUANTEC (Kirkpatrick et al. 2010)
	54 Gy <1 %	
	60 Gy: 6 %	
	61 Gy <10 %	
	69 Gy: 50 %	
Brachial plexus		**Sources**
Maximum point dose	≤60 Gy	Forquer et al. (2009)
	≤66 Gy	PET-Boost[a]

[a]Study protocols

Table 5.3 Dose constraints for normal tissues in the chest as used for stereotactic body radiotherapy (SBRT; fraction dose >5 Gy) according to study protocols and literature reports

Lung			**Sources**
Volume constraints (for lungs minus GTV)	<1,500 cc V12.5 Gy	5 fx	RTOG 0813
	<1,000 cc V13.5 Gy	5 fx	
V20 Gy	≤10 %	3 fx	RTOG 0618
Oesophagus			**Sources**
Maximum dose/volume constraints	≤27 Gy	3 fx	RTOG 0618[a]
	1 cc ≤24 Gy (3 fx)	3 fx	ROSEL[a]
	1 cc ≤27 Gy	5 fx	
	<5 cc≤V27.5 Gy (nonadjacent wall)	5 fx	RTOG 0813[a]
	0.5 cc ≤40 Gy	8 fx	EORTC 22113-08113 LungTech[a]
Heart (or pericardium)			**Sources**
Maximum dose/volume constraints	≤30 Gy	3 fx	RTOG 0618[a]
	1 cc ≤24 Gy	3 fx	ROSEL[a]
	1 cc ≤27 Gy	5 fx	
	<15 cc≤V32 Gy	5 fx	RTOG 0813[a]
	0.5 cc 63 Gy	8 fx	EORTC 22113-08113 LungTech[a]
Spinal cord			**Sources**
	≤18 Gy	3 fx	RTOG 0618[a]
	Any point ≤18 Gy	3 fx	ROSEL[a]
	Any point ≤25 Gy	5 fx	
	30 Gy	5 fx	RTOG 0813[a]
	<0.25 cc≤V22.5 Gy		
	<0.5 cc≤V13.5 Gy		
	0.5 cc 32 Gy	8 fx	EORTC 22113-08113 LungTech[a]
Brachial plexus (ipsilateral)			**Sources**
Maximum dose/volume constraints	≤24 Gy	3 fx	RTOG 0618[a]
	1 cc ≤24 Gy	3 fx	ROSEL[a]
	1 cc ≤27 Gy	5 fx	
	<3 cc≤V30 Gy	5 fx	RTOG 0813[a]
	≤32 Gy		
	0.5 cc 38 Gy	8 fx	EORTC 22113-08113 LungTech[a]
	≤1 cc 15 Gy	1 fx	Forquer et al. (2009)
	≤1 cc 19 Gy	2 fx	
	≤1 cc 22.95 Gy	3 fx	
	≤1 cc 27 Gy	4 fx	
	≤1 cc 31 Gy	5 fx	
	≤1 cc 33.3 Gy	6 fx	
Chest wall			**Sources**
Maximum dose	<30 cc V30 Gy	3–5 fx	Dunlap et al. (2010)
Skin			**Sources**
Maximum dose any point	≤24 Gy	3 fx	RTOG 0618[a]
Great vessels			*Sources*
Volume dose maximum	>10 cc≤V47 Gy	5 fx	RTOG 0813[a]
Trachea and main stem bronchus			**Sources**
Maximum dose	≤30 Gy	3 fx	RTOG 0618[a]
	1 cc ≤30 Gy	3 fx	ROSEL[a]
	1 cc ≤32 Gy	5 fx	
	<4 cc (nonadjacent wall)≤V18 Gy	5 fx	RTOG 0813[a]
	0.5 cc 44 Gy	8 fx	EORTC 22113-08113 LungTech[a]

[a]Study protocols

certain levels (e.g. V20 <35 % or MLD <20 Gy; see Tables 5.2 and 5.3) have been considered "safe", a relevant proportion of patients may still develop severe RILD after lower doses (De Ruysscher et al. 2010).

Furthermore, most toxicity data are derived from conventional 3D conformal radiotherapy, and solid data are lacking relating dosimetric parameters from modern IMRT techniques to toxicity. In this context, it has been suspected that large lung volumes receiving low doses of irradiation may be at risk for RILD (Kristensen et al. 2009). Some groups have therefore recommended a restriction of the V5 (lung volume receiving more than 5 Gy) to, for example, 65 % (Jo et al. 2014).

For a reasonable use of dosimetric parameters, delineation of the lungs should be institutionally standardised. The volumes delineated should include both lungs (separately and jointly) minus the GTV and should exclude air spaces that do not contain lung tissue (like the trachea and main bronchi) and also the free air outside the lung. When automatic contouring algorithms are used, their results must be carefully checked before radiation plan optimisation to assure lower recessus inclusion, to correct erroneous exclusion of lung volumes with increased density or to identify incorrect addition of right and left lungs.

5.2.2.2 Oesophagus

When treating mediastinal pathology with escalating doses, the importance of the oesophagus as a critical structure may even outpace the lungs. This is because in a serial normal tissue (as the oesophagus), small volume of late sequelae like ulcers and fistulae may completely compromise otherwise beneficial treatment effects.

According to a large body of literature, e.g. the QUANTEC data (Werner-Wasik et al. 2010), transient grade 3–4 oesophagitis is rare (<5 %) with conventionally fractionated radiotherapy alone but may rise up to 30 % in the context of concurrent radiochemotherapy for locally advanced NSCLC (Werner-Wasik et al. 2010; De Ruysscher et al. 2007). Multiple parameters, e.g. the mean oesophageal dose (MED), V20, V35, V50, etc., have been shown to correlate with the incidence of oesophagitis (Werner-Wasik et al. 2010; De Ruysscher et al. 2007), of which the most robust parameter may be the MED (Table 5.2). Fortunately, grade 3–4 oesophagitis generally heals within weeks after radio(chemo)therapy, and severe late effects will only occur in less than 1 % of cases. Therefore, the possibility to deliver curative radiochemotherapy should be generally prioritised over the avoidance of acute oesophagitis. In this context, current recommendations allow a rather high risk of acute oesophageal reactions.

In times of SBRT moving more close to the mediastinum, the risk of severe late oesophageal toxicity like strictures, fistulae and ulcers after hypofractionated high-dose radiotherapy will be an issue (Table 5.3). Until now, there are only retrospective estimates and case reports (Onimaru et al. 2003; Senthi et al. 2013) advocating caution with high hypofractionated doses applied to the oesophagus and calling for prospective clinical data collection.

For delineation, the oesophagus is a challenging organ with shifting morphological borders (related to deglutition and various filling) resulting in a large interobserver contour variability (Collier et al. 2003). The organ should be contoured using mediastinal windowing on CT including the mucosa, submucosa and all muscular layers out to the fatty adventitia. To assure accurate use of dose/volume data for planning optimisation, the oesophagus should always be delineated from the cricoid cartilage to the gastric entrance. The identification of the organ may be eased by searching for air-filled parts of the lumen and by the interpolation of contours in order to bridge areas of difficult detectability. Furthermore, side by side reviews of the diagnostic CT scans can be of help. Barium swallows with the planning CT have also been recommended, although this could affect the dose computation and change the anatomic shape of the organ. For standardisation of oesophagus contouring, again the use of an atlas like that of the University of Michigan (Kong et al. 2011) is recommended.

5.2.2.3 Heart

The heart, whose radiosensitivity has been neglected for decades, is a complex organ with several anatomical subvolumes resulting in various

and mainly late radiation-induced changes. Presently, there is only limited data relating dosimetric parameters with cardiac toxicity in patients with lung cancer (Gagliardi et al. 2010). Clinical factors like age, cardiovascular risk factors and comorbidities appear to increase the risk of injury.

Radiotherapy involving the heart has been shown to lead to a measurable increase in the risk of coronary artery disease (CAD) in breast cancer patients. In a prognostically favourable cohort of 2,168 patients with a mean heart dose of 4.9 Gy, this risk starts already at very low doses with an increase of the risk of 7.4 % per Gy mean heart dose (Darby et al. 2013). Beyond CAD, other late effects like pericarditis, myocardial failure and valve dysfunction have been described (Gagliardi et al. 2010). Early effects may show up as arrhythmias. According to the QUANTEC review (Gagliardi et al. 2010), in the context of partial irradiation, conservative (NTCP) model-based estimates predict that a V25 Gy <10 % (in 2 Gy per fraction) will be associated with a <1 % probability of cardiac mortality until 15 years after RT. However, the data supporting these figures have lots of weaknesses, among others the fact that they are all derived from the 2D or 3D planning era and that no subvolume informations are available. Therefore, the generation of prospective dose volume data with subvolume reporting in the situation of modern IMRT techniques will lead to a more solid estimation of risks and more robust dosimetric parameters for plan optimisation and evaluation. Present recommendations for planning restrictions concerning the heart in lung cancer patients are given in Tables 5.2 and 5.3 for conventional fractionation and SBRT, respectively.

For the delineation of the heart, various strategies have been followed. Currently, contouring of the whole organ including the pericardium and the base of the organ is widely recommended, while isolated contouring of the left ventricle as the "only relevant structure" should be regarded obsolete. Contouring should start just below the level in which the pulmonary trunk branches into the left and right pulmonary artery and end inferiorly where the heart blends with the diaphragm (the heart apex). Even if there is no heart muscle visible within the pericardium, this should be included in the contours, as cardiac vessels run in the fatty tissue (Feng et al. 2011). In order to generate data for subvolume effects, the additional contouring of certain subvolumes like the coronary arteries or the valves followed by toxicity evaluation will be of great help.

For contouring the whole organ in clinical routine, again an atlas published by the University of Michigan is a useful tool (Feng et al. 2011).

5.2.2.4 Spinal Cord

The spinal cord tolerance, like in other organs, is a sliding scale, complicated by the fact that due to extremely careful prescriptions, reports on radiotherapy-induced spinal toxicity are very rare. The estimated risk of myelopathy to the full-thickness cord is <1 % after 54 Gy and <10 % after 61 Gy of conventionally fractionated radiotherapy (Kirkpatrick et al. 2010). Among the factors that are most commonly described to influence the incidence of myelopathy are dose, fractionation and treated volume (Tables 5.2 and 5.3). Unfortunately, the symptomatic treatment currently available for spinal cord radiation-induced toxicity is nonspecific and of limited efficacy. Due to the very severe impairment of quality of life by radiation-induced myelitis, tight restrictions of the maximum dose are standard for treatment planning and evaluation (Tables 5.2 and 5.3).

In lung cancer patients, the challenge of re-irradiation may arise. Concerning the spinal cord, solid literature-based recommendations by Nieder et al. are available (Nieder et al. 2006). In their analysis, no case of radiation myelopathy was observed, when the BED of each RT series was below 98 Gy_2, with cumulative BED below 120 Gy_2 (i.e. 60 Gy/2 Gy), and a minimum interval of 6 months had been respected between RT series.

For a safe contouring of the spinal cord, which may not be clearly depicted by the planning CT and whose position within the spinal canal may vary, the bony limits of the spinal canal are considered suitable landmarks. They should be used for routine contouring as most of the published clinical data refer to this kind of reference. With IMRT, the spinal canal should be contoured through the entire planning CT, in order to avoid

spinal cord radiation from a direction which may not be accounted for by the radiation oncologist.

5.2.2.5 Brachial Plexus

Neurotoxicity of the brachial plexus has been more often described among patients with breast cancer (Delanian et al. 2012) who received radiotherapy, but some reports are also available for lung cancer patients leading to the current recommendation to restrict the maximum dose to 66 Gy in conventional fractionation (Table 5.2). Forquer et al. (2009) reported stereotactic body radiotherapy for apical lesions carrying a risk of brachial plexopathy. In their analysis, different grades of brachial plexopathies were noticed in 7/37 patients who received SBRT for apical lung malignancy. Based on these data, the authors suggested to restrict the maximal brachial plexus dose to less than 27 Gy, delivered in 3–4 fractions (Table 5.3). However, there may be cases where even a relatively high risk of a brachial plexus toxicity may be acceptable in order to achieve tumour control.

Contouring of the brachial plexus remains a challenge, due to poor visualisation on planning CTs and significant changes in regional morphology related to arm positioning. Contouring techniques and landmarks have been previously described in the University of Michigan atlas (Kong et al. 2011). Generally, the brachial plexus is situated within the fatty tissue between scalene musculature and subclavian vessels extending in craniocaudal direction from C4/C5 to T1/T2 nerve roots.

5.2.2.6 Chest Wall

Unlike the situation in conventional radiotherapy of lung cancer where chest wall toxicity is negligible, in SBRT the chest wall and ribs are considered organs at risk. In an analysis of 46 consecutive patients, Taremi et al. identified dose, age and female gender as risk factors for the development of chest wall toxicity after SBRT (Taremi et al. 2012). Approximately 5 % of patients will suffer from rib fractures after 3×9 Gy given to a 2 cm^3 chest wall volume (Pettersson et al. 2009). Therefore a dose of less than 30 Gy, delivered in 3–5 fractions on less than 30 cm^3, has been recommended, to limit chest wall toxicity (Dunlap et al. 2010).

The chest wall should be delineated including the ribs and intercostal muscles but excluding the other muscles and skin. If possible it may be auto-segmented starting from the corrected lung edges with a 2 cm expansion in anterior, posterior and lateral directions (Kong et al. 2011).

5.2.2.7 Central Mediastinal Structures in SBRT

Beyond the oesophagus and heart, in times of high-dose hypofractionated radiotherapy moving closer to the midline structures, organs will be at risk, whose toxicity has not played a major role in times of conventional fractionation. The observation of severe bronchial stenosis and fistula as late as >2 years after >80 Gy (Miller et al. 2005) and a high rate of fatal toxicities after SBRT to central tumours (Timmerman et al. 2006) have led to a "no-fly zone" of 2 cm around the bronchial tree. However, the beneficial results of SBRT to peripheral lung tumours call for the propagation of these concepts also for central tumours. The VU Amsterdam group has published a thorough review of reported toxicities after SBRT of central tumours showing a rate of 8.6 % grade III/IV toxicity and a 2.7 % rate of treatment-related mortality (Senthi et al. 2013). However, due to the retrospective character of this study and multiple confounding comorbidities in patient cohorts, the risk of severe toxicity may be underestimated (Nestle et al. 2013). At present, no clear constraints for central mediastinal structures can therefore be given except historical estimates and those which are presently included in several ongoing international multicentre trials on this question (e.g. EORTC 22113-08113 LungTech or RTOG 0813; Table 5.3). The final results of these large studies are expected to provide a better insight into the outcome and toxicity of such treatment concepts.

5.3 Pathology of Tumour Spread

The most recent 7th edition of TNM and ISS classification for lung cancer (Goldstraw et al. 2007) is proposing a complex description of the primary tumour according to its size, location and multicentricity. For regional nodal involvement, ipsi- or contralaterality of metastatic nodes

Table 5.4 TNM classification for lung cancer (7th edition; 2009)

Primary tumour (T)	
T1	Tumour 3 cm or smaller and surrounded by lung or visceral pleura or endobronchial tumour distal to the lobar bronchus, without bronchoscopic evidence of invasion more proximal than the lobar bronchus (i.e. not in the main bronchus)
	T1a: tumour ≤2 cm
	T1b: tumour >2 cm and ≤3 cm
T2	Tumour greater than 3 and up to 7 cm
	T2a: tumour >3 cm and ≤5 cm
	T2b: tumour >5 cm and ≤7 cm
	or
	Invasion of the visceral pleura
	Atelectasis or obstructive pneumonitis that extends to the hilar region but involves less than the entire lung
	Involvement of the main bronchus ≥2 cm or more distal to the carina
T3	Tumour greater than 7 cm
	or
	Tumour with atelectasis or obstructive pneumonitis of the entire lung
	Tumour in the main bronchus within 2 cm of the carina but without involvement of the carina
	Tumour invasion of nonvital structures such as the parietal pleural chest wall (including superior sulcus tumours), mediastinal pleura, diaphragm, phrenic nerve, parietal pericardium
	Separate tumour nodule(s) in the same lobe as the primary tumour
T4	Tumour of any size with
	Invasion of (vital) mediastinal structures: mediastinum, heart, trachea, oesophagus, great vessels, recurrent laryngeal nerve, carina or vertebral body
	Separate tumour nodule(s) in a different ipsilateral lobe to that of the primary tumour
Lymph node metastases (N)	
N0	No locoregional lymph node metastases
N1	Ipsilateral peribronchial and/or ipsilateral hilar nodes and/or intrapulmonary nodes and/or involvement of lymph node regions by direct invasion of primary tumour
N2	Ipsilateral mediastinal and/or subcarinal lymph node metastases
N3	Contralateral mediastinal, contralateral hilar, ipsilateral or contralateral scalene or supraclavicular lymph node metastases
Distant metastasis (M)	
M0	No distant metastasis
M1	Distant metastasis
	M1a: Separate tumour nodule(s) in a contralateral lobe or tumour with pleural nodules or malignant pleural or pericardial effusion
	M1b: Distant metastasis (in extrathoracic organs)

with respect to the primary tumour remains preeminent, while M staging has also been revised to better reflect treatment options (Tables 5.4 and 5.5). An additional classification to account for nodal size and diagnostic pathways has been proposed by Robinson and Ruckdeschel, refining N2 lymph node staging (Robinson et al. 2007). This subclassification of locally advanced disease has proved relevant for the therapy decision-making: surgical resection and neoadjuvant or definitive radiochemotherapy (Table 5.6).

According to actual recommendations (Goeckenjan et al. 2010), staging of small cell lung cancer should also follow the TNM categories. The treatment-relevant distinction between "limited" and "extensive" disease, for which multiple definitions have been proposed in the past, should nowadays be made by M0 vs. M1 stage, i.e. between UICC stages III and IV.

The T, N and M categories, ISS stages and Robinson classification of stage IIIA N2 for lung cancer are shown in Tables 5.4, 5.5 and 5.6.

Table 5.5 ISS stage and TNM

ISS	TNM
I a	T1a N0 M0
	T1b N0 M0
I b	T2a N0 M0
II a	T1a N1 M0
	T1b N1 M0
	T2a N1 M0
	T2b N0 M0
II b	T2b N1 M0
	T3 N0 M0 including separate tumour nodule(s) in the same lobe as the primary tumour
III a	T4 N0–1 M0 including separate tumour nodule(s) in the ipsilateral lung but not in the same lobe as the primary tumour
	T3 N1 M0 including separate tumour nodule(s) in the same lobe as the primary tumour
	T1–3 N2 M0 including separate tumour nodule(s) in the same lobe as the primary tumour
III b	T3 N3 M0 including separate tumour nodule(s) in the same lobe as the primary tumour
	T4 N2 M0 including separate tumour nodule(s) in the ipsilateral lung as the primary tumour
	Any T, N3 M0
IV	Any T, any N, M1a–b including malignant pleural or pericardial effusion

Table 5.6 Subclassification of stage IIIA N2 (Robinson et al. 2007)

IIIA1	Incidental nodal metastases found on final pathology examination of the resection specimen
IIIA2	Nodal (single station) metastases recognised intraoperatively
IIIA3	Nodal metastases (single or multiple stations) recognised by prethoracotomy staging (mediastinoscopy, other nodal biopsies or PET scan)
IIIA4	Bulky or fixed multistation N2 disease

5.4 Visualisation

In accordance with other groups, the actual German S3 guideline (Goeckenjan et al. 2010) recommends the following imaging procedures before curative treatment of lung cancer patients:

- Computed tomography of the chest with i.v. contrast
- MRI of the brain and MRI of the chest in cases of sulcus superior tumours
- FDG-PET/CT, in case of positive findings deciding treatment supplemented by invasive nodal staging

In the context of radiotherapy planning, these imaging methods are also the mainstay of target volume delineation. For any imaging used for this purpose within the planning process beyond side by side viewing, some additional requirements have to be met:

- Patient positioning should be in stable treatment position. For lung cancer, this would usually be a supine position with the arms above the head (possibly supported by arm support), as this permits the widest choice for beam access. For SBRT planning, immobilisation requirements are more strict, and any planning scans should definitely be in the individualised institutionally standardised positioning aids (De Ruysscher et al. 2010).
- A defined approach to tumour motion should be given (see also below). While standard diagnostic imaging in deep inspiration is not suitable for use in RT treatment planning, "conventional" imaging in free breathing should also be avoided in the curative situation. The ideal imaging is the mid-breathing position scan from a 4D acquisition (see below).

Clinical and radiological follow-up imaging should ideally be acquired in or at least seen by the treating centre. Hereby, misunderstandings in the interpretation of treatment-induced radiological changes can be minimised. The standard follow-up scan will always be a chest CT, if necessary supplemented by other imaging like PET/CT. To account for early radiation-induced chances, especially of the lung, a first scan after 3 months should be done, followed by half-yearly scans for the cases treated with curative intent. It should be kept in mind that, especially after SBRT, radiation-induced changes could appear years after treatment and may mimic local tumour recurrence (Huang et al. 2012) (Fig. 5.2). Therefore, a thorough evaluation in the context of prior RT planning and dose delivery will help to avoid unnecessary concerns for the patient.

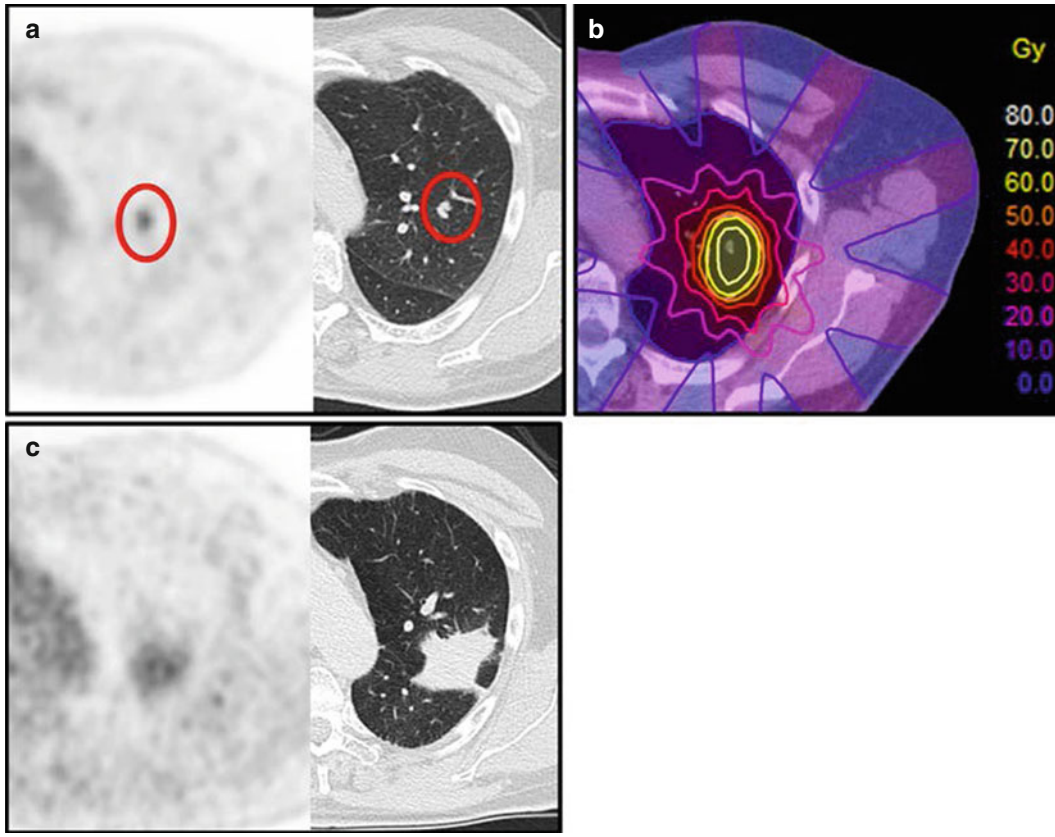

Fig. 5.2 Radiation-induced changes after SBRT. (**a**) Axial FDG-PET and corresponding CT scans of a patient with a malignant pulmonary lesion in the left upper lobe (*red circle*) before SBRT with dose distribution displayed in (**b**). (**c**) PET/CT scan 11 months after treatment with severe dense pulmonary alterations within the high-dose area showing moderate FDG uptake in the fibrosis in the left upper lobe

5.4.1 Computed Tomography (CT)

For initial diagnosis, staging and follow-up of patients with lung cancer, CT with i.v. contrast remains the diagnostic mainstay. Beyond endoscopic information, the determination of T stage mainly depends on CT appearance of the primary tumour. Giving its excellent resolution and good tissue contrast, CT evaluation provides valuable tumour morphologic details, and therefore it should always be performed before more invasive staging procedures. In the diagnosis of solitary pulmonary nodules, CT-based signs of malignancy like spiculae or size increase on follow-up scans play an important role in differentiating benign nodes from those needing intervention. Overall, the specificity of CT for the detection of intrapulmonary nodes is very high, but its specificity is rather low (Wahidi et al. 2007).

For nodal staging, the criterion for malignancy is the size of the node, which obviously leads to a rather low sensitivity and specificity (Wahidi et al. 2007; MacDonald and Hansell 2003). A prior meta-analysis has reported sensitivity and specificity of 62 %, when a CT-derived morphologic criterion (>10 mm in the short axis of the node) was considered as a discriminator for nodal involvement (de Langen et al. 2006).

A chest CT to be used for treatment planning for a lung cancer patient should always include the whole circumference of the patient in the treatment region. It should contain the whole lung volume and extend from the larynx to the upper

abdomen. A slice thickness of 2–3 mm has been recommended (De Ruysscher et al. 2010), as the quality of the resulting digitally reconstructed radiographs (DRRs) will then allow high-precision patient repositioning for treatment verification (Hurkmans et al. 2009). Furthermore, the use of intravenous contrast enables improved delineation of mediastinal structures (Van Sornsen de Koste et al. 2003) clearly outperforming small disadvantages concerning dose calculation.

As mentioned above, a planning CT should be acquired with a concept of how to cope with patient movement and positioning differences, expected during further treatment process. Planning CTs in free breathing should not be used, as the expansion of a random position of tumour and normal tissues by population-based margins may well lead to systematic errors (Slotman et al. 2006). Therefore, if ever available, a 4D planning CT, i.e. a CT scan acquired by respiratory gating, should be used. For about 80 % of SBRT patients and for 60 % of patients with locally advanced lung tumours, the information derived from a 4D CT will allow for smaller margins than population-based ones (Baba et al. 2009; Underberg et al. 2005).

Even the mid-ventilation scan from a 4D CT will improve target volumes, as it allows the correct addition of population-based margins. Beyond this, individual breathing margins like ITVs or a "mid-ventilation/average ventilation" concept (Wolthaus et al. 2008) can be used with such scans. If a 4D CT is not available, the planning CT should be taken in shallow breathing. Institutional standardised protocols using breath-hold CT, cardiac gating or respiratory tracking are possible for both planning and treatment imaging. However, gating and tracking are technically challenging and may only be of value for a small subgroup of patients with significant motion and good compliance (De Ruysscher et al. 2010).

5.4.2 Magnetic Resonance Imaging

Like in other parts of the body, MRI of the chest exhibits a more detailed soft tissue contrast as compared to CT. However, the movements of chest organs place challenges on image acquisition, which have for years prevented MRI from achieving an important role in the imaging of lung tumours. However, MRI proves superior to other morphologic imaging in the diagnosis and evaluation of chest wall infiltration, spinal cord involvement or superior sulcus tumours (MacDonald and Hansell 2003; Komaki et al. 2000; Puderbach et al. 2007).

5.4.3 FDG-PET Imaging

During the past two decades, FDG-PET(-CT) has become a mainstay in the diagnosis and treatment planning of lung cancer patients. The diagnostic superiority of FDG-PET/CT over CT alone concerning N and M staging for NSCLC has been demonstrated by numerous studies, compiled in several meta-analyses (Dwamena et al. 1999; Hellwig et al. 2009). Here, FDG-PET/CT exhibits a higher specificity and sensitivity compared to CT.

For the evaluation of indeterminate lung lesions, the sensitivity and specificity range from 79 to 96 % and from 40 to 83 % (Hellwig et al. 2009). FDG-PET is the non-invasive method with the highest diagnostic accuracy for this question. The main limitation of FDG-PET in the evaluation of lung nodules is false-positive FDG uptake at inflammatory sites and with granulomatous diseases (e.g. sarcoidosis), leading to decreased specificity. Another shortcoming for PET imaging is represented by false-negative results and decreased sensitivity when dealing with small tumours or lesions with decreased FDG avidity (e.g. lepidic tumours).

For the detection of mediastinal involvement, the role of FDG-PET is very well established. Several large series (Hellwig et al. 2009) have reported a higher overall sensitivity of 83 % for PET when compared to 56 % for CT. Adjusting for morphological CT findings, the sensitivity on PET imaging was 91 % for the enlarged nodes and 70 % for normal appearing ones. The overall specificity is also favourable to FDG metabolic imaging when compared to CT (89 % versus 81 %, respectively). Interestingly, when it was adjusted for nodal size,

the specificity of FDG-PET was 70 % for pathological appearing nodes and 94 % for the normally sized ones. These results should be viewed in perspective with mediastinoscopy, which has shown an overall sensitivity of 78 % (82 % when the CT scan shows enlarged lymph nodes and 42 % for normal-sized lymph nodes) and overall specificity of 100 %. However, unlike PET scans, mediastinoscopy does not survey all potentially involved nodes. As the negative predictive value of FDG-PET for mediastinal involvement is about 90 %, while the positive predictive values are lower (Hellwig et al. 2009), current guidelines recommend to biopsy FDG-positive lesions, if they are crucial for treatment decisions (Goeckenjan et al. 2010).

A larger summary of FDG-PET data was published by Gambhir et al. (2001). They evaluated 53 clinical trials published between 1993 and 2000, which included 4,005 patients with lung cancer. In those studies, the average FDG-PET sensitivity and specificity were 83 and 91 %, respectively, whereas for CT they were 64 and 74 %, respectively. Of 1,565 patients evaluated, modification of treatment strategy following FDG-PET staging data was estimated at 37 %. The PLUS multicentre randomised trial compared the conventional workup with conventional workup plus FDG-PET in preoperative assessment of patients suspected for non-small cell lung cancer. FDG-PET prevented unnecessary surgery in one out of five (20 %) cases (van Tinteren et al. 2002). In patients with NSCLC scheduled for radiotherapy, PET scans revealed up to 24 % of cases with unexpected distant metastases, leading to significant impact on therapy decision (MacManus et al. 2001). The presence of a PET scan before multimodal treatment of locally advanced NSCLC showed a higher prognostic impact than complete resection (Eschmann et al. 2007).

The potential use of FDG-PET for radiotherapy planning in lung cancer has been highlighted by numerous publications. Among several reasons for a positive impact of PET imaging, probably the most decisive ones are a higher accuracy for nodal staging as well as improved differentiation between tumour and atelectasis (Nestle et al. 2006). However, caution has to be taken when a PET scan shall be used for RT treatment planning. Here, a range of uncertainties related to technical (e.g. relative calibration between dose calibrator and PET scanner), physical (e.g. image reconstruction parameters), biological (e.g. motion, tumour heterogeneity) and analytical (e.g. region of interest definition method) factors have to be considered.

First of all, the scan should be taken timely before the start of treatment, as it has been shown that locally advanced NSCLC has a probability of progression of 32 % in 24 days (Everitt et al. 2013). A FDG-PET/CT scan taken after induction chemotherapy bears the risk of false-negative findings leading to systematic errors in target volume delineation as the negative predictive value drops to 67 % (Hoekstra et al. 2005). Therefore, this situation should be avoided. If induction chemotherapy is inevitable, a baseline scan should be taken before its onset. Furthermore, PET scans for RT treatment planning should be taken in treatment position using approved quality controlled protocols and be rigidly coregistered. When PET scans shall be used for GTV contouring, a solid communication between nuclear medicine and radiation oncology physicians must be established. Visual co-contouring of colleagues from both specialties, at the planning system using a diagnostically satisfactory window-level setting, has been shown to generate usable GTV contours (Doll 2014). Automated contouring methods as provided by PET manufacturers and RT planning software may speed up the contouring process, but they should be handled with caution after institutional-based calibration by phantom measurements. More technical details and further recommendations for the use of PET/CT in RT planning can be found in the guideline provided by the German working group on nuclear medicine and radiotherapy (Thorwarth et al. 2012).

5.5 Target Volume Delineation

When discussing target volumes for radiotherapy of lung cancer, several distinctive clinical scenarios must be addressed: stereotactic body

radiotherapy (SBRT), neoadjuvant + definitive radiochemotherapy in NSCLC, adjuvant RT in NSCLC and radiochemotherapy in SCLC.

5.5.1 SBRT

The advent of SBRT has in a way revolutionised radiotherapy for lung cancer. With modern high-precision techniques, very high rates of local control and cure can be achieved, which impressively demonstrates the existing dose-effect relation in radiotherapy for lung cancer. SBRT is a well-established approach for patients with peripheral stage I NSCLC (Lagerwaard et al. 2008; Grutters et al. 2010). Even among patients beyond 75 years of age and those with multiple comorbidities, risk-adapted SBRT schemes showed no significant acute toxicity and less than 10 % late grade III toxicity rates (Lagerwaard et al. 2008). Several prior studies have shown no significant lung impairment after SBRT, which appeared overall a safety therapy approach (Harris et al. 1993; Kara et al. 2000; Giraud et al. 2000; Salguero et al. 2013). However, this method has been particularly established in patients with already impaired lung function or after pneumonectomy, which may mask a potentially unfavourable impact from radiation.

As outlined above, the safety limits of SBRT delivered to centrally located lung tumours have not been clearly answered yet. However, presently recruiting trials will hopefully shed more light on this matter. Another clinical scenario which merits attention and further investigation remains SBRT for larger lung tumours.

SBRT target volumes should be delineated in a 4D planning CT. The GTV will be delineated comprising all macroscopic tumours. It has been shown that the subjective appreciation of lung tumour size and extension is dependent on window-level settings (Harris et al. 1993). The best concordance between measured and actual diameters and volumes was obtained by the following window settings: $W = 1{,}600$ and $L = -600$ for parenchyma and $W = 400$ and $L = 20$ for mediastinum. Although of high importance for pre-SBRT staging, the potential impact of (4D) FDG-PET/CT on target volume delineation for SBRT is unclear and may not be important in peripheral tumours. However, current research will show if it may be of help in more central lesions.

The available literature reports deriving recommendations for GTV to CTV margins from surgical series in NSCLC suggest microscopic tumour extension beyond the macroscopic limits (Kara et al. 2000; Giraud et al. 2000). However, most series published on SBRT for lung tumours did not distinguish between GTV and CTV, with the argument that the dose delivered in volume surrounding the GTV may be still high enough to eradicate microscopic disease. However, it has been shown that microscopic disease extension may play a role in locoregional recurrence after SBRT and that this microscopic extension may be predicted by imaging parameters (Salguero et al. 2013).

To cope with movements, the most widely used approach is the delineation of an internal target volume (ITV) according to ICRU 62 (ICRU 1999), i.e. the volume of presence of the tumour at any breathing phase (Fig. 5.3). Practically, the ITV can be generated by adding the GTVs from all or several relevant breathing phases of the 4D CT or by a maximum intensity projection (MIP)-based approach (Hurkmans et al. 2009). Most published data that were generated using this concept showed high rates of tumour control and low toxicity. However, with raising tumour size and higher mobility amplitude, ITVs may expose large areas of normal lung to unnecessary radiation. In an effort to limit toxicity in this subgroup of patients, a statistical approach has been proposed (Wolthaus et al. 2008). Unfortunately, as it needs dedicated software solutions, the statistical approach is yet to be widely disseminated in daily practice.

To adjust for set-up errors, institutionally verified PTV margins will then be added to the ITV or mid-ventilation/average ventilation volume. These margins usually account to several (3–5) mm.

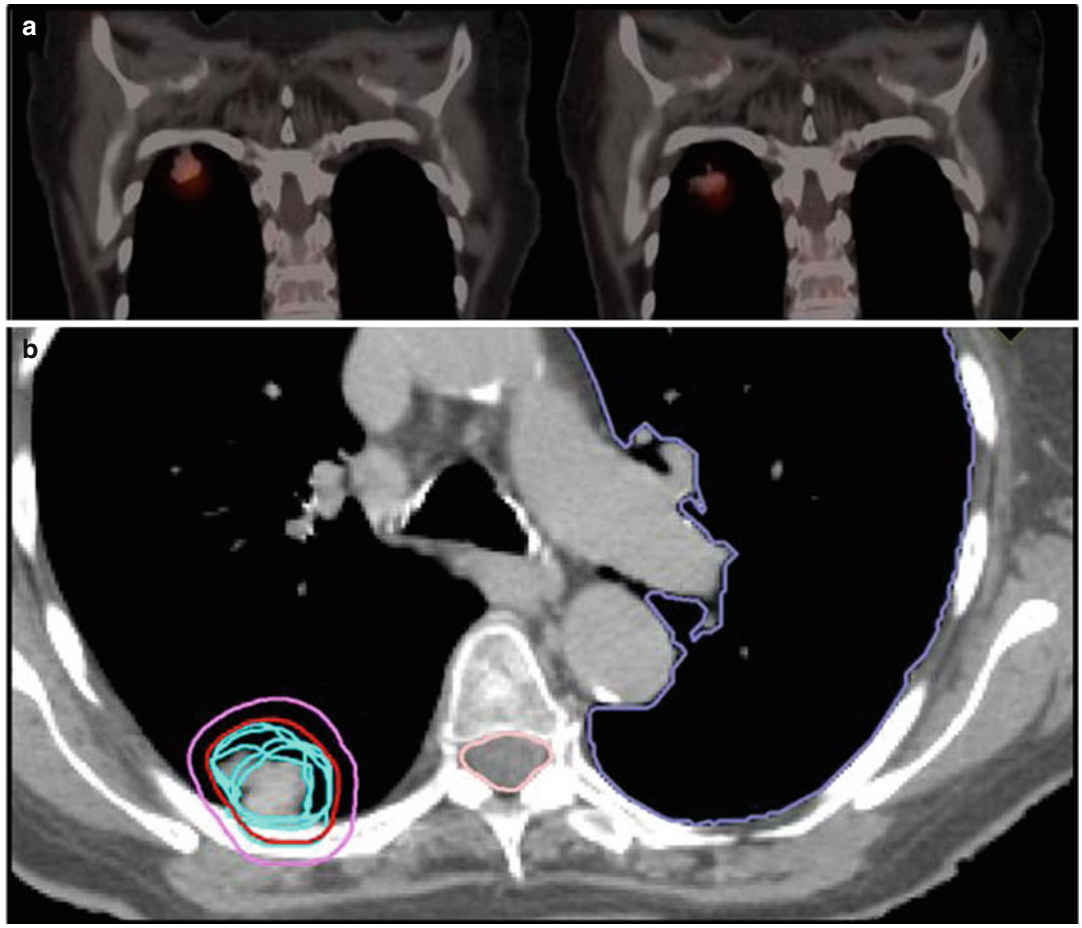

Fig. 5.3 Target volume delineation – SBRT. (**a**) Reconstructed coronal images from 4D PET/CT scan showing breathing movements of a NSCLC; the most cranial and most caudal position is shown. (**b**) Delineation of the target volumes: to account for tumour movement by an ITV approach, GTVs are delineated in all relevant breathing phases (*blue*), whose addition leads to the internal target volume (ITV, *red*). To generate the PTV (*pink*), an isotropic margin is added

5.5.2 Definitive and Neoadjuvant Radiochemotherapy of NSCLC

From the perspective of target volume delineation, the concepts of definitive or neoadjuvant radiochemotherapy of locally advanced NSCLC are essentially similar. Both are widely used in the curative approach for patients with locally advanced NSCLC, with differential indications regulated by multiple national and international guideline recommendations (Goeckenjan et al. 2010). Beyond this, the choice of therapy concept often depends on individual patient's performance status and comorbidities as well as on the local treatment facilities and personnel availability.

For GTV definition, all available clinical and imaging information should be used, including endoscopy reports, results of invasive mediastinal staging (referring to the Mountain-Dresler stations; see above) and CT, MRI and/or PET findings. GTV delineated on planning CT should integrate all these informations, irrespective of their origin. By definition, safety margins and/or prophylactic volumes should not be a part of the GTV. Visually discernible tumour on CT should be delineated using the above-mentioned window-level settings ($W=1{,}600$ and $L=-600$ for parenchyma and $W=400$ and $L=20$ for mediastinum). For PET-based GTV delineation, the procedural and technical recommendations given in Sects. 5.4

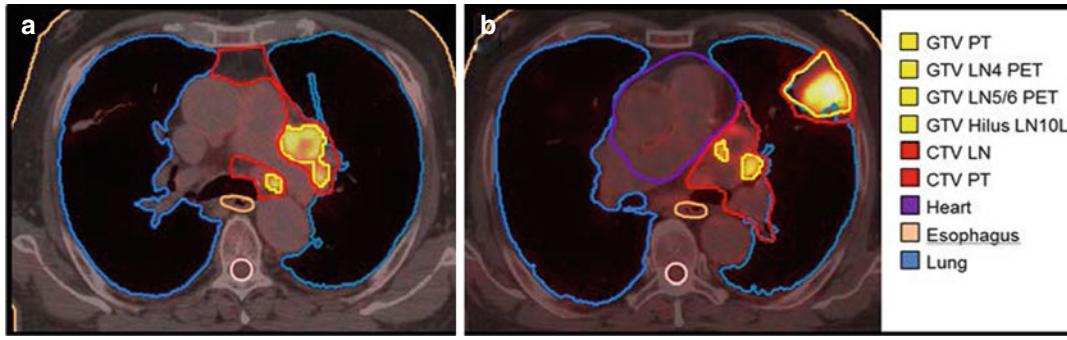

Fig. 5.4 Target volume delineation for definitive radiochemotherapy of NSCLC. Two axial slices of a radiotherapy planning CT fused to FDG-PET scan in identical position for a PET-Plan study patient with NSCLC T2a N2 M0, located in the left upper lobe; PET-positive lymph nodes in lymph node stations 4L, 5, 6, positive biopsy of lymph nodes in 10L. (**a**, **b**) The GTVs of primary tumour and positive lymph nodes are marked in *yellow*, the CTVs (including the whole tumour affected Mountain-Dresler stations) in *red*. (**a**) CTV of lymph node stations 3A, 4L, 5 and 6; (**b**) CTV of primary tumour and lymph node stations 4L, 5 and 10L (left hilum)

and 5.5.1 should be applied in analogy. As outlined above (Sect. 5.4), PET may be particularly helpful to distinguish lung parenchymal atelectasis and to increase the diagnostic accuracy of nodal staging, especially for normal-sized or even invisible lymph nodes. Therefore, in equivocal situations, a positive lymphatic structure on PET should always be included in the GTV, unless the FDG accumulation is beyond any doubt unrelated to malignancy. As the PET acquisition is typically performed during several breathing cycles, a 3D PET-derived volume intrinsically contains some motion information (Caldwell et al. 2003). However, in times of 4D PET/CT, concerns about the representativeness of this fact have been raised. As a generally accepted recommendation, the entire lesion volume with abnormal FDG uptake should be included in the GTV (Fig. 5.4a, b).

To account for microscopic spread surrounding the primary lung tumour, traditional recommendations have proposed GTV to CTV margins of at least 6 mm. However, most actual protocols do not apply such large margins but rather 5 mm or no margin at all (Rosenzweig et al. 2005; De Ruysscher et al. 2008; Hayman et al. 2001). Furthermore, the treated volume may be tailored according to the histology of the primary tumour (Giraud et al. 2000) or to the size of the lymph node (Yuan et al. 2007). In the absence of large trials to correlate GTV to CTV margins with pathological findings and patient outcome, the clinical relevance of this concept remains uncertain. When there is no obvious invasion through distinct anatomical compartments, for example, into adjacent bone or beyond the pleura, CTV delineation should be restricted to omit these normal tissues (De Ruysscher et al. 2010).

CTV concepts for mediastinal treatment have been changing over the years and still remain under discussion. In the past decades, when imaging staging of the mediastinum was unsatisfactory, elective nodal irradiation has been largely used as a routine clinical practice. However, in the absence of solid evidence for better nodal disease control or beneficial outcome, this approach is probably unnecessary today (De Ruysscher et al. 2010). In a compliance analysis on 1,705 patients scheduled for elective nodal irradiation, it was shown that protocol adherence was irrelevant for prognosis (Emami et al. 2003). Hence, a newer CT-based adapted 3D CRT approach has emerged, demonstrating selective nodal irradiation with a rather small number of outfield recurrences (Rosenzweig et al. 2007). Given the diagnostic superiority of FDG-PET, the metabolic information should be incorporated in the initial nodal GTV (Sura et al. 2008; De Ruysscher et al. 2005). As most available literature relates to diagnosis and irradiation of nodal stations, the nodal CTV for definitive and neoadjuvant radiotherapy should, beyond the nodal GTV, contain the whole anatomical Mountain-Dresler stations, which are diagnosed as being tumour affected (Fig. 5.4).

The concepts of selective nodal irradiation have mainly been tested with 3D CRT, which may

Table 5.7 LN regions with probability of affection of >10 % according to Giraud et al. (2006), which could be chosen as target regions for elective nodal irradiation in locally advanced NSCLC

Localisation of primary tumour	Elective nodal irradiation				
Right upper lobe	1R	2R	4R	7	Right hilum
Middle lobe	1R	2R	4R	7	Right hilum
Right lower lobe		2R	4R	7	Right hilum
Right central	1R	2R	4R	7	Right hilum
Left upper lobe	1L	2L	4L	7	Left hilum
Left lower lobe			4L	7	Left hilum
Left central	1L	2L	4L	7	Left hilum

still provide relatively high unintended doses outside the CTV (Jeremic 2004). With expanding use of IMRT providing high-dose radiation with high-precision application, the chance of local control with low toxicity rates will increase. Concerns that remain with this approach are that the outfield recurrences might again reach a relevant level, due to an approximate 10 % rate of false-negative nodes on staging diagnostic imaging (Hellwig et al. 2009). Current and future clinical trials will hopefully answer this question.

If elective nodal irradiation is to be employed beyond the obviously affected lymph nodal stations, the CTV should contain those stations which have been described in the literature to have >10 % risk of undetected (microscopic) spread (Giraud et al. 2006). According to the primary lung tumour location, the nodal stations with increased risk of involvement are summarised in Table 5.7.

The CTV to PTV margins are often chosen to be 8–15 mm. They are applied to account for tumour motions, patient set-up and geometrical uncertainties (Giraud et al. 2000; ICRU 1999). However, if available, 4D planning CT should be used (see Sects. 5.4 and 5.5.1), as it will enable the application of individual breathing margins to the mid-ventilation position of the GTV. In addition to the breathing margins, the set-up and positioning uncertainty should be adjusted by at least 5 mm. In case of the use of gating and/or tracking imaging, individual margin concepts will need to be established institutionally. Manual PTV adaptations should not be performed.

5.5.3 Adjuvant Radiotherapy of NSCLC

Most patients who reach long-term survival after the diagnosis of NSCLC underwent a complete surgical resection, which is only achievable in about 30 % of cases. Moreover, the risk of local and distant failure is high even in this subpopulation, urging for the addition of adjuvant treatment. In contrast to adjuvant chemotherapy, the advantage of adjuvant radiotherapy of the mediastinum has only been shown in older, small populations and sometimes low-quality studies. This has led to the situation that while adjuvant chemotherapy has become standard in N1 and N2 disease, the indications for adjuvant radiotherapy are not completely clear and still subject to ongoing clinical trials. According to the results of the PORT meta-analysis including old series with partly outdated dose and volume concepts (Le Pechoux 2011), postoperative mediastinal irradiation has showed a decreased overall survival, although the risk of locoregional recurrence and the survival among the pN2 subset were improved. Based on these data and supported by more favourable newer studies, some guidelines (Goeckenjan et al. 2010) and specialists from many centres do recommend adjuvant mediastinal irradiation in the pN2 cases and for incomplete resection (R1 situation).

When postoperative radiotherapy is planned, the initial position of the tumour as related to the central mediastinal structures should be known to the radiation oncologist, as should be the detailed pathological report and the results of preoperative mediastinal staging. Clips positioned by the surgeon further ease the identification of the bronchial stump and areas of risk (Fig. 5.5). In case of R1 resection, the additional consultation of the surgeon for delineation of residual tumour volume may be of great help.

The CTV should always include the bronchial stump and the ipsilateral hilum. In addition, due to the frequent unexpected involvement of ipsilateral

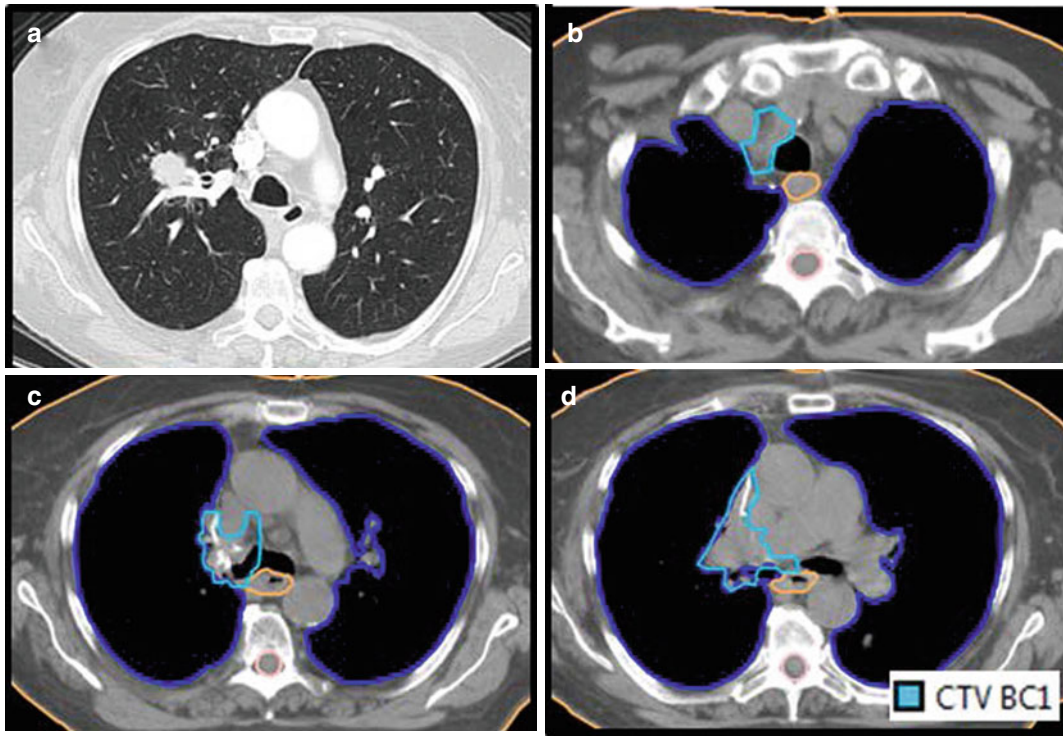

Fig. 5.5 Target volume delineation – adjuvant radiotherapy of NSCLC. (**a**) Preoperative CT scan of a patient with NSCLC in the right upper lobe, pT1a pN2 cM0, R0; histologically positive lymph node in level 4R. (**b**–**d**) Postoperative planning CT with clips positioned by the surgeon. The CTV (*blue*) includes the bronchial stump (**c**, **d**), the ipsilateral hilum (**d**) as well as the ipsilateral nodal stations 2R (**b**), 4R (**c**–**d**) and 7 (**d**)

nodal stations 4 and 7, identified on surgical series, it has been recommended to always include these locations within the CTV (Spoelstra et al. 2010). Beyond this, all lymph node areas with pathologically proved disease involvement should be anatomically included in the CTV. It has been further recommended to include in the treated volume all nodal areas which appear unaffected but are located between noncontiguous involved lymph nodes. Again, the atlas of the University of Michigan can be of help in the anatomical identification and delineation of the Mountain-Dresler stations (Chapet et al. 2005).

5.5.4 Small Cell Lung Cancer

About 15–20 % of lung cancer patients are diagnosed with small cell lung cancer (SCLC). Of those, about 30 % have limited stage disease, i.e. UICC stage < IV with tumours that can be included by a tolerable radiotherapy target volume. Although outcome even in the limited stage of the disease is poor, there is a chance of cure when these patients are given combined radiochemotherapy, which is therefore the standard of care. Although prospective imaging data are less extensive, staging and restaging of SCLC use more or less the same methods as in NSCLC. It has been shown that FDG-PET is diagnostically superior (Brink et al. 2004; Fischer et al. 2007; Pandit et al. 2003) and the accuracy for detection of nodal metastases is higher with PET than with CT.

While the optimum dose and fractionation regimes as well as the optimum timing of the combination of radiation and chemotherapy are subject to clinical studies, there is not much evidence on the best way to delineate target volumes in SCLC. Thus an expert committee discussing the role of elective nodal irradiation concluded that the scope for

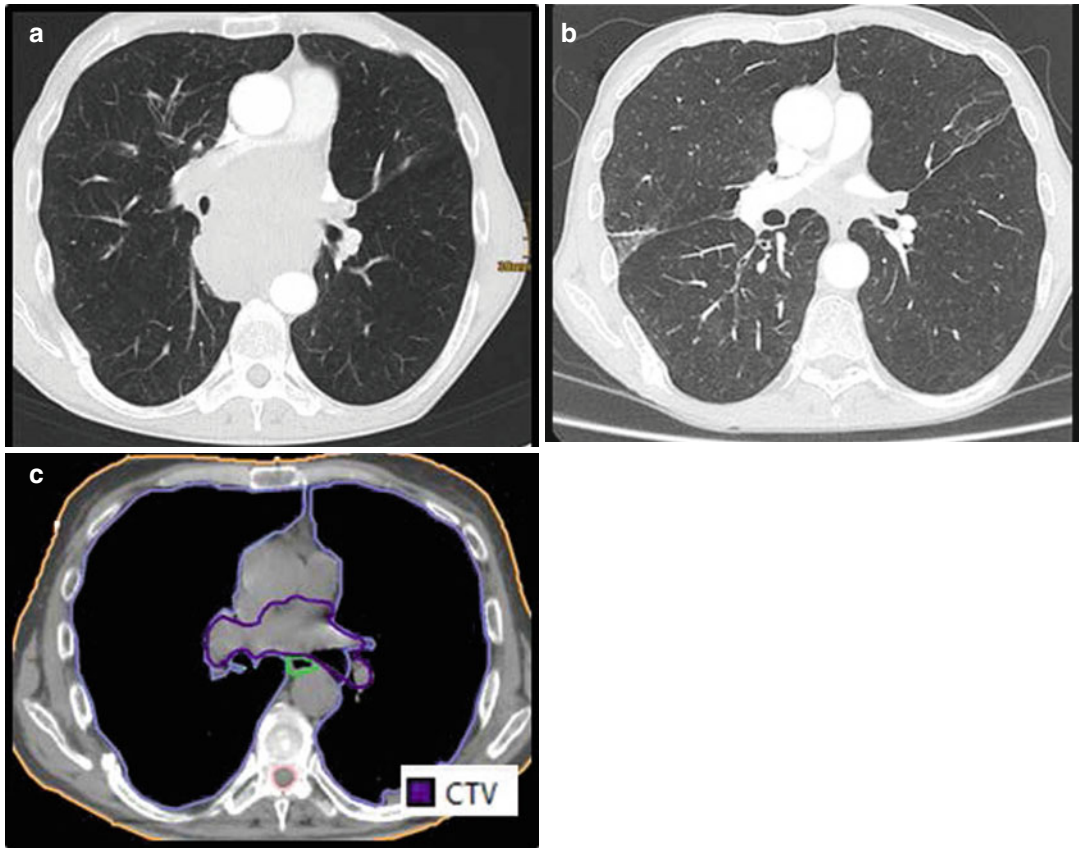

Fig. 5.6 Target volume delineation – small cell lung cancer axial CT scans of a patient at diagnosis of SCLC limited disease (cT3cN3cM0) (**a**), referred for mediastinal radiotherapy after 6 cycles of chemotherapy in partial tumour remission (**b**, **c**) RT planning CT with target volume delineation; the CTV (*purple*) includes the GTV and all nodal regions involved at the time of initial diagnosis

high-level evidence in deciding on the place of ENI in SCLC is very limited (Videtic et al. 2008).

A Dutch study investigated the role of CT-based selective nodal irradiation in SCLC and showed a rate of 11 % isolated outfield recurrences (De Ruysscher et al. 2006). A follow-up study from the same group, using pretreatment FDG-PET-based nodal volumes, revealed a rate of only 3 % isolated outfield recurrences with favourable toxicity profile (van Loon et al. 2008). However, the evidence is still limited and FDG-PET-based target volumes are merely experimental. Furthermore, in clinical routine, pretreatment FDG-PET scans are not always available due to the rapid tumour growth of many SCLC, urging for timely onset of chemotherapy.

Current trial protocols and guidelines (De Ruysscher et al. 2010) recommend to delineate a GTV at the time of RT planning (which may be after the onset of chemotherapy) including all gross disease (primary tumour plus involved nodes) at that time point (Fig. 5.6). For GTV delineation, all methods discussed for NSCLC are applicable, while post-chemotherapy PET should again be used with caution. For the CTV, it is recommended to include all the involved nodal regions at the time of initial diagnosis, if no evidence of progression is identified until radiotherapy planning. Nodal areas should be anatomically delineated in concordance with the atlas of the University of Michigan (Chapet et al. 2005).

References

Auperin A, Le Pechoux C, Rolland E et al (2010) Meta-analysis of concomitant versus sequential radiochemotherapy in locally advanced non-small-cell lung cancer. J Clin Oncol 28:2181–2190

Baba F, Shibamoto Y, Tomita N et al (2009) Stereotactic body radiotherapy for stage I lung cancer and small lung metastasis: evaluation of an immobilization system for suppression of respiratory tumor movement and preliminary results. Radiat Oncol 4:15

Bentzen SM, Harari PM, Tome WA et al (2008) Radiation oncology advances: an introduction. Cancer Treat Res 139:1–4

Brink I, Schumacher T, Mix M et al (2004) Impact of [18 F]FDG-PET on the primary staging of small-cell lung cancer. Eur J Nucl Med Mol Imaging 31:1614–1620

Caldwell CB, Mah K, Skinner M et al (2003) Can PET provide the 3D extent of tumor motion for individualized internal target volumes? A phantom study of the limitations of CT and the promise of PET. Int J Radiat Oncol Biol Phys 55:1381–1393

Chapet O, Kong FM, Quint LE et al (2005) CT-based definition of thoracic lymph node stations: an atlas from the University of Michigan. Int J Radiat Oncol Biol Phys 63:170–178

Collier DC, Burnett SS, Amin M et al (2003) Assessment of consistency in contouring of normal-tissue anatomic structures. J Appl Clin Med Phys 4:17–24

Darby SC, Ewertz M, McGale P et al (2013) Risk of ischemic heart disease in women after radiotherapy for breast cancer. N Engl J Med 368:987–998

de Langen AJ, Raijmakers P, Riphagen I et al (2006) The size of mediastinal lymph nodes and its relation with metastatic involvement: a meta-analysis. Eur J Cardiothorac Surg 29:26–29

De Leyn P, Stroobants S, De Wever W et al (2006) Prospective comparative study of integrated positron emission tomography-computed tomography scan compared with remediastinoscopy in the assessment of residual mediastinal lymph node disease after induction chemotherapy for mediastinoscopy-proven stage IIIA-N2 Non-small-cell lung cancer: a Leuven Lung Cancer Group Study. J Clin Oncol 24:3333–3339

De Ruysscher D, Wanders S, van Haren E et al (2005) Selective mediastinal node irradiation based on FDG-PET scan data in patients with non-small-cell lung cancer: a prospective clinical study. Int J Radiat Oncol Biol Phys 62:988–994

De Ruysscher D, Bremer RH, Koppe F et al (2006) Omission of elective node irradiation on basis of CT-scans in patients with limited disease small cell lung cancer: a phase II trial. Radiother Oncol 80:307–312

De Ruysscher D, Dehing C, Bremer RH et al (2007) Maximal neutropenia during chemotherapy and radiotherapy is significantly associated with the development of acute radiation-induced dysphagia in lung cancer patients. Ann Oncol 18:909–916

De Ruysscher D, Wanders R, van Haren E et al (2008) HI-CHART: a phase I/II study on the feasibility of high-dose continuous hyperfractionated accelerated radiotherapy in patients with inoperable non-small-cell lung cancer. Int J Radiat Oncol Biol Phys 71:132–138

De Ruysscher D, Faivre-Finn C, Nestle U et al (2010) European Organisation for Research and Treatment of Cancer recommendations for planning and delivery of high-dose, high-precision radiotherapy for lung cancer. J Clin Oncol 28:5301–5310

Dehing-Oberije C, De Ruysscher D, van Baardwijk A et al (2009) The importance of patient characteristics for the prediction of radiation-induced lung toxicity. Radiother Oncol 91:421–426

Delanian S, Lefaix JL, Pradat PF (2012) Radiation-induced neuropathy in cancer survivors. Radiother Oncol 105:273–282

Doll C (2014) When there is no expert – ask your colleague! influence of experience and qualification on PET-based target volume delineation. Strahlenther Onkol 190:555–562

Dunlap NE, Cai J, Biedermann GB et al (2010) Chest wall volume receiving >30 Gy predicts risk of severe pain and/or rib fracture after lung stereotactic body radiotherapy. Int J Radiat Oncol Biol Phys 76:796–801

Dwamena BA, Sonnad SS, Angobaldo JO et al (1999) Metastases from non-small cell lung cancer: mediastinal staging in the 1990s–meta-analytic comparison of PET and CT. Radiology 213:530–536

Emami B, Mirkovic N, Scott C et al (2003) The impact of regional nodal radiotherapy (dose/volume) on regional progression and survival in unresectable non-small cell lung cancer: an analysis of RTOG data. Lung Cancer 41:207–214

Eschmann SM, Friedel G, Paulsen F et al (2007) Impact of staging with 18 F-FDG-PET on outcome of patients with stage III non-small cell lung cancer: PET identifies potential survivors. Eur J Nucl Med Mol Imaging 34:54–59

Everitt S, Plumridge N, Herschtal A et al (2013) The impact of time between staging PET/CT and definitive chemo-radiation on target volumes and survival in patients with non-small cell lung cancer. Radiother Oncol 106:288–291

Feng M, Moran JM, Koelling T et al (2011) Development and validation of a heart atlas to study cardiac exposure to radiation following treatment for breast cancer. Int J Radiat Oncol Biol Phys 79:10–18

Fischer BM, Mortensen J, Langer SW et al (2007) A prospective study of PET/CT in initial staging of small-cell lung cancer: comparison with CT, bone scintigraphy and bone marrow analysis. Ann Oncol 18:338–345

Forquer JA, Fakiris AJ, Timmerman RD et al (2009) Brachial plexopathy from stereotactic body radiotherapy in early-stage NSCLC: dose-limiting toxicity in apical tumor sites. Radiother Oncol 93:408–413

Gagliardi G, Constine LS, Moiseenko V et al (2010) Radiation dose-volume effects in the heart. Int J Radiat Oncol Biol Phys 76:S77–S85

Gambhir SS, Czernin J, Schwimmer J et al (2001) A tabulated summary of the FDG PET literature. J Nucl Med 42:1S–93S

Giraud P, Antoine M, Larrouy A et al (2000) Evaluation of microscopic tumor extension in non-small-cell lung cancer for three-dimensional conformal radiotherapy planning. Int J Radiat Oncol Biol Phys 48:1015–1024

Giraud P, De Rycke Y, Lavole A et al (2006) Probability of mediastinal involvement in non-small-cell lung cancer: a statistical definition of the clinical target volume for 3-dimensional conformal radiotherapy? Int J Radiat Oncol Biol Phys 64:127–135

Goeckenjan G, Sitter H, Thomas M et al (2010) Prevention, diagnosis, therapy, and follow-up of lung cancer. Pneumologie 64(Suppl 2):e1–e164

Goldstraw P, Crowley J, Chansky K et al (2007) The IASLC Lung Cancer Staging Project: proposals for the revision of the TNM stage groupings in the forthcoming (seventh) edition of the TNM Classification of malignant tumours. J Thorac Oncol 2:706–714

Grutters JP, Kessels AG, Pijls-Johannesma M et al (2010) Comparison of the effectiveness of radiotherapy with photons, protons and carbon-ions for non-small cell lung cancer: a meta-analysis. Radiother Oncol 95:32–40

Guckenberger M, Allgauer M, Appold S et al (2013) Safety and efficacy of stereotactic body radiotherapy for stage i non-small-cell lung cancer in routine clinical practice: a patterns-of-care and outcome analysis. J Thorac Oncol 8:1050–1058

Harris KM, Adams H, Lloyd DC et al (1993) The effect on apparent size of simulated pulmonary nodules of using three standard CT window settings. Clin Radiol 47:241–244

Hayman JA, Martel MK, Ten Haken RK et al (2001) Dose escalation in non-small-cell lung cancer using three-dimensional conformal radiation therapy: update of a phase I trial. J Clin Oncol 19:127–136

Hellwig D, Baum RP, Kirsch C (2009) FDG-PET, PET/CT and conventional nuclear medicine procedures in the evaluation of lung cancer: a systematic review. Nuklearmedizin 48:59–69, quiz N8-9

Hoekstra CJ, Stroobants SG, Smit EF et al (2005) Prognostic relevance of response evaluation using [18 F]-2-fluoro-2-deoxy-D-glucose positron emission tomography in patients with locally advanced non-small-cell lung cancer. J Clin Oncol 23:8362–8370

Huang K, Dahele M, Senan S et al (2012) Radiographic changes after lung stereotactic ablative radiotherapy (SABR)–can we distinguish recurrence from fibrosis? A systematic review of the literature. Radiother Oncol 102:335–342

Hurkmans CW, Cuijpers JP, Lagerwaard FJ et al (2009) Recommendations for implementing stereotactic radiotherapy in peripheral stage IA non-small cell lung cancer: report from the Quality Assurance Working Party of the randomised phase III ROSEL study. Radiat Oncol 4:1

ICRU (1999) Prescribing, recording and reporting photon beam therapy. Supplement to report 50, in ICRU (ed), International Commission on Radiation Units and Measurements. Bethesda, USA

Jeremic B (2004) Incidental irradiation of nodal regions at risk during limited-field radiotherapy (RT) in dose-escalation studies in nonsmall cell lung cancer (NSCLC). Enough to convert no-elective into elective nodal irradiation (ENI)? Radiother Oncol 71:123–125

Jo IY, Kay CS, Kim JY et al (2014) Significance of low-dose radiation distribution in development of radiation pneumonitis after helical-tomotherapy-based hypofractionated radiotherapy for pulmonary metastases. J Radiat Res 55:105–112

Kara M, Sak SD, Orhan D et al (2000) Changing patterns of lung cancer; (3/4 in.) 1.9 cm; still a safe length for bronchial resection margin? Lung Cancer 30:161–168

Kirkpatrick JP, van der Kogel AJ, Schultheiss TE (2010) Radiation dose-volume effects in the spinal cord. Int J Radiat Oncol Biol Phys 76:S42–S49

Komaki R, Putnam JB Jr, Walsh G et al (2000) The management of superior sulcus tumors. Semin Surg Oncol 18:152–164

Kong FM, Ritter T, Quint DJ et al (2011) Consideration of dose limits for organs at risk of thoracic radiotherapy: atlas for lung, proximal bronchial tree, esophagus, spinal cord, ribs, and brachial plexus. Int J Radiat Oncol Biol Phys 81:1442–1457

Kristensen CA, Nottrup TJ, Berthelsen AK et al (2009) Pulmonary toxicity following IMRT after extrapleural pneumonectomy for malignant pleural mesothelioma. Radiother Oncol 92:96–99

Lagerwaard FJ, Haasbeek CJ, Smit EF et al (2008) Outcomes of risk-adapted fractionated stereotactic radiotherapy for stage I non-small-cell lung cancer. Int J Radiat Oncol Biol Phys 70:685–692

Le Pechoux C (2011) Role of postoperative radiotherapy in resected non-small cell lung cancer: a reassessment based on new data. Oncologist 16:672–681

Liao ZX, Komaki RR, Thames HD Jr et al (2010) Influence of technologic advances on outcomes in patients with unresectable, locally advanced non-small-cell lung cancer receiving concomitant chemoradiotherapy. Int J Radiat Oncol Biol Phys 76:775–781

LoCicero J, Ponn RB, Rusch VW (2005) General thoracic surgery, 6th edn. Lippincott Williams & Wilkins, Philadelphia

MacDonald SL, Hansell DM (2003) Staging of non-small cell lung cancer: imaging of intrathoracic disease. Eur J Radiol 45:18–30

MacManus MP, Hicks RJ, Ball DL et al (2001) Imaging with F-18 FDG PET is superior to Tl-201 SPECT in the staging of non-small cell lung cancer for radical radiation therapy. Australas Radiol 45:483–490

Marks LB, Bentzen SM, Deasy JO et al (2010) Radiation dose-volume effects in the lung. Int J Radiat Oncol Biol Phys 76:S70–S76

Miller KL, Shafman TD, Anscher MS et al (2005) Bronchial stenosis: an underreported complication of high-dose external beam radiotherapy for lung cancer? Int J Radiat Oncol Biol Phys 61:64–69

Mountain CF, Dresler CM (1997) Regional lymph node classification for lung cancer staging. Chest 111:1718–1723

Nestle U, Kremp S, Grosu A (2006) Practical integration of [(18)F]-FDG-PET and PET-CT in the planning of radiotherapy for non-small cell lung cancer (NSCLC): the technical basis, ICRU-target volumes, problems, perspectives. Radiother Oncol 81:209–225

Nestle U, Faivre-Finn C, Deruysscher D et al (2013) Stereotactic body radiotherapy (SBRT) in central non-small cell lung cancer (NSCLC): solid evidence or "no-go"? Radiother Oncol 109:178–179

Nieder C, Grosu AL, Andratschke NH et al (2006) Update of human spinal cord reirradiation tolerance based on additional data from 38 patients. Int J Radiat Oncol Biol Phys 66:1446–1449

Onimaru R, Shirato H, Shimizu S et al (2003) Tolerance of organs at risk in small-volume, hypofractionated, image-guided radiotherapy for primary and metastatic lung cancers. Int J Radiat Oncol Biol Phys 56:126–135

Pandit N, Gonen M, Krug L et al (2003) Prognostic value of [18F]FDG-PET imaging in small cell lung cancer. Eur J Nucl Med Mol Imaging 30:78–84

Pettersson N, Nyman J, Johansson KA (2009) Radiation-induced rib fractures after hypofractionated stereotactic body radiation therapy of non-small cell lung cancer: a dose- and volume-response analysis. Radiother Oncol 91:360–368

Pijls-Johannesma M, De Ruysscher D, Vansteenkiste J et al (2007) Timing of chest radiotherapy in patients with limited stage small cell lung cancer: a systematic review and meta-analysis of randomised controlled trials. Cancer Treat Rev 33:461–473

Puderbach M, Hintze C, Ley S et al (2007) MR imaging of the chest: a practical approach at 1.5T. Eur J Radiol 64:345–355

Robinson LA, Ruckdeschel JC, Wagner H Jr et al (2007) Treatment of non-small cell lung cancer-stage IIIA: ACCP evidence-based clinical practice guidelines (2nd edition). Chest 132:243S–265S

Rosenzweig KE, Fox JL, Yorke E et al (2005) Results of a phase I dose-escalation study using three-dimensional conformal radiotherapy in the treatment of inoperable nonsmall cell lung carcinoma. Cancer 103:2118–2127

Rosenzweig KE, Sura S, Jackson A et al (2007) Involved-field radiation therapy for inoperable non small-cell lung cancer. J Clin Oncol 25:5557–5561

Salguero FJ, Belderbos JS, Rossi MM et al (2013) Microscopic disease extensions as a risk factor for locoregional recurrence of NSCLC after SBRT. Radiother Oncol 109:26–31

Senthi S, Haasbeek CJ, Slotman BJ et al (2013) Outcomes of stereotactic ablative radiotherapy for central lung tumours: a systematic review. Radiother Oncol 106:276–282

Slotman BJ, Lagerwaard FJ, Senan S (2006) 4D imaging for target definition in stereotactic radiotherapy for lung cancer. Acta Oncol 45:966–972

Spoelstra FO, Senan S, Le Pechoux C et al (2010) Variations in target volume definition for postoperative radiotherapy in stage III non-small-cell lung cancer: analysis of an international contouring study. Int J Radiat Oncol Biol Phys 76:1106–1113

Sura S, Greco C, Gelblum D et al (2008) (18) F-fluorodeoxyglucose positron emission tomography-based assessment of local failure patterns in non-small-cell lung cancer treated with definitive radiotherapy. Int J Radiat Oncol Biol Phys 70:1397–1402

Taremi M, Hope A, Lindsay P et al (2012) Predictors of radiotherapy induced bone injury (RIBI) after stereotactic lung radiotherapy. Radiat Oncol 7:159

Thorwarth D, Beyer T, Boellaard R et al (2012) Integration of FDG-PET/CT into external beam radiation therapy planning: technical aspects and recommendations on methodological approaches. Nuklearmedizin 51:140–153

Timmerman R, McGarry R, Yiannoutsos C et al (2006) Excessive toxicity when treating central tumors in a phase II study of stereotactic body radiation therapy for medically inoperable early-stage lung cancer. J Clin Oncol 24:4833–4839

Tofts R, Lee P, Sung A (2013) Interventional pulmonology approaches in the diagnosis and treatment of early stage non small cell lung cancer. Transl Lung Cancer Res 2:316–331

Underberg RW, Lagerwaard FJ, Slotman BJ et al (2005) Benefit of respiration-gated stereotactic radiotherapy for stage I lung cancer: an analysis of 4DCT datasets. Int J Radiat Oncol Biol Phys 62:554–560

van Loon J, Offermann C, Bosmans G et al (2008) 18FDG-PET based radiation planning of mediastinal lymph nodes in limited disease small cell lung cancer changes radiotherapy fields: a planning study. Radiother Oncol 87:49–54

Van Sornsen de Koste JR, de Boer HC, Schuchhard-Schipper RH et al (2003) Procedures for high precision setup verification and correction of lung cancer patients using CT-simulation and digitally reconstructed radiographs (DRR). Int J Radiat Oncol Biol Phys 55:804–810

van Tinteren H, Hoekstra OS, Smit EF et al (2002) Effectiveness of positron emission tomography in the preoperative assessment of patients with suspected non-small-cell lung cancer: the PLUS multicentre randomised trial. Lancet 359:1388–1393

Videtic GM, Belderbos JS, Spring Kong FM et al (2008) Report from the International Atomic Energy Agency (IAEA) consultants' meeting on elective nodal irradiation in lung cancer: small-cell lung cancer (SCLC). Int J Radiat Oncol Biol Phys 72:327–334

Wahidi MM, Govert JA, Goudar RK et al (2007) Evidence for the treatment of patients with pulmonary nodules: when is it lung cancer?: ACCP evidence-based clinical practice guidelines (2nd edition). Chest 132:94S–107S

Werner-Wasik M, Yorke E, Deasy J et al (2010) Radiation dose-volume effects in the esophagus. Int J Radiat Oncol Biol Phys 76:S86–S93

Wolthaus JW, Sonke JJ, van Herk M et al (2008) Comparison of different strategies to use four-dimensional computed tomography in treatment planning for lung cancer patients. Int J Radiat Oncol Biol Phys 70:1229–1238

Yuan S, Meng X, Yu J et al (2007) Determining optimal clinical target volume margins on the basis of microscopic extracapsular extension of metastatic nodes in patients with non-small-cell lung cancer. Int J Radiat Oncol Biol Phys 67:727–734

Liver Tumors

6

Thomas Brunner and Daniel Schanne

Contents

T. Brunner (✉)
Department of Radiation Oncology, University Hospitals of Freiburg, Freiburg im Breisgau, Germany
e-mail: thomas.brunner@uniklinik-freiburg.de

D. Schanne
Department of Radiation Oncology, University Hospitals of Freiburg, Freiburg im Breisgau, Germany

Department of Radiation Oncology, Massachusetts General Hospital, Charlestown, MA, USA
e-mail: Daniel.schanne@uniklinik-freiburg.de

6.1 Anatomy

The liver nestles in the right dome of the diaphragm in the hypochondrium. The dome projects to the 4th rib at maximal expiration and to the 7th rib at maximal inspiration at the junction between the cartilage and the bone. One quarter of the organ is to the left of the median in the epigastrium cranial of the stomach. The caudal liver edge projects from the 10th rib on the right side to the 7th rib on the left side and moves perpendicularly in the craniocaudal direction with respiration. The liver is in close contact with the costal arch and therefore reaches up to the level of the pleural space. The costodiaphragmatic recesses reach the 7th rib in the front and at the 9th rib in the mid-axillary line. In the area of the 9th to the 11th rib, the liver is outside the pleural area.

At the lower surface (facies visceralis), the gallbladder and the inferior vena cava intercalate deeply into the liver tissue creating the fissure sagittalis dextra. The peritoneal sulcus of the left

A.-L. Grosu, C. Nieder (eds.), *Target Volume Definition in Radiation Oncology*,
DOI 10.1007/978-3-662-45934-8_6, © Springer-Verlag Berlin Heidelberg 2015

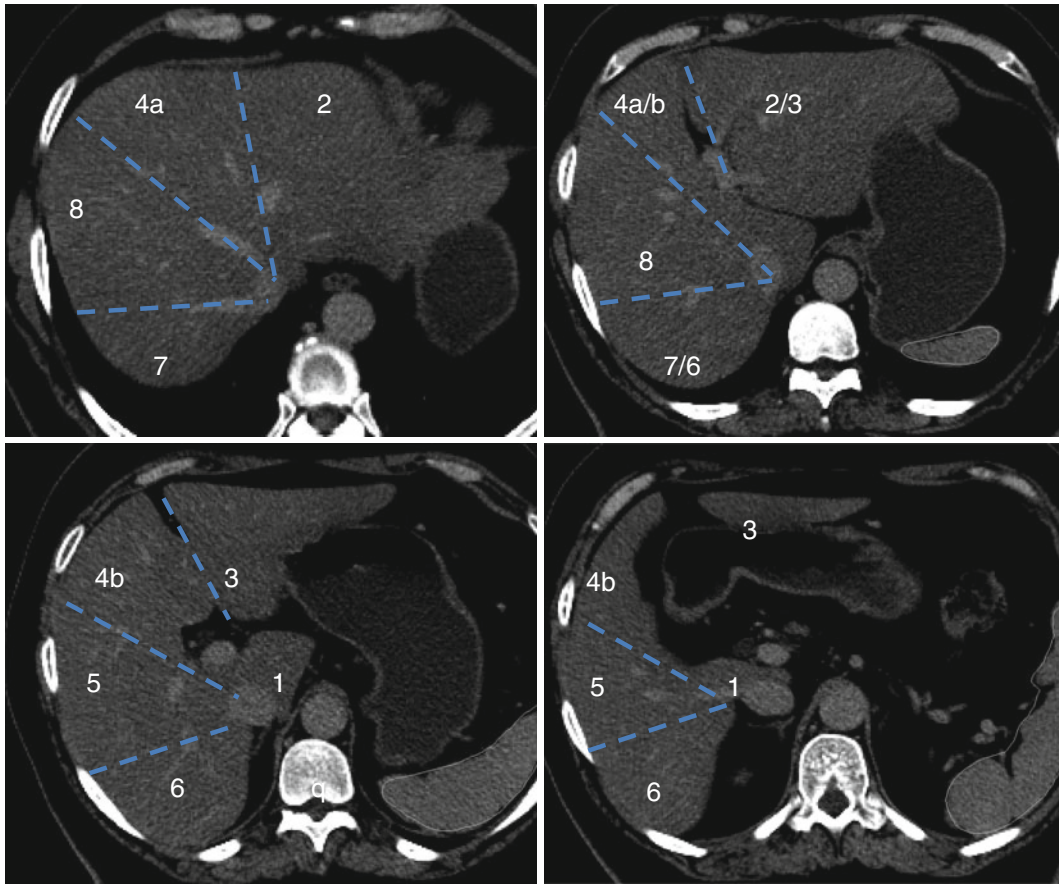

Fig. 6.1 Illustration of the eight liver segments in selected slices of the liver from in a transversal CT scan. Numbers indicate the respective segments of the liver

fissure is interrupted by the caudal process of the caudal lobe. The right liver fissure corresponds to the so-called Sérégé-Cantlie line that constitutes the border between the portal coverage area of the right and of the left liver lobe, and it groups the caudal lobe, the quadratic lobe and the left lobe into an entity. The intrahepatic division of the branches of the portal vein creates a segmental subdivision. Most authors described four segments and eight subsegments.

The main branches of the portal vein have their own respective coverage areas and do not anastomose with each other. They are accompanied by the branches of the A. hepatica propria and of the bile ducts. This so-called hepatic triad of pathways is responsible for the segmentation. The tributaries into the hepatic veins are separate from the triad and locate mostly to the border zones of the segments.

The right liver lobe has an anterior and a posterior segment. In the left liver lobe, there is a medial and a lateral segment. The subsegments form by the subdivision of the branches of the portal vein into an upper and a lower sub-branch.

The eight liver segments (Fig. 6.1) can be localised in computed tomography following the topography of the liver veins and by the portal vein. Similar to the lung the respective segments are drained by the veins running intersegmentally. Usually, three main branches of the liver veins below the diaphragm drain in a star-shaped form into the inferior vena cava. Subdiaphragmatically, the right, middle and left liver vein can be identified in one slice. These subdivide the liver into four vertical sectors which are further discriminated into two horizontal planes by the level of the portal vein. The left liver vein runs sometimes in

the longitudinal fissure dividing the quadrate lobe (segment 4) from the left lateral segments 2 and 3. The middle liver vein is the border between the left and the right liver lobe marking a perpendicularly running plain which caudally ends in the bed of the gallbladder. The right liver vein subdivides the right lobe on one hand into the anterior segments 5 and 8 and on the other hand into the dorsally situated posterior segments 6 and 7. The segments 7 and 8 form the dome of the liver. The caudate lobe corresponds to segment 1, draining via smaller veins directly into the inferior vena cava.

The grouping of the liver segments is independent from the macroscopic architecture of the lobes that are essentially caused by the peritoneal sulcus and by the liver fissures. The left sagittal fissure is caused by the venous ligament (Lig. arantii, a relic of an embryonal anastomosis between the portal vein and the inferior vena cava) and by the falciform ligament containing the obliterated umbilical vein (Lig. teres) in its caudal edge. The peritoneal duplications of the left hepatic fissure embrace the porta hepatis, and they represent the anatomic demarcation between the lobes subdividing the caudal surface into two regions: the hepatorenal space is to the right and the hepatogastric space is to the left. The caudal surface is completely covered by the peritoneum, and therefore it is mobile with respect to the neighbouring organs. The liver slides across the stomach on the left side and across the duodenum, the colonic flexure and the right kidney on the right side. The contact surfaces to these organs are recognised by corresponding impressions of the caudal liver surface.

At the cranial surface of the liver (facies diaphragmatica), the falciform ligament divides into two sheets (Lig. coronarium or triangular hepatis dext. and sin.) enclosing a rhomboidal extraperitoneal field (area nuda or pars affixa). In this area the inferior vena cava intercalates deeply the liver tissue. Additionally the right adrenal and the cranial poles of the kidney are located in this area without peritoneal coverage. The pars affixa almost entirely is in the centrum tendineum of the diaphragm, and it locks the liver in its position. The thoracic pull and the inferior vena cava that receives several liver veins in this area as well as the appendix fibrosa support this effective fixation.

The demarcation of the area nuda is given by the two coronal ligaments (Lig. coronaria) running out into the ligament triangularia and then into the diaphragmal fascia. The peritoneal sulcus behind the liver is often tougher and is called Lig. hepatorenal or Lig. hepatocavoduodenale due to its location.

The pathways have a characteristic layout in the porta hepatis. The portal vein is posterior most, followed ventrally by the hepatic artery and its adventitial and vegetative neural plexus and by the extrahepatic bile ducts as well as the portal lymphatics. The liver veins do not open out into the porta hepatis but directly into the inferior vena cava in the area nuda. The arteries of the liver derive from the branches of the proper hepatic artery that takes its origin from the common hepatic artery and hence from the celiac trunk.

The lymphatic vessels of the liver mainly collect in the porta hepatis, and they reach the celiac lymph nodes and the paraaortic nodes, the cisterna chyli and the thoracic duct. Additionally there is a subserous, superficial lymphatic system on one hand towards the retrosternal and to the anterior mediastinal lymphatics and on the other hand dorsally to the juxtacaval and the posterior mediastinal lymphatics.

6.2 Pathology

Currently, the seventh edition of the UICC classification is in use (Sobin et al. 2009). There is a classification for hepatocellular carcinoma and one for intrahepatic bile ducts. Of relevance for radiotherapy in this context is also the classification of the perihilar extrahepatic bile ducts. The T categories are:

6.2.1 Hepatocellular Carcinoma

- T1: solitary tumour without vascular invasion
- T2: solitary tumour with vascular invasion *or* multiple tumours, none more than 5 cm in greatest dimension
- T3: multiple tumours any more than 5 cm *or* tumour involving a major branch of the portal or hepatic vein(s)

  - T3a: multiple tumours any more than 5 cm
  - T3b: tumour involving a major branch of the portal or hepatic vein(s)
- T4: tumour(s) with direct invasion of adjacent organs other than the gallbladder *or* with infiltration of visceral peritoneum

Together with the lymph node status discriminating N0 (no regional lymph node metastasis) and N1 (regional lymph node metastasis), this leads to the following stage grouping:

Stage	T category	N category	M category
Stage I	T1	N0	M0
Stage II	T2	N0	M0
Stage IIIA	T3a	N0	M0
Stage IIIB	T3b	N0	M0
Stage IIIC	T4	N0	M0
Stage IVA	Any T	N1	M0
Stage IVB	Any T	Any N	M1

6.2.2 Intrahepatic Bile Ducts

- T1: solitary tumour without vascular invasion.
- T2a: solitary tumour with vascular invasion.
- T2b: multiple tumours, with or without vascular invasion.
- T3: tumour perforates the visceral peritoneum or directly invoked adjacent extrahepatic structures.
- T4: tumour(s) with periductal invasion.

Together with the lymph node status discriminating N0 (no regional lymph node metastasis) and N1 (regional lymph node metastasis), this leads to the following stage grouping:

Stage	T category	N category	M category
Stage I	T1	N0	M0
Stage II	T2	N0	M0
Stage III	T3	N0	M0
Stage IVA	T4	N0	M0
	Any T	N1	M0
Stage IVB	Any T	Any N	M1

6.2.3 Extrahepatic Bile Ducts: Perihilar

- T1: tumour confined to the bile duct, with extension up to the muscle layer of fibrous tissue.
- T2a: tumour invades beyond the wall of the bile duct surrounding adipose tissue.
- T2b: tumour invades adjacent hepatic parenchyma.
- T3: tumour invades unilateral branches of the portal vein or hepatic artery.
- T4: tumour invades the main portal vein or its branches bilaterally, of the common hepatic artery, of the second-order biliary radicals bilaterally or unilateral second-ordered biliary radicals with contractual portal vein or hepatic artery involvement.

Together with the lymph node status discriminating N0 (no regional lymph node metastasis) and N1 (regional lymph node metastasis), this leads to the following stage grouping:

Stage	T category	N category	M category
Stage I	T1	N0	M0
Stage II	T2a, T2b	N0	M0
Stage IIIA	T3	N0	M0
Stage IIIB	T1, T2, T3	N1	M0
Stage IVA	T4	N0, N1	M0
Stage IVB	Any T	Any N	M1

6.3 Visualisation

6.3.1 Computed Tomography

Computed tomography (CT) is the most widely used imaging technique because it is commonly available, fast and affordable. It is strongly recommended to acquire a CT with diagnostic quality, using breath holding to yield an anatomically correct image of the tumour without breathing distortion. This image set should then be completed with 4D imaging to incorporate the tumour motion. Unfortunately, liver CT is limited by its inherently low tissue/tumour contrast. Because of this, it is necessary to apply IV contrast in all obtained CT scans. The contrast dye will significantly improve the tissue/tumour contrast and subsequently the ability to delineate the tumour. A recommended image resolution is 1×1 mm in a plane with a 2-mm slice thickness.

When using IV contrast, it is important to acquire the images during the right contrast phase according to the type of examined tumour.

Depending on histology, liver tumours may show a stronger enhancement during the arterial

phase (~30 s after injection) and a lower enhancement during the venous phase (~50–60 s after injection) and the late delayed phase (~180 s after injection) compared to the surrounding liver tissue. This so-called washout phenomenon occurs faster in primary hepatocellular carcinoma (HCC) than in metastases, making it necessary to acquire multiple-phase scans and choose the optimal image set for treatment planning afterwards.

There is also a significant inter-patient variability of contrast dye enhancement that can be accounted for by using a small test bolus of IV contrast preliminary to the actual scan to determine the best time for imaging after IV contrast injection (Bruix and Sherman 2011).

It is also recommended to use oral contrast to facilitate the correct delineation of organs at risk, e.g. the stomach and the intestines.

Due to the differences in CT scanners, contrast dyes and workflows, injection protocols should be optimised for each institution before being used in clinical routine.

Another disadvantage of CT holds up especially for intrahepatic cholangiocarcinoma (CCC). While there is a high sensitivity for detection on IV contrast-enhanced CT, the infiltrative growth pattern of CCC hampers tumour delineation on the acquired images, thereby making alternative imaging (e.g. MRI) obligatory for target volume definition (Charbel and Al-Kawas 2011).

6.3.2 MRI

Compared to CT, magnetic resonance imaging (MRI) offers a higher contrast in soft tissues, especially on non-enhanced scans (Bolog et al. 2011). The variety of available MRI sequences (e.g. T1, T2, diffusion and spectroscopy) allows for detailed conclusions about the size of the investigated lesion, its surrounding edema and infiltration into surrounding tissue which improves target volume delineation and protection of normal tissues. The development of multi-detector CT has recently caught up to MRI concerning sensitivity, but its flexibility in the use of the different sequences and the considerably higher ability to distinguish benign from malignant lesions are still an unrivalled advantage of MRI (Glockner 2007; Ariff et al. 2009).

As in CT, the application of IV contrast after native image acquisition further increases the significance and validity of the MRI scan. Most contrast dyes are based on gadolinium compounds that depict the vascularisation of the investigated tissues. But more advanced agents like gadolinium ethoxybenzyl diethylenetriaminepentaacetic acid (Gd-EOB-DTPA), which are taken up specifically by liver cells, result in a tissue-specific contrast and make it possible to distinguish primary from secondary liver lesions. There are however some limitations to this method, because the cellular uptake of Gd-EOB-DTPA depends on functionally unimpaired liver tissue. This is especially relevant in the diagnosis of HCC due to the cirrhosis that can be appreciated frequently in these patients (Murakami et al. 2012). Another tissue-specific contrast agent is superparamagnetic iron oxide (SPIO), a substance that is taken up by the liver-immanent macrophages of the reticuloendothelial system, thereby leading to a negative contrast, particularly against non-liver tissues.

Disadvantages of MRI include the longer image acquisition time, making 4D imaging more difficult and increasing the dependence on patient compliance. Furthermore it bears higher costs, and the narrow gantry can limit the use of other technical equipment (e.g. stereotactic body frame, abdominal compression, etc.).

6.3.3 FDG-PET/CT

For reliable results, positron emission tomography (PET) should be combined with a co-registered CT scan to offer a better anatomical correlation of tracer enhancement. However, the most commonly used tracer (Hallman et al. 2012) fluorodeoxyglucose (FDG) shows a relatively poor sensitivity of 40–78 % for primary liver lesions and thus is not a useful tool for the improvement of target volume delineation (Goh et al. 2012; Corvera et al. 2008). But this does not hold up to the diagnosis of hepatic metastases, where FDG-PET/CT seems to be among the most reliable imaging techniques with

a sensitivity of up to 95 %, though it will usually not add significant information to the target volume, if CT and MRI are already available (see also 6.5) (Sacks et al. 2011). The main use of FDG-PET/CT is therefore the search for nodal disease and distant metastases of the tumour in question – a very important role, especially in stereotactic, locally curative treatments. In newer studies PET was also deemed useful in treatment follow-up, especially metabolic response evaluation (Solanki et al. 2012).

6.4 4D Imaging

The method uses 4D imaging (CT, MRI, PET) to compensate for tumour motion. The images should be acquired in different breathing phases of the patient to track the complete tumour movement. Many liver tumours are only visible in CT with IV contrast, so identification of the tumour on 4D scans can prove particularly difficult. Prior implantation of fiducial markers can help to overcome this restriction (Fig. 6.2). Alternatively, contrast phases. native cine MRI or 4D-FDG-PET imaging are good solutions to the problem, the latter mostly for liver metastases. Also, the motion of surrogate landmarks, either anatomical (liver incisions/veins/boundary) or artificial ones (fiducials, surgical clips) is useful for contouring of ITV and for IGRT. These surrogates should not be seated too far from the tumour because of the changing anatomical shape of the liver itself during the breathing cycle. Thus, markers directly adjacent or within the lesion lead to the most accurate results (Seppenwoolde et al. 2011). A well-suited marker will reflect not only the translational movements of the target but also the rotational component of the liver motion and is radiopaque to allow for image-guided radiotherapy with cone-beam CT (CBCT) or fluoroscopy. Furthermore it is recommended to use three or more markers in an appropriate distance to one another to enable three-dimensional motion

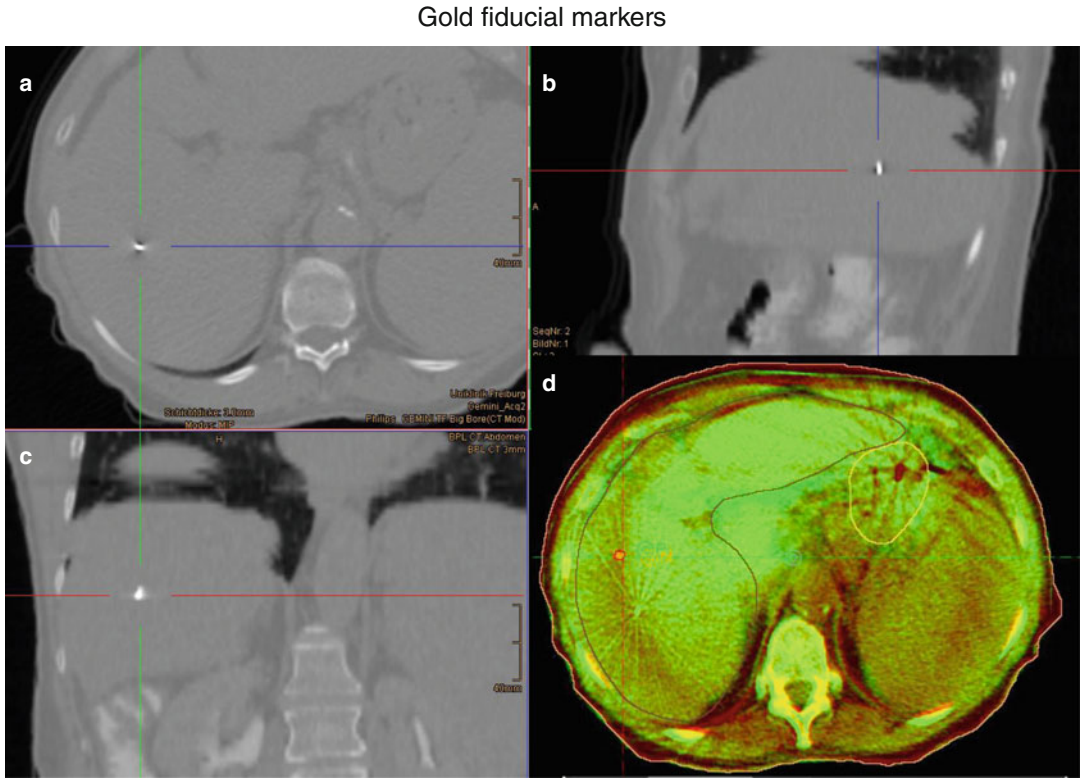

Fig 6.2 Example of a gold fiducial marker in (**a**) transveral, (**b**) sagittal, and (**c**) coronal plane of the planning CT. (**d**) Cone beam CT on treatment of the same patient with positioning of the patient to gold markers

assessment. To achieve optimal results, the obtained 4D scans should be co-registered to the planning CT during target volume delineation.

6.5 Target Volume Delineation

6.5.1 Gross Target Volume Delineation

Prior to delineation, all image sets (CT, MRI, PET, 4D sequences) should be co-registered, if technically possible with deformable registration. The tumour can then be demarcated according to its morphological properties. The basis should be an IV contrast-enhanced CT scan in the appropriate contrast phase, as mentioned earlier. The additional information of a contrast-enhanced MRI can prove to be useful in case of isodense tumours or malignancies with an infiltrative growth pattern. If an MRI with the required quality is not clinically available, PET can facilitate delineation but also bears its own technical difficulties like the correlation of the metabolic PET information to the anatomic position in the planning CT or the relatively high liver-background signal of some tracers (e.g. FDG).

It cannot be overstressed that careful evaluation of all available imaging is of highest importance. This includes previous scans during the course of the diseases and all available current imaging (CT, MRI, FDG-PET, ultrasound). Concerning CT imaging, it is important to actively modify the windowing of the scans individually for best visualisation of the boundaries of a specific lesion.

6.5.2 Clinical Target Volume Delineation

Because there is no general consensus in the published literature, CTV definition depends heavily on specific protocols in individual treatment centres and the clinical experience of the radiation oncologist. But the basis to determine the extent of the CTV is the tumour histology (Sterzing et al. 2014).

For HCC, preliminary correlational studies of radiological findings and histopathology suggest a CTV margin of 4 mm to cope for tumour invasion with 100 % accuracy, although the microscopic invasion can be smaller depending on tumour size, tumour marker level and other factors (Bi et al. 2010). In contrast, intrahepatic CCC with its invasive growth pattern calls for a CTV margin of 5–10 mm to cover 100 % of the microinvasion, again depending mostly on tumour size, histologic grading and tumour marker levels (Tse et al. 2008). Concerning the multitude of different metastases that can affect the liver, the CTV should be adapted according to the primary tumour histology and the radiomorphologic infiltration pattern in these cases with a margin of 0–10 mm around the GTV (Brock 2011). Importantly, after expansion of the GTV/ITV to the CTV the resulting volume has to be carefully evaluated for regions where this would include volumes beyond the limits of the liver. Such areas need to be edited manually if infiltration beyond the organ boundaries is not likely to avoid erroneous expansion into the neighbouring structures potentially leading to increased toxicity.

6.5.3 Planning Target Volume Delineation

The purpose of PTV definition is the compensation of technical inaccuracies (patient set-up, equipment set-up, etc.) and breathing motion. This also means that the PTV has to be adapted to the motion management technique in use, making it necessary to take its respective intra- and interfractional accuracy into account.

The most simplistic possibility is a fixed PTV margin around the CTV. This method however is not suitable in most cases due to the significant breathing motion of the liver, making an approach of asymmetric expansion with larger margins in the CC direction more serviceable. More advanced methods like breath-hold, gating or tracking techniques allow for a significant reduction of safety margins but also come along with a higher demand for technical equipment, patient compliance and staff training, thereby adding further error sources that have to be accounted for in the PTV.

In general, a PTV of 4–5 mm around the CTV is appropriate for stereotactic treatments (SBRT) with larger margins possible according to the individual case and techniques in use.

6.5.4 The Ann Arbor-Toronto Target Volume Delineation Concept

At Ann Arbor and the Princess Margaret Hospital, Toronto, an individualised six-fraction SBRT concept for liver cancer was developed (Tse et al. 2008). This concept is here described because the target volume definition is specific and the concept has gained international reputation. Within that concept dose is allocated dependent on the volume of normal liver irradiated (Ten Haken et al. 1993; Dawson et al. 2006). The reason for this concept is to optimise local control for small and large tumours based on the estimation of normal tissue complication probability (NTCP) for radiation-induced liver disease (RILD). This concept allows prescription of the highest possible save dose on an individual basis with a maximum dose of 60 Gy in six fractions. The NTCP for RILD depends on liver function which is impaired in HCC, and therefore the radiation dose is prescribed to an isodose covering PTV2 (see description below) with a maximum dose of 140 % within the target. The GTV is delineated based on triphasic CT and/or MRI including enhancing large vessel thromboses. For HCC and intrahepatic CCC an 8 mm margin around the GTV within the liver and non-enhancing thromboses is used to create the CTV

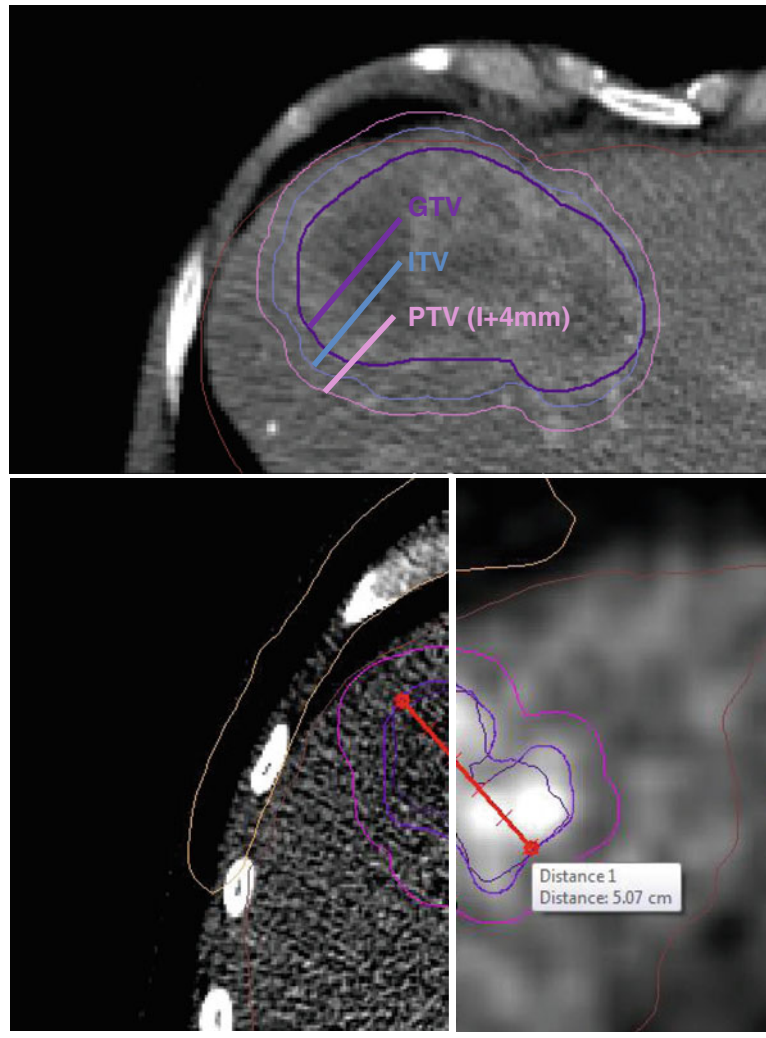

Fig. 6.3 *Top*: Planning CT scan with IV contrast in the portal venous phase for a 10 cm metastasis from breast cancer depicting the respective target volumes. Gross target volume (GTV) as visualised in the planning FDG-PT/CT scan, expansion to the internal target volume (ITV) on the basis of the 4D-PET scan. Direct expansion of the ITV by isotropic 4 mm to obtain the planning target volume (PTV). No clinical target volume was contoured in this case. *Bottom*: Planning FDG-PET/CT scan of 5 cm metastasis from pancreatic cancer shown on the CTV (left) and 4D-PET (right). Same colour coding as above

(Fig. 6.3). This CTV is further expanded to derive PTV1. Margins for both, PTV1 and PTV2, are individualised with a minimum of 5 mm and based on the following criteria: (1) use of breath hold or not, (2) reproducibility of breath hold, (3) liver motion due to breathing and (4) reproducibility of motion (Park et al. 2012). Organs at risk are also contoured, and these are the liver, stomach, small bowel in the irradiated volume, large bowel in the irradiated volume, kidneys, heart and spinal cord. The normal tissue constraints for six-fraction SBRT are for the liver determined by V_{eff}/NTCP (mean <22 Gy); for kidney a mean <12 Gy; for spinal cord a maximum <27 Gy; for stomach, small bowel and large bowel a maximum <30 Gy; for heart a maximum <40 Gy; and for the ribs a maximum <54 Gy.

6.6 Motion Management

Accounting for tumour motion is one of the most important steps in the treatment planning of liver tumours and can lead to a significant reduction in target volume size. The liver is seated directly under the diaphragm and is thus usually subject to substantial movement during breathing cycles. Craniocaudal (CC) movement is the most dominant direction of movement with ranges typically around 9–10 mm and up to several centimetres, but the lesions also frequently move in the anterior/posterior and lateral directions, sometimes even exceeding the CC shift (Hallman et al. 2012; Wolthaus et al. 2006). The American Association of Physicists in Medicine (AAPM) Task Group 76 recommends the implication of motion management techniques for tumours with a motion of >5 mm and thereby evidently underlines the necessity of this topic to be taken into account.

6.6.1 Adjusting the Target Volume/ ITV

One way of dealing with tumour motion is the definition of an internal target volume (ITV) which is the sum of individual tumour volumes in different breathing phases, leading to an enlarged, usually cylindrical volume (because of the dominant CC movement). If 4D scans of the extreme breathing excursions are used, the resulting ITV covers all possible positions the tumour can remain in, but it also bears the risk of being too large because the patient will not constantly inhale and exhale so deeply. This can result in problems, especially in stereotactic treatment if the tumour is seated in delicate positions near critical organs at risk like the small bowel or the stomach. To avoid this, the concept of mid-ventilation can be used, where the target volume encompasses only the part of the ITV in which the tumour is most frequently found during the breathing cycle (Eccles et al. 2006).

6.6.2 Instructed Shallow Breathing

Instructed shallow breathing is one of the simplest methods of tumour motion reduction, and in its most basic approaches, it does not need any technical equipment. The disadvantage, however, is the great amount of patient compliance that is needed to ensure a reproducible result. In order to improve this, the patient can be trained to use breathing coordinating systems which limit inspirational or expirational volume according to a previously defined value. This method has shown a good intrafractional reproducibility but a slightly worse interfractional reproducibility, making regular image guidance necessary (Cerviño et al. 2009).

6.6.3 Breath Hold

Another early technique is the breath-hold method and, as shallow breathing, it holds the advantage of a low technical demand on the treatment equipment. The patient is instructed to inhale or exhale until a predefined breathing state is reached. Then, the treatment is carried out while the patient is holding their breath. Depending on the time span that the patient can

remain in this state, it can be necessary to repeat the procedure and deliver the planned dose over several breath holds. Breath hold requires all planning images to be obtained in the same breathing state as planned for the treatment.

Technically, breath hold does not need image guidance. However, it is especially challenging in patients with co-morbidities and compliance problems. The same holds up for respiratory monitoring, which is also not mandatory, but can increase the reproducibility of the individual breath holds (Wong et al. 1999).

Another useful addition can be an active breathing control (ABC) device, which makes the patient breathe through a tubus in their mouth. A connected valve will shut after a predefined volume of air has passed through after which the treatment can be started. This can improve the treatment, especially for non-compliant patients with problems to follow the instructions properly. If used, the ABC should be applied during all image acquisitions and treatment sessions (Moorrees and Bezak 2012).

There are different concepts described in the literature with treatment delivery in either end-exhalation or end-inhalation state. It has been reported that treatment in exhale position shows a higher intrafractional accuracy of 2.2 ± 2 mm compared to 4.0 ± 3.5 mm in inhale position. In case of cranially seated tumours, deep inspiration breath hold can spare more healthy lung tissue due to the inflated state of the lung although the affected amount of the lung will not be clinically relevant in the treatment of most liver lesions (Brock 2011; Heinzerling et al. 2008).

6.6.4 Abdominal Compression

Compared to instructed shallow breathing, abdominal compression (AC) has the significant advantage of lower dependence on patient compliance. The average reduction in tumour motion that can be achieved with AC is 2–6 mm, allowing for a significant reduction of the safety margins around the target volume, especially in stereotactic treatment (Eccles et al. 2011; Moorees and Bezak 2012). The AC should be applied during all image acquisitions that are used for treatment planning and during the treatment itself. It is recommended to monitor the correct application and the effect of the AC on an interfractional basis.

6.6.5 Gating

Gating is an advanced form of the breath-hold technique. Prior to the radiation treatment, a volume is selected which the tumour passes through during particular states of the breathing cycle. The beam will then repeatedly be turned on while the tumour is in this so-called gate and turned off when it leaves. The preferential gating position is natural exhale due to the minimal organ motion occurring during this state. Treatment planning should utilise 4D imaging with subsequent selection of sequences to ensure the precise determination of the appropriate breathing phase. If 4D imaging is not available, the planning CT can alternatively be obtained only in the desired gating phase after determination of the designated breathing state by preliminary imaging (ultrasound, fluoroscopy, etc.).

To determine the tumour position during radiation treatment, surrogates like respiratory monitoring (e.g. spirometer, breathing belt), fiducial markers or anatomical landmarks in combination with fluoroscopy should be used.

An advantage of gating over the breath-hold technique is the lower dependency on patient compliance because there are no specific instructions the patient has to follow. But this easement is traded in for a higher demand for advanced equipment and thorough planning. Thus, the major difficulties of the gating method are the correct definition of gate position and width to balance the achieved doses in tumour and organs at risk and the precise determination of the tumour position during the treatment session (Heinzerling et al. 2008).

6.6.6 Tracking

The principle of tracking is the constant monitoring of the tumour position in time and the consecutive adaptation of the radiation beam. There are many commercial tracking systems on the market, most of them using surrogate markers like fiducial markers, spirometers, optical markers and others to determine the tumour location. The reported accuracy for these systems ranges between 0.04 and 4.4 mm (Dawson and Ten Haken 2005). In order to maintain the tumour in the radiation beam, most methods rely on couch movement, movement of the radiation source or modification of the multi-leaf collimator arrangement. Which

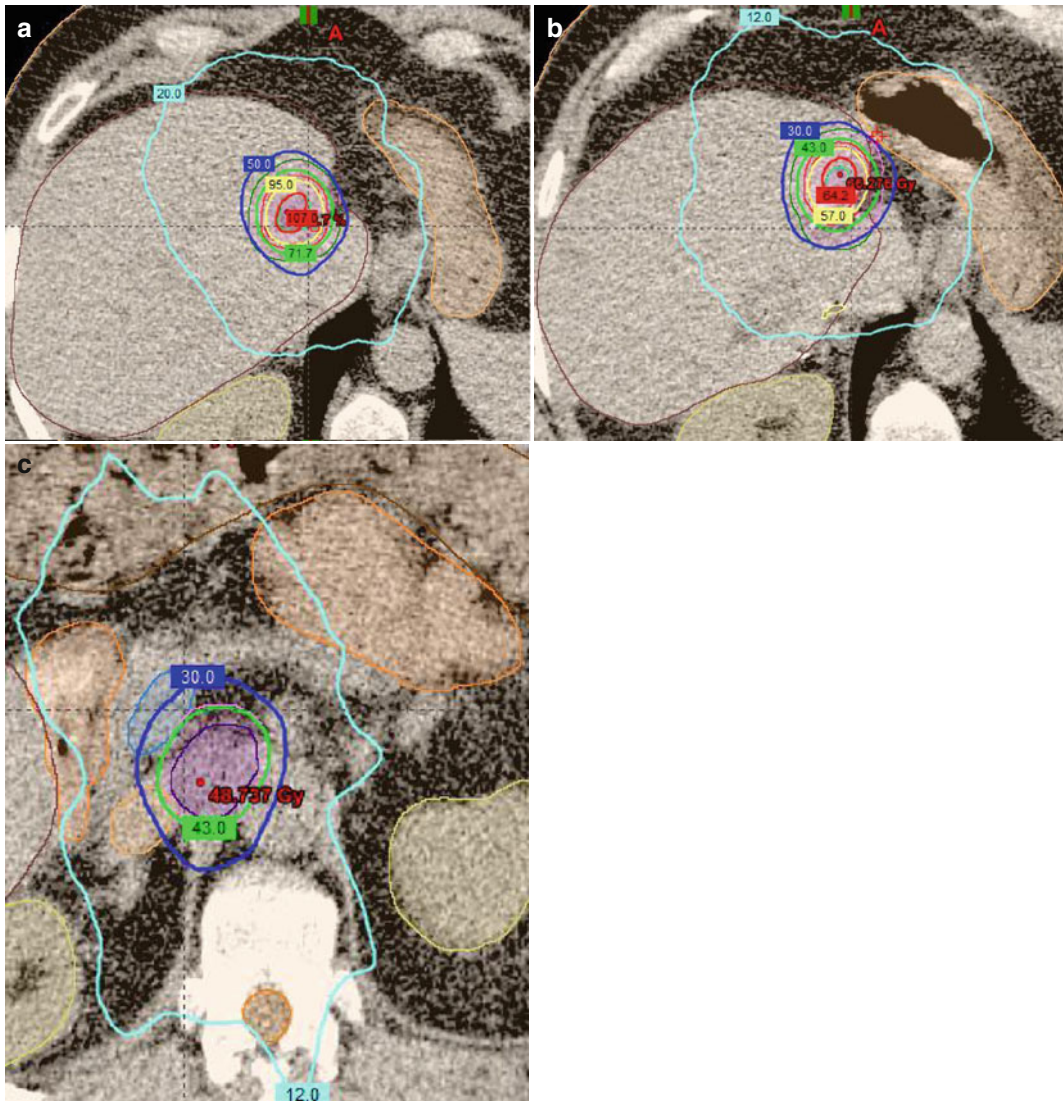

Fig. 6.4 Patient with a liver metastasis from colorectal cancer after two resections for previous liver metastases and FOLFOX chemotherapy at the left edge of the liver. Plan for six fractions of 10 Gy each (EQD2 α/β10 = 100 Gy; BED α/β10 = 120 Gy). (**a**) cranial section with relative isodoses and (**b**) more caudal section with absolute isodoses and proximity to the stomach. (**c**) interaortocaval lymph node treated with six fractions of 7.5 Gray each (EQD2 α/β10 = 65.6 Gy; BED α/β10 = 78.8 Gy)

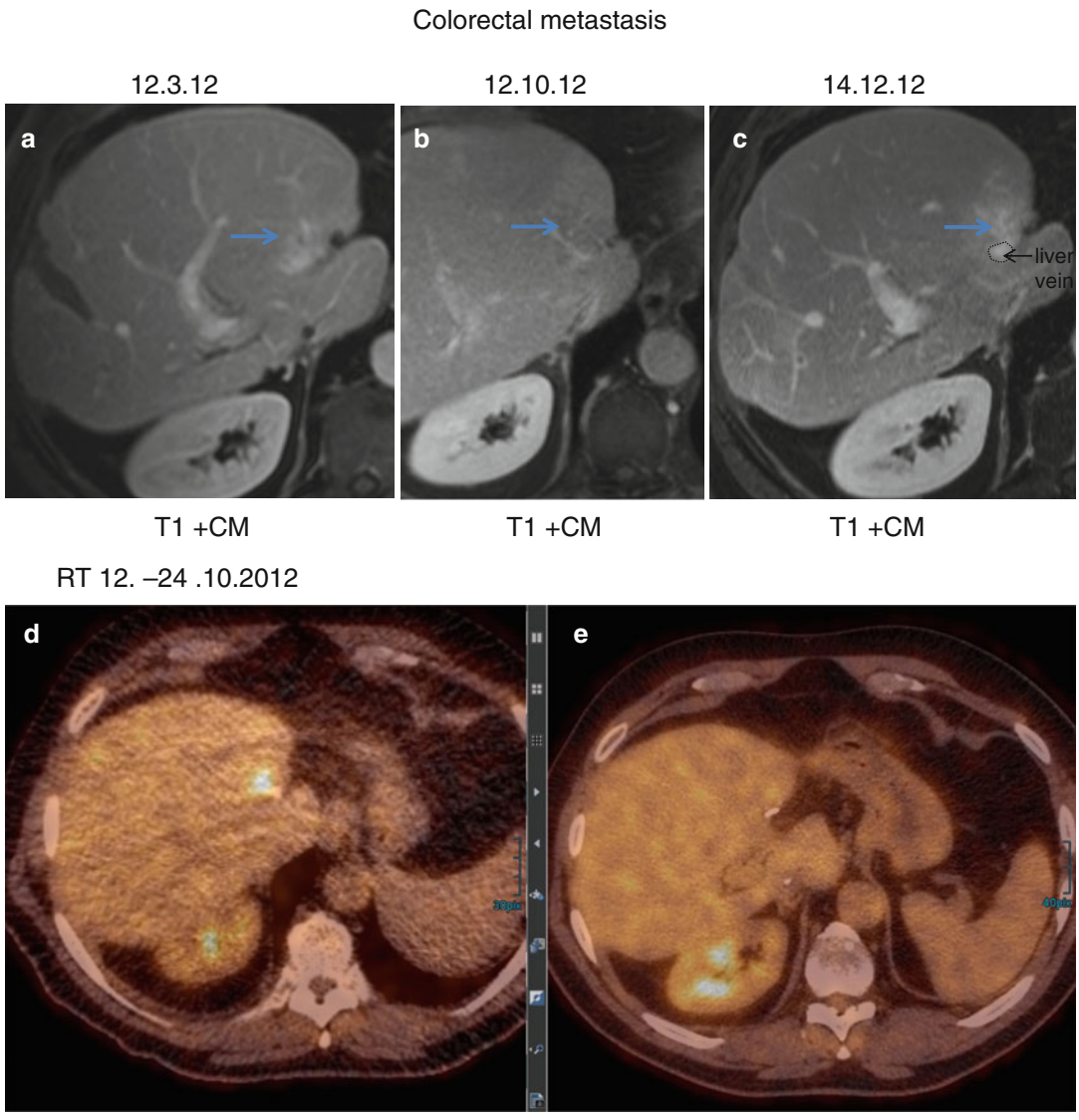

Fig. 6.5 Course of the liver lesion shown in Figure 6.3 (**a** & **b**) prior to treatment (12.3. and 12.10.) and 6 weeks after (14.12.) completion of SBRT. Patient has had left hemihepatectomy; (**a**) arterial phase (T1 vibe after gadolinium): next to a susceptibility artifact in segment 8/5 is a diffuse enhancement with same size as in previous imaging; (**b**) t1 fl_fs after gadolinium: a liver metastasis at the resection margin in segment 8/5, now 1.5 cm in size; (**c**) t1 vibe fs post gadolinium: persisting uptake of the contrast agent after SBRT. (**d**) FDG-PET/CT staging on 24.8.12: FDG take-up typical for malignant disease at the surgical resection margin before SBRT. (**e**) FDG-PET/CT restaging on 07.10.12: no FDG avidity left, i.e. complete metabolic response (mCR) after SBRT. In summary, the MRI re-staging images in comparison with PET are interpreted as post-therapeutic changes in the MRI scan and mCR 6 weeks after SBRT. Local control has been maintained for 30 months after therapy until last follow up

The Ann Arbor-Toronto target volume concept for HCC-and ICC-SBRT in six fractions with individualised dosing

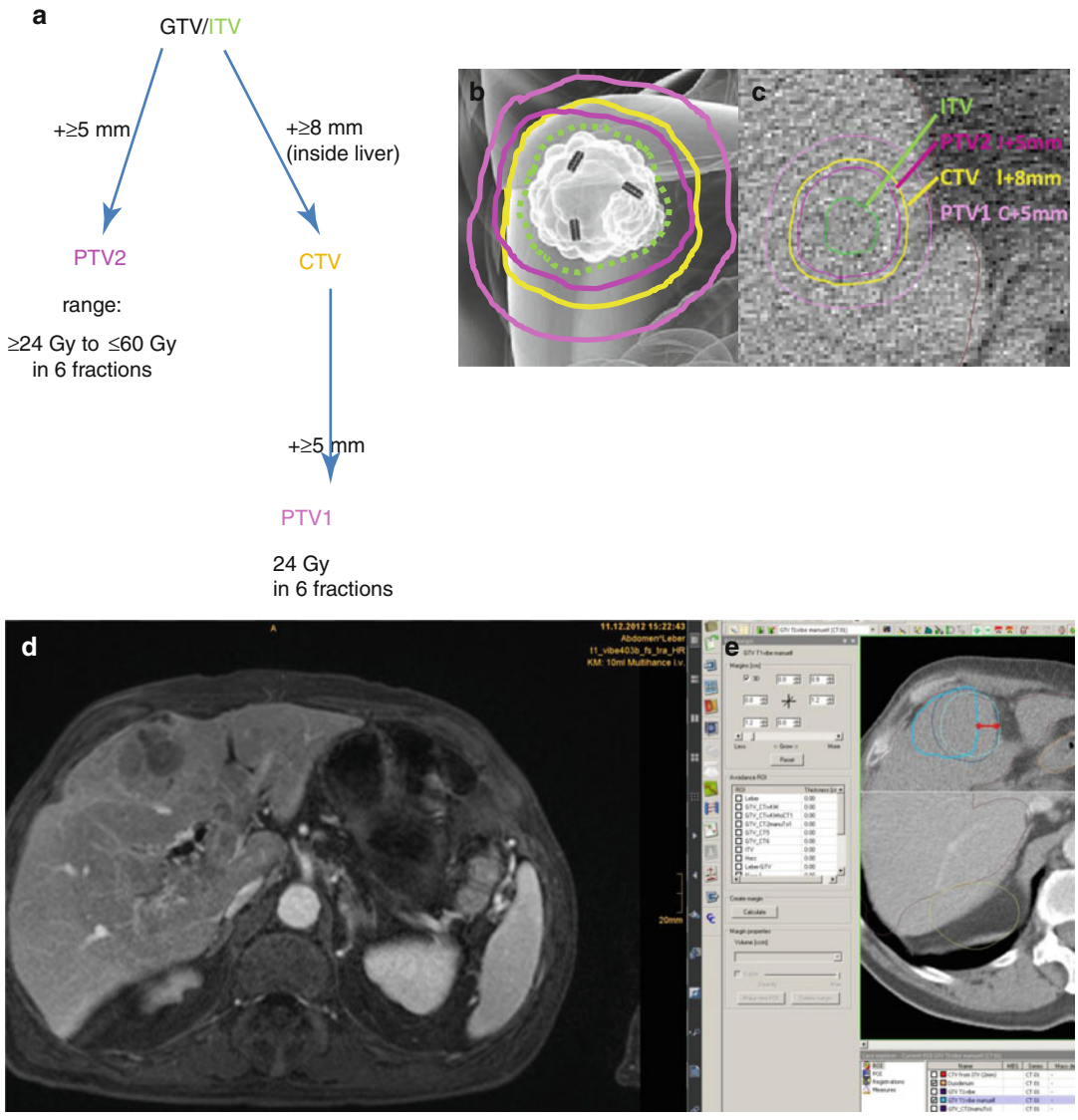

Fig. 6.6 The Ann Arbor-Toronto target volume concept for HCC- and ICC- SBRT in six fractions with individualised dosing. (**a**) *Left panel*: flow chart of the generation of the respective elements of the target volume delineation in a phase I trial escalating dose to PTV2 up to 60 Gy. (**b**) *Middle panel*: note that the CTV (*yellow*) is limited to intrahepatic expansion only. (**c**) *Right panel*: the concept applied to a hepatocellular cancer. (**d**) An example for lateral motion: an MRI scan showing an HCC lesion in segment IVa/b (T1 vibe post gadolinium) and (**e**) showing the large amount of lateral respiratory motion (*red arrow*).

method is the optimal depends on the type of treatment that is planned, staff training and financial budget of each individual institution (Figs. 6.4–6.6).

6.7 Radiation Induced Liver Toxicity (RILD)

Irradiation of the liver can lead to severe toxicity if certain precautions and dose limits are not met. Radiobiologically the liver is a parallel organ at risk, meaning that partial loss of function can be compensated by residual healthy liver tissue, if the mean liver dose does not exceed a threshold value. Thus, the liver – like the lung – is especially suitable for stereotactic high-dose treatment with a steep dose decline to the surrounding liver tissue.

Mean liver doses higher than 30–35 Gy come with a substantial risk of RILD (Lawrence 1995). Patients without preceding liver diseases will typically present several weeks to 4 months after radiation treatment with symptoms like ascites, hepatomegaly and isolated alkaline phosphatase increase but usually without jaundice (classic RILD). The underlying cause is not yet fully understood, but histopathologic studies proposed the model of veno-occlusive disease (VOD), where irradiation leads to damage in endothelial cells of the sinusoids and central veins, which activates the coagulation cascade and thereby leads to fibrinous clots that are soon accompanied by blood cells, particularly erythrocytes. This results in an obstruction of the central veins, causing a hypoxic milieu that damages hepatocytes and can culminate in liver atrophy and hepatic insufficiency (Liang et al. 2006).

In contrast, patients with preexisting liver diseases, like virus hepatitis or cirrhosis, will often develop non-classic RILD. Concerning the clinical symptoms, these patients frequently present with elevated transaminase levels and jaundice (Kim et al. 2007). It was postulated that radiation could induce mitotic catastrophe in regenerating hepatocytes and consequently further impair the already limited organ function.

In carriers of chronic viral hepatitis, irradiation of the liver can lead to a reactivation of the virus. This should be considered in the differential diagnosis of impaired liver function after radiation therapy. To prevent reactivation, clinical studies recommend the prescription of antiviral medication before and during radiation treatment for patients with chronic hepatitis B (Ben-Josef and Lawrence 2005).

Interestingly, RILD is rarely seen in stereotactic treatment, presumably because of the comparably small volumes and the steep dose decline, both leading to a relatively low mean liver dose and thereby preventing the relevant pathophysiologic mechanisms (Dawson et al. 2002).

One of the most eminent problems in clinical practice will be the prediction of side effects from computer-modelled dose calculations and dose-volume histograms. It is recommended to use advanced prediction models like NTCP that have proven to be most reliable (Dawson et al. 2002). If NTCP calculation is not available, methods like dose-volume histogram constraints or mean dose to the liver can be used as a substitute but come with a lower reliability due to their simplicity. To compare different radiation regimes, all doses should be converted into the EQD2 (equivalent dose in 2-Gy fractions) based on the linear-quadratic model. Care should be taken in hypofractionated treatments where this calculation might not depict the truly delivered biologically effective dose (BED).

Now that we have outlined the entire target volume delineation process, a number of figures is given to illustrate how this integrates into treatment of patients. Figure 6.4 shows a plan for liver metastasis from colorectal cancer where the lesion is situated close to the stomach. The same patient also had the para-aortic lymph node which was also treated with SBRT. Figure 6.5 shows a sequence of MRI scans and FDG-PET/CT scans in the same patient to give an idea of the changes that occurred before and after therapy. Of note, metabolic imaging shows a complete response already six weeks after SBRT whereas MRI is difficult to interpret at early time points due to post-therapeutic uptake of gadolinium by inflam-

matory processes. Figure 6.6 illustrates the Ann Arbor-Toronto target volume concept which was first described by this group for a phase I trial in HCC and CCC. One of the advantages of their prescription method is that it is according to ICRU and not to a specific isodose encompassing the PTV (e.g. 60%, 80%).

References

Ariff B, Lloyd CR, Khan S et al (2009) Imaging of liver cancer. World J Gastroenterol 15:1289–1300

Ben-Josef E, Lawrence TS (2005) Radiotherapy for unresectable hepatic malignancies. Semin Radiat Oncol 15:273–278

Bi A-H, Zeng Z-C, Ji Y et al (2010) Impact factors for microinvasion in intrahepatic cholangiocarcinoma: a possible system for defining clinical target volume. Int J Radiat Oncol Biol Phys 78:1427–1436

Bolog N, Andreisek G, Oancea I et al (2011) CT and MR imaging of hepatocellular carcinoma. J Gastrointestin Liver Dis 20:181–189

Brock KK (2011) Imaging and image-guided radiation therapy in liver cancer. Semin Radiat Oncol 21:247–255

Bruix J, Sherman M (2011) Management of hepatocellular carcinoma: an update. Hepatology (Baltimore, MD) 53:1020–1022

Cerviño LI, Gupta S, Rose MA et al (2009) Using surface imaging and visual coaching to improve the reproducibility and stability of deep-inspiration breath hold for left-breast-cancer radiotherapy. Phys Med Biol 54:6853–6865

Charbel H, Al-Kawas FH (2011) Cholangiocarcinoma: epidemiology, risk factors, pathogenesis, and diagnosis. Curr Gastroenterol Rep 13:182–187

Corvera CU, Blumgart LH, Akhurst T et al (2008) 18F-fluorodeoxyglucose positron emission tomography influences management decisions in patients with biliary cancer. J Am Coll Surg 206:57–65

Dawson LA, Ten Haken RK (2005) Partial volume tolerance of the liver to radiation. Semin Radiat Oncol 15:279–283

Dawson LA, Normolle D, Balter JM et al (2002) Analysis of radiation-induced liver disease using the Lyman NTCP model. Int J Radiat Oncol Biol Phys 53:810–821

Dawson LA, Eccles C, Craig T (2006) Individualized image guided iso-NTCP based liver cancer SBRT. Acta Oncol 45:856–864

Eccles C, Brock KK, Bissonnette J-P et al (2006) Reproducibility of liver position using active breathing coordinator for liver cancer radiotherapy. Int J Radiat Oncol Biol Phys 64:751–759

Eccles CL, Patel R, Simeonov AK et al (2011) Comparison of liver tumor motion with and without abdominal compression using cine-magnetic resonance imaging. Int J Radiat Oncol Biol Phys 79:602–608

Glockner JF (2007) Hepatobiliary MRI: current concepts and controversies. J Magn Reson Imaging 25:681–695

Goh V, Sarker D, Osmany S et al (2012) Functional imaging techniques in hepatocellular carcinoma. Eur J Nucl Med Mol Imaging 39:1070–1079

Hallman JL, Mori S, Sharp GC et al (2012) A four-dimensional computed tomography analysis of multi-organ abdominal motion. Int J Radiat Oncol Biol Phys 83:435–441

Heinzerling JH, Anderson JF, Papiez L et al (2008) Four-dimensional computed tomography scan analysis of tumor and organ motion at varying levels of abdominal compression during stereotactic treatment of lung and liver. Int J Radiat Oncol Biol Phys 70: 1571–1578

Kim JH, Park JW, Kim TH et al (2007) Hepatitis B virus reactivation after three-dimensional conformal radiotherapy in patients with hepatitis B virus-related hepatocellular carcinoma. Int J Radiat Oncol Biol Phys 69:813–819

Lawrence TS (1995) Hepatic toxicity resulting from cancer treatment (Conference Paper). Int J Radiat Oncol Biol Phys 31:1237–1248

Liang SX, Zhu XD, Xu ZY et al (2006) Radiation-induced liver disease in three-dimensional conformal radiation therapy for primary liver carcinoma: the risk factors and hepatic radiation tolerance. Int J Radiat Oncol Biol Phys 65:426–434

Moorees J, Bezak E (2012) Four dimensional CT imaging: a review of current technologies and modalities. Australas Phys Eng Sci Med 35:9–23

Moorrees J, Bezak E (2012) Four dimensional radiotherapy: a review of current technologies and modalities. Australas Phys Eng Sci Med 35:399–406

Murakami T, Okada M, Hyodo T (2012) CT versus MR imaging of hepatocellular carcinoma: toward improved treatment decisions. Magn Reson Med Sci 11:75–81

Park JC, Park SH, Kim JH, Yoon SM, Song SY, Liu Z, Song B, Kauweloa K, Webster MJ, Sandhu A, Mell LK, Jiang SB, Mundt AJ, Song WY (2012) Liver motion during cone beam computed tomography guided stereotactic body radiation therapy. Med Phys 39:6431–6442

Sacks A, Peller PJ, Surasi DS et al (2011) Value of PET/CT in the management of liver metastases, part 1. AJR Am J Roentgenol 197:W256–W259

Seppenwolde Y, Wunderink W, Wunderink-van Veen SR, Storchi P, Méndez Romero A, Heijmen BJM. Treatment precision of image-guided liver SBRT using implanted fiducial markers depends on marker-tumour distance. Phys. Med. Biol. 56 (2001):5445–68

Sobin LH, Gospodarowicz MK, Wittekind C (2009) TNM classification of malignant tumors, 7th edn. Wiley-Blackwell, Oxford

Solanki AA, Weichselbaum RR, Appelbaum D et al (2012) The utility of FDG-PET for assessing out-

comes in oligometastatic cancer patients treated with stereotactic body radiotherapy: a cohort study. Radiat Oncol 7:216

Sterzing F, Brunner TB, Ernst I et al (2014) Stereotactic body radiotherapy for liver tumors: principles and practical guidelines of the DEGRO Working Group on Stereotactic Radiotherapy. Strahlenther Onkol 190(10):872–881

Ten Haken RK, Martel MK, Kessler ML et al (1993) Use of Veff and iso-NTCP in the implementation of dose escalation protocols. Int J Radiat Oncol Biol Phys 27:689–695

Tse RV, Hawkins M, Lockwood G et al (2008) Phase I study of individualized stereotactic body radiotherapy for hepatocellular carcinoma and intrahepatic cholangiocarcinoma. J Clin Oncol 26:657–664

Wolthaus JWH, Schneider C, Sonke J-J et al (2006) Mid-ventilation CT scan construction from four-dimensional respiration-correlated CT scans for radiotherapy planning of lung cancer patients. Int J Radiat Oncol Biol Phys 65:1560–1571

Wong JW, Sharpe MB, Jaffray DA et al (1999) The use of active breathing control (ABC) to reduce margin for breathing motion. Int J Radiat Oncol Biol Phys 44: 911–919

Pancreatic Cancer

7

Thomas Brunner and Daniel Schanne

Contents

T. Brunner (✉)
Department of Radiation Oncology, University Hospitals of Freiburg, Freiburg im Breisgau, Germany
e-mail: thomas.brunner@uniklinikfreiburg.de

D. Schanne
Department of Radiation Oncology, University Hospitals of Freiburg, Freiburg im Breisgau, Germany

Department of Radiation Oncology, Massachusetts General Hospital, Charlestown, MA, USA
e-mail: Daniel.schanne@uniklinik-freiburg.de

7.1 Anatomy

The pancreas is 13–15 cm long and is situated retroperitoneally, extending from the duodenum (pancreatic head) to the splenic hilum (pancreatic tail). At the caudal edge, the organ is deeply intercalated by the mesenteric vessels (incisura pancreatitis). The pancreas consists of a ventral and dorsal embryonic part, which are fusing secondarily. The caudal aspect of the pancreatic head and the distal part of the excretory duct (major pancreatic duct, Wirsung) develop from the ventral embryonal part. The larger dorsal part forms the rest of the gland. The proximal part of the excretory duct degenerates in most cases or it yields the accessory pancreatic duct (Santorini) leading into the duodenum at the minor duodenal papilla. The pancreatic head is usually indicated adherent to the duodenal wall. Pancreatic carcinoma of the head often causes an obstruction of the extrahepatic bile duct with the clinical signs of jaundice and a dilated gallbladder that may be palpable (Courvoisier's sign). Excretory ducts pinched off by the tumour may also lead to congested pancreatic secretion and pancreatitis. However, pathologic processes in the pancreatic head do not cause diabetes because the islets of Langerhans are predominantly located in the pancreatic tail and body. At the dorsal aspect of the organ, the splenic vein intercalates deeply into the pancreatic parenchyma. The portal vein forms dorsally of the pancreatic head at the level of the pancreatic incision (incisura pancreatitis)

A.-L. Grosu, C. Nieder (eds.), *Target Volume Definition in Radiation Oncology*,
DOI 10.1007/978-3-662-45934-8_7,

by the confluent of the splenic vein and the superior mesenteric vein. The pancreas superimposes the large vessels of the retroperitoneal space (v. cava inferior, renal vessels and abdominal aorta). These topographic relationships are of importance in pancreatic cancer.

7.1.1 Upper Abdominal Lymphatics

7.1.1.1 Anatomy of Lymph Nodes

Abdominal lymph nodes consist of visceral nodes and lumboaortic nodes. The visceral nodes are grouped along the lymphatic pathways from the abdominal organs. They include the left gastric and right gastric lymph nodes, the pancreaticolienal chain, the hepatic lymph nodes and the superior and inferior mesenteric chains. The lumboaortic nodes can be subdivided into the bilateral lateroaortic group, the pre-aortic group and post-aortic group.

7.1.1.2 Lymph Node Classifications

There are two commonly used classifications: the first is the UICC classification and the second is the Japanese classification. The UICC classification discriminates the lymph nodes as shown in Table 7.1 and differentiates tumours without metastasis/metastases in these nodes (N0) versus tumours with metastasis/matastases (N1) (Sobin et al. 2009). The second is derived from the classification of the Japanese Research Society for Gastric Cancer (JRSGC) originally described in 1962. The numbering of this classification is commonly also employed for pancreatic cancer and other tumours of the upper abdominal region such as liver cancer. For the detailed description of the JRSGC classification, please see the chapter on gastric cancer of this book. The first English edition of the classification of pancreatic carcinoma was published in 1996 (Society 1996). Very different from the UICC, there are three groups of nodes. The first group consists of the nodes that are usually removed during the resection of the head or body/tail of the pancreas. Groups 2 and 3 are subdivided on the basis of lymph flow, rate of involvement by metastasis and outcome. Detection of nodal metastases per group is used to create four categories, N0–N3, with significant prognostic impact (Matsuno 2003).

7.2 Pathology

Currently, the seventh edition of the UICC classification is in use (Sobin et al. 2009). The classification discriminates the anatomical subsites

Table 7.1 Lymph node classifications

UICC subdivisions	Description	JPS	Description
Superior	Sup. to head and body		
Inferior	Inf. to head and body		
Anterior	Ant. pancreaticoduodenal, pyloric[a], proximal mesenteric	Group 1:13a,* 13b,* 17a,* 17b*	Posterior surface of the pancreatic head; anterior surface
Posterior	Posterior pancreaticoduodenal, common bile duct, proximal mesenteric	Group 2: 6,* 8a,* 8p,* 12a,* 12b,* 12p,* 14p,* 14d*	Infrapyloric, common hepatic artery, hepatoduodenal ligament, SMA
Splenic	Hilum of spleen and tail of pancreas[b]	Group 3: 1, 2, 3, 4, 5, 7, 9*, 10, 11p,* 11d, 15, 16a2, 16b1, 18*	(See below table)
Coeliac	[a]		

JPS numbers: *1* right cardial, *2* left cardial, *3* along the lesser curvature of the stomach, *4* along the greater curvature of the stomach, *5* suprapyloric, *6* infrapyloric, *7* along the left gastric artery, *8* along the common hepatic artery, *9* around the celiac artery, *10* splenic hilum, *11* along the splenic artery, *12* in the hepatoduodenal ligament, *13* on the posterior surface of the pancreatic head, *14* along the superior mesenteric artery, *15* along the middle colic artery, *16* around the abdominal aorta, *17* on the anterior surface of the pancreatic head, *18* along the inferior margin of the pancreatic body-tail

[a]Tumours of the head only

[b]Body and tail only

*High risk lymph node regions

head, body and tail of the pancreas for pancreatic ductal adenocarcinoma (PDAC). The definition for tumours of the head of the pancreas is to the right of the left border of the superior mesenteric vein. Consequently, tumours of the body are to the left of this line. The left border of the aorta classifies tumours as located either in the body or tail of the pancreas (Figs. 7.1 and 7.2).

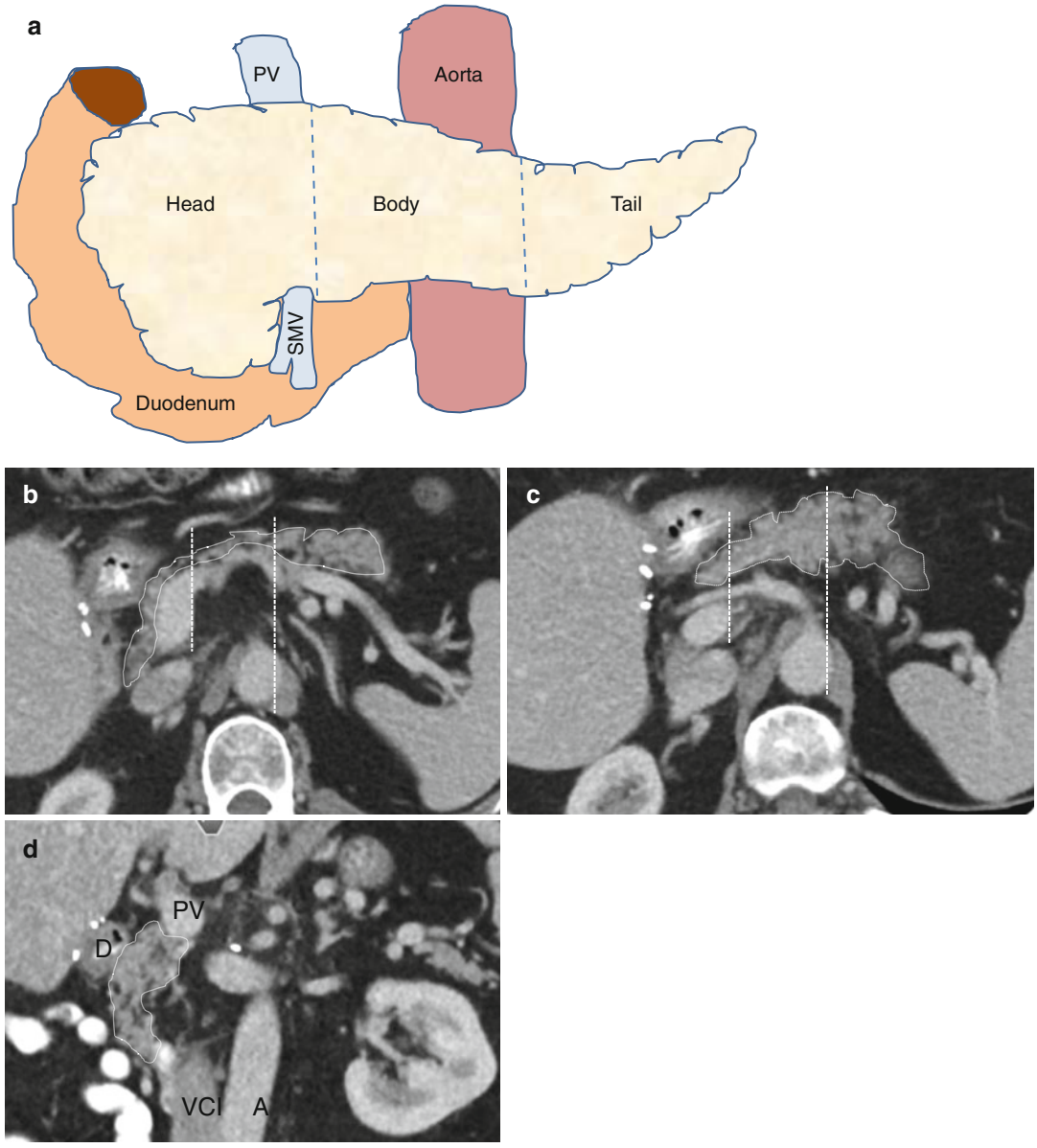

Fig. 7.1 Tumour location. (**a**) Schematic frontal view of the three sections of the pancreas. 1. Head of the pancreas: Tumours arising to the right of the left border of the superior mesenteric vein including the incinate process. 2. Body of the pancreas: Tumours arising between the left border of the superior mesenteric vein and the left border of the aorta. 3. Tail of the pancreas: Tumours arising between left border of the aorta and the splenic hilum. (**b**) and (**c**): two transversal planes depicting the head, body and tail of a healthy pancreas as explained in (**a**). (**d**) Coronal plane showing the head of the pancreas just below the portal vein (*PV*) and its relation to the duodenum (*D*), the vena cava inferior (*VCI*) and the aorta (*A*)

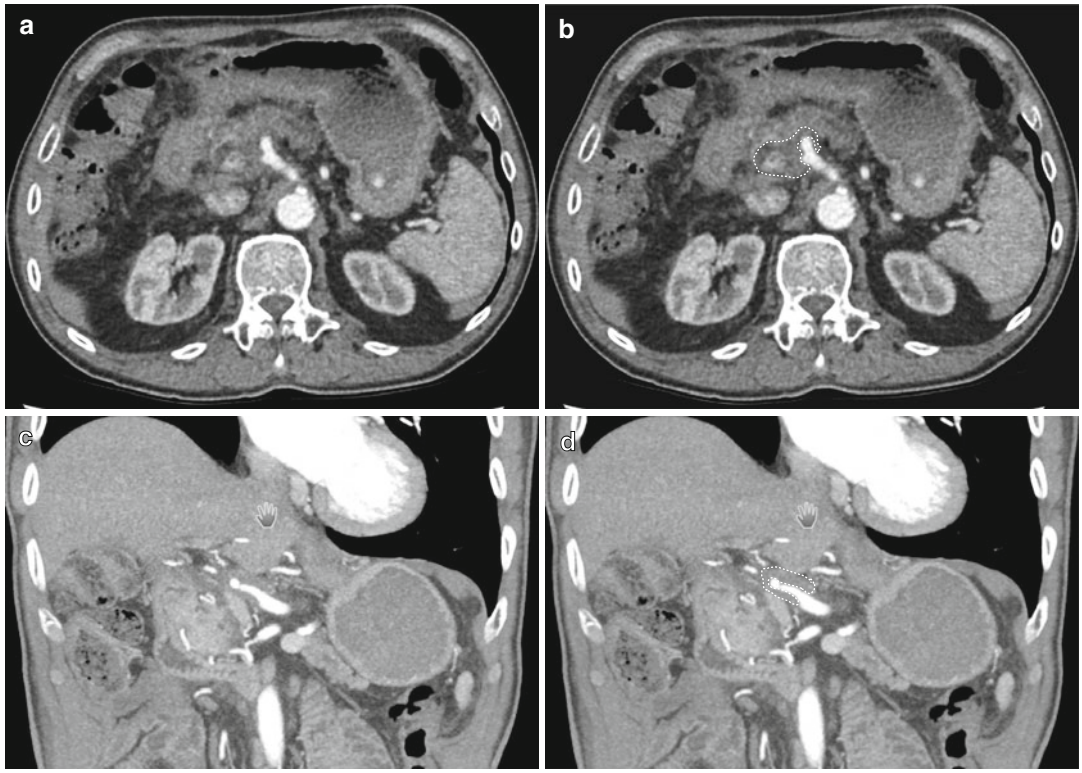

Fig. 7.2 Delineation of the gross target volume. (**a**) Arterial phase CT with a hypodense tumour mass around the common hepatic artery. (**b**) Same as (**a**) with tumour outlined in white dashed line. (**c**) Coronal view of the same tumour (**d**) Same as (**c**) with tumour outlined in white dashed line

The regional lymph nodes for pancreatic tumours are shown in Table 7.1. The T-categories are:

- T1: tumour limited to the pancreas, ≤2 cm in greatest dimension.
- T2: tumour limited to the pancreas, >2 cm in greatest dimension.
- T3: tumour extends beyond the pancreas but without involvement of coeliac axis or superior mesenteric artery.
- T4: tumour involvement of coeliac axis or superior mesenteric artery.

Together with the lymph node status discriminating N0 (no regional lymph node metastasis) and N1 (regional lymph nodes metastasis) based on examination of ≥10 lymph nodes for pN-category, this leads to the following stage grouping:

Stage	T-category	N-category	M-category
Stage IA	T1	N0	M0
Stage IB	T2	N0	M0
Stage IIA	T3	N0	M0
Stage IIB	T1, T2, T3	N1	M0
Stage III	T4	Any N	M0
Stage IV	Any T	Any N	M1

7.3 Visualisation

The role of imaging for pancreatic cancer has to fulfil basically three distinct endpoints: first of all, the primary tumour has to be identified; next, distant metastasis has to be identified to decide whether resection of the tumour is justified. Third, in the absence of distant metastasis, imaging

needs to inform about local tumour resectability. Pancreatic cancers are categorised into resectable, borderline resectable and non-resectable. An expert consensus statement has recently defined these three stages based on contrast-enhanced multi-detector computed tomography (CE-MDCT) (Callery et al. 2009).

7.3.1 Computed Tomography

MDCT is the single most important imaging tool to detect and to stage pancreatic cancer (Prokesch et al. 2003; Shrikhande et al. 2012; Varadhachary et al. 2006; Zeman et al. 1997; Pawlik et al. 2008). A localised tumour mass is the leading criterion in pancreatic cancer. Modern MDCT protocols use a dual-phase technique. 30 s after the intravenous injection of contrast, the arterial phase is acquired, and about 1 min after injection, the portal venous phase is taken. It is necessary to perform a rapid injection (3–5 mL/s) to maximise enhancement of the pancreas and mesenteric vasculature. MDCT has improved spatial and temporal resolution dramatically. The arterial phase images are required for visualisation of the primary tumour as well as evaluation of the arterial vasculature and its relationship with the tumour to predict resectability (Varadhachary et al. 2006). Pancreatic neuroendocrine tumours which are typically hypervascular can also be distinguished best in the arterial phase from PDAC. Compared to the surrounding normal pancreatic parenchyma, most PDACs are hypodense. In 5–10 % of PDACs, there is isoattenuation in both arterial and venous phase images. The subsequent venous phase is required to assess the liver and mesenteric venous vasculature as well as locoregional lymphadenopathy (Horton and Fishman 2002).

Most often water is used as a neutral oral contrast agent for visualisation of the stomach, the duodenum and the jejunum. Typically, thin collimation technique with slice thickness of around 0.6 mm is used with the reconstruction algorithm for 3–5 mm slices for standard interpretation. A second reconstruction at 0.5–0.75 mm is performed to create isotropic multi-planar reformations and 3D reconstructions. Often, two sets of 3D images are created: maximum intensity protection (MIP) and volume-rendered (VR) images. MIP imaging is invaluable for angiographic images to assess the relation of the tumour to the surrounding vasculature. VR allows optimal definition of the soft tissues, muscle, bone, and vasculature to demonstrate complex relationships between different structures at pathology.

For tumour detection, the sensitivity of MDCT is reported between 88 and 98 %. The smaller the tumours, the more difficult they are to visualise. PDACs tend to infiltrate dorsally into the retroperitoneum. Vessel involvement is of highest importance for the staging of local PDAC to classify pancreatic tumours into resectable, borderline resectable and non-resectable. One of the problems of the currently available literature is that discrepancies exist between the definitions of resectability, and therefore, it is highly recommended to consistently use the definition based on expert consensus statement published by Callery (Callery et al. 2009), which defines borderline resectable tumours as:

1. Venous involvement of the superior mesenteric vein (SMV)/portal vein, demonstrating tumour abutment with or without impingement and narrowing of the lumen, encasement of the SMV/portal vein but without encasement of the nearby arteries, or short segment venous occlusion resulting from either tumour thrombus or encasement but with suitable vessel proximal and distal to the area of vessel involvement, allowing for safe resection and reconstruction.
2. Gastroduodenal artery encasement up to the hepatic artery with either short segment encasement or direct abutment of the hepatic artery, without extension to the coeliac axis
3. Tumour abutment of the superior mesenteric artery (SMA) not to exceed >180° of the circumference of the vessel wall (Callery et al. 2009).

Tumour infiltration into the duodenum is important for the radiation oncologist because the duodenum is one of the dose-limiting organs for radiotherapy of pancreatic cancers. The loss of the fat plain between the mass and the duodenum, thickening of the duodenal wall, the extension of the tumour around the duodenum or duodenal obstruction are all signs of duodenal infiltration. A comparison between the tumour dimensions as measured on CT and pathology showed that the sensitivity of CT regarding duodenal invasion is quite low (Arvold et al. 2011). Unfortunately, endoscopic ultrasound is also not very sensitive to detect duodenal infiltration and cannot help to resolve the dilemma between tumour coverage and sparing of the duodenum as an important organ at risk.

Nodal disease is an important prognostic factor in pancreatic cancer, and the seventh classification of the UICC reflects this in defining stage IIB irrespective of T-category. Unfortunately, the ability of CT to distinguish malignant nodes is limited. It is purely based on size threshold of short axis ≥1 cm (Zeman et al. 1997). Correspondingly, the sensitivity of CT for positive nodes may be as low as 22 % (Pawlik et al. 2008). CT is well suited to identify metastatic disease to the liver which is best detected during the portal venous phase.

7.3.2 Magnetic Resonance Imaging

Advantages of MRI over CT are mainly based on the superior tissue contrast (Vachiranubhap et al. 2009). Due to the rich desmoplastic reaction characterised by fibrous stroma, PDAC is good visualised on fat-suppressed T1-weighted images. Tumours tend to be T1 hypointense in comparison with the relatively bright pancreatic parenchyma which avidly enhances on arterial phase images. With time, these tumours tend to increase enhancement on venous and delayed images. Therefore, MRI can be helpful to detect small tumours which can be difficult to visualise on CT especially below a size of 2 cm (Park et al. 2009; Fusari et al. 2010). An important indication for the use of MRI is isoattenuating pancreatic cancer which occurs in about 5–10 % of all pancreatic tumours. In these cases, MRI is an important tool to define the gross tumour volume (GTV) for radiotherapy because of its superior soft tissue contrast (Kim et al. 2010). A comparison between tumour sizes on abdominal MRI with pathologic specimen in resected tumours in 92 patients in 3D VIBE MRI showed that MRI underestimated tumour size by a median difference of 4 mm (range, −34 to 22 mm) (Hall et al. 2013). This is useful information for the expansion of GTV to clinical target volume (CTV). Additionally, alternative sequences can be useful. One of these is magnetic resonance cholangiopancreatography (MRCP) which is helpful to show subtle ductal narrowing (Miller et al. 2006). Diffusion-weighted images (DWI) measuring the random motion of water molecules within tissue render apparent diffusion coefficient (ADC) values. The motion of water is limited within tumours, and therefore, low ADC values can help to identify small lesions (Wang et al. 2011).

Compared to CT, enlarged lymph nodes are more conspicuous on MRI, especially on T2-weighted fat-suppressed sequences. Also, lymph nodes in the mesenteric fat are well visualised on non-fat-suppressed T1-weighted images because in this sequence lymph nodes appear in lower signal compared to the high-signal fat. MRI is particularly good in evaluating hepatic metastasis especially in small lesions where MDCT has limitations. Metastases are slightly hypointense on T1-weighted images and mildly hyperintense on T2-weighted images. Most lesions have peripheral enhancement on post-contrast images and wedge-shaped peripheral enhancement in the arterial phase (Miller et al. 2006).

7.3.3 FDG-PET Imaging

Positron-emission tomography (PET) imaging without a contrast-enhanced CT component is not of use for screening purposes. However, PET-CT with IV contrast may help differentiate benign and malignant pancreatic lesions. The

Table 7.2 Comparison of imaging modalities

	Primary tumour	Resectability	Lymph nodes	Distant metastases	Restaging
MDCT (method of choice)		Very good	Not particularly specific	Good for hepatic metastases >1 cm; poor for peritoneal metastases	Poor: because of desmoplastic reaction
MRT[a]	Preferred for 5–10 % PDAC that are isodense on CT	Inferior	Superior: peripancreatic and mesenteric fat	Depicts small liver lesions	Poor
FDG-PET/CT	Duodenal infiltration	Poor	Poor	Superior	Intermediate: might depict vital tumour cells

[a]See text for the adequate choice of sequences

positive predictive value of PET-CT is up to 91 %, but the negative predictive value of only 64 % is problematic. Therefore, there is a high propensity for false-negative findings. False-negative findings are often observed as a consequence of hypoglycaemia or diabetes. The resolution of PET is best for lesions that are larger than 1 cm in diameter below which there is a high likelihood of false-negative results (Grassetto and Rubello 2011). Another situation where fluorodeoxyglucose (FDG)-PET imaging can be very helpful for tumour delineation is when the tumour infiltrates into the duodenum. Specifically, if patients have had a gastric bypass preventing appropriate oral contrasting of the duodenum, it can be very difficult to appropriately visualise tumour extension, and PET-CT is able to better discriminate duodenum from tumour.

The sensitivity and specificity of PET-CT for locoregional nodal disease have been reported to be only 46 and 63 %, respectively (Pakzad et al. 2006; Kauhanen et al. 2009). The most important reason to explain this poor performance is the insufficient resolution for lesions smaller than 1 cm. However, PET-CT plays a more important role for the detection of distant metastatic disease when combined with contrast-enhanced CT (Table 7.2). One study reported a change in resectability status in 21.5 % of the patients and change of the pretreatment stage in 26.9 % of the patients (Bang et al. 2006).

Evaluation of response to therapy in patients with locally advanced pancreatic cancer is not satisfactory with MDCT. Regression of primary tumours is rarely observed due to the rich desmoplastic reaction in pancreatic tumour masses which cannot be discriminated from viable tumour. PET-CT is superior to MDCT in that respect because it is evaluating viable tumour cells and can discriminate a scar from a true tumour mass (Grassetto and Rubello 2011). However, one pitfall is an inflammatory reaction appearing as a false-positive finding, a typical example for this is cholangitis. A small study in 15 patients before and after chemoradiotherapy showed that tumour response was observed more frequently at PET imaging compared to CT imaging (Bang et al. 2006).

7.4 Target Volume Delineation of the Primary Tumour

7.4.1 GTV Delineation

7.4.1.1 Definitive and Neoadjuvant Treatment

The volumes of interest should be defined in accordance with the ICRU 50/62 guidelines. For GTV definition, the above-described characteristics of tumour visualisation are important. GTV definition relies on a contrast-enhanced thin slice CT planning scan in the arterial contrast phase. Alternatively a planning scan in the venous contrast phase can also be used when an arterial contrast phase scan is registered to the planning scan or visually taken into account on a second monitor for the delineation of the tumour. The GTV is defined as a hypodense

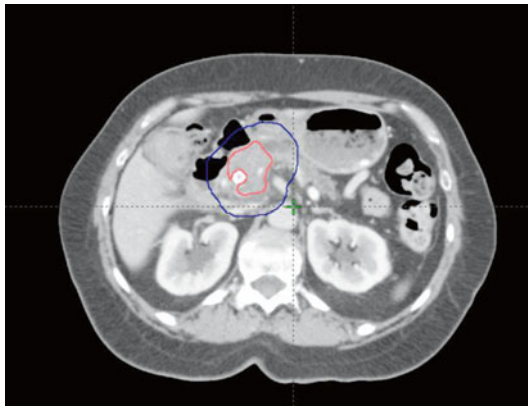

Fig. 7.3 Patient with a tumour in the pancreatic head after insertion of a stent into the common bile duct (*pink* = *GTV*; *blue* = *PTV*)

area in the contrast-enhanced high-resolution CT scan (slice ≤3 mm) as shown in Figs. 7.3 and 7.4. The edge of pancreatic head tumours towards the duodenum can often only reliably be visualised if water as a negative contrast agent is administered prior to the scan. Of note, CT scans have been found to underestimate the extent of infiltration of PDAC into the duodenum (Arvold et al. 2011). Indirect signs of the tumour should also be taken into account. Often dilatation of the pancreatic duct and/or the bile duct (prior to stent insertion) is helpful to determine the border of the tumour at these structures. As the exact margins of pancreatic tumours are often difficult to define, even by experienced radiolo-

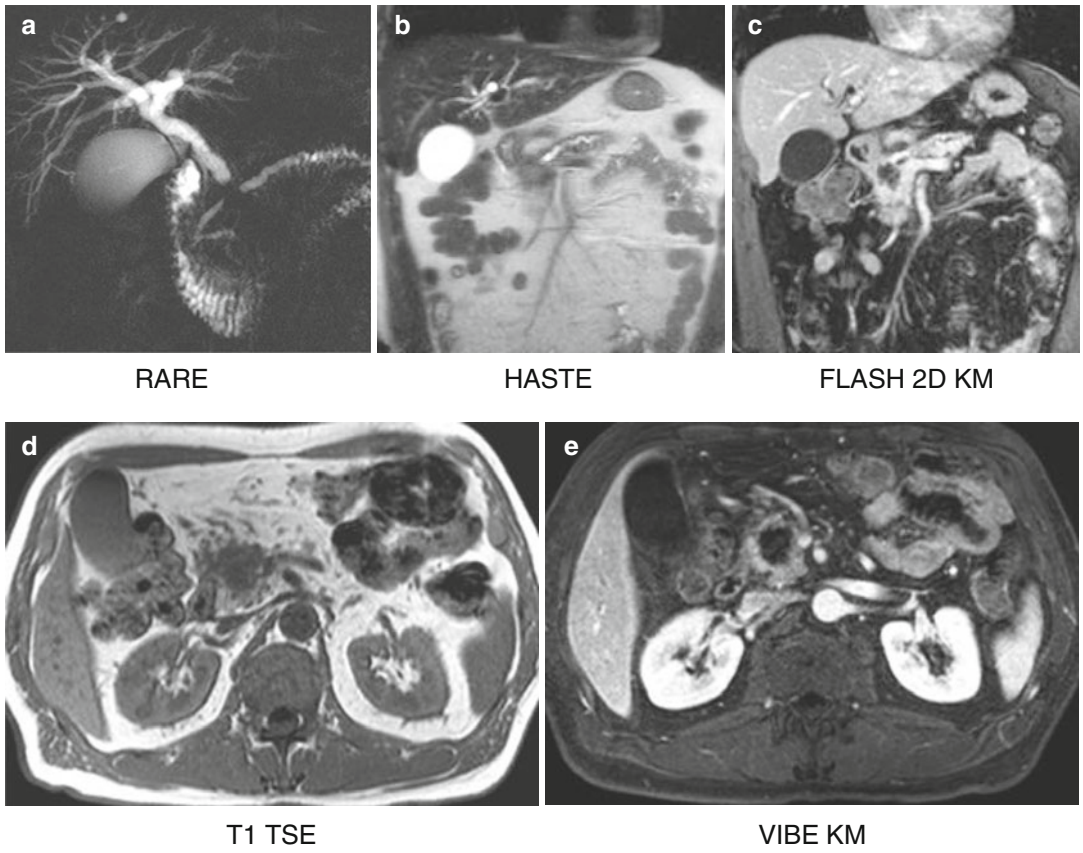

Fig. 7.4 MRI imaging of a pancreatic tumour in a 62-year old patient. (**a**) Double duct sign in the RARE sequence, caused by a mass in the pancreatic head seen in HASTE (**b**); hypointense in FLASH 2D (**c**), T1 TSE (**d**) and VIBE with contrast (**e**); the mass appears hyperintense in DWI (**f**) and (**g**). (**h**) FDG-avid local tumour relapse in PET/CT imaging dorsally to the splenic vein

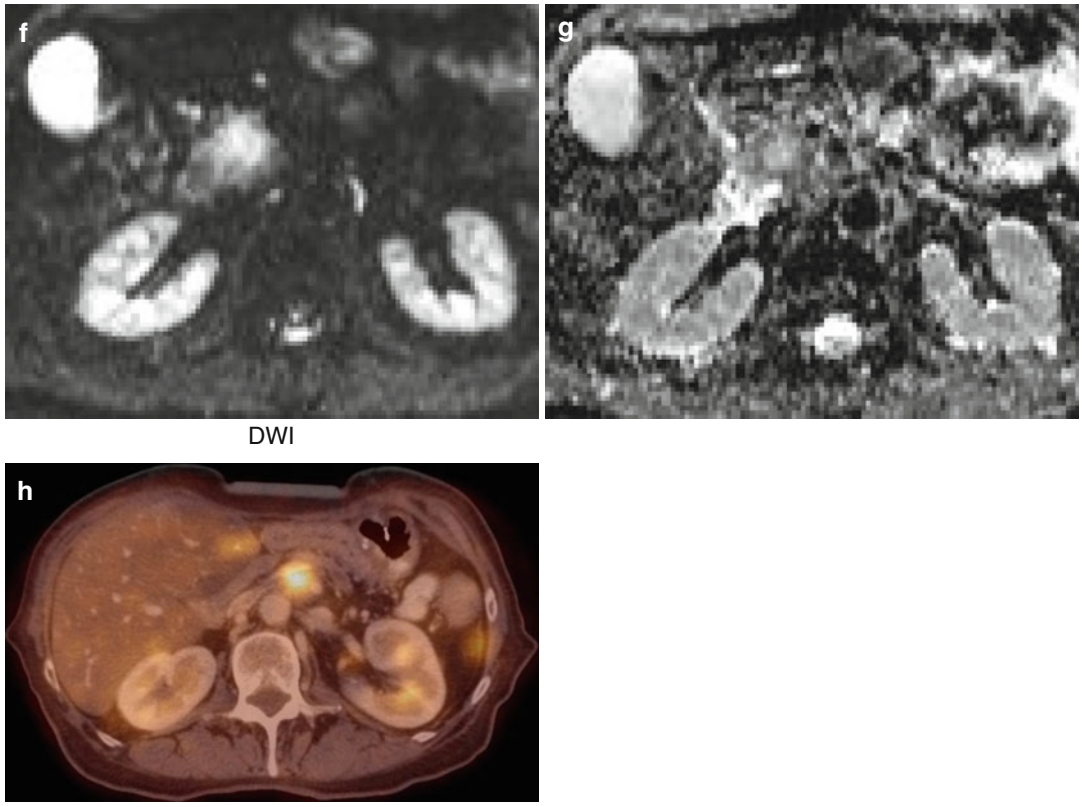

Fig. 7.4 (continued)

gists, GTV delineation should be undertaken in conjunction with, or after discussion with, a radiologist.

As mentioned above, about 5–10 % of pancreatic tumours are isoattenuating. A gadolinium-enhanced MRI (ideally in treatment position) registered to the planning CT should be used for the delineation of the GTV in such cases. If information regarding disease extent from PET scans is available, then this can be used in addition. We have found this helpful to delineate areas of tumour infiltration into the duodenum especially after a gastric bypass procedure where oral contrasting of the bowel is not possible. Accurate delineation of the GTV is of highest importance to fully encompass the tumour with an adequate dose but also to avoid unnecessary enlargement of the treatment volumes to avoid toxicity. The two most critical organs in that respect are the duodenum and the stomach.

7.4.1.2 Adjuvant Treatment

After resection, there is by definition no GTV at the time of radiotherapy (Goodman et al. 2012). In the case of incomplete resection (R1-resection) the surgical, pathologic and preoperative imaging information should be used to identify the region where microscopic tumour has been left. Again, by definition, this is not the GTV, but a CTV.

7.4.2 Clinical Target Volume Delineation of the Primary Tumour

7.4.2.1 Definitive and Neoadjuvant Treatment

There is no clear consensus on the size of the margin around the GTV to derive a CTV, and many institutions will expand the GTV directly into a planning target volume (PTV). Never-

theless, if a CTV of the primary tumour is created, the margin expansion is 5 mm in most reports (McGinn et al. 2001; Muler et al. 2004; Jackson et al. 2010). A detailed analysis comparing pathologic tumour sizes with tumour sizes on CT scans before surgical resection showed that the size on CT scans is significantly smaller compared to pathology measurements (Arvold et al. 2011). This effect was more pronounced in smaller tumours compared to larger tumours. The authors derived an expansion formula from GTV to CTV taking into account the standard error to cover 97.5 % of the tumours: CTV primary expansion in millimetres = 19 mm −1/8 × (CT maximum tumour size in mm). The problem of this formula is that the expansion margins are very large compared to clinical practice. For example, for a tumour measuring 2 cm on CT scan, an expansion margin of 16.5 mm circumferentially would have to be added. Adding such a large margin for GTV to CTV expansion would prevent adequate protection of the duodenum and the stomach in a large number of patients after subsequent further expansion for patient positioning and respiratory movements to obtain the PTV. Therefore, we do not recommend the use of this formula at this time. At our institution, we expand the GTV directly into a PTV.

7.4.2.2 Adjuvant Treatment

For adjuvant treatment, the preoperative tumour volume and the pancreaticojejunostomy are the two regions requiring delineation (Goodman et al. 2012). To delineate the preoperative tumour volume, surgical clips to delineate areas of concern should be included. These are often used to highlight close margins or the uncinate margin. However, it is important to distinguish specifically placed clips pointing to areas at risk of local relapse from clips that are irrelevant for treatment planning. If possible, registration of the preoperative CT scan to the planning CT scan is useful, provided that patient positioning and nutritional status of the patient are not too discrepant between the two sets of imaging. Differences of respiratory phases in imaging need also to be considered. It is important to keep in mind that the post-operative anatomy often varies considerably from preoperative anatomy. The pancreaticojejunostomy is best recognised by identifying the pancreatic remnant first and then the junction with the jejunal loop medially and anteriorly of the remnant. In some cases, pancreaticogastrostomy rather than pancreaticojejunostomy has been performed. Of note, the pancreaticogastrostomy is not included in the CTV because this could lead to increased radiation toxicity.

7.4.3 Planning Target Volume Delineation of the Primary Tumour

As explained above, most commonly, the PTV is directly derived from the GTV skipping the step of creating a CTV. Most commonly, the expansion is 1.5–2 cm in the four directions of the transversal plane (ventral, dorsal, right, left) (Huguet et al. 2012). Due to significant respiratory motion in the craniocaudal direction, most often an expansion of the GTV by 2–3 cm is used in the superior and inferior direction. These expansion margins are problematic if doses up to 60 Gy, as often employed for pancreatic cancer, are intended to be prescribed because the duodenum and the stomach will often be exposed to prohibitively high doses. To avoid this, four-dimensional simulation to assess respiratory motion is strongly recommended. This is described in more detail below in the paragraph on internal target volume (ITV) concepts. 4D information allows to avoid circumferential exposure of the duodenum.

7.4.4 Internal Target Volume Delineation

Studies about pancreatic movement showed that the major direction of movement with respiration is in the superior-inferior direction. MR studies have a tendency to report larger amounts of

movements compared to CT (up to 23.7 mm), and CT studies reported up and down movements of up to 15.3 mm (Bussels et al. 2003; Feng et al. 2009; Gwynne et al. 2009; Mori et al. 2009). Movements in the AP direction are more pronounced and up to 12.1 mm, compared to the left-right direction. Of note there is a high variability between patients of up to ±15.9 mm (Feng et al. 2009). This is a strong argument to use individualised margins creating an internal target volume to reduce the dose to the organs at risk (OAR) (Gwynne et al. 2009). 4D-CT imaging is the most often used technique to define ITVs where a number of breathing cycles are registered to determine respiratory motion. This additional information to the contrast-enhanced planning CT scan can also be used to perform respiratory gating to obtain a further reduction of the margins especially in the craniocaudal direction (Mori et al. 2009).

7.5 Irradiation of Clinically Involved Regional Lymph Nodes

Inclusion of clinically positive lymph nodes in addition to the primary tumour into the target volume is a strategy used by a number of groups. This is an attractive concept which is similar to modern treatment strategies in locally advanced non-small cell lung cancer (NSCLC), avoiding elective nodal irradiation (Senan et al. 2002). However, the problem with this strategy is that in pancreatic cancer CT, the commonly used diagnostic imaging method, is very unreliable to detect metastatic lymph nodes (Roche et al. 2003; Raman et al. 2012). Even PET-CT scanning was found not to be particular superior compared to CT combined with endoscopic ultrasound (Farma et al. 2008). In the light of this situation, we do not recommend to include lymph nodes ≤1 cm in the short axis into the high-dose radiation volume. Patients with borderline resectable pancreatic cancer might benefit more from the inclusion of suspicious nodal areas than patients with clearly non-resectable tumours. If in the latter case the primary tumour is not controlled, the benefit of eradicating microscopic disease is less important compared to borderline resectable disease, where local control by additional surgery can become much more important.

7.6 Prophylactic Irradiation of Uninvolved Regional Lymph Nodes

Lymphatic spread is an important prognostic factor of PDAC (Hidalgo 2010), and the presence of metastatic lymph nodes has been recognised as a predictor of local failure (Asiyanbola et al. 2009). Even though many radiation oncologists choose to include nodal areas into the target volume (McGinn et al. 2001; Brunner et al. 2005, 2006; Van Laethem et al. 2010), others prefer to only irradiate the primary tumour (GTV) without aiming to treat elective lymph nodes (eLNs), to increase the dose delivered to the GTV and/or to prevent toxicity to organs at risk (Murphy et al. 2007; Spalding et al. 2007). It is a matter of great debate among radiation oncologists whether it is necessary to include or not eLNs into the target volume in pancreatic cancer. One of the reasons of this disagreement is that it is difficult if not impossible to prove one or the other opinion. An additional confounding factor is that many nodal areas are so close to the pancreatic tumours that they will be included into PTVs unintentionally. This debate is very similar to the situation in patients with NSCLC where a considerable dose is often delivered incidentally to the high-risk nodal volumes (Zhao et al. 2007) and an analysis comparing four different contouring strategies (RTOG and Oxford with eLN versus SCALOP and Michigan without eLN) confirmed that (1) significant amounts of high-risk eLNs are part of the PTV in concepts not aiming to treat eLN and (2) that incidental exposure of eLNs in these concepts is even larger (Fokas et al. 2013a, b). Inclusion of eLNs has often been criticised for toxicity reasons, and most series where eLNs were part of the treatment volumes had poorly defined delineation guidelines (Fig. 7.5) (Chauffert et al.

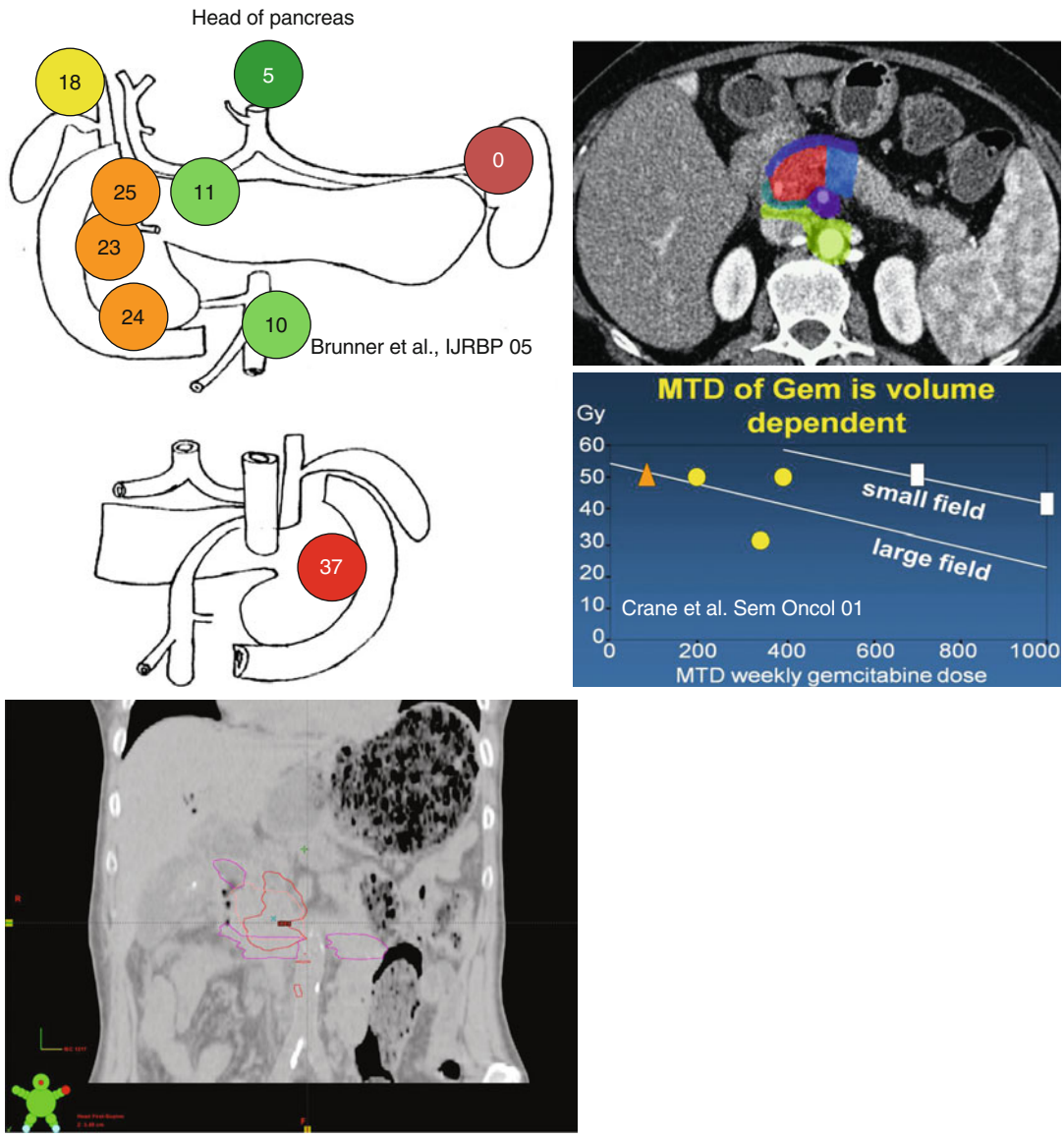

Fig. 7.5 Elective nodal treatment can be considered especially in neoadjuvant and borderline resectable disease. Ventral (**a**) and dorsal (**b**) schematic view of the percentage of nodal spread in pancreatic head tumours at primary resection (regions as in Table 7.3). Based on this analysis a very concise nodal CTV can be tailored (**c**): anterior pancreaticoduodenal (*indigo*), posterior pancreaticoduodenal (*turquoise*), superior mesenteric (*purple*), paraaortic (*green*); (**d**) The relationship of PTV size (*mL*), total dose (*Gy*) and maximal tolerated dose (*MTD*) with concurrent gemcitabine; (**e**) FDG-PET/CT can be very useful for GTV delineation especially in cases with duodenal invasion (duodenum *pink*; PET-GTV *red*; CT-GTV *salmon*)

2008). Therefore, if eLNs are planned to be included, great care must be taken to accurately define the treatment volumes, and this must be based on pathohistological analysis. The pattern of lymph node involvement is commonly reported using the Japanese Pancreatic Society classification of the regional lymph nodes of the pancreas (Table 7.3) (Nagakawa et al. 1993).

A number of studies have reported on how to define the lymph node regions to be treated (McGinn et al. 2001; Brunner et al. 2005, 2006; Caravatta et al. 2012; Sun et al. 2010). Up to

Table 7.3 Pattern of lymph node metastases

JPS (Nagakawa et al. 1993) classification	Nodal area	Percentage of positive nodes
Pancreatic head tumours		
17	Anterior pancreaticoduodenal	23
13	Posterior pancreaticoduodenal	37
–	Suprapancreatic head	25
–	Infrapancreatic head	24
–	Suprapancreatic body	11
12	Hepatoduodenal ligament	18
9	Coeliac trunk	5
14	Superior mesenteric artery	10
16	Para-aortic	22
Pancreatic body/tail tumours		
8	Common hepatic artery	15
9	Coeliac trunk	10
11	Splenic artery	36
14	Superior mesenteric artery	10
16	Para-aortic	16
18	Inferior pancreatic body	24

80 % of all resectable pancreatic head tumours have regional lymphatic metastasis, which suggests that inclusion of lymphatics may enhance locoregional control especially in patients with borderline resectable pancreatic cancer. In an analysis of 175 patients with pancreatic head tumours who underwent primary resection, we analysed the rate of positive lymph nodes for the regional lymphatics (Brunner et al. 2005). Of note, it is expected that patients where chemoradiotherapy is indicated are expected to have more advanced tumours compared to this surgical cohort and therefore also to have higher positive lymph node rates.

Extended retroperitoneal lymphadenectomy was not performed in this study, and therefore, data from the literature on para-aortic lymphatics were additionally analysed for that nodal region (Kayahara et al. 1993, 1999; Nagakawa et al. 1994). The overall frequency of para-aortic disease is reported to be between 15 and 18 % in pancreatic head tumours with much higher rate of micrometastasis. Due to the intricate lymphatic communication between the posterior pancreatic area and the para-aortic area, the adjacent para-aortic area has to be assumed as a common reason for regional local failure (Deki and Sato 1988). On the transversal plane, the region to the right of the inferior vena cava and dorsally to this vessel contained metastatic disease in <5 and >10 % anterior and to the left. All positions around the aorta had a frequency >10 % (Nagakawa et al. 1994). A subsite analysis of the para-aortic area in the craniocaudal direction showed the spread of disease exclusively between the coeliac trunk and the inferior mesenteric artery (Kayahara et al. 1999). Two thirds of para-aortic metastases were situated above and at the level of the root of the renal veins, and metastases below that landmark correlated with a tumour diameter >3 cm (Brunner et al. 2005).

7.6.1 Definitive and Neoadjuvant Treatment

Based on the above-described data, the following elective lymph node regions were selected to be included for:

- Carcinoma of the pancreatic head[1] or of the junction between the head and the body:
  - Superior, inferior, ventral and dorsal pancreaticoduodenal lymph nodes
  - Lymph nodes of hepatoduodenal ligament
  - Superior mesenteric lymph nodes
  - Para-aortic lymph nodes (level of coeliac trunk to superior mesenteric artery)
- Carcinoma at the pancreatic body-tail junction and tumours in the medial third of the pancreatic tail (Sobin et al. 2009)
  - Superior, inferior, ventral and dorsal pancreaticoduodenal lymph nodes
  - Superior mesenteric lymph nodes
  - Para-aortic lymph nodes (level of coeliac trunk to superior mesenteric artery)

[1] For practical purposes, the head of the pancreas lies to the right of the aorta, the body of the pancreas lies in front of the aorta, and the tail of the pancreas lies to the left of the aorta.

- Carcinoma of the lateral two thirds of the pancreatic tail
  - Peripancreatic lymph nodes of the body and tail
  - Coeliac lymph nodes
  - Splenic artery lymph nodes
  - Superior mesenteric lymph nodes
  - Para-aortic lymph nodes (level of coeliac trunk to superior mesenteric artery)

7.6.2 Adjuvant Treatment

For adjuvant therapy, the Radiation Therapy Oncology Group (RTOG) has defined in a consensus panel guidelines for the delineation of the CTV in pancreatic head cancer (Goodman et al. 2012). Additionally to the preoperative tumour volume and the pancreaticojejunostomy, these guidelines define the following four elective nodal volumes: coeliac artery (CA), superior mesenteric artery (SMA), portal vein (PV) and aorta (Table 7.4).

7.6.3 Practical Process of Contouring for Neoadjuvant and Definitive Treatment

- Contouring of the primary tumour:
  - The first step is contouring of the pancreatic tumour on an adequately contrasted CT planning scan and where necessary or available with information from diagnostic MRI or PET-CT.
  - If available, 4D-information should be used to create an ITV.
  - The ITV or the GTV is expanded to create a CTV (most often 5 mm of margin are used).
  - The CTV of the primary tumour is expanded to create a PTV. The margin required depends on institutional setup accuracy and on motion control. Without any motion control and 4D-information, often a margin added to the GTV of 15 mm on the axial plane is used and 20 mm in the craniocaudal direction. If an ITV was created, significantly smaller margins can be used to create the PTV (e.g. CTV to PTV 5 mm in all directions).
- Contouring of involved lymph node(s):
  - This is performed using exactly the same method as for the primary tumour. Depending on the location of the node(s), craniocaudal respiratory motion may differ from the motion of the primary tumour.
- Contouring of elective nodal volumes:
  - Contour the section of the pancreas where the primary tumour is located: for pancreatic head tumours, this is the pancreatic head and body including the uncinate process to the left edge of the aorta.
  - Expand this structure by 5 mm to obtain the peripancreatic nodal CTV. Exclude the duodenum and the stomach from the CTV.
  - Outline the portal vein from the junction of the cystic duct into the CBD to the

Table 7.4 Delineation recommendations

Clinical target volume structures	Definition
Preoperative tumour volume	Including surgical clips (see text in 7.4.2.2)
	Contour of preoperative tumour volume from preoperative imaging
Pancreaticojejunostomy (PJ)	Contour the PJ from the anastomosis with pancreatic remnant to the junction with the jejunal loop
Celiac artery (CA)	The most proximal approximate 1.0–1.5 cm of the CA from its origin from the aorta up to the first branching
Superior mesenteric artery (SMA)	The most proximal approximate 2.5–3.0 cm of the SMA from its origin from the aorta
Portal vein (PV)	Cover the choledochal or hepaticojejunostomy and porta hepatis nodes. Contour the PV from the confluent up to its bifurcation
Aorta	The aorta is contoured from the most superior contour of the CA, PV or pancreaticojejunostomy to the bottom of the lumbar vertebral body 2. The inferior border is lower if the preoperative GTV is more caudal than L2

confluent. Expand the structure by 5 mm in all directions except to the right and to the left.
- Outline the coeliac trunk from its origin in the aorta to the branching and expand by 5 mm in all directions except anteriorly and posteriorly.
- Outline the aorta from the coeliac trunk to the inferior mesenteric artery in tumours >3 cm or to the lower renal vein if smaller. Add a margin of 10 mm in all directions except superiorly and inferiorly. Where this volume extends into bone, manually edit this volume to exclude the vertebral bodies. For tumours of the lateral two thirds of the pancreatic tail, the inferior border is the lower border of the lowermost renal vein.
- Outline the inferior vena cava caudally of the liver parenchyma to the same caudal level as the aorta. Add a margin of 10 mm only to the left and ventrally. Where this volume extends into bone, manually edit this volume to exclude the vertebral bodies.
- Merge the CTV-aorta and the CTV-inferior vena cava to form a CTV-para-aortic.
- Merge all the other CTVs and the CTV-para-aortic to create CTV1.

• Expand CTV1 with an isotropic margin to create PTV1 which needs to contain PTV2 entirely (PTV of the primary tumour).
• Contour the normal structures:
- Stomach
- Duodenum: from the pylorus to the duodenojejunal flexure (ligament of Treitz)
- Small bowel: at least 2 cm superior and inferior of the PTV.
  • Either single loops
  • Or peritoneal cavity (Eppinga et al. 2010) from the cranial level of the pancreas in the caudal direction minus colon
    - Kidneys
    - Liver
    - Spinal cord

• Trim the PTV to avoid circumferential exposure of the duodenum.

References

Arvold ND, Niemierko A, Mamon HJ et al (2011) Pancreatic cancer tumor size on CT scan versus pathologic specimen: implications for radiation treatment planning. Int J Radiat Oncol Biol Phys 80:1383–1390

Asiyanbola B, Gleisner A, Herman JM et al (2009) Determining pattern of recurrence following pancreaticoduodenectomy and adjuvant 5-fluorouracil-based chemoradiation therapy: effect of number of metastatic lymph nodes and lymph node ratio. J Gastrointest Surg 13:752–759

Bang S, Chung HW, Park SW et al (2006) The clinical usefulness of 18-fluorodeoxyglucose positron emission tomography in the differential diagnosis, staging, and response evaluation after concurrent chemoradiotherapy for pancreatic cancer. J Clin Gastroenterol 40:923–929

Brunner TB, Merkel S, Grabenbauer GG et al (2005) Definition of elective lymphatic target volume in ductal carcinoma of the pancreatic head based on histopathologic analysis. Int J Radiat Oncol Biol Phys 62:1021–1029

Brunner TB, Baum U, Grabenbauer GG et al (2006) Large topographic variability of upper abdominal lymphatics and the consequences for radiation treatment planning. Radiother Oncol 81:190–195

Bussels B, Goethals L, Feron M et al (2003) Respiration-induced movement of the upper abdominal organs: a pitfall for the three-dimensional conformal radiation treatment of pancreatic cancer. Radiother Oncol 68:69–74

Callery MP, Chang KJ, Fishman EK et al (2009) Pretreatment assessment of resectable and borderline resectable pancreatic cancer: expert consensus statement. Ann Surg Oncol 16:1727–1733

Caravatta L, Sallustio G, Pacelli F et al (2012) Clinical target volume delineation including elective nodal irradiation in preoperative and definitive radiotherapy of pancreatic cancer. Radiat Oncol 7:86

Chauffert B, Mornex F, Bonnetain F et al (2008) Phase III trial comparing intensive induction chemoradiotherapy (60 Gy, infusional 5-FU and intermittent cisplatin) followed by maintenance gemcitabine with gemcitabine alone for locally advanced unresectable pancreatic cancer. Definitive results of the 2000–01 FFCD/SFRO study. Ann Oncol 19(9): 1592–1599

Deki H, Sato T (1988) An anatomic study of the peripancreatic lymphatics. Surg Radiol Anat 10:121–135

Eppinga W, Lagerwaard F, Verbakel W et al (2010) Volumetric modulated arc therapy for advanced pancreatic cancer. Strahlenther Onkol 186:382–387

Farma JM, Santillan AA, Melis M et al (2008) PET/CT fusion scan enhances CT staging in patients with pancreatic neoplasms. Ann Surg Oncol 15:2465–2471

Feng M, Balter JM, Normolle D et al (2009) Characterization of pancreatic tumor motion using cine MRI: surrogates for tumor position should be used with caution. Int J Radiat Oncol Biol Phys 74:884–891

Fokas E, Eccles C, Patel N et al (2013a) Comparison of four target volume definitions for pancreatic cancer. Guidelines for treatment of the lymphatics and the primary tumor. Strahlenther Onkol 189(5):407–416

Fokas E, Eccles C, Patel N et al (2013b) A treatment planning dosimetric comparison of four target volume contouring techniques for locally advanced pancreatic cancer radiotherapy. Radiother Oncol 107(2): 200–206

Fusari M, Maurea S, Imbriaco M et al (2010) Comparison between multislice CT and MR imaging in the diagnostic evaluation of patients with pancreatic masses. Radiol Med 115:453–466

Goodman KA, Regine WF, Dawson LA et al (2012) Radiation Therapy Oncology Group consensus panel guidelines for the delineation of the clinical target volume in the postoperative treatment of pancreatic head cancer. Int J Radiat Oncol Biol Phys 83:901–908

Grassetto G, Rubello D (2011) Role of FDG-PET/CT in diagnosis, staging, response to treatment, and prognosis of pancreatic cancer. Am J Clin Oncol 34:111–114

Gwynne S, Wills L, Joseph G et al (2009) Respiratory movement of upper abdominal organs and its effect on radiotherapy planning in pancreatic cancer. Clin Oncol (R Coll Radiol) 21:713–719

Hall WA, Mikell JL, Mittal P et al (2013) Tumor size on abdominal MRI versus pathologic specimen in resected pancreatic adenocarcinoma: implications for radiation treatment planning. Int J Radiat Oncol Biol Phys 86(1):102–107

Hidalgo M (2010) Pancreatic cancer. N Engl J Med 362:1605–1617

Horton KM, Fishman EK (2002) Adenocarcinoma of the pancreas: CT imaging. Radiol Clin North Am 40:1263–1272

Huguet F, Goodman KA, Azria D et al (2012) Radiotherapy technical considerations in the management of locally advanced pancreatic cancer: American-French consensus recommendations. Int J Radiat Oncol Biol Phys 83:1355–1364

Jackson AS, Jain P, Watkins GR et al (2010) Efficacy and tolerability of limited field radiotherapy with concurrent capecitabine in locally advanced pancreatic cancer. Clin Oncol (R Coll Radiol) 22:570–577

Kauhanen SP, Komar G, Seppanen MP et al (2009) A prospective diagnostic accuracy study of 18F-fluorodeoxyglucose positron emission tomography/computed tomography, multidetector row computed tomography, and magnetic resonance imaging in primary diagnosis and staging of pancreatic cancer. Ann Surg 250:957–963

Kayahara M, Nagakawa T, Ueno K et al (1993) An evaluation of radical resection for pancreatic cancer based on the mode of recurrence as determined by autopsy and diagnostic imaging. Cancer 72:2118–2123

Kayahara M, Nagakawa T, Ohta T et al (1999) Analysis of paraaortic lymph node involvement in pancreatic carcinoma: a significant indication for surgery? Cancer 85:583–590

Kim JH, Park SH, Yu ES et al (2010) Visually isoattenuating pancreatic adenocarcinoma at dynamic-enhanced CT: frequency, clinical and pathologic characteristics, and diagnosis at imaging examinations. Radiology 257:87–96

Matsuno S (2003) General overview for 20 years in the National Pancreatic Cancer Registry of the Japan Pancreas Society. J Jpn Pancreas Soc 18:97–169

McGinn CJ, Zalupski MM, Shureiqi I et al (2001) Phase I trial of radiation dose escalation with concurrent weekly full-dose gemcitabine in patients with advanced pancreatic cancer. J Clin Oncol 19:4202–4208

Miller FH, Rini NJ, Keppke AL (2006) MRI of adenocarcinoma of the pancreas. AJR Am J Roentgenol 187:W365–W374

Mori S, Hara R, Yanagi T et al (2009) Four-dimensional measurement of intrafractional respiratory motion of pancreatic tumors using a 256 multi-slice CT scanner. Radiother Oncol 92:231–237

Muler JH, McGinn CJ, Normolle D et al (2004) Phase I trial using a time-to-event continual reassessment strategy for dose escalation of cisplatin combined with gemcitabine and radiation therapy in pancreatic cancer. J Clin Oncol 22:238–243

Murphy JD, Adusumilli S, Griffith KA et al (2007) Full-dose gemcitabine and concurrent radiotherapy for unresectable pancreatic cancer. Int J Radiat Oncol Biol Phys 68:801–808

Nagakawa T, Kobayashi H, Ueno K et al (1993) The pattern of lymph node involvement in carcinoma of the head of the pancreas. A histologic study of the surgical findings in patients undergoing extensive nodal dissections. Int J Pancreatol 13:15–22

Nagakawa T, Kobayashi H, Ueno K et al (1994) Clinical study of lymphatic flow to the paraaortic lymph nodes in carcinoma of the head of the pancreas. Cancer 73:1155–1162

Pakzad F, Groves AM, Ell PJ (2006) The role of positron emission tomography in the management of pancreatic cancer. Semin Nucl Med 36:248–256

Park HS, Lee JM, Choi HK et al (2009) Preoperative evaluation of pancreatic cancer: comparison of gadolinium-enhanced dynamic MRI with MR cholangiopancreatography versus MDCT. J Magn Reson Imaging 30:586–595

Pawlik TM, Laheru D, Hruban RH et al (2008) Evaluating the impact of a single-day multidisciplinary clinic on the management of pancreatic cancer. Ann Surg Oncol 15:2081–2088

Prokesch RW, Schima W, Chow LC et al (2003) Multidetector CT of pancreatic adenocarcinoma: diagnostic advances and therapeutic relevance. Eur Radiol 13:2147–2154

Raman SP, Horton KM, Fishman EK (2012) Multimodality imaging of pancreatic cancer-computed tomography, magnetic resonance imaging, and positron emission tomography. Cancer J 18:511–522

Roche CJ, Hughes ML, Garvey CJ et al (2003) CT and pathologic assessment of prospective nodal staging in

patients with ductal adenocarcinoma of the head of the pancreas. AJR Am J Roentgenol 180:475–480

Senan S, Burgers S, Samson MJ et al (2002) Can elective nodal irradiation be omitted in stage III non-small-cell lung cancer? Analysis of recurrences in a phase II study of induction chemotherapy and involved-field radiotherapy. Int J Radiat Oncol Biol Phys 54:999–1006

Shrikhande SV, Barreto SG, Goel M et al (2012) Multimodality imaging of pancreatic ductal adenocarcinoma: a review of the literature. HPB (Oxford) 14:658–668

Sobin LH, Gospodarowicz MK, Wittekind C (2009) TNM classification of malignant tumors, 7th edn. Wiley-Blackwell, Oxford

Society JP (1996) Classification of pancreatic carcinoma. This is actually a report by the Japanes Pancreatic Society and not a book in itself. The data provided is all I could find about it. In: Kanehara (ed),1st English edn. Tokyo

Spalding AC, Jee KW, Vineberg K et al (2007) Potential for dose-escalation and reduction of risk in pancreatic cancer using IMRT optimization with lexicographic ordering and gEUD-based cost functions. Med Phys 34:521–529

Sun W, Leong CN, Zhang Z et al (2010) Proposing the lymphatic target volume for elective radiation therapy for pancreatic cancer: a pooled analysis of clinical evidence. Radiat Oncol 5:28

Vachiranubhap B, Kim YH, Balci NC et al (2009) Magnetic resonance imaging of adenocarcinoma of the pancreas. Top Magn Reson Imaging 20:3–9

Van Laethem JL, Hammel P, Mornex F et al (2010) Adjuvant gemcitabine alone versus gemcitabine-based chemoradiotherapy after curative resection for pancreatic cancer: a randomized EORTC-40013-22012/FFCD-9203/GERCOR phase II study. J Clin Oncol 28:4450–4456

Varadhachary GR, Tamm EP, Abbruzzese JL et al (2006) Borderline resectable pancreatic cancer: definitions, management, and role of preoperative therapy. Ann Surg Oncol 13:1035–1046

Wang Y, Miller FH, Chen ZE et al (2011) Diffusion-weighted MR imaging of solid and cystic lesions of the pancreas. Radiographics 31:E47–E64

Zeman RK, Cooper C, Zeiberg AS et al (1997) TNM staging of pancreatic carcinoma using helical CT. AJR Am J Roentgenol 169:459–464

Zhao L, Chen M, Ten Haken R et al (2007) Three-dimensional conformal radiation may deliver considerable dose of incidental nodal irradiation in patients with early stage node-negative non-small cell lung cancer when the tumor is large and centrally located. Radiother Oncol 82:153–159

Esophageal Cancer

8

Frank B. Zimmermann

Contents

8.1 Introduction and Background

8.1.1 Standard Treatment in Esophageal Cancer

Esophageal cancer is an aggressive malignancy with a high risk of locoregional recurrence and development of distant metastases mainly to the lymph nodes, liver, lung, and peritoneum.

The incidence of squamous cell cancer is still increasing in underdeveloped countries due to rising abuse of alcohol and nicotine during the last decades.

On the other hand, a pronounced rise of adenocarcinoma of the pericardial region in the Western world mainly caused by reflux disease is apparent (Lagergren and Lagergren 2013).

The outcome is poor in all advanced stages, with 5-year survival after R0 resection between 20 and 50 % (Cense et al. 2006).

While esophageal cancer is usually detected in advanced stages, with 70 % of all new cases being stages III and IV, the 5-year survival rate of all patients with esophageal cancer is not above 10 % (Bystricky et al. 2011; Cheng et al. 2013). The type of tumor recurrence after locally aggressive treatment (including trimodality therapy: radiochemotherapy followed by surgery) is a locoregional and a distant one, with up to 50 % of the patients developing both locoregional and systemic recurrences (Bedenne et al. 2007; Sudo et al. 2013).

F.B. Zimmermann
Clinic of Radiotherapy and Radiation Oncology, University Hospital Basel, Petersgraben 4, 4031 Basel, Switzerland
e-mail: FZimmermann@uhbs.ch

A.-L. Grosu, C. Nieder (eds.), *Target Volume Definition in Radiation Oncology*,
DOI 10.1007/978-3-662-45934-8_8, © Springer-Verlag Berlin Heidelberg 2015

Dominant risk factors for tumor recurrence and overall survival are T- and N-stage, in detail the local tumor spread – infiltration of the mediastinum, tracheobronchial tree, and pericardium – and the infiltration of locoregional lymph nodes, with the latter being present in 5 % of mucosal carcinoma, in 30 % of submucosal cancer, and in even more than 80 % in tumors not confined to the esophagus (Hosch et al. 2001), causing about 40 % of all local tumor recurrences. This confirms the relevance of a precise locoregional tumor-staging procedure (Yam et al. 2014).

In principle, the localization of the esophageal cancer and its histopathological subtype influence the regional and distant spread of the tumor and, thereby, the treatment options including resectability (Bystricky et al. 2011).

Surgical resection with or without perioperative radiochemo- or chemotherapy may be the dominant curative procedure of the lower esophagus with adenocarcinoma and with squamous cell carcinoma without contact to the tracheobronchial tree. In all locally advanced tumors of the cervical esophagus and tumors with contact to the tracheobronchial stem, definite radio- or radiochemotherapy may be the treatment of choice (Cooper et al. 1999; Stahl et al. 2005; Bedenne et al. 2007; Allum et al. 2011).

8.1.2 Standard Diagnostic in Esophageal Cancer

Ahead a definite treatment decision, a precise staging has to be conducted. This typically includes at least a computed tomography of the cervical, thoracic, and abdominal region; a cervical ultrasound for tumors of the cervical and upper thoracic esophagus; full endoscopy of the esophagus and the stomach, including an endosonography for the definition of the tumor stage; and a bronchoscopy for all stage uT3–4 tumors of the cervical and upper thoracic area. In advanced tumors, an FDG-PET-CT scan is superior detecting the regional and distant tumor extension and a valuable prerequisite of radiation treatment planning (Vesprini et al. 2008; Allum et al. 2011).

Nevertheless, none of the available imaging techniques can reliably predict the presence of lymph node metastases. The problem with all imaging techniques is that lymphatic spread can only be inferred by the documentation of enlarged nodes or highly increased metabolism, which gives an accuracy of less than 70 % (Siewert et al. 2008).

8.2 Anatomy and Tumor Spread

There are some tumor classifications based on the location of the primary tumor and on the histological subtype. Worldwide, still the dominant histological subtype is squamous cell esophageal cancer. It can be classified according to its location in the proximal, middle, and distal third of the esophagus. Cancer of the upper third of the esophagus usually infiltrates the cervical and mediastinal lymph nodes, while tumors of the middle third mainly metastasize to the mediastinal and upper perigastric lymph nodes and carcinoma of the lower third to the lower mediastinal and abdominal lymph nodes (Gertler et al. 2014).

More recently (Liebermann-Meffert et al. 2001; Cense et al. 2006) and with clinical relevance, the carcinoma of the esophagus is categorized into:

- Tumors of the cervical esophagus (“cervical esophageal cancer”): from the lower edge of the cricoid cartilage to the thoracic inlet behind the suprasternal notch
- Tumors with contact to the tracheobronchial tree above or at the level of the tracheal bifurcation (“suprabifurcal esophageal cancer”; in locally advanced disease, often contact with the left main stem bronchus): from the thoracic inlet to the level of the tracheal bifurcation
- Tumors without contact to the tracheobronchial tree in the lower mediastinum (“infrabifurcal esophageal cancer”) (3)

Both the pattern of lymphatic spread and the selection of treatment strategy are guided by this topographic classification.

The second most common cancer of the esophagus worldwide, but the most common in the Western world and below the tracheal carina, is the adenocarcinoma of the esophagogastric area (AEG). It is

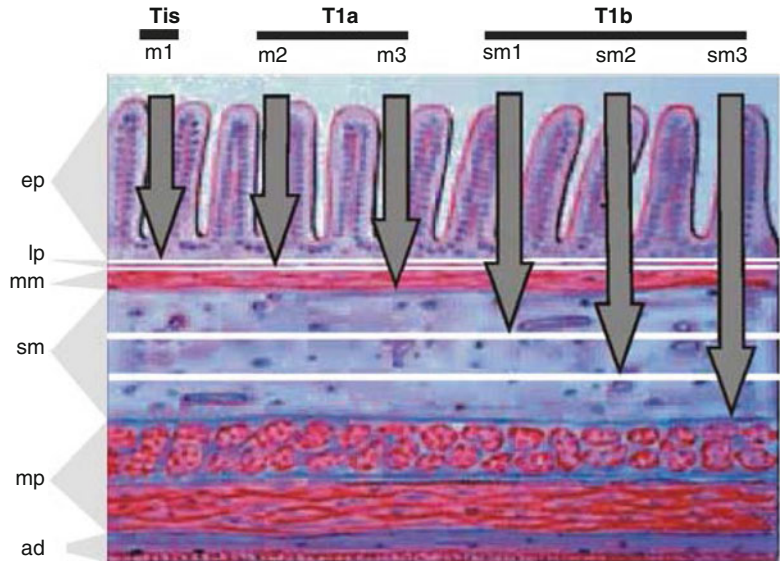

Fig. 8.1 Classification of tumor depth for superficial esophageal cancer. *Ep* epithelium, *lp* lamina propria, *mm* muscularis mucosae, *m* mucosa, *sm* submucosa, *mp* muscularis propria, *ad* adventitia (from Ancona et al. 2008)

subdivided into three subgroups, depending on the anatomic location of the tumor center in relation to the cardia and its natural behavior – AEG I from 5 to 1 cm cranial of the cardia, behaving similar to squamous cell cancer of the distal esophagus, and AEG II and III located in or below the cardia, dealt with like typical gastric cancer:

- AEG type I: Adenocarcinoma of the distal esophagus above the cardia and usually arising from an area with intestinal metaplasia of the esophagus
- AEG type II: True carcinoma of the cardia directly arising from the cardiac epithelium or short segments with intestinal metaplasia at the esophagogastric junction
- AEG type III: Subcardial gastric carcinoma subsequently infiltrating into the esophagogastric junction and distal esophagus

Regarding the regional tumor spread, length of tumor, increasing depth of tumor infiltration, lymphocytic infiltrate, angiolymphatic and neural invasion, as well as poor tumor differentiation and lower age are discussed as relevant risk factors (Bollschweiler et al. 2006; Ancona et al. 2008; Cheng et al. 2013).

In principle, the lymphatic drainage system of the esophagus is complex. There is a longitudinal lymphatic drainage, and especially in the submucosal area it is abundant (Fig. 8.1; Cense et al. 2006; Gertler et al. 2014). For defining the clinical target volume, this early tumor spread via subclinical and diffuse submucosal invasion and also and concurrent the subclinical infiltration of lymph nodes have to be considered in detail (Cheng et al. 2013). Even in early-stage carcinoma (p1sm disease), distant lymph node metastases can be found.

In addition, skip metastases as an intraesophageal spread of tumor cells in submucosal lymphatics are frequently observed in esophageal cancer (Cheng et al. 2013). This influences the target volume, too, with an increasing likelihood from pT1 tumors (about 4 %) to pT4 tumors (about 30 %). It should also be regarded that a metachronous or even synchronous secondary cancer of the upper aerodigestive tract can occur in up to 10 %.

This tumor behavior has major implication on the target volume of definite and preoperative radiotherapy as well. On the other hand, patient's status and comorbidities should be taken into account, not to unnecessarily increase the risk of side effects by unjustified enlargement of the target volume. It is not yet proven if elective nodal irradiation is reasonable (Zhao et al. 2010).

As a basis for treatment planning, the classification of the Japanese Society for Esophageal Diseases may be used (Table 8.1), although only very recent publications with detailed prescription of lymph node spread refer to this terminology (Cheng et al. 2013) (Table 8.2).

Table 8.1 Terminology of the regional lymph nodes in esophageal cancer (according to the Japanese Society of Esophageal Diseases (Fujita et al. 2002; Japanese Society for Esophageal Diseases 2004; Cheng et al. 2013) and according to the RTOG (Korst et al. 1998)

Description of LN position	Numbering (Japanese)	Numbering (RTOG)
Superficial cervical	100 (right, left)	
Cervical paraesophageal	101 (right, left)	
Deep cervical	102 (right, left)	
Peripharyngeal	103 (right, left)	
Supraclavicular	104	1
Upper thoracic paraesophageal	105	
Middle thoracic paraesophageal	108	8 (middle)
Lower thoracic paraesophageal	110	8 (lower)
Recurrent nerve	106 rec	
Pretracheal	106 pre	
Aortopulmonal		5
Paratracheal superior		2 (right, left)
Paratracheal inferior		4 (right, left)
Tracheobronchial	106 tbL (left)	10 (right, left)
Bifurcational	107	7
Main bronchus	109 (right, left)	
Supradiaphragmatic	111	15
Posterior mediastinal	112	3
Ligamentum arteriosum Botallo	113	
Anterior mediastinal	114	6
Cardiac	1 (right), 2 (left)	16
Lesser curvature	3	
Greater curvature	4	
Left gastric artery	7	17
Common hepatic artery	8	18
Splenic artery	11	19
Celiac artery	9	20

In principle, the direction of lymphatic flow is primarily directed to the upper mediastinum and cervical region in patients with suprabifurcal tumors and to the lower posterior mediastinum and celiac axis in patients with infrabifurcal tumors. Tumors located at the level of the tracheal bifurcation tend to metastasize in both directions

Table 8.2 Prediction of lymph node status according to infiltration depth (positive lymph nodes in %)

First author	Pat. No.	T-stage	Histology	
			AD	SCC
Ancona et al. (2008)	27	1 m	0	0
	71	1sm1	8.3	12.5
		1sm2 – 3	42.9	50
Bollschweiler et al. (2006)	16	1 m	0	0
	44	1sm1	22	33
		1sm2	0	17
		1sm3	78	69
Siewert et al. (2008)	1002	1 m	0	22
		1sm1 – 3	18	22
		2	67	50
		3	85	74
		4	89	79
Gockel et al. (2011)	289	1sm1	6	27
	340	1sm2	23	36
	601	1sm3	58	55
Hölscher et al. (2011)	70	1 m	0	0
	101	1 sm1	9	29
		1sm2	13	27
		1sm3	43	76

(Cheng et al. 2013). It should be considered that, especially in squamous cell carcinoma of the esophagus, even very early cancer (T1sm1) may infiltrate lymphatic vessels and disseminate into regional and distant lymph nodes (a detailed recommendation is presented in Table 8.4). Lymphographic studies and histopathological specimen indicate a lymphatic pathway from the lower esophagus upward into the mediastinum and also downward along the celiac axis (Fig. 8.2).

8.3 Target Volume Definition in Trials and Guidelines

The guidelines and recommendations of radiation therapy have been extremely simple in the vast majority of former clinical trials. While the length of treatment portals, later the length of the target volume, has been described just by two numbers in former trials – margins between 3 and 5 cm above and below the primary – it became nowadays obvious that an optimization of radiation

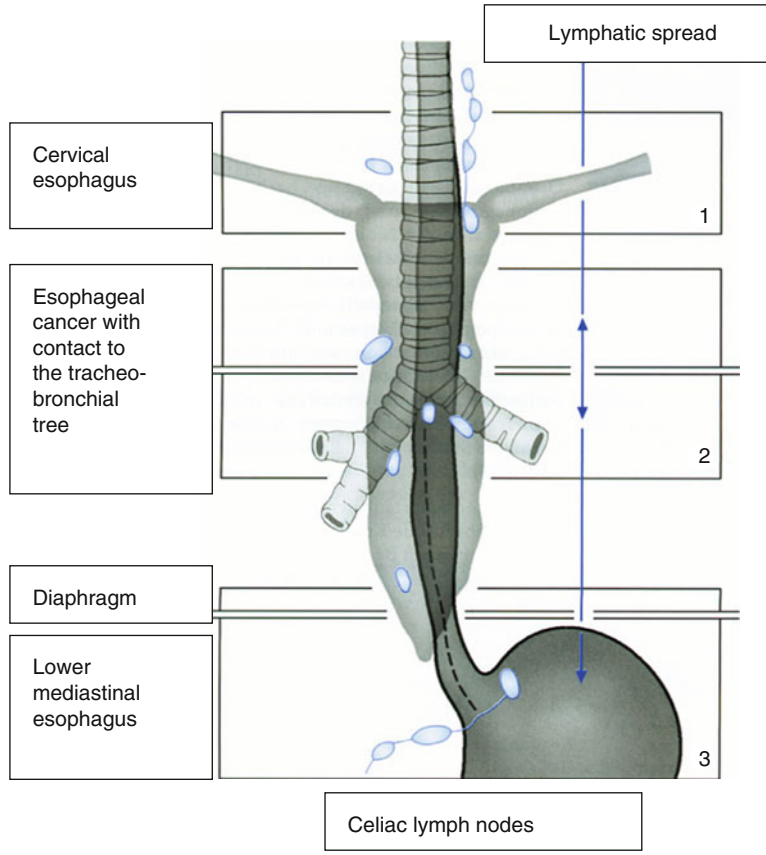

Fig. 8.2 Spread of esophageal cancer into regional lymph nodes: cervical cancer infiltrates predominantly in cranial direction and lower mediastinal cancer to the lower posterior mediastinum and celiac axis. Tumors at the level of the tracheal bifurcation metastasize in both directions

therapy besides an improvement of surgery and further escalating the combinations of chemo- or targeted therapies is essential. Only by optimizing the locoregional control, making the risk of regional tumor recurrences by far less than 40 %, cure can be achieved. On the other hand, normal tissue sparing especially in multimodality concepts is a prerequisite. Therefore, in modern trials, precise definitions of clinical target volumes and dose-volume constraints are standard (Table 8.3).

8.3.1 Target Volume Definition in Definitive Radiation Therapy and Combined Chemoradiation

In patients with squamous cell esophageal cancer, the tumor detected by endoscopy and CT or FDG-PET-CT scan is covered with magins of up to 5 cm in craniocaudal direction, as the vast majority of clinical trials have defined. Carcinoma of the upper cervical esophagus may be treated with smaller margins in cranial direction to spare the vocal cord but to guarantee to fully encompass all tumor extension into the upper esophageal sphincter. No data exist if the margin may be shortened, to avoid severe obstruction of the superior sphincter.

For distal adenocarcinoma of the esophagus, especially in more advanced tumors, lymph nodes of the paracardial region, the posterior lower mediastinum, and the lesser curvature side of the stomach, along the left gastric artery toward the celiac axis, should be included. Due to the low tolerance dose of the stomach, the lymph nodes of the greater curvature should be spared at the latest from 45 Gy (details in Table 8.4, Figs. 8.3, 8.4, and 8.5).

8.3.2 Target Volume Definition in Preoperative Setting

In patients with squamous cell esophageal cancer, a subtotal esophagectomy via a right transthoracic

Table 8.3 Definition of clinical target volume (CTV) in recent clinical trials (without cervical esophageal cancer) and guidelines

First author	Tumor	Oral margin (CTV) (cm)	Aboral margin (CTV) (cm)	Axial margin (CTV) (cm)	Further recommendations
Stahl et al. (2009)	AEG 1-2	5	3	2	All positive LN with 1 cm margin
					Elective nodal irradiation (No. 1, 2, 3, 7, 8, 9, 11)
					Mean dose kidney < 15 Gy
					Mean dose liver < 17 Gy
Crosby et al. (2013)	SCC and AEG 1-2	2	2	1	No nodal irradiation
					V20 lung < 25 %
					V40 heart < 30 %
Tomblyn et al. (2012)	SCC and AEG 1	5	5	1	All positive LN with 2 cm margin
					Elective nodal irradiation for upper (No. 104) and for lower mediastinal cancer (No. 9)
Wang et al. (2012)	SCC	3	3	0.8	V20 lung < 30 %
					V30 lung < 18 %
					Dmean heart <45 Gy
CALGB 9781	SCC and AEG 1	5	5	2	Elective nodal irradiation in upper (No. 104) and in lower mediastinal cancer (No. 9)
French FFCD 9102	SCC and AEG 1	3	3	2	Elective nodal irradiation in upper (No. 104) mediastinal cancer
SAKK 75/08	SCC and AEG 1-2	3.5	3.5	1	All positive LN
					Elective nodal irradiation in upper/middle (No. 105, 108) and distal esophageal cancer (No. 9)
NCCN (2013)	SCC and AEG	3–4	3–4	1	All positive LN with 0.5–1.5 cm margin
					Elective nodal irradiation in cervical (No. 101, 102, 103,104), upper and middle mediastinal cancer (No. 104, 105) and AEG I (No. 110, 9, 3)
					V20 lung < 20 %
					V40 lung < 40 %

AEG adenocarcinoma of the gastroesophageal junction, *SCC* squamous cell carcinoma, *LN* lymph nodes, *No.* LN location according to the Japanese definition, *V20/40* volume receiving 20/40 Gy

and abdominal approach is usually indicated due to the frequent longitudinal submucosal lymphangiosis. It is required for an adequate mediastinal and upper abdominal lymphadenectomy (two-field lymphadenectomy). At most institutions, a two-field lymphadenectomy comprises the following (Fumagalli et al. 1996):

- The periesophageal lymph nodes above the diaphragm and along the vena cava superior
- The lymph nodes at the tracheal bifurcation

Table 8.4 Personal recommendation of defining the clinical target volume in definitive radiation and chemoradiation depending on the location and infiltration depth of the primary (based on Igaki et al. 2005; Tachibana et al. 2005; Dresner et al. 2001; Monig et al. 2002; Feith et al. 2003; Huang et al. 2010; Cheng et al. 2013; Korst et al. 1998; Lazarescu et al. 2013; Meier et al. 2008); the recommendations highly depend on the results of the staging procedures and lung/cardial function tests. All FDG-PET-CT- and endoscopic ultrasound-positive LN should be included in curative settings. If tolerable, the next upper and lower LN positions may also be included by the CTV

Tumor location	Tumor stage	Lymph node CTV according to the Japanese classification (see Table 8.2) (*and in advanced disease according to the RTOG classification*)
Cervical esophagus	T1 m	101, 102, 103, 104
		Tumor and margin cranial up to the upper esophageal sphincter (sparing the vocal cord) and 3 cm caudal
	T 1 sm – T 2	101, 102, 103, 104, 105, 106 rec, 106 pre
	T 2	101, 102, 103, 104, 105, 106 rec, 106 pre
	T 3–4	100, 101, 102, 103 (bilateral neck levels III–VI), 104, 105, 106 rec, 106 pre, 107 (*1, 2 R/L, 3P, 4R/L, homolateral cervical and supraclavicular*)
Upper intrathoracic esophagus with contact to the tracheobronchial tree	T 1 m	105
		Tumor and margin of 3 cm craniocaudal
	T 1 sm – T 2	104 (only the central part), 105, 106 rec, 106 pre, 106 tbL, 107, 108, upper 110, 113, upper 114
		Tumor and margin of 5 cm craniocaudal
	T 3–4	104 (only the central part), 105, 106 rec, 106 pre, 106 tbL, 107, 108, 109 (central part only), 110, 112, 113, 114
		Tumor and margin of 5 cm craniocaudal *(1, 2R/L, 3P, 4R/L, 5, 7, 8 M/L, 9, 10 L/R)*
Lower interthoracic esophagus without contact to the tracheobronchial tree including AEG I	T 1 m	110
		Tumor and margin of 3 cm craniocaudal but not beyond the cardia if not infiltrated
	T 1 sm – T 2	1, 2, 3, 107, 108, 110, 111, 112
		Tumor and margin of 5 cm craniocaudal
	T 3–4	1, 2, 3, 4 (in AEG I), 7, 9, 106 tbL (in AEG I), 107, 108, 109 (in AEG I), 110, 111, 112
		Tumor and margin of 5 cm craniocaudal *(3P, 7, 8 L, 15, 16, 17, 20)*

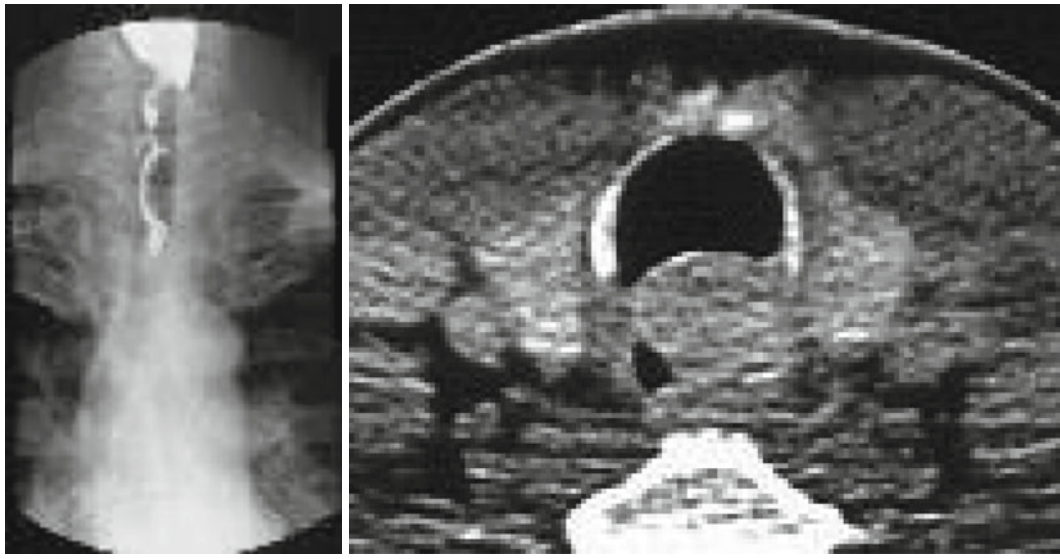

Fig. 8.3 Anterior barium contrast swallowing and CT scan. Locally advanced cervical esophageal cancer: cranial border of the CTV Os hyoid and bilateral cervical LN, lower border 1.5 cm below the bifurcation (No. 100, 101, 102, 103 (bilateral neck levels III–VI), 104, 105, 106 rec, 106 pre, 107)

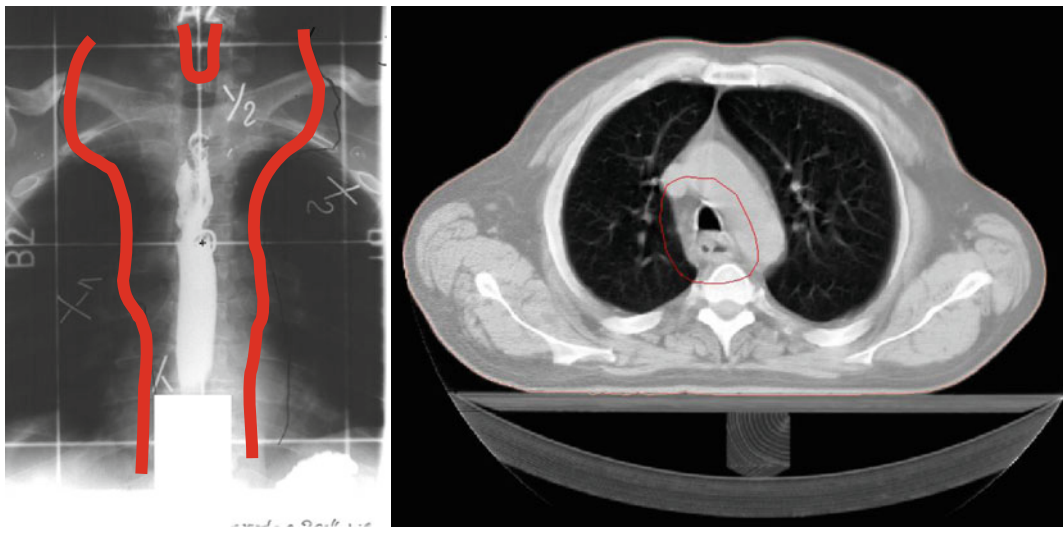

Fig. 8.4 Anterior barium contrast swallowing and CT scan. Locally advanced supracarinal esophageal cancer: cranial border close to the larynx and deep bilateral cervical LN, lower border 5 cm below the bifurcation (104 (only the central part), 105, 106 rec, 106 pre, 106 tbL, 107, 108, 109 (central part only), 110, 112, 113, 114)

- The paratracheal lymph nodes together with the nodes along the left recurrent nerve
- The abdominal suprapancreatic lymphatic compartment along the celiac axis

In patients with adenocarcinoma of the esophagus, especially in more advanced tumors, lymph node metastases occur in decreasing order of prevalence in the paracardial region, the posterior lower mediastinum, the lesser and greater curvature side of the stomach, along the left gastric artery toward the celiac axis, at the superior border of the pancreas along the splenic artery

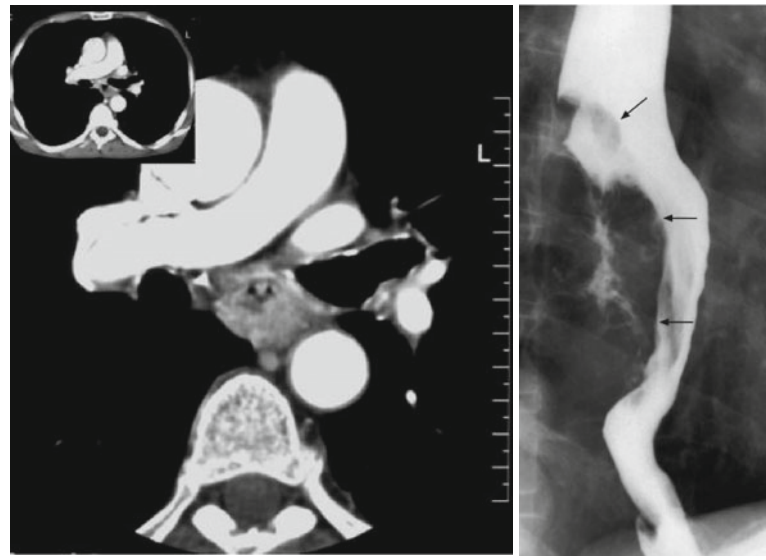

Fig. 8.5 CT-scan and anterior barium contrast swallowing. Locally advanced infracarinal esophageal cancer: Tumor and margin of 5 cm cranio-caudal, cranial border typically 3 cm above the carina, lower border covering the perigastric nodes (lymph nodes of 1, 2, 3, 4 (in AEG I), 7, 9, 106 tbL (in AEG I), 107, 108, 109 (in AEG I), 110, 111, 112)

toward the splenic hilum, and in the area of the left adrenal gland and the left renal vein (Siewert and Stein 1997). Only in patients with advanced cancer and numerous positive locoregional nodes can an infiltration of lymph nodes in the upper mediastinum or cervical region occur. Therefore, an extended lymph node dissection should include the removal of lymph nodes along the splenic artery, at the splenic hilus, and along the left renal vein behind the pancreas. To perform this retroperitoneal lymph node dissection, a left-sided pancreatic resection with splenectomy should be avoided because this procedure is associated with a substantial number of septic complications due to pancreatic fistula and abscess formation.

These aspects have an implication on the target volume definition of a preoperative radiochemotherapy. While lymph node dissection in the upper abdomen is less toxic than radiation therapy, the radiation portals may not be too extended. The lymph nodes along the splenic artery (No. 11), greater curvature (No. 4), common hepatic artery (No. 8), and celiac artery may be spared. A full clearing of the upper mediastinal lymph nodes and especially those with close contact to the tracheobronchial tree is less likely. All these areas should be covered by a sufficient dose of radiation therapy. The procedure should be in detail adjusted with the surgeon, because an increasing target volume means a higher dose to the most critical structure composing the majority of postoperative mortality, the lung.

Besides, the patient also should be evaluated for adequate liver, renal, and bone marrow function. Because preoperative combined radiochemotherapy appears to increase postoperative morbidity after an esophagectomy, a thorough evaluation of the physiologic reserve and general status is essential in these patients to make sure that they can withstand a potentially prolonged and complicated postoperative course (Bartels et al. 1998). Toxicity can be severe, with up to more than 50 % CTC° II–IV hematological and gastrointestinal sequelae each. When offered, besides a perfect treatment planning, an optimal supportive care is essential, including a dedicated intensive ward for perioperative guardianship of the patient (Stein and Siewert 2004).

8.3.3 Target Volume in Postoperative RT und RCT

The rationale for using adjuvant radiation is based on the pattern of failure after a complete resection, being between 12 and 67 % depending on the T- and N-stage (Mei et al. 1989; Gignoux et al. 1987; Teniere et al. 1991).

Although the majority of patients with esophageal cancer die of distant metastasis, the incidence

of local failure after surgery alone is high enough to examine the use of adjuvant radiation therapy.

Although nonrandomized trials have reported encouraging results with postoperative radiation therapy, there is no clear evidence in favor of an adjuvant irradiation (Zieren et al. 1995; Malthaner et al. 2004; Xiao et al. 2003) due to significant increased morbidity. Even in a study with an extraordinary risk of postoperative local tumor progression after incomplete tumor resection, the addition of postoperative radiation therapy did not significantly decrease local or distant failure or improve median survival (Fok et al. 1993). That means there is neither an indication for postoperative radiation after complete nor after incomplete resection. Side effects are increased by postoperative radiotherapy, which may be due to high total doses in some trials (45, 47) and lack of modern conformal radiotherapy with optimal sparing of critical organs as lung in all studies published in the 1990s from trials started in the 1980s. Therefore, postoperative radiotherapy might be offered as an individual decision in a patient recovering fast from preceding surgery. In this situation, the clinical target volume may focus on the former primary site and close resection margins.

Conclusion

Treatment decision and completion in esophageal cancer is a multidisciplinary task – radiologist, endoscopist, surgeon, internal oncologist, and radiation oncologist should be engaged to optimally define the treatment concept and, in case of radiation therapy, the gross tumor volume and the planning target volume.

There is evident data recommending concomitant radiochemotherapy or resection for locally advanced disease with no superiority in either and increasing evidence to combine both – preoperative radiochemotherapy and resection – for unresectable carcinoma in patients under good condition. Even patients with locally advanced carcinoma (stage III) may be cured, with 5-year recurrence-free survival of about 20 % (Cooper et al. 1999; Wong et al. 2003; Malthaner et al. 2004; Patel et al. 2004; Stahl et al. 2005; Bedenne et al. 2007; Allum et al. 2011).

However, combined treatments can cause severe side effects. Pulmonary and cardiovascular complications are most frequent, followed by anastomotic leakage (Ajani et al. 2013). Therefore, an extraordinary experience of the physicians is demanded.

Planning target volume and treatment planning of radiation therapy should follow strict rules established by clinical trials and adapted to the distribution of tumor recurrences in former trials.

Comorbidities have to be taken into account such as chronic obstructive lung disease and cardial insufficiency, in both aggressive dose-escalated radiation therapy and even more relevant in preoperative multimodality concepts. Elective nodal irradiation has to be analyzed and indicated critically (Zhao et al. 2010; Ma et al. 2011). This may be comparable to surgical series, which have not been able to demonstrate a clear overall survival benefit for extended lymphadenectomy in patients with squamous cell carcinoma and adenocarcinoma of the esophagus.

An optimal supportive care program should start immediately after diagnosis, not to compromise the optimal treatment by awaiting the effect of supportive therapy too long.

References

Ajani JA, Xiao L, Roth JA et al (2013) A phase II randomized trial of induction chemotherapy versus no induction chemotherapy followed by preoperative chemoradiation in patients with esophageal cancer. Ann Oncol. doi:10.1093/annonc/mdt339

Allum WH, Blazeby JM, Griffin SM et al (2011) Guidelines for the management of esophageal and gastric cancer. Gut 60:1449–1472

Ancona E, Rampado S, Cassaro M, et al (2008) Prediction of lymph node status in superficial esophageal carcinoma. Ann Surg Oncol 15(11):3278–3288

Bartels H, Stein HJ, Siewert JR (1998) Preoperative risk-analysis and postoperative mortality of oesophagectomy for resectable oesophageal cancer. Br J Surg 85:840–844

Bedenne L, Michel P, Bouche O et al (2007) Chemoradiation followed by surgery compared with chemoradiation alone in squamous cancer of the esophagus: FFCD 9102. J Clin Oncol 25: 1160–1168

Bollschweiler E, Baldus SE, Schröder W et al (2006) High rate of lymph-node metastasis in submucosal esophageal squamous-cell carcinomas and adenocarcinomas. Endoscopy 38(2):149–156

Bystricky B, Okines AFC, Cunningham D (2011) Optimal therapeutic strategies for respectable oesophageal or oesophagogastric junction cancer. Drugs 71:541–555

Cense HA, van Eijck CHJ, Tilanus HW (2006) New insights in the lymphatic spread of oesophageal cancer and its implications for the extent of surgical resection. Best Pract Res Clin Gastroenterol 20:893–906

Cheng J, Kong L, Huang W et al (2013) Explore the radiotherapeutic clinical target volume delineation for thoracic esophageal squamous cell carcinoma from the pattern of lymphatic metastases. J Thorac Oncol 8:359–365

Cooper JS, Guo MD, Herskovic A et al (1999) Chemoradiotherapy of locally advanced esophageal cancer: long-term follow-up of a prospective randomized trial (RTOG 85-01). JAMA 281:1623–1627

Crosby T, Hurt CN, Falk S et al (2013) Chemoradiotherapy with or without cetuximab in patients with oesophageal cancer (SCOPE1): a multicentre, phase 2/3 randomised trial. Lancet Oncol 14(7):627–637

Dresner SM, Lamb PJ, Bennett MK et al (2001) The pattern of metastatic node dissemination from adenocarcinoma of the esophagogastric junction. Surgery 129:103–109

Feith M, Stein HJ, Siewert JR (2003) Pattern of lymphatic spread of Barrett's cancer. World J Surg 27:1052–1057

Fok M, Sham JS, Choy D et al (1993) Postoperative radiotherapy for carcinoma of the esophagus: a prospective, randomized controlled study. Surgery 113:138–147

Fujita H, Sueyoshi S, Tanaka T et al (2002) Three-field dissection for squamous cell carcinoma of the esophagus. Ann Thorac Cardiovasc Surg 8:328–335

Fumagalli U, Panel of Experts (1996) Resective surgery for cancer of the thoracic esophagus. Results of a consensus conference. Dis Esophagus 9:3–19

Gertler R, Stein HJ, Schuster T, Rondak IC, Höfler H, Feith M (2014) Prevalence and topography of lymph node metastases in early esophageal and gastric cancer. Ann Surg 259(1):96–101

Gignoux M, Roussel A, Paillot B et al (1987) The value of preoperative radiotherapy in esophageal cancer: results of a study of the E.O.R.T.C. World J Surg 11: 426–432

Gockel Im Sgourakis G, Lyros O et al (2011) Risk of lymph node metastasis in submucosal esophageal cancer: a review of surgically resected patients. Expert Rev Gastroenterol Hepatol 5:371–384

Hölscher AH, Bollschweiler E, Schröder W et al (2011) Prognostic impact of upper, middle, and lower third mucosal or submucosal infiltration in early esophageal cancer. Ann Surg 254:802–808

Hosch SB, Stoecklein NH, Pichlmeier U et al (2001) Esophageal cancer: the mode of lymphatic tumor cell spread and its prognostic significance. J Clin Oncol 19:1970–1975

Huang W, Li B, Gong H et al (2010) Pattern of lymph node metastases and its implication in radiotherapeutic clinical target volume in patients with thoracic esophageal squamous cell carcinoma: a report of 1077 cases. Radiother Oncol 95:229–233

Igaki H, Kato H, Tachimori Y et al (2005) Surgery for clinical T3 carcinomas of the upper thoracic oesophagus and the need for new strategies. Br J Surg 92:1235–1240

Japanese Society for Esophageal Diseases (2004) Guidelines for clinical and pathological studies on carcinoma of the esophagus, ninth edition. Esophagus 1:107–125

Korst RJ, Rusch VW, Venkatraman E et al (1998) Proposed revision of the staging classification for esophageal cancer. J Thorac Cardiovasc Surg 115:660–670

Lagergren J, Lagergren P (2013) Recent developments in esophageal adenocarcinoma. CA Cancer J Clin 63: 232–248

Lazarescu I, Thureau S, Nkhali L et al (2013) Clinical target volume delineation for radiotherapy of the esophagus. Cancer Radiother 17:453–460

Liebermann-Meffert D, Stein HJ, Duranceau A (2001) Anatomy and embryology of the esophagus. In: Zuidema GD, Yeo CJ (eds) Surgery of the alimentary tract, vol 1, 5th edn. WB Saunders, Philadelphia

Ma JB, Song YP, Yu JM et al (2011) Feasibility of involved-field conformal radiotherapy for cervical and upper-thoracic esophageal cancer. Onkologie 34:599–604

Malthaner RA, Wong RK, Rumble RB, Zuraw L, Members of the Gastrointestinal Cancer Disease Site Group of Cancer Care Ontario's Program in Evidence-based Care (2004) Neoadjuvant or adjuvant therapy for resectable esophageal cancer: a systematic review and meta-analysis. BMC Med 2:35

Mei W, Xian-Zhi G, Weibo Y (1989) Randomized clinical trial on the combination of preoperative irradiation and surgery in the treatment of esophageal carcinoma: report on 206 patients. Int J Radiat Oncol Biol Phys 16:325–327

Meier I, Merkel S, Papadopoulos T et al (2008) Adenocarcinoma of the esophagogastric junction: the pattern of metastatic lymph node dissemination as a rationale for elective lymphatic target volume definition. Int J Radiat Oncol Biol Phys 70:1408–1417

Monig SP, Baldus SE, Zirber TK et al (2002) Topographical distribution of lymph node metastasis in adenocarcinoma of the gastroesophageal junction. Hepatogastroenterology 49:419–422

National Comprehensive Cancer Network: NCCN guidelines Version 1.2015. NCCN.org

Patel M, Ferry K, Franceschi D et al (2004) Esophageal carcinoma: current controversial topics. Cancer Invest 22(6):897–912

Siewert JR, Stein HJ (1997) Barrett's cancer: indications, extent and results of surgical resection. Semin Surg Oncol 13:245–252

Siewert JR, Molls M, Zimmermann F, Lordick F (2008) Chapter 18 – Esophageal cancer: clinical management. In: Kelsen D, Daly J, Kern SE et al (eds) Principles and practice of gastrointestinal oncology. Wolters Kluwer, Lippincott Williams and Wilkins, Philadelphia

Stahl M, Stuschke M, Lehmann N et al (2005) Chemoradiation with and without surgery in patients with locally advanced squamous cell carcinoma of the esophagus. J Clin Oncol 23:2310–2317

Stahl M, Walz MK, Stuschke M et al (2009) Phase III comparison of preoperative chemotherapy compared with chemoradiotherapy in patients with locally advanced adenocarcinoma of the esophagogastric junction. J ClinOncol 27(6):851–856

Stein HJ, Siewert JR (2004) Improved prognosis of resected esophageal cancer. World J Surg 28(6):520–525

Sudo K, Taketa T, Correa AM et al (2013) Locoregional failure rate after preoperative chemoradiation of esophageal adenocarcinoma and the outcomes of salvage strategies. J Clin Oncol 31:4306–4310

Tachibana M, Kingusa S, Yoshimura H et al (2005) Clinical outcomes of extended esophagectomy with three-field lymph node dissection for esophageal squamous cell carcinoma. Am J Surg 189:353–361

Teniere P, Hay JM, Fingerhut A et al (1991) Postoperative radiation therapy does not increase survival after curative resection for squamous cell carcinoma of the middle and lower esophagus as shown by a multicenter controlled trial. French University Association for Surgical Research. Surg Gynecol Obstet 173:123–130

Tomblyn MB, Goldman BH, Thomas CR et al (2012) Cetuximab plus cisplatin, irinotecan, and thoracic radiotherapy as definitive treatment for locally advanced, unresectable esophageal cancer: a phase II study of the SWOG (S0414). J Thorac Oncol 7: 906–912

Vesprini D, Ung Y, Dinniwell R et al (2008) Improving observer variability in target delineation for gastro-esophageal cancer – the role of 18Ffluoro-2-deoxy-D-glucose positron emission tomography/computed tomography. Clin Oncol (R Coll Radiol) 20:631–638

Wang JH, Lu XJ, Zhou H, Wang F (2012) A randomized controlled trial of conventional fraction and late course accelerated hyperfraction three-dimensional conformal radiotherapy for esophageal cancer. Cell Biochem Biophys 62:107–112

Wong RK, Malthaner RA, Zuraw L, Rumble RB, and the Cancer Care Ontario Practice Guidelines Initiative Gastrointestinal Cancer Disease Site Group (2003) Combined modality radiotherapy and chemotherapy in the non-surgical management of localized carcinoma of the esophagus: a practice guideline. Int J Radiat Oncol Biol Phys 55(4):930–942

Xiao ZF, Yang ZY, Liang J et al (2003) Value of radiotherapy after radical surgery for esophageal carcinoma: a report of 495 patients. Ann Thorac Surg 75:331–336

Yam PC, Tong D, Law S (2014) Comparison of sixth and seventh edition of the American Joint Cancer Committee staging systems for esophageal cancer. Ann Surg Oncol 21(2):583–588

Zhao KL, Ma JB, Liu G et al (2010) Three-dimensional conformal radiation therapy for esophageal squamous cell carcinoma: is elective nodal irradiation necessary? Int J Radiat Oncol Biol Phys 76:446–451

Zieren HU, Müller JM, Jacobi CA et al (1995) Adjuvant postoperative radiation therapy after curative resection of squamous cell carcinoma of the thoracic esophagus: a prospective randomized study. World J Surg 19:444–449

Gastric Cancer

9

Tobias Baack, Sabine Mai, and Frederik Wenz

Contents

Abbreviations

3DCRT	3-Dimensional conformal radiation therapy
4D-CT	4-Dimensional computed tomography
5-Fu	5-Fluorouracil
Cal/day	Calories/day
CBCT	Cone-beam CT
CHT	Chemotherapy
CRT	Chemoradiotherapy
CTV	Clinical target volume
DRR	Digitally reconstructed radiograph
DVHs	Dose-volume histograms
EBRT	External beam radiation therapy
EORTC	European Organisation for Research and Treatment of Cancer
EPID	Electronic portal imaging device
GTV	PT gross tumor volume
IGRT	Image-guided radiation therapy
IMRT	Intensity-modulated radiation therapy
ITV	Internal target volume
LN	Lymph node
MRI	Magnetic resonance imaging
OAR	Organs at risk
PET	Positron emission tomography
PPI	Proton pump inhibitors
PT	Primary tumor
ROG	Radiation Oncology Group
RT	Radiotherapy
XELOX	Oxaliplatin/capecitabine

T. Baack (✉)
Department of Internal Medicine,
GRN Clinic Weinheim, Weinheim, Germany
e-mail: Tobias.baack@umm.de

S. Mai • F. Wenz
Department of Radiation Oncology,
University Medical Centre Mannheim,
University of Heidelberg, Mannheim, Germany
e-mail: Sabine.Mai@umm.de;
frederik.wenz@umm.de

A.-L. Grosu, C. Nieder (eds.), *Target Volume Definition in Radiation Oncology*,
DOI 10.1007/978-3-662-45934-8_9, © Springer-Verlag Berlin Heidelberg 2015

9.1 General

Surgical resection is the mainstay of gastric cancer treatment. Total gastrectomy, or whenever possible subtotal gastrectomy, in combination with resection of the lymph nodes and the gastrocolic omentum is performed. The extent of regional lymphadenectomy (D1 or D2) is a subject of controversial discussion.

Gastric cancer is both radio- and chemosensitive. Therefore, local tumor control and overall survival can be enhanced by multimodal treatment strategies such as chemotherapy (CHT) and/or radiotherapy (RT). The phase III Intergroup Trial 0116 showed that adjuvant chemoradiotherapy (CRT, 45 Gy irradiation, and 5-FU plus leucovorin) improved survival versus surgery alone (MacDonald et al. 2001, 2004, 2009).

However, gastric tumors often present in advanced stages and thus surgery is not always possible. Although there is a lack of phase III studies of neoadjuvant CRT compared to surgery alone for gastric cancer, patients with gastroesophageal junction (GEJ) tumors benefit of neoadjuvant CRT (Stahl et al. 2009; van Hagen et al. 2012). Further indications for RT are R1 or R2 resection status and palliative treatment, if obstructive symptoms or local bleeding appears.

Perioperative CT as given in the MAGIC trial enhanced survival compared to surgery alone (Cunningham et al. 2006), but final comparison between perioperative CT and adjuvant CRT is pending.

9.2 Anatomy

The stomach is located between the gastroesophageal junction and the duodenum. It is divided into three major parts: the cranial part is the fundus (cardia), the middle part is the corpus, and the caudal part is the antrum (pylorus). The surface of the stomach is in close contact to several visceral structures. Gastric cancers tend to invade these structures aggressively.

The anterior part of the stomach is adjacent to the liver and the abdominal wall, whereas the back side is in contact to portions of the pancreas, transverse colon, spleen, left kidney, and left suprarenal gland. The complete stomach is covered with peritoneum, except for a small blank region near the gastroesophageal junction.

The lymphatic drainage follows mainly along the celiac axis and can be divided briefly into seven lymph node (LN) regions: LNs along greater and lesser curvatures, suprapancreatic, celiac axis, para-aortics, gastroduodenal, porta hepatic, and splenic hilum. However, gastric cancers located in the upper third can metastasize to paraesophageal LNs as well.

The venous drainage follows predominantly along the portal system to the liver. Hence, liver metastasis can be found in around 30 % of patients (Figs. 9.1 and 9.2).

9.3 Pattern of Failure

Awareness of pattern of failure after surgery, as well as knowledge of the relevant anatomy and organs at risk (OAR), must be the basis for target volume definition. In clinical, reoperative, and pathologic studies, mainly four different sites of failure after surgery have been described: local recurrence, LN failure, peritoneal metastasis, or distant metastasis. Results of pattern of failure based on reoperation series in charge of the University of Minnesota and autopsy studies are summarized in Table 9.1 (Gunderson and Sosin 1982). These findings imply that mainly local recurrence of the tumor bed, in the area of anastomotic junction, and local-regional LN failure appeared after surgery. Some autopsy studies even described local-regional failure rates up to 93 % (Horn 1955). These results demonstrate the potential benefit of local-regional radiotherapy.

Pattern of lymphatic spread differs according to the localization of the primary tumor. On the one hand, tumors localized in the fundus tend to spread to splenic nodes (12–42 %), but less commonly to subpyloric lymph nodes. On the other hand, subpyloric nodes (~50 %) constitute the primary site of lymphatic spread of antral tumors, and splenic nodes are rather rarely involved (<10 %) (Smalley et al. 2002).

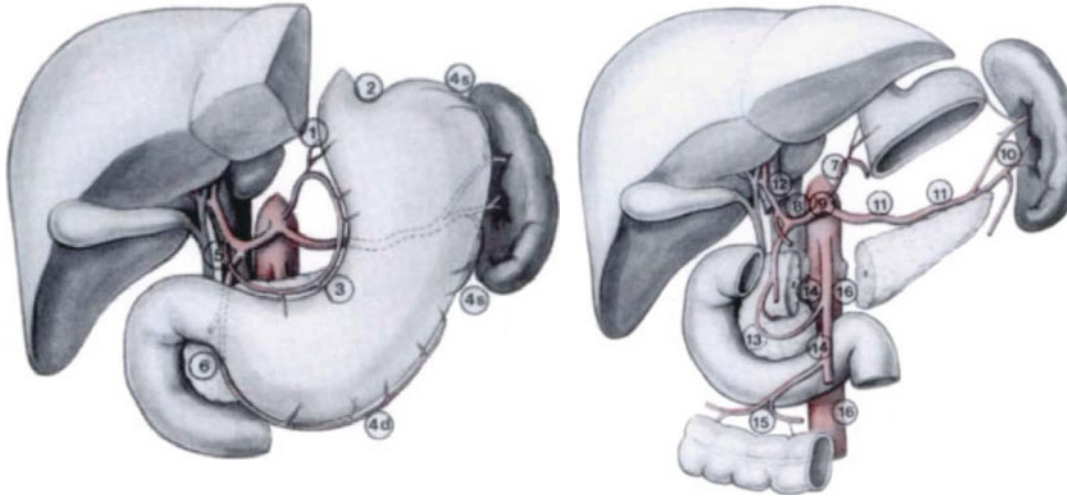

Figs. 9.1 and 9.2 LN drainage: Compartment 1 (DI resection): *1*. right cardial nodes; *2*. left cardial nodes; *3*. nodes along the lesser curvature; *4*. nodes along the greater curvature; *5*. suprapyloric nodes; *6*. infrapyloric nodes. Compartment 2 (D2 resection): *7*. nodes along the left gastric artery; *8*. nodes along the common hepatic artery; *9*. nodes around the coeliac axis; *10*. nodes at the splenic hilus; *11*. nodes along the splenic artery; *12*. nodes in the hepatoduodenale ligament; *13*. nodes at the posterior aspect of the pancreas head; *14*. nodes at the root of the mesenterium; *15*. nodes in the mesocolon of the transverse colon; *16*. paraaortic nodes. (Hartgrink and van de Velde 2005)

Table 9.1 Pattern of failure (Hazard et al. 2006)

	University of Minnesota reoperation series ($n=107$)	Autopsy series
Pattern of relapse	%	%
Gastric bed	55	52–68
Anastomosis	27	54–60
Abdominal wound	5	–
Peritoneal seeding	42	30–43
Lymph nodes	43	52
Local-regional as any site	69	80–93
Local-regional only	23	–
Lymph nodes only	7	–
Lymph nodes only in nodal dissection sites	3	–
Distant metastases	36	50

However, peritoneal seeding is relatively frequent in gastric cancer and has been described in the literature in up to 43 % of postgastrectomy patients (Gunderson and Sosin 1982).

Distant metastasis can be found most commonly in the liver, in approximately 30 % of cases and 10 % in the lung. Yet, with effective locoregional therapy, these secondary failures could be averted (Fig. 9.3).

9.4 Immobilization and Simulation

Patients are usually simulated in supine position with arms raised above the head. For enhancing reproducibility, a variety of immobilization systems, for example, wing boards and vacuum cushions, are available. Legs are placed on knee fixations and patients should be advised to fast for 3 h before simulation.

CT-based radiotherapy planning for gastric cancers is obligatory. CT images should be acquired from above the diaphragm to below the kidneys at the level of vertebrae L4/L5. Application of intravenous contrast is useful to identify the tumor and lymph nodes, but administration of oral contrast medium to visualize gastric distension is only recommended for diagnostic CT, not for planning CT. Surgical clips may be used for matching, but the radiation oncologist must be aware that the anatomy changes after surgery and that clips may not represent the resection margin, but rather vessel clips. Optimally, additional imaging like MRI or PET can be used for treatment planning and available CT slices should not exceed a thickness of 3 mm.

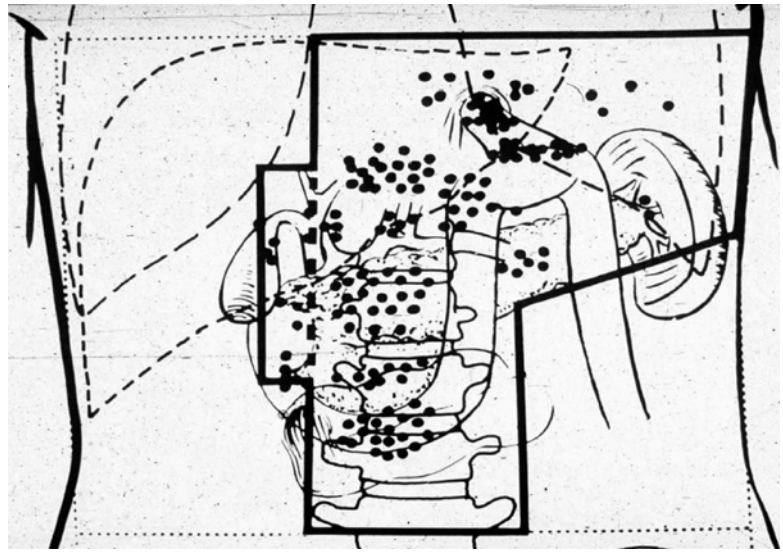

Fig. 9.3 Gunderson cartoon of hypothetical radiotherapy field based on the University of Minnesota reoperation series (Gunderson and Sosin 1982)

9.5 Target Volume Definition

Accurate target volume definition is based on the surgical and pathology reports and the combination of imaging, including CT, endoscopy, and endoscopic ultrasound (EUS) as compulsory and PET as recommended modalities.

9.5.1 Neoadjuvant and Definitive Radiation

For neoadjuvant and definitive radiotherapy treatment, the gross tumor volume (GTV) typically encloses the primary tumor (GTV-tumor) and all involved lymph nodes (GTV-nodal). The clinical target volume (CTV) includes microscopic disease with the primary tumor and their regional lymphatics. In the past, the whole stomach was irradiated, but to minimize toxicity, the target volume now depends on the location of the primary tumor (PT) within the stomach and whether imaging has detected nodal metastasis:

- For PT located in the fundus, the CTV includes the stomach with exclusion of pylorus, antrum, and pancreaticoduodenal lymph node region.
- For PT located in the corpus, the CTV includes the whole stomach with the regional lymph nodes.
- For PT located in the antrum, the CTV includes the stomach without fundus/cardia and splenic lymph node region.

Regardless of the location, a minimum margin of 5 cm in all directions to the GTV must be added. The internal target volume (ITV), which takes the target motion into account, should then be designed. Yet, 4-dimensional computed tomography (4D-CT) planning is not widely available. Therefore, the EORTC-ROG recommends to expand the CTV 1.5 cm distally, 1 cm radially, and 1 cm proximally to create the ITV (Matzinger et al. 2009). At least, a 5 mm 3-D margin is added to the ITV to construct the PTV.

9.5.2 Adjuvant Radiation

Optimally, the GTV has been completely resected at surgery, so the CTV encompasses the tumor bed with a 2 cm range proximally and distally of resection margins, as well as the anastomosis area and the perigastric nodes on the greater and lesser curvature.

Before encompassing the target volume, the radiation oncologist should study surgery and pathology reports carefully. Preoperative images of the GTV are useful to reconstruct the initial tumor localization on the present planning CT.

Adjuvant radiation of the tumor bed in widely resected T1 to T2a tumors is optional, but highly recommended for tumor stages T2b to T4.

In addition, if the margin is less than 5 cm or if lymph nodes are involved, the residual stomach should be included in the CTV. In case of a proximal gastric tumor, 3–5 cm of the distal esophagus should be included in the CTV.

LN irradiation should be performed in any case, but the radiation volume is depending on the site of the primary tumor. If the primary tumor is localized in the upper third of the stomach, infrapyloric and gastroduodenal lymph nodes may be omitted. In the same manner, for small gastric tumors of the lower third, splenic LN may be excluded from CTV.

9.5.3 Organs at Risk (OAR)

To reduce toxicity, the whole volume of all OAR is contoured on the planning CT.

The maximal spinal cord dose must be kept below 45 Gy, which is usually not a problem; 70 % of the volume of each kidney should not receive >20 Gy. Assuming that major parts of the kidney receive more than 20 Gy, the glomerular filtration rate of both kidneys should be measured before RT, to ensure that a sufficient renal function exists. At least 30 % of the liver should not receive beyond 30 Gy (V30 <30 %). Moreover, 30 % of the heart must not receive over 40 Gy and half of the heart must be kept under a total dose of 25 Gy. Attempts should also be made to minimize dose to the lungs, so less than 20 % should receive >20 Gy (V20 <20 %) (Table 9.2).

Table 9.2 Overview of radiation margins and tolerance of OAR

Cranial	Proximal anastomosis plus 2 cm
	For proximal tumors include 3–5 cm of the esophagus (paraesophageal LNs)
Caudal	Inclusion of the subpyloric/pancreaticoduodenal LNs (N3, to the level of L3)
	For proximal tumors with limited LN involvement to the level of L1/2 (truncus coeliacus Th12)
Left	Inclusion of the splenic hilum (LNs)
	For proximal, gastric wall exceeding tumors (≥T3) include left diaphragm
Right	Primary tumor extension (antrum)
	Porta hepatis (LNs)
Ventral	Abdominal wall (peritoneum)
Dorsal	The ventral third of the vertebral body
Kidneys	If both kidneys included, maximum 1/4 of one kidney >20 Gy
	Spare volume according to one kidney
Liver	Maximum 30 % volume <30 Gy
Heart	Maximum 30 % volume <40 Gy
Spinal cord	Usually not a problem, be careful when boost radiation is given
Lungs	Maximum 20 % volume <20 Gy

9.6 Radiation Therapy Techniques

In recent decades, the radiation technique for gastric cancer has made a continual transition from parallel-opposed anteroposterior-posteroanterior (AP-PA) fields based on findings by Gunderson et al. to conformal therapy with 3-dimensional CT planning and, finally, towards modern multiple-fields techniques like intensity-modulated radiation therapy (IMRT). Moreover, intraoperative radiation therapy (IORT) in gastric cancer has been used in the multimodality approach when applied additionally to external beam radiation therapy (EBRT). IORT has the potential to deliver a high dose (10–35 Gy) to the target volume while minimizing radiation exposure to the surrounding tissue, but the precise role of IORT in gastric cancer remains to be determined in further investigations.

Often AP-PA field arrangements were used in the past and resulted in large radiation volumes. Location of the target volume and the proximity of adjacent organs at risk lead subsequently to increased normal tissue toxicity and rates of therapy dropout.

If AP-PA fields are applied, the radiation margins are traditionally defined based on distinctive anatomic structures. Hence, the cranial margin reaches to the left diaphragm, but for proximal tumors, the margin is extended more cranially with inclusion of 3–5 cm of the esophagus. The caudal border is usually placed at the level of L3

to include the pancreaticoduodenal LNs, whereas the left border comprises the LNs of the splenic hilum as well as the greater curvature. The right border encloses the porta hepatis and the preoperative tumor extension.

The supplementation of oblique or lateral fields to AP-PA fields provides a potential benefit in patients with anteriorly located gastric cancer. Nevertheless, by using such techniques, the tolerance of liver and kidneys is limited to <20 Gy.

Whenever preoperative CT scans are available, 3-D planned therapy should be preferred. It is well known that planning in three dimensions allows more precise mapping of high-risk areas. Moreover, by delivering higher doses to the target volume, local control can be considerably improved.

To evaluate doses at OAR and to estimate subsequent toxicity, dose-volume histograms (DVHs) should be used.

Several studies confirm advantages of 3D conformal radiotherapy compared to AP-PA techniques in target volume coverage while protecting OAR (Leong et al. 2005; Ringash et al. 2005). These advantages were gained by dose reduction in kidneys while liver and spinal cord dose remain below the critical tolerance dose. To avoid marginal misses, the target volume must be identified and delineated accurately.

Multiple field arrangements, like IMRT, allow optimally adjusted target dose distributions while reducing the dose to surrounding OAR like the kidneys, heart, liver, and spinal cord (Lohr et al. 2003; Wieland et al. 2004).

Although these modern radiation techniques improved rapidly in the last decade, irradiated volumes may be unavoidably large to take into account setup variations and target motion caused by respiration movement, peristalsis, and intestinal filling. Both interfractional and intrafractional setup variations may influence the accuracy of radiotherapy considerably. IMRT in gastric cancer, with its steep dose gradients and narrow margins around the PTV, should be supplemented whenever possible with image-guided radiation therapy (IGRT). Among various image guidance methods, such as cone-beam CT (CBCT), ultrasound, and electromagnetic signals, CBCT has a dominant position in gastric cancer treatment. It can be performed fast (within 5 min) with relatively low additional radiation exposure (~20 mGy/scan). Various studies suggest daily CBCT or ultrasound imaging prior to radiation to enhance positioning accuracy and shrink PTV margins whereby dose in OAR can be minimized (Boda-Heggemann et al. 2009; Matoba et al. 2012). Image guidance correction can be performed by matching CBCT images automatically or manually with images generated by the planning CT based on bony structures and soft tissue. In general, normal structures such as the truncus coeliacus, kidneys, liver, or parts of the gastrointestinal tract help the oncologist in treatment planning. Additionally, positioning with skin marks compared with laser devices will help for daily patient setup. Electronic portal imaging devices (EPIDs) may be used to adjust treatment setup to digitally reconstructed radiographs (DRR), which are calculated from the CT data set (Figs 9.4 and 9.5).

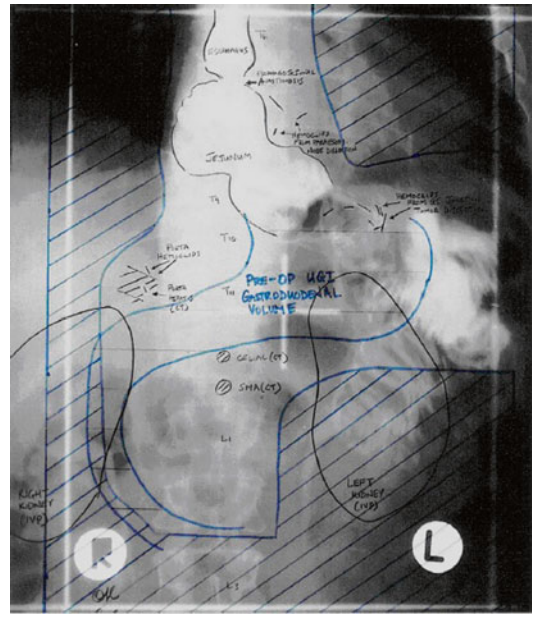

Fig. 9.4 Simulation film for a T4 (diaphragm invasion) gastroesophageal junction tumor with 4 of 15 metastatic involved lymph nodes. With the aid of preoperative CT scans, areas at risk particularly the preoperative tumor bed, anastomotic sites, gastric stump, and regional lymph nodes (celiac axis, greater and lesser curvatures, suprapancreatic, para-aortics, porta hepatic, splenic hilum, and pancreaticoduodenal nodes) can be defined. Notice that three fourths of the right kidney and one third of the left kidney can be spared with such technique (Smalley et al. 2002)

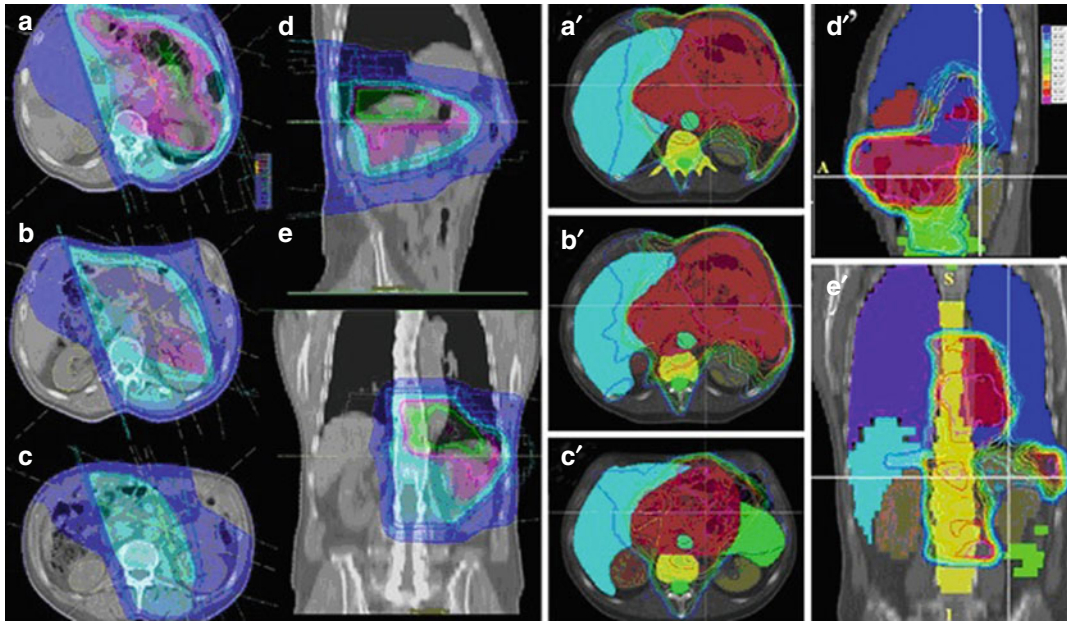

Fig. 9.5 Panel 1: a 3-dimensional conformal radiation therapy (3DCRT) plan for a patient with gastric cancer (45 Gy for the PTV and 5,4 Gy boost for the R1 region). Transversal (**a**–**c**), sagittal (**d**), and coronal (**e**) dose distributions are shown. Cave: the whole cranial part of the left kidney is located in the high-dose area which may result in relevant acute or late renal toxicity. Panel 2: optimized IMRT plan (45 Gy total dose). Transversal (**a**'–**c**'), sagittal (**d**'), and coronal (**e**') dose distributions are shown. IMRT allows sparing the renal cortex as well as the cranial part of the left kidney (Haneder et al. 2012)

9.7 Dose-Fractionation

For neoadjuvant therapy, a total dose of 45 Gy in 25 fractions of 1.8 Gy on 5 days a week is recommended by EORTC-ROG.

For definitive therapy, a dose of 45 Gy in 25 fractions of 1.8 Gy on 5 days a week is conventionally administered. A boost radiation therapy to a total dose of 54–59.4 Gy may be considered.

For adjuvant therapy, chemoradiotherapy consists of a total dose of 45 Gy delivered in 25 fractions, 1.8 Gy daily for 5 days a week with concomitant 5-Fu/leucovorin or oxaliplatin/capecitabine (XELOX) (Hofheinz et al. 2009). A total dose of 50.4–54 Gy seems to be appropriate in patients with residual disease.

9.8 Complications and Toxicity

Side effects and potential complications following radiation are dose and volume dependent and can be minimized if radiation is carefully implemented. Sufficient nutrition (a minimum of 1,500 Cal/day) prior to radiation is warranted and monitored throughout the therapy by assessing the patient's weight at least once a week. Acute side effects may be in particular nausea, anorexia, and fatigue. Premedication 1–3 h before RT with antiemetics, such as 5-HT3-serotonin antagonists, appears to be reasonable. Concomitant chemotherapy can lead to myelosuppression. Therefore, blood counts should be monitored through therapy in regular intervals. However, with total doses below 50 Gy, radiation-induced late effects are in general rare, but incidence increases with doses over 60 Gy and more. The major late effects are ulceration, dyspepsia, and radiation gastritis. For ulcer prophylaxis, proton pump inhibitors (PPI) or H2-blockers are available.

Nevertheless, future studies need to evaluate rates of late effects including secondary cancers in long-term survivors of gastric cancer.

References

Boda-Heggemann J et al (2009) Accuracy of ultrasound-based image guidance for daily positioning of the upper abdomen: an online comparison with cone-beam CT. Int J Radiat Oncol Biol Phys 74(3):892–897

Cunningham D et al (2006) Perioperative chemotherapy versus surgery alone for resectable gastroesophageal cancer. N Engl J Med 355(1):11–20

Gunderson LL, Sosin H (1982) Adenocarcinoma of the stomach: areas of failure in a re-operation series (second or symptomatic look) clinicopathologic correlation and implications for adjuvant therapy. Int J Radiat Oncol Biol Phys 8:1–11

Haneder S et al (2012) Assessment of renal function after conformal radiotherapy and intensity-modulated radiotherapy by functional (1) H-MRI and (23) Na-MRI. Strahlenther Onkol 188(12):1146–1154

Hartgrink HH, van de Velde CJ (2005) Status of extended lymph node dissection: locoregional control is the only way to survive gastric cancer. J Surg Oncol 90(3): 153–165

Hazard L et al (2006) Role of radiation therapy in gastric adenocarcinoma. World J Gastroenterol 12(10):1511–1520

Hofheinz RD et al (2009) Oxaliplatin and capecitabine-based chemoradiotherapy for gastric cancer–an extended phase I MARGIT and AIO trial. Int J Radiat Oncol Biol Phys 73(1):142–147

Horn RC Jr (1955) Carcinoma of the stomach; autopsy findings in untreated cases. Gastroenterology 29(4): 515–523

Leong T et al (2005) 3D conformal radiotherapy for gastric cancer – results of a comparative planning study. Radiother Oncol 74(3):301–306

Lohr F et al (2003) Optimization of dose distributions for adjuvant locoregional radiotherapy of gastric cancer by IMRT. Strahlenther Onkol 179(8):557–563

MacDonald JS et al (2001) Chemoradiotherapy after surgery compared with surgery alone for adenocarcinoma of the stomach or gastroesophageal junction. N Engl J Med 345(10):725–730

MacDonald JS et al (2004) Postoperative combined radiation and chemotherapy improves disease-free survival (DFS) and overall survival (OS) in resected adenocarcinoma of the stomach and gastroesophageal junction: update of the results of Intergroup Study INT-0116 (SWOG 9008). American Society of Clinical Oncology Gastrointestinal Cancer Symposium Abstract no. 6

MacDonald JS et al (2009) Chemoradiation of resected gastric cancer: a 10-year follow-up of the phase III trial INT0116 (SWOG 9008). American Society of Clinical Oncology Annual Meeting Abstract no. 4515

Matoba M et al (2012) Usefulness of 4D-CT for radiation treatment planning of gastric MZBCL/MALT. J Radiat Res 53(2):333–337

Matzinger O et al (2009) EORTC-ROG expert opinion: radiotherapy volume and treatment guidelines for neoadjuvant radiation of adenocarcinomas of the gastroesophageal junction and the stomach. Radiother Oncol 92(2):164–175

Ringash J et al (2005) Post-operative radiochemotherapy for gastric cancer: adoption and adaptation. Clin Oncol (R Coll Radiol) 17(2):91–95

Smalley SR et al (2002) Gastric surgical adjuvant radiotherapy consensus report: rationale and treatment implementation. Int J Radiat Oncol Biol Phys 52(2):283–293

Stahl M et al (2009) Phase III comparison of preoperative chemotherapy compared with chemoradiotherapy in patients with locally advanced adenocarcinoma of the esophagogastric junction. J Clin Oncol 27(6):851–856

van Hagen P et al (2012) Preoperative chemoradiotherapy for esophageal or junctional cancer. N Engl J Med 366:2074–2084

Wieland P et al (2004) IMRT for postoperative treatment of gastric cancer: covering large target volumes in the upper abdomen: a comparison of a step-and-shoot and an arc therapy approach. Int J Radiat Oncol Biol Phys 59(4):1236–1244

Rectal Cancer

10

Jean-Pierre Gerard and Karen Benezery

Contents

J.-P. Gerard (✉) • K. Benezery
Department of Radiation Oncology, Centre Antoine Lacassagne, 33 Avenue de Valombrose, 01689, Nice Cedex 2, France
e-mail: Jean-pierre.gerard@cal.nice.fnclcc.fr

10.1 Introduction

Radiotherapy is playing an important role in the treatment of rectal cancer. Many randomized trials have proven that even with now standard TME (total mesorectal excision) surgery, preoperative radiotherapy (Kapiteijn et al. 2001) or probably better chemoradiotherapy (Sauer et al. 2004; Bosset et al. 2006; Gérard et al. 2010) improves local control. Radiotherapy is mainly given in cases where tumors are located in the distal and middle rectum, and preoperative schedules have been proven to be more efficient and better tolerated than postoperative ones (Sauer et al. 2012; Park et al. 2011).

For that reason this chapter will focus on preoperative radiotherapy for so-called locally advanced rectal cancer (LARC) usually classified as T3, T4, or anterior distal T2 where the risk of local recurrence is significant with surgery alone. Colon cancer where radiotherapy is not frequently used will not be addressed in this chapter.

Radiotherapy technology has evolved gradually since the introduction of computers, digitalized imaging, and robotic guidance (Thariat et al. 2012; Widder et al. 2000). Three-dimensional conformal radiotherapy (3D CRT) is still used as standard technique in many centers and will be described in this chapter although intensity-modulated radiotherapy (IMRT) can be of interest in case of concave target volume shape or of simultaneous integrated boost (SIB) dosing

A.-L. Grosu, C. Nieder (eds.), *Target Volume Definition in Radiation Oncology*,
DOI 10.1007/978-3-662-45934-8_10, © Springer-Verlag Berlin Heidelberg 2015

concepts (Engels et al. 2009). Proton therapy which might provide the best dose distribution is not yet in routine clinical practice (Wolff et al. 2012).

The ICRU report 50 and 62 will be the fundamental basis of the definition of targets and of dose prescription and reporting. It should be noticed that in most of the publications coming from American or Asian institutions, the dose is not reported for the ICRU reference point but at the periphery of the target volume related to an "envelope" isodose, which in practice means that the administered dose is slightly higher than if using the ICRU international recommendations (bringing confusion as in the "Babel Tower").

10.2 A World of Uncertainties and Inhomogeneity

It is really difficult at the present time, which is still a phase of transition between 2D and 3D radiotherapy, to describe a universal standard technique of radiotherapy and target delineation (or contouring) for rectal cancer. This is due to many reasons:

- The *normal tissue contouring* is still controversial. There is a lack of standardized definition of the normal organs at risk (OAR). Even the boarders of the anus and the rectum are not the same when considering different guidelines (Gay et al. 2012). The upper boarder of the rectum is also controversial. The position of the rectosigmoid junction is uncertain. The rectum is a tube and therefore is hollow, but it is unknown if it must be contoured as a solid structure including its content or only as the rectal wall, which is approximately 5 mm in thickness. Moreover, the rectum is a very mobile organ with important shape and volume modifications between simulation and treatment and inter- but also intrafraction changes (Tournel et al. 2008; Nijkamp et al. 2011).
- The *tolerance dose* of the rectum is not fully understood (Gulliford et al. 2010, 2012; Kintzinger et al. 2012).

  The most relevant limiting factor is late rectal toxicity, which is not assessed and scored in a homogeneous way. The Common Terminology Criteria for Adverse Events (CTCAE version 4.0) is often used in clinical trials. Grade 3 late toxicity should be kept below 5 % in the majority of cases. Dose-volume histogram (DVH) analysis appears to be the best way to evaluate this toxicity. The Quantec methodology is a good approach to this challenging task even if important uncertainties remain (Michalski et al. 2010).

  It appears that when considering the whole length of the rectum (a cylinder of 10–12 cm craniocaudal extension), the risk of grade 3 late toxicity is below 5 % for doses not exceeding 44 Gy (2 Gy per fraction). A dose of 70 Gy should not be given to more than 20 % of the rectal volume (V70 < 20 %). It is highly likely that not irradiating the whole circumference of the rectum (whatever the volume) is a factor contributing to better tolerance. The tolerance dose of the anal canal is also not definitively defined. The experience gained through treatment of anal canal carcinoma seems to show that a dose of 60 Gy over 6 weeks to the whole anal canal is unlikely to exceed a 5 % risk of late grade 3 side effects (Ortholan et al. 2005).
- The *lymphatic spread* of rectal cancer is controversial. In many guidelines (Myerson et al. 2009; Roels et al. 2006; Steup et al. 2002) it is recommended to encompass in the clinical target volume (CTV) the obturator or even the external iliac nodes. These recommendations are derived from data of Japanese origin where the latero-pelvic nodes along the hypogastric (internal iliac) vessels are sometimes called obturator nodes, probably because they lie at the origin of the obturator artery. In fact in most of the anatomy books, the obturator nodes are located below the external iliac vein close to the obturator foramina (and nerve). These obturator nodes, located anteriorly in the pelvis, are the first sites of lymphatic spread for cancer of the uterine cervix, prostate, or bladder (Canessa et al. 2004; Arcangeli et al. 2003). They are exceptionally invaded in rectal cancer, and if they are, the survival rate is close to zero (Kobayashi et al. 2011). Moreover when speaking of lymphatic spread in rectal cancer, most of the experts agree that

there is no reliable imaging technique to distinguish between true N0 and N1 stage (Patel et al. 2011).

There are many *guidelines for contouring* the different targets in rectal cancer (Bosset et al. 2011; Krengli et al. 2010; Gay et al. 2012; Mavroidis et al. 2014; Myerson et al. 2009; Roels et al. 2006; Lorchel et al. 2002), and none of them are recommending the same procedure and the same delineation of CTV and other anatomical structures. In practice, techniques are described and used for randomized trials, and their evolution with time is a good way to suggest a contouring proposal. It will be demonstrated in this chapter that the evolution is toward restricted volumes targeting the posterior middle and low pelvis.

The *tumor dose* required in preoperative regimens is also variable with a dose per fraction of 1.8 Gy (not prescribed to the ICRU reference point) in the USA, 2 Gy in some countries, and 5 Gy in northern Europe. The total dose depends on each institution: 25 Gy (5 Gy per fraction) in Scandinavian countries, 45 Gy (1.8 Gy per fraction) in the UK, 50 Gy (2 Gy per fraction) in France (shrinking fields after 44 Gy), 45 Gy (1.8 Gy per fraction) to an "envelope isodose" + boost to a total dose of 50.4–54 Gy in the USA, etc.! It is highly probable that the total dose should be different for differently sized T2, T3, and T4 tumors depending on the strategy (preoperative or exclusive radiotherapy), with or without concurrent chemotherapy. In some recent ongoing trials, the dose of 60 Gy is tested for T4 tumors.

10.3 The Pattern of Local Recurrence: A Major Criterion to Select the "Good CTV"

One of the first attempts to make such an analysis of failure pattern was performed in the 1970s by Gunderson and coworkers (Gunderson and Sosin 1974) using the data of elective second-look surgery after initial radical surgery (often APR) to detect residual or early recurrent cancer in the pelvis. The finding for the rectal tumors treated at that time was that residual cancer was found in the whole pelvis and led to the design (in 2D technique at that time) of the diamond-shape field which is still recommended in some American textbooks today (DeVita et al. 2011).

More recently Nijkamp and coworkers (Nijkamp et al. 2011) have analyzed the pattern of local recurrence of the patients treated in the "Dutch TME trial." Based on 114 local recurrences, they were able to demonstrate that nearly all these recurrences were located in the posterior pelvis and below the S2–S3 interspace. This very important finding led to the conclusion that the cranial border of the CTV can safely be positioned for the majority of patients at or below the S2–S3 interspace with an important reduction in the volume of CTV (usually below 1 l) and a significant sparing of the small bowel.

10.4 Clinical Results from Randomized Trials: The Ultimate Arguments to Define the "Good CTV"

It was obvious when looking at the first randomized trial of preoperative radiotherapy in Sweden (Pählman et al. 1985) or chemoradiotherapy (Boulis-Wassif et al. 1984) that irradiation of large volumes with upper limit at the level of the second lumbar vertebra (L2) or even L4 with 2 simple AP-PA portals was responsible for 1–2 % of treatment-related death or 10–14 % postoperative death. Such large volumes were also possibly responsible for the high late toxicity of postoperative chemoradiotherapy in the USA during the 1980s (O'Connell et al. 1994; Krook et al. 1991), which is not so striking and important in new phase III trials using smaller fields (Park et al. 2011).

On the opposite, with small volumes (less than 1 l) centered on the posterior pelvis with cobalt irradiation, Papillon was able to achieve in the 1980s less than 8 % of local relapse with no serious toxicity (Papillon 1990). This was confirmed by a British randomized study using the same small volume (field size: 10 × 10 cm), which demonstrated that local relapse could be reduced

from 28 to 12 % with no serious toxicity (Marsh et al 1994).

Targeting still smaller volumes with high-dose-rate (HDR) iridium endoluminal brachytherapy, Vuong and coworkers, who treated more than 400 patients, could achieve local control in 95 % of cases without serious toxicity (Vuong et al. 2005).

In France "small posterior" pelvic volumes were recommended in the EORTC trial 22092 (Lorchel et al. 2002; Kouloulias et al. 2002) and the FFCD trial 9203 (Gérard et al. 2006) where it was possible to reduce the rate of local relapse below 10 % in patients treated before the era of TME surgery. In the more recent ACCORD 12 trial, patients were included between 2005 and 2008 presenting with tumors of the middle and distal rectum, all accessible to digital rectal examination (DRE) and all operated according to the TME principle. A clear recommendation was written in this trial not to irradiate a volume exceeding 1.2 l. The upper limit of the CTV was never above the S1–S2 interspace; the anal canal was kept out of the CTV for most of the tumors except if in the distal rectum the tumor was less than 2 cm from the anal canal. The external iliac or obturator lymph nodes were never part of the CTV. Trial participants were not treated with IMRT. After 44 Gy (2 Gy per fraction), a boost dose of 6 Gy in 3 fractions was given to the gross tumor volume (GTV) with a margin (CTV + PTV) of 2 cm. With such a limited PTV, it was possible to achieve after 3 years of follow-up a rate of local recurrence of 4.4 % with less than 5 % of late grade 3 toxicity (CTCAE V3.0) (Gérard et al. 2012).

After reviewing the data of local recurrence and taking into account CTV variation and margins, Nijkamp and coworkers are recommending to contour/create a PTV close to 1,000 ccm (1 l) (Nijkamp et al. 2012).

During long-course radiotherapy, a significant reduction in rectal volume can be seen. When contouring the anterior part of the CTV does not lead to concave (horseshoe) shape, IMRT is not necessary to adequately encompass the PTV. The old-school diamond-shape volume in the DeVita textbook is typically encompassing a volume of 2.5 l (2,500 ccm) which is probably too large. In conclusion small volume (high dose) seems the appropriate strategy, and it is surprising to see that few publications or radiation oncologists are mentioning, when reporting their treatment plans, the volume of the rectal tumor (GTV), of the rectum or anus (OAR), and of the PTV or treated volume. It can be useful to keep in mind the basic mathematical formula of volume to put into perspective the differently contoured and treated volumes for rectal cancer (Appendix 10.1).

10.5 Contouring in Practice

Knowing Where Is the GTV

As most of the local recurrences are close to the GTV, it is crucial to be able to contour as accurately as possible the GTV (the primary rectal tumor) on the CT slices of the treatment planning study. This is the main responsibility of the radiation oncologist. To properly locate the GTV, the radiation oncologist should perform a careful DRE in the position of treatment and if possible a rectoscopy (or have a clear description of such an exam performed by an endoscopist, if possible with photographs). The size in cm of the primary tumor must be measured accurately, and its shape (polypoid, ulcerated, fungating, or infiltrating) must be defined. The distance of the lower pole of the tumor relative to the anal margin must be appreciated, as is the case for the length of the anal canal. It is possible (and easy using a rigid rectoscope) to implant a radiopaque fiducial marker in the rectal wall at the level of the lower pole of the tumor. Such a marker will strongly facilitate the localization of the lower pole of the tumor on the simulation CT scan. Most importantly the clockwise extension and location of the tumor must be accurately defined. A circumferentially infiltrating tumor of the middle rectum ("big T3") is totally different in terms of GTV contouring from a tumor of 3 cm ("small T3") in the distal rectum, and it is also very different if

this tumor encompassing less than half of the rectal circumference is located anteriorly or posteriorly. In any case a sketch of the tumor and its location in the rectum performed by the radiation oncologist is very useful to properly delineate the GTV. Sagittal and transverse axial views provide excellent overview and complement definition of the anatomical structures. Especially the sagittal view can usually in a single image provide an excellent picture of the treatment plane. In the examples presented in this chapter such sagittal views will always be presented. Of course during the process of GTV definition and contouring, the use of appropriate imaging is very important. Magnetic resonance imaging (MRI) of good quality is very helpful especially for "big T3" of the middle rectum where the fat of the mesorectum is more abundant. For early T3 of distal rectum, endoscopic ultrasound (EUS) is sometimes more accurate. If available, positron emission tomography (PET)-CT (tracer: 18-FDG) can add important information to define the GTV. In all situations, being able to perform image fusion with the simulation CT scan will enhance the accuracy of the GTV delineation. It must be stressed when speaking of GTV that there exists no accurate imaging technique to detect metastatic lymph node(s). Even in experienced hands, MRI node classification (N0 vs N1–2) has no correlation with DFS or local recurrence rate. Of course, when suspicious nodes larger than 1 cm short axis diameter are proven metastatic using fine needle aspiration, those should be included in the GTV.

Patient Positioning and Image Acquisition

There is no evidence that the supine or prone position is superior. One advantage of the prone position is to facilitate the accurate introduction of a radiopaque marker of 2.5–3.5 cm in the anal canal. This marker is very useful for good contouring of the anal canal and clear delineation of the anal margin and anorectal junction. Care must be taken when using an anal "marker" not to modify the natural orientation of the anal canal which is always anterior and upward. When a male patient is placed in the prone position, it is important to ask him to position his penis and testis downward in order to avoid direct irradiation of these OAR with the posterior field. The use of belly board remains debatable especially if the treated volume is kept below S1. In very obese patients, belly board technique is probably useful. The small bowel which is the most important OAR to protect is not easy to contour and is highly mobile in the pelvis. Contrast media can be used to facilitate its delineation. The urinary bladder is not required to be full, and there is no special enema to empty the rectum.

Volume Contouring

It is the full responsibility of the radiation oncologist to perform the following steps, which, in collaboration with the dosimetrist and/or physicist, might take 20–30 min. We usually start with the contouring of the rectum and anus. We contour the outer limit of the rectum (limit between muscularis propria and perirectal fat). The lower limit is at the upper part of the anal canal (easily seen with the anal radiopaque marker). The upper limit is at the junction with the sigmoid colon, which is located where the rectum bends anteriorly usually at the level of the S2–S3 interspace and always behind a vertical line passing through the promontorium. This accurate contouring of rectum and anus is crucial, and a regular look at the sagittal view of these two organs is important during this contouring to avoid misleading delineation. It is also important to measure already at that time the length of the anal canal (between 2.5 and 4 cm) and of the rectum (between 10 and 12 cm). The upper limit of the rectum is approximately 15 cm from the anal verge, but of course it is not a straight line as on the sagittal view the anus and rectum are strongly oblique and the rectum is curved.

The contouring of the other OAR can vary from one institution to the other. We usually contour only the femoral heads (a simple sphere close to 50 ccm). It is possible to contour the head and the trochanter. It can be useful to contour the sacrum to evaluate the volume of bone

marrow irradiated especially when concurrent chemotherapy is given in elderly patients and one tries to optimize bone marrow protection. The pubic bone contouring is useful on a sagittal view to see easily the anterior part of the pelvis. One should contour the bladder, the small bowel, the prostate, and the uterus. In female patients it could be helpful to contour the vagina (to reduce sexual side effects), but it is not easy to define this structure on the simulation CT. It could be useful to use a radiopaque marker to visualize it better. The penile bulb of male patients can be contoured even if its protection has not yet proven to reduce erectile dysfunction.

Contouring of the GTV

Primary tumor and metastatic lymph node(s) if biopsy proven or positive based on PET-CT and/or MRI criteria are delineated. It is important to visualize the position of the GTV on the sagittal view to verify its situation in the craniocaudal position and be sure it is in agreement with all the clinical findings previously identified. The GTV must also be visualized on the transverse axial views to check its clockwise location and especially draw it accurately when there is any anterior extension (where the boarder to the OAR is difficult to define). The appropriate contouring of the GTV is the most important step of the treatment planning.

Contouring of the CTV

CTV is a conceptual volume supposed to encompass the subclinical cancer cells "left behind" by the surgeon and supposed to be sterilized by radiotherapy in order to achieve permanent local control (according to ICRU 50). As said previously there are many guidelines recommending the optimal CTV, but none are alike and so far no international consensus has been reached. This is especially true when defining the normal lymph node areas which should be electively included in the CTV. As mentioned above we never electively irradiate "normal" external iliac or obturator nodes. We will include in the CTV: perirectal nodes inside the mesorectum up to the level of S1–S2 or S2–S3 interface and presacral lymph nodes with the same upper limit. We will not try to contour (and to irradiate) the nodes along the inferior mesenteric artery (junction of the upper rectal artery and sigmoid artery at the level of S1). Hypogastric (internal iliac) lymph nodes which include the nodes along the middle rectal artery are included in the CTV. Anteriorly these nodes are following the hypogastric (internal iliac) vessels and are always posterior to the middle of the femoral head and below S1. The rectal wall below the tumor is included in the CTV. At the present time, surgeons agree with a 1 cm limit to avoid a positive distal margin. In case of tumor of the middle rectum, the CTV is 2 cm below the tumor (GTV) along the rectal wall (and not on a vertical line!), and the anal canal is totally outside the CTV. For tumors of the distal rectum (the rectum being more horizontal in the lower part), the CTV is at the upper limit of the anal canal, or if the tumor reaches the upper part of the anal canal, 2/3 of the anal canal might be included in the CTV, but the anal margin (skin) which can be accurately visualized with the anal marker is always outside the CTV as there are never cancer cells in the skin of the anal margin. The mesorectum and especially the "fascia recti" which limit the periphery of the mesorectum in the posterior and lateral planes are not clearly seen on the simulation CT scan. The CTV must be outside of the fascia recti which will be removed entirely by the surgeon. The CTV is close to the sacral bone and lateral bony part of the pelvis along the internal obturator muscle and including a large part of the ischiorectal fossa. The anterior region is the most difficult area for contouring the CTV (especially for an anterior tumor) because the balance between covering the CTV/GTV and protecting the OAR is subtle. Personal perception and interpretation with intra-/extra-observer variability are difficult to avoid in such a situation (as it is for surgical dissection and excision). Medicine is not a fully reproducible arithmetical science! When the CTV is delineated, it is

important to check its position, shape, and size on the sagittal view where the anterior/posterior and upper/lower limits can be seen easily, especially in relation with the location of the GTV, because most of the residual cells will be close (within 2 cm?) to this GTV.

PTV definition is not easy for rectal cancer because "everything is moving" (tumor, rectum, and OAR, mainly small bowel) during inter- and, also to a lesser extent, intrafraction time. Most guidelines recommend an expansion between 0.5 and 1 cm, depending on the institution's immobilization, organ filling, and image guidance policy. The largest expansion is added at the anterior and superior part of the rectum.

Field Definition and Optimization

When contouring of OAR, GTV, and CTV is performed with expansion for the PTV, the treatment planning systems automatically will position the beams. Before a "class solution" must be defined in agreement with the general strategy of the department. We use for most rectal cancers a three-field technique with one posterior and two lateral fields using multileaf collimator (MLC) to shape the fields. It is very important to implement a standard technique in each single department in order to avoid inhomogeneous treatment approaches of varying quality. The boost dose is given with the same three-field technique. It is possible, for the boost, to use a four-field box or if more appropriate a four-field oblique technique.

At this stage the isodose display of the treatment is available, and it is possible to validate the treatment plan. For this validation the DVH is a very useful tool. It is important to check the volume of each OAR, GTV and CTV, and to assess whether ominous discrepancies from expected sizes are observed. Also it is crucial to visualize the isodoses on the sagittal plane (and some transverse axial planes) to assess the satisfactory coverage of the GTV and protection of the main OAR. An ultimate optimization can be performed but will be essentially subjective. The most difficult point is usually at the anterior level of the PTV (or CTV) to find a balance between the desired dose in the GTV/CTV and avoid excessive dose in the OAR (bladder, small bowel, prostate, vagina etc.) and also in case of T4 tumor with invasion of neighboring organs to position properly the boost CTV/PTV.

10.6 Some Practical Examples

Taking into consideration all the above data and recommendations, we will present some cases to illustrate the various treatment plans and volumes contoured, depending mainly on the clinical stage (TNM) and location of the tumor. In all the cases, the strategy recommended by the multidisciplinary team (MDT, or tumor board) was preoperative chemoradiotherapy according to the CAP 50 regimen (Gérard et al. 2012). The dose of radiotherapy prescribed to the ICRU reference point was 50 Gy in 25 fractions over 5 weeks with cone down boost after 44 Gy (2 Gy per fraction). The standard technique (class solution) used in the department of Centre Antoine-Lacassagne in Nice is a three-field technique in the prone position with 18 mV photon beam. In all the cases, the GTV (rectal tumor ± nodes) was accurately assessed by the radiation oncologist who performed careful DRE and rigid proctoscopy. In all cases, EUS and MRI were performed to define the T(N) category. Some patients had additional PET-CT.

In all cases the procedure of contouring was the same:

1. Rectum and anal canal contouring
2. Other OAR contouring
3. GTV (rectal tumor) contouring and positioning in the rectum volume
4. CTV contouring and PTV estimation for the first 44 Gy and for the 6 Gy boost
5. Using the beams eye view software positioning of the fields (one posterior and 2 lateral)

6. Viewing of the isodoses and especially assuring that the 95 % isodose encompasses the PTV
7. If needed optimization of the dose distribution by modification of the field dimension or shape and by changing the relative contribution of each field dose delivery or wedge choice, in order to achieve a good dose homogeneity in the PTV (as defined by ICRU)
8. Dose-volume histogram analysis and control of the volume in ccm of each target and of the volume included in the 95 % isodose. Final validation and signature by the radiation oncologist

During this process a frequent look at the sagittal view of the plan is recommended to ensure "clinical consistency" between the created contours and clinical data of the tumor and patient. The permanent assistance of the dosimetrist or physicist during this process is helpful to ensure fast (20–30 min) and accurate treatment planning.

10.7 Some Clinical Examples

1. T3 NO(X) – distal anterior rectum (male patient, 54 years, tumor 40 % of circumference)

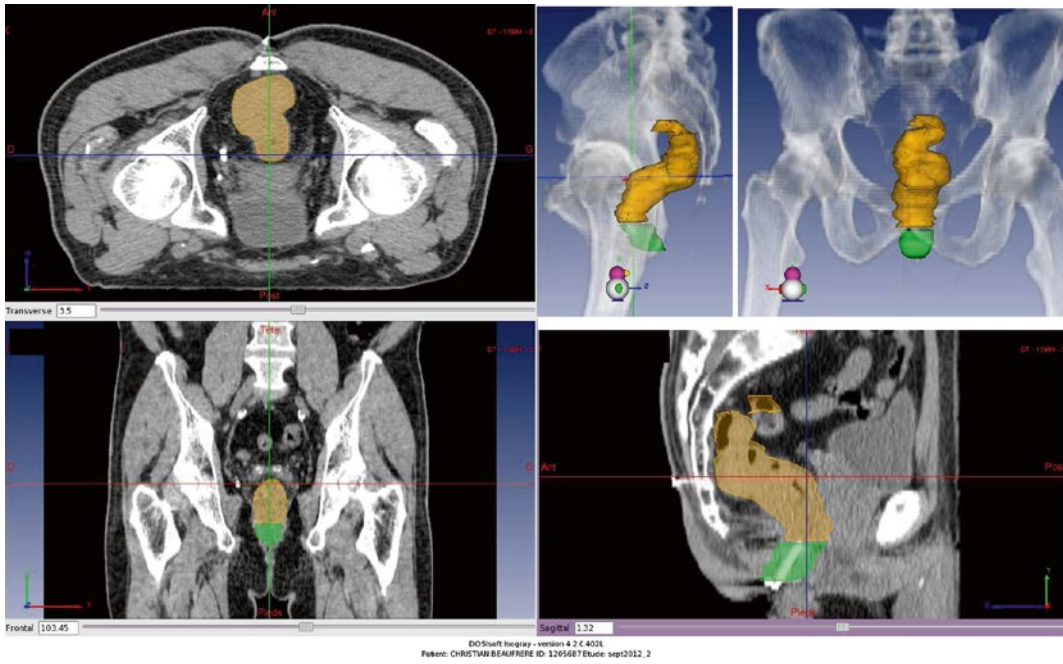

1.1 Contour of rectum (*pale yellow*) and anal canal (*green*). Radiopaque marker seen in the anal canal (3.3 cm long) and visualization of the anal margin (not contoured). The rectum appeared rather large probably containing stools

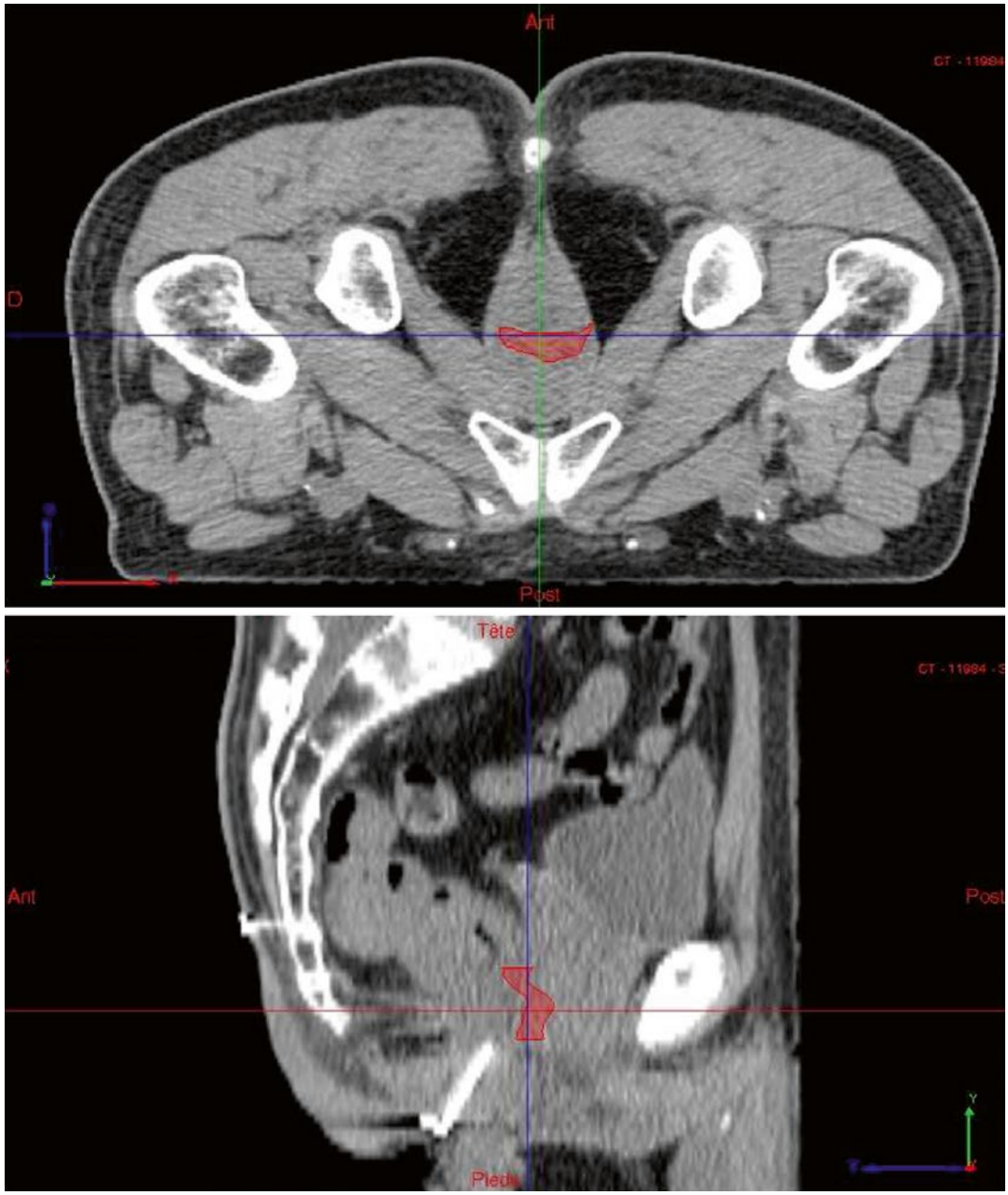

1.3 Rectal tumor contouring and positioning of GTV. Volume of tumor (GTV): 9 ccm

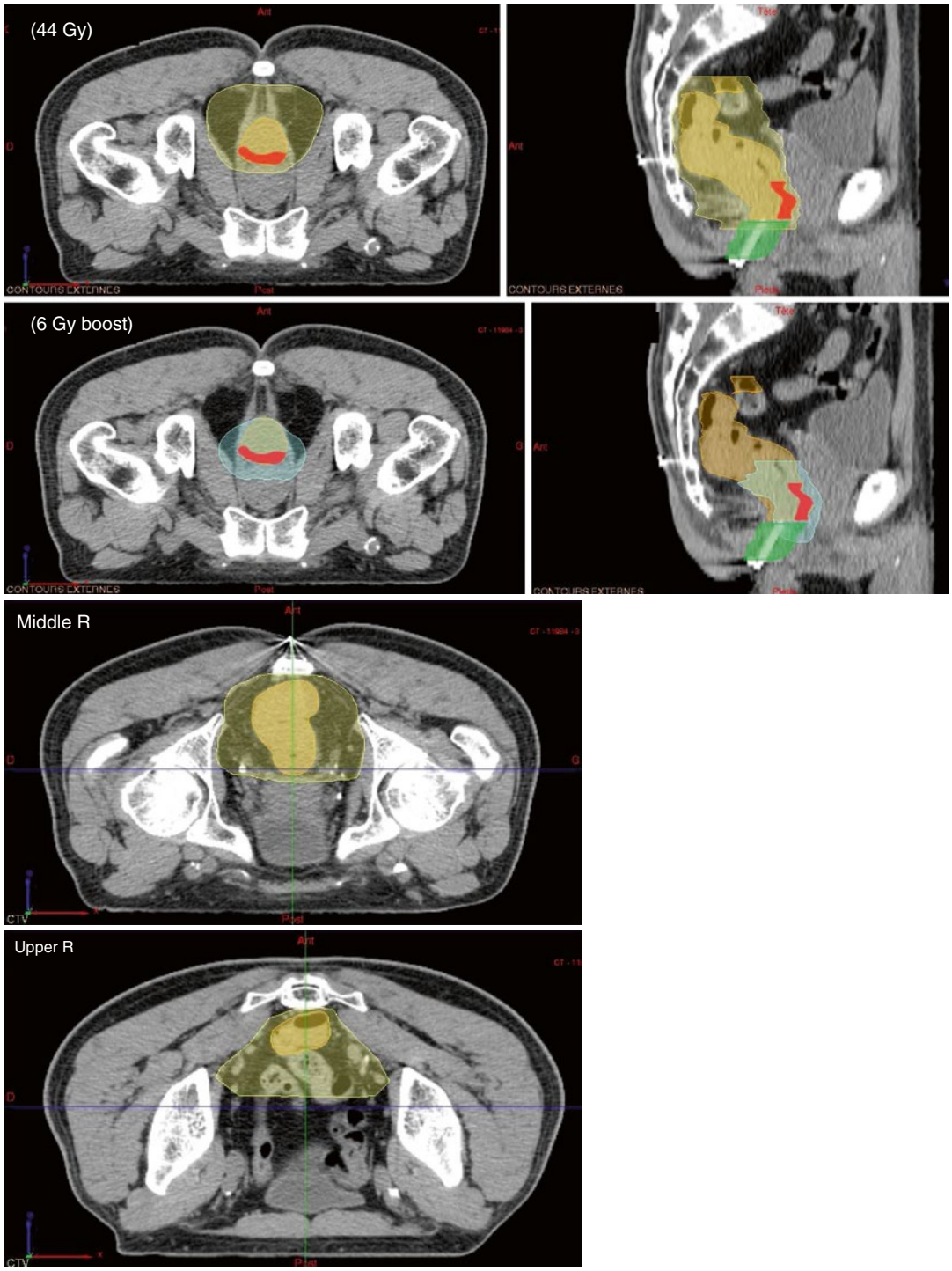

1.4 CTV contouring: CTV 44 Gy (sagittal view; axial view for *low* rectum with GTV, *middle* rectum, *upper* rectum); CTV boost 6 Gy (sagittal and axial views)

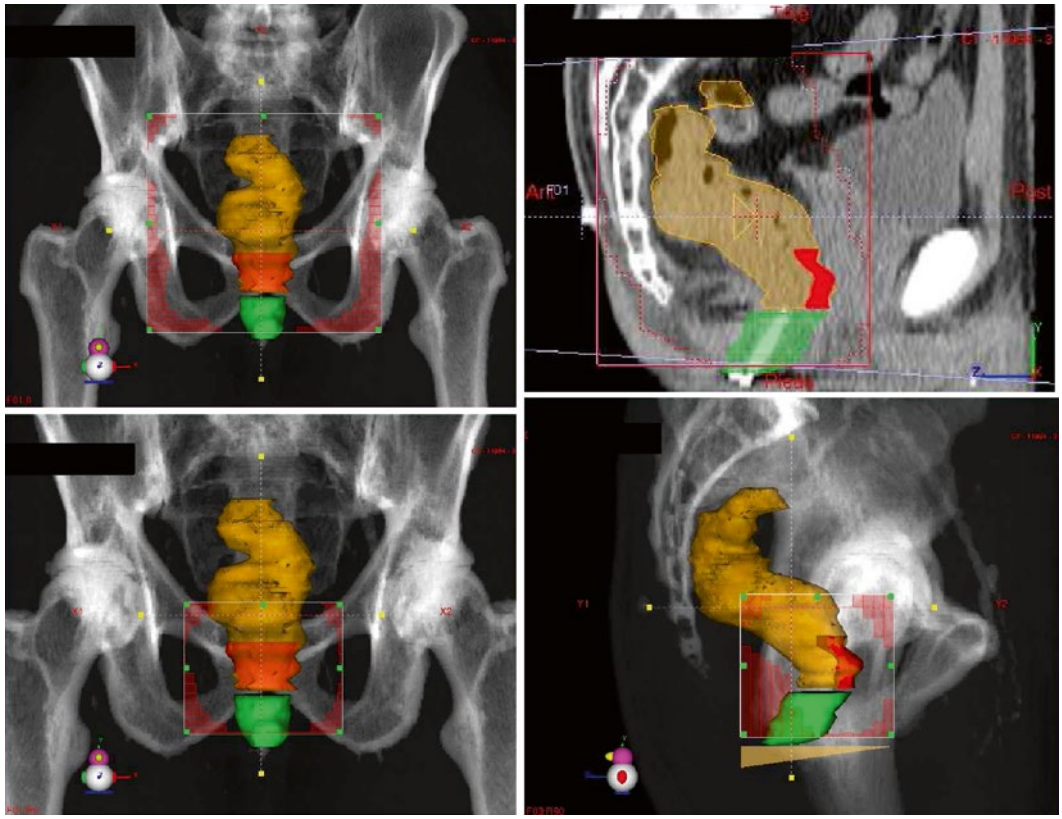

1.5 After PTV definition positioning of fields with MLC: lateral field and posterior field for initial 44 Gy; lateral field and posterior field for 6 Gy boost

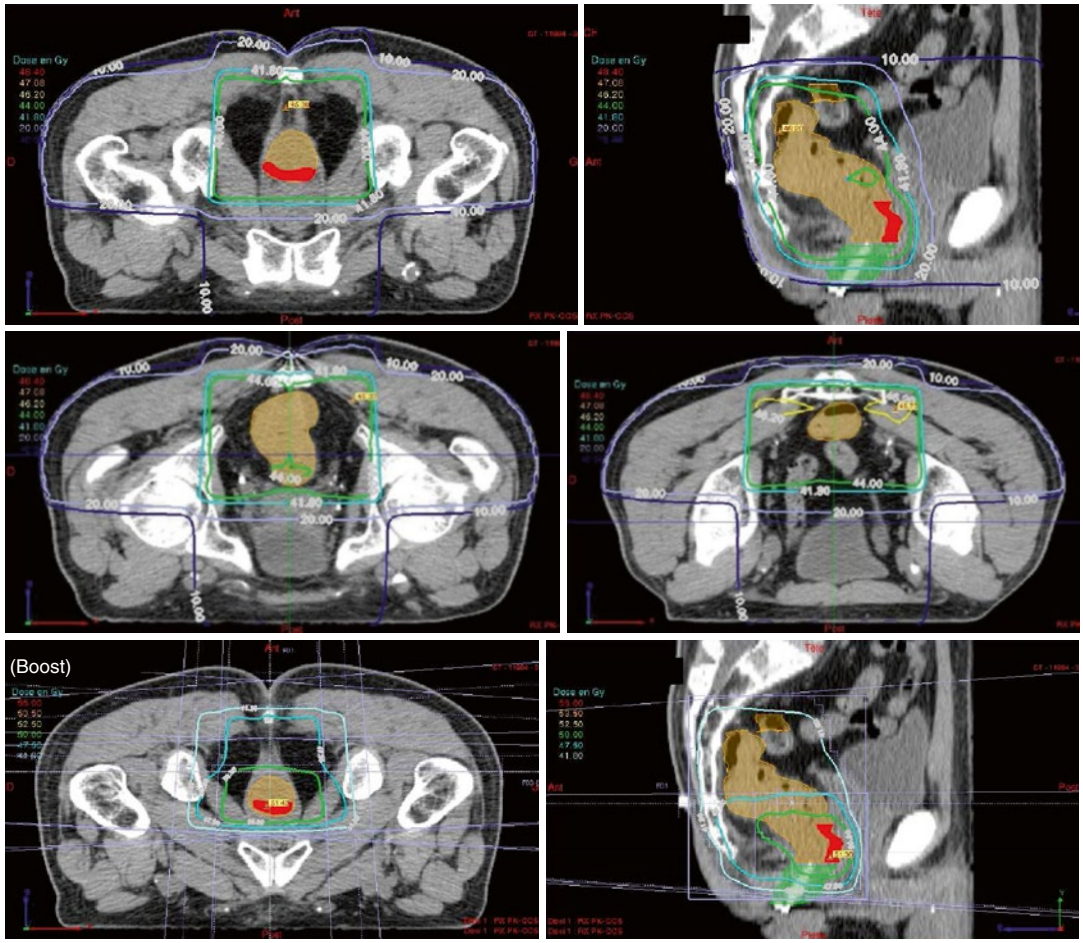

1.6 Isodose display for 44 Gy. Visualization of the 95 % isodose (relative to ICRU reference point) which corresponds to 41.8 Gy (turquoise color); sagittal view and axial view of *low* pelvis with GTV and *middle* and *upper* pelvis. In the *upper plane*, the external iliac arteries, which are calcified, can be easily seen (not included in the CTV due to their anterior location). On the opposite the hypogastric arteries (also calcified) are in the posterior pelvis and well in the CTV with no need for IMRT technique. Isodose display in sagittal plane for 6 Gy boost (95 % isodose, 5.7 Gy) and for 50 Gy. The turquoise isodose is the 41.8 Gy line which is the 95 % isodose relative to the 44 Gy prescription dose and reported for the ICRU point in the middle of the PTV

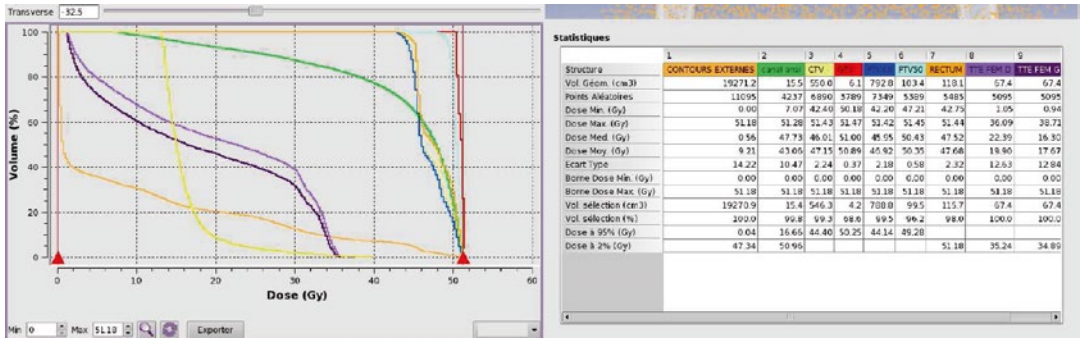

Structure	1 CONTOURS EXTERNES	2 Canal anal	3 CTV	4 [illegible]	5 [illegible]	6 PTV50	7 RECTUM	8 TTE FEM D	9 TTE FEM G
Vol. Géom. (ccm3)	19271.2	15.5	550.0	6.1	792.8	103.4	118.1	67.4	67.4
Points Aléatoires	11095	4237	6890	5789	7349	5389	5485	5095	5095
Dose Min. (Gy)	0.00	7.07	42.40	50.18	42.20	47.21	42.75	1.05	0.94
Dose Max. (Gy)	51.18	51.28	51.43	51.47	51.42	51.45	51.44	36.09	38.71
Dose Med. (Gy)	0.56	47.73	46.01	51.00	45.05	50.43	47.52	22.39	16.30
Dose Moy. (Gy)	9.21	43.65	47.15	50.89	46.92	50.35	47.68	19.46	17.67
Ecart Type	14.22	10.47	2.24	0.37	2.18	0.58	2.32	12.63	12.84
Borne Dose Min. (Gy)	0.00	0.00	0.00	0.00	0.00	0.00	0.00	0.00	0.00
Borne Dose Max. (Gy)	51.18	51.18	51.18	51.18	51.18	51.18	51.18	51.18	51.18
Vol. sélection (ccm3)	19270.9	15.4	546.3	4.2	788.0	99.5	115.7	67.4	67.4
Vol. sélection (%)	100.0	99.8	99.3	68.6	99.5	96.2	98.0	100.0	100.0
Dose à 95% (Gy)	0.04	16.66	44.40	50.25	44.14	49.28			
Dose à 2% (Gy)	47.34	50.96					51.18	35.24	34.89

1.8 The DVH shows the following volumes: anal canal, 15.5 ccm; rectum, 118 ccm; GTV, 9 ccm; CTV, 550 ccm; isodose, 41.8 Gy (envelope isodose encompassing the PTV, 994 ccm). It can be seen that the upper boarder of the envelope isodose (PTV/CTV) is at the level of S2–S3 interspace. Most of the small bowel is above and receives only small doses

2. T3 N1 – middle rectum (male patient, 57 years, tumor 70 % of circumference partly anterior with one node of 1 cm in diameter close to the tumor on the right side of the rectum, which was seen on MRI and palpable on DRE)

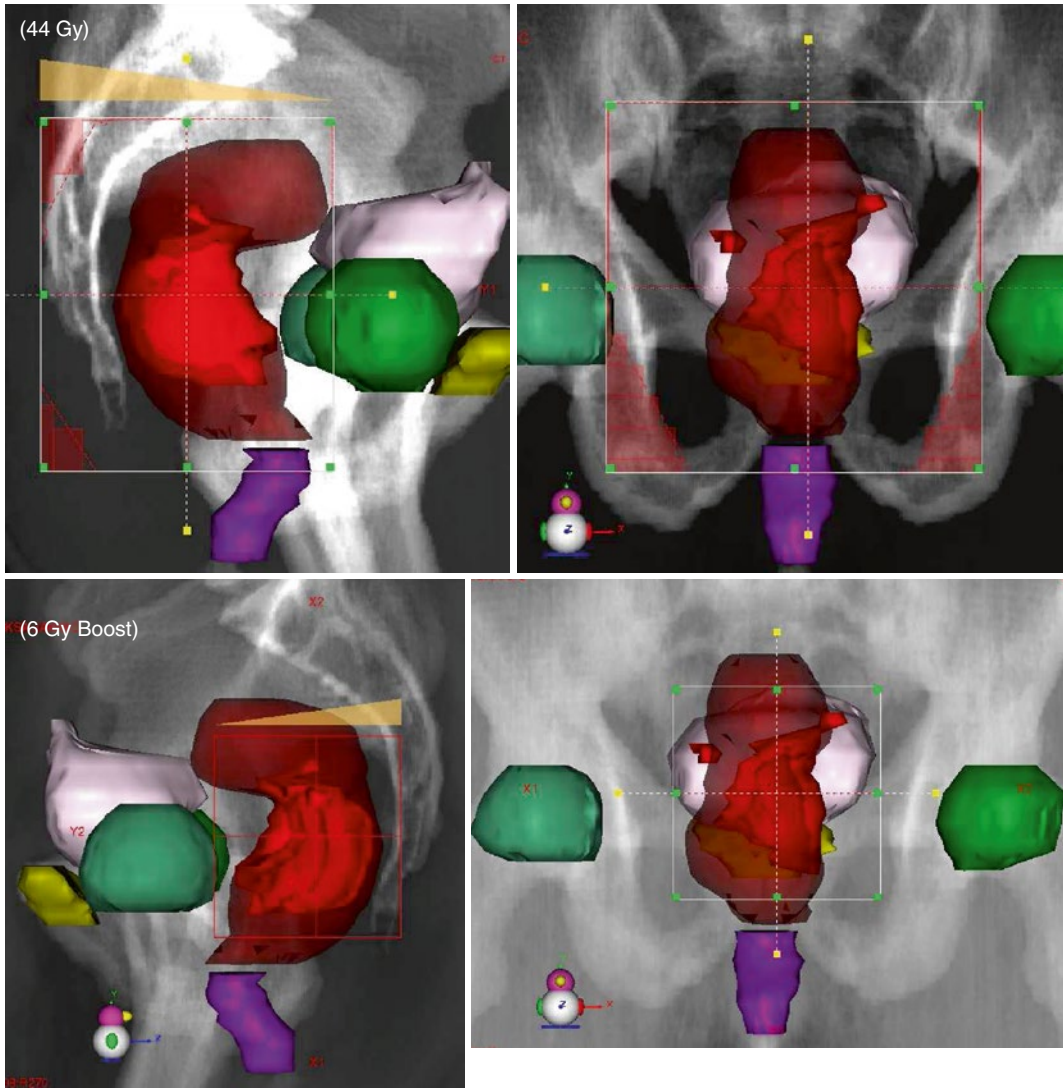

2.5 Positioning of fields with MLC: lateral and posterior fields for 44 Gy; lateral and posterior fields for 6 Gy boost

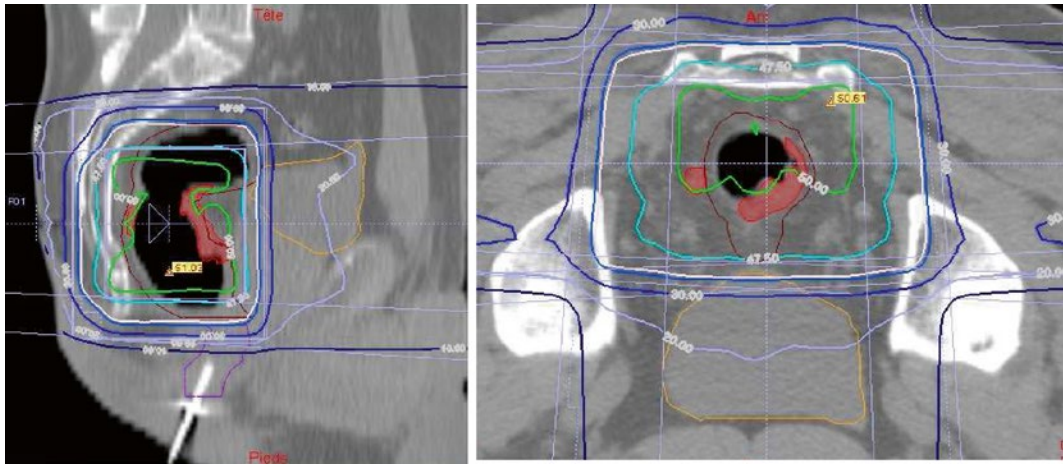

2.6 Isodose display for 50 Gy; sagittal and axial views through the tumor

Statistiques

	1	2	3	4	5	6	7	8	9
Structure	CONTOURS EXTERNES	anus	gtv_tumeur	pubis	rectum	sacrum	tf_d	tf_g	vessie
Vol. Géom. (cm3)	23948.0	14.5	23.3	18.6	169.5	158.3	53.7	54.0	141.7
Points Aléatoires	11119	4205	4455	4334	5763	5709	4947	4952	5623
Dose Min. (Gy)	0.00	1.03	49.06	16.27	39.69	2.36	1.02	1.01	17.05
Dose Max. (Gy)	51.12	40.85	51.26	20.53	51.21	51.08	27.57	28.51	44.64
Dose Med. (Gy)	0.63	5.69	50.16	18.40	50.26	33.85	3.88	4.52	19.87
Dose Moy. (Gy)	7.50	12.28	50.15	18.39	49.36	28.93	6.87	7.77	20.83
Ecart Type	12.56	12.45	0.36	0.91	2.06	17.30	6.71	7.42	3.54
Borne Dose Min. (Gy)	0.00	0.00	0.00	0.00	0.00	0.00	0.00	0.00	0.00
Borne Dose Max. (Gy)	51.26	51.26	51.26	51.26	51.26	51.26	51.26	51.26	51.26
Vol. sélection (cm3)	23947.3	14.5	23.3	18.6	169.5	158.3	53.6	54.0	141.7
Vol. sélection (%)	100.0	100.0	100.0	100.0	100.0	100.0	100.0	100.0	100.0
Dose à 95% (Gy)	0.04	1.26	49.47	16.82	44.45	3.32	1.29	1.30	17.75
Dose à 2% (Gy)	48.05	39.70	50.88	20.15	50.96	50.15	25.41	26.82	33.03

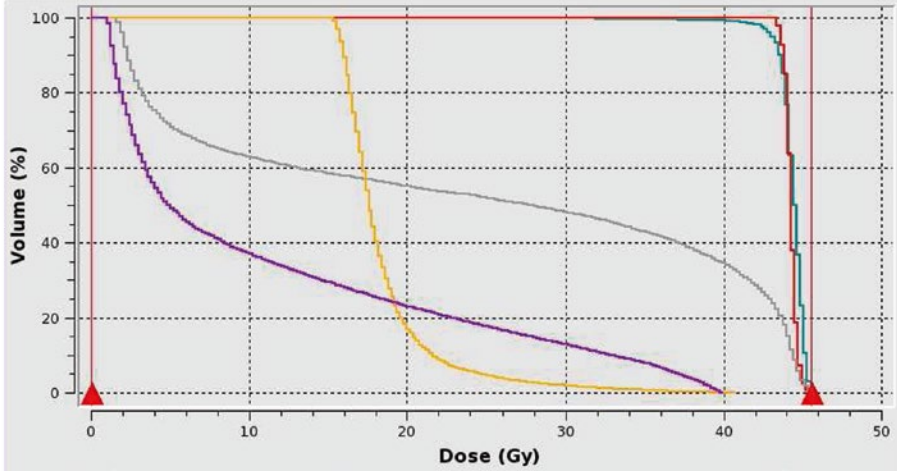

2.8 The DVH showed the following volumes: anal canal, 14.5 ccm; rectum, 169 ccm; GTV, 23 ccm; 95 % isodose of 44 Gy, 1,050 ccm

3. T2 N0 – distal anterior rectum (male patient)

   This 75-year-old patient referred by a surgeon for curative irradiation alone was treated with 50 kV X-ray contact brachytherapy: 110 Gy in 4 fractions, combined with EBRT (CAP 50 regimen derived from the ACCORD 12 trial). Two years later the patient was alive with local control and good bowel function.

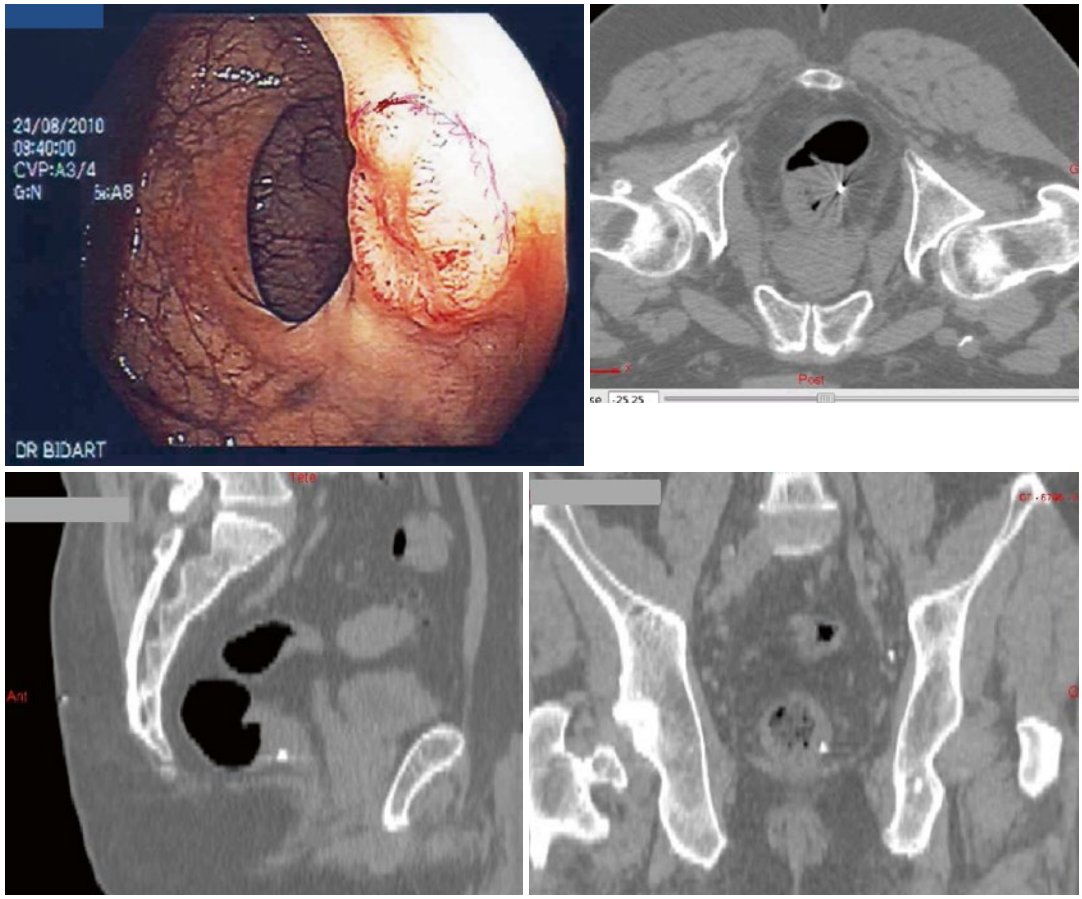

3.1 Endoscopic visualization of the tumor (2.5 cm in diameter). Radiopaque fiducial marker implanted at the lower limit of the tumor (patient prone)

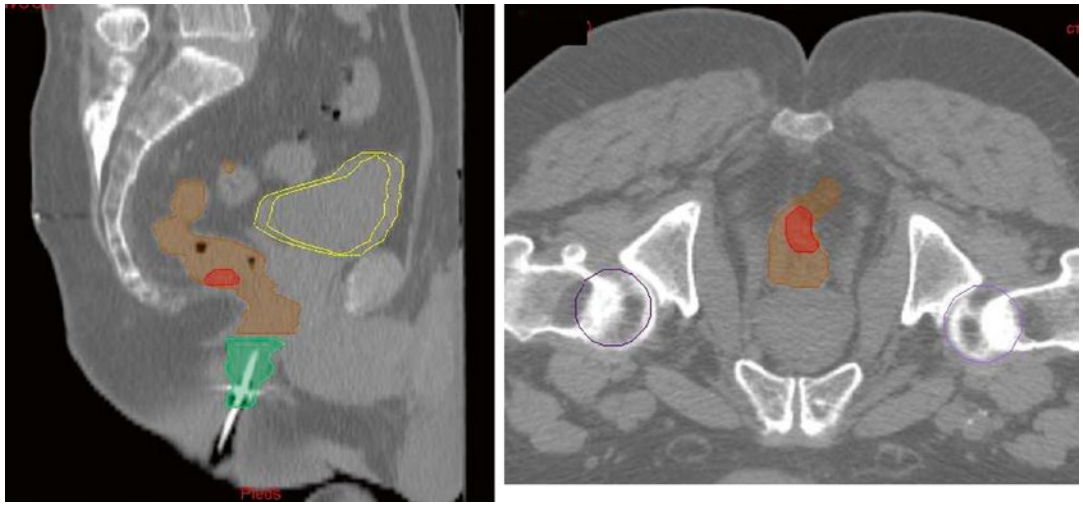

3.3 Rectal tumor (GTV) contouring with OAR (sagittal and axial views)

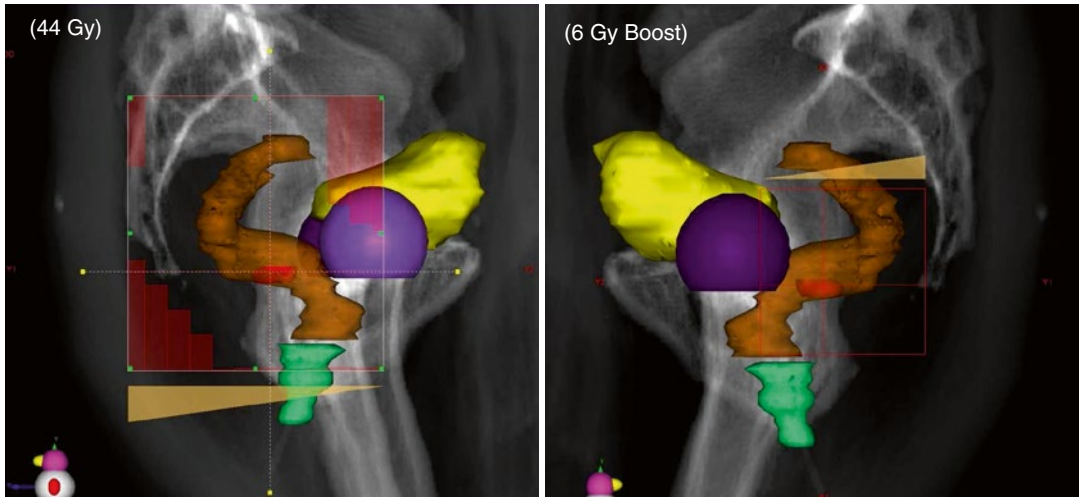

3.5 Positioning of fields with MLC. Lateral field for 44 Gy; lateral field for 50 Gy

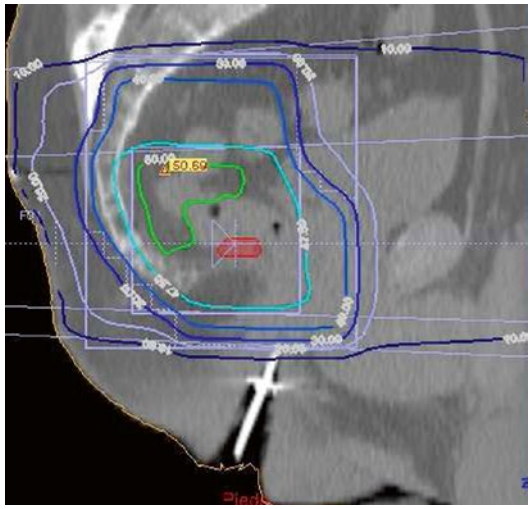

3.6 Isodose display for 50 Gy (sparing of the anal canal; upper limit at S2–S3 interface)

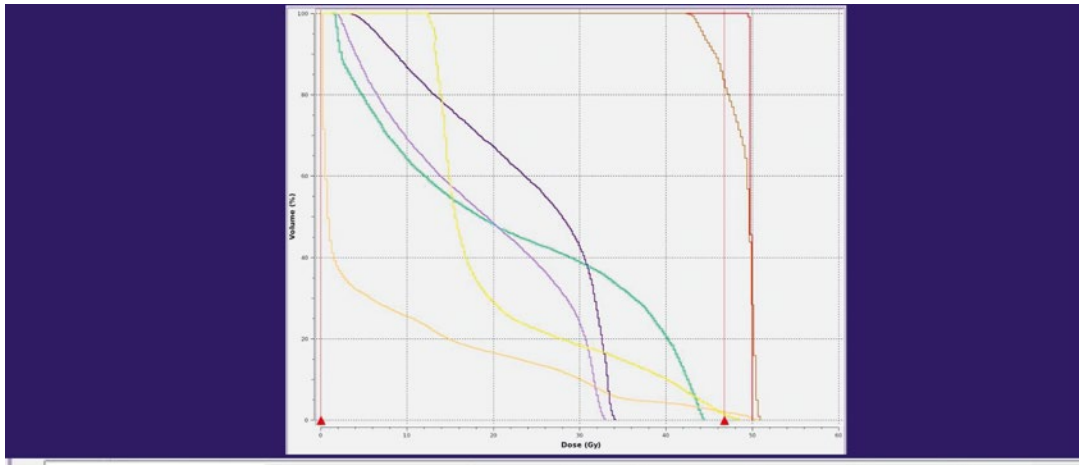

	1	2	3	4	5	6	7
Structure	CONTOURS EXTERNES	canal anal	GTV	RECTUM EXT	TTE FEM D	TTE FEM G	VESSIE
Vol. Géom. (cm3)	20167.8	8.6	1.4	63.3	43.1	43.2	56.0
Points Aléatoires	11100	3946	3193	5054	4812	4813	4974
Dose Min. (Gy)	0.00	1.50	49.45	41.75	1.82	3.17	12.09
Dose Max. (Gy)	50.78	44.45	50.00	50.92	32.96	34.15	48.71
Dose Med. (Gy)	0.75	18.34	49.74	49.54	19.20	27.91	15.55
Dose Moy. (Gy)	7.65	21.53	49.73	48.70	18.53	23.86	20.51
Ecart Type	12.67	15.64	0.11	1.92	10.65	9.44	10.04
Borne Dose Min. (Gy)	0.00	0.00	0.00	0.00	0.00	0.00	0.00
Borne Dose Max. (Gy)	46.73	46.73	46.73	46.73	46.73	46.73	46.73
Vol. sélection (cm3)	19764.0	8.6	0.0	11.0	43.1	43.2	55.3
Vol. sélection (%)	98.0	100.0	0.0	17.4	100.0	100.0	98.8
Dose à 95% (Gy)	0.04	1.88	49.52				
Dose à 2% (Gy)	46.72			50.60	32.45	33.67	46.04

3.8 DVH showing the following volumes: anal canal, 18 ccm; rectum, 63 ccm (small!); GTV, 1.4 ccm (small T2)

4. T4 NX – middle rectum (male patient, tumor fixed to the sacrum)
5. T4 N0 – distal rectum (male patient, tumor fixed to the prostate)

   During surgery 6 weeks after administration of the CAP 50 regimen, a complete (R0) resection could be performed without removal of prostate tissue.
6. Polypoid tumor adenocarcinoma T2 N0, 4.5 cm in diameter ("big polyp"). Middle anterior rectum. Tumor located just in front of a small bowel loop low in the pelvis after a previous hysterectomy. Patient had a traumatic fracture of sacrum after ski accident

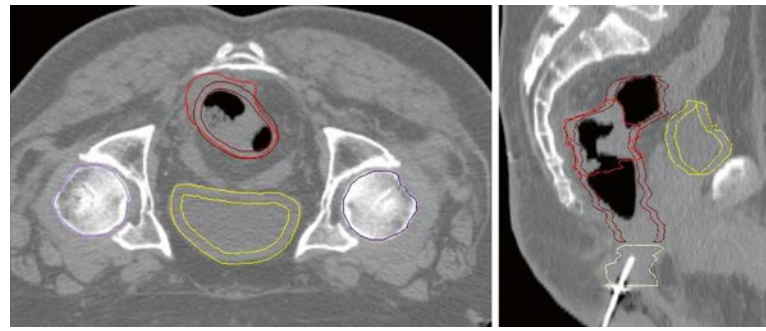

4.3 Rectum and OAR contouring. Contouring of the tumor (GTV) fixed to the left side of the sacrum (patient prone)

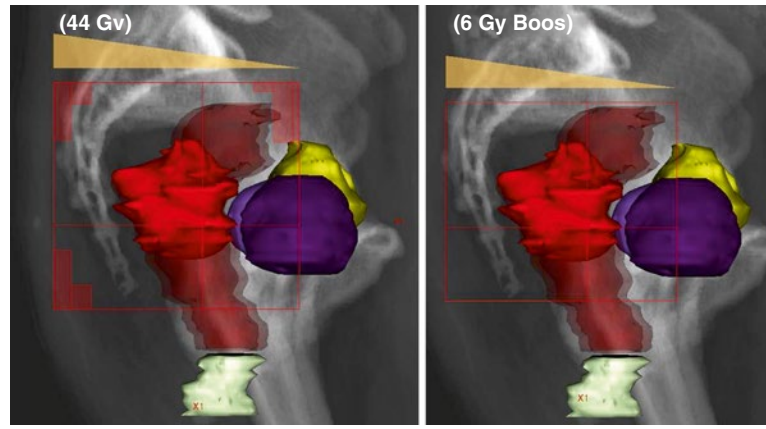

4.4 Positioning of fields with MLC. Lateral field for 44 Gy; lateral field for 50 Gy

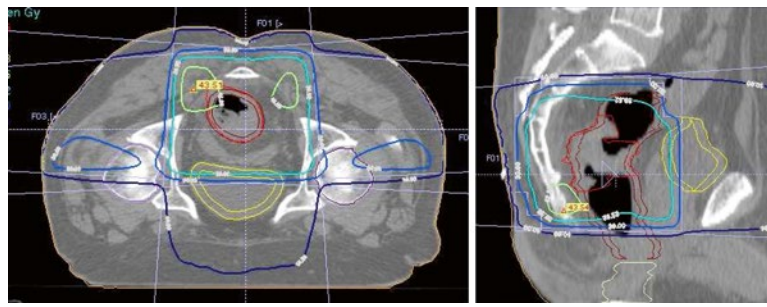

4.6 Isodose display for 44 Gy (sagittal and axial views). Anal canal is spared; sacrum is fully encompassed, upper limit below S1–S2 interface. It would be easily possible to increase the dose to 60–64 Gy to a limited volume (<20 ccm) centered to the area where the tumor is fixed to sacrum with a risk of incomplete R1 or R2 resection

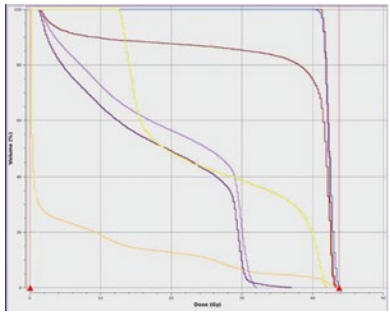

	1	2	3	4	5	6	7	8
Structure	CONTOURS EXTERNES	Canal Anal	[illegible]	[illegible]	RECTUM	TTE FEM D	TTE FEM G	VESSIE
Vol. Géom. (cm3)	29306.4	17.8	82.3	503.9	83.3	76.0	78.5	62.0
Points Aléatoires	11141	4310	5229	6790	5237	5174	5197	5040
Dose Min. (Gy)	0.00	0.41	41.09	39.97	1.41	1.30	1.14	12.42
Dose Max. (Gy)	43.71	1.26	43.33	43.87	43.22	32.20	37.12	42.14
Dose Med. (Gy)	0.28	0.65	42.23	42.27	41.77	24.89	19.24	18.94
Dose Moy. (Gy)	5.59	0.71	42.21	42.28	36.54	19.91	17.72	24.98
Ecart Type	11.09	0.22	0.42	0.59	12.18	10.81	11.18	11.55
Borne Dose Min. (Gy)	0.00	0.00	0.00	0.00	0.00	0.00	0.00	0.00
Borne Dose Max. (Gy)	43.71	43.71	43.71	43.71	43.71	43.71	43.71	43.71
Vol. sélection (cm3)	29304.4	17.8	82.3	503.2	83.3	75.9	78.5	62.0
Vol. sélection (%)	100.0	100.0	100.0	99.9	100.0	100.0	100.0	100.0
Dose à 95% (Gy)	0.02		41.46	41.32				
Dose à 2% (Gy)	41.93	1.19			42.92	31.40	31.14	41.55

4.8 DVH showing the GTV of 82.3 ccm ("big" tumor)

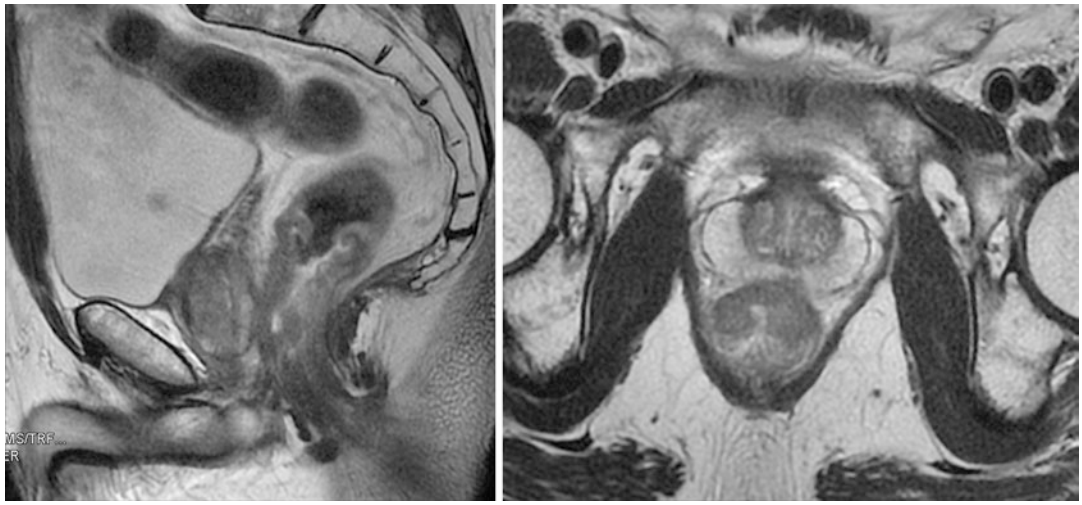

5.0 MRI showing a rectal tumor invading the prostate (sagittal and axial views)

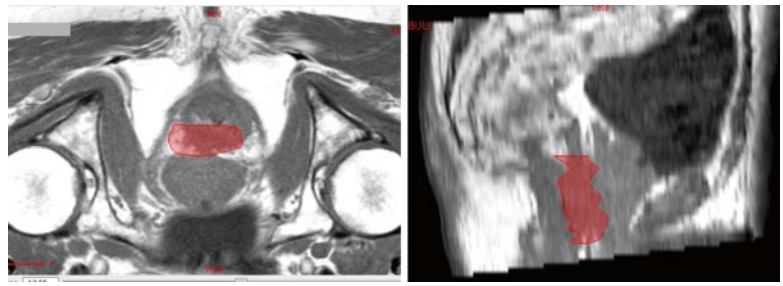

5.3 Rectal tumor (GTV) contouring with the help of image fusion (MRI + simulation CT scan). Axial and sagittal views. The tumor is infiltrating the posterior part of the prostate which was clinically obvious with a fixation on DRE

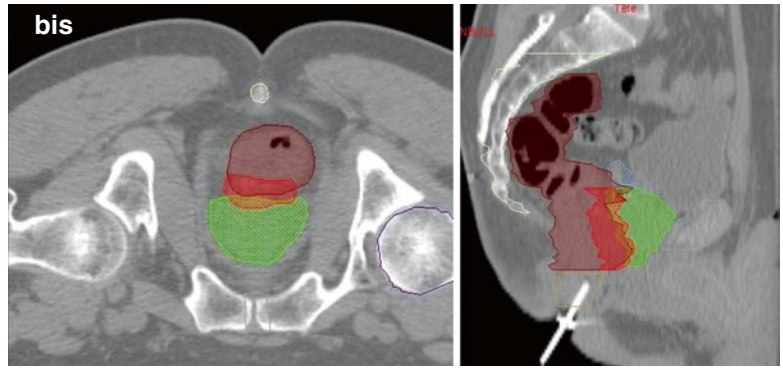

5.3 bis GTV = OAR contouring (rectum and prostate). Radiopaque marker in the anal canal

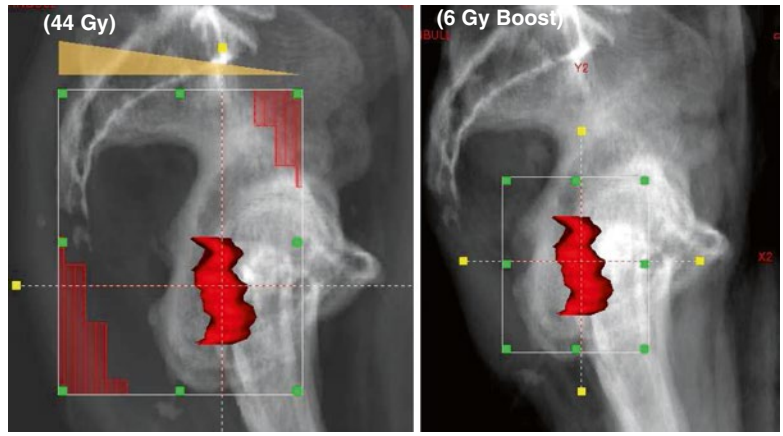

5.5 Field positioning with MLC. Lateral view (44 and 50 Gy)

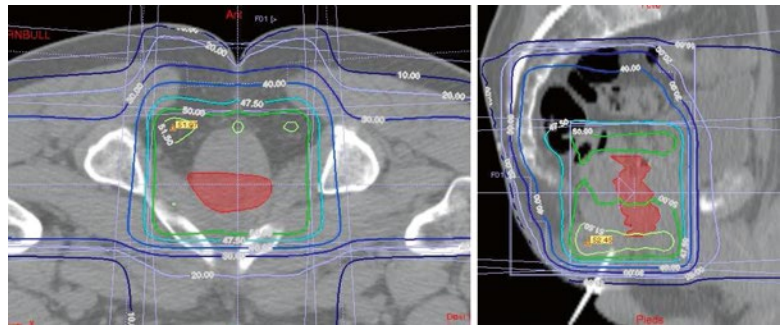

5.6 Isodose display: lateral and axial views for 50 Gy. The anal margin is not in the treated volume (accurate positioning of isodose with the anal marker, prone position)

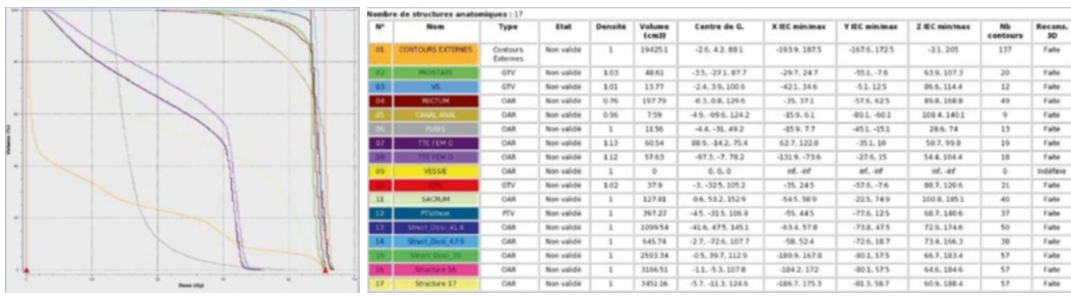

5.8 DVH showing the following volumes: prostate, 48.6 ccm; rectum, 197 ccm; GTV, 37.9 ccm

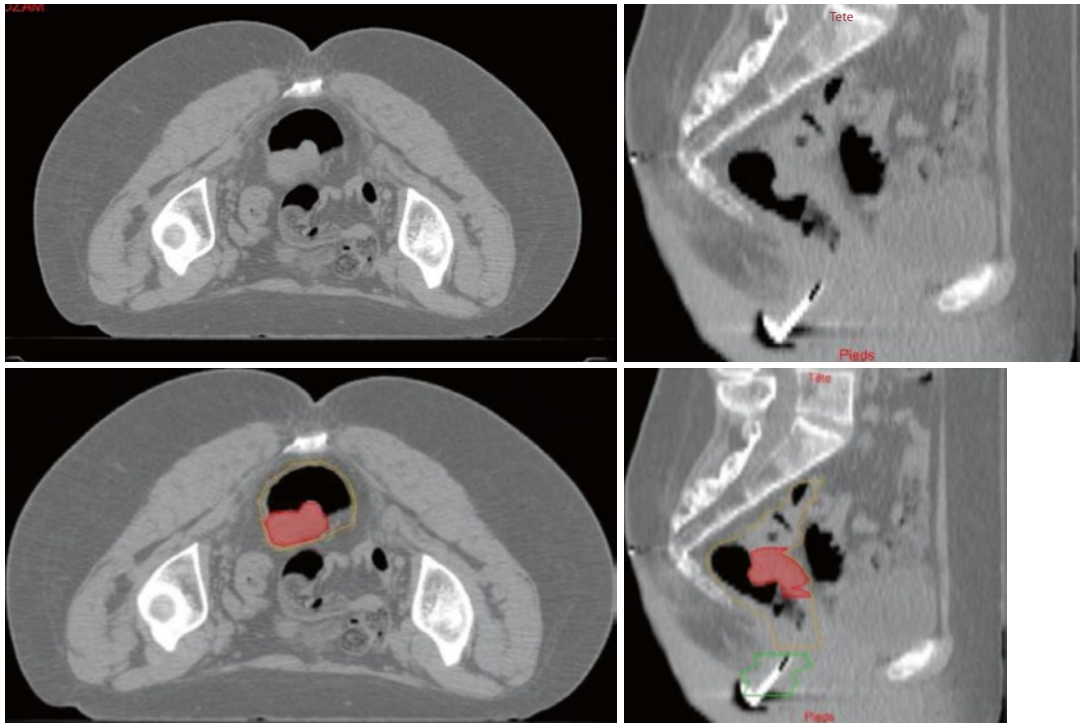

6.3 GTV as seen on simulation CT scan (axial and lateral views). GTV contouring in red (axial and sagittal views)

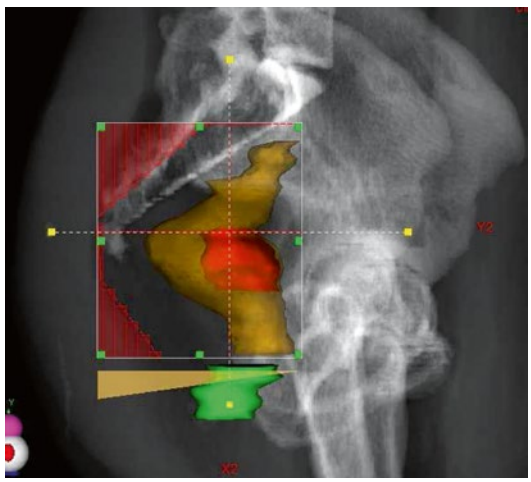

6.5 Field positioning with MLC. Lateral view for 44 Gy

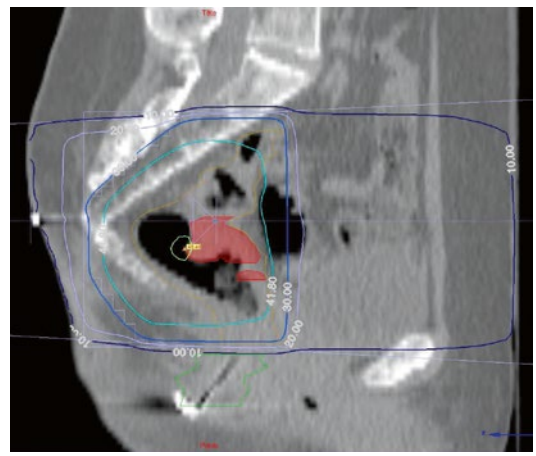

6.6 Isodose display. Sagittal view showing good protection of small bowel

Appendix 10.1

Volume of a sphere

$4/3\pi r^3$: The volume of a tumor of 2 cm in diameter (usually T1) is 4 ccm; 3 cm (T2), 13 ccm; 4 cm (T3), 25 ccm; 5 cm (T4), 49 ccm. A tennis ball is 6.5 cm in diameter (108 ccm). A $10 \times 10 \times 10$ cm field is close to 1 l: 10 times a tennis ball!

A lymph node of 1 cm in diameter corresponds to 0.5 ccm ("very small volume").

Head of femur, which is a sphere close to 5 cm in diameter, is around 50 ccm.

Volume of a cylinder

Surface of circle $(\pi r^2) \times$ height.

A "small rectum": diameter, 4 cm; height, 10 cm; volume "whole rectum," 125 ccm. A "large rectum": diameter, 6 cm; height, 12 cm; volume "whole rectum," 340 ccm.

If the diameter is 9 cm and height 12 cm, to encompass the whole mesorectum and hypogastric nodes, the volume becomes 860 ccm. To encompass such a volume, the width and "thickness" (AP-PA diameter) of the fields usually do not exceed 10–11 cm, and the height is close to 12 cm because the rectum is a "curved" cylinder.

The anal canal together with its sphincters is a cylinder with a surface of 3 cm and height between 2.5 and 4 cm, which corresponds to a volume usually between 5 and 10 ccm.

References

Arcangeli S, Valentini V, Nori SL, Fares C, Dinapoli N, Gambacorta MA (2003) Underlying anatomy for CTV contouring and lymphatic drainage in rectal cancer radiation therapy. Rays 28:331–336

Bosset JF, Collette L, Calais G et al (2006) Chemotherapy with preoperative radiotherapy in rectal cancer. N Engl J Med 355:1114–1123

Bosset JF, Servagi-Vernat S, Créhange G, Azria D, Gérard JP, Hennequin C (2011) Rectal cancer: the radiation basis of radiotherapy, target volume. Cancer Radiother 15:431–435

Boulis-Wassif S, Gerard A, Loygue J et al (1984) Final results of a randomized trial on the treatment of rectal cancer with preoperative radiotherapy alone or in combination with 5-fluorouracil, followed by radical surgery. Trial of the European Organization on Research and Treatment of Cancer Gastrointestinal Tract Cancer Cooperative Group. Cancer 53:1811–1818

Canessa CE, Miegge LM, Bado J, Silveri C, Labandera D (2004) Anatomic study of lateral pelvic lymph nodes: implications in the treatment of rectal cancer. Dis Colon Rectum 47:297–303

DeVita VT Jr, Lawrence TS, Rosenberg SA (2011) DeVita, Hellman, and Rosenberg's Cancer: principles and practice of oncology. Lippincott, Williams and Wilkins

Engels B, De Ridder M, Tournel K et al (2009) Preoperative helical tomotherapy and megavoltage computed tomography for rectal cancer: impact on the irradiated volume of small bowel. Int J Radiat Oncol Biol Phys 74:1476–1480

Gay HA, Barthold HJ, O'Meara E, Bosch WR, El Naqa I, Al-Lozi R et al (2012) Pelvic normal tissue contouring guidelines for radiation therapy: a Radiation Therapy Oncology Group consensus panel atlas. Int J Radiat Oncol Biol Phys 83:e353–e362

Gérard JP, Conroy T, Bonnetain F et al (2006) Preoperative radiotherapy with or without concurrent fluorouracil and leucovorin in T3-4 rectal cancers: results of FFCD 9203. J Clin Oncol 24:4620–4625

Gérard JP, Azria D, Gourgou-Bourgade S et al (2010) Comparison of two neoadjuvant chemoradiotherapy regimens for locally advanced rectal cancer: results of the phase III trial ACCORD 12/0405-Prodige 2. J Clin Oncol 28:1638–1644

Gérard JP, Azria D, Gourgou-Bourgade S et al (2012) Clinical outcome of the ACCORD 12/0405 PRODIGE 2 randomized trial in rectal cancer. J Clin Oncol 30:4558–4565

Gulliford SL, Foo K, Morgan RC et al (2010) Dose-volume constraints to reduce rectal side effects from prostate radiotherapy: evidence from MRC RT01 Trial ISRCTN 47772397. Int J Radiat Oncol Biol Phys 76:747–754

Gulliford SL, Partridge M, Sydes MR, Webb S, Evans PM, Dearnaley DP (2012) Parameters for the Lyman Kutcher Burman (LKB) model of Normal Tissue Complication Probability (NTCP) for specific rectal complications observed in clinical practise. Radiother Oncol 102:347–351

Gunderson LL, Sosin H (1974) Areas of failure found at reoperation (second or symptomatic look) following "curative surgery" for adenocarcinoma of the rectum. Clinicopathologic correlation and implications for adjuvant therapy. Cancer 34: 1278–1292

Kapiteijn E, Marijnen CA, Nagtegaal ID et al (2001) Preoperative radiotherapy combined with total mesorectal excision for resectable rectal cancer. N Engl J Med 345:638–646

Kintzinger C, Demoor-Goldschmidt C, Abderrahmani R, Paris F, Supiot S (2012) Radiation-induced proctitis: symptoms, pathophysiology and treatment. Cancer Radiother 16:372–376

Kobayashi H, Mochizuki H, Kato T, Mori T, Kameoka S, Shirouzu K et al; Study Group for Rectal Cancer Surgery of the Japanese Society for Cancer of the Colon and Rectum (2011) Lymph node ratio is a powerful prognostic index in patients with stage III distal

rectal cancer: a Japanese multicenter study. Int J Colorectal Dis 26:891–896

Kouloulias VE, Bosset JF, van Tienhoven G, Davis BJ, Pierart M, Poortmans P, EORTC Radiotherapy Group. European Organization for Research and Treatment of Cancer (2002) Quality assurance in the EORTC 22921 trial on preoperative radiotherapy with or without chemotherapy for resectable rectal cancer: evaluation of the individual case review procedure. Eur J Cancer 38:1849–1856

Krengli M, Cannillo B, Turri L, Bagnasacco P, Berretta L, Ferrara T et al (2010) Target volume delineation for preoperative radiotherapy of rectal cancer: interobserver variability and potential impact of FDG-PET/CT imaging. Technol Cancer Res Treat 9:393–398

Krook JE, Moertel CG, Gunderson LL, Wieand HS, Collins RT, Beart RW et al (1991) Effective surgical adjuvant therapy for high-risk rectal carcinoma. N Engl J Med 324:709–715

Lorchel F, Maingon P, Crehange G, Bosset M, Bosset JF (2002) Cancer of the rectum: target volumes for preoperative radiotherapy. Cancer Radiother 6(Suppl 1): 93s–99s

Marsh PJ, James RD, Schofield PF (1994) Adjuvant preoperative radiotherapy for locally advanced rectal carcinoma. Results of a prospective, randomized trial. Dis Colon Rectum 37:1205–1214

Mavroidis P, Giantsoudis D, Awan MJ et al (2014) Southwest Oncology Group Radiation Oncology Committee. Consequences of anorectal cancer atlas implementation in the cooperative group setting: radiobiologic analysis of a prospective randomized in silico target delineation study. Radiother Oncol 112(3):418–424

Michalski JM, Gay H, Jackson A, Tucker SL, Deasy JO (2010) Radiation dose-volume effects in radiation-induced rectal injury. Int J Radiat Oncol Biol Phys 76(3 Suppl):S123–S129

Myerson RJ, Garofalo MC, El Naqa I, Abrams RA, Apte A, Bosch WR et al (2009) Elective clinical target volumes for conformal therapy in anorectal cancer: a radiation therapy oncology group consensus panel contouring atlas. Int J Radiat Oncol Biol Phys 74:824–830

Nijkamp J, Kusters M, Beets-Tan RG, Martijn H, Beets GL, van de Velde CJ, Marijnen CA (2011) Three-dimensional analysis of recurrence patterns in rectal cancer: the cranial border in hypofractionated preoperative radiotherapy can be lowered. Int J Radiat Oncol Biol Phys 80:103–110

Nijkamp J, de Haas-Kock DF, Beukema JC, Neelis KJ, Woutersen D, Ceha H et al (2012) Target volume delineation variation in radiotherapy for early stage rectal cancer in the Netherlands. Radiother Oncol 102:14–21

O'Connell MJ, Martenson JA, Wieand HS, Krook JE, Macdonald JS, Haller DG et al (1994) Improving adjuvant therapy for rectal cancer by combining protracted-infusion fluorouracil with radiation therapy after curative surgery. N Engl J Med 331:502–507

Ortholan C, Ramaioli A, Peiffert D, Lusinchi A, Romestaing P, Chauveinc L et al (2005) Anal canal carcinoma: early-stage tumors < or =10 mm (T1 or Tis): therapeutic options and original pattern of local failure after radiotherapy. Int J Radiat Oncol Biol Phys 62:479–485

Påhlman L, Glimelius B, Ginman C, Graffman S, Adalsteinsson B (1985) Preoperative irradiation of primarily non-resectable adenocarcinoma of the rectum and rectosigmoid. Acta Radiol Oncol 24:35–39

Papillon J (1990) Present status of radiation therapy in the conservative management of rectal cancer. Radiother Oncol 17:275–283

Park JH, Yoon SM, Yu CS, Kim JH, Kim TW, Kim JC (2011) Randomized phase 3 trial comparing preoperative and postoperative chemoradiotherapy with capecitabine for locally advanced rectal cancer. Cancer 117:3703–3712

Patel UB, Taylor F, Blomqvist L et al (2011) Magnetic resonance imaging-detected tumor response for locally advanced rectal cancer predicts survival outcomes: MERCURY experience. J Clin Oncol 29:3753–3760

Roels S, Duthoy W, Haustermans K, Penninckx F, Vandecaveye V, Boterberg T, De Neve W (2006) Definition and delineation of the clinical target volume for rectal cancer. Int J Radiat Oncol Biol Phys 65:1129–1142

Sauer R, Becker H, Hohenberger W et al; German Rectal Cancer Study Group (2004) Preoperative versus postoperative chemoradiotherapy for rectal cancer. N Engl J Med 351:1731–1740

Sauer R, Liersch T, Merkel S et al (2012) Preoperative versus postoperative chemoradiotherapy for locally advanced rectal cancer: results of the German CAO/ARO/AIO-94 randomized phase III trial after a median follow-up of 11 years. J Clin Oncol 30(16): 1926–1933

Steup WH, Moriya Y, van de Velde CJ (2002) Patterns of lymphatic spread in rectal cancer. A topographical analysis on lymph node metastases. Eur J Cancer 38:911–918

Thariat J, Hannoun-Levi JM, Sun Myint A et al (2012) Past, present, and future of radiotherapy for the benefit of patients. Nat Rev Clin Oncol 27

Tournel K, De Ridder M, Engels B et al (2008) Assessment of intrafractional movement and internal motion in radiotherapy of rectal cancer using megavoltage computed tomography. Int J Radiat Oncol Biol Phys 71:934–939

Vuong T, Devic S, Moftah B, Evans M, Podgorsak EB (2005) High-dose-rate endorectal brachytherapy in the treatment of locally advanced rectal carcinoma: technical aspects. Brachytherapy 4:230–235

Widder J, Sedlmayer F, Stanek C et al (2000) The 3D conformal approach although less reproducible than 2D (Quality assurance in preoperative radiotherapy of rectal cancer: evaluation of a pre-trial dummy-run. Radiother Oncol 56:341–347

Wolff HA, Wagner DM, Conradi LC et al (2012) Irradiation with protons for the individualized treatment of patients with locally advanced rectal cancer: a planning study with clinical implications. Radiother Oncol 102:30–37

Anal Carcinoma

11

Rob Glynne-Jones, V. Goh, A. Aggarwal, H. Maher, S. Dubash, and R. Hughes

Contents

R. Glynne-Jones (✉) • A. Aggarwal • H. Maher
S. Dubash • R. Hughes
Department of Radiotherapy, Mount Vernon Centre for Cancer Treatment, Mount Vernon Hospital, Northwood, Middlesex HA6 2RN, UK
e-mail: rob.glynnejones@nhs.net

V. Goh
Division of Imaging Sciences and Biomedical Engineering, Kings College London, London, UK

Department of Radiology, Guy's and St Thomas's Hospitals NHS Foundation Trust, London, UK

A.-L. Grosu, C. Nieder (eds.), *Target Volume Definition in Radiation Oncology*,
DOI 10.1007/978-3-662-45934-8_11, © Springer-Verlag Berlin Heidelberg 2015

11.1 Introduction

Squamous cell carcinoma of the anus (SCCA) is a rare cancer but its incidence is increasing throughout the world (Bilimoria et al. 2009; Hartwig et al. 2012; Bentzen et al. 2012; Jin et al. 2011). SCCA spreads in a locoregional manner within and outside the anal canal and to surrounding draining lymph nodes depending on the site of origin. Distant metastases appear relatively late. The primary aim of treatment therefore is to achieve locoregional control and preserve anal function, with the best possible quality of life. Due to these tumours' high sensitivity to chemoradiation, this modality has become the standard of care.

In this chapter we aim to provide a clear practical guide to target delineation (both elective and gross tumour) for external beam radiotherapy (EBRT) in anal cancer. We wanted to determine the optimal imaging modalities for anal cancer and how best to define involved lymph nodes. We review the probability of lymph node metastases within the pelvis and groins and patterns of local recurrence after CRT – although no prospective randomised trials have been able to provide this data in any detail. We describe target volumes, constraints to organs at risk (OARs) and recommendations for external beam radiation therapy (EBRT). We have not addressed the issue of brachytherapy. Also recommendations regarding optimal doses to gross and elective target volumes are beyond the scope of this chapter.

Anatomical textbooks, published studies and reviews with data from lymphangiograms, computerised tomography (CT) and more recently magnetic resonance imaging (MRI) and positron emission tomography (PET) are used to define the anatomical distribution of normal pelvic and inguinal lymph nodes, the boundaries of the anal canal and relevant organs at risk. Historical surgical series document the site of involved lymph nodes. We have examined many old chemoradiation series (Nigro et al. 1983; Leichman et al. 1985; Hughes et al. 1989; Luna-Pérez et al. 1995) and also the results of recent retrospective studies detailing sites and patterns of anal cancer recurrence (Das et al. 2007; Wright et al. 2010; Sebag-Montefiore et al. 2012).

There are several excellent guidelines showing anatomical borders to define the clinical target volumes for anal cancer. The recently published Australasian planning guidelines interpret CT definitions and provide a high-resolution atlas for contouring gross disease and organs at risk (Ng et al. 2012). The descriptions of the elective target volumes or compartments are useful and reproducible. This data therefore complements the existing Radiation Therapy Oncology Group (RTOG) elective nodal anorectal atlas (Myerson et al. 2009). However, we consider that the RTOG recommendations have not integrated specific clinical data and patterns of recurrence but derive from a subjective approach (superposition of targets drawn by a few individual experts), and issues such as genital sparing are insufficiently precise. There are also RTOG pelvic normal tissue contouring guidelines (Gay et al. 2012) available as a CT image atlas on the RTOG website.

However, although comprehensive, we also have issues with accepting without qualification the recommendations of the above (Ng et al. 2012). Many of the Australasian recommendations for CTVs appear unnecessarily extensive in the light of our experience in the UK with the

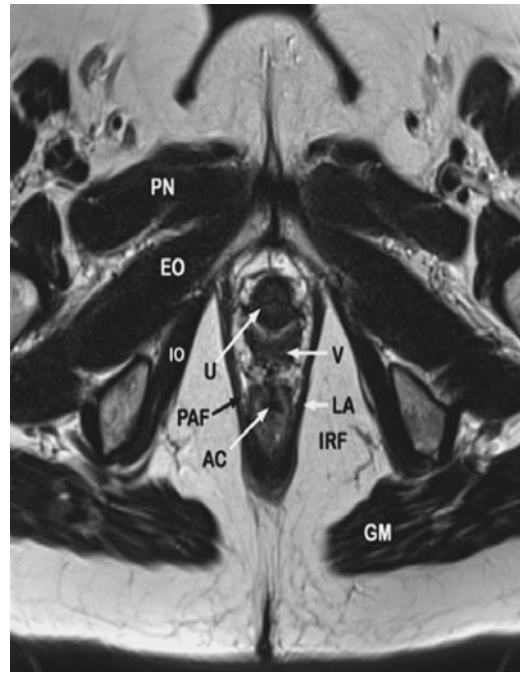

U	Urethra
PAF	Perianal fat
AC	Anal canal
V	Vagina
LA	Levator ani
IRF	Ischiorectal fossa
PN	Pectineus
EO	External obturator
IO	Internal obturator
GM	Gluteus maximus

Fig 11.1 Axial MRI image demonstrating the proximal anal canal in a female

ACT II trial, and it is a 'one-size-fits-all' strategy since they advise all nodal volumes described should be covered for all stages (with the possible exception of frail patients with T1N0 tumours). We have hypothesised that SCCA at the anal margin, involving predominantly the anal canal and finally extending above the dentate line into the rectum, has three anatomically different vascular and lymphatic drainage patterns, which require different approaches and different field sizes.

Conventional pelvic fields have usually referenced anatomical bony structures to deliver pelvic radiation therapy, which achieves suboptimal coverage of the nodal areas. Contouring vessels on CT images is now used as surrogate for lymph node localisation (which is usually not visualised) to achieve more precise and individualised target delineation. We advise the use of CT and co-registration with MRI and/or PET/CT to define appropriate and different algorithms for T1/T2 cancers (<4 cm) and larger (>4 cm (T3, T4)) tumours; see Fig. 11.1. We have incorporated bone, soft tissue and vessel landmarks into an MRI-/CT-based atlas provided by Vicky Goh (consultant radiologist) as part of this group.

11.2 Pathology

More than 80 % of anal SCCs contain one or more subtypes of human papilloma virus (HPV – and usually HPV16 or HPV18). HPV-associated tumours retain wild-type *P53*, and hence patients with HPV-associated tumours appear to have a good response to concurrent chemoradiotherapy, although most of the evidence has been derived from small retrospective studies (Yhim et al. 2011).

SCCA originates from the transitional and squamous mucosa of the anal canal. Terms such as basaloid, transitional or spheroidal and cloacogenic have largely been replaced by the general term squamous cell carcinoma (SCC), because all have a similar natural history and patterns of spread. The biology and prognosis of keratinising and non-keratinising tumours of the anal canal also appear to be similar. Verrucous carcinomas are another variant and are sometimes described as giant condylomas or Buschke-Lowenstein tumours, which

are often enormous exophytic tumours but may have a better prognosis than SCC.

11.2.1 Tumour Grade

Tumours of the anal canal are often defined as poorly differentiated SCC, whereas tumours at the anal margin are well differentiated, but histological grading has been subject to interobserver variability. There is also considerable heterogeneity particularly in larger tumours. Hence, although high-grade tumours are generally accepted to have a worse prognosis, this has not been confirmed in multivariate analysis (Shepherd et al. 1990; Hill et al. 2003).

11.3 Historical Background

Three phase III trials demonstrated that radiotherapy (RT) with concurrent 5FU and mitomycin (MMC) (UKCCCR 1996; Bartelink et al. 1997; Flam et al. 1996) achieves better outcomes in terms of local control and recurrence- or disease-free survival (RFS/DFS) compared to RT alone or RT combined with 5FU alone. In contrast, phase III trials by the Radiotherapy Therapy Oncology Group RTOG 98–11 (Ajani et al. 2008; Gunderson et al. 2012) and the Action Clinique Coordonnees en Cancerologie Digestive ACCORD-03 phase III trial (Peiffert et al. 2012) failed to show benefit for the addition of cisplatin-based neoadjuvant chemotherapy (NACT) prior to CRT in terms of colostomy-free survival (CFS). In the RTOG 9811 trial, the DFS and colostomy rate actually appears inferior with cisplatin (Gunderson et al. 2012). The ACCORD-03 trial also failed to show a benefit in CFS from an increase in the radiotherapy boost dose (Peiffert et al. 2012). Preliminary results of the United Kingdom National Anal Cancer Trial (ACT II) confirm the standard of 5FU/MMC CRT. Results show excellent complete response rates (90 %), with 3-year recurrence-free survival rates overall of 73 % (81 % in T1/T2 tumours, but 64 % for more advanced T3/T4 tumours) (James et al. 2013). The dose and treatment schedule used in the ACT II trial is now the current standard of care in the UK.

11.4 Conventional Radiotherapy Treatment Planning of Anal Cancer

Historically, anal cancer has been treated in all randomised phase III trials with doses of 1.8 Gy per day, using a shrinking-field technique over the course of treatment (UKCCR 1996; Bartelink et al. 1997; Flam et al. 1996; Ajani et al. 2008; Peiffert et al. 2012; James et al. 2013). There have been various previous trial planning techniques. Conventional 2-D large APPA pelvic radiation fields in anal cancer (with generous length and widths of field sizes such that a geometrical miss was extremely unlikely) used the pelvic bones as reference extrapolating the position of the pelvic nodes – based on historical data from studies imaging lymph nodes with lymphangiograms (Davey et al. 1996; Chao and Lin 2002) and early CT scans and from surgical series which defined the sites of pelvic lymph node pathological involvement at laparotomy (Hightower and Judd 1967; Stearns and Quan 1970; Beahrs 1979).

These techniques caused significant acute toxicity of the perineal skin and genitalia; genitourinary, gastrointestinal and haematological toxicity; and poor late function (Ajani et al. 2008; Myerson et al. 2009), often associated with radiotherapy breaks which increase the overall treatment time (OTT), and may compromise efficacy (Allal et al. 1997; Weber et al. 2001; Graf et al. 2003; Huang et al. 2007; Ajani et al. 2008). In April 2012, the National Comprehensive Cancer Network (NCCN) panel agreed that multifield techniques are now preferred over APPA techniques for radiation delivery in anal cancer (Benson et al. 2012). Hence, many institutions are now moving to use multifield techniques, with a range of techniques and different recommended doses.

11.5 Modern Techniques (Intensity-Modulated Radiation Therapy and Volumetric Modulated Arc Therapy)

Delivery of radiotherapy in anal cancer is complex because of the heterogeneity in size, the irregular shape of the target volume and the proximity to

dose-sensitive critical structures (small bowel, femoral heads, perineum and external genitalia). Intensity-modulated radiation therapy (IMRT) and volumetric modulated arc therapy (VMAT) allow sophisticated dose-painting treatment planning. Comparisons between 3D-CRT, IMRT and VMAT in SCCA demonstrate the same dose coverage in the target but 3D-CRT exposes the surrounding tissue and consequently the OAR to much higher doses (Chen et al. 2005; Stieler et al. 2009).

However, the narrow constraints and high precision of treatment raise concerns about potential geographical misses or compromise of target coverage due to systematic or random radiotherapy errors. Clear definitions of target volumes are therefore essential to ensure accurate and reproducible contouring, treatment planning, delivery and quality assurance. This in turn will require strong engagement with the wider multidisciplinary team including physicists and radiographers to optimise treatment outcome for individual patients.

The International Commission on Radiation Units and Measurements (ICRU) report 83 provides additional recommendations on the selection and delineation of the targets volumes and the organs at risk (ICRU 83 2010).

11.6 Image-Guided Radiotherapy (IGRT)

During a treatment course, individual day-to-day tumour position can be variable. On-line daily imaging can correct both systematic and random errors. Off-line imaging should be interpreted by the radiation oncologist for at least the first 3 fractions and then at weekly intervals to deal with systematic errors. The radiation oncologist can therefore use the on-board imaging system (OBI) or the cone beam CT (CBCT). Verification should use bone landmarks, because soft tissues inferiorly are often blurred.

11.6.1 Anatomy

Knowledge of the location and terminology of lymph node groups in the pelvis is essential for accurate staging in a standardised manner.

11.6.2 The Anal Canal

The anal canal is the most distal part of the large bowel beginning at the anorectal junction. It is approximately 4 cm in length, ending at the anal orifice where the true skin is found at the anal margin. Because the dentate line (which defines the level of the upper limit of the internal sphincter) is the most easily identified landmark in the mucosa of the anal canal, many have suggested that the anal canal is divided into infra-dentate and supra-dentate regions (Wendell-Smith 2000). The components of the anal canal of relevance to surgical disease and treatment are demonstrated on axial (Fig. 11.1), sagittal (Fig. 11.2) and coronal (Fig. 11.3) magnetic resonance imaging (MRI) of the anal canal.

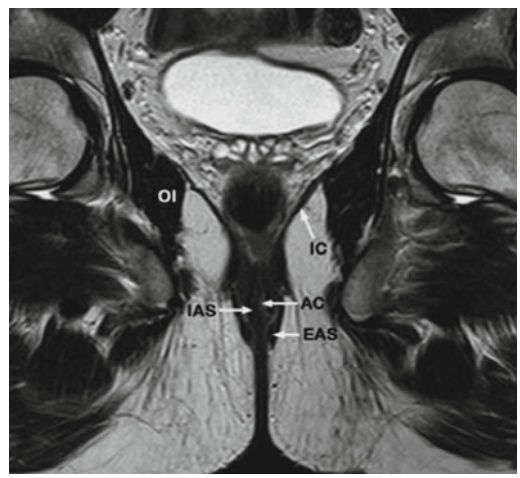

IAS	Internal anal sphincter
EAS	External anal sphincter
AC	Anal canal
IC	Iliococcygeus
OI	Obturator internus

Fig. 11.2 Coronal MRI image demonstrating the anal canal in a female

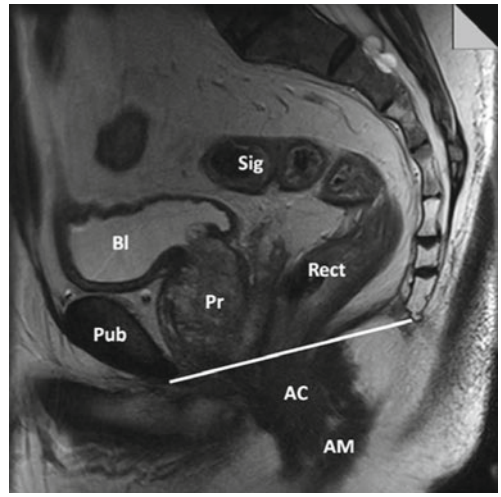

Sig	Sigmoid colon
Rect	Rectum
AC	Anal canal
AM	Anal margin
Pr	Prostate
Bl	Bladder
Pub	Pubis

Fig. 11.3 Sagittal MRI image demonstrating the anal canal in a male

11.6.3 Anal Sphincter

The internal anal sphincter (IAS) is formed by a thickened segment of the circular muscle coat in the distal rectum. From the MRI obtained in the sagittal orientation (Fig. 11.2), the superior aspect of the anal canal can be determined and can usually be defined superiorly by a line joining the tip of the coccyx and the most inferior aspect of the pubis – reflecting the anorectal junction. The ischiorectal fossa, ischial tuberosities and sacrotuberous ligaments lie laterally (best appreciated on MRI obtained in the coronal orientation (Fig. 11.3), the contents of the urogenital triangle anteriorly (Fig. 11.1) and the anal orifice inferiorly (Figs. 11.2 and 11.3)).

11.6.4 Anal Margin

The anal margin is a region of pigmented skin with skin folds surrounding the anus. Although the lateral border of the anal margin has not been defined, anal margin cancer is usually considered as within a radius of approximately 5 cm from the anal orifice.

11.6.5 The Inguinal Nodes

The inguinal nodes are in the inguinal region (*superficial* inguinal nodes are often larger than nodes from other lymphatic areas) anterior to Scarpa's femoral triangle and are bounded superiorly by the inguinal ligament, laterally by the medial border of sartorius and medially by the upper border of adductor longus.

From the *superficial* inguinal nodes, there is an extension to the *deep* inguinal nodes which are within the fatty tissue of the femoral canal and medial side of the femoral vein. If the superficial nodes are clinically negative, it may be reasonable to avoid treating the deep region.

11.6.6 Femoral Nodes

We have rarely if ever seen involvement of the femoral nodes in anal cancer and do not recommend routine contouring of the femoral nodes.

11.6.7 Presacral Nodes

Presacral nodes are sited around lateral and medial sacral arteries. These lie along the lateral borders of the sacrum and anterior to the sacral pelvic surface usually just medial to the foramen.

11.6.8 Pararectal Nodes

Pararectal nodes lie within the mesorectum usually posteriorly on both left and right sides –

probably extending for no more than 4 cm cephalad to the anorectal tumour.

11.6.9 Common Iliac Lymph Nodes

Common iliac lymph nodes are grouped around the common iliac vessel (lateral, intermediate and medial groups).

11.6.10 Internal Iliac Nodes

Internal iliac nodes are sited lateral to the mesorectum and presacral space and are associated with the internal iliac vessels, arising superiorly from the bifurcation of the common iliac artery (at the level of S1) and ending at the level of obturator internus.

11.6.11 External Iliac Nodes

External iliac nodes are usually grouped around the external iliac vessels forming three distinct chains (the lateral, middle and medial groups of external iliac).

Examples of the definitions of the appropriate nodal groups can be found on the ATC website, http://atc.wustl.edu.

11.7 Normal Lymph Node Drainage

Lymphatic drainage depends on the position within the canal. The canal above the dentate line drains to internal pudendal nodes and to the internal iliac system. The canal below the dentate line drains to the medial group of superficial inguinal nodes with further extension to the deep inguinal nodes and some communication superiorly to external iliac nodes and inferiorly with femoral nodes. The upper half of the canal drains mainly by the superior rectal vein to the inferior mesenteric vein and thence potentially to the para-aortic nodes (Hill et al. 2003).

Involvement of regional lymph nodes represents the most common mode of spread from cancer of the anal canal and margin (Kuehn et al. 1968). The perirectal, inguinal, femoral and iliac lymph nodes are the most frequent sites for nodal metastases (Beahrs 1979; Stearns and Quan 1970; Greenall et al. 1985; Gérard et al. 2001). Patients developing inguinal nodal disease invariably do so in the ipsilateral groin (Gérard et al. 2001), unless the tumour is in the midline allowing bilateral nodal recurrence. Nodal involvement is rare if the primary tumour was $\leq$2 cm in maximum diameter but increased to 35 % when the tumour invaded into adjacent pelvic tissues (Boman et al. 1984). Nodal metastases are also more likely in poorly differentiated cancers (Boman et al. 1984).

11.8 Imaging in Anal Cancer

Available imaging modalities are computerised tomography (CT), magnetic resonance imaging (MRI), endo-anal ultrasound (EUS) and positron emission tomography (PET). Together they allow assessment of the local extent including involvement of other structures and spread to inguinal, pelvic and abdominal nodes and distant sites. Each modality has advantages and limitations, the most crucial being the difficulty in differentiating metastatic from uninvolved reactive nodes of equivalent size.

CT scans are conventionally used to image the pelvis and whole body, but some have recorded that CT failed to reveal an anal primary tumour in 10 of 40 patients, i.e. there were 25 % false negatives (Mistrangelo et al. 2012). MRI scans provide the most detailed anatomy of the primary tumour, the sphincter mechanism and the lymphatic network. MRI is now recommended for locoregional staging of anal cancer in European and NCCN guidelines and is routinely performed in the UK (NCCN 2015 - Benson et al. 2012; Glynne-Jones et al. 2010). A comparison of EUS and MRI (Otto et al. 2009) suggested that EUS may be superior to MRI in detecting small superficial tumours.

Anal cancer is FDG avid even in small tumours (1–2 cm), and PET has a high detection rate of the primary tumour of 90–100 % (Cotter et al.

2006; Nguyen et al. 2008; Winton et al. 2009). Hence positron emission tomography (PET)/CT is gaining ground as an initial staging modality since initial descriptions in 2005 and has been part of NCCN treatment guidelines since 2007.

11.8.1 Criteria for Identifying Involvement of Lymph Nodes

Suspicious perirectal and internal iliac nodes on imaging are rarely biopsied so there is significant risk of false positives. There is no international consensus regarding the normal limit for size in the diagnosis of pelvic and inguinal nodal metastases from pelvic tumours. Size criteria also are different for different histologies and different primary sites (Koh et al. 2006). Authors discussing inguinal node recurrences do not clearly define their CT and MRI criteria to determine uninvolved inguinal lymph nodes (Matthews et al. 2011; Ortholan et al. 2012), nor is this feature clear from any of the randomised trials.

Many use 10 mm as a conventional cut-off. Other criteria such as shape, signal intensity pattern, central necrosis and the degree of contrast enhancement in pelvic nodes are often useful but have not been validated.

11.9 Co-registration for Planning

CT is usually ideal for planning in the pelvis, because it provides anatomical detail with the electron density data essential for dosimetry. It is vital to use contrast with the correct windows and take advantage of multiple orthogonal views (axial, sagittal and coronal) to delineate target volumes (Steenbakkers et al. 2005). It is also advisable to involve your radiologist in person in the planning session. However, contouring the target volume with CT alone is difficult and may provide a major source of errors. A major advantage is that contouring vessels on the CT image can now be used as a surrogate for lymph node localisation and can offer a more precise and individualised elective nodal target delineation compared to that achieved previously.

Advances in the quality of MRI and PET/CT now allow us to determine areas of gross tumour volume more accurately and to delineate tumour and organ boundaries more confidently. The conventional planning CT scan can be co-registered with either diagnostic quality MRI imaging or PET.

11.9.1 MRI

There is little movement within the pelvis, and MRI allows the bone structures of the pelvis to be readily co-registered. Diffusion-weighted sequences are particularly useful to delineate the tumour extent, because it is a squamous cell carcinoma. But it is still vital to have the appropriate and high-resolution small field of view. MRI provides excellent anatomical definition of these structures and the components of the sphincter mechanism (see Figs. 11.1 and 11.2) and defines involvement of normal-sized lymph nodes seen on CT. If MRI is to be co-registered, it is important to use a hard couch top to avoid posterior distortion.

11.9.2 PET

An Italian group has found PET/CT useful in target volume delineation (Krengli et al. 2010). PET/CT can define both primary and nodal sites of metabolically active tumour (Bannas et al. 2011), although to our mind PET shows a larger extent than MRI. It is important to note that the positive predictive value of PET for lymph nodes is high, but the negative predictive value is less secure.

11.10 Consensus Atlas

The area of most potential variability and error is between individual radiation oncologists outlining of target and normal tissue volumes. There is a clear role for an agreed consensus/atlas (Nijkamp et al. 2012) with continuous education, training

and cross-collaboration of the radiation oncologist with other specialties especially radiologists to reduce the degree of variability in tumour delineation and enhance the quality assurance within radiotherapy trials. The proposed atlas provides a delineation protocol for anal cancer.

The delineation of pelvic nodes radiologically is described in some relevant pelvic nodal atlases (Portaluri et al. 2005; Taylor et al. 2007; Lengele and Scalliet 2009; Japan Clinical Oncology Group 2010), but these are not sufficiently relevant to anal cancer. It is also curious that there are several different algorithms, which have been proposed for contouring the same pelvic nodes in prostate cancer, anorectal cancer and cervical cancer – and no consensus. The RTOG made suggestions specifically for the definitive treatment of anal cancer based on a consensus of nine experts in radiation oncology (Myerson et al. 2009) partly because of inaccurate contouring in some cases enrolled on RTOG 0529 but confined guidance to elective nodal volumes.

There is a tendency with each new atlas to design larger and larger volumes with more extensive fields and more complex methods, but there is no evidence yet that these developments improve outcome. Hence, there is no widely accepted consensus on proper selection and delineation of lymph node areas for definitive chemoradiation. In general algorithms defining CTV close to bone landmarks carry less variation than those which rely on soft tissue landmarks – particularly landmarks which vary such as the bladder. We have therefore tried to both simplify the structure to produce more compact CTVs and at the same time design individualised targets appropriate to the site of origin and clinical stage. Even then, these targets will vary according to the tumour size and stage, the sex and the individual shape of the patient.

11.11 Clinical Assessment of Primary Tumour

Clinical assessment of the tumour is essential. Information is required on the size and position of the tumour within the anus and whether it is infiltrating or exophytic. It is important to measure the distance the tumour extrudes beyond the anal margin and how far it extends cephalad (i.e. whether it extends above or below the dentate line and levators). Additionally females require a vaginal examination particularly in anterior tumours to assess if the vagina itself is directly involved or if the tumour is palpable by involving the rectovaginal septum. However should pain prevent per rectal (PR) examination, an EUA (examination under anaesthetic) should be considered. It is recommended that the treating radiation oncologist is present during the procedure to ensure that precise measurements are noted, facilitating target volume delineation and treatment planning. We consider a clinical proforma an absolute essential for accurate target delineation (clinical proforma – see Appendix 11.2).

11.12 Clinical Assessment of Inguinal Nodes

Clinical assessment of inguinal nodes is also required. Involved nodes tend to be found medially, just lateral to the pelvic tubercle, and are firm, almost analogous to a hard marble. Fixed nodes may be palpated more laterally beyond these areas in patients presenting with more extensive T3/T4 tumours.

11.13 Details of Imaging Proforma for Each Patient (Appendix 11.3)

An imaging proforma based on MRI should be completed by the MDT radiologist.

11.14 Planning

The use of a planning CT scan with target volumes delineated (primary and nodal) on each slice- and pixel-based inhomogeneity correction is considered standard practice. There are arguments for planning both in the supine and prone positions. We recommend patients should be

simulated and planned in the supine position because it is more stable and reproducible without any custom immobilisation device. Although we accept that local practices may vary, some prefer that patients with very exophytic tumours extending well outside the anal canal are planned prone and bolus used. Hence, appropriate immobilisation and a treatment position with which the centre is familiar should ideally be used.

11.15 Patient Data Acquisition

The CT scan limits are the superior aspect of L3 superiorly to the mid-femur or 6 cm below a radio-opaque marker/ball bearing indicating the anal verge or the inferior extent of tumour, whichever is more inferior and can be wired. The recommended slice thickness is 3 mm. Immobilisation devices such as Vac-Lok are recommended. All patients must be scanned with a comfortably full bladder (>250 ml). For optimal set-up techniques, it is important to consider patient interventions which promote ideal imaging and the patient keeping still, i.e. advice on diet, bowel preparation, pain relief and even methods of relaxation.

11.15.1 Contrast

Intravenous contrast is mandatory unless contraindicated by virtue of allergy or renal impairment. Small bowel contrast is recommended if the small bowel is intended to be contoured as an OAR. Gastrografin 20 ml in water 45–60 min prior to the planning scan or dilute contrast agents in routine diagnostic use are useful. An intravaginal marker should be used in females.

11.15.2 Bolus

Application of bolus is more difficult if the patient is placed supine. If there are concerns, to ensure adequate dose at the anal margin, as an alternative to bolus, the patient's buttocks can be taped together at the time of simulation and for treatment, although this position may not be easily reproducible. Bolus is not recommended to the skin overlying the groins unless tumour extends to skin surface, because the oblique incidence of the IMRT beams usually increase the superficial dose. Anyway we aim to spare the most superficial 5 mm of skin unless there are fungating nodes in the groin. However, it may be important to provide adequate photon fluence in air near the skin in these areas to account for set-up variations.

11.16 Definition of Target Volumes

Definition of target volumes and OARs has been standardised in ICRU reports 50 (ICRU 50 1993) and ICRU 62 (ICRU 62 1999).

Details of imaging proforma for each patient (Appendix 11.3)

Additional information will be available from CT, MRI and PET/CT.

11.16.1 The Primary Gross Tumour Volume

The primary gross tumour volume (GTVp), and the nodal GTV (GTVn), i.e. all involved nodal regions (on imaging or biopsy proven), should be defined and outlined on each CT slice, using all radiological imaging available, and ideally co-registered with the planning scan. The overall GTV is defined but described separately by all macroscopic tumour together with the entire circumference of the anal canal wall (GTVp) and the involved nodes' GTVn. GTVp will extend from either the ball-bearing marker or the demarcated inferior aspect of the tumour extending below the anal margin – whichever is more inferior. Where the primary tumour cannot be identified on the CT images – often Tx (excisional biopsy with positive margins but no macroscopic disease), the anal sphincter complex, will be contoured (in addition to any observed perianal tumour extension) and will be designated as the CTVa.

Whether using a single-phase DP-IMRT or two phases (IMRT and conformal), it is

recommended that all phases of treatment are planned at the same time, as the primary site and even involved lymph nodes may regress rapidly on commencement of CRT.

11.16.2 The Primary Tumour Clinical Target Volume (CTV)

The clinical target volume (CTV) represents extension around tumour and subclinical disease which cannot be seen or imaged. The CTV needs to encompass gross primary tumour CTVp, involved lymph nodes and lymph node stations potentially at risk of microscopic disease (CTVn), the mesorectum (CTVm) and the entire anal canal (CTVa). Defined landmarks should be easy to recognise.

A CTVp should be created by expanding the GTVp anisotropically by 10 mm radially to cover microscopic spread and by 15 mm superiorly and 15 mm inferiorly. This volume is created according to a computer-generated algorithm and therefore does not follow anatomical landmarks. However, anatomical boundaries should be respected, so CTVp in air, bone or any tissues, normally considered natural barriers to tumour infiltration and hence not at risk for microscopic spread, should be manually edited to avoid overlap into these nontarget areas.

11.16.3 The Primary Tumour Planning Target Volume (PTV)

A further expansion to allow for set-up and day-to-day internal organ movement should be created. 10-mm expansion is recommended on CTVps to generate these PTVs. Very little data exists for the use of IGRT and adaptive treatment plans for anal cancer. It may be necessary to insert fiducial markers into or close to the primary tumour and the anal margin to track the movement of these to provide confidence regarding tumour position. Alternatively cone beam CT scanning may be used with off-line correction. Due to the relatively poor visualisation with cone beam imaging, visualisation of the primary tumour may be difficult, and a surrogate of potential tumour movement might be required, for example, the degree of rectal gas distortion. Daily imaging and a knowledge of the department's systematic and random errors may allow the clinician to reduce the CTV to PTV margin to 5–7 mm particularly for patients treated in the supine position. Hence, each department should audit its margin of errors to ensure the PTV margins allocated are reasonable.

11.16.4 Elective Volumes

11.16.4.1 Anal Canal CTV (CTVa)

We believe that the whole anal cancer should be considered at risk of microscopic disease and, if not covered in the initial GTV expansion, should be delineated separately and then expanded to form part of the CTV, i.e. CTVa alongside the primary tumour CTVp to create the primary tumour PTVp + a. This is rarely the case as expansion of 15 mm caudal and cephalad means the anal canal will invariably be included in the CTVp, unless the tumour involves the rectum above the dentate line. The superior extent of the anal canal can be determined on MRI scans and is usually defined superiorly by a line joining the tip of the coccyx and the most inferior aspect of the pubis. However, we do not agree with the Australasian atlas (Ng et al. 2012) that the entire ischiorectal fossa should be contoured as CTVa.

11.16.4.2 Mesorectum (CTVm)

The perirectal mesorectal region should be contoured to include perirectal nodes, but the lower part of the mesorectum is poorly visualised on CT and is even less clear more superiorly, particularly anteriorly, because other structures are not available to define its boundaries. Hence there may be a need to be more generous anteriorly. The archives suggest that in anal cancer Papillon did not formally treat the lymph nodes – although he used arc therapy. He is said to have commented that recurrences were always within the reach of his finger (i.e. 6–9 cm) and probably reflect recurrent mesorectal lymph nodes. We do

not therefore recommend treatment of the upper portion or the entire mesorectum unless tumour extends to the peritoneal reflection and enlarged presacral nodes are imaged. The lower portion of the mesorectum to a maximum distance of 5 cm cephalad to the tumour should be sufficient for CTVm unless tumour extends from the anal canal above the dentate line. We suggest that CTVm = mesorectum with no further expansion + 10 mm for PTV will then suffice.

11.17 Elective Nodal Volumes (CTVn)

Much of the basis of pelvic atlases and anatomical details have been defined in patients with cervical cancers, where it was apparent that conventional techniques for cervix irradiation based on bone references often failed to encompass the planning target volume (Zunino et al. 1999).

Inclusion of the common iliac nodes, and full coverage of the entire internal iliac nodal system, by defining an upper CTV border at, or near, the sacral promontory (Das et al. 2007; Wright et al. 2010) remains an area of discussion. In the RTOG and European CTV recommendations, the elective nodal regions include common iliac nodes up to the 5th lumbar vertebra to a dose of 45 Gy. Yet, common iliac nodal involvement appears rare (1 %), and few recurrences are observed in this site. Standard inclusion within the radiotherapy field may therefore not be justified. In the Norwegian National Population Cohort (Bentzen et al. 2012), the standard superior border was at the level of the lower border of the SI joints. Only if the primary cancer extended into rectal mucosa or the nodes were considered involved did the field extend to the sacral promontory. Thus despite the fact that approximately 50 % of patients had a field extending to the lower end of the SI joint, no recurrences were observed above this treatment field (Bentzen et al. 2012).

In ACT II the superior aspect of the initial APPA field was defined as 2 cm *above* the inferior aspect of the sacroiliac joints, i.e. usually at the S1/S2 interface, and with the beam divergence, the estimated dose to the common iliac nodes was small (Aggarwal et al. 2012). Very few isolated recurrences are observed above this field in the ACT II dataset (Sebag-Montefiore et al. 2012).

We therefore recommend that only the more advanced (T3/T4) cancers with presacral nodes may need higher superior border extending the nodal/elective CTV to the origin of external and internal iliac nodes.

Normal-sized but potentially involved nodes cannot be reliably seen on CT or routine pelvic MRI scans. Three-dimensional lymph node mapping with the aid of lymphangiograms has been used to generate a nodal CTV guideline for gynaecologic malignancies (Chao and Lin 2002). Meticulous pioneering work by Taylor et al. (2005 and 2007) proposed the targeting of pelvic lymph nodes determined upon their predicted relationship to the pelvic vasculature which can be easily identified on CT scan especially following the administration of intravenous contrast.

The use of a margin of 7 mm was shown to cover 91, 98, 94 and 98.6 % of the common iliac, medial external iliac, anterior external iliac, and internal iliac lymph nodes, respectively. Although this study was performed in gynaecological cancer, it has gained acceptance as the basis for lymph node outlining in many pelvic cancers including high-risk prostate, bladder and penile cancer. The outlining of the vessels and subsequent expansion according to Taylor was used by the Australasian Gastrointestinal Tumour Group (AGITG) to form the basis of their atlas for IMRT planning of anal cancer (Ng et al. 2012). We have therefore recommended a 7-mm margin for elective nodal CTV around vessels.

11.17.1 External Iliac Nodes

The external iliac vessels extend anteriorly along the pelvic sidewall as they descend through the pelvis. In terms of definition, the external iliac nodes refer to those above the inguinal ligament distinguishing them from the inguinal nodes which lie below. The lateral external nodes are less well covered using the 7-mm margin. Hence

a wider 10-mm margin following the iliopsoas margin should be considered. Consideration should be given to contouring the superficial iliac circumflex vein in clinically node-positive patients.

11.17.2 Internal Iliac Nodes

The internal iliac vessels sometimes have subdivisions which should be outlined and then expanded by 7 mm. Care should be taken to extend the target volume to the pelvic sidewall.

11.17.3 Obturator Node

The obturator node is not well covered using a simple expansion from the pelvic blood vessels. To cover this nodal group, a strip of 15–18 mm along the pelvic sidewall connecting the external iliac nodes to the internal iliac nodes is recommended.

11.17.4 Inguinal Lymph Nodes

Agreed boundaries of the inguinal region and the position of uninvolved inguinal lymph nodes are difficult to determine on CT imaging alone. We agree with the RTOG suggestion that the inguinal region should be contoured as a compartment (Myerson et al. 2009), rather than just using vessels. The inguinal node positions were not defined within the Taylor proforma (Taylor et al. 2007). The original ACT II protocol called for a 3-cm margin to field inferior to the anal verge treating the inguinal and femoral nodes inferiorly to this distance. This would seem to extend unnecessarily far inferiorly.

The inguinal nodes lie below the inguinal ligament (not easily visible on CT scans). We consider the inguinal compartment as extending from the superior aspect of the femoral head to 1–2 cm below the junction of the saphenous vein and femoral vein. The superficial inguinal lymph nodes form a T-shape: one row (the horizontal group) is running parallel to and below the inguinal ligament, while the other superficial row (the vertical group) is arranged vertically along the femoral/great saphenous vein. We have rarely if ever seen clinical involvement of the femoral nodes in anal cancer, unless the inguinal nodes are already grossly involved, and do not therefore recommend routine contouring of the femoral nodes.

Sartorius may be a difficult landmark. Anteriorly, the skin is not part of the volume, and the first 5 mm can be spared except in case of skin invasion from involved nodes. We prefer to use a faint line anteriorly defining the fascia and the spermatic cord more medially. Posteriorly is the deep femoral vein. The edge of the iliopsoas muscle defines the lateral border, and the edge of the adductor longus muscle, the medial border. Again there is considerable variability on the medial aspect.

The RTOG 0529 RT guidelines recommend that if there are no positive nodes (on biopsy or imaging) in the inguinal/femoral nodal region, the caudad extent of elective CTV groin coverage should be at the level of the takeoff of the profunda femoris vessels (approximately the inferior aspect of the obturator foramina). The caudad extent of the inguinal region (CTVC) should be 2 cm caudad to the saphenous/femoral junction (which usually lies 4 cm below and 4 cm lateral to the pubic tubercle) and cranially should extend to the upper edge of the superior pubic rami.

11.18 Planning Target Volume (PTV)

The RTOG 0529 acknowledges that set-up variations can occur and recommend a PTV margin of about 10 mm to be appropriate. Specifying margins around a CTV for PTV is by no means an exact science.

We distinguish between primary CTVp (anisotropic expansion as above) and involved nodal CTVn, where we recommend an isotropic 10-mm expansion to be added to generate the PTV. In contrast, the elective nodal CTVs are only expanded by 5 mm.

11.19 Summary of Volume Definitions

The AGITG guidelines and atlas for IMRT in anal cancer are also available for a pictorial atlas of some of these volumes (Ng et al. 2012).

- *GTVp* = includes the gross primary and anal tumour volume
- *GTVn* = includes all involved nodal regions
- GTV combined (*GTV comb*) = GTVp + GTVn
- *CTVp* = GTVp + 10-mm expansion radially and 15 mm sup/inf
- *CTVa* = the entire anal canal
- *CTVp* + *a* = includes the GTVp and the entire anal canal from the anorectal junction to the anal verge including the internal and external anal sphincters
- *CTVn* = includes GTVn with a 10-mm expansion
- *CTVn elective* = uninvolved nodal regions
  CTVcombined(*CTVcomb*) = CTVp(+a) + CTVn
  PTV = *CTV comb* + 10 mm circumferentially
  PTV elective = *CTVn elective* + 7-mm margin

11.20 The Pelvic Organs at Risk (OARs)

The pelvic organs at risk (OARs) include the anal canal, small bowel, bladder, skin, external genitalia/perineal skin (penis and scrotum in men and vulva in women), iliac crests (from the bony top to the superior part of acetabulum inferiorly), femoral heads (from the bony top to the lesser trochanter inferiorly) and lumbosacral plexus. It is recommended that all these radiation-sensitive structures are outlined as part of the planning process by the radiation oncologist. Guidelines on dose constraints may be found per the RTOG 0529 closed study protocol (http://www.rtog.org). The tolerance of these structures will be contextual in that exceeding some OAR doses is never acceptable, while others are relative. Imaging an organ does not necessarily mean that IMRT plans can be designed to spare it, because the organ's location with respect to the target may not allow this. Nevertheless, objectives (desired achievements) and constraints (necessary achievements) will need to be set for clinical targets and critical structures with priorities or weighting for these structures.

11.20.1 The Anal Canal

The anal canal is a radiation-sensitive structure. Its function is compromised by high doses of radiotherapy leading to late complications (Buettner et al. 2012; Peeters et al. 2006; Heemsbergen et al. 2006; Vordermark et al. 1999) and occasionally necessitating a stoma. In some ways it should be considered as an OAR. However, this is also the site of primary disease, and it is therefore not possible to restrict the dose prescribed to the anal canal as this may compromise disease control.

11.20.2 Lumbosacral Plexus

Some have contoured the lumbosacral plexus (Badin et al. 2008) from the L4–5 interspace to the level of the sciatic nerve in the greater sciatic foramen caudal to piriformis.

11.20.3 Femoral Head and Neck

The entire femoral head and neck should be contoured using bone windows down to the lesser trochanter and considered as an organ at risk. The incidence of insufficiency fractures in the hips and femoral heads and late pathological fracture has been shown to be increased after pelvic radiotherapy especially in women (Baxter et al. 2005; Tomaszewski et al. 2012). The present authors have experience of hip fractures in this elderly female treated population.

11.20.4 Bone Marrow

Mell and colleagues (Mell et al. 2008) showed that the volume of bone marrow receiving 10–20 Gy was associated with increased toxicity. Functional bone marrow is difficult to visualise

but can be assisted with the use of dynamic MRI sequences which are fused to the planning CT. A recent UK study of IMRT suggested that haematological toxicity could be minimised by using the low superior field border (standard in UK), and therefore sparing the bone marrow (Petkar et al. 2012). Our recommendations do not give concern for overall pelvic bone marrow doses, but there may be implications of IMRT on bone marrow volume irradiated – and particularly the impact of using VMAT as there will be a low-dose bath.

11.20.5 Urinary Bladder

The external outline of the bladder wall should be contoured. Patients should have a comfortably full bladder pretreatment (≥250 ml). This may help move small bowel out of the pelvis and reduce toxicity, as the bladder is relatively radioresistant compared to the small bowel.

11.20.6 Small Bowel

There is a significant correlation between small bowel volumes receiving at least 15 Gy and acute grade 3 gastrointestinal toxicity (Robertson et al. 2010).

Tolerance of small bowel reflects the volume of small bowel receiving 15 Gy (threshold of 100–200 cm^3) – and 30 and 50 Gy (thresholds of 35–300 cm^3) (Martin et al. 2010). Devisetty found a significant correlation between dosimetric parameters and acute GI toxicity for a V30 >450 cm^3 (33 % GI toxicity) (Devisetty et al. 2009).

Since small bowel is a mobile organ which extends into the upper abdomen, it is not practical to outline the whole organ. Some contour small bowel from the rectosigmoid junction to at least 20 mm above the superior extent of any PTV as individual bowel loops. We consider that the small bowel should be contoured tightly around the bowel wall as individual bowel loops to 3 cm above the PTV. The RTOG recommended three separate dose volume constraints for small bowel (Kachnic et al. 2013). In contrast, we have 4 constraints outside the PTV (<200 cm^3 to more than 30 Gy, <150 cm^3 to more than 35 Gy, <30 cm^3 to more than 45 Gy and none to more than 50 Gy).

11.20.7 External Genitalia and Perineum

In males the testes are highly sensitive to the effects of radiation, and it is unlikely that an IMRT plan would be sufficiently conformal to spare the testis to prevent loss of spermatogenesis. We contour from the base of the penis inferiorly. Little data exists regarding scrotal skin tolerance as a specific organ of risk; however, the development of skin toxicity around the external genitalia is one of the most distressing side effects of anal cancer RT. In females, there is an even greater lack of data regarding tolerance of clitoris, labia majora and labia minora. The vulva and soft tissues should be contoured up to the level of the mons pubis.

11.20.8 Radiotherapy Dose Prescription

Elective – 42 Gy in 28 fractions (1.5 Gy per fraction) in 5.5 weeks

Macroscopic disease – 50.4–52 Gy in 28 fractions (1.8–1.86 Gy per fraction) in 5.5 weeks

11.21 Discussion

The RTOG guidelines are a one-size-fits-all consensus of experts for elective volumes (Myerson et al. 2009). However, anal cancer is not really a single disease entity but has different modes of spread depending on whether the tumour is large or small; demonstrates involved nodes or not; is lateral, anterior or posterior; or lies in the upper canal/extends above the dentate line or low canal or beyond the margin. Hence, the CTV needs customising according to clinical and MRI staging and tumour site. Much of the present guidance is

merely judgement, based on experience and not an exact science. Each recommendation will be trading off perceived advantages and disadvantages, but the delineation needs to be in the main reproducible. However, it is not designed to be a rigid framework, because diagnosing a clinically involved node in a particular site may persuade the radiation oncologist to extend the CTV beyond our recommended constructs.

Conclusions

In this chapter we have presented guidelines for imaging and contouring gross disease and elective nodal and anatomical volumes for target delineation in anal cancer for EBRT based on stage and location, which represents our 'index' suggested algorithm. We recommend both a clinical proforma (Appendix 11.1) and an imaging proforma (Appendix 11.2) and a planning proforma as an absolute essential for accurate target delineation, for quality assurance and to facilitate audit. We hope these proposals will decrease uncertainties and observer variation, while also facilitating training. In future, we also need to agree exacting dose constraints by European consensus.

We are not aware of any ongoing phase III trials for anal cancer in any country. We hope therefore that this chapter and the recommendations will be helpful in combination with the RTOG and Australasian atlases – each has strengths and limitations. Ongoing education and real-time quality assurance will be essential for future phase III studies incorporating IMRT or VMAT. But it should be stressed that there is no 'gold standard' for target delineation in anal cancer. All recommendations will inevitably change, develop and be modified till we have international consensus.

Appendices

Appendix 11.1

APPENDIX 1
Proforma for documenting initial clinical extent of anal cancer: please draw on diagrams from exam under anaesthetic (EUA) or clinical and/or MRI measurements

Patient Number ☐☐☐☐☐☐☐☐ Initials ☐☐☐
EUA yes ☐ no ☐

Clinical staging

Site Canal ☐ Margin ☐ Rectum ☐ Not known ☐

T* stage T1 ☐ T2 ☐ T3 ☐ T4 ☐ TX ☐

N* stage N0 ☐ N1 ☐ N2 *(canal only)* ☐ N3 *(canal only)* ☐ NX ☐

caudal extent above dentate line ☐ or **below dentate line** ☐

Canal tumours **Caudal Extent** **Margin tumours** **Nodes**

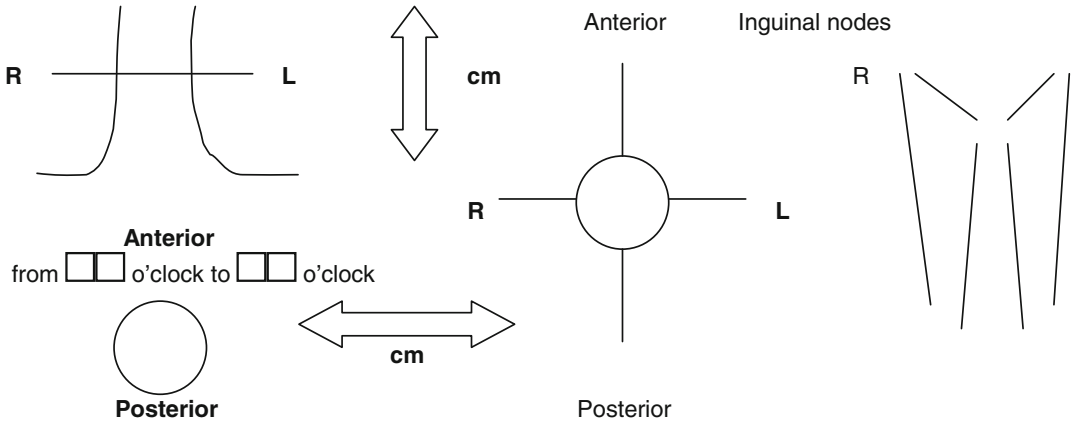

Pathology **Tumour type** Squamous ☐ Basaloid ☐

Differentiation Poor ☐ Moderate ☐ Well ☐

Margins N/A biopsy ☐ Not clear ☐ Excision Clear ☐

***Staging of Anal Cancers – TNM**

	Anal Canal	**Anal Margin**
T1	2 cm or less in greatest dimension	2 cm or less in greatest dimension
T2	> 2 cm but ≤5 cm in greatest dimension	>2 cm but ≤ 5 cm in greatest dimension
T3	>5 cm in greatest dimension	>5 cm in greatest dimension
T4	Tumour of any size invading adjacent organ/s e.g. vagina, urethra, bladder (sphincter muscle involvement alone is not T4)	Tumour invades deep extradermal structures i.e. muscle, bone etc.
N0	No regional lymph node metastasis	No regional lymph node involvement
N1	Peri-rectal lymph node involvement	Ipsilateral inguinal lymph node involvement
N2	Unilateral internal iliac &/or inguinal lymph node/s	-
N3	Peri-rectal & inguinal lymph nodes &/or bilateral internal iliac &/or inguinal lymph node involvement	-

Appendix 11.2

TNM staging for anal canal cancer

Primary tumour (*T*)	
Tx	Primary tumour cannot be assessed
Tis	Carcinoma in situ [Bowen's disease, high-grade intraepithelial lesion (HSIL), anal intraepithelial neoplasia (AIN) II–III]
T1	Tumour less than 2 cm in greatest dimension
T2	Tumour between 2 and 5 cm in greatest dimension
T3	Tumour more than 5 cm in greatest dimension
T4	Tumour invading adjacent organs [vagina, urethra, bladder, sacrum]
Regional lymph nodes (*N*)	
NX	Regional nodes cannot be assessed
N0	No regional lymph node metastasis
N1	Metastasis in perirectal nodes
N2	Metastasis in unilateral internal iliac and/or inguinal nodes
N3	Metastasis in perirectal and/or bilateral internal iliac or inguinal nodes
Distant metastasis (*M*)	
M0	No distant metastasis
M1	Distant metastasis

Appendix 11.3: MRI Protocol for ANAL CANCER – Acquisition and Reporting

High-resolution MRI is an accurate tool for locoregional staging and response assessment. MRI provides an accurate depiction of tumour site and tumour size, defines the relationship of the tumour to adjacent structures and enables locoregional lymph nodes to be assessed.

The aim in anal cancer is to:

- Identify patients with T3- or T4- and/or node-positive disease who have a poorer prognosis
- Define the locoregional extent of disease to assist radiotherapy planning
- Define the locoregional extent and degree of disease regression post therapy in order to tailor further treatment

Patient Preparation

In terms of patient preparation, we do not advocate the routine use of bowel cleansing (purgative or enema) or luminal distension. The use of an antiperistaltic (Buscopan or glucagon IM) may be helpful.

Table 11.1 MRI acquisition

Pelvis	Sequences and orientation
5 mm/no gap	T1 axial
To enable evaluation of locoregional lymphadenopathy and pelvic metastatic disease	T2 axial
	T2 sagittal
	DWI axial: $b=0$, 100, 1,000, 1,200 s/mm^2
Primary tumour	
3 mm/no gap	STIR and T2 axial and coronal
To enable evaluation of tumour extent and involvement of local structures	T2 axial and coronal
	STIR axial and coronal
	DWI axial: $b=0$,100, 500, 800 s/mm^2

The posttreatment MRI sequences should match the orientation and angles of the pretreatment MRI

Table 11.2 Node size criteria. The following maximal size criteria are used to define the upper limit of normal nodes

Sites	Size (mm)
Perirectal	5
Inguinal	15
External iliac	10
Internal iliac	7
Common iliac	9

Sequences

Imaging may be performed on 1.5- or 3-T systems. Following localisation sequences, pelvic and tumour sequences are acquired. Pelvic sequences provide an overview of the entire pelvis and locoregional nodes reflecting the lymphatic drainage of the tumour. The axial sequences are from the level of L5/S1 to below the symphysis pubis. Tumour sequences are taken axial and coronal to the anal tumour and canal.

Table 11.1 summarises the sequences applied. These include T1-weighted, T2-weighted and diffusion-weighted sequences.

MRI Reporting

MRI reporting should reflect the site and locoregional extent of the tumour and the presence and site of nodal disease and provide the maximal tumour dimension (RECIST 1.1.) and an overall stage (TNM).

At baseline, reports should include:

- .Involvement of the anterior urogenital triangle
- Lymph node disease including the location and size of nodes
- TNM stage
- RECIST

Posttreatment reports should include:

- Site of tumour (low, mid- or upper anal canal)
- Size (maximal transaxial dimension) of the primary tumour
- Maximal length of the primary tumour
- Height of tumour from the anal verge
- Morphologic appearance of tumour including any necrotic component
- Extent of extramural spread, which should be reflected by descriptors of locoregional extent:
  - Involvement of the rectum
  - Involvement of the levator ani
  - Involvement of the ischiorectal fossa
  - Involvement of the anterior urogenital triangle
  - Lymph node disease including the location and size of nodes
  - TNM: tumour downstaging, lymph node downstaging
  - RECIST response
  - Presence of post-CRT changes: fibrosis, desmoplasia, inflammatory change, submucosal oedema and necros*is*

RECIST Response

This is as per RECIST 1.1 and the maximal tumour length is used.

Appendix 11.4

Lymph node volumes should follow vessels as defined by contrast CT using asymmetric manual expansions to nodes along tissue planes as defined in the table below from Taylor et al. *Clinical Oncology*. 2007;19:542–550

Lymph node group	Recommended margins
Common iliac	7-mm margin around vessels; extend posterior and lateral borders to psoas and vertebral body
External iliac	7-mm margin around vessels; extend anterior border by additional 10 mm anterolaterally along iliopsoas muscle to include lateral external iliac nodes
Obturator	Join external and internal iliac regions with 18-mm-wide strip along pelvic sidewall
Internal iliac	7-mm margin around vessels; extend lateral borders to pelvic sidewall
Presacral	10-mm strip over anterior sacrum
Inguinal	Not described

Appendix 11.5: Algorithm for Planning According to Site and Stage

1. Anal canal – T1/T2			
Site: *anal canal*	Recommended GTV/CTV/PTV	Imaging	Additional
Stage T1,T2 N0[a] IMRT or VMAT or 3D conformal IMRT or VMAT	(i) GTV primary + 10 mm ant/post/laterally + 15 mm sup and inf = CTVp CTVp + 10 mm = PTVp (ii) CTVm mesorectal nodes to 5 cm CTVn = vessels + 7 mm External iliac, internal iliac obturator nodes from the level of S2 inferiorly (ACT II – 2 cm above the most inferior aspect of SI joints) Inguinal nodes as compartment (CTVm + CTVn) + 5 mm = PTVn	TRUS and/or MRI and CT scanning	Patient supine Fiducial markers only if involved field only for small T1 Anal canal (see Table 11.1) Nodes (see Table 11.2)
B			
Stage T1,T2, N1[b] (metastasis in lower perirectal nodes) IMRT or VMAT or 3D conformal	(i) GTV primary + 10 mm ant/post/laterally + 15 mm sup and inf = CTVp CTVp + 10 mm = PTVp (ii) CTVm mesorectal nodes to superior rectal artery + presacral nodes CTVn = vessels + 7 mm Pelvic nodes below bifurcation of common iliac vessels, i.e. external iliac, internal iliac, obturator nodes Inguinal nodes as compartment (CTVm + CTVn) + 5 mm = PTVn	TRUS and/or MRI and CT scanning PET/CT recommended	Patient supine Anal canal (see Table 11.1) Nodes (see Table 11.2)
C			
Stage T1,T2, N2–N3[c] (N2-metastasis in unilateral internal iliac and/or inguinal nodes or N3) IMRT or VMAT or 3D conformal	(i) GTV primary + 10 mm ant/post/laterally + 15 mm sup and inf = CTVp CTVp + 10 mm = PTVp (ii) GTV nodes + 10 mm = CTVn (iii) CTVm mesorectal nodes + presacral nodes CTVn = vessels + 7 mm Pelvic nodes below bifurcation of common iliac vessels, i.e. external iliac, internal iliac, obturator nodes Inguinal nodes as compartment extending inferiorly if involved superficial inguinal nodes (CTVm + CTVn) + 5 mm = PTVn	TRUS and/or MRI and CT scanning PET/CT highly recommended	Patient supine Anal canal (see Table 11.1) Nodes (see Table 11.2)

2. Anal canal – T3/T4			
Anal canal/anal margin/rectum			
C			
Stage T3,T4, N0–N3 (N2-metastasis in unilateral internal iliac and/or inguinal nodes or N3) IMRT or VMAT or 3D conformal	(i) GTV primary + 10 mm ant/post/laterally + 15 mm sup and inf = CTVp CTVp + 10 mm = PTVp (ii) GTV nodes + 10 mm = CTVn (iii) CTVm mesorectal nodes + presacral nodes CTVn = vessels + 7 mm Pelvic nodes below bifurcation of common iliac vessels, i.e. external iliac, internal iliac, obturator nodes Inguinal nodes as compartment extending more inferiorly if involved superficial inguinal nodes (CTVm + CTVn) + 5 mm = PTVn	TRUS and/or MRI and CT scanning PET/CT highly recommended	Patient supine Anal canal (see Table 11.1) Nodes (see Tables 11.2 and 11.3)

[a]T1/T2N0 and T1/T2N1 (inguinal nodes) anal margin treat as above A, except ensuring adequate coverage inferiorly
[b]Anal canal/rectum, i.e. anal canal extending >1 cm above dentate line, treat whole mesorectum/presacral area as for rectal cancer, but also the whole anal canal to the anal margin as CTV, i.e. treat as C above
[c]For T3/T4 cancers at any site – use algorithm C above even if cNO

Appendix 11.6: Anal IMRT Planning Sheet

Diagnosis: Squamous Cell Carcinoma Anus

Stage:.....

Date:.....

Patient Sticker

Organ	OAR / Target	Dose constraint	Dose received	Signature
PTV	95 % of PTV	Min 95 %		/
	99 % of PTV	Min 90 %		/
	50 % of PTV	Between 99 % – 101 %		/
	5 % of PTV	Max 105 %		/
	2 % of PTV	Max 107 %		/
				/
Small Bowel	>30 Gy	<200 cc		/
	>35 Gy	<150 cc		/
	>45 Gy	<20 cc		/
	>50 Gy	0 cc		/
				/
Femoral Heads	>30 Gy	<50 %		/
	>40 Gy	<35 %		/
	>44 Gy	<5 %		/
Pelvic bone marrow/iliac crests				/
				/
Genitalia				/
				/
Bladder				/
				/

Table 11.3 Various guidelines for pelvic node CTV drawing

	Common iliac	External iliac	Internal iliac	Obturator
Portaluri et al. (2005)	Cranial: aortic bifurcation	Cranial: common iliac bifurcation (L5–S1)	Cranial: common iliac bifurcation (L5–S1)	Cranial: cranial sections of the obturator muscle
	Caudal: common iliac bifurcation	Caudal: femoral ring (disappearance of lateral muscles of the abdominal wall, artery becomes lateral)	Caudal: cranial sections of the coccygeal muscle	Caudal: superior margin inferior branch of the pubic bone
	Anterior: mesocolon	Anterior: fat of small bowel, deferent duct or round ligament	Anterior: bladder, uterus	Anterior: external iliac vein
	Lateral: psoas muscles	Lateral	Lateral	Lateral
	Posterior: sacrum	Cranial: psoas, int iliac vein, iliac bone, sacroiliac joint	Cranial: psoas muscle, int iliac vein, iliac bone, sacroiliac joint	Cranial: acetabulum
		Caudal: piriformis muscle, internal obturator muscle	Caudal: piriformis muscle, int obturator muscle	Caudal: internal obturator muscle
		Posterior	Posterior	Posterior: internal obturator muscle
		Cranial: ext iliac vessels	Cranial: sacral wing	Medial: bladder
		Caudal: pubic bone (superior branch)	Caudal: piriformis muscle	
		Medial: mesocolon, uterus, bladder	Medial: mesocolon, uterus, bladder	
Taylor et al. (2005, 2007)	7 mm around common iliac vessels, extending posterior and lateral borders to psoas and vertebral body	7 mm around ext iliac vessels, extending anterior border by additional 10 mm anterolaterally along the iliopsoas muscle to include lateral external iliac nodes	7-mm margin around int iliac vessels, extending lateral borders to pelvic sidewall	18-mm-wide strip along pelvic sidewall joining external and internal iliac regions
Shih et al. (2005)	2.0-cm expansion around the distal 2.5 cm of common iliac vessels superior to bifurcation	2.0-cm expansion around ext iliac vessels for 9 cm from common iliac bifurcation	2.0-cm expansion around int iliac vessels for 8.5 cm extending from common iliac bifurcation	Not specified
RTOG 0418	7 mm around common iliac vessels, with superior border at 7 mm below L4–L5 interspace	7 mm around ext iliac vessels, terminating at the level of the femoral head	7 mm around int iliac vessels	Not specified
Australasian atlas (Ng et al. 2012)	Not specifically recommended	7 mm around ext iliac vessels, from bifurcation of common iliac terminating at the level within the pelvis	7 mm around int iliac vessels, from bifurcation of common iliac terminating at obturator canal	From the acetabulum to obturator canal (3–5 mm)

References

Aggarwal A, Gayadeen S, Robinson D et al (2012) Clinical target volumes in anal cancer; calculating what dose was likely to have been delivered in the UK ACT II protocol. Radiother Oncol 103:341–346

Ajani JA, Winter KA, Gunderson LL et al (2008) Fluorouracil, mitomycin and radiotherapy vs fluorouracil, cisplatin and radiotherapy for carcinoma of the anal canal: a randomised controlled trial. JAMA 199:1914–1921

Allal JS, Mermillod B, Roth AD et al (1997) The impact of treatment factors on local control in T2-T3 anal carcinomas treated by radiotherapy with or without chemotherapy. Cancer 79(12):2329–2335

Badin S, Iqbal A, Sikder M, Chang VT (2008) Persistent pain in anal cancer survivors. J Cancer Surviv 2(2):79–83

Bannas P, Weber C, Adam G, Frenzel T, Derlin T, Mester J, Klutmann S (2011) Contrast-enhanced [(18)F] fluorodeoxyglucose-positron emission tomography/computed tomography for staging and radiotherapy planning in patients with anal cancer. Int J Radiat Oncol Biol Phys 81(2):445–451

Bartelink H, Roelofsen F, Eschwege F et al (1997) Concomitant radiotherapy and chemotherapy is superior to radiotherapy alone in the treatment of locally advanced anal cancer: results of a phase III randomized trial of the European Organization for Research and Treatment of Cancer Radiotherapy and Gastrointestinal Cooperative Groups. J Clin Oncol 15:2040–2049

Baxter NN, Habermann EB, Tepper JE, Durham SB, Virnig BA (2005) Risk of pelvic fractures in older women following pelvic irradiation. JAMA 294(20):2587–2593

Beahrs OH (1979) Management of cancer of the anus. Am J Roentgenol 133:790–795

Benson AB 3rd, Arnoletti JP, Bekaii-Saab T et al (2012) Anal Carcinoma, Version 2.2012: featured updates to the NCCN guidelines. J Natl Compr Canc Netw 10(4):449–454

Bentzen AG, Guren MG, Wanderås EH, Frykholm G, Tveit KM, Wilsgaard T, Dahl O, Balteskard L (2012) Chemoradiotherapy of anal carcinoma: survival and recurrence in an unselected national cohort. Int J Radiat Oncol Biol Phys 83(2):e173–e180, Epub 2012 Mar 19

Bilimoria KY, Bentrem DJ, Rock CE, Stewart AK, Ko CY, Halverson A (2009) Outcomes and prognostic factors for squamous-cell carcinoma of the anal canal: analysis of patients from the National Cancer Data Base. Dis Colon Rectum 52(4):624–631

Boman BM, Moertel CG, O'Connell MJ et al (1984) Carcinoma of the anal canal. A clinical and pathologic study of 188 cases. Cancer 54:114–125

Buettner F, Gulliford SL, Webb S, Sydes MR, Dearnaley DP, Partridge M (2012) The dose–response of the anal sphincter region–an analysis of data from the MRC RT01 trial. Radiother Oncol 103(3):347–352

Chao KS, Lin M (2002) Lymphangiogram-assisted lymph node target delineation for patients with gynecologic malignancies. Int J Radiat Oncol Biol Phys 54(4):1147–1152

Chen YJ, Liu A, Tsai PT, Vora NL, Pezner RD, Schultheiss TE, Wong JY (2005) Organ sparing by conformal avoidance intensity-modulated radiation therapy for anal cancer: dosimetric evaluation of coverage of pelvis and inguinal/femoral nodes. Int J Radiat Oncol Biol Phys 63(1):274–281

Cotter SE, Grigsby PW, Siegel BA, Dehdashti F, Malyapa RS, Fleshman JW et al (2006) FDG-PET/CT in the evaluation of anal carcinoma. Int J Radiat Oncol Biol Phys 65(3):720–725

Das P, Bhatia S, Eng C et al (2007) Predictors and patterns of recurrence after definitive chemoradiation for anal cancer. Int J Radiat Oncol Biol Phys 68(3):794–800

Davey P, Saibil EA, Wong R (1996) Bipedal lymphography in the management of carcinoma of the anal canal. Br J Radiol 69(823):632–635

Devisetty K, Mell LK, Salama JK et al (2009) A multi-institutional acute gastrointestinal toxicity analysis of anal cancer patients treated with concurrent intensity-modulated radiation therapy (IMRT) and chemotherapy. Radiother Oncol 93(2):298–301

Flam M, John M, Pajak TF et al (1996) Role of mitomycin in combination with fluorouracil and radiotherapy and of salvage chemoradiation in the definitive nonsurgical treatment of epidermoid carcinoma of the anal canal: results of a phase III randomized Intergroup Study. J Clin Oncol 14:2527–2539

Gay HA, Barthold HJ, O'Meara E, Bosch WR, El Naqa I, Al-Lozi R, Rosenthal SA, Lawton C, Lee WR, Sandler H, Zietman A, Myerson R, Dawson LA, Willett C, Kachnic LA, Jhingran A, Portelance L, Ryu J, Small W Jr, Gaffney D, Viswanathan AN, Michalski JM (2012) Pelvic normal tissue contouring guidelines for radiation therapy: a Radiation Therapy Oncology Group consensus panel atlas. Int J Radiat Oncol Biol Phys 83(3):e353–e362, Epub 2012 Apr 6

Gérard JP, Chapet O, Samiel S, Morignat E, Isaac S, Paulin C et al (2001) Management of inguinal lymph node metastases in patients with carcinoma of the anal canal: experience in a series of 270 patients treated in Lyon and review of the literature. Cancer 92:77–84

Glynne-Jones R, Northover JM, Cervantes A (2010) Anal cancer: ESMO clinical practice guidelines for diagnosis, treatment and follow-up. Ann Oncol 21(Suppl 5):v8

Graf R, Wust P, Hilderbrant B et al (2003) Impact of overall treatment time on local control of anal cancer treated with radiochemotherapy. Oncology 65:14–22

Greenall MJ, Quan SH, Urmacher C, DeCosse JJ (1985) Treatment of epidermoid carcinoma of the anal canal. Surg Gynecol Obstet 161(6):509–17.7–92

Gunderson LL, Winter KA, Ajani JA et al (2012) Long-term update of US GI intergroup RTOG 98–11 phase III trial for anal carcinoma: survival, relapse, and colostomy failure with concurrent chemoradiation involving fluorouracil/mitomycin versus fluorouracil/cisplatin. J Clin Oncol 30:4344–4351

Hartwig S, Syrjänen S, Dominiak-Felden G, Brotons M, Castellsagué X (2012) Estimation of the epidemiological burden of human papillomavirus-related cancers and non-malignant diseases in men in Europe: a review. BMC Cancer 12:30, Review

Heemsbergen WD, Peeters ST, Koper PC, Hoogeman MS, Lebesque JV (2006) Acute and late gastrointestinal toxicity after radiotherapy in prostate cancer patients: consequential late damage. Int J Radiat Oncol Biol Phys 66(1):3–10

Hightower BM, Judd ES (1967) Squamous cell carcinoma of the anal canal and anus: current status of therapy. Mayo Clin Proc 42:271

Hill J, Meadows H, Haboubi N, Talbot IC, Northover JM (2003) Pathological staging of epidermoid anal cancer for the new era. Colorectal Dis 5(3):206–213

Huang K, Haas-Kogan D, Weinberg V, Krieg R (2007) Higher radiation dose with a shorter treatment duration improves outcome for locally advanced carcinoma of anal canal. World J Gastroenterol 13(6):895–900

Hughes LL, Rich TA, Delclos L, Ajani JA, Martin RG (1989) Radiotherapy for anal cancer experience from 1979–1987. Int J Radiat Oncol Biol Phys 17(6): 1153–1160

ICRU (2010) Prescribing, recording and reporting photon-beam intensity-modulated radiation therapy (IMRT). ICRU report 83. ICRU, Bethesda.

ICRU (1993) Prescribing, recording and reporting photon beam therapy, ICRU Report 50. ICRU, Bethesda, Oxford University Press, Oxford.

ICRU (1999) Prescribing, recording and reporting photon beam therapy, ICRU Report 62 (Supplement to ICRU Report 50). ICRU, Bethesda, Oxford University Press, Oxford.

James RD, Glynne-Jones R, Meadows HM et al (2013) Mitomycin or cisplatin chemoradiation with or without maintenance chemotherapy for treatment of squamous-cell carcinoma of the anus (ACT II): a randomised, phase 3, open-label, 2×2 factorial trial. Lancet Oncol 14:516–524

Japan Clinical Oncology Group, Toita T, Ohno T, Kaneyasu Y et al (2010) A consensus-based guideline defining the clinical target volume for pelvic lymph nodes in external beam radiotherapy for uterine cervical cancer. Jpn J Clin Oncol 40(5):456–463

Jin F, Stein AN, Conway EL et al (2011) Trends in anal cancer in Australia, 1982–2005. Vaccine 29(12):2322–2327

Kachnic LA, Winter K, Myerson RJ et al (2013) RTOG 0529: a phase 2 evaluation of dose-painted intensity modulated radiation therapy in combination with 5-fluorouracil and mitomycin-C for the reduction of acute morbidity in carcinoma of the anal canal. Int J Radiat Oncol Biol Phys 86:27–33

Koh DM, Hughes M, Husband JE (2006) Cross-sectional imaging of nodal metastases in the abdomen and pelvis. Abdom Imaging 31:632–643

Krengli M, Milia ME, Turri L, Mones E, Bassi MC, Cannillo B et al (2010) FDG-PET/CT imaging for staging and target volume delineation in conformal radiotherapy of anal carcinoma. Radiat Oncol 5:10

Kuehn PG, Eisenberg H, Reed JF (1968) Epidermoid carcinoma of the perianal skin and anal canal. Cancer 22:932–938

Leichman L, Nigro N, Vaitkevicius VK et al (1985) Cancer of the anal canal. Model for preoperative adjuvant combined modality therapy. Am J Med 78(2):211–215

Lengele B, Scalliet P (2009) Anatomical bases for the radiological delineation of lymph node areas. Part III: pelvis and lower limbs. Radiother Oncol 92(1): 22–33

Luna-Pérez P, Fernández A, Labastida S, Lira-Puerto V, Vázquez-Curiel JA, Herrera L (1995) Patterns of recurrence in squamous cell carcinoma of the anal canal. Arch Med Res 26(3):213–219, Review

Martin E, Pointreau Y, Roche-Forestier S, Barillot I (2010) Normal tissue tolerance to external beam radiation therapy: small bowel. Cancer Radiother 14(4–5):350–353

Matthews JH, Burmeister BH, Borg M, Capp AL, Joseph D, Thompson KM, Thompson PI, Harvey JA, Spry NA (2011) T1–2 anal carcinoma requires elective inguinal radiation treatment–the results of Trans Tasman Radiation Oncology Group study TROG 99.02. Radiother Oncol 98(1):93–98

Mell LK, Schomas DA, Salama JK et al (2008) Association between bone marrow dosimetric parameters and acute haematologic toxicity in anal cancer patients treated with concurrent chemotherapy and intensity-modulated radiotherapy. Int J Radiat Oncol Biol Phys 71:1431–1437

Mistrangelo M, Pelosi E, Bellò M et al (2012) Role of positron emission tomography-computed tomography in the management of anal cancer. Int J Radiat Oncol Biol Phys 84(1):66–72

Myerson RJ, Garofalo MC, El Naqa I, Abrams RA, Apte A, Bosch WR, Das P, Gunderson LL, Hong TS, Kim JJ, Willett CG, Kachnic LA (2009) Elective clinical target volumes for conformal therapy in anorectal cancer: a radiation therapy oncology group consensus panel contouring atlas. Int J Radiat Oncol Biol Phys 74(3):824–830

National Comprehensive Cancer Network (NCCN) (2015) Clinical guidelines in oncology. Anal carcinoma, version 2. National Comprehensive Cancer Network. http:// www.nccn.org/professional/physicians_gls/pdf/analpdf. Accessed 2 February 2015

Ng M, Leong T, Chander S et al (2012) Australasian Gastrointestinal Trials Group (AGITG) contouring atlas and planning guidelines for intensity-modulated radiotherapy in anal cancer. Int J Radiat Oncol Biol Phys 83:1455–1462

Nguyen BT, Joon DL, Khoon V, Quong G, Chao M, Wada M et al (2008) Assessing the impact of FDG-PET in the management of anal cancer. Radiother Oncol 87:376–382

Nigro MD, Seydel HG, Considine B et al (1983) Combined preoperative radiation and chemotherapy for squamous cell carcinoma of the anal canal. Cancer 51(10):1826–1829

Nijkamp J, de Haas-Kock DF, Beukema JC et al (2012) Target volume delineation variation in radiotherapy for early stage rectal cancer in the Netherlands. Radiother Oncol 102(1):14–21, Epub 2011 Sep 6

Ortholan C, Resbeut M, Hannoun-Levi JM, Teissier E, Gerard JP, Ronchin P, Zaccariotto A, Minsat M, Benezery K, François E, Salem N, Ellis S, Azria D, Champetier C, Gross E, Cowen D (2012) Anal canal cancer: management of inguinal nodes and benefit of prophylactic inguinal irradiation (CORS-03 Study). Int J Radiat Oncol Biol Phys 82(5):1988–1995

Otto SD, Buhr HJ, Frericks B et al (2009) Staging anal cancer: prospective comparison of transanal endoscopic ultrasound and magnetic resonance imaging. J Gastroinst Surg 13:1292–1298

Peeters ST, Hoogeman MS, Heemsbergen WD et al (2006) Rectal bleeding, fecal incontinence, and high stool frequency after conformal radiotherapy for prostate cancer: normal tissue complication probability modeling. Int J Radiat Oncol Biol Phys 66(1):11–19

Peiffert D, Tournier-Rangeard L, Gérard JP et al (2012) Induction chemotherapy and dose intensification of the radiation boost in locally advanced anal canal carcinoma: final analysis of the randomized UNICANCER ACCORD 03 trial. J Clin Oncol 30:1941–1948

Petkar I, Lee Y, Brooks C et al (2012) Intensity Modulated Radiation Therapy (IMRT) with concurrent chemotherapy for Anal Cancer – Retrospective study evaluating toxicity profile and response rates In: National Cancer Research Institute (NCRI) (ed) Cancer conference 2012, NCRI, Liverpool, 4–7 Nov 2012. Abstract RCR22 Available from: http://www.ncri.org.uk/ncriconference/2012abstracts/naviation/search.html

Portaluri M, Mambace S, Perez C et al (2005) A three-dimensional definition of nodal spaces on the basis of CT images showing enlarged nodes for pelvic radiotherapy. Int J Radiat Oncol Biol Phys 63(4):1101–1107

Robertson JM, Söhn M, Yan D (2010) Predicting grade 3 acute diarrhea during radiation therapy for rectal cancer using a cutoff-dose logistic regression normal tissue complication probability model. Int J Radiat Oncol Biol Phys 77(1):66–72

Sebag-Montefiore D, James R, Meadows H, et al (2012) The pattern and timing of disease recurrence in squamous cancer of the anus: mature results from the NCRI ACT II trial. J Clin Oncol 30(Suppl; abstr 4029)

Shepherd NA, Scoffield JH, Love SB et al (1990) Prognostic factors in anal squamous carcinoma: a multi variant analysis of clinical, pathological and flow cytometric perimeters in 235 cases. Histopathology 16:545–555

Shih HA, Harisinghani M, Zietman AL et al (2005) Mapping of nodal disease in locally advanced prostate cancer: rethinking the clinical target volume for pelvic nodal irradiation based on vascular rather than bony anatomy. Int J Radiat Oncol Biol Phys 63: 1262–1269

Stearns MW Jr, Quan SH (1970) Epidermoid carcinoma of the anorectum. Surg Gynecol Obstet 131:953–957

Steenbakkers RJ, Duppen JC, Fitton I, Deurloo KE, Zijp L, Uitterhoeve AL, Rodrigus PT, Kramer GW, Bussink J, De Jaeger K, Belderbos JS, Hart AA, Nowak PJ, van Herk M, Rasch CR (2005) Observer variation in target volume delineation of lung cancer related to radiation oncologist-computer interaction: a 'Big Brother' evaluation. Radiother Oncol 77(2): 182–190

Stieler F, Wolff D, Lohr F et al (2009) A fast radiotherapy paradigm for anal cancer with volumetric modulated arc therapy (VMAT). Radiat Oncol 4:48

Taylor ARA, Rockall A, Reznek RH et al (2005) Mapping pelvic lymph nodes: guidelines for delineation in intensity-modulated radiotherapy. Int J Radiat Oncol Biol Phys 63:1604–1612

Taylor A, Rockall AG, Powell ME (2007) An atlas of the pelvic lymph node regions to aid radiotherapy target volume definition. Clin Oncol (R Coll Radiol) 19(7):542–550

Tomaszewski JM, Link E, Leong T et al (2012) Twenty-five-year experience with radical chemoradiation for anal cancer. Int J Radiat Oncol Biol Phys 83(2):552

UKCCCR Anal Cancer Working Party (1996) Epidermoid anal cancer: results from the UKCCCR randomised trial of radiotherapy alone versus radiotherapy, 5-fluorouracil and mitomycin. Lancet 348:1049–1054

Vordermark D, Sailer M, Flentje M, Thiede A, Kölbl O (1999) Curative-intent radiation therapy in anal carcinoma: quality of life and sphincter function. Radiother Oncol 52(3):239–243

Weber DC, Kurtz J, Allal AS (2001) Impact duration of local control in anal canal carcinoma treated by split course radiotherapy and concomitant chemotherapy. Int J Radiat Oncol Biol Phys 50:675–680

Wendell-Smith CP (2000) Anorectal nomenclature. Fundamental terminology. Dis Colon Rectum 43:1349–1358

Winton E, Heriot AG, Ng M, Hicks RJ, Hogg A, Milner A et al (2009) The impact of 18-fluorodeoxyglucose positron emission tomography on the staging, management and outcome of anal cancer. Br J Cancer 100(5):693–700

Wright JL, Patil S, Temple L et al (2010) Squamous cell carcinoma of the anal canal: patterns and predictors of failure and implications for intensity modulated radiation treatment planning. Int J Radiat Oncol Biol Phys 78(4):1064–1072

Yhim HY, Lee NR, Song EK et al (2011) The prognostic significance of tumor human papillomavirus status for patients with anal squamous cell carcinoma treated with combined chemoradiotherapy. Int J Cancer 129(7):1752–1760

Zunino S, Rosato O, Lucino S, Jauregui E, Rossi L, Venencia D (1999) Anatomic study of the pelvis in carcinoma of the uterine cervix as related to the box technique. Int J Radiat Oncol Biol Phys 44(1): 53–59

Sarcomas

12

Barbara Röper, Hans Rechl, Katja Specht,
and Klaus Wörtler

Contents

12.1 Introduction

Sarcomas are a rare entity that accounts for less than 1 % of all malignant tumors with 0.6–0.7 % for soft tissue sarcomas and 0.2 % for bone sarcomas in adults (5.9 and 4.5 % in children, respectively). The annual incidence of soft tissue sarcomas is approximately 3.0–3.8/100,000 inhabitants and of bone sarcomas 0.8–1.1/100,000

All authors are members of the Center for Musculoskeletal Tumors (Sarcoma) at the Klinikum rechts der Isar, Technische Universität München, with support from the Wilhelm Sander-Foundation

B. Röper, MD (✉)
Klinik und Poliklinik für Strahlentherapie und Radiologische Onkologie, Klinikum rechts der Isar, Technische Universität München,
Ismaninger Straße 22, 81675 München, Germany
e-mail: Barbara.Roeper@lrz.tum.de

H. Rechl, MD
Klinik für Orthopädie und Sportorthopädie der Technischen Universität München,
Klinikum rechts der Isar, München, Germany

K. Specht, MD
Institut für Allgemeine Pathologie und Pathologische Anatomie der Technischen Universität München,
Klinikum rechts der Isar, München, Germany

K. Wörtler, MD
Institut für diagnostische und interventionelle Radiologie der Technischen Universität München,
Klinikum rechts der Isar, München, Germany

A.-L. Grosu, C. Nieder (eds.), *Target Volume Definition in Radiation Oncology*,
DOI 10.1007/978-3-662-45934-8_12, © Springer-Verlag Berlin Heidelberg 2015

inhabitants (Siegel et al. 2012). Sarcomas can occur in any anatomic region. About 60–75 % of soft tissue sarcomas are located in the extremities, 10 % in the trunk wall, 15 % in the retroperitoneum, and <10 % in the head and neck region or other sites. Predilection sites for bone tumors are the corresponding long bones around the knee (43 %) as well as the proximal extremity girdles and the pelvic region (31 %), which is the most common site for chondrosarcoma and Ewing sarcoma. The WHO classification in its revised form (Fletcher et al. 2013) differentiates between benign, malignant, and intermediate lesions which are subcategorized in "locally aggressive" or "rarely metastasizing." At present, there are 53 different malignant subtypes of soft tissue tumors and another 26 soft tissue tumors of "unspecified, borderline, or uncertain behavior." For bone tumors, 28 malignant and 7 "unspecified, borderline, or uncertain" subtypes are described. Thus, the heterogeneity of histologies, sites, and biological behavior of sarcomas is a challenge even in interdisciplinary expert management. Given the rarity and the complexity of the disease, treatment of sarcomas should be reserved to centers with special expertise.

This chapter concentrates on those entities the radiation oncologist is confronted with more frequently, i.e., (1) soft tissue sarcomas, (2) desmoid-type fibromatosis, (3) osteosarcomas, (4) Ewing sarcoma, (5) chondrosarcomas, and (6) chordomas.

12.2 General Aspects of Radiation Treatment Planning in Sarcomas

In curative radiation treatment of sarcomas, high total doses are in use. Thus, reproducible positioning is of utmost importance. Immobilization aids like vacuum mattresses for the body and thermoplastic masks for head and neck or distal extremity sites should be used routinely in order to keep margins between the clinical target volume (CTV) and the planning target volume (PTV, see ICRU-reports 50, 83) as small as reasonably possible. For photon treatment, the use of intensity-modulated radiation therapy (IMRT) in combination with image guidance (IGRT) is strongly encouraged. With IMRT, chances are high to achieve sufficient dose coverage of any irregularly shaped PTV and to realize steep dose gradients to critical organs at risk (OAR) in close proximity to the tumor site. IGRT helps to reduce the margin for positioning uncertainty, thus, reducing the high dose volume as well. Other high-precision techniques such as stereotactic radiotherapy, interstitial brachytherapy, or intraoperative radiotherapy may be of special value in sarcoma treatment in order to improve the therapeutic ratio for uncomplicated cure. For some entities like chondrosarcoma and chordoma, particle therapy has been reported to be very successful. For curative treatment in pediatric patients, protons are a valuable option because of the reduced dose-wash outside the PTV in comparison to photon IMRT techniques. The high linear energy transfer (LET) of heavy particles like carbon ions may bring along additional biological advantages in slowly growing tumors, but for most histological entities, experience is still very limited so far.

12.3 Soft Tissue Sarcomas

12.3.1 Anatomy and Histopathology

Soft tissue tumors are derived from mesenchymal cells and are classified according to their line of differentiation into adipocytic tumors, fibroblastic–/–myofibroblastic tumors, so-called fibrohistiocytic tumors, smooth muscle tumors, pericytic tumors, skeletal muscle tumors, vascular tumors, chondro-osseous tumors, gastrointestinal stromal tumors, nerve sheath tumors, and tumors of uncertain differentiation as well as undifferentiated/unclassified tumors. *Benign* soft tissue tumors are at least 100 times more frequent than *malignant* soft tissue tumors. In terms of both prognosis and therapeutic decisions, grading of malignant tumors is crucial. In addition to the categories of benign and malignant tumors, there is the category of *intermediate malignancy*: Tumors belonging to the latter category either display a locally aggressive behavior e.g., desmoid-type fibromatosis) or

show the ability to give rise to metastasis (e.g., dermatofibrosarcoma protuberans, giant cell tumor of soft tissues). In terms of sarcomas, there is a couple of grading systems in use, all of which correlating with prognosis. The two most widely used are those proposed by the NCI (National Cancer Institute) and the FNCLCC (French Fédération Nationale des Centres de Lutte Contre le Cancer) (Coindre 2006), the latter showing superior prognostic prediction. It comprises three independent prognostic factors: (i) tumor differentiation according to histological type, (ii) the mitotic count in 10 HPF, and (iii) the presence/extent of necrosis. Factors are scored separately and added to a sum score, corresponding to the three-grade system. Translated into a two-grade system, grade I tumors are rated *low grade*, whereas grade II and grade III tumors are considered to be *high grade*. If alternatively a four-grade system is applied, then grades I–II is regarded as *low grade* and grades III–IV as *high grade*, respectively.

In the TNM-staging system for STS in its 7th edition (Sobin et al. 2009), "T" stands for size of the primary tumor (T1: ≤5 cm, T2: >5 cm). The location is described in relation to the fascia (suffix "a," superficial tumor site with no fascial contact; suffix "b," fascial involvement). "N" stands for absence or presence of regional nodal (N0, N1) and "M" for distant metastases (M0, M1). In contrast to the UICC classification of carcinomas, the UICC classification of sarcomas in the 7th edition considers the grading as the most important prognostic factor, with UICC stage I reserved for low-grade sarcomas.

The most frequently encountered soft tissue sarcomas are undifferentiated pleomorphic sarcoma (formerly: malignant fibrous histiocytoma (MFH)) which cannot be assigned to a certain cell line, liposarcoma (adipocytic tumor), leiomyosarcoma (smooth muscle tumor), myxofibrosarcoma (fibroblastic tumor, see Fig. 12.1), synovial sarcoma (uncertain differentiation, *not* arising from synovial cells!), and malignant peripheral nerve sheath tumors. These entities account for approximately 75 % of all soft tissue sarcomas, three quarters of them being high grade.

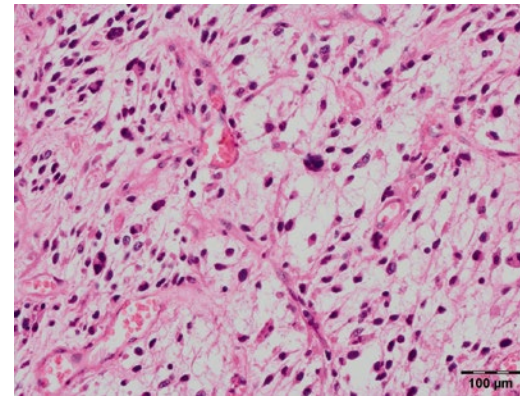

Fig. 12.1 Myxofibrosarcoma, G2. Intermediate grade myxofibrosarcoma showing mildly atypical, hyperchromatic tumor cells in a myxoid stroma and a characteristic vascular pattern with curvilinear, thin-walled blood vessels

12.3.2 Imaging of STS

Soft tissue sarcomas presenting as a mass of a certain size can be visualized on CT, which is particularly helpful to detect calcifications and secondary changes of adjacent bony elements. However, the preferred diagnostic tool is magnetic resonance imaging (MRI) which allows depiction of several *tissue components* on the basis of intrinsic signal characteristics. For example, high signal intensity on T1- and T2-weighted images and signal loss on fat-suppressed images indicate fatty tissue; intermediate signal intensity on T1-weighted and high signal intensity on T2-weighted images is seen with cystic, necrotic, or myxoid tumor components, whereas low signal intensity on images with T2 contrast is compatible with the presence of calcifications, collagen, or hemosiderin deposits. In most cases, the application of contrast medium is indicated in order to further characterize the tumor with respect to its *vascularization, homogeneity*, and *extent of necrosis*. Furthermore, the *margins of the lesion* can be visualized, ranging from well demarcated to infiltrative. Benign lesions may be encapsulated, but even high-grade sarcomas might be surrounded by a relatively well-defined zone of compressed normal tissue, which is referred to as the *pseudocapsule*. On the other hand, locally aggressive lesions such as

desmoid-type fibromatosis may exhibit diffusely infiltrating margins. Thus, the *growth pattern*, as displayed by MRI, does not necessarily correlate with the malignancy of a soft tissue tumor, but is crucial for the radiation oncologist with regard to target volume delineation. MRI visualizes *tumor localization* (subcutaneous, intramuscular, intermuscular, etc.), *fascial involvement*, *transcompartmental spread*, as well as *infiltration of adjacent tissues* such as bone. There may be clear evidence of involvement of major vessels or nerves if they are entirely encased by the tumor or noninvolvement if these structures are clearly separated from the tumor by a layer of normal tissue. If the tumor abuts major vessels or nerves, the infiltration probability can be estimated from the degree of circumferential contact.

Peritumoral edema represents a common MR finding in soft tissue sarcomas, which is visualized as an ill-defined area of high signal intensity on fat-suppressed, T2-weighted, and STIR images as well as on contrast-enhanced T1-weighted images with fat suppression. In STS of the extremities, peritumoral edema can be quite extensive longitudinally and might even exceed the length of the solid tumor. It should be regarded as potentially contaminated by tumor cells, although compression of venous and/or lymphatic vessels may contribute to formation of edema distal to the mass as well.

The value of *positron emission tomography* with glucose-labelled tracers (e.g., FDG-PET-CT) is limited for the delineation of the primary tumor. A threshold-based approach in 17 patients produced large standard deviations between the gross tumor volume (GTV) based on PET-CT in comparison with contrast-enhanced MRI for all SUV (standardized uptake value) thresholds (Karam et al. 2009). Nevertheless, FDG-PET-CT could be of help in defining the clinically relevant portion of peritumoral edema in sarcomas producing a substantial FDG uptake in the primary tumor. In a study of 7 superficial sarcomas (6 "MFHs"), SUVs were correlated with histopathological findings at regular intervals of 1 cm up to 5 cm away from the primary tumor defined by contrast-enhanced MRI. Mean SUV_{max} was 2.2 (range 0.3–3.8) at 1 cm, 1.1 (0.85–1.47) at 2 cm, and 0.83 (0.65–1.15) at 3 cm from the tumor margin. Mapping of the resected tissue revealed absence of tumor cells in areas where SUV_{max} was below 1.0 (Yokouchi et al. 2011).

12.3.3 Target Volume Delineation in STS

Generally, visualization of the tumor with MRI is the basis for target volume definition in STS. Thus, the use of a contouring software that allows for import of MRI sequences and registration with the planning CT is strongly recommended. For visualization of the primary tumor, a contrast-enhanced T1-weighted sequence with fat suppression is appropriate, supplemented by a T2-weighted sequence for fatty components, if indicated. For visualization of the peritumoral edema, fat-suppressed T2-weighted images are most suitable, covering the whole extent of soft tissue edema longitudinally.

12.3.3.1 Target Volume Delineation in Extremity Soft Tissue Sarcoma (ESTS)

ESTS, Target Volume Delineation for Preoperative Radiotherapy

Ideally, diagnostic MRI is performed in the same position as radiation treatment, allowing for exact registration with the planning CT and delineation of the primary tumor and perifocal edema. The GTV encompasses the visible primary tumor. The inclusion of edema is a matter of controversy. There is a consensus that it should in any case be included into the CTV which generally covers the whole volume of potential microscopic tumor involvement, but one could argue that visible changes in the MRI signals reflect a macroscopic tumor involvement and the edema should be regarded as GTV.

Historically, in *extremity soft tissue sarcoma (ESTS)*, radiation treatment fields were chosen that encompassed the visible tumor with a 2 cm margin in anterior-posterior and lateral directions and a 5 cm or wider margin longitudinally up to a dose of approximately 50 Gy (Mundt et al. 1995; Wylie et al. 1999). This had to be translated into the ICRU concept with definitions of CTV and PTV margins (ICRU reports 50, 83).

According to a meeting of radiation oncologists involved in STS Radiation Therapy Oncology Group (RTOG) studies, their view of CTV definition for preoperative radiotherapy of intermediate-to-high-grade sarcoma (tumor size ≥5 cm) followed the RTOG 0630 protocol, expanding the GTV with a radial margin of 1.5 cm and a longitudinal margin of 3 cm, shortened at the end of a compartment. Inclusion of suspicious edema defined on MRI T2 images beyond the margins mentioned above was left to the clinical judgement of the radiation oncologist. It could be excluded from the CTV in case the risk of tumor cell occurrence seemed to be low or the irradiation caused excessive toxicity (Wang et al. 2011).

In a later consensus meeting of experts in radiation oncology from Canadian, American, and European sarcoma centers, for high-grade tumors, a CTV definition was advocated expanding the GTV in all radial directions by 1.5 cm and longitudinally by 4 cm (Haas et al. 2012). The edema was not included in the GTV but in the CTV, expanding the CTV beyond the geometrical margins wherever edema was visible. Uninvolved fascia and bones were regarded as being effective barriers to tumor spread. Thus, restricting the CTV to their surfaces and to the skin was found to be sufficient (Hong et al. 2004). The longitudinal margin of 4 cm was supported by a histopathological study in 15 patients, which reported changes in T2-weighted MRI signal in a distance up to 0–7 cm, contrast enhancement in 0–5 cm, and tumor cells up to 4 cm away from the main tumor mass, as was confirmed in the corresponding surgical specimens (White et al. 2005). For definition of the PTV, an institutional margin for positioning uncertainty should be applied around the CTV, which may be 1 cm or more for variable sites like the thigh or reduced to 0.5 cm in case of reproducible mask fixation of the target and/or daily image guidance with visualization of the soft tissue (Haas et al. 2012; Dickie et al. 2010).

After analysis of 60 recurrences (7.8 %) in a cohort of 768 STS patients treated with pre- or postoperative radiotherapy between 1990 and 2006, PTV encompassing the GTV with longitudinal margins of 5 cm and 1–2 cm axially appeared sufficient, as 49 relapses were in-field, 2 were marginal, and only 9 were out-of-field (1.1 % overall) (Dickie et al. 2012).

Bearing in mind the success rates of adjuvant brachytherapy in ESTS with margins of not more than 1.5–3 cm and the more precise imaging and dose application techniques available today, the margin width for CTV and PTV definitions is under discussion. At the MGH, Boston, good results in preoperative radiotherapy of ESTS were achieved with a margin of 1–1.5 cm radially and 3.5 cm longitudinally to the GTV for the definition of the CTV and another 0.5–0.7 cm expansion for the PTV. After a median follow-up of 41 months, 5 local recurrences occurred in 56 patients (5-year actuarial local control rate of 88.5 %), of which three were located in the CTV and two within and beyond the CTV (Kim et al. 2010).

To reduce margins between CTV and PTV, immobilization aids have been proven to be effective (Dickie et al. 2009). If daily image guidance with cone beam or MV-CT is performed, a 0.5 cm CTV expansion for the PTV is permitted (O'Sullivan et al. 2013).

In preoperative radiotherapy of extremity STS, wound complication is an issue of note. The OAR is the skin and subcutaneous tissue around the tumor that receives a relevant radiation dose and is involved in the wound healing process after tumor resection. In a phase III randomized trial on extremity STS, the arm with preoperative radiotherapy to a total dose of 50 Gy followed by surgery was associated with a 35 % wound complication rate, whereas in the other arm with surgery upfront followed by postoperative radiotherapy to a total dose of 66 Gy, a 17 % wound complication rate was observed (O'Sullivan et al. 2002).

In a phase II study on preoperative IMRT (50 Gy) and IGRT for lower extremity STS, the CTV was defined as the GTV plus a radial margin of 1.5 cm and a longitudinal margin of 4 cm. The PTV encompassed the CTV plus a 0.5 cm margin in all directions. A high radiation dose to planned excision sites and tissue qualifying for surgical skin flaps was carefully avoided. A 30.5 % incidence of wound complications was found in 59 evaluable patients. This was numerically lower

than the risk of 43 % for lower limb STS derived from the preoperative arm of the randomized trial cited above, but did not reach statistical significance (O'Sullivan et al. 2013). Image-guided IMRT reduced the need for tissue transfer and was associated with low chronic morbidity.

Another phase II study of preoperative image-guided IMRT to a total dose of 50 Gy for ESTS stages II–III, aiming for a reduction of wound complication rate (primary endpoint), was initiated in 2011 at the Technical University of Munich (PREMISS: *P*reoperative *R*adiotherapy for Sarcomas of the *E*xtremities with Intensity-*M*odulation, *I*mage-guidance and *S*mall *S*afety margins, NCT01552239), (National Cancer Institute 2013). In the PREMISS protocol, the GTV encompasses the tumor and the peritumoral edema, with a 1 cm expansion in axial and a 2.5 cm expansion in longitudinal directions for the CTV and another 0.5 cm margin for the PTV. An example is given in Fig. 12.2.

In order to quantify the sparing of organs at risk, namely, the bone and the soft tissue outside the PTV ($Bone_{exPTV}$, $SoftTissue_{exPTV}$), these structures are contoured from each 3 cm proximal to the first and distal to the last CT slice containing the PTV. Intensity-modulated treatment planning aims for keeping the percentage of "$Bone_{exPTV}$" encompassed by the 40 Gy isodose (V_{40Gy}) below 50 %. Likewise, the V_{30Gy} of the "$SoftTissue_{exPTV}$" is kept below 50 %.

ESTS, Target Volume Delineation for Postoperative Radiotherapy

In soft tissue sarcoma of the extremity with no prior radiation treatment, postoperative radiotherapy is usually indicated with the exception of low-grade tumors after R0 resection and atypical lipomatous tumors (ALT) after marginal resection. Generally, the dose administered to the tumor site (PTV_{boost}) may vary between 60 and 70 Gy, according to histological subtype, grade, and resection margin. For a larger volume including all surgically manipulated tissue (PTV_{large}), the prescribed dose is often between 45 and 56 Gy. Careful review of surgical and pathological reports as well as postoperative MRI will help to identify areas in need of irradiation and facilitate the choice of boost dose.

With IMRT, simultaneous integrated boost techniques became available, leading to concepts of slightly enhanced single doses ($\leq$2.2 Gy) for the PTV_{boost} and/or slightly reduced single doses ($\geq$1.7 Gy) for the PTV_{large} compared to conventional fractionation. An example is given in Fig. 12.3.

At the time of planning CT, all surgical scars and drainage sites should be marked with radiopaque linings. As there is no "GTV" after macroscopical complete tumor resection, any attempt should be made to coregistrate the planning CT with pre- and postoperative MRI in order to reconstruct the GTV contact planes ($GTV_{contact}$) in the postoperative anatomy. The comparison of preoperative and postoperative MRI helps to differentiate between perifocal edema arising from the tumor and postoperative edematous changes. The resection site might exhibit slight contrast enhancement, and scarring might be visible through soft tissue deformation.

The clinical target volume for the boost dose (i.e., CTV_{boost}) encompasses the $GTV_{contact}$ plus a margin of 1.5 cm, the initially suspicious perifocal

Fig. 12.2 Myxoid liposarcoma (cT2b cN0 cM0 G2) of the right lateral gastrocnemius muscle in a 41-year-old man. (**a**) Axial contrast-enhanced T1-weighted image with fat suppression, tumor size 10.5 cm×7.2 cm. (**b**) Coronal STIR image, solid lesion of 14.3 cm in length, marked distal soft tissue edema following a fascial plane (*arrow*). (**c**–**d**) Target volume definition for preoperative radiotherapy to a total dose of 50 Gy, visualized on a coronal STIR image and a coronal reconstruction of the planning CT: solid primary tumor, *yellow*; GTV, *orange* (including edema); CTV, *pink* (GTV plus 1 cm margin in axial and 2.5 cm margin in longitudinal directions in soft tissue); and PTV, *red* (CTV plus 0.5 cm margin, including GTV plus 1 cm margin, regardless of bone or air). (**e**) Four weeks after radiotherapy, axial contrast-enhanced T1-weighted image with fat suppression: tumor size 8 cm×5.3 cm, decreased contrast enhancement of tumor tissue, increased proportions of myxoid changes, and necrosis. (**f**) Coronal STIR image 4 weeks after RT, solid tumor 12.6 cm in length ("no change" according to RECIST version 1.1), regression of soft tissue edema. After limb-preserving tumor resection, all resection margins were found free of tumor (R0 resection), and the percentage of vital tumor cells quantified to be approximately 5 %

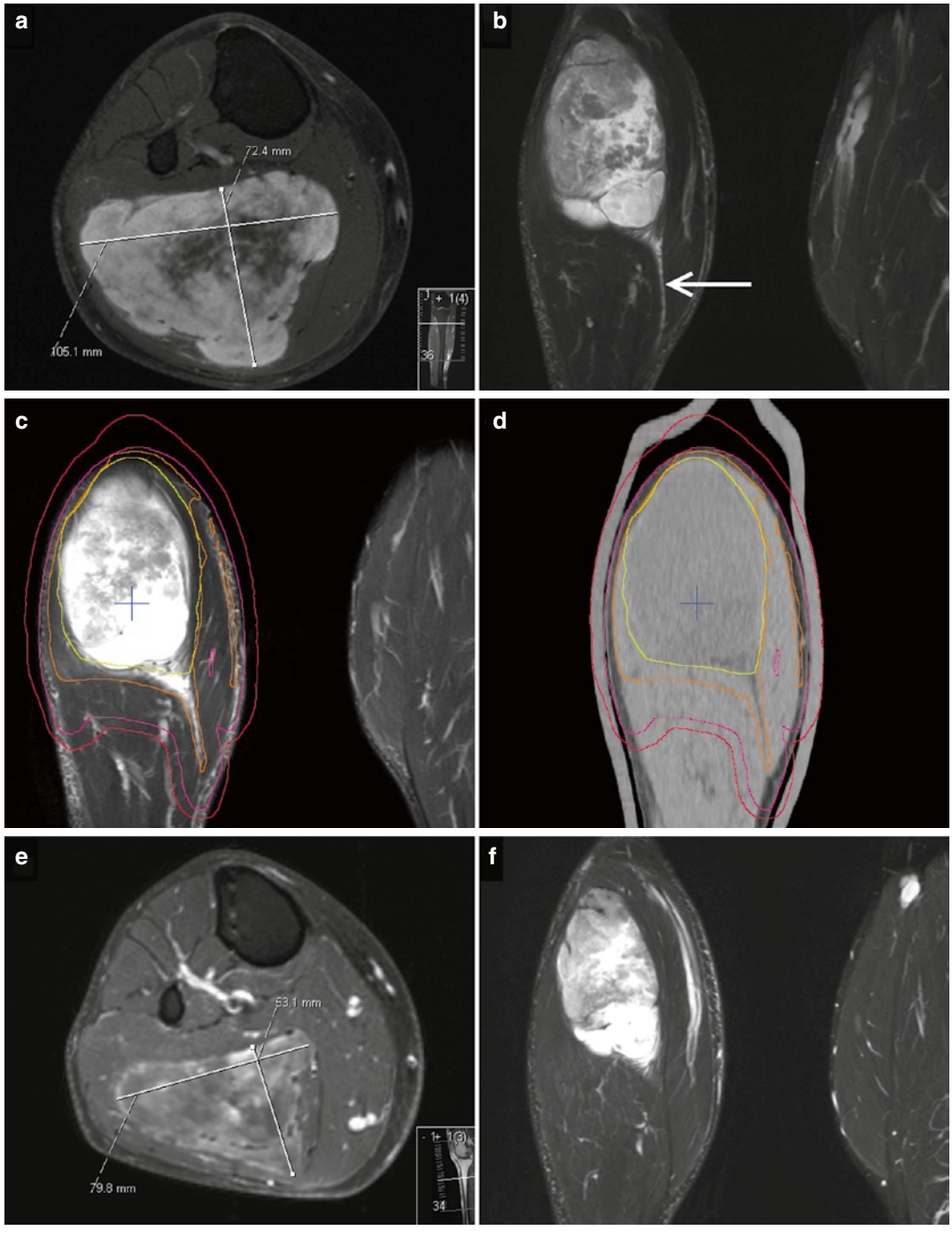
a
72.4 mm
105.1 mm
1(4)
36
b
c
d
e
53.1 mm
79.8 mm
1(3)
34
f

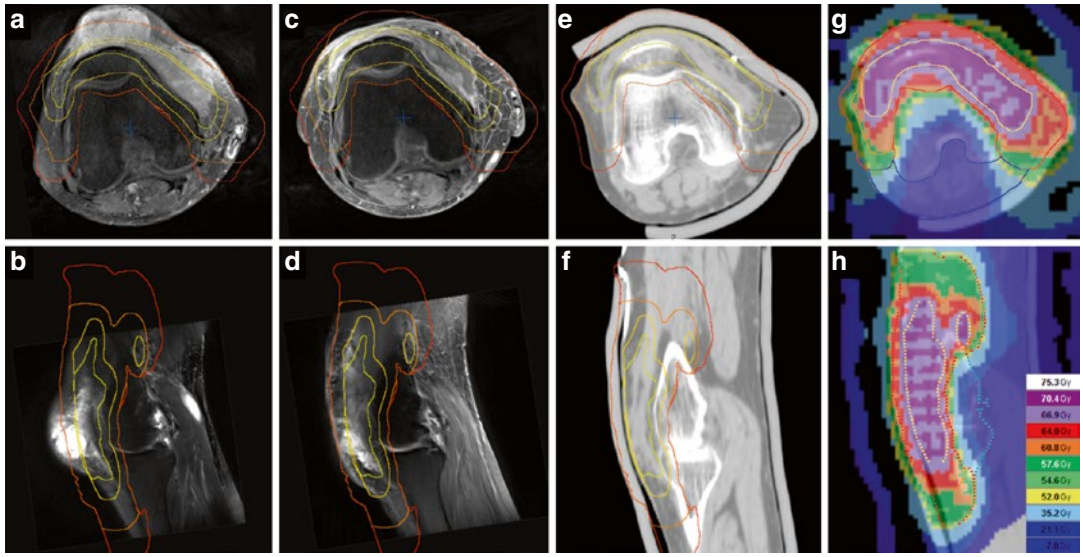

Fig. 12.3 Epitheloid myxofibrosarcoma of the right knee in a 73-year-old woman. (**a**) Axial contrast-enhanced T1-weighted and (**b**) sagittal T2-weighted images with fat suppression showing pretibial tumor with extensions to the medial femoral condyle and to the tibial tuberosity. (**c**–**d**) Postoperative situation (pT2b cN0 cM0 G2, ≥R1) after tumor resection in another facility, displayed on axial and sagittal T1-weighted fat-suppressed images: contrast enhancement of the resection cavity, residual tumor cannot be excluded, in particular medial to the patella and at the tibial tuberosity. The patient refused amputation, radical local tumor resection would result in a loss of function in the knee joint, therefore postoperative/definitive radiotherapy was offered. (**e**) Axial and (**f**) sagittal planning CT reconstruction, target volume definition for simultaneous integrated boost technique: tumor contact and resection cavity ($GTV_{contact/postop}$), *yellow*; PTV_{SIB2}, *light orange* (GTV plus 0.5 cm axial margin and 1.5 cm proximodistal margin, with 0.2 cm skin sparing) to a total dose of 70.4 Gy in 32 fractions of 2.2 Gy; PTV_{SIB1}, *orange* (postoperative edemal changes plus 1 cm axial margin and 2 cm longitudinal margin) to a total dose of 64 Gy in fractions of 2.0 Gy; CTV_{large}, not shown (postoperative edemal changes plus 1.5 cm axial margin and 4.5 cm longitudinal margin, in soft tissue); and PTV_{large}, *red* (CTV_{large} plus 0.5 cm margin) to a total dose of 57.6 Gy in fractions of 1.8 Gy. (**g**) Axial and (**h**) sagittal view of the dose distribution (tomotherapy planning)

edema, and the resection cavity with a 0.5–1.5 cm margin. According to institutional protocols and reproducibility of patient positioning, the PTV_{boost} expands the CTV_{boost} with a margin of 0.5–1 cm.

The clinical target volume for the lower dose (CTV_{large}) encompasses the $GTV_{contact}$ with a more generous margin of 4 cm in longitudinal and 1.5 cm in radial directions, restricted to anatomic borders respected by the tumor, and all surgically manipulated tissue including scars and drainage sites with a 0.5–1 cm margin. Again, another 0.5–1 cm margin is applied to generate the PTV_{large}.

12.3.3.2 Target Volume Delineation in Retroperitoneal Soft Tissue Sarcoma (RPS)

In *retroperitoneal soft tissue sarcomas (RPS)* institutional series with intraoperative radiotherapy, proton or carbon ion therapy have produced promising results (Sindelar et al. 1993; Petersen et al. 2002; Pawlik et al. 2006; Serizawa et al. 2009; Yoon et al. 2010; Pezner et al. 2011), though the data from epidemiological studies is conflicting (Sampath et al. 2010; Tseng et al. 2011). The current concept of preoperative radiotherapy is especially helpful in retroperitoneal STS, as the tumor displaces the surrounding bowel, the normal tissues with tumor contact are in place for target volume definition, and the limited total dose of 50 Gy is feasible in the abdomen (Pawlik et al. 2006). In 2012, a multicenter phase III randomized controlled trial has been initiated to elucidate the effect of preoperative radiotherapy (50.4 Gy) on abdominal recurrence-free survival (STRASS: *S*urgery With or Without Radiation Therapy in *T*reating Patients With Previously Untreated Nonmetastatic

Retroperitoneal *S*oft Tissue Sarcoma, EORTC-protocol 22092, NCT01344018) (EORTC 2013). A consensus meeting on target volume definition for RPS outside study protocols is in preparation.

Generally, in the retroperitoneal space, liposarcoma is the predominant histology, followed by leiomyosarcoma, accounting for 50 and 26 % of RPS, respectively, according to a SEER database with 1,365 patients undergoing resection of RPS in the years 1988–2005 (Nathan et al. 2009). Whereas for atypical lipomatous tumors of the limbs (ALT), even in case of microscopic incomplete resection, the indication for postoperative radiation therapy is rarely given, and the estimated risk of dedifferentiation is below 2 %; for retroperitoneal ALT, it might exceed 20 %. In ALT of the retroperitoneum, spermatic cord or mediastinum tumor-free resection margins are rarely achieved and may ultimately lead to death in the following 10–20 years in >80 % of patients due to repeated, locally uncontrolled recurrences or dedifferentiation with development of metastases. For dedifferentiated liposarcoma at first presentation, a local recurrence rate of 40 % after 5 years is reported for all sites, but for a retroperitoneal site, nearly all tumors eventually recur if patients are followed up for 10 years or longer. Factors relevant for survival in RPS are the histological subtype, the histological grade, and the tumor invasion of adjacent structures, whereas tumor size has no impact on overall survival (Nathan et al. 2009).

For target volume delineation in retroperitoneal sarcoma, a contrast-enhanced computed tomography is needed which can be complemented with registration of MRI. 4D-CT helps to quantify the organ movement due to breathing. The extent of dedifferentiation may vary grossly within a tumor. In case of low-grade liposarcoma, it may be extremely difficult to determine the GTV as there is often no "capsule" between ALT and normal fatty tissue, and tissue densities/signal intensities may not differ. The displacement of bowel is indicative of the presence of a tumor mass as well as a "blurred" aspect of the fatty tissue, which may result from streaks of collagen or an inflammatory component of the tumor.

Perifocal edema is less common in RPS in comparison with ESTS and, if present, should at least be included in the CTV. Institutional protocols for the GTV-to-CTV margin may vary in the order of 0.5–2 cm, according to the adjacent tissue. We suggest a general margin of 1.5 cm in all directions around the primary tumor plus perifocal edema. In the direction of anatomic barriers, e.g., uninvolved liver, we reduce the margin to the extent of breathing movement as visible in a 4D-CT. There should be clear communication with the surgeon if the ipsilateral kidney is to be removed later, in which case a compromise in the target volume delineation for ipsilateral kidney sparing is not indicated, and sparing of the contralateral kidney is mandatory. With image-guided IMRT, we apply a margin of 0.5 cm around the CTV to derive the PTV. The dose (i.e., 50.4 Gy) is prescribed to the median, aiming for a target dose coverage of 95 % of the nominal dose in at least 95 % of the target volume ($D_{95\%} \geq 47.8$ Gy). The intersection of the PTV and small or large bowel is derived from the contoured structures and subjected to a dose of 47.8–50.4 Gy in the optimization process, with steep dose gradients in the bowel outside the PTV. In the spinal cord, we allow for a dose maximum of 50.4 Gy. For other organs like the stomach, duodenum, liver, pancreas, spleen, and lungs, the planning optimization is generally aiming for organ sparing outside the PTV, but without limitation of the dose maximum in the intersection zone between the PTV and organs at risk. An example is given in Fig. 12.4.

In a pilot study of 18 patients with retroperitoneal liposarcoma, the CTV was restricted to the posterior abdominal wall from where the tumor derived. After a total dose of 50 Gy in fractions of 2 Gy, acute toxicity was tolerable and all tumors could be resected. With a median follow-up of 27 months, 2 local recurrences developed (Bossi et al. 2007). In another pilot study on 16 patients with RPS, a total dose of 45 Gy in 25 fractions was applied to the entire tumor plus 1–1.5 cm margins and a simultaneous dose escalation to a total dose of 57.5 Gy (in fractions of 2.3 Gy) to the volume predicted as being at high risk for a tumor-positive surgical margin (contoured in consultation with the operating surgeon). Acute morbidity was manageable, and 14 patients underwent macroscopic complete tumor

resection. Two recurrences were seen after a median follow-up of 28 months (Tzeng et al. 2006). A retrospective analysis of the recurrence pattern in 33 patients treated with preoperative RT for RPS (GTV plus 1–1.5 cm margin for CTV and another 0.5 cm for PTV) and 32.9 months of median follow-up identified only 4 patients with a local recurrence within the treatment field that theoretically might have been prevented with local dose escalation. Another 12 patients developed a failure outside the PTV or at regional, distant, or a combination of sites. The authors concluded that the approach of dose escalation might be limited, and strategies for appropriate patient selection were needed (McBride et al. 2013). However, 10 of 33 patients in this series additionally had a postoperative I-125 brachytherapy implant at the tumor resection site with a median dose of 77.5 Gy. Thus, it remains unclear how many further local recurrences might have already been prevented by this boost technique.

12.3.3.3 Target Volume Delineation in STS of Other Sites

Soft tissue sarcoma can occur at any site of the body and at all ages. In adults, the limbs (see Sect. 12.3.3.1) and the retroperitoneal space (see Sect. 12.3.3.2) are the most frequent sites of STS, but up to 10 % of tumors may arise each in the head and neck region and the trunk/pelvis. Target volume definition follows the same principles as described for extremity STS. Nevertheless, the growth directions of the tumors might be more complex and have to be considered individually. The margins for definition of the CTV may be shortened in a way just to encompass the surface of uninvolved anatomic barriers like bones or to exclude critical radiosensitive structures. If a combination of surgery and radiotherapy is indicated in STS of the head and neck, the advantages of preoperative radiation therapy (lower doses, smaller treatment volumes, etc.) are particularly valuable. In case of radical tumor resection probably resulting in large defects requiring plastic surgery, again preoperative radiotherapy may be preferred in order to omit irradiation of the transferred flap tissue.

If a radical tumor resection is not feasible because of the tumor site or extent (e.g., large STS of the tongue, extensive angiosarcoma of the face/scalp, etc.), definitive radiation therapy is considered. An example is given in Fig. 12.5. Total doses of 70 Gy or more may be applied, e.g., with shrinking fields, a simultaneous integrated boost technique, or with brachytherapy. For CTV definition of the boost, margins of 2 cm around the GTV are often not feasible and thus substantially reduced, depending on histology, site, organs at risk, and irradiation technique.

12.3.3.4 Target Volume Delineation in Pediatric STS

In children, STS represents the fifth most common tumor group with an incidence of 1/100,000 per year. The most frequent STS histology is rhabdomyosarcoma (RMS), accounting for approximately half of all STS in children. All pediatric sarcoma patients should be treated within prospective interdisciplinary protocols (like the Intergroup Rhabdomyosarcoma Studies (IRS), studies from the Children's Oncology Group in North America, SIOP-MMT studies in Europe, Italian Cooperative Group RMS studies, German Cooperative CWS protocols, etc.) that also guide target volume definitions. In comparison with recommendations for radiotherapy of STS in adults, a reduction of margins and doses seems to be feasible in children (Curtis et al. 2009; Krasin et al. 2010; Wolden et al. 2005; Eaton et al. 2013). Techniques to reduce the integral dose to the body like brachytherapy and particle therapy are of particular value in this age group (Blank et al. 2010; Combs et al. 2012; Cotter et al. 2011; Childs et al. 2012; Laskar et al. 2007; Lee et al. 2005; Timmermann et al. 2007; Viani et al. 2008).

In the Children's Oncology Group D9602 study for low-risk RMS, a cumulative incidence of local/regional failure not higher than 15 % after 5 years was reported. The study included 342 eligible patients, of which 172 received radiotherapy to stage-adapted total doses of 36 Gy, 41.4 Gy, or 50.4 Gy as part of their

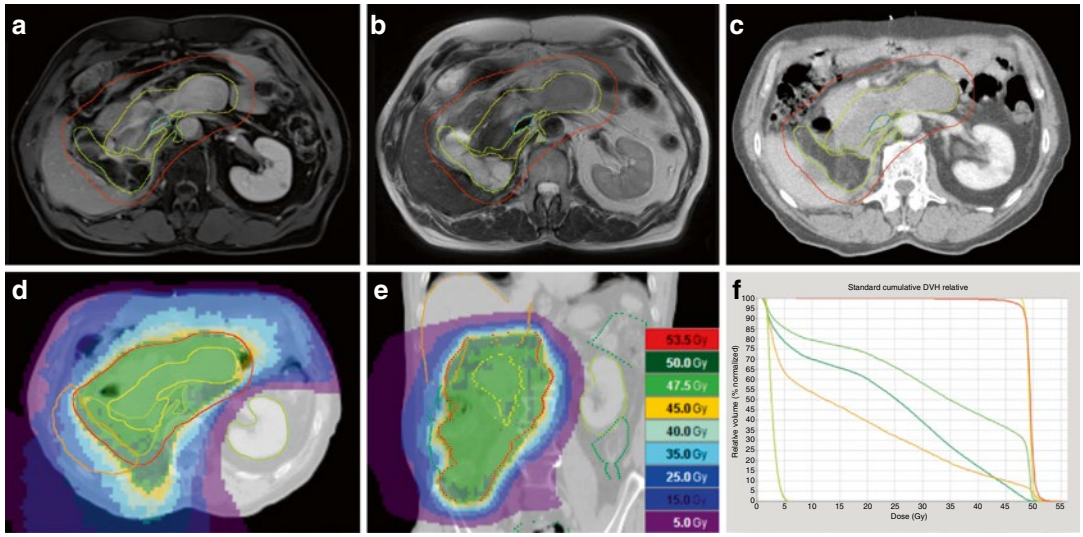

Fig. 12.4 Fourth recurrence of a retroperitoneal liposarcoma (rcT2b N0 M0 ≥ G1) within 8 years in a 74-year-old man having undergone several tumor resections, including right nephrectomy and adrenalectomy, cholecystectomy, right hemicolectomy, and partial resections of involved diaphragm, small bowel, and sigma. (**a**) Axial contrast-enhanced T1-weighted image with fat suppression, showing a bimorphic tumor: a non-lipomatous component in the midline closely related to duodenum and pancreas, displaying high signal intensity due to contrast enhancement (*bright yellow* structure) and a lipomatous (well-differentiated) component (*light yellow* structure) with low signal intensity due to suppression of fat signal, extending from the right liver lobe to the iliac crest. (**b**) Axial T2-weighted image: hypointense signal intensity of the non-lipomatous portion and isointensity to fat of the well-differentiated portion. (**c**) Target volume definition for preoperative radiotherapy to a total dose of 50 Gy in 25 fractions of 2 Gy: GTVs, *yellow* and PTV, *red*, including the non-lipomatous portion of the recurrence plus 1.5 cm margins and the well-differentiated portion with 1.0 cm margins for CTV (not shown), plus a 0.5 cm margin for positioning uncertainty. In the direction of the sole kidney, the margins were locally restricted to a sum of 1.5 cm. Vena cava inferior – *blue* (for alignment purposes of MRI and CT). The hypodense subcapsular liver lesion is a residual known to be caused by trauma. (**d**) Axial and (**e**) coronal view of the dose distribution, optimized for dose sparing of the kidney (tomotherapy planning). (**f**) Dose volume histograms (from right to left): GTV, *yellow*; PTV, *red*; bowel, *green*; bowel outside PTV (subvolume of bowel), *darker green*; liver, beige; and sole kidney, *light green*. Six weeks later, a macroscopic complete resection of the non-lipomatous portion of the recurrence including partial duodenectomy and bowel resections was achieved as well as a debulking of the well-differentiated tumor recurrence. The most recent follow-up 1.5 years after combined treatment showed a stable situation with remnants of well-differentiated tumor

multimodal treatment. The gross tumor was defined as the pretherapeutic extent of tumor, excluding the intra-abdominal or intrathoracic portion that had initially displaced organs but then had vanished under chemotherapy or debulking surgery, letting the organs return to their normal anatomic position. The CTV_{large} was defined as the GTV plus 1.5 cm and included the entire lymph node chain in case of lymph node involvement. The CTV_{boost} beyond a dose of 36 Gy to the primary site was defined as the GTV plus 0.5 cm. Generally, the PTV was defined as the CTV plus an institution-specific margin, which was 0.5 cm in most patients (Breneman et al. 2012).

In the COG 9803 study, for intermediate-risk RMS, again a combined margin of 2 cm around the GTV was used to derive the PTV. The cumulative 5-year failure rate of locoregional control was similar for patients receiving 3D-conformal radiotherapy (3D-CRT) or IMRT with 18 and 15 %, respectively. IMRT improved the target dose coverage compared with 3D-CRT, which according to the authors might become a relevant issue when lowering radiation doses or margins in future studies (Lin et al. 2012). An example of an extensive,

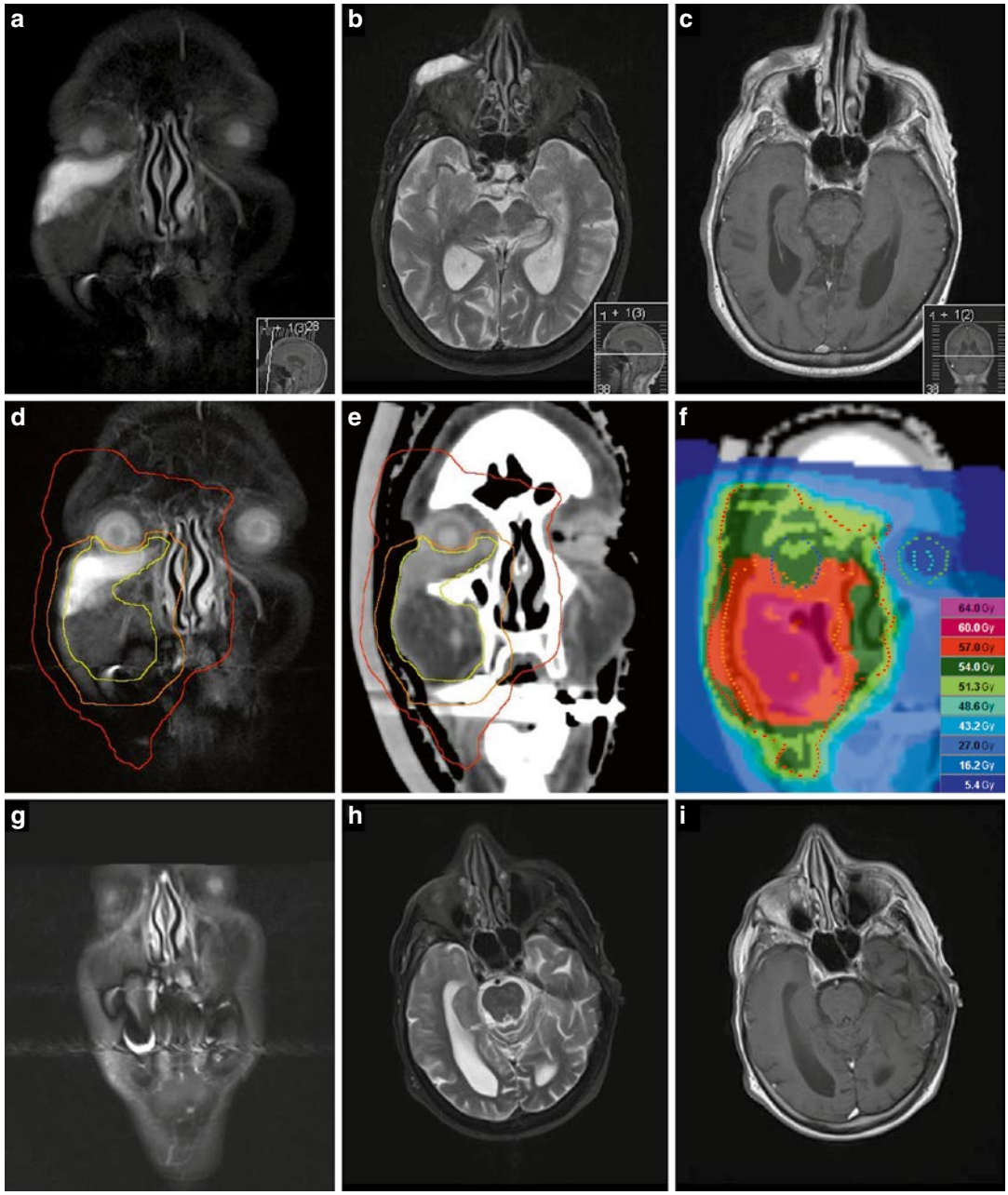

Fig. 12.5 Rapidly growing right midfacial angiosarcoma (cT2b cN1 cMx G3) in a 90-year-old woman. (**a**) Coronal and (**b**) axial STIR image displaying an infraorbital tumor affecting the right lower eyelid and anterior buccal tissue (submandibular lymph node metastasis not shown). (**c**) Axial contrast-enhanced T1-weighted image showing premaxillary tumor tissue with hypointense signal. (**d**) Target volume delineation for definitive (palliative) radiotherapy, visualized on a coronal STIR image and (**e**) in the coronal planning CT reconstruction: GTV, *yellow* (including high-risk buccal tissue); PTV_{SIB}, *orange* (GTV of primary tumor (and affected lymph node, not shown) plus 1 cm margin, shortened in the direction of the eye bulb); and PTV_{large}, *red* (GTV plus 3 cm margin, shortened in the direction of the oral cavity (and submandibular nodal region, not shown)). (**f**) Coronal view of the dose distribution (tomotherapy planning). In fact, 25 of 30 planned fractions of 2.0 Gy to the PTV_{SIB} and of 1.8 Gy to the PTV_{large} of this plan were actually delivered. For the remaining 5 fractions, both target volumes were cranially restricted to just include the lower eyelid in order to spare orbital structures. (**g**) Coronal and (**h**) axial STIR images and (**i**) axial contrast-enhanced T1-weighted image, 6 weeks after radiotherapy, showing nearly complete remission of tumor

irregularly shaped primary tumor not feasible for 3D-CRT but for IMRT is given in Fig. 12.6.

Special attention is given to STS of parameningeal location. In consecutive IRS protocols, target volume definition for parameningeal STS with high risk for meningeal extension changed considerably over time, with inclusion of whole-brain radiation therapy (WBRT) in 1978 (IRS-II), elimination of WBRT for a subgroup of patients in 1987 (IRS-III), and for all patients in 1991 (IRS-IV). The margin around the primary tumor at the skull base was changed from 2 cm in IRS-II to 5 cm in IRS-III and resumed to 2 cm in IRS-IV. In many circumstances, to spare critical surrounding structures, the 2 cm margin had to be smaller to minimize risks of toxicity. The cumulative 5-year failure rate for all 595 eligible parameningeal RMS patients (including 38 % RMS with intracranial extension) was 17 %. No significant differences in the incidence of local failure by protocol era from IRS-II to IRS-IV were detected. Thus, WBRT and larger margins could safely be omitted (Michalski et al. 2004).

In a small series of 17 parameningeal STS patients, including 9 tumors with intracranial extension, radiotherapy to a median prescribed dose of 50.4 Gy (relative biological effectiveness (RBE)) was delivered with protons. The CTV was individually drawn and a margin of 0.75–1 cm added to account for setup uncertainty and penumbra lateral to the beam direction. After a median follow-up of 5 years for survivors, the crude local failure rate was 18 % (3 of 17) and thus comparable to the studies cited above. Rates of late effects from proton radiotherapy compared favorably to reports from photon-treated cohorts (Childs et al. 2012).

In an institutional series of 55 RMS patients including 18 parameningeal tumors, treated between 2000 and 2010, a PTV cone-done boost was applied in 28 patients (51 %) with a median relative reduction in PTV volume of 56 %. The PTV_{large} was based on the pretherapeutic gross tumor ($GTV_{initial}$) with a 0.5–1.5 cm margin to derive the CTV and an additional margin of 0.5–1.0 cm to account for setup uncertainty and target motion. For patients who received a cone-down boost after delivery of 36–41.4 Gy, a PTV_{boost} was created based on residual gross tumor after induction chemotherapy ($GTV_{postCTx}$) with the margins applied accordingly. In total, 5 local failures were observed, all occurring within the high-dose target volumes. Thus, the receipt of a response-based boost in conjunction with delayed RT had no discernible impact on local control in most patients, but allowed for considerable sparing of normal tissue. However, in the subset of patients with parameningeal RMS and intracranial extension, a high rate of leptomeningeal recurrences was observed after application of a cone-down boost, which prompted the authors to advise for wider margin RT for this subgroup (Eaton et al. 2013).

12.3.3.5 Target Volume Delineation in Metastatic Sites of STS

There is some evidence that treating metastatic sites of RMS with curative doses of radiotherapy might be beneficial. In a group of 13 *children*, including 8 RMS patients and 5 with Ewing sarcoma, radiotherapy to total doses above 40 Gy in each metastatic site led to an actuarial local control rate of 92 % after 5 years. Overall survival was 35 % at 5 years (Liu et al. 2011).

In our practice, metastatic sites of RMS (and Ewing sarcoma) in children are treated with a simultaneous integrated boost (SIB) technique (see Fig. 12.6 and also Fig. 12.14 in Sect. 12.6). The PTV_{large} is defined as the visible GTV including edema plus a 0.5 cm margin for the CTV_{large} and another 0.5 cm margin for positioning inaccuracies. In vertebral metastasis, the whole affected vertebra is included in the CTV_{large}; in a long bone, its full thickness at the affected level; and in lymph node metastasis, the affected nodal region. For the PTV_{large}, a total dose of 45 Gy in fractions of 1.8 Gy is prescribed. A simultaneous integrated boost (SIB) to a total dose of 50 Gy in fractions of 2.0 Gy is applied to a PTV_{boost}, encompassing the GTV plus a 0.5 cm margin.

Metastatic sites of soft tissue sarcoma *in adults* might be treated by radiosurgery or hypofractionated stereotactic radiotherapy, applying the established concepts of treatment for intracranial, pulmonal, hepatic, or osseous metastases. Review of 21 sarcoma patients treated with radiosurgery to a marginal dose of 16 Gy in 60 cerebral lesions resulted in a local control rate of 88 %. The median survival after diagnosis of

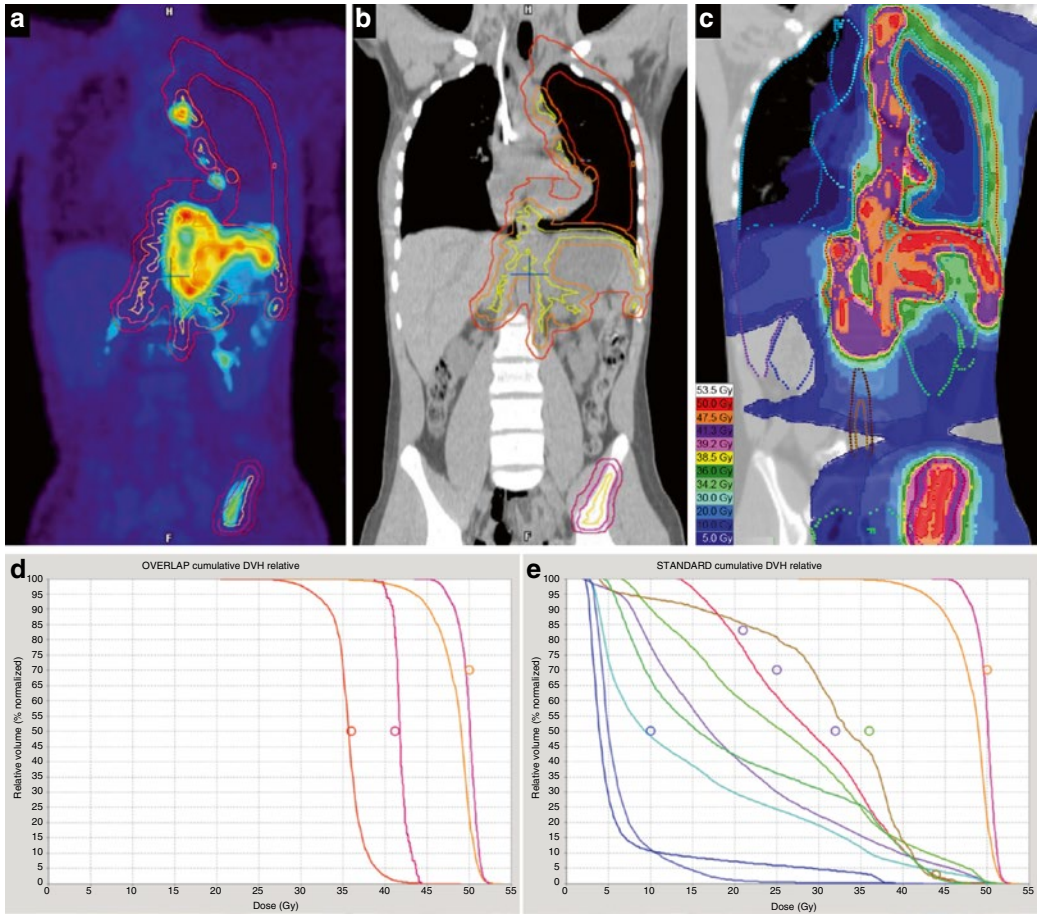

Fig. 12.6 Stage IV alveolar rhabdomyosarcoma cT2b cN1 cM1 (LYM, PLE, OSS) G3 in a 16-year-old boy. The main tumor mass is located in the posterior mediastinum and midline upper abdomen (axial width 11 cm) with infiltration of the diaphragm, the neuroforamen Th11/12, several lymph node metastases at the mediastinum, the paraaortal and truncal region, and the internal mammarian chain, diffuse pleural involvement on the left side with numerous nodular tumor deposits and pleural effusion, peritoneal tumor nodules contacting the spleen, and left iliac bone metastasis. (**a**) Pretherapeutic FDG-PET, coronal view, showing elevated glucose uptake of primary tumor and metastatic sites. (**b**) Target volume delineation for definitive radiotherapy of all tumor sites after good response to four cycles of chemotherapy according to CWS-guidance protocol (complete remission), coronal planning CT reconstruction: GTV1, *yellow* (thoracoabdominal tissue contacting the initial tumor/metastases or residual lesions); GTV2, *yellow* (extent of initial tumor in the left iliac bone); $PTV1_{SIB50Gy}$, *orange* (GTV1 plus 0.5 cm margin); $PTV2_{SIB50Gy}$, *pink* (GTV in left iliac bone plus 0.5 cm margin) to a total dose of 50 Gy in 25 fractions of 2.0 Gy; $PTV2_{large\ 41.4Gy}$, *purple* (GTV2 in left iliac bone plus 1 cm margin) to a total dose of 41.25 Gy in fractions of 1.65 Gy; and $PTV1_{large36Gy}$, *red* (GTV1 plus 0.5 cm margin without lung tissue for CTV1, plus another 0.5 cm margin for positioning uncertainty, including on the left side the whole parietal pleura, diaphragm, and peritoneal surfaces of high risk plus 1 cm margin, restricted to 0.5 cm into the left kidney) to a total dose of 36 Gy in fractions of 1.44 Gy). (**c**) Coronal view of the dose distribution (tomotherapy planning), including pleural irradiation on the left side. Irradiation time per fraction was 17.5 min. (**d**) Dose volume histograms for target volumes displayed in "overlap mode," showing exclusively those parts of target volumes not included in others of higher planning priority (right to left): $PTV2_{SIB50Gy}$, *pink*; $PTV1_{SIB50Gy}$, *orange*; $PTV2_{large\ 41.4Gy}$, *purple*; and $PTV1_{large36Gy}$, *red*. (**e**) Dose volume histograms displayed in "standard mode" for $PTV2_{SIB50Gy}$, *pink*, and $PTV1_{SIB50Gy}$, *orange*, and the following OARs (right to left on the level of median dose): spinal cord, *brown* (maximal dose (D_{max}) 50 Gy); left ventricle of heart, *red* (mean heart dose (D_{mean}) 26 Gy, volume receiving 40 Gy (V_{40Gy}) 9 %); left lung, *green* (V_{20Gy} 62 %, V_{30Gy} 40 %, D_{mean} 26 Gy); liver, *violet* (V_{30Gy} 22 %); left kidney, *darker green* (V_{18Gy} 45 %); whole lung, *pale blue* (D_{mean} 15.6 Gy); right lung, *blue* (D_{mean} 6.3 Gy); and right kidney, *dark blue* (V_{18Gy} 8 %). The radiation therapy was delivered simultaneously to the 5th and 6th cycle of chemotherapy (dosage of substances reduced to 67 %) in a split-course manner with a planned break of 2 weeks after the 13th fraction and transplantation of autologous stem cells after both cycles. After additional high-dose chemotherapy and allogeneic transplantation, the patient is disease free and in good performance status. Late effects of radiation therapy do not exceed grade I° according to RTOG/EORTC (last follow-up so far 2.4 years after diagnosis)

intracranial metastasis was 16 months (Flannery et al. 2010). In a series of 52 patients with multimodality treatment of their lung metastases of STS, including 15 patients and 74 lesions treated with extracranial stereotactic radiotherapy between 1990 and 2006 (preferred concept of 50 Gy total dose in 5 fractions), actuarial local control at 5 years was 82 %. Median overall survival was 2.1 years for patients receiving stereotactic radiotherapy and 0.6 years for those who never received it ($p = 0.002$) (Dhakal et al. 2012). After stereotactic radiotherapy to spinal metastases in 58 patients with 65 lesions, isolated local failure of the unirradiated adjacent vertebral bodies occurred in 3 % (Klish et al. 2011). Thus, restricting the PTV to the affected vertebral level seems to be safe.

In bone metastases of STS amenable to stereotactic radiotherapy, we adopted the concept of 5 fractions of 6 Gy to the PTV_{large} (definition as stated above for metastatic sites in children) with a simultaneous integrated boost (SIB) of 8 Gy per fraction to the GTV plus a 0.5 cm margin (PTV_{boost}).

For larger STS metastasis of any site not suitable for stereotactic radiotherapy, a hypofractionated concept aiming at local control is offered with 22 fractions of 2.0 Gy to the PTV_{large} and of 2.5 Gy to the PTV_{boost} as defined above, with an optional SIB2 of 2.7 Gy to the GTV(= PTV_{boost2}), resulting in nominal total doses of 44 Gy, 55 Gy, and – if applicable without additional risk – 59.4 Gy, respectively. An example is given in Fig. 12.7. Target volume definition is generally based on image fusion of planning CT with diagnostic MRI and treatment delivered with IMRT and daily image guidance.

For palliative treatment of STS metastases, hypofractionated treatment with single doses of 3 Gy to a total dose of, e.g., 39 Gy may be offered safely (Soyfer et al. 2010).

12.4 Desmoid-Type Fibromatosis

12.4.1 Anatomy and Histopathology

Desmoid-type fibromatosis is a locally aggressive (myo)fibroblastic neoplasm that usually arises in deep soft tissues. According to the WHO classification 2013, it is a soft tissue tumor of borderline malignancy due to locally aggressive growth with a high tendency toward local recurrence, but lacks metastatic potential. Mesenteric fibromatosis may be associated with Gardner-type familial adenomatous polyposis (FAP). The pathogenesis of sporadic lesions is thought to be multifactorial, with trauma (e.g., from surgery) and endocrine changes (e.g., gestation) playing a role. Abdominal fibromatosis may arise from the musculoaponeurotic structures of the abdominal wall (e.g., rectus or internal oblique muscles) or intra-abdominally in the mesentery or pelvis. Extra-abdominal fibromatosis can occur at any anatomical site; predilection sites are the shoulder, chest wall, back, thigh, and the head and neck region. The macroscopic aspect resembles scar tissue. Histopathologically, the lesions are typically poorly circumscribed with infiltration of the surrounding soft tissue structures. There is a spindle cell proliferation (fibroblasts or myofibroblasts with low mitotic activity and without cytological atypia) in a collagenous stroma, arranged into ill-defined long fascicles, containing prominent blood vessels and sometimes perivascular edema (see Fig. 12.8). Especially in mesenteric or pelvic lesions, myxoid change may be found (Goldblum and Fletcher 2013).

12.4.2 Imaging in Desmoid-Type Fibromatosis

MRI represents the imaging modality of choice in desmoid-type fibromatosis. For imaging of abdominal fibromatosis, computed tomography still has its role and MRI can be used supplementarily. The intermuscularly located lesions usually exhibit predominantly low signal intensity on T1-weighted MR images and show considerable contrast enhancement (see Fig. 12.9a, b). On T2-weighted images, the signal intensity may vary interlesionally and intralesionally, depending on the extent and distribution of collagen deposits and more cellular areas. Dense areas of collagen typically present as band-like areas of low signal intensity. High T2-weighted signal intensity was found to be associated with a higher contrast enhancement ratio, suggesting that this might reflect greater cellularity and

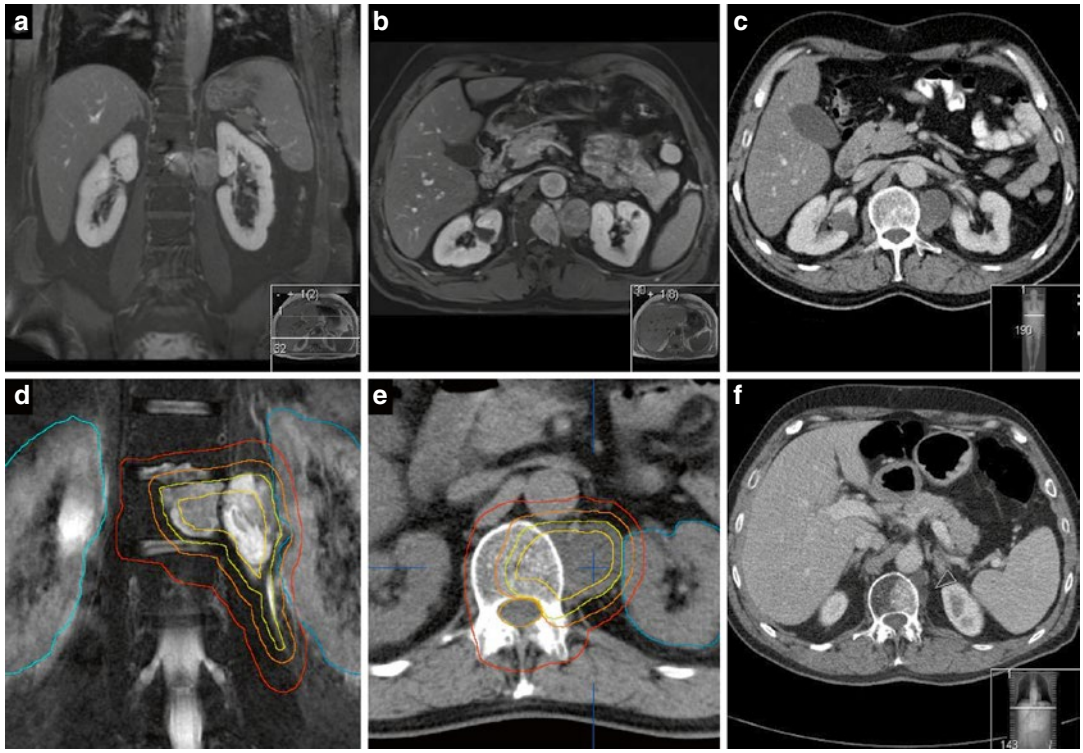

Fig. 12.7 Osseous metastasis of a liposarcoma in the first lumbar vertebra with soft tissue extension into the left psoas muscle (and a further lesion each to the left iliac bone and to the proximal femur, not shown) in a 55-year-old man, 10 years after R0 resection with intra- and postoperative radiotherapy of a 21-cm-sized primary of the left thigh and 2 years after R1 resection and postoperative radiotherapy of a 12-cm-sized sternal metastasis. (**a**) Coronal and (**b**) axial contrast-enhanced T1-weighted MR image displaying the intraosseous and extraosseous portion of the lumbar metastasis with elevated signal intensity compared to unaffected vertebral body and muscle signaling. (**c**) Axial CT image at the level of the affected vertebra, subtle morphological changes in the vertebral body, hypodensity, and enlargement of the left psoas muscle. (**d**) Target volume definition for definitive radiotherapy in a simultaneous integrated boost technique, visualized on a coronal STIR image and (**e**) in the axial planning CT: GTV, *pale yellow* (including soft tissue mass at the level L1-2 and fascial involvement of psoas muscle down to the level L3); PTV_{SIB1}, *orange* (GTV plus 0.5 cm margin, without spinal canal) to a total dose of 55 Gy in 22 fractions of 2.5 Gy; and PTV_{large}, *red* (GTV plus 1 cm margin in axial, 1.5 cm in cranial and 2.0 cm in caudal directions, including the whole affected vertebral body plus 1 cm margin, reduced in the direction of the right kidney) to a total dose of 44 Gy in fractions of 2.0 Gy. PTV_{SIB2} – inner *yellow* contour (GTV with a negative margin of 0.5 cm, minimal distance to spinal canal 1.0 cm) to a prescribed total dose of 59.4 Gy in fractions of 2.7 Gy. (A similar concept was used for radiation treatment of the metastatic sites in the pelvis, not shown.) The maximum point dose in the spinal canal was restricted to 51.5 Gy. The average dose (D_{mean}) to the left and right kidney was 17.9 and 8.2 Gy, the volume receiving 18 Gy or more (V_{18Gy}) 32.5 and 5 %, respectively. (**f**) Contrast-enhanced CT image 1 year after definitive radiation treatment: complete remission with recalcification of the vertebral lesion and shrinkage of the soft tissue extension in the left psoas muscle (*arrow*). No deterioration of renal function parameters

vascularization of a potentially aggressive desmoid tumor (Sinha et al. 2012). Usually, the margins of the lesion are ill defined, reflecting the diffuse infiltration of neighboring tissues. Streaks of high signal intensity in fat-suppressed, contrast-enhanced T1-weighted images or inversion recovery T2 images may exceed the main tumor mass by several centimeters and may indicate the extent of fascial involvement or direction of growth.

12.4.3 Target Volume Delineation in Desmoid-Type Fibromatosis

Local recurrences are common after surgical resection alone, as a histological complete resection is difficult to achieve or would require mutilating surgery with gross functional deficits in individual cases. In a review of 22 publications on treatment of extra-abdominal fibromatosis, the 5-year local control rate was 72 % in case of complete tumor resections (R0) and 41 % in case of tumor-involved surgical margins (R1), whereas rates of 94 and 75 % were reported for a combined treatment with postoperative radiotherapy, respectively. Radiotherapy alone was more effective than surgery alone with control rates of 78 % versus 61 % (Nuyttens et al. 2000). The treatment of recurrences results in higher recurrence rates than treatment of newly diagnosed tumors (Zlotecki et al. 2002), and reported doses vary between 50 and 60 Gy with conflicting data on the issue, whether or not doses above 56 Gy are of further benefit (Gluck et al. 2011; Guadagnolo et al. 2008; Micke and Seegenschmiedt 2005; Rutenberg et al. 2011; Zlotecki et al. 2002).

As spontaneous arrest of the growth was found in approximately 50 % of patients during follow-up with either medical therapy or no therapy at all, modern management of desmoid-type fibromatosis aims for a conservative approach whenever possible, including pharmacotherapy like tamoxifen or imatinib (Bonvalot et al. 2012). In growing tumors, surgery aims for complete resection. Nevertheless, in a substantial percentage of cases, the final resection margins are very close or positive, in which case, additive radiotherapy is indicated (Baumert et al. 2007; Mullen et al. 2012). Irresectable tumors might be referred for definitive radiotherapy; an example is given in Fig. 12.9.

Given the rarity of the disease, details for target volume delineation are sparse, apart from the general advice for generous margins and the risk of failure at the edges of the radiation fields (Zlotecki et al. 2002; Gluck et al. 2011).

In a series of 65 patients treated with postoperative or definitive radiotherapy at the University of Florida between 1970 and 2000, RT portals encompassed the full tumor extent and/or the entire operative bed with the addition of generous, 5–10 cm, margins. After a median total dose of 54 Gy, 11 local failures occurred, two within the RT fields and nine at a margin of the RT field. The authors recommend to choose the size of irradiation ports large enough to cover the tumor bed and the full extent of all operative fields with sufficient margins to cover potential fibromatosis infiltration along the paths of the neurovascular bundles, fascial planes, and other potential paths of least resistance (Zlotecki et al. 2002).

Of 68 patients with radiotherapy for desmoid-type fibromatosis included in a study of a European rare cancer network, 17 developed a recurrence. Eleven recurrences (65 %) occurred at the field border or in areas of the target volume receiving less than 50 Gy of total dose. Thus, the authors supported the recommendation to add wide radiation field margins of at least 5 cm around the tumor or the surgical bed in the direction of possible infiltrative growth (Baumert et al. 2007).

In the series of 115 patients treated at the MD Anderson Cancer Center between 1965 and 2005, radiation portal margins were retrospectively calculated as one half of the difference between the maximal tumor dimension and the largest portal dimension, resulting in values <5 cm in 33 %, 5–7 cm in 22 %, and >7 cm in 44 %. The local control rates after 10 years for the three groups were 66, 88, and 73 %, showing no statistically significant difference. Similar values for local control were found regarding subgroups of patients with and without surgery. The current clinical practice at this institution at the time of publication was to include the surgical bed with a 5–7 cm margin to a dose of 50 Gy in case of marginal tumor resection. For gross disease, treatment of gross tumor volume plus 5–7 cm margins to a dose of 50 Gy was recommended, to be followed by a boost to the GTV with 2–3 cm margins to a cumulative dose of 56 Gy (Guadagnolo et al. 2008).

A series of 31 patients from a single institution was managed with a combination of tumor resection and intraoperative electron irradiation (IOERT) to a median dose of 12 Gy, followed by

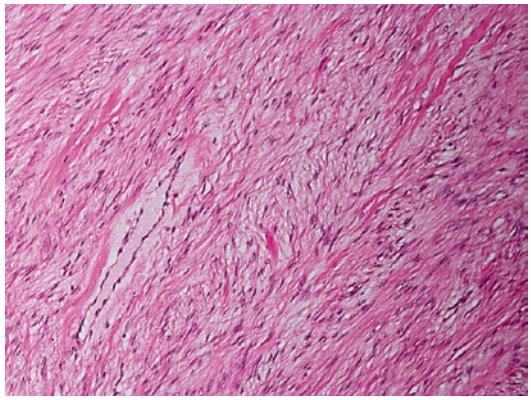

Fig. 12.8 Fibromatosis. Fascicles of bland spindle cells separated by collagen

fractionated postoperative external-beam radiotherapy (EBRT) to a median dose 45 Gy. The IOERT boost was intended to cover the surgical bed with a margin of 1 cm as visually defined in correspondence with the surgeon. In fact, the median applicator size was 9 cm (range 5–14 cm), whereas the reported median tumor size was 9 cm as well (range 4–25 cm). The EBRT target volume included the surgical bed (and macroscopically residual tumor, if present), with a safety margin of 5–7 cm. After a median follow-up of 32 months, 5 recurrences were noted, classified as in-field IOERT in three, in-field EBRT in one, and at the border of the EBRT field in one case. The estimated 5-year local control for the whole group was 73 % and within the IORT-field 82 %, respectively (Roeder et al. 2010).

In our institution, the general principles of sarcoma treatment are applied (see above). Apart from the main tumor mass, we include all streaky changes of high MRI signal intensity in contrast-enhanced, fat-suppressed T1-weighted images and in STIR images into the GTV. Definitive radiotherapy is applied in IMRT technique with a simultaneous integrated boost concept and daily image guidance (see Fig. 12.9). The boost volume, consisting of the GTV plus a 0.5 cm margin to derive the CTV_{boost} and another 0.5 cm margin to derive the PTV_{boost}, is treated to a total dose of 60 Gy with single fractions of 2.0 Gy. The CTV_{large} considers the GTV with margins of 1.5–4.5 cm, depending on the anatomical site and the directions of growth. The PTV_{large}, including the CTV_{large} plus a 0.5 cm margin, is to be treated to a total dose of 54 Gy with single fractions of 1.8 Gy. The 2–4.5 cm margins are applied in the directions of suspected tumor growth, i.e., along the fascial planes and neurovascular bundles, and the smaller 1.5–2 cm margins in the direction perpendicular to these planes. In case of tumor adherence to bone, a maximal slice of 1 cm thickness of the bone is included in the PTV_{large}.

In the postoperative setting, apart from reconstructing the contact zones of the removed tumor mass, all manipulated tissue from previous tumor resections including scars are identified and in our practice included in the "GTVpostop." Applying the margins as described above, the PTV_{large} is derived. Drainage sites are at least included in the CTV_{large} with 0.5 cm margins. In case of microscopically involved resection margins (R1 resection), treatment of a boost volume based on the contact zones of the resected tumor and the resection cavity with 1 cm margins is discussed individually. In case of localized macroscopic residual tumor (R2 resection), a boost volume is treated to a total dose of 60 Gy, consisting at least of the residual tumor plus a 1 cm margin.

12.5 Osteosarcoma

12.5.1 Anatomy and Histopathology

Bone tumors account for less than 0.2 % of all malignant tumors. The annual incidence of osteosarcoma (OS) is approximately 0.2–0.3/100,000 with a peak incidence of 0.8–1.1/100,000 in the age group 15–19 years and a smaller peak in older adults (0.4/100,000 for people aged ≥60 years). The vast majority of osteosarcomas arise in the long bones of the extremities, especially in the distal femur (30 %), proximal tibia (15 %), and proximal humerus (15 %), i.e., the sites of the most proliferative growth plates. In long bones, the metaphysis is the predilection site with 90 %. In adolescents, up to 70 % of tumors are located around the knee. Tumors of the axial or craniofacial skeleton are primarily observed in adults.

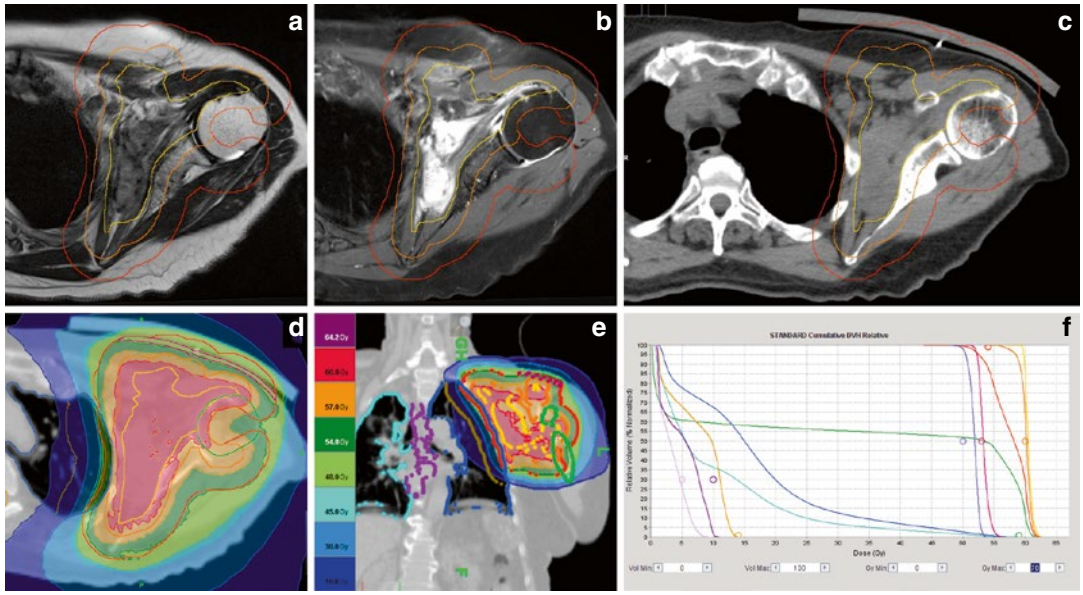

Fig. 12.9 Desmoid-type fibromatosis of the left axilla, affecting the subscapularis, the anterior serratus, and the supraspinatus muscle in a 70-year-old woman. Target volume delineation for definitive radiotherapy visualized (**a**) on an axial T2-weighted image showing an ill-defined mass of low signal intensity and (**b**) elevated signal intensity on a contrast-enhanced T1-weighted image with fat suppression. Note typical MR morphology with band-like areas of low signal intensity on T2-weighted as well as contrast-enhanced T1-weighted image. (**c**) Planning CT: GTV – *yellow*, including all visible extensions along the involved muscles and ventral capsule of the shoulder joint. PTV_{SIB}, *orange* (GTV plus 1 cm margin, excluding lung tissue) to a total dose of 60 Gy in 30 fractions of 2 Gy, and PTV_{large}, *red* (GTV plus 2.5 cm margin, but not beyond 0.5 cm into lung tissue and 0.8 cm into humerus or air. (**d**) Axial and (**e**) coronal view of dose distribution (tomotherapy planning). (**f**) Dose volume histograms for target volumes and OARs (right to left): GTV, *yellow*; PTV_{SIB}, *orange*, dose to 95 % of this volume ($D_{95\%}$) 58.4 Gy; PTV_{large}, *red* (including the SIB-volume); PTVlarge-in-skin, *dark red* (subvolume of PTV_{large} intersecting with a 0.3 cm interior wall of the body); $PTV_{large\text{-}in\text{-}air}$, *violet* (subvolume of PTV_{large} outside the body); humerus, *green*; left lung, *dark blue* (volume receiving 20 Gy or more (V_{20Gy}) 30 %, V_{30Gy} 12.6 %, mean dose (D_{mean}) 16.5 Gy); subvolume of left lung used for lung-sparing optimization, beige; whole lung, *light blue* (D_{mean} 10.5 Gy); esophagus, *violet*; and right lung, *light pink*. During the following year, repetitive MR imaging revealed slow but steady reduction of tumor size and contrast enhancement

For primary osteosarcomas, i.e., in cases of normal underlying bone, different genetic syndromes such as Li-Fraumeni, hereditary retinoblastoma, and others are predisposing conditions. Secondary osteosarcoma can occur after previous radiotherapy (2.7–5.5 % of all osteosarcomas are radiation induced), after transformation in Paget's disease of the bone, or rarely in the context of bone infarction or benign tumors (fibrous dysplasia), all typically affecting older patients.

Histopathologically, most high-grade osteosarcomas are conventional osteosarcomas, subclassified according to the predominant matrix into osteoblastic OS (76–80 %), chondroblastic OS (10–13 %), fibroblastic OS (10 %), or other rare histological subtypes. Less common are telangiectatic OS (<4 % of all osteosarcoma), small cell OS (1.5 %), or high-grade surface OS (<1 %). Conventional osteosarcoma has a broad morphologic spectrum and grows permeatively, replacing the marrow space, eroding preexisting trabeculae, and expanding haversian systems. An essential component for the diagnosis of OS is the presence of neoplastic bone or unmineralized matrix (osteoid). In osteoblastic OS, the principal matrix is neoplastic bone with variation between thin trabeculae to compact bone (see Fig. 12.10). In chondroblastic OS, the neoplastic cartilage is usually hyaline, but may be myxoid (e.g., in tumors of the jaw). The cartilage may be the

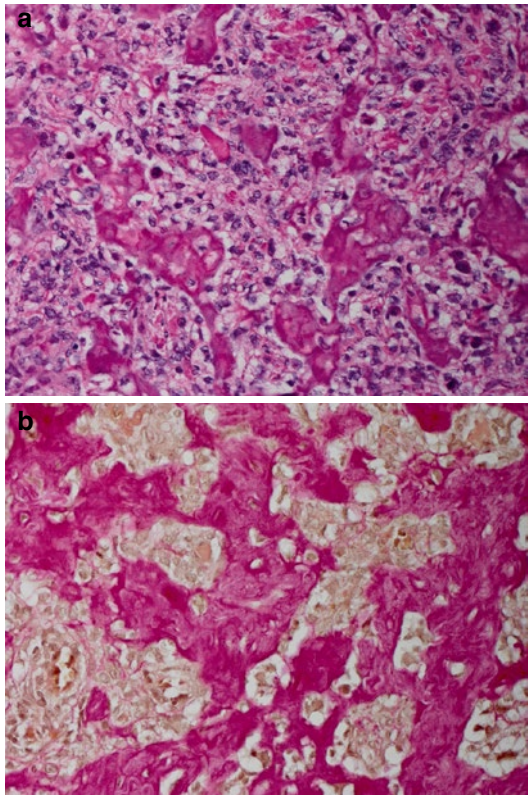

Fig. 12.10 Osteoblastic osteosarcoma, high grade, G3. Trabeculae of immature bone ("osteoid") are produced by anaplastic tumor cells. (**a**) H&E and (**b**) van Gieson stains

dominating component over neoplastic bone. In fibroblastic OS, the tumor cells are often spindled with severe atypia and associated with extracellular collagen. Conventional OS typically arises in the medullary cavity of the metaphysis with ultimate destruction of the cortex, circumferential extraosseous soft tissue formation, and displacement of the periosteum (Fletcher et al 2013).

12.5.2 Imaging in Osteosarcoma

On conventional radiographs, osteosarcoma typically shows a geographic growth pattern of moth-eaten or permeative bone destruction. Mineralized tumor matrix can produce "cloud-like" or "ivory-like" areas of increased radiodensity which occurs in combination with lytic portions. Exclusively blastic or lytic lesions are rare. The tumor usually destroys the bony cortex and causes an interrupted or complex periosteal reaction in 90 % of the cases. Osteoblastic osteosarcomas can be associated with radiating spicules of periosteal bone formation giving the lesion a "sunburst" appearance.

CT can visualize the destruction of cancellous and cortical bone, bone sclerosis, matrix mineralizations, and the extraosseous tumor component (see Fig. 12.11a). Its ability to define the exact intraosseous extent of the lesion is however limited.

MRI represents the most advantageous imaging modality for local staging. The intraosseous tumor extent is best visualized on T1-weighted pulse sequences orientated along the long axis and covering the entire affected bone. Tumor tissue causes complete bone marrow replacement with a signal intensity that is at least as low as that of normal muscle tissue. Intraosseous tumor can thus be distinguished from reactive edema which might obscure the tumor margins on T2-weighted or contrast-enhanced images.

The extraosseous tumor component is usually best displayed on short-axis T2-weighted or contrast-enhanced T1-weighted sequences. Osteosarcomas can show various signal intensities on T1- as well as T2-weighted images dependent on their histologic composition/subtype. On T2-weighted images, areas of low signal intensity are more likely to represent osteoblastic or fibroblastic components (see Fig. 12.11b), whereas areas of high signal intensity might correspond to chondroblastic or telangiectatic elements. Paraneoplastic edema is of high signal intensity on T2-weighted and STIR sequences. With a high level of confidence, MRI allows for the diagnosis of tumor involvement of the epiphysis or the adjacent joint as well as neurovascular encasement. The tumor may be highly vascularized with an erratic pattern of neoplastic vessels (Freyschmidt et al. 2010).

12.5.3 Target Volume Delineation in Osteosarcoma

Osteosarcoma of low-grade (central OS, parosteal OS) and of intermediate-grade malignancy

(periosteal/chondroblastic OS) has a good prognosis with overall survival rates of 85–90 % after surgical resection alone with wide margins. In high-grade osteosarcomas, the combination of chemotherapy (active substances: doxorubicin, cisplatin, high-dose methotrexate, ifosfamide) and surgery leads to a disease-free survival rate of >60 %, whereas surgery alone is associated with a DFS of only 10–20 %.

Generally, patients should be treated in prospective trials. Even in metastatic osteosarcoma, 30 % long-term survival can be achieved if treated as aggressively as primary tumors. If (secondary) resection of all metastatic sites is possible, a long-term survival of 40 % is possible. In case of recurrence, long-term survival drops below 20 %. Substances like ifosfamide, etoposide, and carboplatin are under discussion for second-line chemotherapy, but there is a consensus that again local therapy (attempt of complete removal of all tumor manifestations) is of utmost importance for cure.

Currently, the indication for radiotherapy is reserved for individual cases of marginal or incomplete tumor resection or definitive treatment of irresectable tumors. Adjuvant/additive radiotherapy may be applied preoperatively in order to increase the chance of resectability or postoperatively in order to improve local control in case of close or positive resection margins. An example is given in Fig. 12.11. Classifying a lesion as unresectable should include a central assessment from a reference surgeon before planning definitive radiotherapy. This may apply to primary tumors as well as to metastatic lesions or recurrences.

Within the COSS (Cooperative Osteosarcoma Study Group) protocol, total doses of 54–60 Gy are recommended for preoperative radiotherapy and at least 60 Gy, or better ≥70 Gy, for postoperative and definitive radiotherapy. Because of the high doses necessary to control the tumor, advanced techniques like IMRT/IGRT and other high-precision techniques are helpful to spare dose to organs at risk and to increase the chance of uncomplicated cure. If feasible, patients should be included into studies elucidating the role of hadron therapy like protons or carbon ions, namely, for osteosarcoma of axial site.

Preliminary experience with helium and/or neon ions in 17 patients with bone sarcomas of the axial site was reported from Berkeley. Fifteen patients presented with gross tumor; six were treated for recurrent tumors. MRT was integrated into the planning process as soon as available. After total dose of 52–76 Gy (relative biological effectiveness (RBE)), mean 64 Gy (RBE), with variation in dose per fraction from 2.0 to 3.0 Gy (RBE), the local control rate after 5 years was 48 % for all 17 patients and 53 % for 13 patients with osteosarcoma. The 5-year overall survival rate was 41 % (Uhl et al. 1992).

In a series of 41 osteosarcoma patients treated with additive or definitive radiotherapy at the MGH in Boston between 1980 and 2002, 23 had parts of their total dose delivered with protons (10–80 Gy (RBE), median 66 Gy (RBE)) for critical tumor sites like the skull base, paranasal, sinuses, and spine. The local control rate according to the extent of resection was 78 % for gross total or subtotal resection and 40 % for biopsy only, respectively. The corresponding overall survival rate was 74 and 25 %, respectively. Patients with spinal, pelvic, recurrent extremity, and trunk lesions were treated with 20 Gy preoperatively followed by completion of RT postoperatively. For target volume definition, the CTV_{large} encompassed the tumor plus 2 cm margins. The surgical scars were included in the postoperative RT if no preoperative radiotherapy was applied and the resulting field was not impracticably large. The CTV_{boost} would include the tumor plus a 1 cm margin, which was tightened for sparing critical organs at risk like the spinal cord, brain, and optic structures. In case of R0 resection, 55–60 Gy was administered, 60–68 Gy for R1 resections, and ≥68 Gy for gross disease (DeLaney et al. 2005).

Schwarz et al. evaluated the role of radiotherapy in osteosarcoma from the experience in 100 patients included in the COSS registry between 1980 and 2007. The calculated local control rates were 40 % in 66 primary tumors and 17 % in 11 local recurrences, whereas none of the 23 cases of metastatic disease could ultimately be controlled. Local control rates for combined surgery and RT were significantly better than those for RT alone (48 % versus 22 %). Overall survival

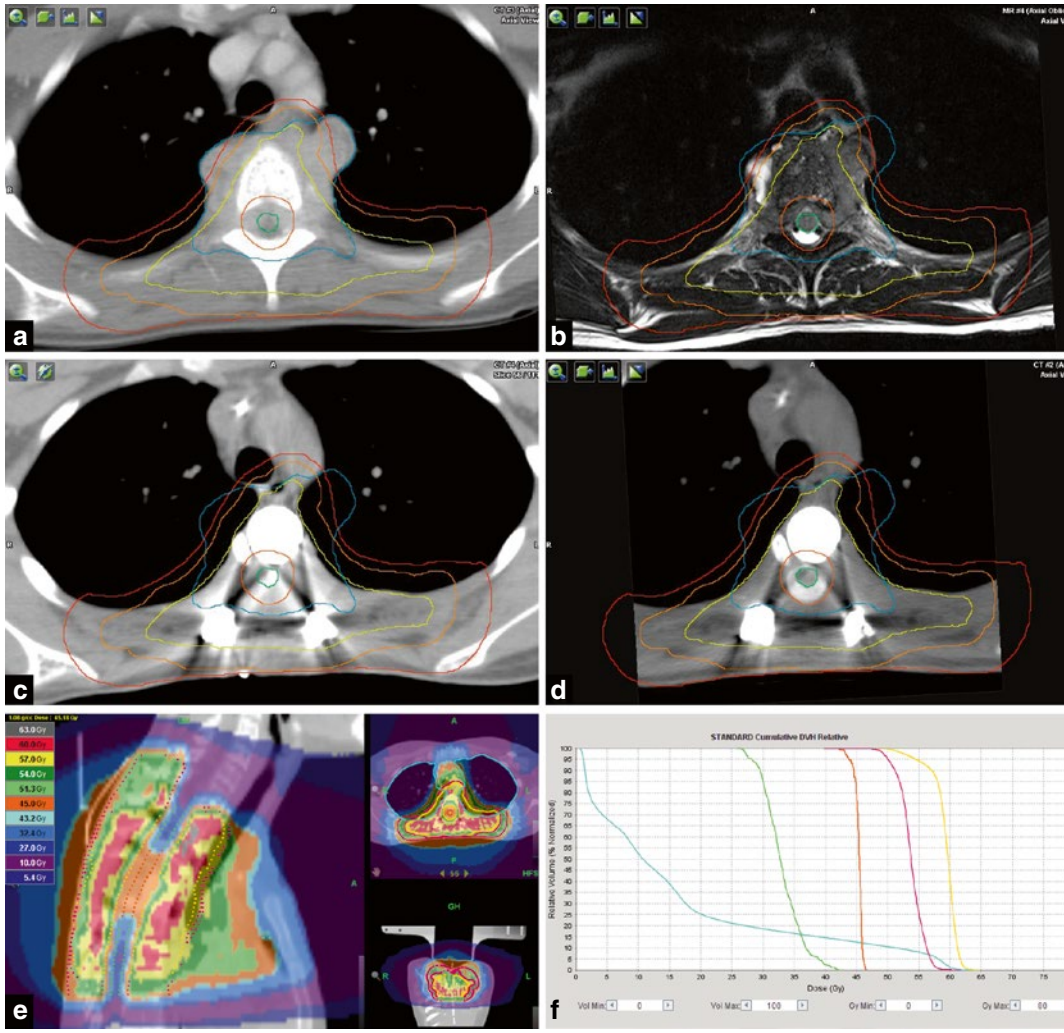

Fig. 12.11 Osseous metastasis of a high-grade osteosarcoma affecting the 4th thoracic vertebra in a 19-year-old woman, 3 years after multimodal curative treatment of the primary in the left distal femur. (**a**) Pretreatment diagnostic CT: eburnation of the vertebral body and spiculated periostal reaction, large extraosseous paravertebral tumor component. (**b**) T2-weighted MR image displaying an inhomogeneous tumor mass of low signal intensity, contacting anteriorly the esophagus, aorta, and origin of left subclavian artery, bilaterally the pleura and protruding into the spinal canal. In order to release beginning paraplegia, sensory deficits, and pain, gross tumor resection was performed, proving tumor infiltration of the mediastinum, bilateral pleura, and vertebral ligaments extending just to involve level Th3 and Th5 (R1 resection). The resected vertebral body was reconstructed with a titanium cage, and the spine surgically stabilized from Th2 to Th6. Second-line chemotherapy (carboplatin, etoposide) was initiated and additive radiation therapy planned to be given simultaneously to the 3rd and 4th cycle. (**c**) Planning CT displaying the postoperative situation with artifacts due to stabilization material. For contouring and planning, an MV-CT was registered as well as (**d**) a myelo-CT for exact delineation of the spinal cord – *green*. Target volume delineation was based on the $GTV_{contact/postop}$, *yellow* (tissue contacting the initial tumor, the resection cavity and surgically manipulated tissue), rather than on the $GTV_{initial}$, *blue* (tumor mass at diagnosis). PTV_{SIB}, *orange* ($GTV_{contact/postop}$ plus 1 cm margin, restricted to 0.5 cm into lung and mediastinal tissues and to a distance of 0.6 cm to the spinal cord) with a prescribed total dose of 60 Gy in 30 fractions of 2 Gy, and PTV_{large}, *red* ($GTV_{contact/postop}$ plus a 2 cm margin, restricted to 1 cm into lung and mediastinal tissues and to a distance of 0.6 cm to the spinal cord) with a prescribed total dose of 54 Gy in fractions of 1.8 Gy. (**e**) Sagittal view of the dose distribution (tomotherapy planning). At the level of tumor initially contacting the spinal cord (lower part of Th3 to upper part of Th5), a total dose of 45 Gy (*orange*) is prescribed, with maximal myelon sparing above and below. (**f**) Dose volume histograms: $PTV_{SIB60Gy}$, *yellow*; $PTV_{large54Gy}$, *red*; spinal cord at high risk (Th3-5), *orange*; spinal cord beyond high-risk level, *green*; and whole lung, *blue*. The maximal dose at a distance of 0.3 cm to the spinal cord was 50.2 Gy and at a distance of 0.6 cm 58.0 Gy, respectively

rates were 55 % for RT of the primary, 15 % for recurrences, and 0 % for metastatic disease, respectively (Schwarz et al. 2009).

A series of 78 patients with inoperable osteosarcoma of the trunk treated with definitive carbon ion radiotherapy (CIRT) between 1996 and 2009 was reported from Chiba Cancer Center, Japan. The tumor site was the pelvis in 61 patients, paraspinal in 15, and others in 2. After a median total dose of 70.4 Gy (RBE) (dose escalation phase I/II study with 52.8–73.6 Gy (RBE), fixed dose of 70.4 Gy (RBE) after April 2000) delivered in 16 fractions over 4 weeks, the 5-year local control rate was 62 % with an overall survival rate of 46 %.

The CTV encompassed the gross tumor volume and all tissues displaying contrast enhancement in CT or MR imaging. The area that was considered subclinical disease was added to the CTV as well. The median maximum tumor size was 10 cm (range 2–18 cm) and the median reported CTV 510 cm^3 (range 60–2,299 cm^3) (Matsunobu et al. 2012).

In 2010, a trial with 45 Gy (RBE) of protons to a PTV_{large} and a 15–21 Gy (RBE) carbon ion boost for non-resectable osteosarcoma was designed at the university of Heidelberg, Germany (NCT01005043). The local therapy as defined by the study should be embedded in current chemotherapy concepts. Within the protocol, the GTV is delineated according to MRI/CT-scan/PET-CT. The CTV contains the visible GTV plus the subclinical microscopic malignant disease, guided by the initial (pre-chemotherapy) tumor extension. In axial tumors, expansion of the GTV aims for a clinical safety margin of 2 cm. For extremity sarcomas, a margin of 4–5 cm around the GTV is preferred. The PTV is delineated in collaboration with the radiation physicist taking into account organ and patient movement and inaccuracies in beam and patient setup (Blattmann et al. 2010).

Given the rarity of the disease and the indication for RT, it is generally advised to discuss each case individually with the reference radiation oncologist from ongoing studies.

12.6 Ewing Sarcoma

12.6.1 Anatomy and Histopathology

Ewing sarcoma is relatively rare, accounting for 6–8 % of primary malignant bone tumors. However, it is the second most common osseous malignancy in children and young adults. Nearly 80 % of patients are younger than 20 years, the peak incidence is during the second decade of life, with a slight male predominance of 1.4:1 (M:F). The annual incidence is estimated at 0.06–0.1/100,000.

The most prevalent sites are – in descending order – the diaphysis or metaphyseal-diaphyseal portion of long bones (femur, tibia, humerus), the pelvis and ribs, and other bones such as the skull, vertebra, scapula, etc. About 10–20 % of cases are extraskeletal. At diagnosis, metastases are found in approximately 25 % of patients. Typical metastatic sites are the lung and bones and, less frequently, the lymph nodes.

Ewing sarcoma is a tumor thought to arise from mesenchymal stem cells. It consists of small, blue, round primitive-appearing tumor cells displaying varying degrees of neuroectodermal differentiation. Recurrent balanced translocations involving the *EWSR1* gene on chromosome 22 and a member of the *ETS* family coding transcription factors are characteristic for Ewing sarcoma. In approximately 85 % of Ewing sarcoma, the *EWSR1* fusion partner is *FLI1*, generating the hybrid *EWSR1-FLI1* oncoprotein which is responsible for transcriptional gene dysregulations. Numerous other chromosomal rearrangements are found in Ewing sarcoma involving the EWSR1 or related genes.

"Classical Ewing sarcoma" is composed of uniformly small, round cells with round nuclei containing fine chromatin, often with cytoplasmatic glycogen deposits and indistinct cytoplasmatic membranes (see Fig. 12.12). In "atypical Ewing sarcoma" cells are larger and have prominent nuclei and irregular contours. Tumors with higher degree of neuroectodermal differentiation (e.g., forming pseudorosettes) may be termed

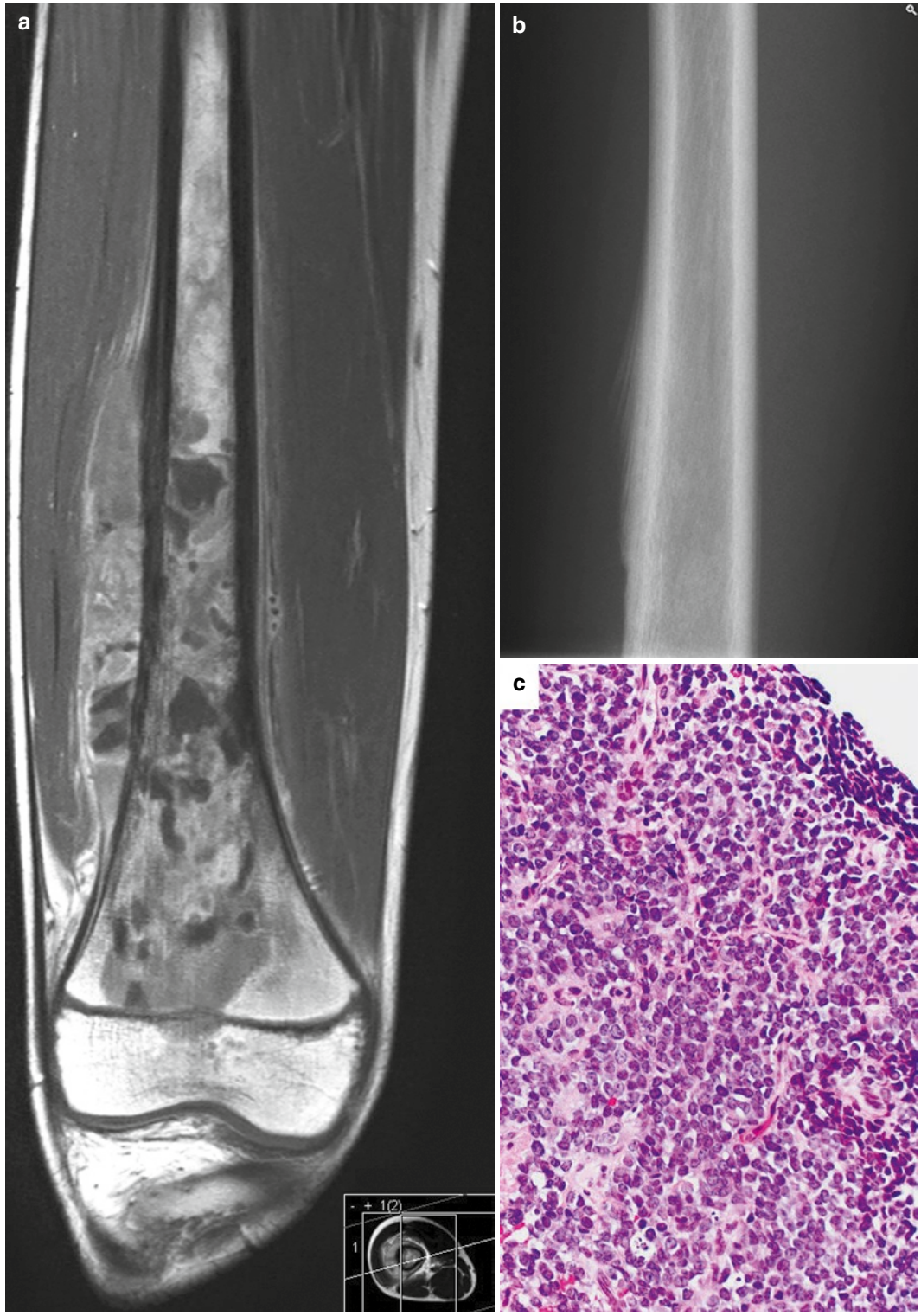

Fig. 12.12 Ewing sarcoma of the right femur in an 11-year-old boy. (**a**) Coronal contrast-enhanced T1-weighted MR image shows the intraosseus and extraosseous tumor component and the extension beyond the epiphyseal plate. (**b**) Conventional radiograph displaying the periostal reaction. (**c**) Histology shows small round cells with uniform nuclei containing fine chromatin

"peripheral neuroectodermal tumor (PNET)." The emerging group of "Ewing-like sarcoma" is more heterogeneous in morphology and molecular findings, but up to now, classified and treated like other Ewing sarcomas. "Askin tumor" is a synonym for Ewing sarcoma of the chest wall.

Ewing sarcoma of the bone typically arises in the medullary shaft with destruction of the cortex and varying degree of extraosseous soft tissue extension. Ewing sarcoma primarily arising in soft tissue may be associated with a large peripheral nerve. Generally, the tumor has destructive borders with invasive margins, often showing necrotic or hemorrhagic regions, e.g., intramedullary or subperiosteal (De Alava et al. 2013).

12.6.2 Imaging in Ewing Sarcoma

Imaging findings in Ewing sarcoma can be unspecific and may mimic other conditions, such as osteomyelitis, Langerhans cell histiocytosis, osteosarcoma, and metastatic neuroblastoma. Conventional radiographs usually show permeative and/or moth-eaten osteolytic changes which commonly lack a geographic component. In approximately two thirds of cases, lytic changes are predominant, whereas in the remaining cases (reactive), osteosclerosis may be visible or even predominant, in particular if flat bones are affected. The bone changes are typically associated with an interrupted or complex periosteal reaction, most often of the lamellated ("onion skin") or spiculated subtypes. In cases with extensive cortical destruction, pathological fracture may occur (16 % at time of diagnosis). An extraosseous tumor component is usually large and clinically apparent as a mass. The full extent of the lesion is visualized on cross-sectional imaging.

In lytic and sclerotic bone destruction, periosteal changes and soft tissue extension can be displayed in more detail with CT. The extent of medullary involvement and the soft tissue component are however best demonstrated by MRI (see Fig. 12.12a). The T1- and T2-weighted signal intensities of Ewing sarcomas are usually unspecific. The main portion of the tumor is mostly solid and demonstrates avid contrast enhancement. Peritumoral edema is usually circumscribed and appears bright on T2-weighted and STIR sequences.

A whole-body MRI with the use of T1-weighted and STIR sequences can be performed to exclude or identify skeletal metastases, which is highly relevant for therapy planning (see Fig. 12.14b, c). MRI represents the most reliable imaging technique to quantify therapy-induced changes of tumor volume (see Fig. 12.13a, b and Fig. 12.14j, k). A volume reduction of less than 25 % is regarded as predictive of poor histological response. On FDG-PET, a reduction of an initially raised SUV (standardized uptake value) to a post-chemotherapeutic maximum value of <2 was found to be correlated with a good histological response and a favorable prognosis (Freyschmidt et al. 2010).

12.6.3 Target Volume Delineation in Ewing Sarcoma

Treatment of Ewing sarcoma patients worldwide is organized in cooperative trials (such as POG-CCG (Intergroup, United States), REN-3 (Italy), EW-88 (France), SSG IX (Scandinavia), ET-2 (United Kingdom, MRC), EURO-EWING99 (European Intergroup), and EWING2008 (European and North American Cooperative Groups)), aiming to further improve treatment outcome. Cure can only be achieved with a combination of both systemic and local control. Current treatment schedules favor primary induction chemotherapy, followed by local therapy and adjuvant chemotherapy (Bernstein et al. 2006). Usually, neoadjuvant chemotherapy is initiated as soon as the diagnosis is confirmed by biopsy and staging procedures are completed, utilizing a combination of active substances such as adriamycin, vincristine, actinomycin D, etoposide, ifosfamide, or cyclophosphamide. Meanwhile, the appropriate local therapy approach should be scheduled according to the discussion within the interdisciplinary medical team caring for the patient and to the vote of the study reference center. Surgical treatment is the preferred option

for the primary tumor if it is feasible without causing major functional deficits, as retrospective data has shown favorable local control rates in patients in whom surgery is possible. These data are usually confounded by a selection bias favoring resectable tumors. To date, there is no randomized data comparing local therapy modalities. Indication for radiotherapy and dosage is tailored to the patient's individual risk profile and may result in preoperative, postoperative, or definitive radiotherapy. Definitive radiation treatment is indicated if only an intralesional resection is possible, as debulking procedures do not improve local control (Bernstein et al. 2006).

Target volume definition has to consider the pretherapeutic MRI displaying the initial tumor extent as well as the restaging MRI displaying the current tumor extent at the time of radiation treatment planning. Neoadjuvant chemotherapy may have led to a substantial shrinkage of extraosseous tumor volume, whereas a relevant difference in intraosseous tumor extent cannot be expected. Definition of the PTV_{large} is based on the pretherapeutic gross tumor volume ($GTV_{initial}$) except for subvolumes initially bulging into preformed cavities like the chest or the pelvis that have shown a regression under neoadjuvant chemotherapy. Within these cavities, the GTV is confined to the current tumor contour. Thus, the initial "contact zones" of the tumor are taken for the $GTV_{contact}$ and – according to the protocol in use – a margin of 1 cm is applied for generation of the CTV_{large} with an additional institutional setup margin to produce the PTV_{large}, or a general margin of 2 cm is applied around the GTV_{large} to derive the PTV_{large}, respectively. Treatment of the whole tumor-bearing compartment showed no better results than treating the visible tumor and additional safety margins (Donaldson et al. 1998). For preoperative or definitive radiotherapy, the CTV_{large}/PTV_{large} also includes the biopsy site and for postoperative radiotherapy additionally, the whole cavity of tumor resection with all scars and drainage sites. The PTV_{large} is usually treated to a total dose of 45–50.4 Gy in conventional fractionation.

According to the individual constellation of risk factors, higher total doses may be indicated, e.g., 54 Gy in preoperative radiotherapy or 54–60 Gy in definitive radiotherapy or selected cases of postoperative radiotherapy with poor response to induction chemotherapy and/or marginal/intralesional resection. Target definition for the boost dose above 45–50 Gy considers only the gross disease after induction chemotherapy ($GTV_{postCTx}$) plus a margin of 1 or 2 cm for definition of the CTV_{boost} or PTV_{boost}, respectively. For application of total doses above 54 Gy, a further reduction of margins is allowed (shrinking field technique). Translated into a SIB concept, total doses of 45, 54, and 60 Gy in a single-treatment plan of 30 fractions can be applied with fraction sizes of 1.5, 1.8, and 2.0 Gy for the PTV_{large}, PTV_{boost1}, and PTV_{boost2}, respectively. An example is given in Fig. 12.13 for definitive treatment of an irresectable pelvic Ewing sarcoma. For the 45 Gy volume, this might raise concerns about the effectivity of small daily fractions. Alternatively, single doses below 1.8 Gy can be avoided with the help of two consecutive plans, containing 25 fractions of 1.8 Gy to PTV_{large} and of 2.0 Gy to PTV_{boost2} in the first plan, to be followed by 5 fractions of 1.8 Gy to PTV_{boost1} and 2.0 Gy to PTV_{boost2} in the second plan.

In a combined analysis of all 1058 patients treated within the trials CESS 81, CESS 86, and EICESS 92 for localized Ewing tumors, the rate of local failure was 7.5 % after surgery with and without postoperative radiotherapy, 5.3 % after preoperative, and 26.3 % after definitive radiotherapy. Irradiated patients represented a negatively selected population with unfavorable tumor sites (70.7 % axial). In CESS 81, the whole tumor-bearing compartment was irradiated to a dose of 36 Gy. For definitive RT, the PTV_{boost} included the initial tumor with a 5 cm margin. In CESS 86 and EICESS 92, the PTV_{large} consisted of the pretherapeutic tumor size plus a 5 cm margin to a dose of 44 Gy and the PTV_{boost} of the pretherapeutic tumor size plus a 2 cm margin. Generally, the authors advise for resection, if marginal or wide resection is feasible. Risk factors like poor histological response to chemotherapy and marginal or intralesional resection should prompt postoperative radiotherapy. As results for definitive radiotherapy were comparable to those achieved by intralesional resection plus postoperative radiotherapy, debulking procedures should be avoided and RT given instead, possibly followed by tumor resection (Schuck et al. 2003).

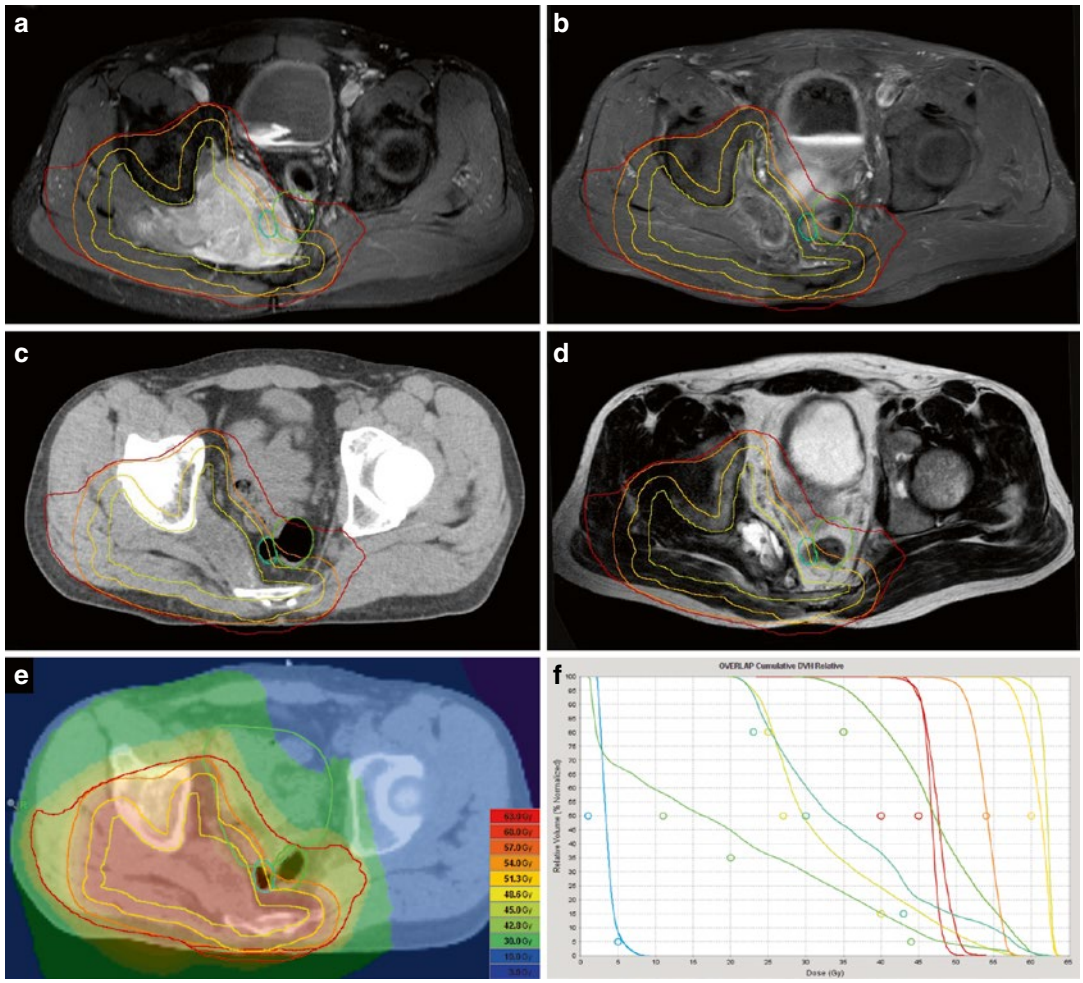

Fig. 12.13 PNET/Ewing sarcoma (cT2 cN0 cM0 G4) of the right pelvis in a 30-year-old man. (**a**) Pretherapeutic axial contrast-enhanced T1-weighted MR image with fat suppression. The tumor involves the acetabulum and sacral bone including the lumbosacral plexus on the right side and extends through the greater sciatic foramen into the gluteal muscles. The pelvic organs are grossly displaced. (**b**) Good partial remission after 6 cycles of chemotherapy according to EWING 2008 protocol (VIDE), residual tumor centered in the greater sciatic foramen, and pelvic organs less displaced as visualized on contrast-enhanced T1-weighted image with fat suppression. (**c**) Planning CT for definitive radiotherapy (**d**) and axial T2-weighted MR image registered for target volume delineation: $GTV_{contact}$, *yellow* (including all surfaces initially contacted by the tumor and the parts of the muscles initially involved); PTV_{SIB2}, *light orange* (GTV plus 1 cm margin, 1,489 cm^3) to a total dose of 60 Gy in 30 fractions of 2 Gy; PTV_{SIB1}, *orange* (GTV plus 2 cm margin, manually shortened in the direction of pelvic organs, 2,623 cm^3) to a total dose of 54 Gy in fractions of 1.8 Gy; and PTV_{large}, *red* (including the sacral bone to the contralateral sciatic foramen and greater portions of the gluteus maximus muscle, 3,916 cm^3) to a total dose of 45 Gy in fractions of 1.5 Gy. (**e**) Axial view of the dose distribution (tomotherapy planning). (**f**) Dose volume histograms for target volumes (GTV, PTV_{SIB2}, PTV_{SIB1}, PTV_{large}, see above for colors) and organs at risk: rectum, *green*; sigmoid colon, *light blue*; urinary bladder, *yellow*; intestine, *light green*; and genitals, *blue*. Reevaluation with PET-CT and MR imaging after radiotherapy resulted in complete remission

12.6.3.1 Extremities

In Ewing tumors of the extremities, the PTV_{large} usually includes the tumor volume with a 5 cm margin in proximodistal directions (Bacci et al. 2009). In case of extensive intramedullary involvement or evidence of intramedullary skip

Fig. 12.14 Ewing sarcoma cT2 cN0 cM1 (PUL, OSS, LYM) G4 in a 17-year-old boy. The primary tumor arises from the proximal fibula. Multiple metastases are found in the lungs, the pleura, the spine (Th8, Th11, L5, S1, S2), and the pelvic bones (close to the sacroiliac joints and in the right acetabulum) and suspected in an external iliac lymph node. Treatment was guided by the META-EICESS protocol, including radiation therapy to each of the initially visible lesions. (**a**) Sagittal planning CT reconstruction at midline, target volumes for irradiation of the lungs, *blue* (lung tissue plus visible pleura according to 4D-CT plus a margin of 1 cm), to a total dose of 18 Gy in 12 fractions of 1.5 Gy, and to thoracic, *red*, and lumbosacral lesions, *purple*. (**b**) Pretherapeutic whole-body MRI detects bone metastases of high signal intensity on coronal STIR images and (**c**) low signal intensity on corresponding T1-weighted images, as exemplarily displayed for the lesions in Th8 and Th11 – *yellow*. (**d**) Corresponding coronal planning CT reconstruction after 4 cycles of chemotherapy (VIDE): hypodense lesions with peripheral sclerotic rims, indicating recalcification as a response to chemotherapy. PTV_{SIB} – *orange* (GTV plus 1 cm margin, reduced to 0.5 cm after completion of whole-lung irradiation) to a total dose of 50 Gy in 25 fractions of 2.0 Gy and PTV_{large} (affected vertebra plus 1 cm margin) to a total dose of 45 Gy in fractions of 1.8 Gy. The thoracic irradiation was delivered in two consecutive plans of 12 and 13 fractions, including the whole-lung irradiation in the first plan only, which was delivered in 10.8 min per fraction. (**e**) Coronal reconstruction of thoracoabdominal planning CT. The pelvic target volumes, *purple*, were treated with a separate plan, delivered in 5.5 min per fraction. *Second row*: Target volume delineation for the primary tumor on contrast-enhanced T1-weighted MR images with fat suppression. (**f**) Sagittal and (**g**) coronal MR images display a tumor arising from the right proximal fibula with soft tissue edema extending along the whole length of the calf. (**h**) Coronal image obtained after 4 cycles of chemotherapy (VIDE) displays shrinkage of the main tumor mass, reduction of contrast enhancement, and regression of soft tissue edema. (**i**) Coronal planning CT reconstruction: GTV, *yellow* (the residual tumor, all initial contact tissues and the edema remaining after chemotherapy); $PTV_{SIB60Gy}$, *orange* (GTV plus 0.5 cm axial and 1.0 cm longitudinal margin) to a total dose of 60 Gy in 30 fractions of 2.0 Gy; and PTV_{large}, *red* (GTV plus 1 cm axial and 2 cm longitudinal margin, including the whole initial edema with a 0.5 cm margin) to a total dose of 54 Gy in fractions of 1.8 Gy. (**j**) Corresponding axial MR images obtained before and (**k**) after application of 4 cycles of chemotherapy. The GTV – *yellow* – considers the initial tumor extensions transferred to the postchemotherapeutic anatomy. Irradiation time for a single fraction was 5.5 min. All target volumes were treated simultaneously with the 5th and 6th cycle of chemotherapy (omission of doxorubicin and general dose reduction to 75 %) in a split-course manner with a planned break after the first 14 (of maximal 30) fractions. The total amount of red bone marrow included in radiation treatment fields was estimated to be 40 %. Further treatment consisted of repeated high-dose chemotherapy, autologous stem cell rescue, and later also allogeneic haploidentical stem cell transplantation. The patient suffered from severe fungal pneumonia during the phase of aplasia after the first high-dose chemotherapy but recovered and remained in complete remission. Apart from a mild Graft-versus-host disease and a palsy of the right fibular nerve caused by the tumor, the patient is asymptomatic (last follow-up 2 years after diagnosis)

lesions, whole-bone irradiation might be adequate. Uninvolved epiphyseal plates should be spared, if possible.

12.6.3.2 Vertebral Column

In tumors of the vertebral column, the PTV_{large} usually includes one unaffected vertebra above and below the affected bone. In a dose escalation study on one patient with the scenario "tumor restricted to a single vertebral body," the possibility of applying up to 70 Gy to the PTV_{boost} while keeping the $D_{2\%}$ of the spinal cord below 50 Gy was shown for advanced techniques like stereotactic radiotherapy, VMAT, helical tomotherapy, and proton therapy. For the scenario "involvement of the vertebral foramen and paraspinal tissues," helical tomotherapy was the only technique enabling a total dose of 59.2 Gy to the PTV_{boost} while keeping the $D_{2\%}$ of the spinal cord below 44 Gy (Vogin et al. 2013a).

In a French cohort of 75 patients with localized spinal Ewing tumors treated between 1988 and 2009 within successive protocols, the only prognostic factor for local control was the tumor site (favorable versus unfavorable vertebral compartment). Overall local control at 5 years was 78 % without significant differences between a surgical and a definitive radiooncological approach. Twelve of 13 patients suffering from long-term neurological sequelae had initially presented with central neurological deficits and had decompressive surgery. The authors concluded that initial decompressive surgery should be avoided and rather an effective chemotherapy initiated immediately. Seventy-three percent of patients were affected by orthopedic problems,

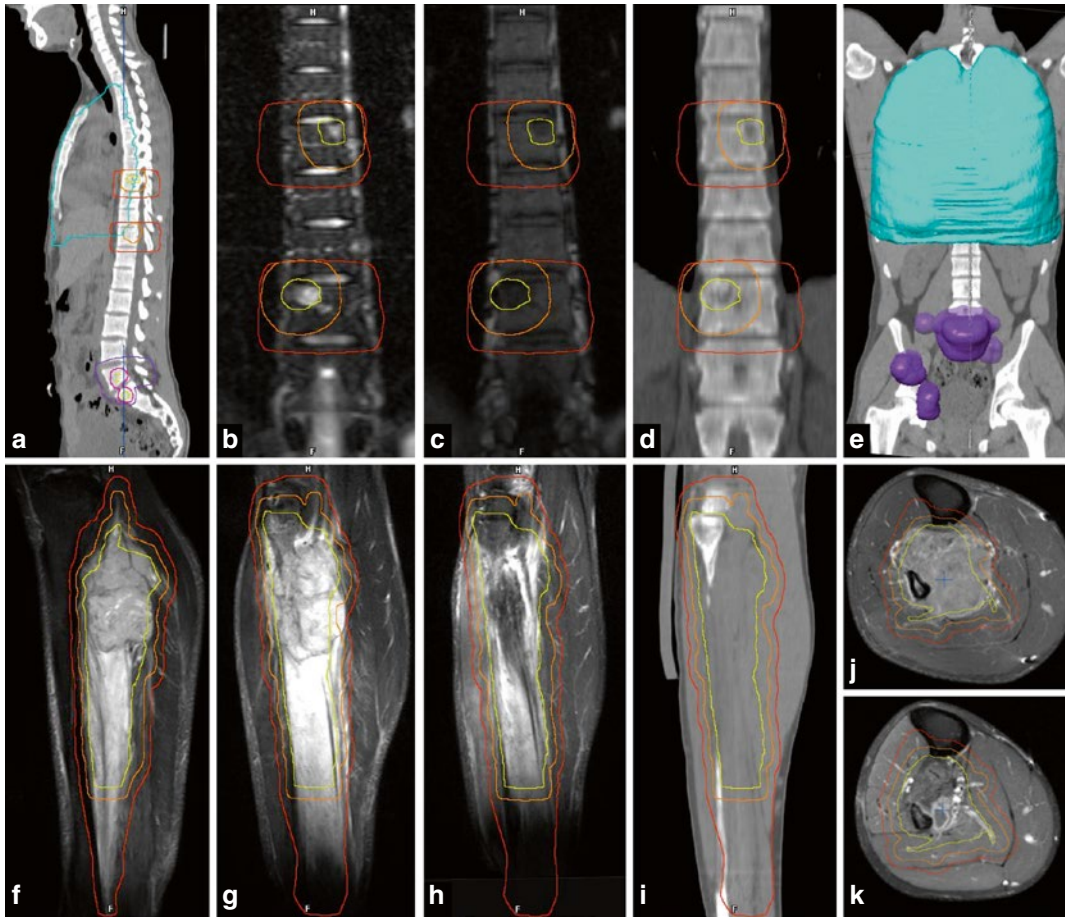

mainly spinal mobility reduction (40 %), spinal curvature deformation (35 %), growth retardation (28 %), and spinal pain (25 %). Vertebrae affected asymmetrically by radiation therapy showed anterior or lateral wedging of the vertebral body, leading to subsequent kyphosis and/or scoliosis. Fibrosis and contracture of the irradiated soft tissue may have accelerated the progression of the deformity, namely, in adolescence. Thus, symmetrical irradiation of vertebrae is strongly recommended (Vogin et al. 2013b).

In a series of 27 patients treated at the University of Florida between 1965 and 2007 with radiotherapy for spinal and paraspinal Ewing tumors (21 definitive, 1 preoperative, 4 postoperative, 1 total body irradiation only), the PTV_{large} generally encompassed the whole affected vertebra plus one grossly uninvolved vertebra superior and inferior to the tumor. For paraspinal soft tissue involvement, the pretherapeutic infiltrating borders were surrounded by a 2–4 cm margin, if applicable. Every effort was made to avoid partial vertebral irradiation and to minimize the dose to the spinal cord and lungs (three-dimensional conformal planning introduced in 1994). Target doses of 45–50 Gy for microscopic disease and 55–60 Gy for gross disease were reported without further details for the definition of boost volumes. Ten patients received also total body irradiation (TBI), adding 8–12 Gy to the primary site. The 5-year actuarial local control rate was 84 % after definitive radiotherapy and 100 % after combined treatment. The 5-year overall survival was 62 % for the whole group and 71 % for 22 nonmetastatic patients. Three out of ten severe complications (according to Common Terminology Criteria

for Adverse Events grade III or greater) were attributable to radiotherapy, including esophageal stricture, intractable nausea, and bladder hypertrophy causing bilateral hydronephrosis (Indelicato et al. 2010).

Of 116 patients with vertebral Ewing tumors enrolled in the European cooperative studies CESS 81, CESS 86, or EICESS 92 between 1981 and 1999, 64.6 % received definitive radiotherapy, 3.4 % definitive surgery, and 27.5 % combined treatment. Target volumes shrinked with successive protocols: in CESS 81, the PTV_{large} (36 Gy) encompassed the tumor-bearing compartment and the PTV_{boost} (46–60 Gy) the initial tumor extent plus a 5 cm margin. In CESS 86, the PTV_{large} (44 Gy) consisted of the initial tumor extent plus 5 cm and the PTV_{boost} (60 Gy) of the pretherapeutic tumor plus 2 cm. In EICESS 92, the PTV included one uninvolved vertebra above and below the affected vertebra and the pretherapeutic soft tissue component of the tumor with a 2–3 cm margin (44–54 Gy). There was no statistical difference in the incidence of local recurrences for patients receiving definitive radiotherapy or combined treatment (22.6 % versus 18.7 %) (Schuck et al. 2005). This did not differ from the results of definitive radiotherapy for other tumor sites, as analysis of 266 CESS and EICESS patients with definitive radiotherapy for all sites showed 26 % local recurrences (Schuck et al. 2003). Local relapse analysis was available in 14 of 23 irradiated patients with local or combined local and systemic recurrence. Of these, 13 were classified as in-field; 1 was a marginal relapse. The authors concluded that local recurrence in nearly all cases is attributable to tumor cell resistance to radiation, rather than insufficient radiation volumes (Schuck et al. 2005).

The reported series of 30 pediatric Ewing sarcoma treated in Boston with proton radiotherapy included 14 patients with spinal/paraspinal tumor sites. The CTV_{large} consisted of any bony or soft tissue tumor and any tumor edema seen on pretherapeutic MRI/CT/PET scans plus a 1–2 cm anatomically constrained margin (prescribed dose 30.6–50.4 Gy (relative biological effectiveness (RBE)), median 45 Gy (RBE) in fractions of 1.8 Gy (RBE)). The CTV_{boost} included the initial bony tumor and the post-chemotherapeutic soft tissue component with a 1–2 cm anatomically constraint margin (prescribed dose 45–55.8 Gy (RBE), median 50.4 Gy (RBE)). For the definition of PTVs, apart from the positioning uncertainties, the specific necessities of passively scattered proton therapy were taken into account.

At a median follow-up of 38 months, the 3-year local control rate was 86 % for all 30 patients. Five of 14 patients with vertebral body primary tumors developed scoliosis/kyphosis (3 mild, 1 moderate, 1 severe). All patients who developed spine deformities had laminectomies before proton treatment. Secondary hematological malignancy was an issue with 4 of 30 patients developing an acute myelocytic leukemia or a myelodysplastic syndrome (Rombi et al. 2012).

12.6.3.3 Pelvis

From the University of Florida, a series of 35 patients with localized Ewing tumors of the pelvis and sacral bones treated between 1970 and 2005 have been reported. Twenty-six patients received definitive radiotherapy, 7 patients had preoperative, and 2 postoperative radiotherapy, each to a median dose of 55 Gy. Planning target volumes were generally shrinking with the availability of superior imaging in the modern era. Fourteen patients also received TBI adding 8–13.5 Gy to the primary site. The 15-year actuarial local control rate was 64 % after definitive radiotherapy and 100 % after combination with surgery. During follow-up, 27 % of patients presented with severe complications, including osteoradionecrosis requiring hip replacement, hip fractures, hemorrhagic cystitis, severe sympathetic dystrophy/radiculopathy, bowel perforation, and development of 2 osteosarcomas.

In a planning study comparing three-dimensional conformal radiotherapy (3D-CRT) and intensity-modulated radiation treatment (IMRT) planning in a set of 8 patients with pelvic Ewing sarcomas, IMRT showed significantly better results regarding dose conformity and bowel sparing at doses above 30 Gy, which is valuable for dose escalation (Mounessi et al. 2013).

12.6.3.4 Chest Wall

In another institutional series of the University of Florida, 39 patients diagnosed with Ewing tumors of the chest wall between 1966 and 2006 were analyzed. In 22 patients, local treatment consisted of radiotherapy alone, including eight out of nine patients with metastatic disease. The remaining 17 patients received surgery with or without adjuvant radiotherapy. Apart from irradiation to the primary site to a median biological effective dose of 59 Gy_{10} (range 33.6–84 Gy_{10}), five of 39 patients received hemithorax RT to a dose of 10–15 Gy (in 1 Gy per fraction), 2 patients had bilateral lung RT (15–18 Gy in 1–1.2 Gy per fraction), and another 11 patients total body irradiation, adding 8–13.5 Gy to the primary site. The 5-year rates of local control and overall survival were 72 and 34 % for the whole group and 79 and 44 % for the nonmetastatic subset, respectively. 26 % of patients experienced toxicity of grade III or higher (according to CTCAE criteria), including two pulmonary deaths. The authors stress the need for improved RT techniques in order to reduce morbidity (Indelicato et al. 2011).

Analyses of 138 patients with nonmetastatic Ewing tumors of the chest wall treated in the CESS 86 or EICESS 92 protocol between 1985 and 1996 revealed the value of hemithorax irradiation. Forty-two patients who received hemithorax irradiation to a dose of 15–20 Gy were negatively selected, yet the rate of event-free survival after 7 years was better (63 %) than for the 86 patients without hemithorax irradiation (46 %), mainly due to a reduction of systemic relapse rates (22 % versus 39 %, respectively) (Schuck et al. 2002).

12.6.3.5 Lymph Node Metastasis

Based on SEER data on 1,452 patients below 40 years of age, diagnosed between 1973 and 2008, the incidence of regional lymph node involvement in the Ewing tumor family was found to be 3.2 % in skeletal tumors and 12.4 % in extraskeletal primary tumors. On multivariate analysis, lymph node involvement was an independent predictor for inferior overall survival (Applebaum et al. 2012).

Apart from systemic treatment, all involved lymph node sites should be treated locally, either by regional lymph node dissection or by definitive radiotherapy similar to the treatment of the primary tumor.

12.6.3.6 Distant Metastasis

Approximately 25 % of patients present with metastatic disease, mainly to the lung or the bone/bone marrow. In case of lung metastases, whole-lung irradiation (WLI) is recommended even after chemotherapy-induced clinical complete remission. Retrospective analysis of the EICESS 92 data on 99 patients with pulmonary metastases revealed a trend toward better overall survival after 5 years with 61 % for 70 patients with WLI as compared to 49 % for 29 patients without WLI (Bolling et al. 2008).

In an institutional review of 31 patients with metastatic Ewing tumors, a 5-year overall survival rate of 22.1 % was found. None of the patients receiving chemotherapy alone survived. All long-term survivors had local therapy including radiotherapy to metastatic bony sites and whole-lung irradiation for pulmonary metastasis (Paulino et al. 2013).

Analysis of 120 patients with primary disseminated multifocal disease registered into the European Ewing Tumor Working Initiative of National Groups (EURO-E.W.I.N.G. 99) trial revealed a 3-year event-free survival of 39 % in patients who received local therapy to the primary site and all metastases compared with 17 % in patients with any local treatment and 14 % in patients with no local therapy. Multivariate analysis showed absence of local treatment to be the major risk factor (HR = 2.21). Thus, surgery or radiotherapy with curative doses should be applied to metastatic sites wherever possible (Haeusler et al. 2010). In a comparison of 11 patients with multifocal bone disease depicted in whole-body MRI, radiation therapy to each tumor site and high-dose chemotherapy with stem cell rescue, a prolonged survival was found compared to a matched group of 26 patients treated in the European Intergroup Cooperative Ewing Sarcoma Study-92 (EICESS-92). Overall survival at 5 and 10 years was 45 and 27 % for

patients with intensified local and systemic treatment, compared to 8 and 8 % for those without (Burdach et al. 2010).

In primary disseminated multifocal Ewing tumors, we treat all localized metastatic sites (GTV) that show tracer uptake in bone scintigraphy or PET imaging or localized hypointense signals on T1-weighted images and hyperintense signals in T2-weighted inversion recovery images of a whole-body MRI. An example is given in Fig. 12.14. In our practice, the CTV_{large} encompasses the GTV plus a 0.5 cm margin, in case of spinal metastasis including the whole affected vertebral body, in case of long bones including the whole cross section at the affected level, respectively. The PTV_{large} encompasses the CTV_{large} plus a 0.5 cm margin and is treated to a total dose of 45 Gy in single fractions of 1.8 Gy with IMRT and daily image guidance. A simultaneous integrated boost (SIB) is applied to the GTV plus a 0.5 cm margin accounting for positioning uncertainties to a total dose of 50 Gy in single fractions of 2.0 Gy.

12.7 Chondrosarcoma

12.7.1 Anatomy and Histopathology

Chondrosarcomas are defined as neoplasms producing cartilaginous matrix. In analogy to the reclassification of "liposarcoma grade I" into "atypical lipomatous tumor," the 4th edition of the WHO classification 2013 redefines the former "chondrosarcoma grade I" into "atypical cartilaginous tumor" in order to emphasize the local aggressiveness but lack of metastatic potential in these well-differentiated tumors.

A chondrosarcoma arising centrally in the bone without a benign precursor is called primary central chondrosarcoma. This lesion predominantly affects patients over the age of 50 years and accounts for 20 % of malignant bone tumors and 85 % of all chondrosarcomas. Thus, it is the third most common primary malignancy of bone after myeloma and osteosarcoma. Predilection sites are the trunk and the proximal extremity girdles, accounting for about 75 % of chondrosarcomas (pelvis, proximal and distal femur, proximal humerus, and ribs). The hands, feet, spine, and craniofacial bones (skull base) are rare locations.

The histomorphology varies widely with grade. Grading takes into account nuclear size, hyperchromasia, cellularity, and mitosis. Atypical cartilaginous tumors can be difficult to separate from enchondroma, displaying areas of lobulated cartilage matrix and few cells with little variation in size and shape and absence of mitoses. There may be areas of myxoid or mucoid material and cystic changes. Entrapment of preexistent bone is typical. With higher grade, tumors are more cellular and pleomorphic, with increasing number of mitoses. An example is given in Fig. 12.15. In grade III chondrosarcoma, cells at the periphery of cartilage lobules may be spindled. In a series of 338 patients, 61 % of chondrosarcomas were

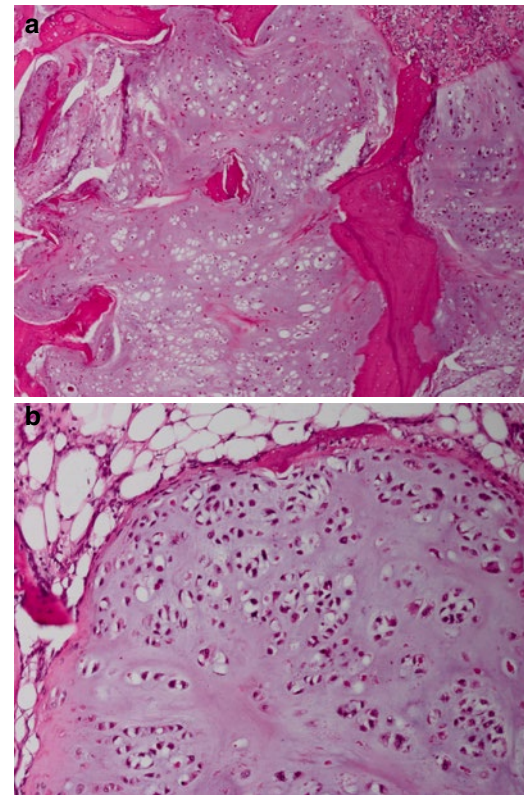

Fig. 12.15 Chondrosarcoma, grade II. (**a**) Cartilaginous nodules permeating between bony trabeculae. (**b**) High-power view shows tumor cells with pleomorphic and hyperchromatic nuclei

grade I, 36 % were grade II, and 3 % were grade III (Bjornsson et al. 1998).

As in every sarcoma, tumor grade is of utmost importance for prognosis. Five-year survival of patients with grade I tumors is >80 %, with most lesions controlled after curettage or surgical resection with the exception of problematic sites like the pelvis and skull base. Chondrosarcomas of higher grade have a worse prognosis; these combined groups have a 5-year survival of 53 %. They should be treated with en bloc resection and wide margins (Gelderblom et al. 2008).

Secondary central chondrosarcoma arises in a preexisting enchondroma. Patients with Ollier's disease or Maffucci syndrome (diseases with multiple enchondromas) have a markedly increased risk (around 40–50 %) of developing these secondary chondrosarcomas.

Secondary peripheral chondrosarcoma arising in preexisting cartilaginous caps of osteochondromas should be suspected if the cartilage cap exceeds 1.5–2 cm in thickness. Primary periosteal chondrosarcomas, i.e., malignant hyaline cartilage tumors originating from the periosteum on the bone surface, are rare (Hogendoorn et al. 2013).

Dedifferentiated chondrosarcoma is a highly malignant subtype with areas of low-grade chondrosarcoma and abrupt transition into areas of a high-grade, non-cartilaginous sarcoma (e.g., spindle cell sarcoma, pleomorphic sarcoma). It can be expected in 10–15 % of central chondrosarcomas. The prognosis is exceptionally poor with rapid progression into metastatic disease. Data for a beneficial effect of chemotherapy or radiation therapy on prognosis is lacking (Inwards and Hogendoorn 2013).

Mesenchymal chondrosarcoma accounts for <3 % of all primary chondrosarcomas with a peak incidence in the second and third decade of life. Origin in craniofacial bones, ribs, and vertebrae is more frequent than in conventional chondrosarcoma. Primary extraskeletal soft tissue involvement is frequent, namely, of the meninges. The tumor has a biphasic pattern with poorly differentiated small round to oval cells (resembling Ewing sarcoma) mixed with islands of hyaline cartilage and a myopericytoma-like vascular pattern. The clinical course may be prolonged, but systemic spread is observed even after >20 years. In this aggressive tumor, chemotherapy is a therapeutic option (Nakashima et al. 2013).

12.7.2 Imaging in Chondrosarcoma

The imaging appearance of a chondrosarcoma varies with the subtype, location, and histological grade of the tumor.

Central chondrosarcomas typically cause lytic bone destruction on radiographs, which can range from geographic and well-defined lesions to a highly aggressive appearance with a moth-eaten or even permeative pattern. The affected bone might appear expanded, and a periosteal shell (neocortex) represents the most common type of periosteal reaction. In approximately 50 % of the cases, mineralization of the chondroid matrix can be detected as areas of punctuate, flocculent, or ring-like radiodensities. The most reliable findings in the distinction between a central chondrosarcoma and an enchondroma are cortical penetration and an extraosseous tumor component. Like in other malignant bone tumors, MR imaging represents the best-suited imaging modality to define the local tumor extent. Highly differentiated chondrosarcomas typically show a lobulated architecture and exhibit low signal intensity on T1-weighted images, very high signal intensity on T2-weighted and STIR images, as well as a characteristic septonodular pattern of contrast enhancement ("rings and arcs"). An example is given in Fig. 12.16a, b. Less differentiated tumors or tumor components usually have a more unspecific MR appearance.

Peripheral (exostotic) chondrosarcomas are composed of an osseous stalk and a cartilaginous cap and thus, radiographically resemble osteochondromas. The osseous stalk can reveal signs of secondary destruction by the cartilaginous component, which might be identified in case of mineralization. CT and MR imaging can both be used to determine the thickness of the cartilage cap; however, due to its higher soft tissue contrast, MR represents the preferred modality for local staging. A cartilage cap thickness of more than

2 cm in adults and more than 3 cm in children is regarded as a criterion to distinguish a peripheral chondrosarcoma from an osteochondroma. Since most exostotic chondrosarcomas are low-grade lesions, the cartilage component typically shows the abovementioned signal characteristics of a well-differentiated chondrogenic tumor.

Dedifferentiated chondrosarcomas often show an "enchondroma-like" component as well as an aggressive component with cortical destruction on plain radiographs, reflecting the histologic bimorphism of this entity (Inwards and Hogendoorn 2013). On MR imaging, the well-differentiated component presents the typical features of a chondrogenic tumor, whereas the dedifferentiated component shows intermediate to low instead of high signal intensity on T2-weighted images and diffuse instead of peripheral enhancement following intravenous contrast administration. This component often penetrates the cortex and extends into the surrounding soft tissues.

12.7.3 Target Volume Delineation in Chondrosarcoma

The treatment of chondrosarcoma is tailored to the histological grade and tumor site. Atypical cartilaginous tumor/grade I chondrosarcoma in the long bones can be treated with curettage and have a good prognosis. Approximately 10 % of tumors that recur show an increase in the degree of malignancy. The 5-year survival is 83 % for all sites, and patients die from locally recurrent tumor that is difficult to manage surgically (e.g., pelvis or skull) (Gelderblom et al. 2008).

Favorable data on skull base chondrosarcomas grades I–II treated with particle therapy, namely, protons or carbon ions, demonstrate that definitive radiotherapy to a total dose of approximately 65–70 Gy (relative biological effectiveness (RBE)) is highly successful. Institutional series from different particle therapy centers in North America, Europe, and Japan uniformly report on 5-year local control rates of 85–100 % for patients with low-grade chondrosarcoma of the skull base after definitive or postoperative radiotherapy to total doses of 60–79.2 Gy (RBE) (Weber et al. 2005; Schulz-Ertner et al. 2007b; Hug et al. 1999; Noel et al. 2004; Habrand et al. 2008; Ares et al. 2009; Schulz-Ertner et al. 2004; Combs et al. 2009; Munzenrider and Liebsch 1999; Tsujii and Kamada 2012). Thus, particle therapy in a center with expertise in skull base chondrosarcomas has become the treatment of first choice for affected patients. If this cannot be organized, high-precision photon treatment is a valuable option, as good results have been achieved with fractionated stereotactic radiotherapy as well (Debus et al. 2000). For details about the target volume definition in this site, the reader is referred to the corresponding chapter in this textbook (Chap. 3). At the Heidelberg Ionenstrahl-Therapie (HIT) center, a clinical phase III trial is open for patients with skull base chondrosarcoma, who will be randomized between either 45/60 Gy (RBE) of carbon ion or 50–56/70 Gy (RBE) of proton radiation therapy. In the publication on the background and methodology of the study, its principles of target volume definition are reported (Nikoghosyan et al. 2010).

For other sites like cervical, thoracic, lumbar, and sacral spine/paraspinal chondrosarcomas, local control is more difficult to achieve and curettage or local excision alone is usually not sufficient. Surgery should aim for en bloc resection. If this is not feasible or results in microscopic or macroscopic residual tumor, radiotherapy is indicated (Boriani et al. 2009). In a series of 60 patients with newly diagnosed extracranial chondrosarcoma (31 extremity/pelvis, 8 head and neck, 13 chest wall, and 10 spine/paraspinal) considered of being at high risk for local recurrence, a combination of surgery and photon radiotherapy resulted in local control rates of 100, 94, and 42 % after R0, R1, and R2 resections, respectively (Goda et al. 2011). Figure 12.16 gives an example of postoperative radiotherapy for a thoracic chondrosarcoma after R1 resection.

In a phase II study of high-dose photon and proton radiotherapy for spine sarcomas at the Harvard Medical School in Boston, 8 of 14 chondrosarcomas could be controlled after a median follow-up of 4 years. Of 6 patients with local

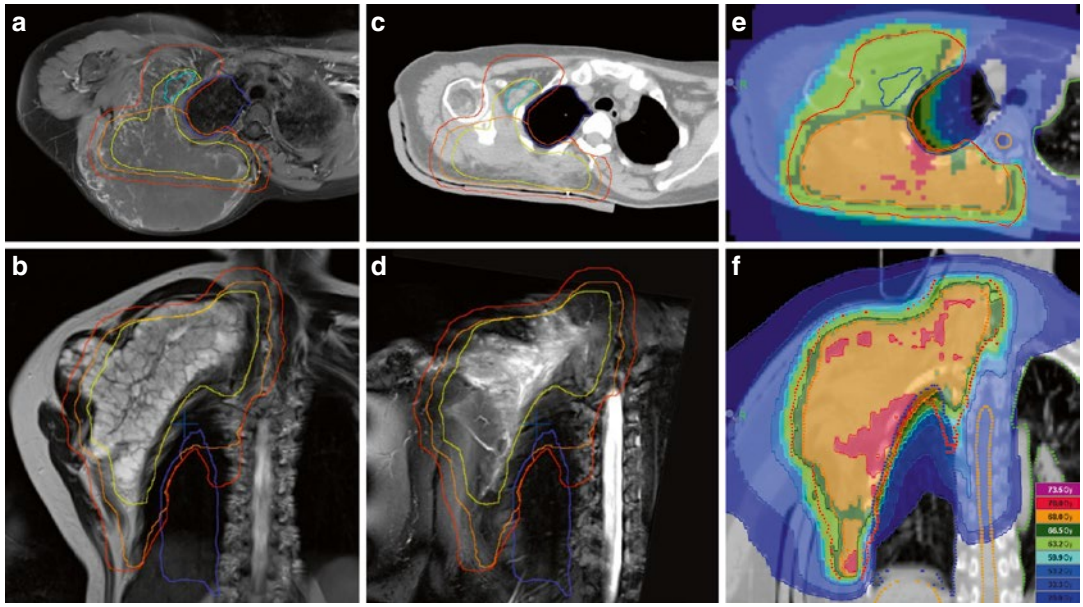

Fig. 12.16 Low-grade chondrosarcoma (cT2 cN0 cM0 G1) of the right shoulder girdle/thoracic region in a 51-year-old woman with Ollier's disease, a rare, nonhereditary sporadic disorder where multiple intraosseous enchondromas develop and secondary chondrosarcomas may occur. (**a**) Axial contrast-enhanced T1-weighted fat-suppressed MR image displaying the large tumor encasing the superior thoracic aperture on the right side. The tumor shows the typical lobulated architecture with low signal intensity on the T1-weighted image and a septonodular pattern of contrast enhancement. (**b**) Coronal T2-weighted image displaying the lobulated tumor with high signal intensity of the chondroid matrix. (**c**) Axial planning CT and (**d**) coronal STIR image in the postoperative situation: the resection specimen was 20 cm × 20 cm × 12 cm with proof of tumor cells at several sites of all resection margins. $GTV_{contact}$, *yellow* (including all contact tissue of the initial tumor extension and the portion of pronounced postoperative edema), and $PTV_{SIB70Gy}$,*orange* (GTV plus 0.5 cm margin for CTV_{SIB}, plus another 0.5 margin for positioning uncertainty, not exceeding 0.3 cm into the right lung, *blue*, restricted to the body with 0.3 cm skin sparing and to the portion posterior to the lymphatic drainage of the arm/course of the brachial plexus, *light blue*) to a prescribed total dose of 70 Gy in 35 fractions of 2.0 Gy. PTV_{large}, *red* (GTV plus 1.5 cm margin for CTV_{large}, including all postoperative changes, plus another 0.5 cm margin for positioning uncertainty, not exceeding 0.3 cm into lung tissue, 0.5 cm into humerus, and 0.5 cm beyond the skin, with a distance of at least 1.2 cm to the spinal cord), to a dose of 66.5 Gy in 35 fractions of 1.9 Gy. (**e**) Axial and (**f**) coronal view of the dose distribution (tomotherapy planning). The average dose (D_{mean}) to the right lung was 23.6 Gy, the median dose 14.3 Gy, and the maximal dose to the spinal cord 48.9 Gy (D_{max})

failures (4 thoracic, 1 lumbar, 1 sacrum), 4 had been treated for locally recurrent tumors, and two also developed distant metastases (sacral and lumbar chondrosarcoma) (DeLaney et al. 2009). The target volume definition and dose prescriptions in this study have been reported in detail: The CTV_{large} included the GTV plus tissues suspected of subclinical tumor invasion. For preoperative RT, this was defined as the gross tumor with 1 cm or more of soft tissue margin on extraosseous tumor, as well as grossly involved vertebrae plus one vertebra above and below. Where the CTV_{large} would extend beyond a fascial barrier, i.e., pleura or peritoneum, the volume was reduced to encompass but not extend beyond the fascia. Biopsy sites were included. For patients undergoing only postoperative RT, the CTV_{large} was to include all surgically manipulated tissues (scars, drain sites, and stabilization hardware). Generally, the CTV_{large} plus an institutional setup margin (of 0.5 cm for photons and 0.3 cm laterally for protons) was treated to a dose of 50.4 Gy (RBE). In case of macroscopic complete tumor resection, the CTV_{boost} including the initial GTV was treated to an additional proton dose of 19.8 Gy (RBE) (i.e., cumulative dose

70.2 Gy (RBE)). For unresected patients, this volume received another 7.2 Gy (RBE) in 4 proton fractions (i.e., cumulative dose 77.4 Gy (RBE)). For grossly incomplete resections, the boost above 70.2 Gy (RBE) was administered to a CTV_{boost2} including only the postoperative residual tumor to a total dose of 77.4 Gy (RBE). Spinal cord center dose was limited to 54 Gy (RBE) and cord surface dose to 63 Gy (RBE) over a length of 5 cm or less. The cauda equina was constrained to 70.2 Gy (RBE), except for areas in direct contact with the tumor. In lateralized sacral lesions, the contralateral sacral nerves were tried to be spared. Apart from a contralateral sacral insufficiency fracture 4 months after treatment, no other grade III complications have been reported for these 14 chondrosarcoma patients (DeLaney et al. 2009).

In the pediatric series treated at the Paul Scherrer Institute with spot-scanning proton radiation therapy between 2000 and 2010, 7 patients with chondrosarcoma (5 skull base, 1 cervical, 1 thoracic spine) received a mean total dose of 66 (range 54–72) Gy (RBE). The GTV was defined as the macroscopic tumor identified on the planning CT and MRI performed after the last surgery at the time of proton therapy planning. The CTV included the GTV (if tumor resection was subtotal) plus preoperative tumor extension modified anatomically, plus high-risk area for microscopic involvement. The PTV_{large} encompassed the CTV plus a 0.5 cm margin, the PTV_{boost} was defined as the GTV plus a 0.5 cm margin. Dose constraints to organs at risk were determined as maximum dose (D2) of 54.0 and 63.0 Gy (RBE) to the center and surface of the brainstem or spinal cord, respectively. After a mean follow-up of 4 years, 1 local recurrence of a high-grade tumor arising from the cervical paraspinal region was observed after 2.7 years, leading to death 1.3 years later. In this patient, the in-field recurrence was detected in the area of the initial gross residual tumor abutting the spinal cord, where target volume coverage in the PTV_{boost} was compromised because of spinal cord sparing. The other 6 patients remained locally controlled, including 4 patients with gross disease at the time of radiotherapy (Rombi et al. 2013).

In an update on the clinical results of carbon ion radiotherapy at the National Institute of Radiological Sciences (NIRS) in Chiba, Japan, a 5-year local control rate of 88 % was reported for 76 patients with skull base and paracervical tumors, including 14 chondrosarcomas (Tsujii and Kamada 2012). From 1996 to 2009, a total of 71 patients with chondrosarcomas of all sites received definitive carbon ion RT at the NIRS. The clinical target volumes ranged between 25 and 2,900 cm^3 (median 488 cm^3). A 5-year local control rate of 60 % was achieved with only 4 patients experiencing grade III and/or IV skin/soft tissue late reactions (Tsujii and Kamada 2012).

12.8 Chordoma

12.8.1 Anatomy and Histopathology

Chordoma is a rare, malignant tumor showing notochordal differentiation. It accounts for approximately 1–2 % of all malignant bone tumors. The tumor is thought to arise from ectopic intraosseous notochordal remnants of the spine, predominantly from sacrococcygeal bones or the skull base. The typical histological findings are large cells with clear to eosinophilic cytoplasm separated into lobules by prominent fibrous septa with good vascularization. Tumor cells are often extensively vacuolated, referred to as "physaliphorous cells." Their nuclei show immunoreactivity for brachyury. Smaller cells are arranged in ribbons and cords, often embedded in vast amounts of extracellular myxoid matrix (see Fig. 12.17). In "chondroid chordoma," the matrix resembles hyaline cartilage. The appearance is indistinguishable from a cartilaginous tumor except that the cells express keratin and brachyury. "Dedifferentiated chordoma" is a biphasic tumor, with chordoma histology and undifferentiated spindle cell tumor or osteosarcoma next to each other (Flanagan and Yamaguchi 2013).

12.8.2 Imaging in Chordoma

Chordomas are midline tumors that typically occur in the sacrococcygeal junction (50–60 %),

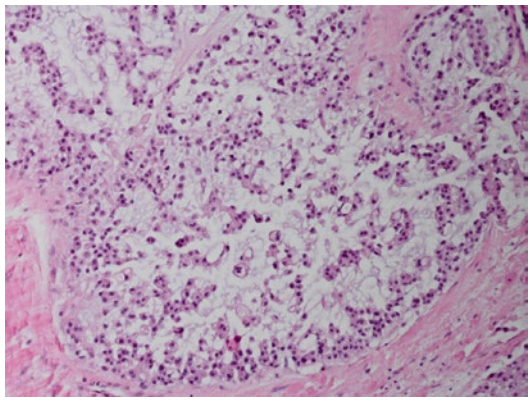

Fig. 12.17 Chordoma. Lobulated appearance of chordoma, with cords and nests of tumor cells set in a myxoid matrix

the clivus, and less frequently, the mobile spine. Lytic destruction of the affected bone is more commonly seen on radiography and CT than (reactive) osteosclerosis. Some chordomas show amorphous calcifications which might resemble the matrix calcifications of chondrosarcomas. In the majority of cases, a soft tissue component is present at the time of diagnosis.

MR imaging typically shows a lobulated mass with an extraosseous component, which is often larger than the intraosseous portion of the tumor. The tumor tissue appears hypointense on T1- and markedly hyperintense on T2-weighted images. Contrast enhancement is usually moderate and does not reveal a specific pattern (diffuse enhancement) (see Fig. 12.18a, b). Adjacent organs are more likely to be displaced than infiltrated by the soft tissue mass.

12.8.3 Target Volume Delineation in Chordoma

Treatment of chordomas remains a challenge. Tumors are believed to grow slowly and metastasize rarely, but their local aggressiveness is exceptionally and uncontrolled local disease is eventually fatal. Radical tumor resection would be the treatment of choice but is often hampered by the proximity or involvement of neurovascular structures. In several series from different particle therapy centers in North America, Europe, and Japan, favorable local control rates could be achieved with radiation treatment employing protons, helium, or carbon ions. For skull base chordomas, 5-year local control rates of 60–80 % are reported, which are lower than for chondrosarcomas at this site but better than the average outcome for skull base chordoma reported in the literature (Munzenrider and Liebsch 1999; Noel et al. 2001; Schulz-Ertner et al. 2007a; Jensen et al. 2011; Ares et al. 2009). A recent meta-analysis on skull base chordomas treated with surgery and adjuvant radiotherapy considered 23 observational studies published between 1999 and 2010 including 807 patients (Di Maio et al. 2011). The weighted average 5-year progression-free survival and overall survival were 50.8 and 78.4 %, respectively. Patients with incomplete tumor resection were 3.83 times more likely to experience a recurrence and 5.85 times more likely to die at 5 years versus patients with complete resection. There was no difference in 5-year overall survival by type of adjuvant radiation, although 5-year PFS was lower in patients receiving Gamma Knife radiosurgery relative to carbon ion radiotherapy on paired z-test (Di Maio et al. 2011). Postoperative stereotactic fractionated radiotherapy to a median total dose of 66.6 Gy for residual tumor resulted in a local control rate of 50 % at 5 years in a series from Heidelberg including 37 patients, which is in line with the average results from the meta-analysis (Debus et al. 2000).

The experience with Gamma Knife stereotactic radiosurgery for residual or recurrent skull base chordomas is presented in a pooled analysis of 71 patients treated in 6 North American centers between 1988 and 2008. Of note, 21 patients underwent prior RT (median total dose of 55.8 Gy). A median margin dose of 15 Gy (9–25 Gy) and a median maximum dose of 32 Gy (18–50 Gy) were delivered with radiosurgery to a median target volume of 7.1 cm^3 (range 0.9–109 cm^3). The 5-year "treated tumor control rate" was 66.4 %, with 23 of 71 patients developing tumor progression in the treatment volume. Another 14 patients suffered from progression "adjacent to the prescribed treatment volume" and further 7 patients from "remote tumor recurrence," which means that 41 of 71 patients experienced some sort of local failure

(Kano et al. 2011). This underlines the necessity to carefully consider all infiltrative tumor extensions in the treatment of a chordoma and to care for the surgical pathway, as tumor seeding is an important issue (Rombi et al. 2013; Wang et al. 2012).

Very good results for skull base chordoma have been obtained with carbon ion therapy at the National Institute of Radiological Sciences (NIRS) in Chiba, Japan: a 5-year local control rate of 88 % was reported after a median dose of 60.8 Gy (relative biological effectiveness (RBE)) delivered in 16 fractions to 47 patients with gross tumor (Tsujii and Kamada 2012). For details about the target volume definition in the skull base, the reader is referred to the corresponding chapter in this textbook (Chap. 3).

For chordoma of the spine, the literature is sparse. In the phase II study of high-dose photon/proton radiotherapy in the management of spine sarcomas from Boston, 29 chordomas were included. After a median follow-up of 4 years, among 23 primary chordomas, none recurred locally versus 3 of 6 treated for locally recurrent chordoma after prior surgery. Details of the target volume delineation are also given in section 5.3 of this chapter (Target Volume Delineation in Chondrosarcoma). In brief, the CTV_{large} contained the GTV plus 1 cm soft tissue margin on extraosseous tumor plus one vertebra above and below the grossly involved vertebrae and all surgically manipulated tissue. The PTV_{large} encompassed the CTV_{large} with an institutional set-up margin and was treated to a dose of 50.4 Gy (RBE). For the PTV_{boost}, only the initial GTV plus an institutional setup margin was considered and treated to a total dose of 70.2 Gy (RBE) after complete resection or to a total dose of 77.4 Gy (RBE) after biopsy, respectively. In case of R2 resection, the fields were coned down again after 70.2 Gy (RBE) to treat the residual gross tumor with institutional setup margin to the total dose of 77.4 Gy (RBE). The doses to the spinal cord center and surface were constrained to 54 Gy (RBE) and 63 Gy (RBE), respectively. The cauda equina should not receive doses above 70.2 Gy (RBE), except for areas in direct contact with tumor. During follow-up, 2 patients developed sacral neuropathy with unilateral leg weakness 4 and 5.5 years after doses of 77.12 Gy (RBE) and 77.4 Gy (RBE) for sacral chordoma. Recommended posterior skin dose was 66 Gy RBE or less. Apart from an insufficiency fracture of the contralateral sacrum (1 month after surgery and 19.8 Gy of preoperative radiotherapy, obviously not related to radiotherapy), a case of erectile dysfunction, and a rectal bleed, no other grade III complications occurred in 29 patients with chordoma (DeLaney et al. 2009).

The experience from the Paul Scherrer Institute with spot-scanning-based proton therapy comprises 40 patients with extracranial chordoma (16 cervical, 4 thoracic, 10 lumbar spine, and 11 sacrum). Nineteen of 40 patients had gross residual disease between 13 and 495 cm^3 (mean 69.1 cm^3) which seemed not suitable for further resection. The CTV encompassed the presurgical tumor extension plus the dorsal surgical pathway (but not the abdominal pathway) and surgical instrumentations. The PTV was derived from the CTV plus a margin of 0.3–0.5 cm in all three dimensions for cervical chordomas and a margin of 0.5–1.0 cm for all other sites. The mean dose to the PTV was 72.5 Gy (RBE) (range, 59.4–75.2 Gy (RBE)) in conventional fractionation. Dose to the surface and the center of the spinal cord was constrained to 63 Gy (RBE) and 54 Gy (RBE), respectively. After a median follow-up of 43 months, 13 patients developed local failure, resulting in a 5-year local control rate of 62 % for the entire cohort. All 19 patients without prior surgical stabilization had local tumor control at 5 years (100 %) with one local failure observed subsequently at 71 months. In contrast, 12 of 21 patients with surgical stabilization (i.e., vertebral body reconstruction with titanium cage placement +/− posterior stabilization) developed local failures, yielding a 5-year local control rate of only 30 %. The difference was highly significant ($p=0.0003$). The 5-year local control rate for patients with and without gross residual disease was 47 and 66 %, respectively ($p=0.048$). No late grade III neurotoxicity occurred. A case of osteonecrosis of an irradiated

lumbar vertebra 13 months after proton treatment with 71 Gy (RBE) and a case of subcutaneous fistula in the sacral region requiring several wound debridements were reported, the latter patient also developing a leiomyosarcoma of the urinary bladder (Staab et al. 2011).

The pediatric series from the same institution included 19 chordomas, of which 5 were located at the cervical spine and one each at the lumbar spine and sacrum. Dose prescription and constraints were determined as summarized above for adult patients, and a maximum dose (D2) of 64 Gy (RBE) was defined to the center of cauda equina and sacral nerve roots. A mean dose of 74 Gy (RBE) was applied (range, 73.8–75.6 Gy (RBE)). All spinal tumors remained controlled during follow-up, and no high-grade toxicity occurred (Rombi et al. 2013).

In an institutional series of 23 spinal chordomas, 6 of which were located in the cervical spine; four, tumors involving L5, S1, or S2 level; and 13, tumors of S3 level and below, only in five of ten patients in the latter group the tumor could be controlled by wide excision alone. Of three tumors managed by biopsy and radiation therapy, two remained controlled with stereotactic treatment. All other patients with a surgical approach upfront eventually developed a local failure, in spite of postoperative radiation therapy applied to most of them (details of radiation therapy were not reported) (Eid et al. 2011).

Based on observations from surgeons, chordomas are tumors with less vasculature, despite the fact that they often cause heavy bleeding intraoperatively, which is assumed to be due to the aggressive extension of the neoplasm encasing the surrounding abundant vasculatures. They are "relatively fluid" compared with other solid tumors, can easily break through the bony cortex, and are prone to invade the paravertebral soft tissue. These features might explain the problem of seeding in the surgical field, and surgical techniques should be applied to minimize tumor seeding (Wang et al. 2012). In a series of 14 cervical chordoma patients managed surgically with special regard to minimize tumor seeding and with application of postoperative radiotherapy to a median dose of 66 Gy (range 44–80 Gy), 5-year disease-free survival was 50 % (Wang et al. 2012).

Thus, for postoperative radiotherapy of chordoma, inclusion of the surgically manipulated tissue is mandatory and treatment of the whole surgical bed to high total doses is justified. An example is given in Fig. 12.18.

Very favorable results have been reported for definitive carbon ion radiotherapy from Chiba, Japan. Between 1996 and 2007, 95 patients with unresectable sacral chordomas including 11 recurrences following previous resection were treated to a median total dose of 70.4 Gy (RBE) (range, 52.8–73.6 Gy (RBE)) delivered in 16 fractions within 4 weeks. Patients were positioned in a customized cradle and immobilized with a thermoplastic sheet, usually in prone position. Respiratory gating of both the acquired CT images and the therapy beam was performed. The median CTV was 370 cm^3 (range, 47–1,468 cm^3), the PTV included the CTV plus a 5 mm margin for positioning uncertainties. The CTV received at least 90 % of the prescribed dose. In cases where the tumor was located very close to critical organs, such as the bowel and skin, the margin was reduced and consequently <90 % of the dose was applied to some tumors. After a median follow-up of 42 months, six local recurrences were observed; the 5-year local control rate was 88 %. Two patients had grade III late skin reactions. Two patients with a total dose of 73.6 Gy (RBE) experienced grade IV late skin and soft tissue complications requiring skin grafts. Fifteen patients required continuing medication for sciatic nerve neuropathy. Five of these 15 patients received a total dose of 73.6 Gy (RBE). The authors mentioned in the discussion an analysis of dose-volume histograms of 44 sciatic nerves in 22 patients receiving 70.4–73.6 Gy (RBE) and followed for >2 years, indicating that a length of >10 cm and a total dose of >70 Gy (RBE) were possible thresholds for sciatic nerve injury (Imai et al. 2010, 2011).

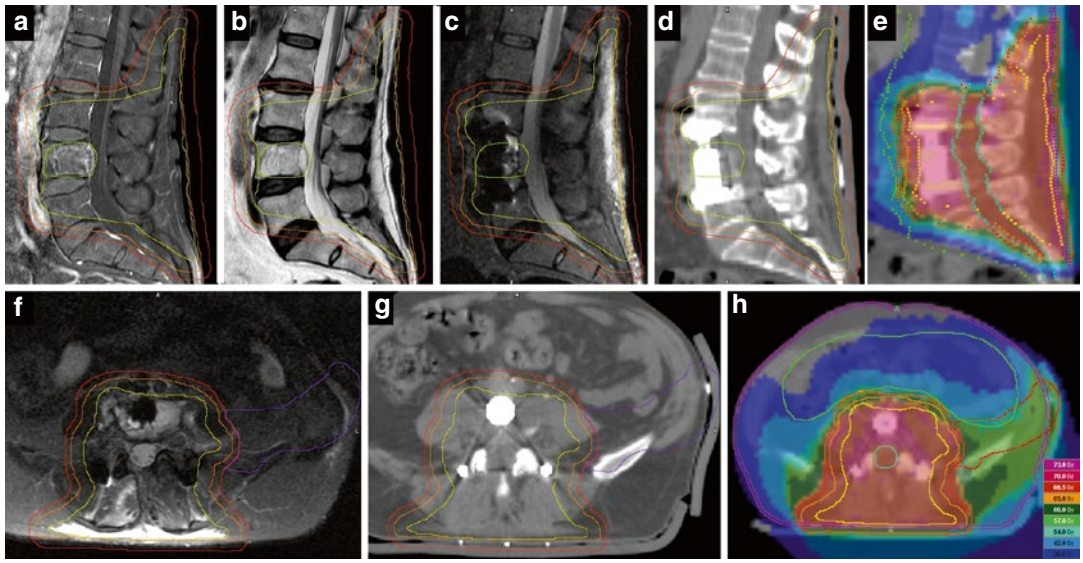

Fig. 12.18 Chordoma of the 4th lumbal vertebra in a 62-year-old man. (**a**) Sagittal contrast-enhanced T1-weighted MR image with fat suppression and (**b**) T2-weighted image, revealing the tumorous destruction of the vertebral body and extension into the epidural space. The patient presented with right lower back pain that was relieved after interlaminar fenestration of L4/L5, partial tumor resection using a paravertebral access, and dorsal stabilization by percutaneous instrumentation of level L3 to L5. Histopathologically, chordoma was confirmed (MIB-1 proliferation index of 5 %). 4 weeks later, tumor debulking with total vertebrectomy of L4, partial vertebrectomy of L3/L5 and intervertebral discs, as well as obelisk insertion was performed over a left lateral retroperitoneal surgical access. (**c**) Postoperative sagittal STIR image showing artifacts induced by metallic implants, normalized anterior contour of the spinal canal, and gross postoperative edema in the posterior subcutaneous tissue. (**d**) Sagittal reconstruction of the planning CT for additive radiotherapy: $GTV_{initial}$, *light green*; GTV_{postop}, *yellow* (resection cavity and high-risk area of tumor-cell contamination due to surgical procedures); PTV_{SIB}, *orange* (GTV_{postop} plus 0.5 cm margin for CTV, manually shortened to allow for sparing of kidneys and bowels, plus 0.5 cm margin for positioning uncertainty, excluding 3 mm skin) to a total dose of 70 Gy in 35 fractions of 2.0 Gy; and PTV_{large1}, *red* (GTV_{postop} plus 1.0 cm margin with inclusion of $GTV_{initial}$ plus 1.5 cm margin in body plus vertebrae L3 and L5 for CTV, plus 0.5 cm margin for positioning uncertainty) to a total dose of 60 Gy in fractions of 1.71 Gy. (**e**) Sagittal view of dose distribution (tomotherapy planning): Full dose to the spinal nerves within level L3–S2, *light blue*, with a median dose of 68.9 Gy and a point dose maximum (D_{max}) of 71.4 Gy. Sparing of the spinal canal at and above level L2 (D_{max} 51.8 Gy) and of the bowel – *green* (D_{mean} 23.2 Gy, D_{max} 58.2 Gy). (**f**) Postoperative axial STIR image and (**g**) axial planning CT at the level of L4. Apart from the target volumes described above, the retroperitoneal surgical access was included in a PTV_{large2} – *purple* – according to the postoperative changes along the psoas muscle, the anterior surface of the left iliac bone, and the left lateral abdominal wall. (**h**) In order to apply single doses not lower than 1.71 Gy per fraction to the PTV_{large2} (as prescribed for the PTV_{large1}), the main treatment plan was calculated for a prescribed total dose of 60 Gy in 35 fractions to the PTV_{large2} but replaced for the last 3 fractions with a plan not further considering this target volume, resulting in a total dose of 54.7 Gy for the PTV_{large2}

References

Applebaum MA, Goldsby R, Neuhaus J, DuBois SG (2012) Clinical features and outcomes in patients with Ewing sarcoma and regional lymph node involvement. Pediatr Blood Cancer 59:617–620

Ares C, Hug EB, Lomax AJ, Bolsi A, Timmermann B, Rutz HP, Schuller JC, Pedroni E, Goitein G (2009) Effectiveness and safety of spot scanning proton radiation therapy for chordomas and chondrosarcomas of the skull base: first long-term report. Int J Radiat Oncol Biol Phys 75:1111–1118

Bacci G, Palmerini E, Staals EL, Longhi A, Barbieri E, Alberghini M, Ferrari S (2009) Ewing's sarcoma family tumors of the humerus: outcome of patients treated with radiotherapy, surgery or surgery and adjuvant radiotherapy. Radiother Oncol 93:383–387

Baumert BG, Spahr MO, Von Hochstetter A, Beauvois S, Landmann C, Fridrich K, Villa S, Kirschner MJ, Storme G, Thum P, Streuli HK, Lombriser N, Maurer R, Ries G, Bleher EA, Willi A, Allemann J, Buehler

U, Blessing H, Luetolf UM, Davis JB, Seifert B, Infanger M (2007) The impact of radiotherapy in the treatment of desmoid tumours. An international survey of 110 patients. A study of the Rare Cancer Network. Radiat Oncol 2:12

Bernstein M, Kovar H, Paulussen M, Randall RL, Schuck A, Teot LA, Juergens H (2006) Ewing's sarcoma family of tumors: current management. Oncologist 11: 503–519

Bjornsson J, McLeod RA, Unni KK, Ilstrup DM, Pritchard DJ (1998) Primary chondrosarcoma of long bones and limb girdles. Cancer 83:2105–2119

Blank LE, Koedooder K, van der Grient HN, Wolffs NA, van de Kar M, Merks JH, Pieters BR, Saeed P, Baldeschi L, Freling NJ, Koning CC (2010) Brachytherapy as part of the multidisciplinary treatment of childhood rhabdomyosarcomas of the orbit. Int J Radiat Oncol Biol Phys 77:1463–1469

Blattmann C, Oertel S, Schulz-Ertner D, Rieken S, Haufe S, Ewerbeck V, Unterberg A, Karapanagiotou-Schenkel I, Combs SE, Nikoghosyan A, Bischof M, Jakel O, Huber P, Kulozik AE, Debus J (2010) Non-randomized therapy trial to determine the safety and efficacy of heavy ion radiotherapy in patients with non-resectable osteosarcoma. BMC Cancer 10(96):96

Bolling T, Schuck A, Paulussen M, Dirksen U, Ranft A, Konemann S, Dunst J, Willich N, Jurgens H (2008) Whole lung irradiation in patients with exclusively pulmonary metastases of Ewing tumors. Toxicity analysis and treatment results of the EICESS-92 trial. Strahlenther Onkol 184:193–197

Bonvalot S, Desai A, Coppola S, Le Péchoux C, Terrier P, Domont J, Le Cesne A (2012) The treatment of desmoid tumors: a stepwise clinical approach. Ann Oncol 23(Suppl 10):x158–x166

Boriani S, Saravanja D, Yamada Y, Varga PP, Biagini R, Fisher CG (2009) Challenges of local recurrence and cure in low grade malignant tumors of the spine. Spine (Phila Pa) 34:S48–S57

Bossi A, De Wever I, Van Limbergen E, Vanstraelen B (2007) Intensity modulated radiation-therapy for preoperative posterior abdominal wall irradiation of retroperitoneal liposarcomas. Int J Radiat Oncol Biol Phys 67:164–170

Breneman J, Meza J, Donaldson SS, Raney RB, Wolden S, Michalski J, Laurie F, Rodeberg DA, Meyer W, Walterhouse D, Hawkins DS (2012) Local control with reduced-dose radiotherapy for low-risk rhabdomyosarcoma: a report from the Children's Oncology Group D9602 study. Int J Radiat Oncol Biol Phys 83:720–726

Burdach S, Thiel U, Schoniger M, Haase R, Wawer A, Nathrath M, Kabisch H, Urban C, Laws HJ, Dirksen U, Steinborn M, Dunst J, Jurgens H (2010) Total body MRI-governed involved compartment irradiation combined with high-dose chemotherapy and stem cell rescue improves long-term survival in Ewing tumor patients with multiple primary bone metastases. Bone Marrow Transplant 45:483–489

Childs SK, Kozak KR, Friedmann AM, Yeap BY, Adams J, MacDonald SM, Liebsch NJ, Tarbell NJ, Yock TI (2012) Proton radiotherapy for parameningeal rhabdomyosarcoma: clinical outcomes and late effects. Int J Radiat Oncol Biol Phys 82:635–642

Coindre JM (2006) Grading of soft tissue sarcomas: review and update. Arch Pathol Lab Med 130: 1448–1453

Combs SE, Nikoghosyan A, Jaekel O, Karger CP, Haberer T, Munter MW, Huber PE, Debus J, Schulz-Ertner D (2009) Carbon ion radiotherapy for pediatric patients and young adults treated for tumors of the skull base. Cancer 115:1348–1355

Combs SE, Kessel KA, Herfarth K, Jensen A, Oertel S, Blattmann C, Ecker S, Hoess A, Martin E, Witt O, Jakel O, Kulozik AE, Debus J (2012) Treatment of pediatric patients and young adults with particle therapy at the Heidelberg Ion Therapy Center (HIT): establishment of workflow and initial clinical data. Radiat Oncol 7:170–177. doi:10.1186/1748-717X-7-170

Cotter SE, Herrup DA, Friedmann A, MacDonald SM, Pieretti RV, Robinson G, Adams J, Tarbell NJ, Yock TI (2011) Proton radiotherapy for pediatric bladder/prostate rhabdomyosarcoma: clinical outcomes and dosimetry compared to intensity-modulated radiation therapy. Int J Radiat Oncol Biol Phys 81:1367–1373

Curtis AE, Okcu MF, Chintagumpala M, Teh BS, Paulino AC (2009) Local control after intensity-modulated radiotherapy for head-and-neck rhabdomyosarcoma. Int J Radiat Oncol Biol Phys 73:173–177

De Alava E, Lessnik SL, Sorensen PH (2013) Ewing sarcoma. In: Fletcher CDM, Bridge JA, Hogendoorn PCW, Mertens F (eds) WHO classification of tumours of soft tissue and bone, 4th edn. IARC, France

Debus J, Schulz-Ertner D, Schad L, Essig M, Rhein B, Thillmann CO, Wannenmacher M (2000) Stereotactic fractionated radiotherapy for chordomas and chondrosarcomas of the skull base. Int J Radiat Oncol Biol Phys 47:591–596

DeLaney TF, Park L, Goldberg SI, Hug EB, Liebsch NJ, Munzenrider JE, Suit HD (2005) Radiotherapy for local control of osteosarcoma. Int J Radiat Oncol Biol Phys 61:492–498

DeLaney TF, Liebsch NJ, Pedlow FX, Adams J, Dean S, Yeap BY, McManus P, Rosenberg AE, Nielsen GP, Harmon DC, Spiro IJ, Raskin KA, Suit HD, Yoon SS, Hornicek FJ (2009) Phase II study of high-dose photon/proton radiotherapy in the management of spine sarcomas. Int J Radiat Oncol Biol Phys 74: 732–739

Dhakal S, Corbin KS, Milano MT, Philip A, Sahasrabudhe D, Jones C, Constine LS (2012) Stereotactic body radiotherapy for pulmonary metastases from soft-tissue sarcomas: excellent local lesion control and improved patient survival. Int J Radiat Oncol Biol Phys 82:940–945

Di Maio S, Temkin N, Ramanathan D, Sekhar LN (2011) Current comprehensive management of cranial base chordomas: 10-year meta-analysis of observational studies. J Neurosurg 115:1094–1105

Dickie CI, Parent A, Griffin A, Craig T, Catton C, Chung P, Panzarella T, O'Sullivan B, Sharpe M (2009) A device and procedure for immobilization of patients receiving limb-preserving radiotherapy for soft tissue sarcoma. Med Dosim 34:243–249

Dickie CI, Parent AL, Chung PW, Catton CN, Craig T, Griffin AM, Panzarella T, Ferguson PC, Wunder JS, Bell RS, Sharpe MB, O'Sullivan B (2010) Measuring interfractional and intrafractional motion with cone beam computed tomography and an optical localization system for lower extremity soft tissue sarcoma patients treated with preoperative intensity-modulated radiation therapy. Int J Radiat Oncol Biol Phys 78: 1437–1444

Dickie CI, Griffin AM, Parent AL, Chung PW, Catton CN, Svensson J, Ferguson PC, Wunder JS, Bell RS, Sharpe MB, O'Sullivan B (2012) The relationship between local recurrence and radiotherapy treatment volume for soft tissue sarcomas treated with external beam radiotherapy and function preservation surgery. Int J Radiat Oncol Biol Phys 82:1528–1534

Donaldson SS, Torrey M, Link MP, Glicksman A, Gilula L, Laurie F, Manning J, Neff J, Reinus W, Thompson E, Shuster JJ (1998) A multidisciplinary study investigating radiotherapy in Ewing's sarcoma: end results of POG #8346. Pediatric Oncology Group. Int J Radiat Oncol Biol Phys 42:125–135

Eaton BR, McDonald MW, Kim S, Marcus RB Jr, Sutter AL, Chen Z, Esiashvili N (2013) Radiation therapy target volume reduction in pediatric rhabdomyosarcoma: implications for patterns of disease recurrence and overall survival. Cancer 119:1578–1585

Eid AS, Chang UK, Lee SY, Jeon DG (2011) The treatment outcome depending on the extent of resection in skull base and spinal chordomas. Acta Neurochir (Wien) 153:509–516

EORTC (2013) A phase III randomized study of preoperative radiotherapy plus surgery versus surgery alone for patients with retroperitoneal sarcomas (RPS) – STRASS. http://www.eortc.be/clinicaltrials/trial number 62092. Accessed 1 July 2013

Flanagan AM, Yamaguchi T (2013) Chordoma. In: Fletcher CDM, Bridge JA, Hogendoorn PCW, Mertens F (eds) WHO classification of tumours of soft tissue and bone, 4th edn. IARC, France

Flannery T, Kano H, Niranjan A, Monaco EA III, Flickinger JC, Kofler J, Lunsford LD, Kondziolka D (2010) Gamma knife radiosurgery as a therapeutic strategy for intracranial sarcomatous metastases. Int J Radiat Oncol Biol Phys 76:513–519

Fletcher CDM, Bridge JA, Hogendoorn PCW, Mertens F (2013) WHO classification of tumours of soft tissue and bone, 4th edn. IARC, France

Freyschmidt J, Ostertag H, Jundt G (2010) Knochentumoren, 3rd edn. Springer, Heidelberg

Gelderblom H, Hogendoorn PC, Dijkstra SD, van Rijswijk CS, Krol AD, Taminiau AH, Bovee JV (2008) The clinical approach towards chondrosarcoma. Oncologist 13:320–329

Gluck I, Griffith KA, Biermann JS, Feng FY, Lucas DR, Ben-Josef E (2011) Role of radiotherapy in the management of desmoid tumors. Int J Radiat Oncol Biol Phys 80:787–792

Goda JS, Ferguson PC, O'Sullivan B, Catton CN, Griffin AM, Wunder JS, Bell RS, Kandel RA, Chung PW (2011) High-risk extracranial chondrosarcoma: long-term results of surgery and radiation therapy. Cancer 117:2513–2519

Goldblum JR, Fletcher JA (2013) Desmoid-type fibromatosis. In: Fletcher CDM, Bridge JA, Hogendoorn PCW, Mertens F (eds) WHO classification of tumours of soft tissue and bone, 4th edn. IARC, France

Guadagnolo BA, Zagars GK, Ballo MT (2008) Long-term outcomes for desmoid tumors treated with radiation therapy. Int J Radiat Oncol Biol Phys 71:441–447

Haas RL, DeLaney TF, O'Sullivan B, Keus RB, Le PC, Olmi P, Poulsen JP, Seddon B, Wang D (2012) Radiotherapy for management of extremity soft tissue sarcomas: why, when, and where? Int J Radiat Oncol Biol Phys 84:572–580

Habrand JL, Schneider R, Alapetite C, Feuvret L, Petras S, Datchary J, Grill J, Noel G, Helfre S, Ferrand R, Bolle S, Sainte-Rose C (2008) Proton therapy in pediatric skull base and cervical canal low-grade bone malignancies. Int J Radiat Oncol Biol Phys 71:672–675

Haeusler J, Ranft A, Boelling T, Gosheger G, Braun-Munzinger G, Vieth V, Burdach S, van den Berg H, Juergens H, Dirksen U (2010) The value of local treatment in patients with primary, disseminated, multifocal Ewing sarcoma (PDMES). Cancer 116:443–450

Hogendoorn PCW, Bovée JVMG, Nielsen GP (2013) Chondrosarcoma (grades I-III), including primary and secondary variants and periosteal chondrosarcoma. In: Fletcher CDM, Bridge JA, Hogendoorn PCW, Mertens F (eds) WHO classification of tumours of soft tissue and bone, 4th edn. IARC, France

Hong L, Alektiar KM, Hunt M, Venkatraman E, Leibel SA (2004) Intensity-modulated radiotherapy for soft tissue sarcoma of the thigh. Int J Radiat Oncol Biol Phys 59:752–759

Howlader N, Noone AM, Krapcho M, Garshell J, Neyman N, Altekruse SF, Kosary CL, Yu M, Ruhl J, Tatalovich Z, Cho H, Mariotto A, Lewis DR, Chen HS, Feuer EJ, Cronin KA (eds) (2013) SEER cancer statistics review, 1975–2010, National Cancer Institute. Bethesda, http://seer.cancer.gov/csr/1975_2010/, based on November 2012 SEER data submission, posted to the SEER web site

Hug EB, Loredo LN, Slater JD, DeVries A, Grove RI, Schaefer RA, Rosenberg AE, Slater JM (1999) Proton radiation therapy for chordomas and chondrosarcomas of the skull base. J Neurosurg 91:432–439

ICRU, International Commission on Radiation Units and Measurements (1993) ICRU report 50: prescribing, recording, and reporting photon-beam therapy. Bethesda, http://www.icru.org/home/reports/prescribing-recording-and-reporting-photon-beam-therapy-report-50

ICRU, International Commission on Radiation Units and Measurements (2010) ICRU report 83: prescribing,

recording, and reporting intensity-modulated photon-beam therapy (IMRT). Bethesda, http://www.icru.org/testing/reports/prescribing-recording-and-reporting-intensity-modulated-photon-beam-therapy-imrt-icru-report-83

Imai R, Kamada T, Tsuji H, Sugawara S, Serizawa I, Tsujii H, Tatezaki S (2010) Effect of carbon ion radiotherapy for sacral chordoma: results of Phase I-II and Phase II clinical trials. Int J Radiat Oncol Biol Phys 77:1470–1476

Imai R, Kamada T, Sugahara S, Tsuji H, Tsujii H (2011) Carbon ion radiotherapy for sacral chordoma. Br J Radiol 84(Spec No 1):S48–S54. doi:10.1259/bjr/13783281

Indelicato DJ, Keole SR, Shahlaee AH, Morris CG, Gibbs CP Jr, Scarborough MT, Pincus DW, Marcus RB Jr (2010) Spinal and paraspinal Ewing tumors. Int J Radiat Oncol Biol Phys 76:1463–1471

Indelicato DJ, Keole SR, Lagmay JP, Morris CG, Gibbs CP Jr, Scarborough MT, Islam S, Marcus RB Jr (2011) Chest wall Ewing sarcoma family of tumors: long-term outcomes. Int J Radiat Oncol Biol Phys 81:158–166

Inwards C, Hogendoorn PCW (2013) Dedifferentiated chondrosarcoma. In: Fletcher CDM, Bridge JA, Hogendoorn PCW, Mertens F (eds) WHO classification of tumours of soft tissue and bone, 4th edn. IARC, France

Jensen AD, Munter MW, Debus J (2011) Review of clinical experience with ion beam radiotherapy. Br J Radiol 84(Spec No 1):S35–S47. doi:10.1259/bjr/71511359

Kano H, Iqbal FO, Sheehan J, Mathieu D, Seymour ZA, Niranjan A, Flickinger JC, Kondziolka D, Pollock BE, Rosseau G, Sneed PK, McDermott MW, Lunsford LD (2011) Stereotactic radiosurgery for chordoma: a report from the North American Gamma Knife Consortium. Neurosurgery 68:379–389

Karam I, Devic S, Hickeson M, Roberge D, Turcotte RE, Freeman CR (2009) PET/CT for radiotherapy treatment planning in patients with soft tissue sarcomas. Int J Radiat Oncol Biol Phys 75:817–821

Kim B, Chen YL, Kirsch DG, Goldberg SI, Kobayashi W, Kung JH, Wolfgang JA, Doppke K, Rosenberg AE, Nielsen GP, Raskin KA, Springfield DS, Schwab JH, Gebhardt MC, Yoon SS, Hornicek FJ, DeLaney TF (2010) An effective preoperative three-dimensional radiotherapy target volume for extremity soft tissue sarcoma and the effect of margin width on local control. Int J Radiat Oncol Biol Phys 77:843–850

Klish DS, Grossman P, Allen PK, Rhines LD, Chang EL (2011) Irradiation of spinal metastases: should we continue to include one uninvolved vertebral body above and below in the radiation field? Int J Radiat Oncol Biol Phys 81:1495–1499

Krasin MJ, Davidoff AM, Xiong X, Wu S, Hua CH, Navid F, Rodriguez-Galindo C, Rao BN, Hoth KA, Neel MD, Merchant TE, Kun LE, Spunt SL (2010) Preliminary results from a prospective study using limited margin radiotherapy in pediatric and young adult patients with high-grade nonrhabdomyosarcoma soft-tissue sarcoma. Int J Radiat Oncol Biol Phys 76:874–878

Laskar S, Bahl G, Ann MM, Puri A, Agarwal MG, Patil N, Shrivastava SK, Dinshaw KA (2007) Interstitial brachytherapy for childhood soft tissue sarcoma. Pediatr Blood Cancer 49:649–655

Lee CT, Bilton SD, Famiglietti RM, Riley BA, Mahajan A, Chang EL, Maor MH, Woo SY, Cox JD, Smith AR (2005) Treatment planning with protons for pediatric retinoblastoma, medulloblastoma, and pelvic sarcoma: how do protons compare with other conformal techniques? Int J Radiat Oncol Biol Phys 63: 362–372

Lin C, Donaldson SS, Meza JL, Anderson JR, Lyden ER, Brown CK, Morano K, Laurie F, Arndt CA, Enke CA, Breneman JC (2012) Effect of radiotherapy techniques (IMRT vs. 3D-CRT) on outcome in patients with intermediate-risk rhabdomyosarcoma enrolled in COG D9803–a report from the Children's Oncology Group. Int J Radiat Oncol Biol Phys 82:1764–1770

Liu AK, Stinauer M, Albano E, Greffe B, Tello T, Maloney K (2011) Local control of metastatic sites with radiation therapy in metastatic Ewing sarcoma and rhabdomyosarcoma. Pediatr Blood Cancer 57:169–171

Matsunobu A, Imai R, Kamada T, Imaizumi T, Tsuji H, Tsujii H, Shioyama Y, Honda H, Tatezaki S (2012) Impact of carbon ion radiotherapy for unresectable osteosarcoma of the trunk. Cancer 118:4555–4563

McBride SM, Raut CP, Lapidus M, Devlin PM, Marcus KJ, Bertagnolli M, George S, Baldini EH (2013) Locoregional recurrence after preoperative radiation therapy for retroperitoneal sarcoma: adverse impact of multifocal disease and potential implications of dose escalation. Ann Surg Oncol 20:2140–2147

Michalski JM, Meza J, Breneman JC, Wolden SL, Laurie F, Jodoin M, Raney B, Wharam MD, Donaldson SS (2004) Influence of radiation therapy parameters on outcome in children treated with radiation therapy for localized parameningeal rhabdomyosarcoma in Intergroup Rhabdomyosarcoma Study Group trials II through IV. Int J Radiat Oncol Biol Phys 59: 1027–1038

Micke O, Seegenschmiedt MH (2005) Radiation therapy for aggressive fibromatosis (desmoid tumors): results of a national Patterns of Care Study. Int J Radiat Oncol Biol Phys 61:882–891

Mounessi FS, Lehrich P, Haverkamp U, Willich N, Bolling T, Eich HT (2013) Pelvic Ewing sarcomas. Three-dimensional conformal vs intensity-modulated radiotherapy. Strahlenther Onkol 189:308–314

Mullen JT, DeLaney TF, Kobayashi WK, Szymonifka J, Yeap BY, Chen YL, Rosenberg AE, Harmon DC, Choy E, Yoon SS, Raskin KA, Petur NG, Hornicek FJ (2012) Desmoid tumor: analysis of prognostic factors and outcomes in a surgical series. Ann Surg Oncol 19:4028–4035

Mundt AJ, Awan A, Sibley GS, Simon M, Rubin SJ, Samuels B, Wong W, Beckett M, Vijayakumar S, Weichselbaum RR (1995) Conservative surgery and adjuvant radiation therapy in the management of adult soft tissue sarcoma of the extremities: clinical and

radiobiological results. Int J Radiat Oncol Biol Phys 32:977–985
Munzenrider JE, Liebsch NJ (1999) Proton therapy for tumors of the skull base. Strahlenther Onkol 175(Suppl 2):57–63
Nakashima Y, de Pinieux G, Ladanyi M (2013) Mesenchymal chondrosarcoma. In: Fletcher CDM, Bridge JA, Hogendoorn PCW, Mertens F (eds) WHO classification of tumours of soft tissue and bone, 4th edn. IARC, France
Nathan H, Raut CP, Thornton K, Herman JM, Ahuja N, Schulick RD, Choti MA, Pawlik TM (2009) Predictors of survival after resection of retroperitoneal sarcoma: a population-based analysis and critical appraisal of the AJCC staging system. Ann Surg 250:970–976
National Cancer Institute (2013) Preoperative radiotherapy for sarcomas of the extremities with intensity-modulation, image-guidance and small safety-margins (PREMISS). http://www.cancer.gov/clinicaltrials/search/view?cdrid=729085&version=HealthProfessional&protocolsearchid=12212638. Accessed 1 July 2013
Nikoghosyan AV, Rauch G, Munter MW, Jensen AD, Combs SE, Kieser M, Debus J (2010) Randomised trial of proton vs. carbon ion radiation therapy in patients with low and intermediate grade chondrosarcoma of the skull base, clinical phase III study. BMC Cancer 10:606–610. doi:10.1186/1471-2407-10-606
Noel G, Habrand JL, Mammar H, Pontvert D, Haie-Meder C, Hasboun D, Moisson P, Ferrand R, Beaudre A, Boisserie G, Gaboriaud G, Mazal A, Kerody K, Schlienger M, Mazeron JJ (2001) Combination of photon and proton radiation therapy for chordomas and chondrosarcomas of the skull base: the Centre de Protontherapie D'Orsay experience. Int J Radiat Oncol Biol Phys 51:392–398
Noel G, Feuvret L, Ferrand R, Boisserie G, Mazeron JJ, Habrand JL (2004) Radiotherapeutic factors in the management of cervical-basal chordomas and chondrosarcomas. Neurosurgery 55:1252–1260
Nuyttens JJ, Rust PF, Thomas CR Jr, Turrisi AT III (2000) Surgery versus radiation therapy for patients with aggressive fibromatosis or desmoid tumors: a comparative review of 22 articles. Cancer 88:1517–1523
O'Sullivan B, Davis AM, Turcotte R, Bell R, Catton C, Chabot P, Wunder J, Kandel R, Goddard K, Sadura A, Pater J, Zee B (2002) Preoperative versus postoperative radiotherapy in soft-tissue sarcoma of the limbs: a randomised trial. Lancet 359:2235–2241
O'Sullivan B, Griffin AM, Dickie CI, Sharpe MB, Chung PW, Catton CN, Ferguson PC, Wunder JS, Deheshi BM, White LM, Kandel RA, Jaffray DA, Bell RS (2013) Phase 2 study of preoperative image-guided intensity-modulated radiation therapy to reduce wound and combined modality morbidities in lower extremity soft tissue sarcoma. Cancer 119:1878–1884
Paulino AC, Mai WY, Teh BS (2013) Radiotherapy in metastatic Ewing sarcoma. Am J Clin Oncol 36: 283–286
Pawlik TM, Pisters PW, Mikula L, Feig BW, Hunt KK, Cormier JN, Ballo MT, Catton CN, Jones JJ, O'Sullivan B, Pollock RE, Swallow CJ (2006) Long-term results of two prospective trials of preoperative external beam radiotherapy for localized intermediate- or high-grade retroperitoneal soft tissue sarcoma. Ann Surg Oncol 13:508–517
Petersen IA, Haddock MG, Donohue JH, Nagorney DM, Grill JP, Sargent DJ, Gunderson LL (2002) Use of intraoperative electron beam radiotherapy in the management of retroperitoneal soft tissue sarcomas. Int J Radiat Oncol Biol Phys 52:469–475
Pezner RD, Liu A, Chen YJ, Smith DD, Paz IB (2011) Full-dose adjuvant postoperative radiation therapy for retroperitoneal sarcomas. Am J Clin Oncol 34: 511–516
Roeder F, Timke C, Oertel S, Hensley FW, Bischof M, Muenter MW, Weitz J, Buchler MW, Lehner B, Debus J, Krempien R (2010) Intraoperative electron radiotherapy for the management of aggressive fibromatosis. Int J Radiat Oncol Biol Phys 76: 1154–1160
Rombi B, DeLaney TF, MacDonald SM, Huang MS, Ebb DH, Liebsch NJ, Raskin KA, Yeap BY, Marcus KJ, Tarbell NJ, Yock TI (2012) Proton radiotherapy for pediatric Ewing's sarcoma: initial clinical outcomes. Int J Radiat Oncol Biol Phys 82:1142–1148
Rombi B, Ares C, Hug EB, Schneider R, Goitein G, Staab A, Albertini F, Bolsi A, Lomax AJ, Timmermann B (2013) Spot-scanning proton radiation therapy for pediatric chordoma and chondrosarcoma: clinical outcome of 26 patients treated at Paul Scherrer Institute. Int J Radiat Oncol Biol Phys 86:578–584
Rutenberg MS, Indelicato DJ, Knapik JA, Lagmay JP, Morris C, Zlotecki RA, Scarborough MT, Gibbs CP, Marcus RB (2011) External-beam radiotherapy for pediatric and young adult desmoid tumors. Pediatr Blood Cancer 57:435–442
Sampath S, Hitchcock YJ, Shrieve DC, Randall RL, Schultheiss TE, Wong JY (2010) Radiotherapy and extent of surgical resection in retroperitoneal soft-tissue sarcoma: multi-institutional analysis of 261 patients. J Surg Oncol 101:345–350
Schuck A, Ahrens S, Konarzewska A, Paulussen M, Frohlich B, Konemann S, Rube C, Rube CE, Dunst J, Willich N, Jurgens H (2002) Hemithorax irradiation for Ewing tumors of the chest wall. Int J Radiat Oncol Biol Phys 54:830–838
Schuck A, Ahrens S, Paulussen M, Kuhlen M, Konemann S, Rube C, Winkelmann W, Kotz R, Dunst J, Willich N, Jurgens H (2003) Local therapy in localized Ewing tumors: results of 1058 patients treated in the CESS 81, CESS 86, and EICESS 92 trials. Int J Radiat Oncol Biol Phys 55:168–177
Schuck A, Ahrens S, von Schorlemer I, Kuhlen M, Paulussen M, Hunold A, Gosheger G, Winkelmann W, Dunst J, Willich N, Jürgens H (2005) Radiotherapy in Ewing tumors of the vertebrae: treatment results and

local relapse analysis of the CESS 81/86 and EICESS 92 trials. Int J Radiat Oncol Biol Phys 63:1562–1567
Schulz-Ertner D, Nikoghosyan A, Thilmann C, Haberer T, Jakel O, Karger C, Kraft G, Wannenmacher M, Debus J (2004) Results of carbon ion radiotherapy in 152 patients. Int J Radiat Oncol Biol Phys 58:631–640
Schulz-Ertner D, Karger CP, Feuerhake A, Nikoghosyan A, Combs SE, Jakel O, Edler L, Scholz M, Debus J (2007a) Effectiveness of carbon ion radiotherapy in the treatment of skull-base chordomas. Int J Radiat Oncol Biol Phys 68:449–457
Schulz-Ertner D, Nikoghosyan A, Hof H, Didinger B, Combs SE, Jakel O, Karger CP, Edler L, Debus J (2007b) Carbon ion radiotherapy of skull base chondrosarcomas. Int J Radiat Oncol Biol Phys 67:171–177
Schwarz R, Bruland O, Cassoni A, Schomberg P, Bielack S (2009) The role of radiotherapy in oseosarcoma. Cancer Treat Res 152:147–164
Serizawa I, Kagei K, Kamada T, Imai R, Sugahara S, Okada T, Tsuji H, Ito H, Tsujii H (2009) Carbon ion radiotherapy for unresectable retroperitoneal sarcomas. Int J Radiat Oncol Biol Phys 75:1105–1110
Siegel R, Naishadham D, Jemal A (2012) Cancer statistics, 2012. CA Cancer J Clin 62:10–29
Sindelar WF, Kinsella TJ, Chen PW, DeLaney TF, Tepper JE, Rosenberg SA, Glatstein E (1993) Intraoperative radiotherapy in retroperitoneal sarcomas. Final results of a prospective, randomized, clinical trial. Arch Surg 128:402–410
Sinha A, Hansmann A, Bhandari S, Gupta A, Burling D, Rana S, Phillips RK, Clark SK, Goh V (2012) Imaging assessment of desmoid tumours in familial adenomatous polyposis: is state-of-the-art 1.5 T MRI better than 64-MDCT? Br J Radiol 85:e254–e261
Sobin LH, Gospodarowicz MK, Wittekind CH (2009) UICC: TNM classification of malignant tumors, 7th edn. Wiley-Blackwell, Oxford
Soyfer V, Corn BW, Kollender Y, Tempelhoff H, Meller I, Merimsky O (2010) Radiation therapy for palliation of sarcoma metastases: a unique and uniform hypofractionation experience. Sarcoma 2010:927972
Staab A, Rutz HP, Ares C, Timmermann B, Schneider R, Bolsi A, Albertini F, Lomax A, Goitein G, Hug E (2011) Spot-scanning-based proton therapy for extracranial chordoma. Int J Radiat Oncol Biol Phys 81:e489–e496
Timmermann B, Schuck A, Niggli F, Weiss M, Lomax AJ, Pedroni E, Coray A, Jermann M, Rutz HP, Goitein G (2007) Spot-scanning proton therapy for malignant soft tissue tumors in childhood: first experiences at the Paul Scherrer Institute. Int J Radiat Oncol Biol Phys 67:497–504
Tseng WH, Martinez SR, Do L, Tamurian RM, Borys D, Canter RJ (2011) Lack of survival benefit following adjuvant radiation in patients with retroperitoneal sarcoma: a SEER analysis. J Surg Res 168:e173–e180
Tsujii H, Kamada T (2012) A review of update clinical results of carbon ion radiotherapy. Jpn J Clin Oncol 42:670–685
Tzeng CW, Fiveash JB, Popple RA, Arnoletti JP, Russo SM, Urist MM, Bland KI, Heslin MJ (2006) Preoperative radiation therapy with selective dose escalation to the margin at risk for retroperitoneal sarcoma. Cancer 107:371–379
Uhl V, Castro JR, Knopf K, Phillips TL, Collier JM, Petti PL, Daftari I (1992) Preliminary results in heavy charged particle irradiation of bone sarcoma. Int J Radiat Oncol Biol Phys 24:755–759
Viani GA, Novaes PE, Jacinto AA, Antonelli CB, Pellizzon AC, Saito EY, Salvajoli JV (2008) High-dose-rate brachytherapy for soft tissue sarcoma in children: a single institution experience. Radiat Oncol 3:9
Vogin G, Biston MC, Marchesi V, Amessis M, De ML, Lacroix F, Leroy A, Gassa F, Zefkili S, Helfre S (2013a) Localized Ewing sarcoma of the spine: a preliminary dose-escalation study comparing innovative radiation techniques in a single patient. Cancer Radiother 17:26–33
Vogin G, Helfre S, Glorion C, Mosseri V, Mascard E, Oberlin O, Gaspar N (2013b) Local control and sequelae in localised Ewing tumours of the spine: a French retrospective study. Eur J Cancer 49:1314–1323
Wang D, Bosch W, Roberge D, Finkelstein SE, Petersen I, Haddock M, Chen YL, Saito NG, Kirsch DG, Hitchcock YJ, Wolfson AH, DeLaney TF (2011) RTOG sarcoma radiation oncologists reach consensus on gross tumor volume and clinical target volume on computed tomographic images for preoperative radiotherapy of primary soft tissue sarcoma of extremity in Radiation Therapy Oncology Group studies. Int J Radiat Oncol Biol Phys 81:e525–e528
Wang Y, Xiao J, Wu Z, Huang Q, Huang W, Zhu Q, Lin Z, Wang L (2012) Primary chordomas of the cervical spine: a consecutive series of 14 surgically managed cases. J Neurosurg Spine 17:292–299
Weber DC, Rutz HP, Pedroni ES, Bolsi A, Timmermann B, Verwey J, Lomax AJ, Goitein G (2005) Results of spot-scanning proton radiation therapy for chordoma and chondrosarcoma of the skull base: the Paul Scherrer Institut experience. Int J Radiat Oncol Biol Phys 63:401–409
White LM, Wunder JS, Bell RS, O'Sullivan B, Catton C, Ferguson P, Blackstein M, Kandel RA (2005) Histologic assessment of peritumoral edema in soft tissue sarcoma. Int J Radiat Oncol Biol Phys 61: 1439–1445
Wolden SL, Wexler LH, Kraus DH, Laquaglia MP, Lis E, Meyers PA (2005) Intensity-modulated radiotherapy for head-and-neck rhabdomyosarcoma. Int J Radiat Oncol Biol Phys 61:1432–1438
Wylie JP, O'Sullivan B, Catton C, Gutierrez E (1999) Contemporary radiotherapy for soft tissue sarcoma. Semin Surg Oncol 17:33–46
Yokouchi M, Terahara M, Nagano S, Arishima Y, Zemmyo M, Yoshioka T, Tanimoto A, Komiya S (2011) Clinical implications of determination of safe surgical margins by using a combination of CT and

18FDG-positron emission tomography in soft tissue sarcoma. BMC Musculoskelet Disord 12(166):166

Yoon SS, Chen YL, Kirsch DG, Maduekwe UN, Rosenberg AE, Nielsen GP, Sahani DV, Choy E, Harmon DC, DeLaney TF (2010) Proton-beam, intensity-modulated, and/or intraoperative electron radiation therapy combined with aggressive anterior surgical resection for retroperitoneal sarcomas. Ann Surg Oncol 17:1515–1529

Zlotecki RA, Scarborough MT, Morris CG, Berrey BH, Lind DS, Enneking WF, Marcus RB Jr (2002) External beam radiotherapy for primary and adjuvant management of aggressive fibromatosis. Int J Radiat Oncol Biol Phys 54:177–181

Lymphomas

13

Pretesh R. Patel and Chris R. Kelsey

Contents

Abbreviations

ABVD	Adriamycin, bleomycin, vinblastine, dacarbazine
CT	Computed tomography
CTV	Clinical target volume
DLBCL	Diffuse large B-cell lymphoma
ESR	Erythrocyte sedimentation rate
GTV	Gross tumor volume
IFRT	Involved-field radiation therapy
IMRT	Intensity-modulated radiation therapy
INRT	Involved-node radiation therapy
ISRT	Involved-site radiation therapy
MALT	Mucosa-associated lymphoid tissue
MLC	Multi-leaf collimators
NLPHL	Nodular lymphocyte-predominant Hodgkin lymphoma
PCNSL	Primary central nervous system lymphoma
PET	Positron emission tomography
PTV	Planning target volume
RT	Radiation therapy
WBRT	Whole-brain radiation therapy

13.1 Introduction

Thomas Hodgkin first described lymphoma as "[the] morbid appearance of the absorbent glands and spleen" in 1832. Since that time, it has been recognized that lymphoma is in fact comprised of a diverse group of diseases. The World Health Organization 2008 classification lists some 80

P.R. Patel, MD • C.R. Kelsey, MD (✉)
Department of Radiation Oncology,
Duke Cancer Institute,
Duke University Medical Center,
Morris Building, Room 05125A, 201 Trent Drive,
Durham, NC, 27710, USA
e-mail: christopher.kelsey@duke.edu

A.-L. Grosu, C. Nieder (eds.), *Target Volume Definition in Radiation Oncology*,
DOI 10.1007/978-3-662-45934-8_13, © Springer-Verlag Berlin Heidelberg 2015

subtypes of B- and T-cell hematopoietic and lymphoid neoplasms, Hodgkin lymphoma among them (Swerdlow and Harris 2008). The history of Hodgkin lymphoma is illustrative of the systematic advance in the treatment of lymphoma generally, and three key lessons from this history influence therapy today.

First, advanced radiation techniques can lead to improvements in the therapeutic ratio. For many decades after Hodgkin's first description, Hodgkin lymphoma was considered to be a systemic and incurable disease. Initially, patients were generally treated with primitive radiation machines to sites of palpable disease using a wide range of doses. Two important concepts emerged from work at Stanford University. The first concept was radiation dose response when used as the sole modality (Kaplan 1966). A dose of ~35–40 Gy was necessary to achieve local control. The second concept was the nature of Hodgkin lymphoma to spread to contiguous lymph nodes (Rosenberg and Kaplan 1966). Thus, prophylactic treatment to clinically uninvolved but high-risk adjacent sites led to higher rates of disease control. For many decades patients with early stage disease were treated with definitive radiation therapy using full doses and large fields (subtotal nodal irradiation).

Second, effective eradication of subclinical disease with systemic drug therapy can allow for safe reductions in RT volumes and dose. For Hodgkin lymphoma, subtotal nodal irradiation has been supplanted by combined modality therapy. In the setting of effective systemic therapy, randomized studies have confirmed that RT treatment volumes and dose can be decreased without loss of clinical efficacy (Bonadonna et al. 2004; Engert et al. 2003, 2010). In essence, chemotherapy is relied upon to eradicate subclinical disease, and radiation therapy is utilized to optimize local control at originally involved sites. A lower dose is typically adequate when used as an adjunct to effective systemic therapy.

Third, the quality of survivorship takes on greater importance with increasing treatment efficacy and higher cure rates. It is well-documented that reductions in the intensity of RT, i.e., lower dose and smaller field size, are associated with lower rates of acute and long-term morbidity (Bonadonna et al. 2004; Koontz et al. 2006). Secondary malignancies (Hodgson et al. 2007) and cardiac complications (Schellong et al. 2010) are two of the most important late complications of lymphoma survivors – both of which appear to be associated with radiation dose and volume. Similarly, the preference of chemotherapy, ABVD (doxorubicin, bleomycin, vinblastine, dacarbazine) over MOPP (mechlorethamine, vincristine, procarbazine, prednisone), for example, is largely based on the improved toxicity profile of the former.

Lymphoma management continues to evolve, and the issues mentioned above have ushered in new paradigms for radiotherapy for both Hodgkin and non-Hodgkin lymphoma. Herein, modern guidelines for design and delivery of RT will be presented. The influences of advances in diagnostic imaging, systemic therapy, and RT delivery systems will be highlighted. Finally, case-based discussions of commonly encountered disease entities will highlight nuances of radiation treatment planning and delivery.

13.2 General Considerations

13.2.1 Volumetric Treatment Planning

Classic lymphoma radiation fields – going by such names as total nodal, subtotal nodal, mantle, inverted Y, and involved field – are largely based on two-dimensional osseous anatomy. The definitions of anatomic regions in the Ann Arbor staging classification were never intended to define RT fields but have bolstered this concept nonetheless. Modern imaging and RT treatment planning have rendered obsolete this approach in favor of volumetrically defined targets.

Cross-sectional and functional imaging is widely available and ubiquitously used to stage and monitor lymphoma. Both online electronic fusion and manual matching of diagnostic and radiation treatment planning images are now possible. As such, irradiation volumes may be more

precisely defined. The familiar concepts of gross tumor volume (GTV), clinical target volume (CTV), and planning target volume (PTV) as defined in ICRU Report 83 (ICRU 2010) should be used in lymphoma treatment planning.

In general, the GTV should include all clinically detectable disease. In the case of consolidation RT following systemic therapy, both pre- and post-chemotherapy GTVs should be delineated. The most critical component of modern treatment planning is definition of the CTV. This volume should ideally include all sites of gross *and* microscopic disease.

In the most optimal setting, it may be possible to define a highly conformal CTV which only includes the involved nodes. Involved-node radiation therapy (INRT) requires meticulous review of diagnostic imaging, initiation of radiation treatment planning prior to initiation of chemotherapy, advanced RT techniques to avoid marginal miss, and effective systemic therapy to successfully eradicate subclinical disease in the immediately adjacent area. Standard guidelines for INRT have been published by the EORTC-GELA (Girinsky et al. 2008) and German Hodgkin Study Group (Eich et al. 2008). Those who implement INRT as part of a combined modality program are encouraged to adopt strict adherence to these criteria.

In the alternate extreme – inadequate diagnostic and/or treatment planning imaging, suboptimal RT delivery techniques, or inadequate systemic therapy – a more generous CTV, similar to the involved field, may be more appropriate. Most cases will fall between these two extremes. In that setting, the CTV should be more generous than the INRT CTV but need not include the entire lymph node region. This strategy is recommended for most clinical scenarios in which both chemotherapy and radiation therapy are utilized and is termed involved site radiotherapy (ISRT). In defining the ISRT CTV, the quality of diagnostic imaging, response to systemic therapy, disease-specific spread patterns, and adjacent at-risk organs should be considered (see summary Fig. 13.1). INRT is generally not recommended for diseases treated with RT alone (e.g., stage I follicular lymphoma).

The CTV is then expanded to create the PTV to account for setup uncertainty and target motion. A margin for penumbra in three-dimensional conformal radiotherapy is also necessary. Thoughtful patient positioning and immobilization can minimize the PTV margin, thereby sparing normal tissues. In addition, internal target motion, most commonly encountered in the thorax and upper abdomen, can be addressed in a variety of ways. ICRU Report 62 (ICRU 1999) defines the internal target volume (ITV) as the CTV plus a margin to account for changes in target position and shape. When applicable, the ITV should be defined using 4D CT simulation and/or fluoroscopy. In cases where clinically significant irradiation of normal tissues may occur due to tumor motion, strategies to minimize the ITV margin should be employed. A variety of

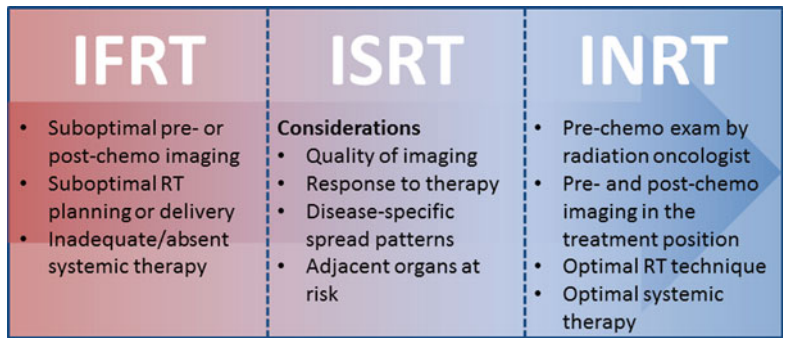

Fig. 13.1 Clinical target volume (CTV) considerations The extent of the CTV is dependent upon several factors. Increasing confidence in the delineation and control of subclinical disease may allow more conformal target volumes. *IFRT* involved field radiotherapy, *ISRT* involved site radiotherapy, *INRT* involved node radiotherapy

approaches exist including deep inspiratory breath hold, gating, active-breathing control, and abdominal compression, among others.

Finally, volumetric delineation of organs at risk (OAR) should be included in RT treatment planning. The dose delivered to critical normal structures should then be considered in treatment planning. When appropriate, motion of OARs and setup uncertainties should be accounted for utilizing a planning organ at risk volume.

13.2.2 Simulation

Patient setup and immobilization can significantly influence the exposure of critical normal structures to radiation. The RT dose, organs at risk, and treatment verification plan should be considered prior to simulation. Strategies that optimize reproducibility, patient comfort, and geographic avoidance of normal structures are best. Patient instructions, such as full bladder or empty stomach, may further optimize normal tissue avoidance.

With rare exception, a CT simulation should be completed for treatment planning. Contiguous 2.5–5 mm slices should be obtained through the intended treatment volume. The use of IV contrast during simulation should be personalized and may not be necessary, particularly if a patient has achieved a complete response to chemotherapy. For abdominal and pelvic locations, oral contrast is often helpful to delineate the bowels. As noted above, target motion should be assessed and incorporated into treatment planning. For superficial targets, bolus may be required and should be placed at the time of simulation. In some centers, simulation MR and/or PET may be obtained in the treatment position and fused with the CT for treatment planning.

When applicable, all diagnostic images that will influence target volume delineation should be electronically fused with the simulation CT. A key first step in treatment planning is manual verification of all electronic fusions. When fusion is not possible, for instance, due to positioning differences between scans, careful manual transfer with concurrent review of both datasets should be carried out by the treating radiation oncologist.

13.2.3 Treatment Technique

Standard techniques, 3D conformal RT (3DCRT) or electron therapy, should be used whenever possible. In select cases with critical normal tissues in close proximity to irradiation targets, advanced RT techniques may be advantageous. These include IMRT, volumetric arc-based therapy, and proton therapy. Recommendations regarding the best technique for an individual case cannot be made and high-level data are lacking.

The use of more conformal techniques, such as IMRT or arc-based therapy, often results in greater sparing of high dose to critical normal structures at the cost of greater low-dose irradiation. In addition, the potential for geographic miss may be greater. Vigorous treatment verification, with image guidance, for example, should be considered when advanced techniques are used.

In cases with superficial disease involvement (e.g., conjunctival or cutaneous disease), electron irradiation may be preferred. Machine-specific depth dose characteristics of commissioned electron energies should be used for clinical treatment planning. CT simulation is recommended when faithful dose calculation algorithms (e.g., Monte Carlo) are available. Electron therapy is discussed in more detail below.

13.3 Disease-Specific Recommendations

Building on the target delineation and treatment planning principles noted above, this section presents clinical scenarios and provides more detail regarding the nuances of RT design and delivery. For comparison, Table 13.1 lists the standard anatomic definitions of the involved field.

Many of the principles discussed thus far are applicable to nearly all types of Hodgkin and

Table 13.1 Involved fields using osseous anatomy

	Superior	Inferior	Medial	Lateral	Notes
Cervical	1–2 cm above mastoid tip and chin	2 cm below clavicle	Ipsilateral transverse process	Include medial 2/3 clavicle	Add laryngeal block after 19.8 Gy
Mediastinum	C5–6 interspace	Lower of 5 cm below carina and 2 cm below pre-chemo disease	N/A	Post-chemo volume with 1.5 cm margin	Include hilum with 1 cm margin (1.5 cm if involved)
Axilla	C5–6 interspace	Lower of tip of scapula or 2 cm below lowest axillary node	Ipsilateral transverse process	Flash axilla	Include lung block
Para-aortic	Higher of T11 or 2 cm above pre-chemo disease	Lower of L4 and 2 cm below pre-chemo disease	N/A	Transverse process or 2 cm margin on post-chemo volume	Kidney blocks may be necessary
Inguinal	Middle of the sacroiliac joint	5 cm below lesser trochanter	Medial border of obturator foramen with 2 cm margin on pre-chemo disease	Greater trochanter or 2 cm lateral to pre-chemo disease	

non-Hodgkin lymphoma. In addition to disease-specific discussion, site-specific recommendations are also presented below. Both the treatment site and the disease entity should be considered in the delineation of the target volume. For a given site, however, many aspects of simulation and treatment delivery remain unchanged regardless of disease. While the following sections are not divided by site, the following list may be helpful to direct interested readers to site-specific discussion:

- Neck nodes – Sects. 3.1.2 (Figs. 13.2a and 13.3), 3.1.3 (Fig. 13.4), and 3.4.2 (Fig. 13.6)
- Mediastinum – Sects. 3.1.2 (Fig. 13.3) and 3.1.3 (Fig. 13.4)
- Axilla – Sects. 3.1.2 (Fig. 13.2) and 3.3.2 (Fig. 13.8)
- Para-aortic – Sect. 3.1.3 (Fig. 13.4)
- Inguinal – Sect. 3.2.2 (Fig. 13.5)
- Head and neck – Sects. 3.4.2 (Fig. 13.6), 3.5.4.1 (Figs. 13.12 and 13.13), and 3.7.2 (Figs. 13.15 and 13.16)
- Orbital – Sects. 3.4.2 (Fig. 13.7) and 3.5.3.1 (Figs. 13.10 and 13.11)
- Gastric – Sect. 3.5.2.1 (Fig. 13.9)
- CNS – Sect. 3.6.2 (Fig. 13.14)
- Cutaneous – Sect. 3.8 (Figs. 13.17 and 13.18)

13.3.1 Classical Hodgkin Lymphoma

13.3.1.1 Overview

Until the 1990s, most patients with early-stage Hodgkin lymphoma were treated with full-dose (35–40 Gy) subtotal nodal irradiation, treating both involved nodal sites and adjacent uninvolved areas. The addition of chemotherapy to radiotherapy was shown to decrease the risk of relapse (Ferme et al. 2007; Specht et al. 1998). Further randomized studies demonstrated that in the setting of systemic therapy, smaller radiation doses and fields were adequate (Bonadonna et al. 2004; Engert et al. 2003, 2010). Currently, the most effective treatment is chemotherapy, typically ABVD (doxorubicin, bleomycin, vinblastine, dacarbazine) followed by low-dose, conformal radiotherapy to originally involved areas (Aviles and Delgado 1998; Laskar et al. 2004; Meyer et al. 2012; Noordijk et al. 2005; Pavlovsky et al. 1988; Picardi et al. 2007; Wolden et al. 2012; Herbst et al. 2010). Most randomized studies that have evaluated RT in the context of a combined modality treatment program have utilized the involved field concept (Fig. 13.2).

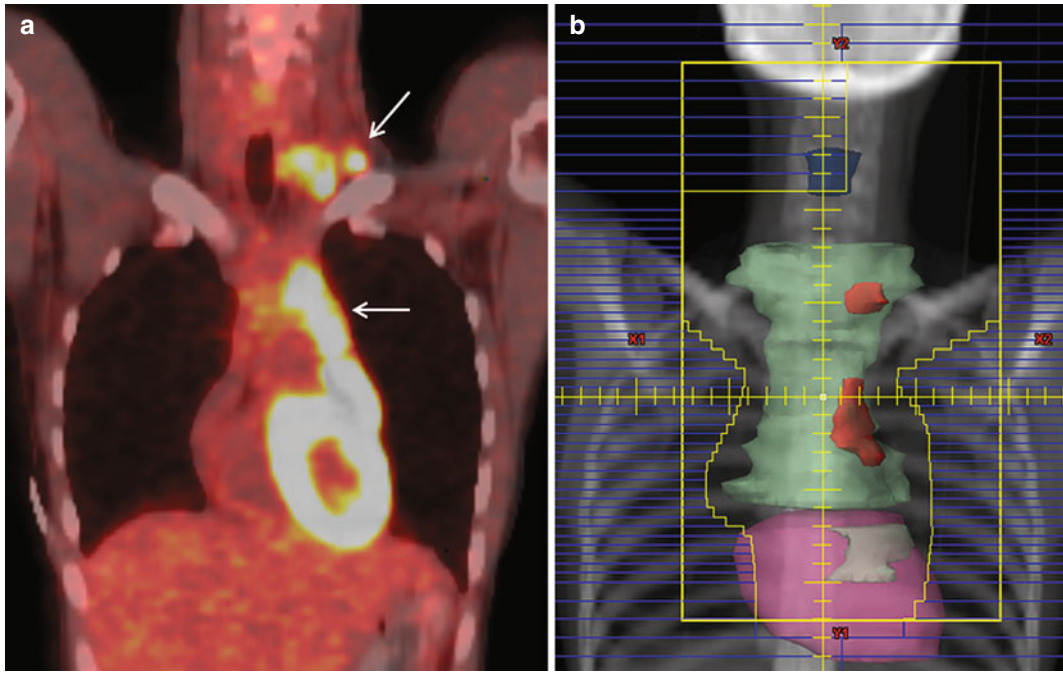

Fig. 13.2 Hodgkin lymphoma – involved field

Case	22-year-old female with stage IIA nodular sclerosis Hodgkin lymphoma with erythrocyte sedimentation rate (ESR) of 65 (early-stage unfavorable) with complete response to four cycles of ABVD. Panel **a** – pre-chemotherapy PET/CT scan. *White arrows* indicate sites of disease involvement. Sites of involvement include the left neck, mediastinum, and pericardial lymph nodes
Prescription	23.4 Gy (1.8 Gy/fraction)
Simulation	CT simulation without contrast, supine, free breathing, immobilized on indexed wing board with arms up
Treatment planning	AP/PA treatment fields. Panel **b** – consolidation radiotherapy portal with custom multi-leaf collimators (MLC). *Red volume* represents residual CT abnormalities. *Green volume* represents the CTV. *Blue volume* is the larynx. *Pink volume* is the heart

13.3.1.2 Consolidation RT

The principles of volumetric treatment planning discussed above can be used to define consolidation RT target volumes in early stage Hodgkin lymphoma. The volume of the CTV should be defined with careful consideration of the factors listed in Fig. 13.1. In general, the superior and inferior extent of the CTV should include the pre-chemotherapy extent of disease with 2 cm margin regardless of treatment response. The post-chemotherapy width, particularly in the mediastinum and retroperitoneum, is utilized to define the CTV. In cases where there is concern for residual disease, a shrinking field boost technique may be considered.

The treatment fields utilized in Hodgkin lymphoma are presently in flux. Three treatment options are shown in Fig. 13.3 for a patient with early stage, favorable Hodgkin lymphoma involving the left supraclavicular and axillary lymph nodes receiving consolidation RT after two cycles of ABVD. Treatment of an anatomically defined target volume, IFRT, is shown in panel a (see Table 13.1). ISRT and INRT are shown in panels b and c, respectively. Compared to IFRT, the ISRT field includes the axial extent of the involved lymph node stations with smaller superior-inferior margins and no prophylactic irradiation of uninvolved adjacent regions. In this case, the more generous IFRT was used as indicated by the

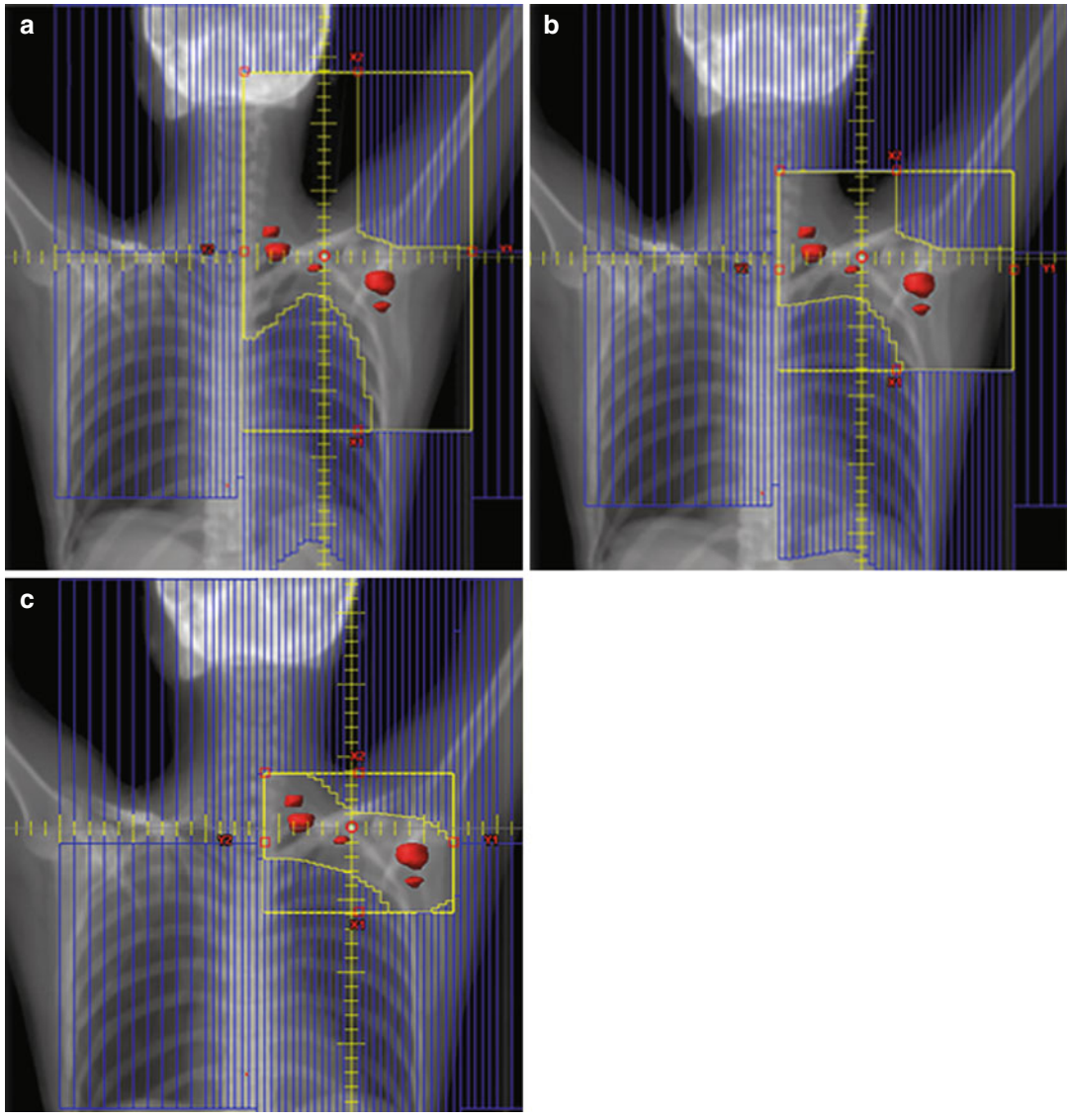

Fig. 13.3 Hodgkin lymphoma – IFRT, ISRT, INRT

Case	26-year-old female with favorable stage IIA nodular sclerosis Hodgkin lymphoma with ESR 20 (early-stage favorable) with complete response to two cycles of ABVD
Prescription	19.8 Gy (1.8 Gy /fraction)
Simulation	CT simulation with contrast, supine, free breathing, immobilized on indexed wing board with arms up
Treatment planning	AP/PA treatment fields. Pre-chemotherapy GTV shown in *red contour*. IFRT includes the ipsilateral cervical, supraclavicular, and axillary anatomic regions (panel **a**). The superior and inferior extent of irradiation is reduced in ISRT (panel **b**). INRT includes only initial sites of disease (panel **c**). IFRT used in this case due to two cycles of chemotherapy

From *ONCOLOGY* 2012:26:1182 (used with permission)

recently published German HD10 study (Engert et al. 2010). In this study, only two cycles of ABVD were administered, and radiation therapy was given to an involved field. Whether involved site or involved-node radiotherapy is adequate in patients receiving only two cycles of ABVD is not clear.

13.3.1.3 Subtotal Nodal Irradiation (STNI)

Though infrequent, full-dose STNI is still employed in the contemporary management of Hodgkin lymphoma. A recent trial showed no difference in progression-free or overall survival in patients with favorable disease treated with either ABVD or STNI (Meyer et al. 2012). However, a combined modality approach is still generally pursued given the known late effects of STNI. More commonly, STNI is pursued when a patient has localized (stage I-II) disease that is refractory to multiple chemotherapy regimens.

The initial treatment fields are anatomically defined (Table 13.1) and include the lymph nodes in the bilateral cervical, supraclavicular, axillary, mediastinal, and hilar regions (mantle field). A dose of ~30 Gy to this area is followed by a ~10 Gy boost to sites of gross disease. Prophylactic treatment of para-aortic lymph nodes and the spleen typically follows after a 2-week break. Figure 13.4 shows a standard STNI field setup. Strategies to optimize accurate matching of supra- and infradiaphragmatic fields are needed. In the presented case (Fig. 13.4), a complete response was achieved after STNI, and the patient was then considered for a stem cell transplant.

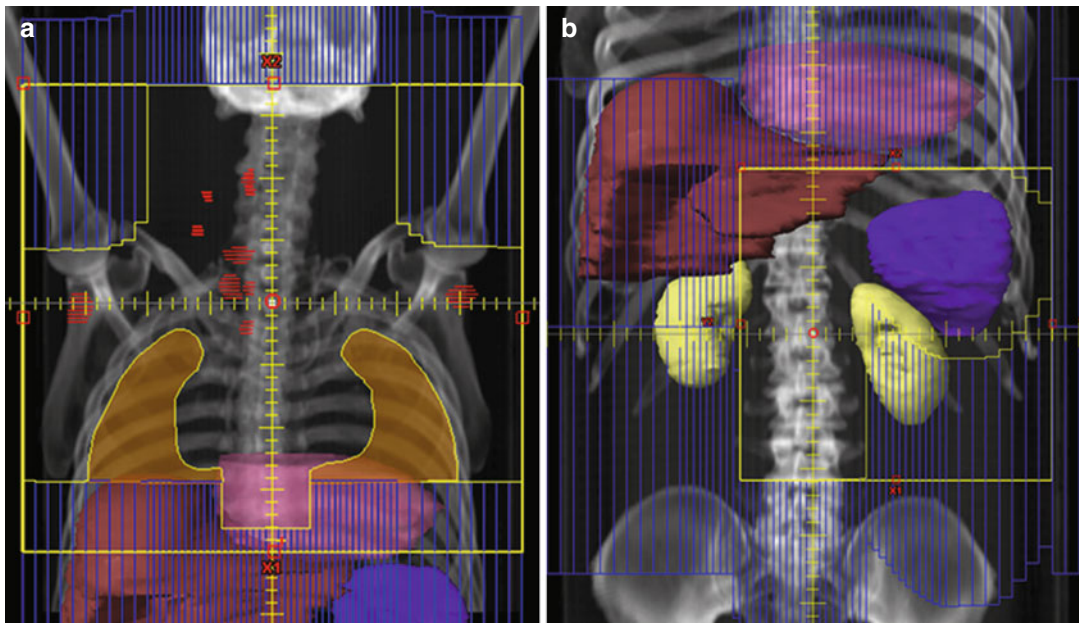

Fig. 13.4 Hodgkin lymphoma – subtotal nodal irradiation (STNI)

Case	26-year-old female with stage IIA refractory Hodgkin lymphoma with disease in left neck and mediastinum unresponsive to ABVD and ICE, undergoing definitive radiation therapy
Prescription	Mantle field (30.6 Gy) followed by boost to involved areas (10.8 Gy); para-aortic/spleen field (25.2 Gy) using 1.8 Gy fractions
Simulation	CT simulation without contrast, supine, head extended, free breathing, immobilized in customized body mold
Treatment planning	AP/PA treatment fields. Panel **a** – mantle field. Boosts fields not shown. Panel **b** – para-aortic/spleen field

From *ONCOLOGY* 2012:26:1182 (used with permission)

13.3.2 Nodular Lymphocyte-Predominant HL (NLPHL)

13.3.2.1 Overview

Nodular lymphocyte-predominant Hodgkin lymphoma (NLPHL) is an unusual subtype of Hodgkin lymphoma, consisting of ~5 % of cases. It has a distinct immunophenotype (CD15 and CD30 negative, CD20 and CD45 positive), presentation, and natural history. While overall relapse rates are similar between classical Hodgkin lymphoma and NLPHL, patients with the latter tend to relapse later and survive relapses better (Nogova et al. 2008; Diehl et al. 1999). The optimal treatment is not clear, and given the rarity of this disease, randomized trials will be difficult to perform. For patients with localized disease, RT alone is generally recommended (Nogova et al. 2005; Chen et al. 2010). However, at least one study has suggested that the addition of chemotherapy may be associated with better outcomes (Savage et al. 2011).

13.3.2.2 RT Considerations

The same principles of volumetric treatment planning should be applied to NLPHL. In cases where systemic therapy is not used, a more generous CTV is recommended. On the other hand, following a good clinical response to systemic therapy, more conformal CTV volumes may be more appropriate.

For instance, Fig. 13.5 shows two clinical target volumes for a patient with NLPHL involving a single left inguinal lymph node. In the presented case, no systemic therapy was utilized, and the larger clinical target volume was treated (panel a) with a boost to the smaller clinical target volume (panel b), as RT was utilized to eradi-

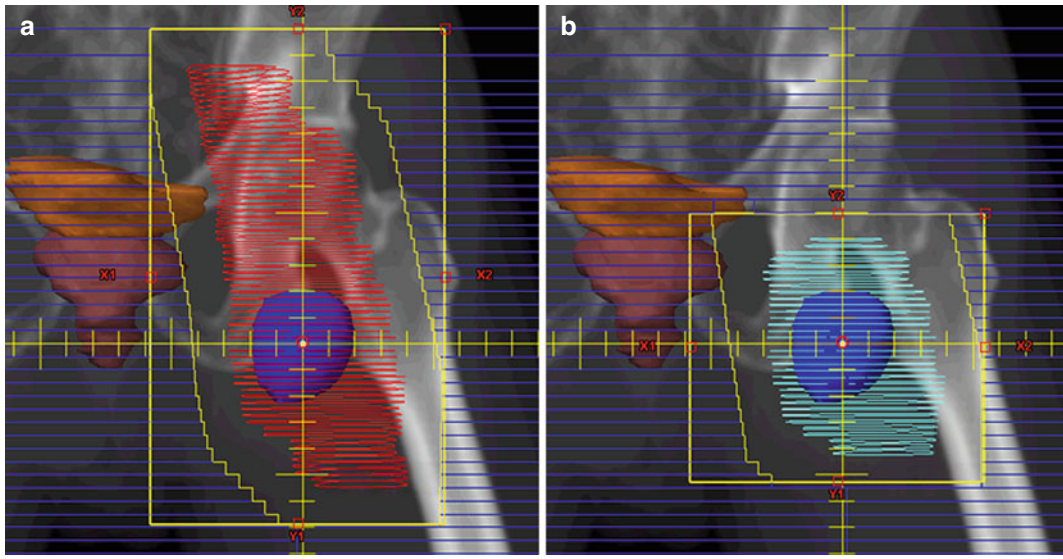

Fig. 13.5 Nodular lymphocyte-predominant Hodgkin lymphoma (NLPHL)

Case	52-year-old male with stage IA NLPHL involving a single left inguinal LN (*dark blue contour*). Treated with radiation therapy alone. Therefore, the initial clinical target volume includes the low pelvic and inguinal lymph nodes with a boost to gross disease
Prescription	30 Gy (2 Gy/ fraction) to CTV1 (*red contour*) (**a**); 2 Gy qd to 6 Gy to CTV2 (*aqua contour*) (**b**); total dose –36 Gy
Simulation	CT Simulation without contrast, supine, with legs frog-legged. For male patients, position genitalia out of field and shield testicles with clam shell
Treatment planning	2-field 3D (AP and PA). The bladders (*brown contour* and *orange contour*) are adequately spared

cate both clinical and subclinical disease. Theoretically, however, if systemic therapy had been given, it may have been more appropriate to irradiate the smaller CTV (panel b). For treatment of the inguinal region, the patient should be positioned frog-legged in order to separate the leg from the external genitalia and minimize skin folds. When possible the genitalia should be positioned out of the field, and the testicles should be shielded in men.

13.3.3 Diffuse Large B-Cell Lymphoma

13.3.3.1 Overview

Historically, RT was the preferred treatment for localized diffuse large B-cell lymphoma (DLBCL). Single-institution studies demonstrated that long-term disease control was achieved in ~40–45 % of patients (Vaughan Hudson et al. 1994; van der Maazen et al. 1998; Kaminski et al. 1986). Subsequent randomized trials demonstrated that the addition of chemotherapy to RT significantly decreased the risk of disease recurrence (Landberg et al. 1979; Monfardini et al. 1980; Nissen et al. 1983). Currently, the majority of patients are treated initially with immunochemotherapy, mostly commonly R-CHOP (rituximab, cyclophosphamide, doxorubicin, vincristine, prednisone). Most (Horning et al. 2004; Martinelli et al. 2009; Miller et al. 2001), but not all (Bonnet et al. 2007), studies have shown that consolidation RT decreases the risk of recurrence after chemotherapy, and a combined modality approach has become a standard of care in localized DLBCL.

13.3.3.2 RT Considerations

The principles of target volume delineation and treatment are similar to that of Hodgkin lymphoma for nodal DLBCL. DLBCL involves extranodal sites more commonly than Hodgkin

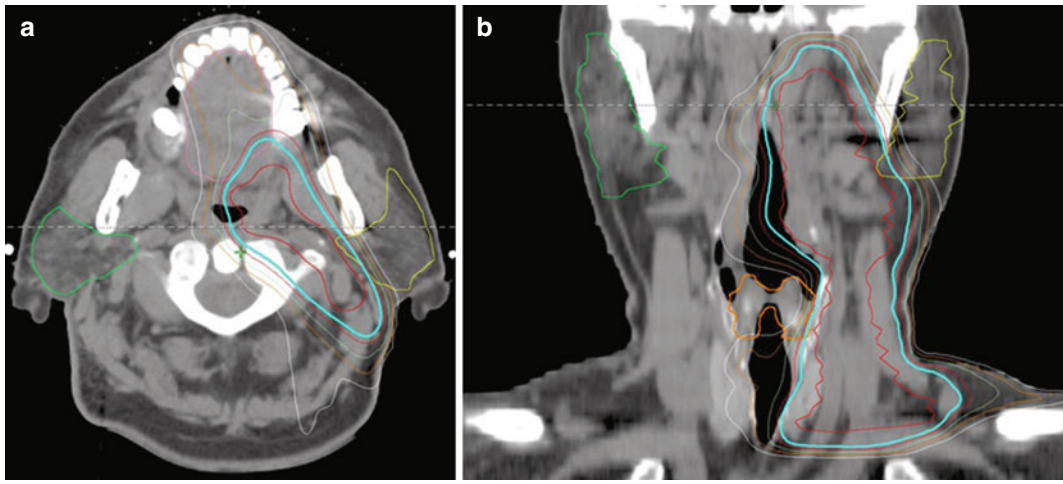

Fig. 13.6 Diffuse large B-cell lymphoma (DLBCL)

Case	62-year-old male with stage IIA DLBCL involving the left tonsil and a level II cervical lymph node s/p left tonsillectomy. He received six cycles of R-CHOP chemotherapy with complete response by PET/CT
Prescription	30 Gy (2 Gy/ fraction)
Simulation	CT simulation without contrast, supine, head extended, immobilized with thermoplastic mask, with arms down. IV contrast can be considered
Treatment planning	9-field IMRT plan. The CTV includes the left tonsillar fossa and ipsilateral neck (*red contour*). Critical normal structures include the left and right parotid glands (*yellow* and *green contour*, respectively), the larynx (*orange contour*, panel **b**), and the oral cavity (*pink contour*, panel **a**). The prescription isodose line is shown in cyan

lymphoma. When treating extranodal sites, clinical judgment is necessary to determine how much of the structure should be included in the clinical target volume. This will depend on the site treated as well as quality of diagnostic imaging. Figure 13.6 depicts the treatment plan for a patient with stage IIA DLBCL involving the left tonsil and ipsilateral level 2 neck. An ISRT CTV was delineated using the pre-chemotherapy PET/CT to include the entire tonsil and ipsilateral neck. Due to the proximity of the CTV to critical normal structures, namely, the parotid gland and oral cavity, IMRT was utilized to improve conformality. The prescription isodose contour is shown in cyan with simultaneous coverage of the CTV (red contour) and avoidance of the left parotid (yellow contour) and oral cavity (pink contour). IMRT is often advantageous for irradiation of targets in the head and neck due to proximity of many dose-limiting normal structures.

Figure 13.7 shows the opposed lateral treatment fields utilized in the consolidative irradiation of a patient with ocular DLBCL. In this case, the retina and vitreous were the targets for irradiation. The isocenter of treatment was placed at the anterior edge of the globe in order to minimize tangential irradiation of the cornea. Tissue-compensating wedges were used to improve dose homogeneity.

13.3.4 Follicular Lymphoma (FL)

13.3.4.1 Overview

Follicular lymphoma is the second most common subtype of non-Hodgkin lymphoma. Most present with advanced disease and are primarily managed with systemic immunochemotherapy. Low-dose RT can complement systemic therapy by providing very effective palliation of symptomatic areas (4 Gy in 1–2 fractions). For the minority of

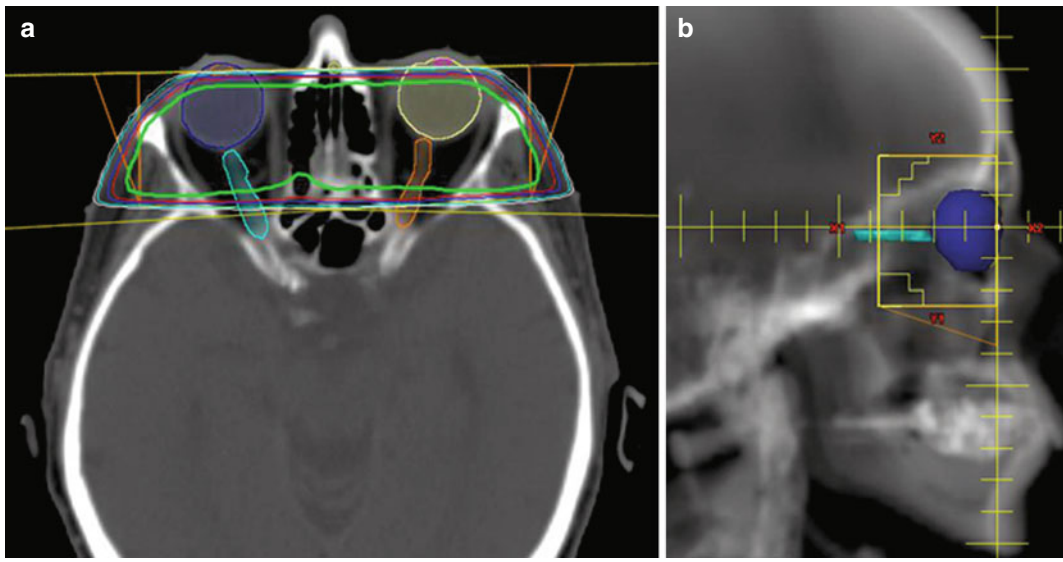

Fig. 13.7 Primary intraocular lymphoma

Case	76-year-old female with bilateral intraocular lymphoma s/p high-dose methotrexate
Prescription	30 Gy (2 Gy/fraction)
Simulation	CT simulation without contrast, supine, immobilized with thermoplastic mask
Treatment planning	2-field 3D plan (LAO, RPO). Opposed treatment fields were angled to match anterior divergence to minimize tangential irradiation of the cornea (panel **a**). Custom MLC blocking was utilized to target the posterior globe and distal optic nerves bilaterally (panel **b**). The prescription isodose line is shown in *green*. The right and left optic nerve are contoured in cyan and *orange*, respectively (panel **a**)

patients with localized disease, most published guidelines recommend RT alone (24–30 Gy). This recommendation is based on multiple studies with long follow-up showing 10-year failure-free survival of ~50 % (Vaughan Hudson et al. 1994; Campbell et al. 2010; Guadagnolo et al. 2006; Mac Manus and Hoppe 1996), with few relapses occurring thereafter. A study using data from the Surveillance, Epidemiology, and End Results (SEER) program demonstrating superior survival in patients who receive RT for stage I follicular lymphoma supports this approach (Pugh et al. 2010).

13.3.4.2 RT Considerations

Diagnostic imaging, preferably contrast-enhanced PET/CT, should be used to delineate the GTV. In most cases, localized follicular lymphoma will be treated with RT alone. Thus, RT is relied upon to eradicate clinically apparent and microscopic disease in the immediate region. Hence, IFRT is preferred over INRT. Most patients with stage I follicular lymphoma present with disease in the inguinal region, axilla, or neck. Treatment of these sites, compared to those more centrally located, is associated with a low risk of morbidity. Figure 13.8 depicts the GTV (red contour) and CTV (green contour) for a patient with stage IA FL of the left axilla treated with RT alone. The medial axillary lymph nodes are located where the axillary vessels cross the lateral aspect of the pectoralis minor. Since no systemic therapy was given, the medial lymph nodes are included as well as the lymph nodes in the supraclavicular fossa. Full humeral head blocking should be avoided when treating the axilla.

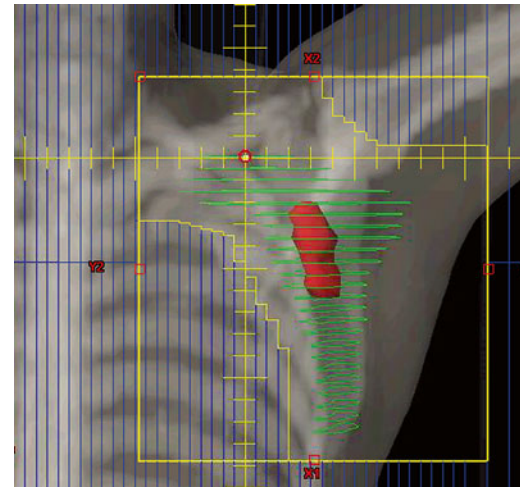

Fig. 13.8 Follicular lymphoma (FL)

Case	72-year-old female with stage IA FL involving the left axilla staged by PET/CT and bone marrow biopsy
Prescription	24 Gy (2 Gy/fraction)
Simulation	CT simulation without contrast, supine, immobilized on indexed wing board with arms up
Treatment planning	2-field 3D (AP and PA). The GTV is delineated in red and the CTV in *green*. Custom MLC blocking is utilized to irradiate the involved lymph nodes and regions at risk of harboring microscopic disease in the involved region

13.3.5 Marginal Zone Lymphoma (MZL)

13.3.5.1 Overview

Marginal zone lymphoma is the third most common non-Hodgkin lymphoma and consists of three entities – extranodal marginal zone lymphoma of mucosa-associated lymphoid tissue (MALT lymphoma), splenic marginal zone lymphoma, and nodal marginal zone lymphoma. The latter two entities are fairly rare and will not be discussed further. Most patients with MALT lymphoma present with localized disease. The most commonly involved sites include the stomach, orbital adnexa, salivary glands, thyroid, skin, and lungs (Goda et al. 2010). Though patients with localized MALT lymphoma are often treated with RT alone, the simulation and treatment planning approach vary widely. The most common sites of involvement receive additional attention below.

13.3.5.2 Stomach

The microorganism *Helicobacter pylori* is the causative agent of gastric MALT lymphoma for many patients. Eradication of the bacterium results in lymphoma regression and long-term

disease-free survival in ~50 % of patients (Wundisch et al. 2005; Schechter et al. 1998). RT is used in those patients without an apparent *H. pylori* infection or who have refractory or progressive disease despite antibiotics. RT results in lymphoma eradication and long-term disease control in >90 % of patients.

RT Considerations

The target for irradiation is the entire stomach. Therefore, patients are asked to fast for 2–3 h prior to simulation and treatment to facilitate a smaller target volume. A small amount of oral contrast can be used to improve visualization of the stomach, and IV contrast should be considered in cases with concomitant regional lymph node involvement. Immobilization with a customized body mold is recommended. Respiratory motion can be assessed with 4D CT simulation and/or fluoroscopy. In general, more generous margins should be considered due to internal target motion in the treatment of gastric MALT.

Given the possibility of internal target motion, conformal IMRT techniques should be used with caution. The kidneys, liver, and heart are the critical organs of interest and should be contoured. Differential kidney function may be assessed via nuclear imaging prior to irradiation. The use of oblique and multiple fields should be customized to minimize irradiation of normal tissues. Figure 13.9 depicts the opposed oblique treatment fields (right anterior oblique [RAO] shown) used in the treatment of a patient with *H. pylori* negative gastric MALT lymphoma.

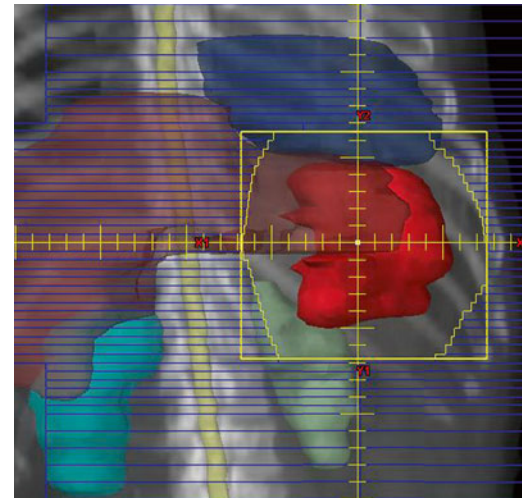

Fig. 13.9 Extranodal marginal zone lymphoma of mucosa-associated lymphoid tissue (stomach)

Case	61-year-old male with *Helicobacter pylori* negative, stage IEA MALT lymphoma of the stomach
Prescription	30 Gy (1.5 Gy/ fraction)
Simulation	4D CT simulation with oral contrast, supine, with arms up. Immobilization with custom body mold. Patient fasting for 3 h prior to simulation
Treatment planning	2-field 3D plan (RAO [shown above] and LPO). The CTV includes the entire stomach (*red contour*), taking into account organ motion during respiratory cycle. Beam angles and custom MLC blocks were designed to minimize irradiation of critical normal structures including the left kidney (*light green contour*), right kidney (*cyan contour*), liver (*brown contour*), heart (*dark blue contour*), and spinal cord (*yellow contour*). Patient treated with prophylactic antiemetics

13.3.5.3 Orbital Adnexa

The most common orbital sites involved by MALT lymphoma include the bulbar and palpebral conjunctiva, lacrimal gland, and periorbital soft tissues. Though an association with the bacterium *Chlamydia psittaci* has been demonstrated (Ferreri et al. 2005), as well as evidence of lymphoma regression with antibiotic therapy, this has not been universally confirmed, and the role of antibiotics in orbital MALT lymphoma is controversial. Presently, RT is the preferred approach for localized disease.

RT Considerations

Appropriate diagnostic testing to confirm localized disease should be performed. A combination of CT, PET, and/or MRI should be used to detect involvement of adnexal soft tissue structures. It should be noted though that MALT lymphoma is often not FDG avid on PET. MRI is the preferred imaging modality to assess the extent of orbital involvement. In addition, formal evaluation by

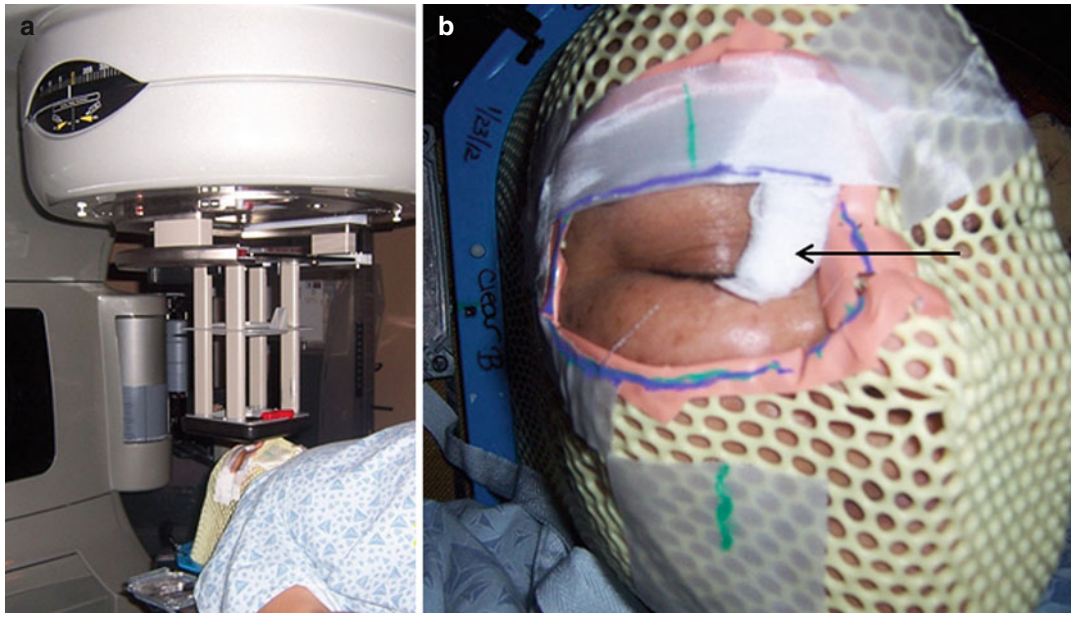

Fig. 13.10 Extranodal marginal zone lymphoma of mucosa-associated lymphoid tissue (conjunctiva)

Case	58-year-old female with stage IEA MALT lymphoma of the right conjunctiva
Prescription	24 Gy (2 Gy/fraction)
Simulation	Clinical simulation with patient immobilized in thermoplastic mask, supine, with arms down. Right eye cut out of the mask
Treatment planning	En face 6 MeV electrons prescribed to 90 % isodose line (panel **a**). Target volume delineated clinically (*purple contour*, panel **b**). Custom gauze fashioned to fill tissue defect near the medial canthus (*black arrow*, panel **b**). One cm bolus used daily (not shown)

ophthalmology should be obtained prior to treatment.

In cases of disease limited to the superficial conjunctiva, en face electron irradiation is preferred. Clinical simulation with immobilization in a thermoplastic mask is helpful. The mask can be cut to expose the affected eye (Fig. 13.10). Due to the depth-dose characteristics of electron irradiation, a generous margin should be used to define field borders. Tissue defects should be smoothed with tissue-simulated material. To obtain adequate surface dose, daily bolus is typically required.

When disease involvement is more extensive, electron irradiation may not provide adequate depth-dose. In general, if there is periorbital soft tissue involvement, treatment of the entire eye is recommended. 3DCRT or IMRT may be used in this clinical setting. For example, Fig. 13.11 depicts the case of a patient with stage IEA MALT lymphoma involving the left conjunctiva with extension to the retrobulbar space. A 3DCRT wedged-pair technique is used to obtain adequate depth dose, encompassing the entire eye and periorbital region, while completely avoiding irradiation of the contralateral eye. For bilateral disease, opposed lateral fields are generally preferred.

13.3.5.4 Salivary Glands/Thyroid

Patients with the autoimmune diseases, Hashimoto thyroiditis, and Sjogren syndrome appear to be at higher risk of developing MALT lymphoma of the thyroid and salivary glands, respectively (Holm et al. 1985; Talal and Bunim 1964). MALT lymphomas can arise in any of the salivary glands in the head and neck region, though the parotid is most frequently involved.

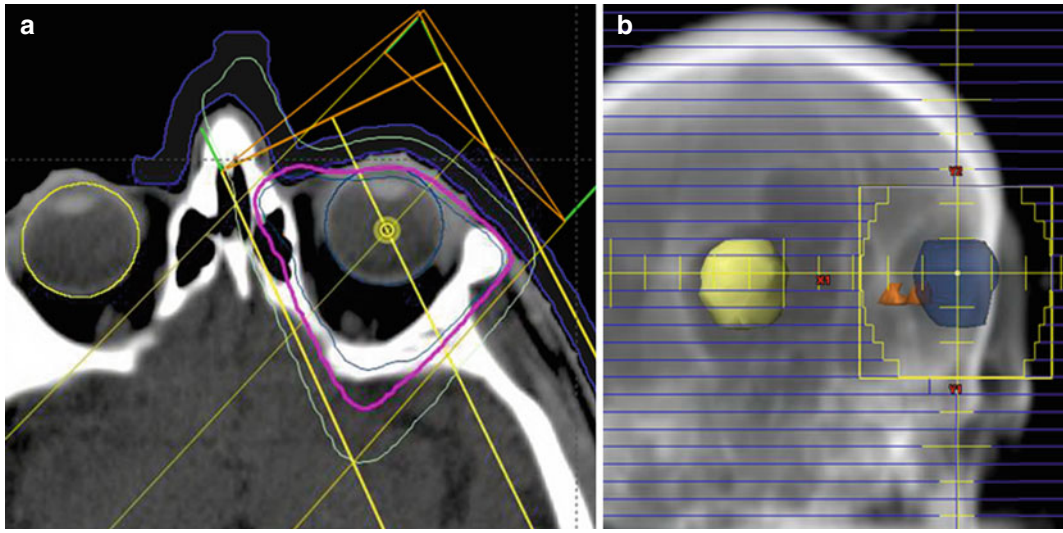

Fig. 13.11 Extranodal marginal zone lymphoma of mucosa-associated lymphoid tissue (orbit)

Case	66-year-old male with stage IEA MALT lymphoma of the left conjunctiva with extension to the left lacrimal gland and retrobulbar space
Prescription	24 Gy (2 Gy/ fraction)
Simulation	CT simulation without contrast, supine, with patient immobilized in thermoplastic mask
Treatment planning	2-field 3D plan (LAO and RAO, panel **a**). Wedged-pair technique with custom MLC blocking designed to irradiate the left eye and surrounding soft tissues (RAO, panel **b**). Prescription isodose shown in *magenta* and contralateral eye in *yellow* (panel **a**). One centimeter bolus used daily (*dark blue contour*, panel **a**)

RT Considerations

Detailed imaging of the region with CT, PET, and/or MRI should be obtained. In addition, if minor salivary gland involvement is suspected, fiberoptic laryngoscopy may also be helpful. In general, the target volume is the entire structure with any local extension. Treatment with 3DCRT or IMRT should be considered on an individualized basis. Many of the usual difficulties with conventional 3DCRT treatment of the head and neck are eliminated on account of the relatively low dose required. Figure 13.12 shows an AP/PA treatment plan for a patient with right parotid MALT lymphoma. In Fig. 13.13, the thyroid and postsurgical bed are irradiated with a differentially weighted 75 % AP and 25 % PA treatment plan. Generous margins are used due to clinical uncertainty regarding the initial extent of disease (partial thyroidectomy with no presurgical imaging). Daily bolus was used given the superficial position of the thyroid.

13.3.6 Primary Central Nervous System Lymphoma (PCNSL)

13.3.6.1 Overview

Primary central nervous system lymphoma (PCNSL) is a rare extranodal non-Hodgkin lymphoma that occurs in both immunocompetent and immunosuppressed individuals. The most common histologic subtype is DLBCL. The current standard of care is chemotherapy incorporating high-dose methotrexate. The contribution of whole-brain radiation therapy (WBRT) after high-dose methotrexate is controversial. Although WBRT may decrease the risk of relapse, it is often counterbalanced by increased toxicity (Abrey et al. 2000). In older patients (>60 years), conventional doses of WBRT (45 Gy) have been associated with unacceptably high rates of severe neurotoxicity, including dementia (Omuro et al. 2005). When a complete response is achieved, lower doses of RT (23.4 Gy)

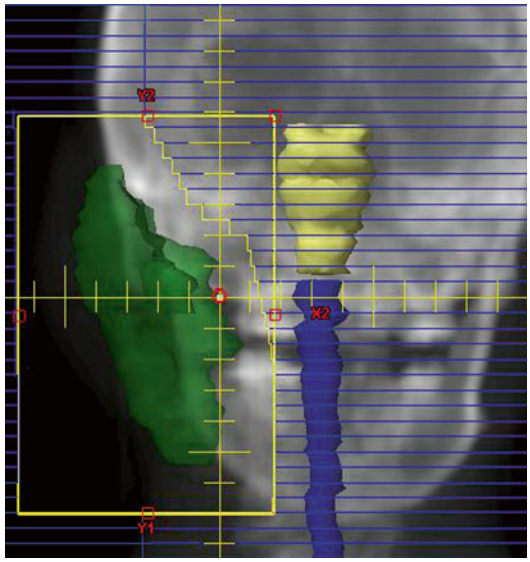

Fig. 13.12 Extranodal marginal zone lymphoma of mucosa-associated lymphoid tissue (parotid)

Case	78-year-old male with stage IEA marginal zone lymphoma of the right parotid gland
Prescription	24 Gy (2 Gy/fraction)
Simulation	CT simulation without contrast, supine, immobilized with thermoplastic mask, with arms down
Treatment planning	2-field 3D plan (AP and PA). The parotid gland, including deep and accessory lobes, was considered the CTV and contoured (*green*). Custom MLC blocking was designed to irradiate the whole parotid while minimizing irradiation of the ipsilateral eye, oral cavity, spinal (*blue contour*), and brain stem (*yellow contour*)

may decrease the risk of relapse but avoid the toxicity of full-dose WBRT (Shah et al. 2007).

13.3.6.2 RT Considerations

WBRT for PCNSL is similar to standard WBRT used in other clinical settings. Patients should be simulated supine and immobilized in a thermoplastic mask. The key difference in the delineation of WBRT fields for PCNSL is the inclusion of posterior globe and optic nerves. Figure 13.14 shows a right lateral field with inclusion of the posterior orbits. The isocenter is placed anteriorly to minimize tangential corneal irradiation.

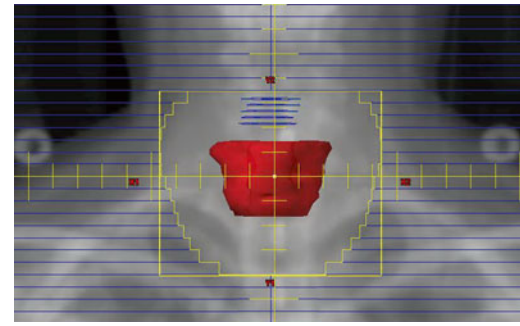

Fig. 13.13 Extranodal marginal zone lymphoma of mucosa-associated lymphoid tissue (thyroid)

Case	58-year-old male with stage IAE MALT lymphoma of the thyroid s/p partial thyroidectomy with no presurgery diagnostic imaging
Prescription	30 Gy (2 Gy/fraction)
Simulation	CT Simulation without contrast, supine, immobilized with thermoplastic mask, with arms down
Treatment planning	2-field 3D plan (AP 75 % weighting, PA 25 %). The residual thyroid and operative bed are delineated (*red contour*). The larynx is in close proximity and cannot be spared (*blue contour*). The field takes into account uncertainty regarding extent of soft tissue extension. One centimeter bolus utilized daily

13.3.7 Extranodal NK/T-cell Lymphoma, Nasal Type

13.3.7.1 Overview

The upper aerodigestive tract, including the nasal cavity, nasopharynx, palate, and paranasal sinuses, is the most commonly involved site of for extranodal NK/T-cell lymphoma, nasal type. It is a rare entity and only a limited number of clinical trials have been performed assessing different management paradigms. Thus the optimal treatment approach, particularly the choice and timing of chemotherapy, has not been established. RT appears to be an important component in patients with localized disease (Li et al. 2006). Many patients have disease in close proximity to critical structures including the eyes, brain, and parotid glands, and advanced radiation techniques, including IMRT, are often necessary.

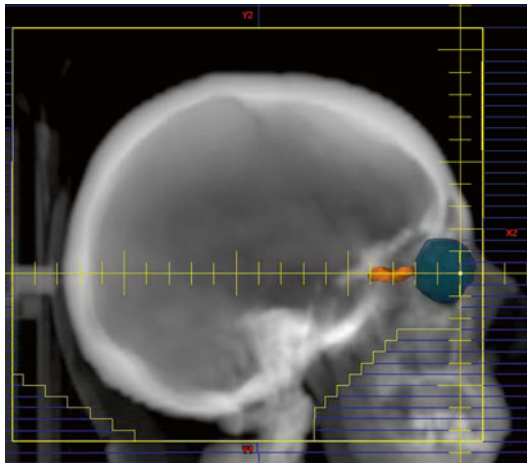

Fig. 13.14 Primary central nervous system lymphoma

Case	58-year-old female with primary CNS lymphoma s/p high-dose methotrexate with complete response
Prescription	23.4 Gy (1.8 Gy/ fraction)
Simulation	CT simulation without contrast, supine, immobilized with thermoplastic mask
Treatment planning	2-field plan (opposed laterals). Custom MLC blocking designed to irradiate the whole brain with particular attention to include the posterior globe (*dark blue contour*) and optic nerves (*orange contour*)

13.3.7.2 RT Considerations

The principles of volumetric treatment planning described above apply to NK/T-cell lymphoma. The target for irradiation is defined by the initial extent of disease. Therefore, optimal pre-chemotherapy imaging and diagnostic assessment are necessary for conformal irradiation. CT, PET, and MRI all provide important information regarding the extent of disease within the intricate anatomy of the sinonasal region. Pre-chemotherapy fiberoptic laryngoscopy is critical to document disease extent.

The optimal treatment approach for nasal NK/T-cell lymphoma is not established. Studies have used RT alone as well as RT with either concurrent or sequential chemotherapy. If patients receive chemotherapy before RT, it is ideal to undergo CT simulation in the treatment position before the start of treatment. At the time of simulation, an external bite block with tongue depressor can be used to minimize acute toxicity. Patients should be immobilized in a thermoplastic mask. All diagnostic information should be used in the delineation of the CTV. Several critical normal structures near the nasal cavity and paranasal sinuses should be contoured as avoidance structures including the bilateral eyes, optic nerves, optic chiasm, brain stem, mandible, spinal cord, oral cavity, and parotid glands.

Studies have also utilized different RT field designs, including treatment of the GTV with margin only as well as GTV + paranasal sinuses, with or without prophylactic treatment of cervical lymph nodes. IMRT is often, but not always, necessary to minimize irradiation of adjacent normal structures. Figure 13.15 depicts the dose distribution achieved by a 9-field IMRT plan. There is conformal irradiation of the CTV extending superiorly into the ethmoid sinuses between the two eyes (panels a, b). On the other hand, with more limited disease involving the hard palate, the patient depicted in Fig. 13.16 was irradiated with 3DCRT. Excellent sparing of the bilateral parotid glands was achieved without the use of IMRT in this case.

13.3.8 Cutaneous Lymphomas

13.3.8.1 Overview

The skin is a common extranodal site for lymphoma involvement. The most common T-cell entities include mycosis fungoides and primary cutaneous anaplastic large-cell lymphoma (which must be distinguished from lymphomatoid papulosis). The most common B-cell entities include primary cutaneous follicle center lymphoma, marginal zone lymphoma (MALT) of the skin, and primary cutaneous DLBCL, leg type. RT plays a central role in the definitive management of most cutaneous lymphomas (Senff et al. 2007; Bekkenk et al. 2000; Liu et al. 2003; Wilson et al. 1998), particularly localized presentations, and can be used for any histology for palliation if necessary (Navi et al. 2011; Thomas et al. 2013; Neelis et al. 2009).

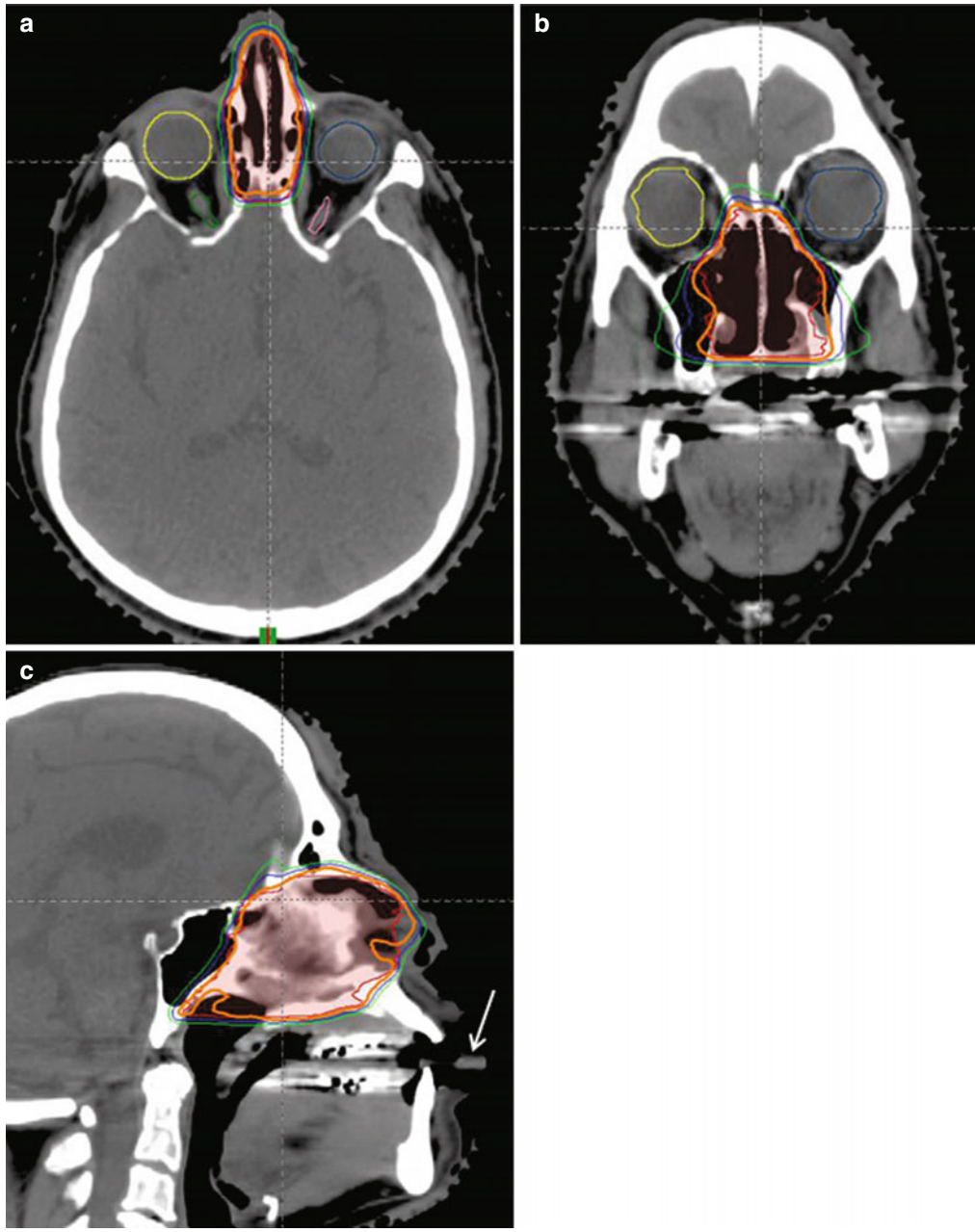

Fig. 13.15 Extranodal NK/T-cell lymphoma, nasal type (case 1)

Case	51-year-old male with EBV-positive, stage IEA NK/T-cell lymphoma of the nasal cavity bilaterally and nasopharynx status post 6 cycles of ICE chemotherapy with PET CR
Prescription	50.4 Gy (1.8 Gy/fraction)
Simulation	CT simulation without contrast, supine, immobilized in customized thermoplastic mask with neck slightly extended. External bite block (*white arrow*, panel **c**) used to depress the oral tongue
Treatment planning	9-field IMRT plan selected to optimize target coverage and avoid normal tissues. Avoidance structures include the optic chiasm, optic nerves (*dark green* and *pink contour*, panel **a**), bilateral eyes (*yellow* and *blue contour*, panel **b**), mandible, brain stem, and spinal cord. Isodose distributions shown in axial plane (**a**), coronal (**b**), and sagittal planes (**c**). *Red volume* represents the PTV. Isodose contours shown include 50.4 Gy (*orange contour*), 45 Gy (*blue contour*), and 40 Gy (*green contour*). *Dashed gray lines* indicate cut lines for each view.

13.3.8.2 RT Considerations

The first step in RT treatment planning is a total skin exam with careful delineation of all sites and extent of cutaneous disease. Palpation of disease to identify dermal extension should be done. Ideally, interdisciplinary agreement should be sought with dermatology. Photo documentation of all sites of disease and irradiation targets should be included in the patient chart.

In the vast majority of cases, superficial electron irradiation is used. All irradiation targets should be marked on the skin with adequate bolus. The electron depth-dose is best characterized using advanced dosimetric algorithms (e.g., Monte Carlo method). If such techniques are available, CT simulation should be done with radiopaque demarcation of irradiation targets. In general, target volumes with margins of 2–3 cm are recommended. Figure 13.17 shows the electron irradiation target (purple dots) for a patient with primary cutaneous B-cell lymphoma with follicle center histology. Figure 13.18 depicts the initial extent of involvement (panel a), the volume of irradiation (panel b), and treatment outcome (panel c) in a patient with localized anaplastic large-cell lymphoma of the skin.

Mycosis fungoides, and occasionally other entities, is often treated with total skin irradiation.

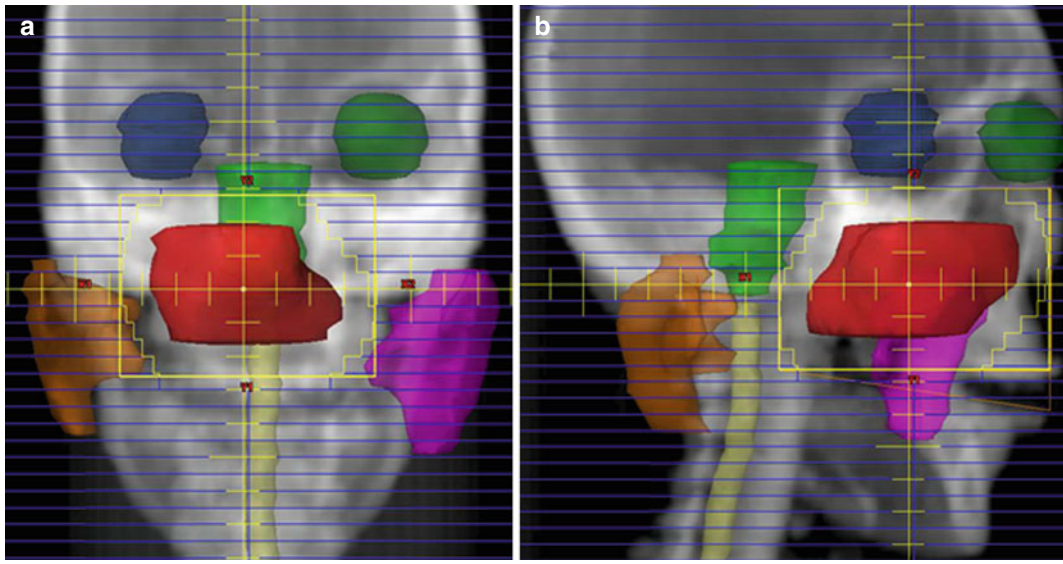

Fig. 13.16 Extranodal NK/T-cell lymphoma, nasal type (case 2)

Case	30-year-old male with EBV-positive, stage IEA NK/T-cell lymphoma of the hard palate treated with concurrent radiation therapy and DeVIC (dexamethasone, etoposide, ifosfamide, carboplatin)
Prescription	50 Gy (2 Gy/fraction)
Simulation	CT simulation without contrast, supine, immobilized in customized thermoplastic mask with neck slightly extended. External bite block used to depress oral tongue.
Treatment planning	3-field 3D plan (AP, panel **a**; RAO, panel **b**; LAO, not shown) selected to irradiate the CTV (*red contour*), representing GTV + 1.5 cm margin. Avoidance structures include the bilateral eyes (*dark green* and *blue contour*), mandible, brain stem (*green contour*), spinal cord (*yellow contour*), and bilateral parotid glands (*orange* and *magenta contours*). Mean dose to each parotid <10 Gy

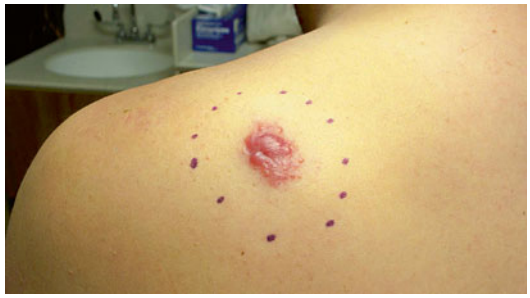

Fig. 13.17 Primary cutaneous B-cell lymphoma (follicle center)

Case	45-year-old male with primary cutaneous B-cell lymphoma of the left shoulder
Prescription	36 Gy (2 Gy/fraction)
Simulation	Patient positioned on stomach with arms above his head
Treatment planning	One en face electron field with 2.5 cm margin on palpable/visible disease. 9 MeV electrons prescribed to 90 % with 1 cm bolus

This requires commissioning of a linear accelerator to perform such treatment and is most commonly performed at specialized centers. Guidelines for total skin irradiation have been published (Hoppe 2003).

13.3.9 Plasma Cell Neoplasms

13.3.9.1 Overview

Multiple myeloma is the most common plasma cell neoplasm. A small percentage of patients will present with localized plasmacytomas. These can arise from either osseous or, less commonly, extraosseous sites. Solitary plasmacytoma may be cured with RT alone. Generally, the recommended dose in this setting is higher than that recommended for patients with multiple myeloma (40–45 Gy versus 15–30 Gy). While local control is achieved in most patients, a significant number of patients with solitary plasmacytomas progress to myeloma. The risk of myeloma development is ~70 % in patients with osseous plasmacytomas and ~35 % with extraosseous disease (Ozsahin et al. 2006).

13.3.9.2 RT Considerations

Using all available diagnostic imaging, the extent of osseous and/or extraosseous disease should be contoured on a treatment planning CT. Generous margins to account for intra-osseous extension should be used. Treatment of the entire bone and prophylactic irradiation of adjacent vertebral bodies are not necessary (see Figs. 13.19 and 13.20), though they are often included after expanding the field to take into account setup error and penumbra. For extraosseous disease, which commonly develops in the head and neck region, proximity of critical normal structure may require advanced treatment techniques such as IMRT.

Painful lytic lesions from multiple myeloma are a common indication for palliative RT. A relatively low dose of RT is usually sufficient for pain relief, and hypofractionation is typically utilized (8 Gy in 1 fraction or 20–30 Gy in 4–10 fractions). The volume of irradiation should be determined using a combination of diagnostic imaging and physical exam findings. A generous margin should be used around the clinical target volume without attempting to include all adjacent asymptomatic disease. Sparing of bone marrow in patients eligible for autologous stem cell transplant is imperative. Disease in weight-bearing bones, such as the femur, can be evaluated by orthopedic oncologists for prophylactic nailing to prevent fracture.

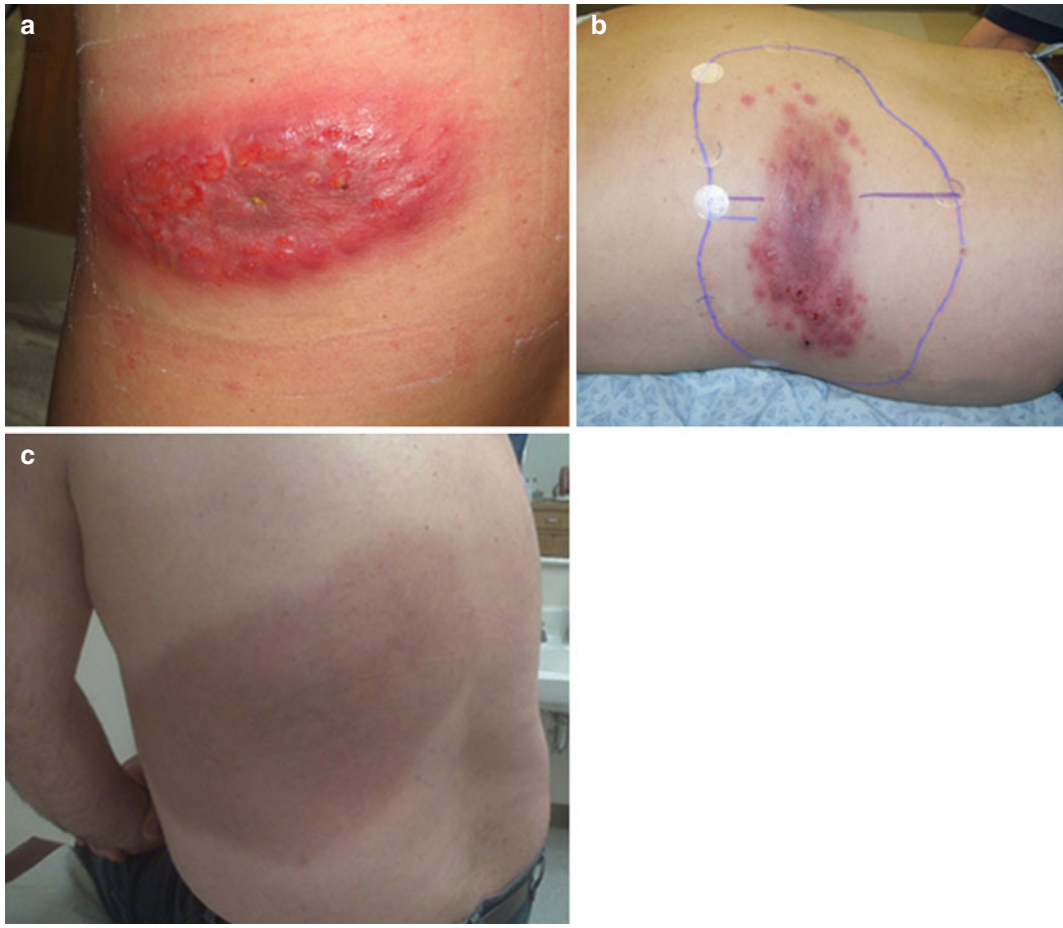

Fig. 13.18 A patient with primary cutaneous ALCL of the left back (**a**). The electron field demarcated in purple (**b**). The patient 3 months after completing radiation therapy (**c**)

Case	45-year-old male with 4-month history of painful rash. Biopsy showed a CD30 positive lymphoproliferative disorder
Prescription	40 Gy (2 Gy/fraction)
Simulation	Patient positioned on stomach with arms above his head
Treatment planning	Two en face electron fields with 3 cm margin on palpable/visible disease. 9 MeV electrons prescribed to 90 % using 1 cm bolus. Junction feathered at 20 Gy

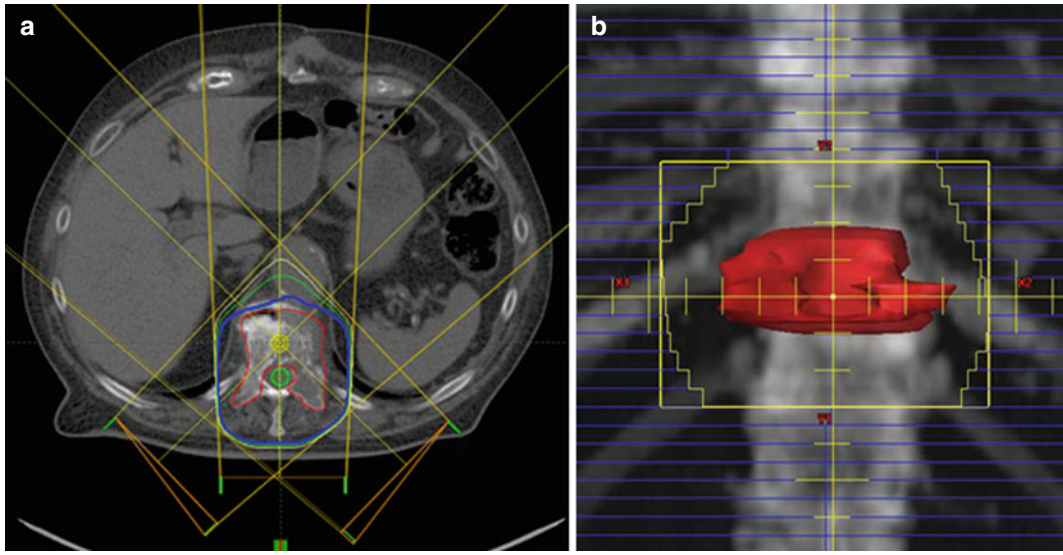

Fig. 13.19 Solitary plasmacytoma of the bone

Case	77-year-old male with solitary plasmacytoma of T11 with pathologic fracture
Prescription	44 Gy (2 Gy/fraction)
Simulation	CT simulation without contrast, supine, and arms up
Treatment planning	3-field 3D plan (PA, RPO, LPO). GTV contoured to include the entire T11 vertebral body including extension to pedicles bilaterally (panel **a**, *red contour*). Each field designed with custom MLC blocking (panel **b**, PA field). Prescription isodose line shown in blue (panel **a**)

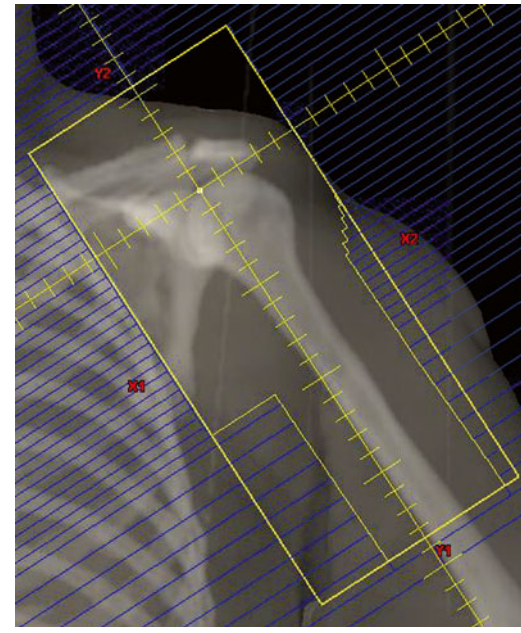

Fig. 13.20 Multiple myeloma

Case	74-year-old female with multiple myeloma s/p multiple systemic therapies with painful left shoulder lytic lesions. Left shoulder X-ray reveals lytic lesions involving the proximal-mid humerus, distal clavicle, and scapula
Prescription	20 Gy (4 Gy/fraction)
Simulation	CT simulation without contrast, supine, with the left arm slightly akimbo
Treatment planning	2-field 2D plan (AP, PA). Custom MLC blocking utilized to avoid circumferential limb irradiation

References

Abrey LE, Yahalom J, DeAngelis LM (2000) Treatment for primary CNS lymphoma: the next step. J Clin Oncol 18(17):3144–3150

Aviles A, Delgado S (1998) A prospective clinical trial comparing chemotherapy, radiotherapy and combined therapy in the treatment of early stage Hodgkin's disease with bulky disease. Clin Lab Haematol 20(2):95–99

Bekkenk MW, Geelen FA, van Voorst Vader PC, Heule F, Geerts ML, van Vloten WA, Meijer CJ, Willemze R (2000) Primary and secondary cutaneous CD30(+) lymphoproliferative disorders: a report from the Dutch Cutaneous Lymphoma Group on the long-term follow-up data of 219 patients and guidelines for diagnosis and treatment. Blood 95(12):3653–3661

Bonadonna G, Bonfante V, Viviani S, Di Russo A, Villani F, Valagussa P (2004) ABVD plus subtotal nodal versus involved-field radiotherapy in early-stage Hodgkin's disease: long-term results. J Clin Oncol 22(14):2835–2841

Bonnet C, Fillet G, Mounier N, Ganem G, Molina TJ, Thieblemont C, Ferme C, Quesnel B, Martin C, Gisselbrecht C, Tilly H, Reyes F (2007) CHOP alone compared with CHOP plus radiotherapy for localized aggressive lymphoma in elderly patients: a study by the Groupe d'Etude des Lymphomes de l'Adulte. J Clin Oncol 25(7):787–792. doi:10.1200/JCO.2006.07.0722, JCO.2006.07.0722 [pii]

Campbell BA, Voss N, Woods R, Gascoyne RD, Morris J, Pickles T, Connors JM, Savage KJ (2010) Long-term outcomes for patients with limited stage follicular lymphoma: involved regional radiotherapy versus involved node radiotherapy. Cancer 116(16):3797–3806. doi:10.1002/cncr.25117

Chen RC, Chin MS, Ng AK, Feng Y, Neuberg D, Silver B, Pinkus GS, Stevenson MA, Mauch PM (2010) Early-stage, lymphocyte-predominant Hodgkin's lymphoma: patient outcomes from a large, single-institution series with long follow-up. J Clin Oncol 28(1):136–141. doi:10.1200/JCO.2009.24.0945, JCO.2009.24.0945 [pii]

Diehl V, Sextro M, Franklin J, Hansmann ML, Harris N, Jaffe E, Poppema S, Harris M, Franssila K, van Krieken J, Marafioti T, Anagnostopoulos I, Stein H (1999) Clinical presentation, course, and prognostic factors in lymphocyte-predominant Hodgkin's disease and lymphocyte-rich classical Hodgkin's disease: report from the European Task Force on Lymphoma Project on Lymphocyte-Predominant Hodgkin's Disease. J Clin Oncol 17(3):776–783

Eich HT, Muller RP, Engenhart-Cabillic R, Lukas P, Schmidberger H, Staar S, Willich N (2008) Involved-node radiotherapy in early-stage Hodgkin's lymphoma. Definition and guidelines of the German Hodgkin Study Group (GHSG). Strahlenther Onkol 184(8):406–410

Engert A, Schiller P, Josting A, Herrmann R, Koch P, Sieber M, Boissevain F, De Wit M, Mezger J, Duhmke E, Willich N, Muller RP, Schmidt BF, Renner H, Muller-Hermelink HK, Pfistner B, Wolf J, Hasenclever D, Loffler M, Diehl V (2003) Involved-field radiotherapy is equally effective and less toxic compared with extended-field radiotherapy after four cycles of chemotherapy in patients with early-stage unfavorable Hodgkin's lymphoma: results of the HD8 trial of the German Hodgkin's Lymphoma Study Group. J Clin Oncol 21(19):3601–3608

Engert A, Plutschow A, Eich HT, Lohri A, Dorken B, Borchmann P, Berger B, Greil R, Willborn KC, Wilhelm M, Debus J, Eble MJ, Sokler M, Ho A, Rank A, Ganser A, Trumper L, Bokemeyer C, Kirchner H, Schubert J, Kral Z, Fuchs M, Muller-Hermelink HK, Muller RP, Diehl V (2010) Reduced treatment intensity in patients with early-stage Hodgkin's lymphoma. N Engl J Med 363(7):640–652. doi:10.1056/NEJMoa1000067

Ferme C, Eghbali H, Meerwaldt JH, Rieux C, Bosq J, Berger F, Girinsky T, Brice P, Van't Veer MB, Walewski JA, Lederlin P, Tirelli U, Carde P, Van den Neste E, Gyan E, Monconduit M, Divine M, Raemaekers JM, Salles G, Noordijk EM, Creemers GJ, Gabarre J, Hagenbeek A, Reman O, Blanc M, Thomas J, Vie B, Kluin-Nelemans JC, Viseu F, Baars JW, Poortmans P, Lugtenburg PJ, Carrie C, Jaubert J, Henry-Amar M (2007) Chemotherapy plus involved-field radiation in early-stage Hodgkin's disease. N Engl J Med 357(19):1916–1927. doi:10.1056/NEJMoa064601, 357/19/1916 [pii]

Ferreri AJ, Ponzoni M, Guidoboni M, De Conciliis C, Resti AG, Mazzi B, Lettini AA, Demeter J, Dell'Oro S, Doglioni C, Villa E, Boiocchi M, Dolcetti R (2005) Regression of ocular adnexal lymphoma after Chlamydia psittaci – eradicating antibiotic therapy. J Clin Oncol 23(22):5067–5073. doi:10.1200/JCO.2005.07.083, JCO.2005.07.083 [pii]

Girinsky T, Specht L, Ghalibafian M, Edeline V, Bonniaud G, Van Der Maazen R, Aleman B, Paumier A, Meijnders P, Lievens Y, Noordijk E, Poortmans P (2008) The conundrum of Hodgkin lymphoma nodes: to be or not to be included in the involved node radiation fields. The EORTC-GELA lymphoma group guidelines. Radiother Oncol 88(2):202–210. doi:10.1016/j.radonc.2008.05.012, S0167-8140(08)00241-7 [pii]

Goda JS, Gospodarowicz M, Pintilie M, Wells W, Hodgson DC, Sun A, Crump M, Tsang RW (2010) Long-term outcome in localized extranodal mucosa-associated lymphoid tissue lymphomas treated with radiotherapy. Cancer 116(16):3815–3824. doi:10.1002/cncr.25226

Guadagnolo BA, Li S, Neuberg D, Ng A, Hua L, Silver B, Stevenson MA, Mauch P (2006) Long-term outcome and mortality trends in early-stage, grade 1–2 follicular lymphoma treated with radiation therapy. Int J Radiat Oncol Biol Phys 64(3):928–934. doi:10.1016/j.ijrobp.2005.08.010, S0360-3016(05)02375-8 [pii]

Herbst C, Rehan FA, Brillant C, Bohlius J, Skoetz N, Schulz H, Monsef I, Specht L, Engert A (2010) Combined modality treatment improves tumor control and overall survival in patients with early

stage Hodgkin's lymphoma: a systematic review. Haematologica 95(3):494–500. doi:10.3324/haematol.2009.015644, haematol.2009.015644 [pii]

Hodgson DC, Gilbert ES, Dores GM, Schonfeld SJ, Lynch CF, Storm H, Hall P, Langmark F, Pukkala E, Andersson M, Kaijser M, Joensuu H, Fossa SD, Travis LB (2007) Long-term solid cancer risk among 5-year survivors of Hodgkin's lymphoma. J Clin Oncol 25(12):1489–1497. doi:10.1200/JCO.2006.09.0936, JCO.2006.09.0936 [pii]

Holm LE, Blomgren H, Lowhagen T (1985) Cancer risks in patients with chronic lymphocytic thyroiditis. N Engl J Med 312(10):601–604. doi:10.1056/NEJM198503073121001

Hoppe RT (2003) Mycosis fungoides: radiation therapy. Dermatol Ther 16(4):347–354, 01647 [pii]

Horning SJ, Weller E, Kim K, Earle JD, O'Connell MJ, Habermann TM, Glick JH (2004) Chemotherapy with or without radiotherapy in limited-stage diffuse aggressive non-Hodgkin's lymphoma: Eastern Cooperative Oncology Group study 1484. J Clin Oncol 22(15):3032–3038. doi:10.1200/JCO.2004.06.088, JCO.2004.06.088 [pii]

ICRU (1999) International Commission on Radiation Units and Measurements. Prescribing, recording, and reporting photon therapy (Supplement to ICRU Report 50). ICRU Report 62

ICRU (2010) Definition of volumes. J ICRU 10(1):41–53. doi:10.1093/jicru/ndq009

Kaminski MS, Coleman CN, Colby TV, Cox RS, Rosenberg SA (1986) Factors predicting survival in adults with stage I and II large-cell lymphoma treated with primary radiation therapy. Ann Intern Med 104(6):747–756

Kaplan HS (1966) Evidence for a tumoricidal dose level in the radiotherapy of Hodgkin's disease. Cancer Res 26(6):1221–1224

Koontz BF, Kirkpatrick JP, Clough RW, Prosnitz RG, Gockerman JP, Moore JO, Prosnitz LR (2006) Combined-modality therapy versus radiotherapy alone for treatment of early-stage Hodgkin's disease: cure balanced against complications. J Clin Oncol 24(4):605–611

Landberg TG, Hakansson LG, Moller TR, Mattsson WK, Landys KE, Johansson BG, Killander DC, Molin BF, Westling PF, Lenner PH, Dahl OG (1979) CVP-remission-maintenance in stage I or II non-Hodgkin's lymphomas: preliminary results of a randomized study. Cancer 44(3):831–838

Laskar S, Gupta T, Vimal S, Muckaden MA, Saikia TK, Pai SK, Naresh KN, Dinshaw KA (2004) Consolidation radiation after complete remission in Hodgkin's disease following six cycles of doxorubicin, bleomycin, vinblastine, and dacarbazine chemotherapy: is there a need? J Clin Oncol 22(1):62–68

Li YX, Yao B, Jin J, Wang WH, Liu YP, Song YW, Wang SL, Liu XF, Zhou LQ, He XH, Lu N, Yu ZH (2006) Radiotherapy as primary treatment for stage IE and IIE nasal natural killer/T-cell lymphoma. J Clin Oncol 24(1):181–189

Liu HL, Hoppe RT, Kohler S, Harvell JD, Reddy S, Kim YH (2003) CD30+ cutaneous lymphoproliferative disorders: the Stanford experience in lymphomatoid papulosis and primary cutaneous anaplastic large cell lymphoma. J Am Acad Dermatol 49(6):1049–1058. doi:10.1016/S0190, S0190962203024848 [pii]

Mac Manus MP, Hoppe RT (1996) Is radiotherapy curative for stage I and II low-grade follicular lymphoma? Results of a long-term follow-up study of patients treated at Stanford University. J Clin Oncol 14(4):1282–1290

Martinelli G, Gigli F, Calabrese L, Ferrucci PF, Zucca E, Crosta C, Pruneri G, Preda L, Piperno G, Gospodarowicz M, Cavalli F, Moreno Gomez H (2009) Early stage gastric diffuse large B-cell lymphomas: results of a randomized trial comparing chemotherapy alone versus chemotherapy + involved field radiotherapy. (IELSG 4). [corrected]. Leuk Lymphoma 50(6):925–931. doi:10.1080/10428190902912478, 911751509 [pii]

Meyer RM, Gospodarowicz MK, Connors JM, Pearcey RG, Wells WA, Winter JN, Horning SJ, Dar AR, Shustik C, Stewart DA, Crump M, Djurfeldt MS, Chen BE, Shepherd LE (2012) ABVD alone versus radiation-based therapy in limited-stage Hodgkin's lymphoma. N Eng J Med 366(5):399–408. doi:10.1056/NEJMoa1111961

Miller TP, LeBlanc M, Spier C (2001) CHOP alone compared to CHOP plus radiotherapy for early stage aggressive non-Hodgkin's lymphomas: update of the Southwest Oncology Group (SWOG) randomized trial. Blood 98:724a

Monfardini S, Banfi A, Bonadonna G, Rilke F, Milani F, Valagussa P, Lattuada A (1980) Improved five year survival after combined radiotherapy-chemotherapy for stage I–II non-Hodgkin's lymphoma. Int J Radiat Oncol Biol Phys 6(2):125–134

Navi D, Riaz N, Levin YS, Sullivan NC, Kim YH, Hoppe RT (2011) The Stanford University experience with conventional-dose, total skin electron-beam therapy in the treatment of generalized patch or plaque (T2) and tumor (T3) mycosis fungoides. Arch Dermatol 147(5):561–567. doi:10.1001/archdermatol.2011.98, 147/5/561 [pii]

Neelis KJ, Schimmel EC, Vermeer MH, Senff NJ, Willemze R, Noordijk EM (2009) Low-dose palliative radiotherapy for cutaneous B- and T-cell lymphomas. Int J Radiat Oncol Biol Phys 74(1):154–158. doi:10.1016/j.ijrobp.2008.06.1918, S0360-3016(08)02951-9 [pii]

Nissen NI, Ersboll J, Hansen HS, Walbom-Jorgensen S, Pedersen-Bjergaard J, Hansen MM, Rygard J (1983) A randomized study of radiotherapy versus radiotherapy plus chemotherapy in stage I-II non-Hodgkin's lymphomas. Cancer 52(1):1–7

Nogova L, Reineke T, Eich HT, Josting A, Muller-Hermelink HK, Wingbermuhle K, Brillant C, Gossmann A, Oertel J, Bollen MV, Muller RP, Diehl V, Engert A (2005) Extended field radiotherapy, combined modality treatment or involved field radiotherapy for patients with stage IA lymphocyte-

predominant Hodgkin's lymphoma: a retrospective analysis from the German Hodgkin Study Group (GHSG). Ann Oncol 16(10):1683–1687

Nogova L, Reineke T, Brillant C, Sieniawski M, Rudiger T, Josting A, Bredenfeld H, Skripnitchenko R, Muller RP, Muller-Hermelink HK, Diehl V, Engert A (2008) Lymphocyte-predominant and classical Hodgkin's lymphoma: a comprehensive analysis from the German Hodgkin Study Group. J Clin Oncol 26(3):434–439. doi:10.1200/JCO.2007.11.8869, JCO.2007.11.8869 [pii]

Noordijk EM, Thomas J, Ferme C, van't Veer MB, Brice P, Divine M, Morschhauser F, Carde P, Eghbali H, Henry-Amar M (2005) First results of the EORTC-GELA H9 randomized trials: the H9-F trial (comparing 3 radiation dose levels) and H9-U trial (comparing 3 chemotherapy schemes) in patients with favorable or unfavorable early stage Hodgkin's lymphoma (HL). Proceedings of ASCO 23(June 1 Suppl):6505

Omuro AM, Ben-Porat LS, Panageas KS, Kim AK, Correa DD, Yahalom J, Deangelis LM, Abrey LE (2005) Delayed neurotoxicity in primary central nervous system lymphoma. Arch Neurol 62(10):1595–1600. doi:10.1001/archneur.62.10.1595, 62/10/1595 [pii]

Ozsahin M, Tsang RW, Poortmans P, Belkacemi Y, Bolla M, Dincbas FO, Landmann C, Castelain B, Buijsen J, Curschmann J, Kadish SP, Kowalczyk A, Anacak Y, Hammer J, Nguyen TD, Studer G, Cooper R, Sengoz M, Scandolaro L, Zouhair A (2006) Outcomes and patterns of failure in solitary plasmacytoma: a multicenter Rare Cancer Network study of 258 patients. Int J Radiat Oncol Biol Phys 64(1):210–217. doi:10.1016/j.ijrobp.2005.06.039, S0360-3016(05)02223-6 [pii]

Pavlovsky S, Maschio M, Santarelli MT, Muriel FS, Corrado C, Garcia I, Schwartz L, Montero C, Sanahuja FL, Magnasco O et al (1988) Randomized trial of chemotherapy versus chemotherapy plus radiotherapy for stage I-II Hodgkin's disease. J Natl Cancer Inst 80(18):1466–1473

Picardi M, De Renzo A, Pane F, Nicolai E, Pacelli R, Salvatore M, Rotoli B (2007) Randomized comparison of consolidation radiation versus observation in bulky Hodgkin's lymphoma with post-chemotherapy negative positron emission tomography scans. Leuk Lymphoma 48(9):1721–1727. doi:10.1080/10428190701559140, 781796832 [pii]

Pugh TJ, Ballonoff A, Newman F, Rabinovitch R (2010) Improved survival in patients with early stage low-grade follicular lymphoma treated with radiation: a Surveillance, Epidemiology, and End Results database analysis. Cancer 116(16):3843–3851. doi:10.1002/cncr.25149

Rosenberg SA, Kaplan HS (1966) Evidence for an orderly progression in the spread of Hodgkin's disease. Cancer Res 26(6):1225–1231

Savage KJ, Skinnider B, Al-Mansour M, Sehn LH, Gascoyne RD, Connors JM (2011) Treating limited-stage nodular lymphocyte predominant Hodgkin lymphoma similarly to classical Hodgkin lymphoma with ABVD may improve outcome. Blood 118(17): 4585–4590. doi:10.1182/blood-2011-07-365932, blood-2011-07-365932 [pii]

Schechter NR, Portlock CS, Yahalom J (1998) Treatment of mucosa-associated lymphoid tissue lymphoma of the stomach with radiation alone. J Clin Oncol 16(5):1916–1921

Schellong G, Riepenhausen M, Bruch C, Kotthoff S, Vogt J, Bolling T, Dieckmann K, Potter R, Heinecke A, Bramswig J, Dorffel W (2010) Late valvular and other cardiac diseases after different doses of mediastinal radiotherapy for Hodgkin disease in children and adolescents: report from the longitudinal GPOH follow-up project of the German-Austrian DAL-HD studies. Pediatr Blood Cancer 55(6):1145–1152. doi:10.1002/pbc.22664

Senff NJ, Hoefnagel JJ, Neelis KJ, Vermeer MH, Noordijk EM, Willemze R (2007) Results of radiotherapy in 153 primary cutaneous B-Cell lymphomas classified according to the WHO-EORTC classification. Arch Dermatol 143(12):1520–1526. doi:10.1001/archderm.143.12.1520, 143/12/1520 [pii]

Shah GD, Yahalom J, Correa DD, Lai RK, Raizer JJ, Schiff D, LaRocca R, Grant B, DeAngelis LM, Abrey LE (2007) Combined immunochemotherapy with reduced whole-brain radiotherapy for newly diagnosed primary CNS lymphoma. J Clin Oncol 25(30):4730–4735. doi:10.1200/JCO.2007.12.5062, 25/30/4730 [pii]

Specht L, Gray RG, Clarke MJ, Peto R (1998) Influence of more extensive radiotherapy and adjuvant chemotherapy on long-term outcome of early-stage Hodgkin's disease: a meta-analysis of 23 randomized trials involving 3,888 patients. International Hodgkin's Disease Collaborative Group. J Clin Oncol 16(3):830–843

Swerdlow SHCE, Harris NL (2008) World Health Organization classification of tumours of haematopoietic and lymphoid tissues. IARC Press, Lyon

Talal N, Bunim JJ (1964) The development of malignant lymphoma in the course of Sjogren's syndrome. Am J Med 36:529–540

Thomas TO, Agrawal P, Guitart J, Rosen ST, Rademaker AW, Querfeld C, Hayes JP, Kuzel TM, Mittal BB (2013) Outcome of patients treated with a single-fraction dose of palliative radiation for cutaneous T-cell lymphoma. Int J Radiat Oncol Biol Phys 85(3):747–753. doi:10.1016/j.ijrobp.2012.05.034, S0360-3016(12)00750-X [pii]

van der Maazen RW, Noordijk EM, Thomas J, Raemaekers JM, Meerwaldt JH (1998) Combined modality treatment is the treatment of choice for stage I/IE intermediate and high grade non-Hodgkin's lymphomas. Radiother Oncol 49(1):1–7

Vaughan Hudson B, Vaughan Hudson G, MacLennan KA, Anderson L, Linch DC (1994) Clinical stage 1 non-Hodgkin's lymphoma: long-term follow-up of patients treated by the British National Lymphoma Investigation with radiotherapy alone as initial therapy. Br J Cancer 69(6):1088–1093

Wilson LD, Kacinski BM, Jones GW (1998) Local superficial radiotherapy in the management of minimal stage

IA cutaneous T-cell lymphoma (Mycosis Fungoides). Int J Radiat Oncol Biol Phys 40(1):109–115, S0360-3016(97)00553-1 [pii]

Wolden SL, Chen L, Kelly KM, Herzog P, Gilchrist GS, Thomson J, Sposto R, Kadin ME, Hutchinson RJ, Nachman J (2012) Long-term results of CCG 5942: a randomized comparison of chemotherapy with and without radiotherapy for children with Hodgkin's lymphoma – a report from the Children's Oncology Group. J Clin Oncol 30(26):3174–3180. doi:10.1200/JCO.2011.41.1819, JCO.2011.41.1819 [pii]

Wundisch T, Thiede C, Morgner A, Dempfle A, Gunther A, Liu H, Ye H, Du MQ, Kim TD, Bayerdorffer E, Stolte M, Neubauer A (2005) Long-term follow-up of gastric MALT lymphoma after Helicobacter pylori eradication. J Clin Oncol 23(31):8018–8024. doi:10.1200/JCO.2005.02.3903, JCO.2005.02.3903 [pii]

Prostate Cancer

14

Dirk Böhmer

Contents

D. Böhmer
Department of Radiation Oncology,
Charité University Medicine,
Campus Virchow Klinikum,
Augustenburger Platz 1,
Berlin 13353, Germany
e-mail: dirk.boehmer@charite.de

14.1 Introduction

In general target delineation is not depending on radiotherapy technique, whether 3D conformal, IMRT, or rotation techniques are used. Tumor-related risk factors such as transcapsular tumor spread or tumor grading rather determine the extent of target volume delineation. Regarding prostate cancer delineation, the determining factors are clinical tumor extension according to the UICC tumor stage, the Gleason score, as well as the number of positive biopsies defined by random prostate biopsy and the PSA level. The European Organization for Research and Treatment of Cancer (EORTC) radiation oncology group (ROG) developed the first comprehensive guideline on target volume definition for primary radiotherapy in prostate cancer which was published in 2006. They provide thorough information on target and organ at risk volume definition, imaging, patient setup, and treatment verification (Boehmer et al. 2006). This chapter refers to clinical or prognostic risk factors which are the commonly known factors as defined according to the National Comprehensive Cancer Network (NCCN) and Anthony D'Amico.

Table 14.1 summarizes the risk group classification.

A.-L. Grosu, C. Nieder (eds.), *Target Volume Definition in Radiation Oncology*,
DOI 10.1007/978-3-662-45934-8_14, © Springer-Verlag Berlin Heidelberg 2015

Table 14.1 Risk group definition according to D'Amico and NCCN

Risk group	Low	Intermediate	High
NCCN			
T-stage	cT1c + cT2a and	cT2b – 2c and/or	cT3 or
PSA	<10 ng/ml and	>10–20 ng/ml and/or	>20 ng/ml or
Gleason sum	<7	=7	8–10
D'Amico et al. (1997a, 1998, 1999)			
T-stage	cT1c – 2a and	cT2b and/or	cT2c – cT3 or
PSA	<10 ng/ml and	>10–20 ng/ml and/or	>20 ng/ml or
Gleason sum	<7	=7	8–10

Note that the two classifications differ only by clinical stage in intermediate- and high-risk tumors

14.2 International Commission on Radiation Units and Measurements (ICRU) Volumes Definition

ICRU 50, ICRU 62, and ICRU 82 provide a comprehensive definition of target volumes and organs at risk (OAR) in radiotherapy. The ICRU 50, published in 1993, presented the first concept of standardizing definitions of target volume delineation and organs at risk (International Commission on Radiation Units and Measurements 1993). The 1999 supplement (ICRU 62) introduced additional volumes that would change the extension of target volumes based on published data on internal organ motion and positioning uncertainties (International Commission on Radiation Units and Measurements 1999). In its latest modification from 2010, the ICRU report 83 takes into consideration new developments in imaging modalities as well as new radiation techniques and their influence on target volume definition (International Commission on Radiation Units and Measurements 2010).

The gross tumor volume (GTV) comprises the macroscopic tumor extension. These are all tumor manifestations that are visible clinically as defined by the TNM system. Additional information is derived from imaging techniques such as ultrasound, computed tomography (CT), magnetic resonance imaging (MRI), functional MRI, or position emission tomography (PET), respectively. It may not only include the primary tumor but also lymph node metastases or distant tumor manifestations.

The clinical target volume (CTV) is defined as the GTV plus a volume that is considered at risk of containing subclinical or microscopic disease. The extent of this margin differs widely among different tumor locations or different tumor histologies. Until now there is no consensus on how the risk of subclinical disease is defined but typically a probability of occult disease of 5–10 % is assumed to require treatment. The consideration of the consequences of failure and the expected feasibility of salvage treatment furthermore influence the clinical judgment (International Commission on Radiation Units and Measurements 2010).

The planning target volume (PTV) comprises the CTV with an additional margin derived from internal organ movement and patient setup error. The PTV is the only target structure of which the size changes depending on the precision of the applied radiotherapy technique. Without any measures to determine the exact position of the prostate before or during the treatment fraction, the CTV–PTV margin should cover the mentioned errors to provide a high probability of CTV coverage of the applied radiotherapy.

The internal target volume (ITV) was introduced first in the ICRU report 62. The aim was to take into account possible changes of the CTV in terms of size, shape, and position. In prostate cancer these changes may be attributed to varying volumes of adjacent organs, namely, rectum and bladder, which may cause altering CTV volumes.

The planning organ at risk volume (PRV) is directly associated with the ITV. Due to varying filling states of organs at risk, the ITV allows for an improved determination of doses received by organs at risk during a treatment course. As volumes may vary substantially, a precise measurement of these doses is not possible as the volume of an OAR may change not only between

Table 14.2 Summary of target volume definitions in the published phase III trials

Phase III trials	CTV definition	CTV–PTV margin
Arcangeli et al. (2012)	Prostate + SV	10 mm uniform
Lukka et al. (2005)	Prostate	15, 10 mm at PRI
Pollack et al. (2006)	Prostate +9 mm inferiorly + proximal SV (intermediate risk); whole SV + LN (high risk)	Conv. IMRT: 8, 5 mm at PRI hypo. IMRT: 7, 3 mm at PRI
Norkus et al. (2009)	Prostate + base of SV	8–10 mm
Yeoh et al. (2011)	Prostate	2D-RT: 15, 20 mm superior + inferior 3D-RT: 15 mm uniform
MD Anderson (Kuban et al. 2008)	Prostate + SV	Ant. + inf.: 12.5–15 mm post. + sup.: 7.5–10 mm
Dutch trial (Al-Mamgani et al. 2011)	Prostate ± SV	Arm A: 10 mm (68 Gy)
		Arm B: 10 mm (68 Gy)
		Arm B: 5 mm (last 10 Gy)
PROG96-09 (Zietman et al. 2005)	Prostate +5 mm	7–10 mm
GETUG 06 (Beckendorf et al. 2011)	46 Gy: prostate + SV	10 mm (5 mm posteriorly)
	Arm A: prostate (24 Gy)	
	Arm B: prostate (34 Gy)	
MRC RT01 (Dearnaley et al. 2007)	Low risk: prostate + base of SV +5 mm intermediate + high-risk: prostate + SV +5 mm	5–10 mm

Hypo-FX hypofractionation, *SV* seminal vesicles, *LN* lymph nodes, *IMRT* intensity-modulated radiotherapy, *RT* radiotherapy, *PRI* prostate–rectum interface

treatment fractions but also within a single fraction (inter- and intrafraction deviation). Furthermore a larger OAR volume may be advantageous as well as a distinct disadvantage in certain clinical situations. The rectum, for instance, may receive a significantly lower dose when fully extended by the use of an endorectal balloon, as the PTV positioned anteriorly will be treated in a constant position. In a systematic review, a reduction of the rectal wall dose was shown in planning studies when an endorectal balloon was used. Yet there are no clinical studies to confirm whether rectal toxicities are reduced as well (Smeenk et al. 2010). Furthermore an extended rectum may shift the prostate anteriorly and thus may result in an increased rectal dose when no image-guided radiotherapy is applied.

Current randomized trials have used a variety of target delineations. Table 14.2 gives an overview of the available randomized trials on hypofractionation and dose escalation in primary prostate cancer radiotherapy. Obviously the target volume definition is different in each trial although prostate plus seminal vesicles were used as the CTV in most trials. The definitions of the PTV margins are variable as well, ranging from 3 to 20 mm.

The following paragraphs will collect and sum up the available evidence on target volume definition.

14.3 Pathological Considerations for Prostate Cancer Clinical Target Volume Delineation

14.3.1 CTV Delineation in Low-Risk Prostate Cancer

Knowledge of the natural spread of prostate cancer is crucial for determination of reasonable clinical target volumes. The most comprehensive data on this issue can be derived from pathological studies. The tumor-related bottleneck factors for CTV definitions are (a) the presence of extracapsular extension (ECE) and (b) seminal vesicle invasion (SVI).

In 1997 D'Amico et al. found in a retrospective analysis of 749 prostatectomy specimens that the

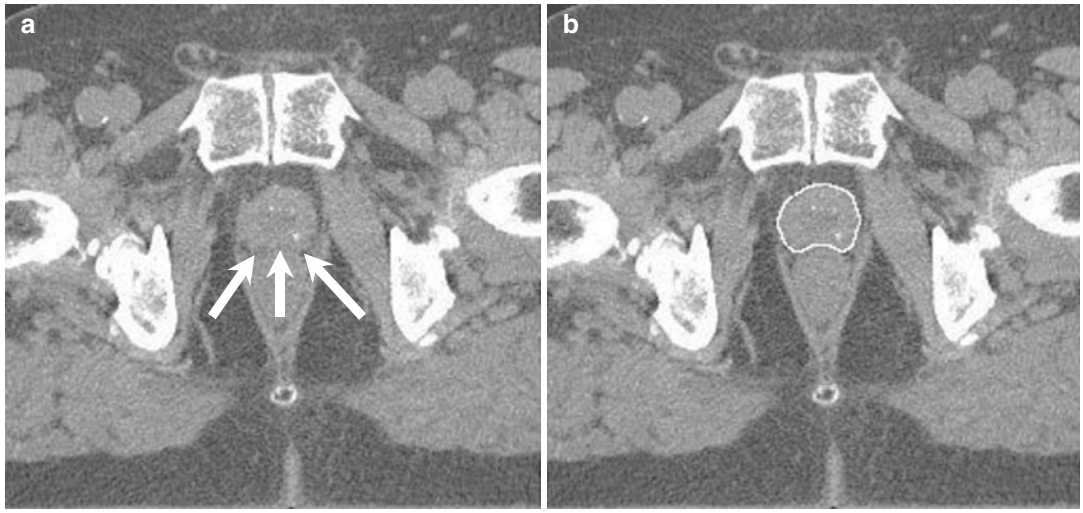

Fig. 14.1 Typical CT slice in the mid-gland region. *Arrows* indicate the fat layer at the prostate–rectum interface (**a**). CTV contour of the same CT slice (**b**)

risk of pathologic SVI as well as macroscopic extracapsular tumor extension is only 2 % in low-risk patients. They furthermore found that the risk of PSA relapse is similar in patients undergoing radical prostatectomy or radiotherapy when patients without clinical risk factors were included (D'Amico et al. 1997b). These factors were defined as PSA <10 ng/ml, clinical stage <T2c, and Gleason score <7, respectively. Further pathological studies confirmed these results (Kestin et al. 2002). Taking these findings into account, there is no sensible reason to include the seminal vesicles into the CTV in patients with low-risk prostate cancer. As the risk of ECE is similarly low, it is obvious to delineate the prostate only as CTV defined by the visible boundaries on planning computed tomography or magnetic resonance imaging. An example of CTV delineation is shown in Fig. 14.1b.

Does this hold true for patients *with* clinical risk factors?

14.3.2 CTV Delineation in Intermediate- and High-Risk Prostate Cancer

To shed light on this question, it is useful to focus on the two most relevant factors of tumor recurrence after definitive therapy, namely, extracapsular tumor extension and seminal vesicle involvement. It is well understood that the risk for these factors rises with increasing clinical risk factors. The question whether the degree of extracapsular extension may influence treatment outcome has been addressed by many authors. Just recently van Veggel published an outcome study after radical prostatectomy, focusing on the associated pathological ECE evaluation. Evaluation of the biochemical relapse rate of 134 patients according to different definitions of ECE revealed a significant association of the extent of ECE with the rate of biochemical relapse rates (van Veggel et al. 2011). Their results confirmed studies from various other authors (Epstein et al. 1993; Wheeler et al. 1998; Davis et al. 1999). To be able to apply these results to target volume definition in prostate cancer radiotherapy, it is necessary to evaluate the specific amount of extracapsular tumor extension. In the largest published series, Teh et al. found that, among all prostatectomy specimens with extracapsular tumor extension, only 2.8 % show an extension of more than 5 mm from the capsule (Teh et al. 2003). Several pathological studies have confirmed that more than 90 % of all patients who present with ECE have a radial tumor extension from the capsule of less than 4–5 mm (Davis et al. 1999; Schwartz et al. 2007; Sohayda et al. 2000).

CTV definition of the prostate gland plus an additional circumferential margin of 5 mm would

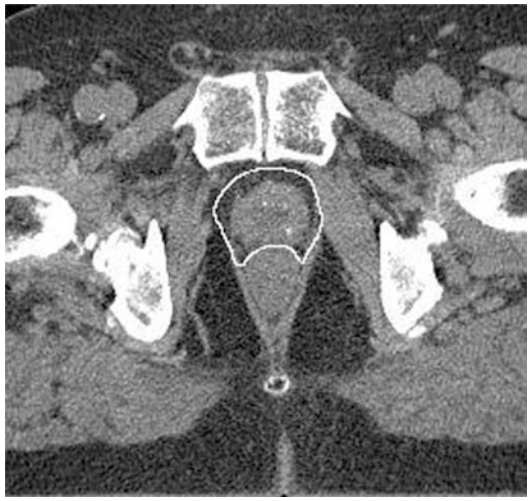

Fig. 14.2 Contouring of the prostate plus a 5 mm margin to include the possible periprostatic extension in patients with risk factors

thus cover more than 90 % of tumor extensions outside the prostate. At the prostate–rectum interface, the anterior rectal wall represents a solid boundary for tumor cells so that the CTV can be reduced posteriorly. An example is shown in Fig. 14.2.

Kestin and colleagues reviewed 344 prostatectomy specimens with regard to SVI. They found that the tumor never involves the whole SV; the most distant cancer found was 1.5 cm apart from the SV tip. Including the proximal 2 cm of the SV into the CTV would include 90 % of pathologically involved seminal vesicles. In terms of certainty of CT definitions of the seminal vesicle compared to pathological measurements, they furthermore found that the two methods are in good agreement (Kestin et al. 2002). Given that 38 % of all patients showed at least one high-risk feature, it seems advisable to include the proximal 2.0–2.5 cm of the seminal vesicles into CTV in order to cover more than 90 % of all SVI. Finally only 1 % of low-risk patients had an SVI which confirms not to include SVs into CTV in this patient group. With each prognostic high-risk factor, the rate of SVI rises from 15 % with one high-risk factor, 28 % with two, to 58 % with three high-risk factors, respectively.

With regard to CTV definition, it may be reasonable to include the base of the seminal vesicles (proximal 2–2.5 cm) into the CTV for all patients with high-risk features. Yet one must be aware that with only one high-risk factor the number of patients who are treated with a larger CTV without having an SVI is considerably high. The treating physician must refer to the available data to gain informed consent with the patient.

14.4 CT/MRI and Target Delineation

CT scans are still considered standard for target delineation. There are two main reasons indicating that this will not change thoroughgoing within the next 10 years. Firstly CT scanners are available at the disposal of all radiotherapy units and are mainly used as dedicated imaging systems. Secondly treatment planning systems are nowadays continuing to calculate tissue-specific doses based on Hounsfield units. Just recently the Department of Oncology of the University Hospital in Helsinki, Finland, commissioned an MRI-only-based treatment planning procedure for external beam radiotherapy of prostate cancer (Kapanen et al. 2012). Yet the use of MRI-based systems across the board will not be realistic within the next decade.

Using CT scans for prostate cancer treatment planning is known to contain inaccuracies. An analysis of the pathologic prostate volume and the CTV delineated in 10 patients whose preoperative CT scans were available showed an almost twofold increase of the respective volumes (Teh et al. 2003). Although the significance of this result is limited due to the small number of analyzed CT scans, the issue of volume overestimation must be scrutinized.

It is a well-known fact that CT scans overestimate the "true" prostate volume by 20–60 % when compared with MRI scans. Yet there is a lack of precise information on the exact regions of overestimation. In a multiobserver study on CT–MRI prostate delineation, the volume overestimation was 40 %, favoring the CT scans. The authors point out that the CT volume did not encompass the whole MRI volume, indicating that the differences in size between CT and MRI are not evenly distributed around the delineated prostate (Rasch et al. 1999). The largest

differences are seen at the apex of the prostate where the MRI is able to clearly distinguish between the apex, the urogenital diaphragm, and the plexus Santorini. The soft tissue contrast in MRI allows for an easily visible boundary layer just as well at the prostate base, with the higher signal intensity of the seminal vesicles compared to the prostatic tissue. These two regions showed the largest CT–MRI volume differences among the observers.

These findings are of crucial relevance in terms of target volume definition. Whereas the risk of transcapsular extension is very small in the anterior or anterolateral parts of the gland, it is highest in the posterior and posterolateral parts. Thus the periprostatic region at the prostate–rectum interface is at the highest risk of tumor recurrence when underdosed by radiotherapy.

That implies that we have to focus on the CT-based overestimation in these anatomic areas. To our knowledge there is no study or paper giving details about this special issue throughout the literature. But we do know that CT can often discriminate precisely the posterolateral area cranially of the apex region where there is usually a thin fatty layer between the posterior surface of the prostate and the rectal wall. Figure 14.1a shows an example of this area. Figure 14.1b shows the prostate contour of this CT slice.

Considering a patient with intermediate- or high-risk factors who has a substantial risk of transcapsular spread and furthermore assuming the extracapsular extension to be in most cases not larger than 5 mm, the resulting contour for the CTV is shown in Fig. 14.2. Note that any anatomic boundary such as rectal wall, bone, or muscle represents a demarcation line which is usually not crossed by tumor cells except in locally advanced T4 tumors. Thus the CTV contour should include this boundary but should not include the given organ. Figure 14.3 provides examples of MRI, which can be fused with planning CT scans.

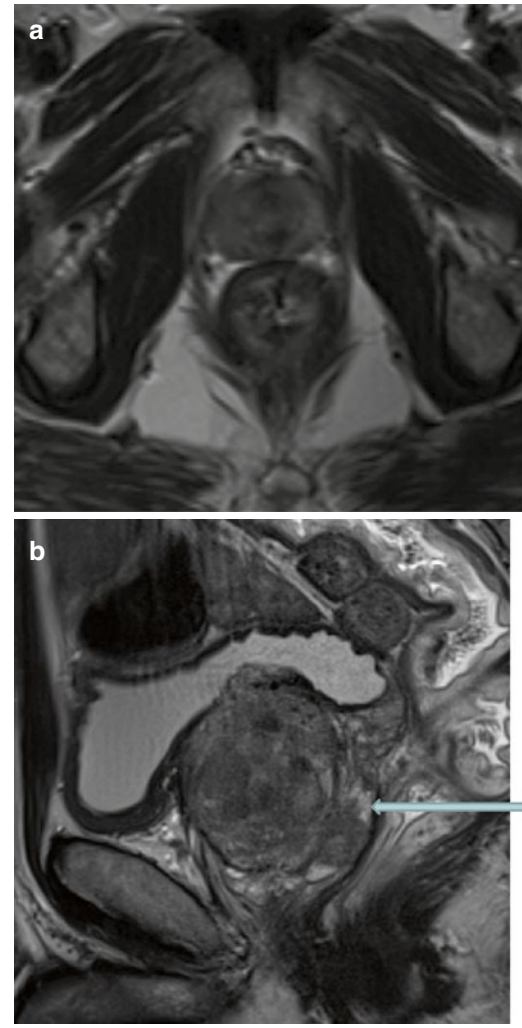

Fig. 14.3 (**a**) Magnetic resonance imaging (axial T2 TSE) of the prostate gland. (**b**) Magnetic resonance imaging (sagittal T2 TSE) of T3a prostate cancer with infiltration through the posterior part of the capsule (*arrow*)

14.5 CTV–PTV Margin

The PTV represents a security margin encompassing the CTV that considers daily setup errors of the patient and the individual internal organ motion (see Sect. 14.3.2). This margin may be defined uniformly or may be smaller toward the prostate–rectum interface.

There is consensus that the PTV is being contoured by a computer planning system as an automatically generated margin. The PTV must not be generated by hand as for an individual observer it is not possible to draw a three-dimensional margin encompassing the CTV.

The CTV–PTV margin is depending on the type and precision of the verification method of the patients' daily treatment as well as intrafraction motion but not on the type of therapy, e.g.,

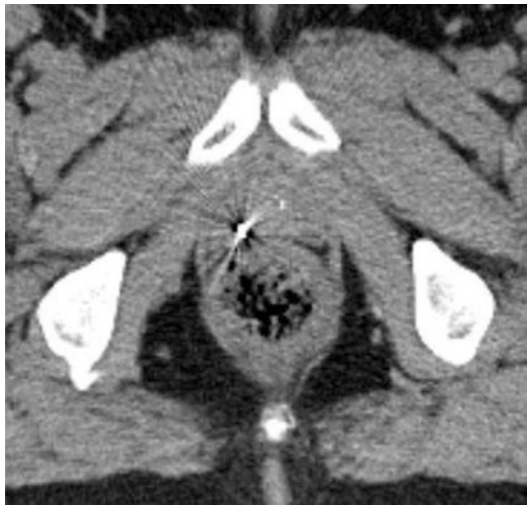

Fig. 14.4 Fiducial gold marker used for image-guided radiotherapy. Note that artifacts might influence delineation of the prostate

3D conformal or IMRT. Obviously a daily online setup verification and correction requires smaller PTV margins compared to an offline verification protocol that is performed once or twice weekly. Recently image-guided radiotherapy has emerged as a tool to verify and if necessary correct the patients' position before each treatment by using cone beam CT, ultrasound, intraprostatic fiducial markers (Fig. 14.4), or implanted electronic devices. These systems are able to minimize interfraction motion to a great extent.

There are numerous studies that tried to define the CTV–PTV margin based on analyses of the number of verifications performed per week. The largest study with regard to image guidance and inter- as well as intrafraction motion was performed by Kotte et al. (2007). They analyzed more than 11,000 measurements of online setup verifications of 427 patients who were treated with a 5-field IMRT. All patients had implanted fiducial gold markers and verification was performed before each treatment session and before each treated field. They found that there is substantial intrafraction motion with 66 % of all measurements with a motion outside a range of 2 mm and 28 % outside a range of 3 mm. The authors were able to demonstrate that with a daily setup correction, systematic and random setup errors were smaller than 1 mm. In conclusion they recommend a minimum CTV–PTV margin of 2 mm when a daily setup verification of the prostate position is performed before each treatment session.

Graf et al. conducted a study on 23 prostate cancer patients with implanted gold markers and calculated the necessary CTV–PTV margin relative to the frequency of setup verifications and corrections (Graf et al. 2009). Table 14.3 shows their main results.

Margins were calculated using a formula developed by van Herk (2004). The key message of this analysis states that with daily setup corrections a CTV–PTV margin of 5 mm is appropriate, whereas once weekly or no correction requires 10 mm margins (Graf et al. 2009).

The relevance of a constant or reproducible filling status of the rectum and/or the bladder has not been of major concern for decades. In 2005 De Crevoisier published a landmark study of an increased risk of biochemical relapse after prostate radiotherapy if the rectum had been distended (filled) during planning CT. The authors

Table 14.3 PTV margins calculated from the frequency of setup corrections

Random σ and systematic Σ error [mm]							PTV margin [mm]		
Direction	LR		SI		AP		LR	SI	AP
	Σ	σ	Σ	σ	Σ	σ			
No correction	2.0	2.9	2.7	3.9	2.6	4.3	7.0	9.5	9.5
Correction 1×/week	1.9	2.8	2.3	3.5	2.4	3.9	6.7	8.2	8.7
Correction 3×/week	1.6	2.5	1.8	3.0	1.7	3.3	5.8	6.6	7.7
Correction 5×/week	1.4	2.0	1.4	2.3	1.3	2.2	4.9	5.1	4.8

Adapted from Graf et al. (2009)
LR left–right, *SI* superior–inferior, *AP* anterior–posterior

found on multivariate analysis that rectal distension was an independent risk factor for biochemical failure with a hazard ratio of 3.89 (95 % CI, 1.58–9.56, $p=0.003$) (de Crevoisier et al. 2005). This was confirmed in a subgroup analysis of the Dutch dose-escalation trial. The authors found an increased risk of failure in patients with a 25 % risk of seminal vesicle involvement and a risk of geometric miss defined by anorectal volume >90 cm^3 and symptoms of diarrhea at least 25 % of the treatment time (Heemsbergen et al. 2007).

Results from these studies provide evidence that an empty rectum during planning CT provides improved biochemical control in patients undergoing definitive radiotherapy for prostate cancer. This involves only patients who are treated with conventional verification techniques, e.g., offline correction protocols. In the case of image-guided radiotherapy, the risk of a geographic miss is reduced substantially because the image guidance positions the prostate irrespective of the distension of the rectum.

The relevance of patient instructions with regard to constant filling status of the rectum and bladder was explored in a study to evaluate whether this patient preparation yields an improvement of target stability. The authors were able to demonstrate that with proper patient instructions, the calculated CTV–PTV margins would be as low as with image-guided radiotherapy (Graf et al. 2012).

In summary, CTV–PTV margins must be adapted to the type of patient setup verification and the frequency of these verifications. With regard to treatment precision in prostate cancer radiotherapy, radiation oncologists may select from a variety of verification options, namely, implanted fiducial markers or electronic devices, cone beam or MV-CT, or ultrasound However, these procedures are not yet available throughout the radiotherapy community.

The significance of bladder and rectal filling status is important and may help to reduce deviations in the position and shape of the prostate.

References

Al-Mamgani A, van Putten WL, van der Wielen GJ, Levendag PC, Incrocci L (2011) Dose escalation and quality of life in patients with localized prostate cancer treated with radiotherapy: long-term results of the Dutch randomized dose-escalation trial (CKTO 96–10 trial). Int J Radiat Oncol Biol Phys 79(4):1004–1012. doi:10.1016/j.ijrobp.2009.12.039

Arcangeli S, Strigari L, Gomellini S, Saracino B, Petrongari MG, Pinnaro P, Pinzi V, Arcangeli G (2012) Updated results and patterns of failure in a randomized hypofractionation trial for high-risk prostate cancer. Int J Radiat Oncol Biol Phys 84(5):1172–1178. doi:10.1016/j.ijrobp.2012.02.049

Beckendorf V, Guerif S, Le Prise E, Cosset JM, Bougnoux A, Chauvet B, Salem N, Chapet O, Bourdain S, Bachaud JM, Maingon P, Hannoun-Levi JM, Malissard L, Simon JM, Pommier P, Hay M, Dubray B, Lagrange JL, Luporsi E, Bey P (2011) 70 Gy versus 80 Gy in localized prostate cancer: 5-year results of GETUG 06 randomized trial. Int J Radiat Oncol Biol Phys 80(4):1056–1063. doi:10.1016/j.ijrobp.2010.03.049

Boehmer D, Maingon P, Poortmans P, Baron MH, Miralbell R, Remouchamps V, Scrase C, Bossi A, Bolla M (2006) Guidelines for primary radiotherapy of patients with prostate cancer. Radiother Oncol 79(3):259–269. doi:10.1016/j.radonc.2006.05.012

D'Amico AV, Whittington R, Kaplan I, Beard C, Schultz D, Malkowicz SB, Tomaszewski JE, Wein A, Coleman CN (1997a) Equivalent 5-year bNED in select prostate cancer patients managed with surgery or radiation therapy despite exclusion of the seminal vesicles from the CTV. Int J Radiat Oncol Biol Phys 39(2):335–340

D'Amico AV, Whittington R, Schultz D, Malkowicz SB, Tomaszewski JE, Wein A (1997b) Outcome based staging for clinically localized adenocarcinoma of the prostate. J Urol 158(4):1422–1426

D'Amico AV, Whittington R, Malkowicz SB, Schultz D, Blank K, Broderick GA, Tomaszewski JE, Renshaw AA, Kaplan I, Beard CJ, Wein A (1998) Biochemical outcome after radical prostatectomy, external beam radiation therapy, or interstitial radiation therapy for clinically localized prostate cancer. JAMA 280(11):969–974

D'Amico AV, Whittington R, Malkowicz SB, Fondurulia J, Chen MH, Kaplan I, Beard CJ, Tomaszewski JE, Renshaw AA, Wein A, Coleman CN (1999) Pretreatment nomogram for prostate-specific antigen recurrence after radical prostatectomy or external-beam radiation therapy for clinically localized prostate cancer. J Clin Oncol 17(1):168–172

Davis BJ, Pisansky TM, Wilson TM, Rothenberg HJ, Pacelli A, Hillman DW, Sargent DJ, Bostwick DG (1999) The radial distance of extraprostatic extension of prostate carcinoma: implications for prostate brachytherapy. Cancer 85(12):2630–2637

de Crevoisier R, Tucker SL, Dong L, Mohan R, Cheung R, Cox JD, Kuban DA (2005) Increased risk of biochemical and local failure in patients with distended rectum on the planning CT for prostate cancer radiotherapy. Int J Radiat Oncol Biol Phys 62(4):965–973. doi:10.1016/j.ijrobp.2004.11.032

Dearnaley DP, Sydes MR, Graham JD, Aird EG, Bottomley D, Cowan RA, Huddart RA, Jose CC, Matthews JH, Millar J, Moore AR, Morgan RC, Russell JM, Scrase CD, Stephens RJ, Syndikus I, Parmar MK (2007) Escalated-dose versus standard-dose conformal radiotherapy in prostate cancer: first results from the MRC RT01 randomised controlled trial. Lancet Oncol 8(6):475–487. doi:10.1016/S1470-2045(07)70143-2

Epstein JI, Carmichael MJ, Pizov G, Walsh PC (1993) Influence of capsular penetration on progression following radical prostatectomy: a study of 196 cases with long-term follow-up. J Urol 150(1):135–141

Graf R, Wust P, Budach V, Boehmer D (2009) Potentials of on-line repositioning based on implanted fiducial markers and electronic portal imaging in prostate cancer radiotherapy. Radiat Oncol 4:13. doi:10.1186/1748-717X-4-13

Graf R, Boehmer D, Nadobny J, Budach V, Wust P (2012) Appropriate patient instructions can reduce prostate motion. Radiat Oncol 7:125. doi:10.1186/1748-717X-7-125

Heemsbergen WD, Hoogeman MS, Witte MG, Peeters ST, Incrocci L, Lebesque JV (2007) Increased risk of biochemical and clinical failure for prostate patients with a large rectum at radiotherapy planning: results from the Dutch trial of 68 GY versus 78 Gy. Int J Radiat Oncol Biol Phys 67(5):1418–1424. doi:10.1016/j.ijrobp. 2006.11.014

International Commission on Radiation Units and Measurements (1993) Prescribing, recording, and reporting photon beam therapy. ICRU report 50, Oxford University Press, Oxford

International Commission on Radiation Units and Measurements (1999) Prescribing, recording, and reporting photon beam therapy (Supplement to ICRU report 50). ICRU Report 62, Oxford University Press, Oxford

International Commission on Radiation Units and Measurements (2010) Prescribing, recording, and reporting photon-beam intensity-modulated radiation therapy (IMRT). ICRU report 83, Oxford University Press, Oxford 10(1). doi:10.1093/jicru/ndq002

Kapanen M, Collan J, Beule A, Seppala T, Saarilahti K, Tenhunen M (2012) Commissioning of MRI-only based treatment planning procedure for external beam radiotherapy of prostate. Magn Reson Med. doi:10.1002/mrm.24459

Kestin L, Goldstein N, Vicini F, Yan D, Korman H, Martinez A (2002) Treatment of prostate cancer with radiotherapy: should the entire seminal vesicles be included in the clinical target volume? Int J Radiat Oncol Biol Phys 54(3):686–697

Kotte AN, Hofman P, Lagendijk JJ, van Vulpen M, van der Heide UA (2007) Intrafraction motion of the prostate during external-beam radiation therapy: analysis of 427 patients with implanted fiducial markers. Int J Radiat Oncol Biol Phys 69(2):419–425. doi:10.1016/j.ijrobp.2007.03.029

Kuban DA, Tucker SL, Dong L, Starkschall G, Huang EH, Cheung MR, Lee AK, Pollack A (2008) Long-term results of the M.D. Anderson randomized dose-escalation trial for prostate cancer. Int J Radiat Oncol Biol Phys 70(1):67–74. doi:10.1016/j.ijrobp.2007.06.054

Lukka H, Hayter C, Julian JA, Warde P, Morris WJ, Gospodarowicz M, Levine M, Sathya J, Choo R, Prichard H, Brundage M, Kwan W (2005) Randomized trial comparing two fractionation schedules for patients with localized prostate cancer. J Clin Oncol 23(25): 6132–6138. doi:10.1200/JCO.2005.06.153

Norkus D, Miller A, Kurtinaitis J, Haverkamp U, Popov S, Prott FJ, Valuckas KP (2009) A randomized trial comparing hypofractionated and conventionally fractionated three-dimensional external beam radiotherapy for localized prostate adenocarcinoma : a report on acute toxicity. Strahlenther Onkol 185(11):715–721. doi:10.1007/s00066-009-1982-z

Pollack A, Hanlon AL, Horwitz EM, Feigenberg SJ, Konski AA, Movsas B, Greenberg RE, Uzzo RG, Ma CM, McNeeley SW, Buyyounouski MK, Price RA Jr (2006) Dosimetry and preliminary acute toxicity in the first 100 men treated for prostate cancer on a randomized hypofractionation dose escalation trial. Int J Radiat Oncol Biol Phys 64(2):518–526. doi:10.1016/j.ijrobp.2005.07.970

Rasch C, Barillot I, Remeijer P, Touw A, van Herk M, Lebesque JV (1999) Definition of the prostate in CT and MRI: a multi-observer study. Int J Radiat Oncol Biol Phys 43(1):57–66

Schwartz DJ, Sengupta S, Hillman DW, Sargent DJ, Cheville JC, Wilson TM, Mynderse LA, Choo R, Davis BJ (2007) Prediction of radial distance of extraprostatic extension from pretherapy factors. Int J Radiat Oncol Biol Phys 69(2):411–418. doi:10.1016/j.ijrobp. 2007.03.016

Smeenk RJ, Teh BS, Butler EB, van Lin EN, Kaanders JH (2010) Is there a role for endorectal balloons in prostate radiotherapy? A systematic review. Radiother Oncol 95(3):277–282. doi:10.1016/j.radonc.2010.04.016

Sohayda C, Kupelian PA, Levin HS, Klein EA (2000) Extent of extracapsular extension in localized prostate cancer. Urology 55(3):382–386

Teh BS, Bastasch MD, Wheeler TM, Mai WY, Frolov A, Uhl BM, Lu HH, Carpenter LS, Chiu JK, McGary J, Woo SY, Grant WH 3rd, Butler EB (2003) IMRT for prostate cancer: defining target volume based on correlated pathologic volume of disease. Int J Radiat Oncol Biol Phys 56(1):184–191

van Herk M (2004) Errors and margins in radiotherapy. Semin Radiat Oncol 14(1):52–64. doi:10.1053/j.semradonc.2003.10.003

van Veggel BA, van Oort IM, Witjes JA, Kiemeney LA, Hulsbergenvan de Kaa CA (2011) Quantification of extraprostatic extension in prostate cancer: different parameters correlated to biochemical recurrence after

radical prostatectomy. Histopathology 59(4):692–702. doi:10.1111/j.1365-2559.2011.03986.x

Wheeler TM, Dillioglugil O, Kattan MW, Arakawa A, Soh S, Suyama K, Ohori M, Scardino PT (1998) Clinical and pathological significance of the level and extent of capsular invasion in clinical stage T1–2 prostate cancer. Hum Pathol 29(8):856–862

Yeoh EE, Botten RJ, Butters J, Di Matteo AC, Holloway RH, Fowler J (2011) Hypofractionated versus conventionally fractionated radiotherapy for prostate carcinoma: final results of phase III randomized trial. Int J Radiat Oncol Biol Phys 81(5):1271–1278. doi:10.1016/j.ijrobp.2010.07.1984

Zietman AL, DeSilvio ML, Slater JD, Rossi CJ Jr, Miller DW, Adams JA, Shipley WU (2005) Comparison of conventional-dose vs. high-dose conformal radiation therapy in clinically localized adenocarcinoma of the prostate: a randomized controlled trial. JAMA 294(10): 1233–1239. doi:10.1001/jama.294.10.1233

Gynecological Cancer

15

Nina A. Mayr, Larissa Lee, and Catherine Yashar

Contents

N.A. Mayr, MD (✉)
Department of Radiation Oncology,
Ohio State University, Columbus, OH, USA
e-mail: Nina.Mayr@osumc.edu

L. Lee, MD
Department of Radiation Oncology, Brigham and Women's Hospital, Harvard Medical School, Boston, MA, USA

C. Yashar, MD
Department of Radiation Oncology, University of California San Diego, San Diego, CA, USA

15.1 Cervical Cancer

15.1.1 Anatomy, Pathology

The uterus consists of the body and cervix, which are connected by the isthmus. The cervix is a fibro-glandular structure connecting the uterus with the vagina and divided into the ectocervix, which is covered with squamous epithelium, and endocervix lined with glandular epithelium. The principal supporting ligaments of the uterus are the broad, round, uterosacral, and cardinal ligament, which are common pathways of invasion in cervical cancer.

The uterus derives its blood supply from several sources that form a rich network of anastomosing vessels. The primary blood supply is from the uterine artery, an anterior branch of the internal iliac artery. The uterine artery enters the uterus after crossing the ureter at the isthmus/level of the internal os. The ovarian artery enters at the level of the fundus through the ovarian ligament. Vaginal arteries anastomose with the uterine vessels inferiorly.

Lymphatic vessels form a rich subserosal plexus that drains from four trunks. The more superior vessels travel through the broad ligament, parallel to the fallopian tube, and drain to the external iliac nodes. More inferiorly, the vessels cross through the broad ligament to the nodes at the bifurcation of the common iliac into the internal and external iliac vessels. At the junction of the fallopian tube and the uterine body are trunks that

A.-L. Grosu, C. Nieder (eds.), *Target Volume Definition in Radiation Oncology*,
DOI 10.1007/978-3-662-45934-8_15,

may pass directly to the para-aortic lymph nodes through the ovarian pedicle. Lymphatics near the round ligament can pass directly along the ligament to the femoral lymph nodes.

15.1.2 Routes of Spread

Cervical cancer spreads by local extension along adjacent ligamentous structures of the parametria and uterosacral and cardinal ligaments, along the endocervix to the corpus and distally to the vagina.

Lymphatic spread in cervical cancer occurs predominantly through the lateral and posterior lymphatic trunks (Fig. 15.1) along the obturator, external, and internal iliac nodes and less commonly to the superior rectal and presacral nodes. Lymphatic spread generally progresses sequentially from echelon to echelon. Obturator nodes, which are part of the medial external iliac nodes (located near the obturator internal muscle) (Walsh et al. 1980), drain to the more proximal external iliac, common iliac to para-aortic nodes, and finally through the cisterna chyli at the level of L1–L2 to the left supraclavicular nodes. Spread through the posterior trunk to the superior rectal and presacral nodes also occurs, particularly in advanced tumors. Among the visceral lymph nodes, the parametrial nodes are commonly involved.

15.1.3 Imaging Modalities

15.1.3.1 Computed Tomography

CT remains the most widely used diagnostic imaging modality for staging and is the most frequently employed imaging modality for target delineation in cervical cancer. It is excellent in delineating lymph node regions (although its accuracy to differentiate normal from tumor-involved nodes is inferior to PET/CT). CT readily depicts the morphology of presacral target tissues and normal structures, including the small and large bowel, bladder, other abdominal organs, kidneys, and bone. CT is superior in delineating surgical clips and implanted vaginal gold markers. CT allows delineation of the uterus but does not differentiate tumor from the normal uterus, which generally is sufficient for the purposes of

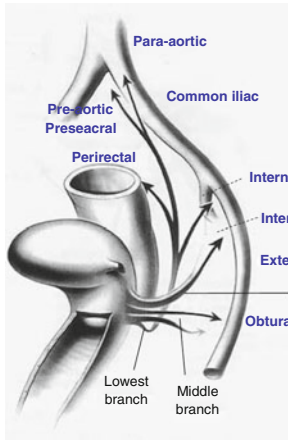

Cervical lymphatics drain in 3 dominant lymphatic trunks: lateral trunk (the largest), posterior and anterior trunk.

The **lateral trunk** (Figure on left)

consists of:	→ drains to :
- upper branch	→ upper internal iliac LN[1)]
- middle branch	→ obturator LN[2)]
- lowest branch	→ gluteal, common iliac, presacral LN
The **posterior trunk**	→ superior rectal LN
	→ sub-aortic LN (sacral promontory)
The **anterior trunk**	→ distal external iliac

Lymphatic spread occurs in stepwise fashion successively from echelon to echelon. LN spread along lymphatic echelons includes:
- obturator LN → external iliac → common iliac → para-aortic
internal iliac → common iliac → para-aortic

Adapted from Plentl AA, Friedman EA, Lymphatic system of the female genitalia. Philadelphia. WB Saunders, 1971 p.83.

Fig. 15.1 Lymphatic drainage of the cervix. The lymphatic trunks are presented and lymph node echelons are tabulated. [2]Obturator *ln* are part of the medial subgroup of the external ilian *ln*, located close to the obturator internus muscle. [1]The term *hypogastric* node is used variably, to describe the most cephalic of the internal iliac nodes or the entire internal iliac node chain (2). Adapted from Plentl AA, Friedman EA, Lymphatic system of the female genitalia. Philadelphia. WB Saunders, 1971 p.83.

external beam radiation. However, substructures of the uterus, cervix, isthmus, corpus, and fundus are challenging to delineate on CT. Because of its lacking tissue differentiation between the tumor and normal soft tissue structures, CT is limited in delineating the tumor extent within the uterus. Its accuracy in parametrial involvement is inferior compared to MRI (Mitchell et al. 2006; Subak et al. 1995). Therefore, MRI is the preferred imaging modality for high-precision delineation of the primary tumor/extent as required for image-guided brachytherapy.

15.1.3.2 Magnetic Resonance Imaging (MRI)

High-precision assessment of the primary tumor volume and extent is best assessed by MRI in cervical cancer (Bhosale et al. 2010; Balleyguier et al. 2011; Hricak 1991). With its superior soft tissue contrast, MRI is superior to CT in delineating the tumor within the cervix and differentiating it from the uterus and adjacent pelvic tissues, including bladder invasion, parametrial extension, and rectal and perirectal involvement (Mitchell et al. 2006; Subak et al. 1995). This high precision is particularly important for image-based brachytherapy, more so than in external beam radiation, where target volumes include the parauterine structures. Vaginal extension is more accurately delineated by MRI (Sala et al. 2007). MRI is superior to CT in assessing serial subtle morphologic changes in tumor volume/extent (Mayr et al. 2010), which is relevant for longitudinal imaging during therapy for adaptive therapy and for image-guided brachytherapy.

For the assessment and morphologic depiction of regional lymph nodes and postoperative seromas, CT and MRI are generally equivalent (Mitchell et al. 2006; Subak et al. 1995). For both CT and MRI, the identification of *involved* lymph nodes is limited to morphologic criteria, including shape and internal architecture. Configuration criteria for involvement include size (>1 cm in short axis), short-axis-to-long-axis ratio (i.e., more round shape is more consistent with involvement), and margin irregularity. Architectural criteria include central necrosis on contrast-enhanced CT (Yang et al. 2000) or MRI, signal intensity irregularity on T2-weighted MRI (Brown et al. 2003), and loss of the fatty hilum (Koh et al. 2006). With the overall limited accuracy, a combination of size, configuration, and internal architecture should be used.

MRI is helpful in identifying incidental, non-tumor-related findings that may influence therapy including distortion or retroversion of the uterus, fibroids, ovarian findings, and other pelvic abnormalities. The cervical tumor is best delineated on T2-weighted imaging, fast spin echo, or turbo spin-echo sequences, which provide high resolution, while gradient echo sequences are more susceptible to artifacts. T2-weighted sequences are superior to T1-weighted and contrast-enhanced imaging (Sironi et al. 1993). Diffusion imaging may be helpful, particularly when T2-weighted images are equivocal (Charles-Edwards et al. 2008). The use of 3 T MRI does not improve the accuracy over 1.5 T (Hori et al. 2009).

15.1.3.3 Positron Emission Tomography (PET)

The staging and target delineation of cervical cancer have been further advanced by the introduction of fluorodeoxyglucose (^{18}F)(FDG) PET and PET/CT. While CT and MRI identify lymph node involvement, assessment is limited to morphologic size and architectural criteria. The metabolic characterization of lymph nodes by PET/CT provides the most sensitive assessment of pelvic and para-aortic lymph node involvement.

15.1.3.4 Imaging–Surgical–Pathology Correlations

In imaging–surgical–pathology correlation studies, CT has been reported to have an accuracy of 70–80 % for evaluation of lymph node involvement based on size. Accuracy improves to 93 % with a cutoff value of 1 cm (Hawnaur 1993; Hardesty et al. 2001; Bellomi et al. 2005).

In MRI–pathology correlation studies, MRI has been shown to provide better staging than clinical exam in early stage cervical cancer (Bhosale et al. 2010; Balleyguier et al. 2011; Hricak 1991). For tumor volume and delineation, MRI–histologic correlation was found to be 98 % in comparisons of tumor volume from 3D MRI with digitized giant histologic tissue sections

(Burghardt et al. 1989; Greco et al. 1989). These studies established the high accuracy of MRI for the delineation of tumor extent in cervical cancer. In surgical–pathology correlation studies, MRI showed better sensitivities (40–57 %) and specificities (77–80 %) than CT for parametrial invasion (Siegel et al. 2012).

The sensitivity for PET ranges from 79 to 91 % (Siegel et al. 2012) with most misses related to microscopic involvement (Lin et al. 2003). PET/CT, with the added spatial resolution from CT, has a sensitivity of 58–72 %, a specificity of 93–99 %, and an accuracy of 85–99 % for lymph node involvement in cervical cancer (Choi et al. 2006; Sironi et al. 2006).

15.1.4 Target Delineation

15.1.4.1 Simulation Procedure

For cervical cancer, it is critical to incorporate the information from *both* imaging *and clinical* (*pelvic*) *examination* into the radiation therapy planning. Visible and/or palpable and mucosal vaginal involvement is essentially impossible to assess by axially oriented CT imaging and can also be missed on MRI. Placement of radiopaque seed markers into the cervix or into the most distal visible or palpable vaginal tumor extent assists the delineation and the target volume design. Gold markers are recommended for this purpose as ferromagnetic materials will cause metallic artifacts on MRI preventing proper imaging. A dry tampon, which provides negative contrast for CT or MRI, is a simple method to delineate the vagina and lower extent of the cervix/tumor. However, rigid vaginal markers, rectal markers, and rectal contrast administration are not recommended as they may cause upward displacement of the cervix and distension of the rectum with ensuing displacement of the cervix, respectively. If target delineation is based on such displaced anatomy, geographical tumor miss may occur during actual treatment, as daily therapy is delivered without markers/rectal distension. Vaginal tampons have been shown to not cause displacement (Weidner et al. 1999). If excessive rectal distention is noted at the time of simulation, repeat scanning after evacuation or bowel preparation regimen may increase target reproducibility. This is particularly important in postoperative radiation therapy, where mobility of the vaginal target has been well documented and overall target volumes in the pelvis tend to be smaller (Chan et al. 2008; Taylor and Powell 2008).

For CT simulation, intravenous contrast is helpful for the differentiation of regional lymph nodes from vessels, depiction of nodal architecture (see Sect. 1.3.2), and delineation of the bladder. Oral contrast given 1–1.5 h before the simulation can improve differentiation of the bowel from lymph nodes (Figs. 15.2, 15.3, 15.4, 15.5, 15.6, and 15.7), vascular structures, and tumor. However, the effect on dose calculations (Williams et al. 2002) has to be addressed during dosimetry by correcting the inhomogeneity value of the contrast-opacified bowel to water density. For MRI simulation, T2-weighted sequences to delineate the primary tumor, parametria, vagina, and lymph nodes without contrast are used, as the bladder and bowel are readily delineated on these sequences. Contrast is not needed for primary tumor delineation.

If IMRT is used, two scans, one with full and one with empty bladder, are highly recommended, particularly in postoperative patients. This allows delineation of an internal target volume (ITV) accounting for interfractional organ motion from random organ motion and variable bladder and rectal filling (Chan et al. 2008; Taylor and Powell 2008). Full/empty bladder scans are discussed in more detail in Sect. 2.4.2.

15.1.4.2 Target Volume Delineation

Guidelines for target delineation have been developed by the RTOG (Lim et al. 2011; Small; Small et al. 2008) and are used in RTOG and GOG studies.

The *primary tumor GTV* includes the cervical tumor and parametrial and vaginal tumor extensions (if MRI is used). If CT is used, which cannot differentiate tumor from the normal uterus, the entire uterus may have to be delineated as GTV, as well as CT evidence of parametrial and vaginal tumor extensions (Fig. 15.6).

The *primary tumor CTV* includes the cervix (if not already included in the GTV), uterus, parametria, ovaries, and a vaginal margin of at least 2 cm distal to the cervix or lowest vaginal tumor extent based on imaging evidence and per implanted

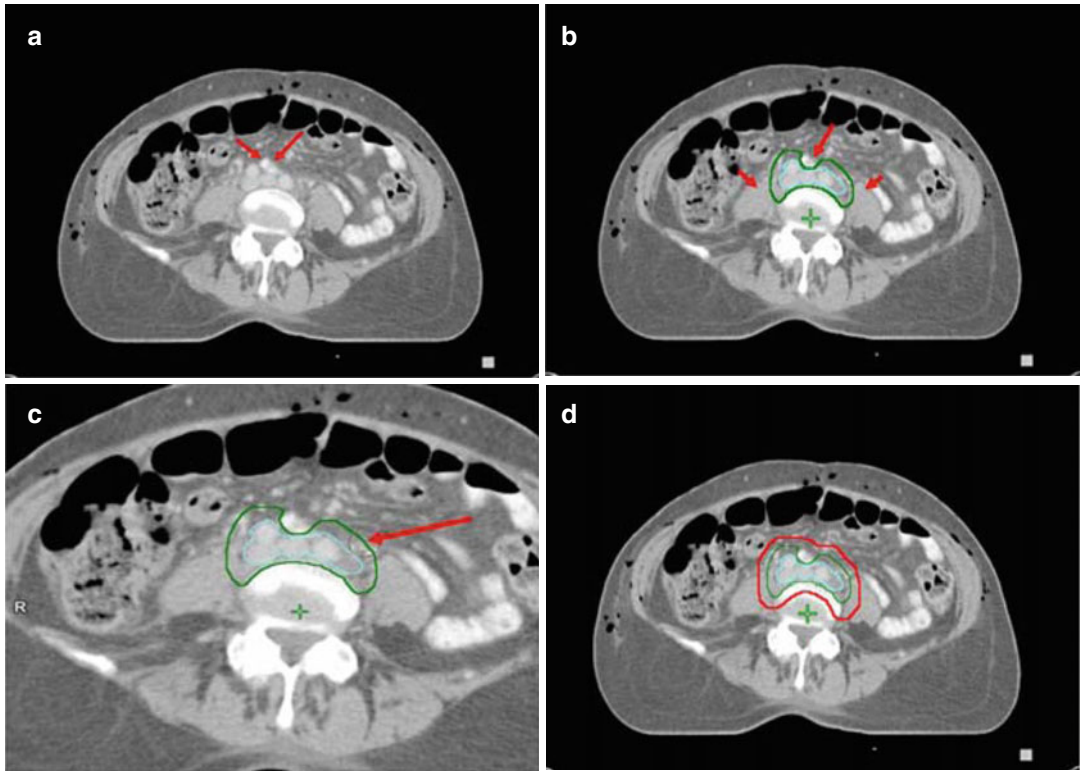

Fig. 15.2 Contouring of the upper common iliac lymph node target. (**a**) The right and left common iliac arteries and veins are seen at the level just below the aortic bifurcation. The different contrast properties of the barium in the small bowel, compared to vascular contrast, help differentiate bowel from vessels and nodal structures. (**b**) The vessels and adjacent lymphatic regions have been contoured (*aqua*) for reference. The lymph node CTV is shown in green. (**c**) Separate delineation of the vessels and lymph nodes (*aqua*) may not be needed. Instead the lymph node CTV (*green*) can be outlined directly at a distance of 0.7 cm from vessels/nodes using the circle cursor (*arrow*), set at 0.7 cm, or a similar drawing tool (**c**), simultaneously excluding psoas, bowel and bone in uninvolved lymph node sites. (**d**) For the lymph node PTV (*red*) a margin of 0.7–1 cm is added to the CTV

markers (Fig. 15.6d). The boundaries of the parametria extend from the upper border of the fallopian tube superiorly to the pelvic floor muscles inferiorly and the posterior wall of the bladder anteriorly to the mesorectal fascia and uterosacral ligaments posteriorly. Separate delineation of the parametria is challenging on CT and is not mandatory because the PTV usually encompasses the intervening tissues between the uterus and the lymph node target at the pelvic side wall (Fig. 15.6b). If uterosacral ligaments are involved by palpation or imaging, the mesorectum and perirectal lymph nodes should be included.

In patients with known involved lymph node(s), the *lymph node GTV* contour encompasses the involved node on CT or MRI. Contrast CT to characterize the involved nodes by internal architectural features and/or necrosis or close consideration to architectural MRI features (Sect. 1.3.2) can be helpful. Coregistration of PET and PET/CT (even a diagnostic scan) is most useful in identifying and localizing the involved node(s). However, the delineation should be based on its morphologic geometry and margin on the CT or MRI.

The *lymph node CTV* contour encompasses the iliac vessels and pelvic lymph nodes, including obturator, external iliac, internal iliac, and common iliac lymph nodes (Figs. 15.2, 15.3, 15.4, 15.5, and 15.6) and 0.7 cm of the perinodal tissue for uninvolved and 1.5 cm for involved lymph nodes. Psoas and piriformis muscles at the pelvic wall and bone are excluded if the lymph nodes are uninvolved. The intraperitoneal small bowel is excluded (Figs. 15.2, 15.3, 15.4, and 15.5).

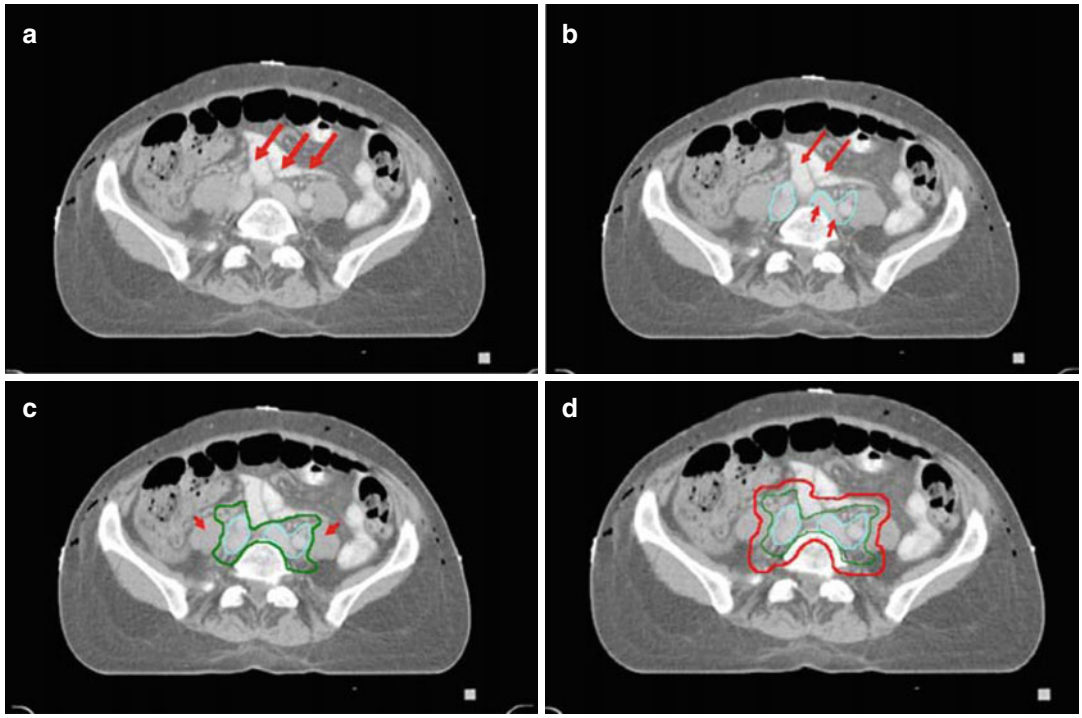

Fig. 15.3 Contouring of the mid common iliac lymph node target. (**a**) The right and left common iliac arteries, veins and lymph nodes are seen medial to the psoas muscles with bowel (*arrows*) in close proximity. (**b**) The left common iliac vein (*short arrows*) is sectioned longitudinally. Vessels and adjacent lymphatic regions have been contoured (*aqua*) for reference. (**c**) The CTV (*green*) again adds a 0.7 cm margin to vessels and adjacent lymphatic tissue, excluding small bowel and psoas. (**d**) For the lymph node PTV (*red*) an additional margin of 0.7 cm is added to the CTV

Surgical clips and seromas (Mayr et al. 2011) are included where applicable. The superior extent of the lymph node CTV is typically 0.7 cm below the L4/L5 interspace (so that the PTV, which adds 0.7 cm, extends to the L4/L5 interspace).

However, the traditional 2D-based landmark of L4/L5 has been challenged as the upper border of the common iliac nodes. Significant viability of the aortic bifurcation has been found, and 40 % of common iliac lymph nodes are reported to be located above the L4/L5 interspace (Marnitz et al. 2006). Therefore, the superior border of the lymph node target should be individualized. If high common iliac lymph nodes are involved and no lymph node dissection has been performed, inclusion of the para-aortic lymph nodes should be considered. The inferior extent of the nodal target is just proximal to the inguinal canal, which represents the lower extent of the external iliac nodes. The presacral lymph nodes are included by contouring a 1–2 cm margin of tissue anterior to the sacrum from the sacral levels of S1–S3 (Figs. 15.4 and 15.5); this volume also includes the insertion of the uterosacral ligaments.

For the *PTV*, an additional margin of 1.5–2 cm is added to the CTV, which varies based on the degree of image guidance and modality (IMRT vs. 3D CRT) used. The distal vaginal margin adds 1 cm to the vaginal PTV, resulting in a total of 3 cm margin from the GTV. The sum of the primary tumor PTV and lymph node PTV results in a confluent final PTV that encompasses the nodal regions, tumor, uterus and parametria, uterosacral ligaments, and presacral lymph nodes (Fig. 15.6).

For the *postoperative target*, which is described in more detail in Sect. 2.4.2, vaginal, paravaginal, and parametrial CTVs are contoured. Delineation of the lymph node CTV follows the same principles as for intact cervical cancer.

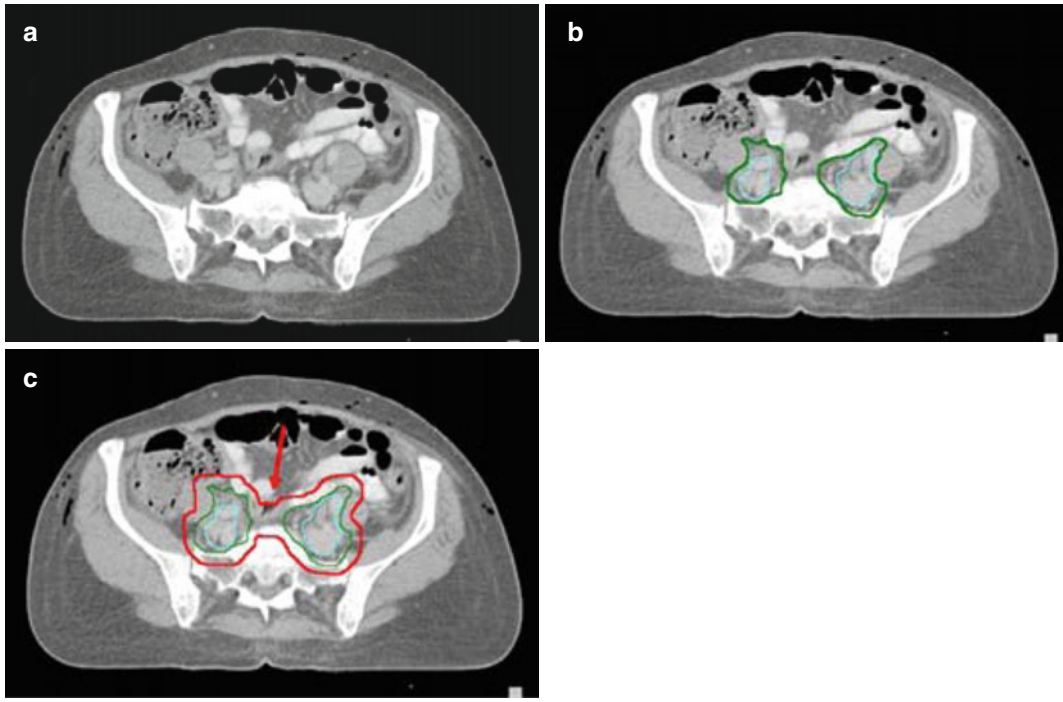

Fig. 15.4 Contouring of the upper external and internal iliac lymph node target. (**a**) At the level just below the bifurcation of the common iliac arteries and veins, the right and left external and internal iliac arteries, veins and lymph nodes are seen medial to the psoas muscles. (**b**) Vessels and lymph nodes are contoured for reference (*aqua*). (**c**) The CTV (*green*) adds a 0.7 cm margin to vessels and adjacent lymphatic tissue, excluding small bowel and psoas. (**d**) For the lymph node PTV (*red*) adds an additional margin of 0.7. In addition a 2 cm strip of tissue anterior to the sacrum (*arrow*) is added to include the presacral lymph nodes

15.1.4.3 Critical Normal Tissue Delineation

Normal structures including the rectum (up to the rectosigmoid junction), bowel including the large bowel above the rectum, and intraperitoneal contents (small bowel and mesentery) within 5 cm above the upper border of the target volume, as well as the bladder and femoral heads, are contoured.

15.2 Endometrial Cancer

15.2.1 Anatomy, Pathology

Pathology

The most common histology is adenocarcinoma; less common histologies include adenosquamous, squamous cell, and mucinous carcinoma. Histologies that infer a worse prognosis and have altered routes of spread include carcinosarcomas, papillary serous carcinomas, and clear cell carcinomas.

The uterus derives its blood supply from several sources that form a rich network of anastomosing vessels. The primary blood supply is from the uterine artery, an anterior branch of the internal iliac artery. The uterine artery enters the uterus after crossing the ureter at the isthmus/level of the internal os. The ovarian artery enters at the level of the fundus through the ovarian ligament. Vaginal arteries anastomose with the uterine vessels inferiorly.

Lymphatic vessels form a rich subserosal plexus that drains from four trunks. The more superior vessels travel through the broad ligament, parallel to the fallopian tube, and drain to the external iliac nodes. More inferiorly, the vessels cross through the broad ligament to the nodes at the bifurcation of the common iliac into the internal and external iliac vessels. At the junction

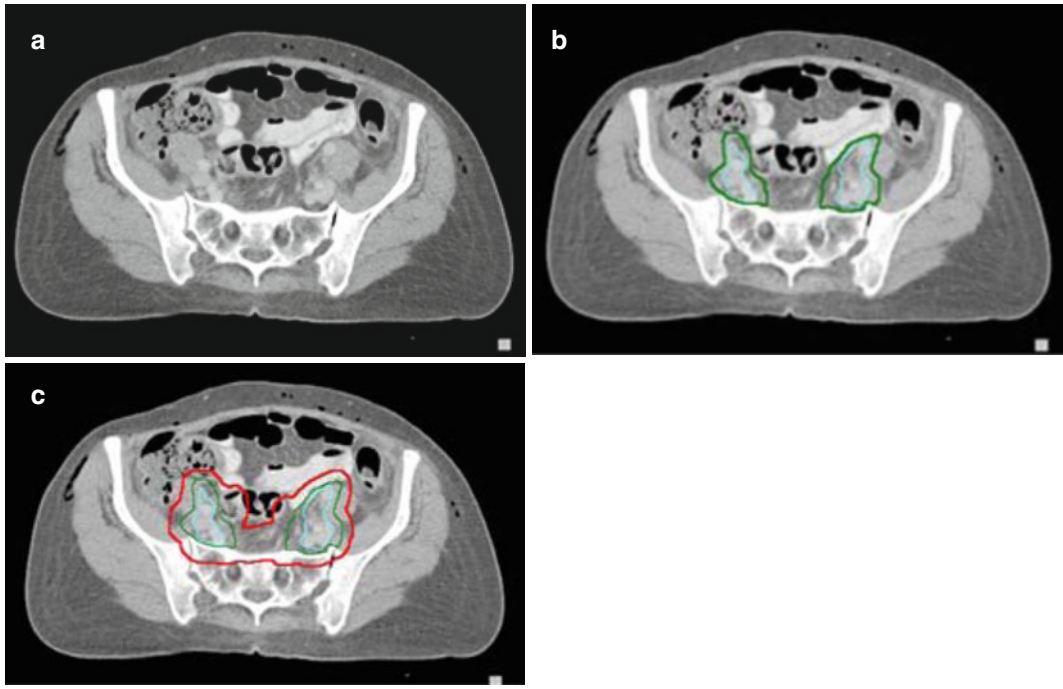

Fig. 15.5 Contouring of the mid external and internal iliac lymph node target. (**a**) Below the level in Fig. 4 external iliac vessles and nodes are seen anteriorly, internal iliac posteriorly and con. (**b**) Vessels and lymph nodes and lymph node CTV (*green*) are contoured as in Figs. 3–4. (**d**) For the lymph node PTV (*red*) adds an additional margin of 0.7. and a 2 cm strip of tissue anterior to the sacrum as in Fig. 4

of the fallopian tube and the uterine body are trunks that may pass directly to the para-aortic lymph nodes through the ovarian pedicle. Lymphatics near the round ligament can pass directly along the ligament to the femoral lymph nodes, although this is rare.

15.2.2 Routes of Spread

Endometrial carcinomas initially spread locally, traveling along the mucosa or invading into the myometrium and at times into the cervix. Direct extension into the parametria, bladder, or rectum can occur as can peritoneal spread via the fallopian tubes or through direct serosal extension. Hematogenous spread occurs primarily to the lung and liver.

A landmark surgicopathologic study was published by the Gynecologic Oncology Group and to this day remains the standard work on spread of stage I and occult stage II endometrial carcinoma (Creasman et al. 1987). It demonstrated that the likelihood of spread outside the uterus depends on a combination of factors including grade and depth of myometrial invasion. Overall, in those patients thought to have disease confined to the uterus, 22 % had extrauterine disease including 11 % with pelvic and/or para-aortic disease, 12 % with positive abdominal cytology, 5 % with adnexal involvement, and 6 % with gross peritoneal disease. It is important to note, however, that the more serious prognosis and different routes of spread seen by papillary serous and clear cell carcinoma were not recognized at the time of this study, and those tumors were not separated and evaluated independently. Unlike cervical cancer, lymphatic spread is not limited to a strictly sequential pattern from pelvic to para-aortic lymph nodes, but can occur directly to the para-aortic nodes through the lymphatics along the ovarian vessels, particularly when extensive tumor is present in the upper corpus or fundus.

Tumors with more aggressive histologies tend to metastasize to the lymph nodes and peritoneum,

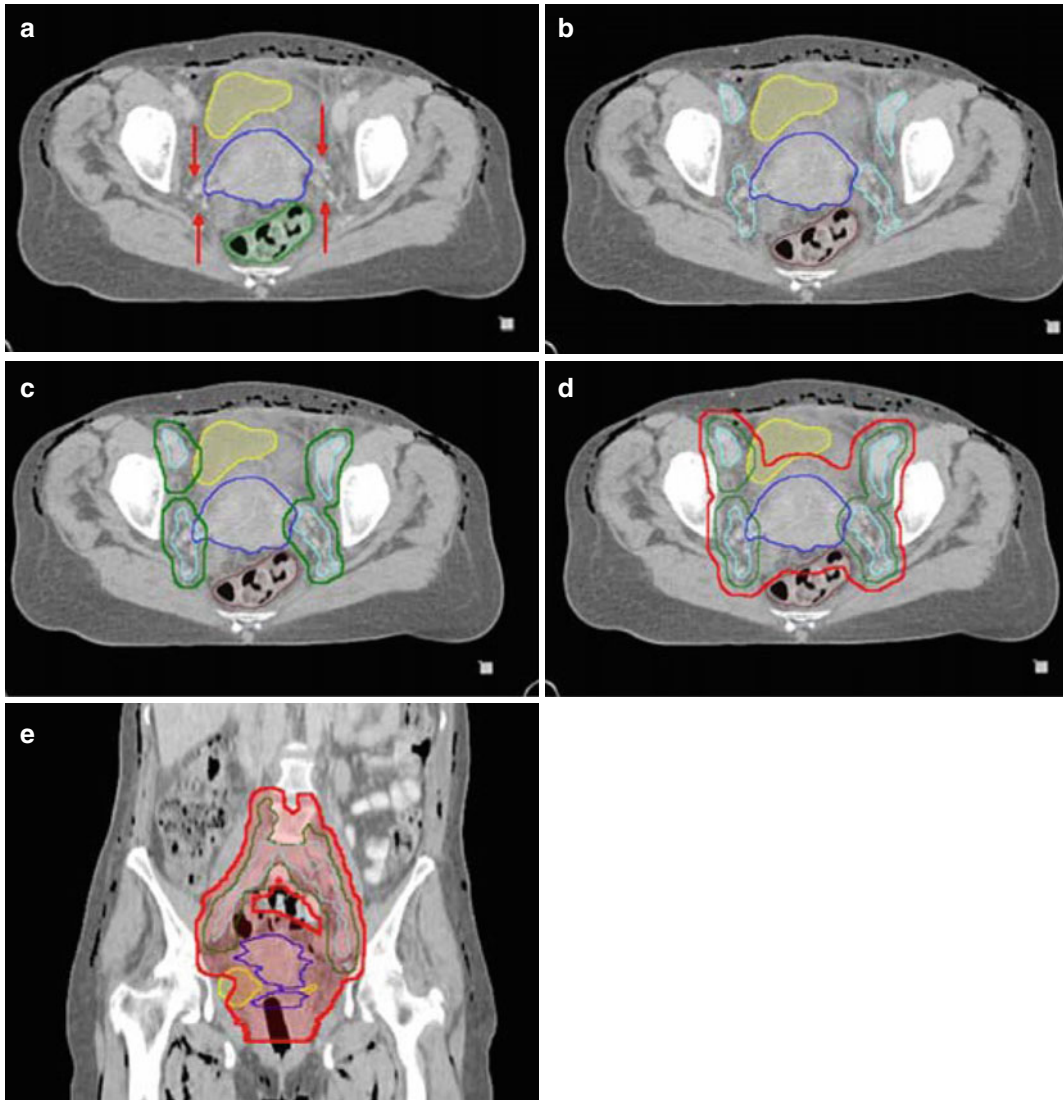

Fig. 15.6 Contouring of the GTV and distal lymph node target. (**a**) The cervical tumor and uterus (*blue*), bladder (*yellow*) and rectum (*light green*) are contoured. Precise delineation of paramtrial extension is challenging with CT and indistinguishable fro parametrial lymph nodes and vessels. (**b**) Delineation of the external and internal iliac lymph nodes (*aqua*) and shows that extension to the paramtetrial nodal regions (*arrows in* (**a**)) can be confluent with obturator and medial internal iliac node lymph node regions. (**c**) The lymph node CTV is countoured (*green*). (**d**) The final PTV (*red*) includes the nodal regions and a 1–1.5 cm margin around the cervical tumor/uterus, allowing partial bladder and rectal sparing. (**e**) A coronal view of the total PTV shows the lymph node CTV, cervical tumor/uterus GTV. The vagina is well delineated using a dry tampon

including the upper abdomen, more commonly, although differentiating the behavior of these tumors from aggressive grade 3 tumors is controversial (Alektiar et al. 2002).

Contemporary surgical management includes evaluation of the abdominopelvic cavity with targeted biopsy, collection of peritoneal fluid for cytology, and extrafascial hysterectomy and bilateral salpingo-oophorectomy.

Lymph node dissection is now predicated on risk of nodal spread. Distally, the dissection extends to the circumflex iliac vein and proximally to the bifurcation of the aorta into the common iliac vessels. Laterally, the dissection

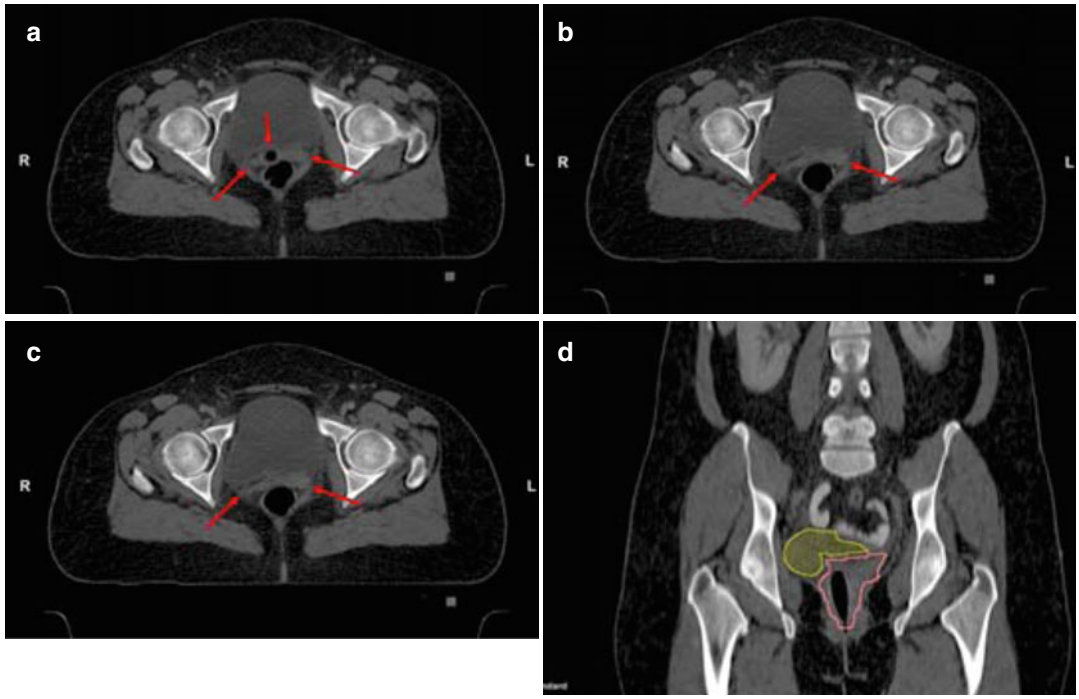

Fig. 15.7 Contouring of the postoperative target: vaginal tissues. (**a**) The vaginal tissues can extend well above the vaginal markers or tampon (*arrows*). The upper extent of the vaginal tampon is visible (*middle arrow* in **a**); (**b**) shows a more superior section. (**c**) The vaginal cuff is contoured (*pink*). (**c**) Coronal view shows the full superior extent of the vaginal tissues; bowel is displaced from the target by bladder (*yellow*) filling on the right, but close to the vagina on the left

extends to the genitofemoral nerve that runs along the pelvic sidewall and medially to the superior vesical artery. The most posterior landmark is the obturator nerve. If the intention is to sample the para-aortic nodes, the dissection extends cephalad either to the inferior mesenteric artery (IMA) or the renal vessels. Two large randomized trials did not demonstrate an improvement in survival with surgical staging (Group 2009; Benedetti Panici et al. 2008), and only 30–40 % of patients have formal dissection in the United States (Sharma et al. 2011). The outlines of the dissection should reflect the target for irradiation if it is to substitute for nodal treatment or if added for potential residual disease postoperatively.

Familiarity of the nodal risk based on uterine risk factors such as depth of invasion, grade, and lymphovascular space invasion is essential to assist in the decision to recommend pelvic irradiation in the absence of nodal dissection. What determines an adequate level of risk is debatable, but generally the chance of serious complications from irradiation such as chronic bowel or bladder complaints or lymphedema is reported in the 2–10 % range (van Creutzberg et al. 2000; Keys et al. 2004).

15.2.3 Imaging Modalities, Surgical–Pathology Correlation

Available imaging modalities have limitations in detecting spread of disease, as spread in most patients is microscopic. Local/regional staging is commonly performed utilizing CT with and without intravenous contrast and with bowel contrast. CT has been reported to have an accuracy of 70–80 % for evaluation of nodal disease based on size. Accuracy improves to 93 % with a cutoff value of 1 cm (Hawnaur 1993; Hardesty et al. 2001; Bellomi et al. 2005), and CT is the main

modality to delineate lymph node regions and normal structures.

In patients treated for intact endometrial cancer, MRI is excellent in assessing the extent of myometrial and cervical invasion and extrauterine extension (Shin et al. 2011; Cade et al. 2011; Whittaker et al. 2009), which may determine treatment regimens and the decision for brachytherapy alone versus combined external plus brachytherapy. In addition, response of the tumor to external radiation can be assessed to individualize brachytherapy planning.

The (^{18}F)PET/CT has demonstrated a 78 % sensitivity and a 93 % negative predictive value. An ongoing GOG study is evaluating the role of PET/CT in cervical and endometrial carcinoma (Signorelli et al. 2009). Magnetic resonance imaging (MRI) has demonstrated a 75–90 % accuracy rate in assessing nodal spread and invasion into the cervix or myometrium (Rockall et al. 2005; Messiou et al. 2006).

15.2.4 Target Delineation

The principles of target delineation for definitive radiation to the intact uterus follow that of cervical cancer. As primary surgical management is far more common than definitive radiation for uterine cancer, this chapter will focus on largely delineation of the postoperative target.

Defining the target for postoperative pelvic radiation has been the subject of investigation and has sparked national trials (RTOG study 0418) and an atlas (http://www.rtog.org/CoreLab/ContouringAtlases/GYN.aspx) for the postoperative treatment of cervical or uterine carcinomas (Small et al. 2008; Jhingran et al. 2012).

15.2.4.1 Simulation Procedure

Computed tomography should be performed, preferably with intravenous contrast. Bowel contrast can be helpful as well, as long as dosimetric adjustments of the high-density contrast in the bowel are made, which can affect dose calculations (Williams et al. 2002). Consideration should be given to a bowel regimen to minimize stool and gas prior to simulation, as excessive distension displaces the vaginal target anteriorly. If the patient subsequently experiences diarrhea, posterior movement of the vagina can lead to exclusion of the target from the PTV (planning target volume). If excessive rectal distention is noted at the time of simulation, repeat scanning after evacuation or bowel prep may increase target reproducibility. Alternatively, including more of the anterior rectal wall in the CTV (clinical target volume) can be considered, but without image-guided radiation therapy, there is the concern that alteration of the rectal filling will lead to excessive variability in vaginal position.

15.2.4.2 Target Volume Delineation for Postoperative Endometrial Cancer

The *postoperative CTV* should include the draining lymph nodes as outlined above including the common, external, and internal iliac vessels with a 0.7 cm margin with the upper border as discussed for cervical cancer (Sect. 1.4.2) typically 0.7 cm below the L4/L5 interspace. Contouring of the presacral region to the bottom of S3 should be included for patients with cervical stromal invasion. Inferiorly, the nodal contours will split into a right and left contour, and when the internal iliac vessels are more difficult to visualize, the contours should extend from the external iliac node region anteriorly to the piriformis muscle posteriorly. The nodal CTV continues until the level of the femoral heads, just before the external iliacs exit the pelvis. For postoperative radiation, there is no GTV.

An *internal target volume* (*ITV*) is recommended by RTOG 0418 to account for motion of the vaginal structures with variable bladder filling. This is accomplished by performing the simulation CT with both a full and an empty bladder, contouring the CTV and merging the vaginal CTVs, thereby including the vagina and vaginal cuff with both scenarios. Care should be taken to include all vaginal tissue which at times can extend superiorly to the vaginal marker. The lateral extent of the vaginal CTV should extend to the pelvic musculature, and the upper 3 cm of the vagina should be contoured, or alternatively the CTV

should be extended to 1 cm above the bottom of the obturator foramen, whichever is lower.

For the *lymph node CTV*, as for cervical cancer, the typical volume expansion from the vessels and lymph nodes is 0.7 cm and excludes the bone and the psoas and piriformis muscles but should include any visible lymph nodes or pertinent clips from surgical dissection (Messiou et al. 2006). At times, large lymphoceles are noted on the postoperative CT, and these should be included in the CTV. However, with a negative dissection, the risk of tumor contamination is low, and it should be noted that inclusion of the lymphoceles into the CTV will decrease normal tissue sparing. Anterior to the vertebral bodies and the sacrum, the CTV should include 1.5 cm of tissue while excluding the bone. It is not necessary to extend the CTV into the sacral foramina, but caution should be used to include the potential space medial to the psoas muscle and lateral to the vertebral body (Fontanilla et al. 2013).

The *para-aortic CTV* is contoured if the para-aortic nodes have not been sampled or if involved nodes are found. The vertebral interspace of the level T11/T12 vertebra has been historically the upper extent of the treatment volume, for surgical dissection extends to the inferior mesenteric artery or renal vessels. If concurrent chemotherapy is given, consideration should be given to lowering the fields below the T11/T12 level. The cisterna chyli lies posterior to the aorta just superior to the renal vessels, anterior to the first or second lumbar vertebra.

For the *PTV*, variability exists in recommendations for the PTV margin. RTOG 0418 recommended a 0.7 cm margin on the nodal and vaginal CTV/ITV, but earlier studies, especially those without an ITV, used margins of 1 cm (Lujan et al. 2003; Georg et al. 2006). Without an ITV, consideration should be given to daily image guidance or larger PTV margins. Motion studies have demonstrated differential movement laterally and anteriorly/posteriorly, and target motion has ranged from 1.5 to 2.3 cm, primarily due to bladder filling and emptying (Jürgenliemk-Schulz et al. 2011; Harris et al. 2011). Positional change with rectal filling/emptying has been variably reported.

15.2.4.3 Target Volume Delineation for Intact Endometrial Cancer

Treatment with external beam and/or brachytherapy for medically inoperable uterine carcinoma has not received the same scrutiny as medically inoperable uterine cancer is uncommon. However, guidelines for external beam irradiation generally mimic those recommended for intact cervical carcinoma.

For *brachytherapy in intact uterine cancer*, several different brachytherapy systems are available for intact uterine cancer, including single tandem, dual tandem (Y-tandem), triple tandem, and Heyman packing (Nag et al. 2000a; Coon et al. 2008; Bauer et al. 1991; Weitmann et al. 2005). In addition, both low-dose-rate and high-dose-rate deliveries are acceptable.

The system used should be chosen based on the ability to cover the tumor and full uterine wall and vaginal thickness (Mock et al. 1998). With new MRI imaging, the ability to discern the location and depth of tumor invasion is far more sophisticated (Shin et al. 2011; Cade et al. 2011; Whittaker et al. 2009). The choice between ovoids and cylinder for coverage of the vagina depends on preference, unless there is vaginal extension below the dosimetric coverage of the ovoids. In that instance, a vaginal cylinder should be used for full coverage. If gross disease is present, it is prudent to mark the inferior extent of disease with a radiopaque gold marker to assure full coverage, especially if external beam irradiation is given initially as the tumor may regress prior to the brachytherapy boost. Historically, with 2D dosimetry, the dose was prescribed 2 cm from the uterine tandem. Ideally, 3D imaging should be used, and assurance of coverage of the entire uterine serosa and targeted vagina should be covered by the prescription isodose line. Detailed suggestions on treatment, coverage, dose specification, and optimization have been published by the American Brachytherapy Society (Nag et al. 2000b).

Vaginal cuff brachytherapy alone has become increasingly more common for postoperative endometrial carcinoma. Cylinders and ovoids have been used with advantages and disadvantages to both (Kim et al. 2002). In addition, there

are molds, shielded cylinders, and multichannel applicators available for customization of dosimetry. Most importantly, the largest vaginal cylinder should be used to maximize dosimetry and avoid air gaps between the cylinder and the mucosa and to avoid underdosing the target (Richardson et al. 2010). Different fractionation schemes and lengths of the vagina treated are used, and a summary of choices with detailed recommendations for postoperative cuff treatment and treatment of cuff recurrences has been published by the American Brachytherapy Society and recently updated (Small et al. 2012, 2005). Most physicians choose to treat only the upper portion of the vagina adjuvantly and treat the entire length of the vagina only in cases of positive margins, recurrent disease, or with other high-risk pathological findings. For gross disease, the thickness of tumor should not exceed 5 mm if intracavitary brachytherapy is planned. If this thickness is exceeded, it is best to treat with interstitial therapy according to established guidelines (Beriwal et al. 2012).

15.3 Vulvar Cancer

15.3.1 Anatomy, Pathology

As the vulva is covered by a keratinized squamous epithelium, the most common histology for vulvar cancer is squamous cell carcinoma. Adenocarcinoma of the vulva may arise from Bartholin's glands, eccrine sweat glands, Paget's disease, or ectopic breast tissue. Other less common histologies include melanoma and basal cell carcinoma. Soft tissue sarcomas are rare in the vulva, although leiomyosarcoma, malignant fibrous histiocytoma, liposarcoma, angiosarcoma, rhabdomyosarcoma, epithelioid sarcoma, and Kaposi's sarcoma have all been described. Metastatic involvement of the vulva may also occur, most commonly from primary genitourinary or gastrointestinal cancers.

The vulva encompasses the mons pubis, labia majora, labia minora, clitoris, vaginal vestibule, perineal body, and the supporting subcutaneous tissues. The vulva is bordered superiorly by the anterior abdominal wall and inferiorly by the anus. The lateral extent of the vulva is the labiocrural fold at the medial thigh. The distal vagina and the urethra open onto the vestibule of the vulva.

The course of the vulvar lymphatic channels has been well described by extensive surgical mapping studies (Parry-Jones 1963). The vulvar lymphatics travel anteriorly through the labia majora, then laterally at the mons pubis to drain into the superficial inguinal lymph nodes. In general, the lymphatics do not extend laterally beyond the labiocrural folds or cross midline for well-lateralized structures. Lymphatic drainage of midline structures, such as the clitoris or perineal body, is more commonly bilateral to the inguinal lymph nodes. A small proportion of lymphatic drainage from the clitoris travels under the pubic symphysis directly to the pelvic lymph nodes.

15.3.2 Routes of Spread

The most common site of primary vulvar cancer is the labia majora, although invasive disease may arise from any of the vulvar structures, including the Bartholin's glands. Local growth at the primary site may lead to extension into the adjacent organs, including the urethra, clitoris, vagina, and anus. The risk of lymph node involvement is related to tumor size, poor differentiation, depth of stromal invasion, and lymphovascular invasion (Homesley et al. 1993). The primary echelon nodes for vulvar cancer, the superficial inguinal lymph nodes, are located within the femoral triangle formed by inguinal ligament superiorly, sartorius muscle laterally, and adductor longus muscle medially. Lymphatic drainage from superficial to deep inguinal nodes penetrates the cribriform fascia medial to the femoral vein. The most superior of the deep nodes, Cloquet's node, is located under the inguinal ligament and directly drains to the external iliac nodal chain. Although tumor emboli from the primary site travel to the inguinal lymph nodes, in-transit skin metastases are rare in the absence of bulky groin involvement. Metastases to the contralateral groin or pelvis are uncommon in the absence of ipsilateral nodal involvement.

15.3.3 Imaging Modalities

15.3.3.1 Magnetic Resonance Imaging

The local extent of a primary vulvar cancer is assessed clinically to determine resectability, although MRI may provide additional information pertinent for surgical and radiation therapy planning. Similar to cervical cancer, vulvar cancers are isointense to the muscle on T1-weighted images and intermediate to high signal intensity on T2-weighted scans (Sohaib et al. 2002). In locally advanced cases, invasion into adjacent pelvic structures such as the urethra, bladder, or rectum may be visualized by MRI. For lesions smaller than 2 cm in diameter, MRI does not provide reliable evaluation, particularly for plaque-like lesions as the primary site may not be visualized.

15.3.3.2 CT, PET/CT, Ultrasound

CT is the most commonly employed modality to delineate pelvic anatomy for treatment planning and particularly depth of inguinal lymph nodes. Assessment of regional nodal involvement in vulvar cancer may be performed by CT, PET, or ultrasound. CT has a relatively low sensitivity and specificity for the detection of nodal involvement and is primarily used for radiation treatment planning. The sensitivity of PET for the detection of nodal involvement and distant metastatic spread is higher than CT (Lamoreaux et al. 2005) and is often incorporated in the initial staging evaluation for women with locally advanced disease. In the setting of unresectable nodal spread, PET may be used to identify involved nodes for dose escalation. CT and ultrasound have been used in conjunction with fine-needle aspiration to confirm inguinal nodal involvement in preoperative or definitive cases. As discussed below, none of the available imaging modalities are able to replace surgical staging and pathologic assessment of the inguinal lymph nodes.

15.3.3.3 Imaging–Surgical–Pathology Correlations

Preoperative MRI has been shown to have moderate correlation with clinicopathologic findings for staging of the primary site in vulvar cancer. In a prospective study of 22 women, MRI accurately predicted tumor stage in 70 % of cases (Sohaib et al. 2002). However, the primary tumor was not visualized in 50 % of the patients although the imaging parameters may not have been optimal, and tumor delineation improved with higher resolution and thinner sectioning.

As clinical exam is largely inaccurate in assessing groin node involvement, prospective imaging studies to evaluate the inguinal nodes have been performed with pathologic correlation by surgical staging. In a study of preoperative MRI in 60 patients with vulvar cancer, 2 radiologists evaluated nodal size and characteristics, including the presence of a fatty hilum, margin, and shape, prior to lymph node dissection or sentinel node biopsy. The operating characteristics for MRI showed a sensitivity, specificity, positive predictive value, and negative predictive value of 52 %, 85–89 %, 46–52 %, and 87–89 %, respectively (Bipat et al. 2006). A second study of MRI for nodal staging found a sensitivity, specificity, PPV, and NPV of 86, 82, 64, and 94 %, respectively, when size, shape, and STIR/T2 signal abnormality were considered on radiologic review (Singh et al. 2006). The variability in the operating characteristics between studies may be explained by the differences in imaging technique as well as the study population, as the second study included a significant proportion of patients with advanced disease. PET has also been shown to have relatively low sensitivity but high specificity for inguinal nodal involvement. In a surgical correlation study of 15 patients with 29 analyzed groins, the sensitivity, specificity, PPV, and NPV for PET for the detection of lymph node involvement were 67, 95, 86, and 86 %, respectively (Cohn et al. 2002). Imaging assessment by CT or ultrasound with pathologic assessment by fine-needle aspirate has also been explored, although its use has again been limited by relatively low sensitivity for the detection of metastatic involvement, ranging from 58 % for CT (Land et al. 2006) and 80–83 % for ultrasound (Moskovic et al. 1999). Given the morbidity and mortality of groin recurrence, the false-negative rates with preoperative

imaging remain unacceptably high and should not be considered a replacement for nodal dissection or sentinel node biopsy. In appropriately selected patients, sentinel lymph node biopsy has shown considerable promise in prospective, multi-institutional trials of clinically node-negative vulvar cancer patients, with a sensitivity of 91 % and false-negative predictive value of 3.7 % (Levenback et al. 2012). Sentinel lymph node biopsy also reduces the rates of acute and long-term groin complication compared to inguinal nodal dissection (Van der Zee et al. 2008).

15.3.4 Target Delineation

15.3.4.1 Simulation Procedure

For the CT simulation, patients are placed in an immobilization device (e.g., VacLoc) in "frog-legged" position to expose the groins and prevent skin blousing. Visible and/or palpable and mucosal involvement of the vagina should be localized with implanted radiopaque markers. The patient should be instructed for bladder filling. IV and bowel contrast should be considered.

15.3.4.2 Target Volume Delineation for the Postoperative Vulvar Cancer

Target delineation for vulvar cancer requires a thorough understanding of the primary and nodal patterns of spread, the extent of surgical staging, and the radiation intent. In patients with operable disease, postoperative radiotherapy may be delivered to the primary site, inguinal nodal region, and/or pelvis based on surgical–pathologic factors. Indications for vulvar radiation include close surgical margins or other risk factors for local relapse defined by the Heaps criteria (Heaps et al. 1990). The clinical target volume should include the entire vulva with the anatomic boundaries described above. Vulvar radiation should also be delivered in all patients with nodal involvement as use of a midline block is associated with increased rates of local recurrence (Dusenbery et al. 1994). In patients with inguinal nodal involvement, the nodal CTV should include the ipsilateral and contralateral inguinal nodes, as well as the pelvic lymph nodes. Most commonly, the superior border of the radiation field is set at the L5/S1 vertebral interspace to cover the bifurcation of the common iliac nodes. The nodal basins at risk in the pelvis are the bilateral external iliac, internal iliac, obturator, and presacral nodes.

Of note, contouring guidelines for IMRT in vulvar cancer have not yet been established, although clinical experience from single institutional series has been reported (Beriwal et al. 2006, 2008). Some of the principles for the delineation of inguinal region are gleaned from RTOG contouring guidelines for anorectal cancer.

The *inguinofemoral lymph node CTV* should be contoured inferiorly to the level of the ischial tuberosity or lesser trochanter or alternatively 2 cm inferior to the saphenous–femoral junction as recommended by the RTOG contouring guidelines for anorectal cancer (Myerson et al. 2009). For the inguinal lymph nodes, a larger contouring margin is recommended around the femoral vessels than commonly applied in pelvic nodes. In a study of 22 women with gynecologic cancer and clinical or pathologic inguinal nodal involvement, the margins around the femoral vessels required to cover at least 90 % of the disease were 35 mm in the anteromedial direction, 23 mm anterior, 25 mm anterolateral, 22 mm medial, 9 mm posterior, and 32 mm lateral (Kim et al. 2012). The corresponding anatomic boundaries were laterally, the medial border of the iliopsoas; medially, the lateral border of the adductor longus or medial end of the pectineus; posteriorly, the iliopsoas muscle laterally and anterior aspect of the pectineus muscle; and medially and anteriorly, the anterior edge of the sartorius muscle. None of the patients had involved posterior or lateral nodes alone without involvement of the anterior or anteromedial positions. The authors suggest that the inguinal lymph nodes are contoured as a compartment defined by anatomic landmarks rather than a uniform expansion around the vessels.

The *pelvic lymph node CTV* should encompass the external and internal iliac vessels and

adjacent suspicious nodes with a 0.7–1 cm margin while excluding the bone, muscle, and bowel.

The presacral nodal region should connect the bilateral iliac nodal volume to approximately the level of S2 when the piriformis muscle is visualized.

15.3.4.3 Target Volume Delineation for Intact Vulvar Cancer

The *primary tumor GTV* for preoperative or definitive radiotherapy in locally advanced cases should encompass the gross primary tumor and its extensions based on clinical examination findings, MRI, CT, or PET-CT. This may include vaginal extension as delineated by imaging or radiopaque implanted markers based on physical examination. The GTV further includes tumor involvement of lymph nodes based on examination findings, MRI, CT, or PET-CT.

For the *primary tumor CTV*, a 1–2 cm expansion is added to the GTV. In addition, regional lymphatics in the pelvis are contoured as described for cervical cancer (Sect. 1.4.2), and inguinal lymphatics (which have not already been included in the GTV) are delineated as described for vulvar cancer (Sects. 3.4.2 and 3.4.3).

The PTV adds a 0.7 cm margin to the CTV. Bolus of the skin bridge is not required in the absence of dermal spread, although bolus over the vulva should be considered to adequately dose the skin in this area.

15.3.4.4 Target Delineation for Brachytherapy

Select patients with unresectable disease involving the vulva are candidates for interstitial brachytherapy to deliver additional dose escalation. Extrapolating from current guidelines for cervical cancer, the GTV should include residual disease at the time of brachytherapy, supplemented by imaging findings on MRI, CT, or PET. The HR-CTV should include a margin of 1–2 cm around the GTV. Particular caution is advised with the use of interstitial brachytherapy for vulvar cancer, as high rates of necrosis and nonhealing ulcer have been reported (Thibault et al. 2012; De Ieso et al. 2012).

15.4 Vaginal Cancer

15.4.1 Anatomy, Pathology

The vagina is a long muscular organ that extends from the cervix to vulva with an average length of 8 cm. The normal tissue structures that are closely opposed to the vagina are the bladder and urethra anteriorly and the rectum posteriorly.

The mucosa of the vagina is composed of a nonkeratinizing stratified squamous epithelium, which overlies a highly vascular stroma with a rich lymphatic network. The lymphatics of the upper vagina follow the path of the cervical lymphatics to the paracervical, parametrial, obturator, hypogastric, external iliac, and common iliac lymph nodes. The lymphatic drainage of the posterior vagina empties to the inferior gluteal, anorectal, and presacral nodes. From the distal vagina, the lymphatic channels course to the inguinal and femoral nodes, similar to the primary drainage of the vulva. Due to the complex lymphatic network, lymph node drainage from the vagina is not well lateralized.

Primary vaginal cancer is a rare malignancy and represents 3 % of gynecologic cancers (Siegel et al. 2011). Approximately 2,600 women are diagnosed with vaginal cancer in the United States annually (Cancer facts and figures 2012), although metastatic involvement of the vagina is not uncommon. By the FIGO definition, tumors that involve the cervix or vulva are not considered vaginal cancers and are classified as cervical or vulvar cancers, even if the disease bulk is centered in the vagina (Aerts et al. 2009). The most common histology for primary vaginal cancer is squamous cell carcinoma, accounting for 85 % of cases and frequently associated with HPV infection (Daling et al. 2002). As the vaginal epithelium does not contain glandular elements, primary adenocarcinoma of the vagina is rare, although adenocarcinoma may arise in areas of vaginal adenosis, foci of endometriosis, or Wolffian rests. The clear cell variant of vaginal adenocarcinoma is associated with in utero exposure to the synthetic estrogen diethylstilbestrol (DES) (Herbst et al. 1971), although the peak incidence is well passed. Other less frequent his-

tologic subtypes include melanoma, lymphoma, and sarcoma, specifically rhabdomyosarcoma, leiomyosarcoma, endometrial stromal sarcoma, and malignant mixed Müllerian tumor.

15.4.2 Routes of Spread

Vaginal cancers most commonly arise in the upper vagina and may extend directly into the adjacent paravaginal tissues, parametrium, or pelvic sidewall. Anterior or posterior extension may result in bladder or rectal invasion. Tumors arising in the mid to lower vagina can penetrate the vaginal wall and involve the urogenital diaphragm, levator ani muscles, or pelvic fascia.

Pathologic examination from full-thickness biopsy or partial vaginectomy specimens has shown that 95 % of the lymphatic channels are located within 3 mm depth from the vaginal surface (Choo et al. 2005). Due to the complex lymphatic network, lymph node drainage from the vagina is not well lateralized. Tumors with access to the lymphatic channels of the upper third of the vagina drain to the pelvic nodal groups, while lymphatics of the lower one-third of the vagina spread to the inguinal–femoral nodes as described above. Tumors with involvement of the rectovaginal septum have an increased risk of perirectal and presacral nodal spread.

15.4.3 Imaging Modalities

15.4.3.1 Magnetic Resonance Imaging

Given the rarity of vaginal cancer, prospective imaging studies have not been performed, although the utility of advanced imaging modalities may be extrapolated from other disease sites. Given its superior soft tissue resolution, MRI may supplement physical exam in assessing tumor volume and extent of tumor in paravaginal tissues. Similar to cervical cancer, primary vaginal tumors are best visualized on T2-weighted imaging and appear hyperintense (Taylor et al. 2007). Visualization of the vaginal tumor may be improved with the instillation of vaginal gel, which distends the vaginal walls and allows for assessment of tumor thickness. This imaging-based thickness assessment is valuable for decisions regarding the type of brachytherapy and to individualize brachytherapy dose prescription.

15.4.3.2 PET

PET/CT, which has become a standard diagnostic tool for cervical cancer (Schwarz et al. 2007; Selman et al. 2008), has similar applicability for vaginal cancer, as the sensitivity for the detection of the primary vaginal tumor and involved pelvic lymph nodes is greater than CT alone (Lamoreaux et al. 2005). The detection of nodal involvement may also influence the extent of the radiation fields and delivered dose.

15.4.3.3 Imaging–Surgical–Pathology Correlations

Correlative studies of imaging and pathologic findings have not been well described for vaginal cancer, as the majority of patients are treated with definitive radiation therapy. However, several surgical series have demonstrated the association between tumor stage and the risk of lymph node involvement, which ranges from 0 to 6 % for stage I, 21–26 % for stage II, and 78–83 % for stages III and IV, respectively (Rubin et al. 1985; Senekjian et al. 1988). For patients with early stage disease that are candidates for vaginal brachytherapy, dose is prescribed to cover the tumor thickness and vaginal lymphatics.

15.4.4 Target Delineation

15.4.4.1 Simulation Procedure

For lower vaginal tumors, where inguinal nodes are included into the treatment volume, the patient positioning a preparation resembles that for vulvar cancer (Sect. 3.4.1) and for upper vaginal tumors that for cervical cancer (Sect. 1.4.1).

15.4.4.2 Target Volume Delineation for External Beam Radiation

The gross *GTV* for vaginal cancer is defined as the clinically apparent visible/palpable tumor involvement based on examination findings, CT, MRI, and/or PET. Delineation of the GTV at

diagnosis should encompass visible and palpable and imaging evidence of gross tumor at the primary site, as well as any involved lymph nodes in the pelvis, inguinal, and/or para-aortic regions.

The *CTV* represents the regions at risk for microscopic spread, including the GTV with a 1–2 cm margin, full vaginal length, paravaginal tissues, and bilateral pelvic lymph nodes, specifically the external iliac, internal iliac, obturator, presacral, and perirectal nodes. If the distal one-third of the vagina is involved, the inguinal lymph node regions should also be contoured in the nodal CTV.

The superior border of the *PTV* generally extends to L5/S1 (to include the common iliac lymph nodes), and the inferior field border should cover the full vaginal length. If IMRT is planned, the PTV margins should take into account the movement of the vagina with organ filling, which may be displaced by 1.5–2 cm on average in the anterior–posterior direction (Jhingran et al. 2012; Harris et al. 2011). In patients with lymph node involvement, the next echelon nodes should be included in the treatment field. A 3D conformal or IMRT boost may be used to deliver a cumulative dose of 60–64 Gy to gross nodal disease accounting for the brachytherapy contribution.

15.4.4.3 Target Volume Delineation for Brachytherapy

In the definitive treatment of vaginal cancer, intracavitary or interstitial brachytherapy is used for dose escalation to areas of gross disease to deliver a cumulative dose of 70–85 Gy. The choice of brachytherapy modality depends on the residual tumor thickness following external beam radiotherapy. In tumors with a thickness of less than 5 mm, vaginal cylinder brachytherapy may be used to deliver the additional boost, while interstitial implants are appropriate for patients where larger residual tumors and/or tumor thickness is more than 1 cm. Target contouring may be adopted from the GEC-ESTRO guidelines for image-guided cervical cancer brachytherapy (Haie-Meder et al. 2005). At the time of brachytherapy, the GTV is defined as the gross residual disease based on examination and MRI findings, and the HR-CTV represents the adjacent regions with a high risk of local recurrence. At the University of Vienna, the HR-CTV for vaginal cancer encompasses the GTV, as well as the gray zones on MRI and the adjacent vaginal circumference at the level of the residual tumor (Dimopoulos et al. 2012). For CT-based planning, placement of fiducial markers may be used to demarcate the superior, inferior, and lateral extent of the tumor for contouring purposes. The IR-CTV includes the initial extent of tumor as well as the full vaginal length given the risk of submucosal spread through the vaginal lymphatics. The IR-CTV should receive a minimum of 60 Gy including the external beam and brachytherapy contribution. Although the tolerance of the vagina is ill defined, dose limits of 120–150 Gy for the upper vagina and 80–100 Gy for the lower vagina have been adopted based on retrospective data (Hintz et al. 1980).

References

Aerts HJ, van Baardwijk A, Petit SF, Offermann C, Loon JV, Houben R, Dingemans AM, Wanders R, Boersma L, Borger J, Bootsma G, Geraedts W, Pitz C, Simons J, Wouters BG, Oellers M, Lambin P, Bosmans G, Dekker AL, Ruysscher DD (2009) Identification of residual metabolic-active areas within individual NSCLC tumours using a pre-radiotherapy (18) Fluorodeoxyglucose-PET-CT scan. Radiother Oncol 91(3):386–392

Alektiar KM, McKee A, Lin O, Venkatraman E, Zelefsky MJ, McKee B, Hoskins WJ, Barakat RR (2002) Is there a difference in outcome between stage I-II endometrial cancer of papillary serous/clear cell and endometrioid FIGO Grade 3 cancer? Int J Radiat Oncol Biol Phys 54(1):79–85

American Cancer Society (2012) Cancer facts and figures 2012. Atlanta. http://www.cancer.org/research/cancerfactsstatistics/cancerfactsfigures2012/

Balleyguier C, Sala E, Da Cunha T et al (2011) Staging of uterine cervical cancer with MRI: guidelines of the European Society of Urogenital Radiology. Eur Radiol 21(5):1102–1110

Bauer M, Schulz-Wendtland WR, van t' Hooft E, Richard F (1991) The new development of an afterloading applicator for the primary treatment of endometrial carcinoma. The first clinical empirical report. Strahlenther Onkol 167:545–548

Bellomi M, Bonomo G, Landoni F, Villa G, Leon ME, Bocciolone L, Maggioni A, Viale G (2005) Accuracy of computed tomography and magnetic resonance imaging in the detection of lymph node involvement in cervix carcinoma. Eur Radiol 15:2469–2474

Benedetti Panici P, Basile S, Maneschi F et al (2008) Systematic pelvic lymphadenectomy versus no lymphadenectomy in early-stage endometrial carcinoma: randomized clinical trial. J Natl Cancer Inst 100:1707–1716

Beriwal S, Heron DE, Kim H et al (2006) Intensity-modulated radiotherapy for the treatment of vulvar carcinoma: a comparative dosimetric study with early clinical outcome. Int J Radiat Oncol Biol Phys 64(5): 1395–1400

Beriwal S, Coon D, Heron DE et al (2008) Preoperative intensity-modulated radiotherapy and chemotherapy for locally advanced vulvar carcinoma. Gynecol Oncol 109(2):291–295

Beriwal S, Demanes DJ, Erickson B et al (2012) American Brachytherapy Society consensus guidelines for interstitial brachytherapy for vaginal cancer. Brachytherapy 11(1):68–75

Bhosale P, Peungjesada S, Devine C et al (2010) Role of magnetic resonance imaging as an adjunct to clinical staging in cervical carcinoma. J Comput Assist Tomogr 34(6):855–864

Bipat S, Fransen GA, Spijkerboer AM et al (2006) Is there a role for magnetic resonance imaging in the evaluation of inguinal lymph node metastases in patients with vulva carcinoma? Gynecol Oncol 103(3): 1001–1006

Brown G, Richards C, Bourne MW, Newcombe RG, Radcliffe AG, Dallimore NS, Williams GT (2003) Morphologic predictors of lymph node status in rectal cancer with use of high-spatial-resolution MR imaging with histopathologic comparison. Radiology 227(2):371–377

Burghardt E, Hofmann H, Ebner F et al (1989) Magnetic resonance imaging in cervical cancer: a basis for objective classification. Gynecol Oncol 33:61–67

Cade TJ, Quinn MA, McNally OM et al (2011) Predictive value of magnetic resonance imaging in assessing myometrial invasion in endometrial cancer: is radiological staging sufficient for planning conservative treatment? Int J Gynecol Cancer 20(7):1166–1169

Chan P, Dinniwell R, Haider MA et al (2008) Inter- and intrafractional tumor and organ movement in patients with cervical cancer undergoing radiotherapy: a cinematic-MRI point-of-interest study. Int J Radiat Oncol Biol Phys 70:1507–1515

Charles-Edwards EM, Messiou C, Morgan VA, De Silva SS, McWhinney NA, Katesmark M, Attygalle AD, DeSouza NM (2008) Diffusion-weighted imaging in cervical cancer with an endovaginal technique: potential value for improving tumor detection in stage Ia and Ib1 disease. Radiology 249(2):541–550

Choi HJ, Roh J, Seo SS, Lee S, Kim JY, Kim SK, Kang KW, Lee JS, Jeong JY, Park SY (2006) Comparison of the accuracy of magnetic resonance imaging and positron emission tomography/computed tomography in the presurgical detection of lymph node metastases in patients with uterine cervical carcinoma: a prospective study. Cancer 106(4):914–922

Choo JJ, Scudiere J, Bitterman P et al (2005) Vaginal lymphatic channel location and its implication for intracavitary brachytherapy radiation treatment. Brachytherapy 4(3):236–240

Cohn DE, Dehdashti F, Gibb RK et al (2002) Prospective evaluation of positron emission tomography for the detection of groin node metastases from vulvar cancer. Gynecol Oncol 85(1):179–184

Coon D, Beriwal S, Heron DE, Kelley JL, Edwards RP, Sukumvanich P, Zorn KK, Krivak TC (2008) High-dose-rate Rotte "Y" applicator brachytherapy for definitive treatment of medically inoperable endometrial cancer: 10-year results. Int J Radiat Oncol Biol Phys 71:779–783

Creasman WT, Morrow C, Bundy BN et al (1987) Surgical pathologic spread patterns of endometrial cancer: a Gynecologic Oncology Group study. Cancer 60: 2035–2041

Daling JR, Madeleine MM, Schwartz SM et al (2002) A population-based study of squamous cell vaginal cancer: HPV and cofactors. Gynecol Oncol 84(2):263–270

De Ieso PB, Mullassery V, Shrimali R et al (2012) Image-guided vulvovaginal interstitial brachytherapy in the treatment of primary and recurrent gynecological malignancies. Brachytherapy 11(4):306–310

Dimopoulos JC, Schmid MP, Fidarova E et al (2012) Treatment of locally advanced vaginal cancer with radiochemotherapy and magnetic resonance image-guided adaptive brachytherapy: dose-volume parameters and first clinical results. Int J Radiat Oncol Biol Phys 82(5):1880–1888

Dusenbery KE, Carlson JW, LaPorte RM et al (1994) Radical vulvectomy with postoperative irradiation for vulvar cancer: therapeutic implications of a central block. Int J Radiat Oncol Biol Phys 29(5): 989–998

Fontanilla HP, Klopp A, Lindberg ME, Jhingran A, Kelly P, Takiar V, Iyer RB, Levenback CF, Zhang Y, Done L, Eifel PJ (2013) Anatomic distribution of [18F] fluorodeoxyglucose-avid lymph nodes in patients with cervical cancer. Pract Radiat Oncol 3(1):45–53

Georg P, Georg D, Hillbrand M, Kirisits C, Pötter R (2006) Factors influencing bowel sparing in intensity modulated whole pelvic radiotherapy for gynaecological malignancies. Radiother Oncol 80:19–26

Greco A, Mason P, Leung AWL et al (1989) Staging of carcinoma of the uterine cervix: MRI-surgical correlation. Clin Radiol 40(4):401–405

Group AS (2009) Efficacy of systematic pelvic lymphadenectomy in endometrial cancer (MRC ASTEC trial): a randomized study. Lancet 373:125–136

Haie-Meder C, Potter R, Van Limbergen E et al (2005) Recommendations from Gynaecological (GYN) GEC-ESTRO Working Group (I): concepts and terms in 3D image based 3D treatment planning in cervix cancer brachytherapy with emphasis on MRI assessment of GTV and CTV. Radiother Oncol 74(3):235–245

Hardesty SJ, Sumkin J, Hakim C et al (2001) The ability of helical CT to preoperatively stage endometrial carcinoma. Am J Roentgenol 176:603–606

Harris EE, Latifi K, Rusthoven C, Javedan K, Forster K (2011) Assessment of organ motion in postoperative

endometrial and cervical cancer patients treated with intensity-modulated radiation therapy. Int J Radiat Oncol Biol Phys 15:e645–e650

Hawnaur JM (1993) Staging of cervical and endometrial carcinoma. Clin Radiol 47:7–13

Heaps JM, Fu YS, Montz FJ et al (1990) Surgical-pathologic variables predictive of local recurrence in squamous cell carcinoma of the vulva. Gynecol Oncol 38(3):309–314

Herbst AL, Ulfelder H, Poskanzer DC (1971) Adenocarcinoma of the vagina. Association of maternal stilbestrol therapy with tumor appearance in young women. N Engl J Med 284(15):878–881

Hintz BL, Kagan AR, Chan P et al (1980) Radiation tolerance of the vaginal mucosa. Int J Radiat Oncol Biol Phys 6(6):711–716

Homesley HD, Bundy BN, Sedlis A et al (1993) Prognostic factors for groin node metastasis in squamous cell carcinoma of the vulva (a Gynecologic Oncology Group study). Gynecol Oncol 49(3): 279–283

Hori M, Kim T, Murakami T, Imaoka I, Onishi H, Tomoda K, Tsutsui T, Enomoto T, Kimura T, Nakamura H (2009) Uterine cervical carcinoma: preoperative staging with 3.0-T MR imaging–comparison with 1.5-T MR imaging. Radiology 251(1):96–104

Hricak H (1991) Cancer of the uterus: the value of MRI pre-and post-irradiation. Int J Radiat Oncol Biol Phys 21:1089–1094

Jhingran A, Winter K, Portelance L, Miller B, Salehpour M, Gaur R, Souhami L, Small W Jr, Berk L, Gaffney D (2012) A phase II study of intensity modulated radiation therapy to the pelvis for postoperative patients with endometrial carcinoma: radiation therapy oncology group trial 0418. Int J Radiat Oncol Biol Phys 84:e23–e28

Jürgenliemk-Schulz IM, Toet-Bosma M, de Kort GA, Schreuder HW, Roesink JM, Tersteeg RJ, van der Heide UA (2011) Internal motion of the vagina after hysterectomy for gynaecological cancer. Radiother Oncol 98:244–248

Keys HM, Roberts JA, Brunetto VL et al (2004) A phase III trial of surgery with or without adjunctive external pelvic radiation therapy in intermediate risk endometrial adenocarcinoma: a Gynecologic Oncology Group study. Gynecol Oncol 92(3):744–751

Kim RY, Pareek P, Duan J, Murshed H, Brezovich I (2002) Postoperative intravaginal brachytherapy for endometrial cancer; dosimetric analysis of vaginal colpostats and cylinder applicators. Brachytherapy 1:138–144

Kim C, Olson A, Kim H et al (2012) Contouring inguinal and femoral nodes; how much margin is needed around the vessels? Pract Radiat Oncol 2(4):274–278

Koh DM, Hughes M, Husband JE (2006) Cross-sectional imaging of nodal metastases in the abdomen and pelvis. Abdom Imaging 31(6):632–643

Lamoreaux WT, Grigsby PW, Dehdashti F et al (2005) FDG-PET evaluation of vaginal carcinoma. Int J Radiat Oncol Biol Phys 62(3):733–737

Land R, Herod J, Moskovic E et al (2006) Routine computerized tomography scanning, groin ultrasound with or without fine needle aspiration cytology in the surgical management of primary squamous cell carcinoma of the vulva. Int J Gynecol Cancer 16(1):312–317

Levenback CF, Ali S, Coleman RL et al (2012) Lymphatic mapping and sentinel lymph node biopsy in women with squamous cell carcinoma of the vulva: a gynecologic oncology group study. J Clin Oncol 30(31): 3786–3791

Lim K, Small W Jr, Portelance L et al (2011) Consensus guidelines for delineation of clinical target volume for intensity-modulated pelvic radiotherapy for the definitive treatment of cervix cancer. Int J Radiat Oncol Biol Phys 79(2):348–355

Lin WC, Hung Y, Yeh LS, Kao CH, Yen RF, Shen YY (2003) Usefulness of (18)F-fluorodeoxyglucose positron emission tomography to detect para-aortic lymph nodal metastasis in advanced cervical cancer with negative computed tomography findings. Gynecol Oncol 89(1):73–76

Lujan AE, Mundt A, Yamada SD, Rotmensch J, Roeske JC (2003) Intensity-modulated radiotherapy as a means of reducing dose to bone marrow in gynecologic patients receiving whole pelvic radiotherapy. Int J Radiat Oncol Biol Phys 57:516–521

Marnitz S, Köhler C, Schneider A, Seiler F, Hinkelbein W (2006) Interindividual variability of lymph drainages in patients with cervical cancer. Implication on irradiation planning. Strahlenther Onkol 182(2):80–85

Mayr NA, Wang JZ, Lo SS et al (2010) Translating response during therapy into ultimate treatment outcome: a personalized 4-dimensional MRI tumor volumetric regression approach in cervical cancer. Int J Radiat Oncol Biol Phys 76(3):719–727

Mayr NA, Huang Z, Eisenhauer E, Lo SS, Wang JZ, Yuh WTC (2011) Postoperative seromas following robotic/laparoscopic lymph node dissection in patients with radiation/chemotherapy for gynecologic cancers. Presented as a scientific exhibit at the 53rd Annual Meeting of the American Society of Radiation Oncology, Miami, FL, October 2–6, 2011 (abst). Int J Radiat Oncol Biol Phys 81(2):S462

Messiou C, Spencer J, Swift SE (2006) MR staging of endometrial cancer. Clin Radiol 61:822–832

Mitchell D, Snyder B, Coakley F et al (2006) Early invasive cervical cancer: tumor delineation by magnetic resonance imaging, computed tomography, and clinical examination, verified by pathologic results, in the ACRIN 6651/GOG 183 Intergroup Study. J Clin Oncol 24:5687–5694

Mock M, Knocke T, Fellner C, Pötter R (1998) Analysis of different application systems and CT-controlled planning variants in treatment of primary endometrial carcinomas. Is brachytherapy treatment of the entire uterus technically possible? Strahlenther Onkol 174:320–328

Moskovic EC, Shepherd JH, Barton DP et al (1999) The role of high resolution ultrasound with guided cytol-

ogy of groin lymph nodes in the management of squamous cell carcinoma of the vulva: a pilot study. Br J Obstet Gynaecol 106(8):863–867
Myerson RJ, Garofalo MC, El Naqa I et al (2009) Elective clinical target volumes for conformal therapy in anorectal cancer: a radiation therapy oncology group consensus panel contouring atlas. Int J Radiat Oncol Biol Phys 74(3):824–830
Nag S, Erickson B, Thomadsen B, Orton C, Demanes JD, Petereit D (2000a) The American Brachytherapy Society recommendations for high-dose-rate brachytherapy for carcinoma of the cervix. Int J Radiat Oncol Biol Phys 48:201–211
Nag S, Erickson B, Parikh S, Gupta N, Varia M, Glasgow G (2000b) The American Brachytherapy Society recommendations for high-dose-rate brachytherapy for carcinoma of the endometrium. Int J Radiat Oncol Biol Phys 48:779–790
Parry-Jones E (1963) Lymphatics of the vulva. J Obstet Gynaecol Br Commonw 70:751–765
Richardson S, Palaniswaamy G, Grigsby PW (2010) Dosimetric effects of air pockets around high-dose rate brachytherapy vaginal cylinders. Int J Radiat Oncol Biol Phys 1:276–279
Rockall AG, Sohaib S, Harisinghani MG et al (2005) Diagnostic performance of nanoparticle enhanced magnetic resonance imaging in the diagnosis of lymph node metastases in patients with endometrial and cervical cancer. 2. J Clin Oncol 25:2813–2821
Rubin SC, Young J, Mikuta JJ (1985) Squamous carcinoma of the vagina: treatment, complications, and long-term follow-up. Gynecol Oncol 20(3):346–353
Sala E, Wakely S, Senior E et al (2007) MRI of malignant neoplasms of the uterine corpus and cervix. AJR Am J Roentgenol 188(6):1577–1587
Schwarz JK, Siegel BA, Dehdashti F et al (2007) Association of posttherapy positron emission tomography with tumor response and survival in cervical carcinoma. JAMA 298(19):2289–2295
Selman TJ, Mann C, Zamora J et al (2008) Diagnostic accuracy of tests for lymph node status in primary cervical cancer: a systematic review and meta-analysis. CMAJ 178(7):855–862
Senekjian EK, Frey KW, Stone C et al (1988) An evaluation of stage II vaginal clear cell adenocarcinoma according to substages. Gynecol Oncol 31(1):56–64
Sharma C, Deutsch I, Lewin S, Burke W et al (2011) Lymphadenectomy influences the utilization of adjuvant radiation treatment for endometrial cancer. Am J Obstet Gynecol 205:e1–e9
Shin KE, Park BK, Kim CK et al (2011) MR staging accuracy for endometrial cancer based on the new FIGO stage. Acta Radiol 52(7):818–824
Siegel R, Ward E, Brawley O et al (2011) Cancer statistics, 2011: the impact of eliminating socioeconomic and racial disparities on premature cancer deaths. CA Cancer J Clin 61(4):212–236
Siegel CL, Andreotti R, Cardenes HR, Brown DL, Gaffney DK, Horowitz NS, Javitt MC, Lee SI, Mitchell DG, Moore DH, Rao GG, Royal HD, Small W Jr, Varia MA, Yashar CM, American College of Radiology (2012) ACR appropriateness Criteria® pretreatment planning of invasive cancer of the cervix. J Am Coll Radiol 9(6):395–402
Signorelli M, Guerra L, Buda A et al (2009) Role of integrated FDG PET/CT in the surgical management of patients with high risk clinical early stage endometrial cancer: detection of pelvic nodal metastases. Gynecol Oncol 115:231–235
Singh K, Orakwue CO, Honest H et al (2006) Accuracy of magnetic resonance imaging of inguinofemoral lymph nodes in vulval cancer. Int J Gynecol Cancer 16(3): 1179–1183
Sironi S, Cobelli F De, Scarfone G, Colombo E, Bolis G, Ferrari A, DelMaschio A (1993) Carcinoma of the cervix: value of plain and gadolinium-enhanced MR imaging in assessing degree of invasiveness. Radiology 188(3):797–801
Sironi S, Buda A, Picchio M, Perego P, Moreni R, Pellegrino A, Colombo M, Mangioni C, Messa C, Fazio F (2006) Lymph node metastasis in patients with clinical early-stage cervical cancer: detection with integrated FDG PET/CT. Radiology 238(1):272–279
Small W Jr. RTOG Gynecologic pelvic atlas. http://www.rtog.org/atlases/contour.html. Accessed 25 Feb 2015
Small W Jr, Erickson B, Kwakwa F (2005) American Brachytherapy Society survey regarding practice patterns of postoperative irradiation for endometrial cancer: current status of vaginal brachytherapy. Int J Radiat Oncol Biol Phys 63:1502–1507
Small W Jr, Mell LK, Anderson P et al (2008) Consensus guidelines for delineation of clinical target volume for intensity-modulated pelvic radiotherapy in postoperative treatment of endometrial and cervical cancer. Int J Radiat Oncol Biol Phys 71(2):428–434
Small W Jr, Beriwal S, Demanes DJ, Dusenbery KE, Eifel P, Erickson B, Jones E, Rownd JJ, De Los Santos JF, Viswanathan AN, Gaffney D, American Brachytherapy Society (2012) American Brachytherapy Society consensus guidelines for adjuvant vaginal cuff brachytherapy after hysterectomy. Brachytherapy 11:58–67
Sohaib SA, Richards PS, Ind T et al (2002) MR imaging of carcinoma of the vulva. AJR Am J Roentgenol 178(2):373–377
Subak L, Hricak H, Powell CB et al (1995) Cervical carcinoma: computed tomography and magnetic resonance imaging for preoperative staging. Obstet Gynecol 86(1):43–50
Taylor A, Powell M (2008) An assessment of interfractional uterine and cervical motion: implications for radiotherapy target volume definition in gynaecological cancer. Radiother Oncol 88:250–257
Taylor MB, Dugar N, Davidson SE et al (2007) Magnetic resonance imaging of primary vaginal carcinoma. Clin Radiol 62(6):549–555
Thibault I, Lavallee MC, Aubin S et al (2012) Inverse-planned gynecologic high-dose-rate interstitial

brachytherapy: clinical outcomes and dose–volume histogram analysis. Brachytherapy 11(3):181–191

van Creutzberg CL, Putten WL, Koper P, Lybeert ML, Jobsen JJ, Wárlám-Rodenhuis CC, De Winter KA, Lutgens LC, van den Bergh AC, van de Steen-Banasik E, Beerman H, van Lent M (2000) Surgery and postoperative radiotherapy versus surgery alone for patients with stage-1 endometrial carcinoma: multicentre randomised trial. PORTEC Study Group. Post Operative Radiation Therapy in Endometrial Carcinoma. Lancet 355:1404–1411

Van der Zee AG, Oonk MH, De Hullu JA et al (2008) Sentinel node dissection is safe in the treatment of early-stage vulvar cancer. J Clin Oncol 26(6):884–889

Walsh JW, Amendola M, Konerding KF, Tisnado J, Hazra TA (1980) Computed tomographic detection of pelvic and inguinal lymph-node metastases from primary and recurrent pelvic malignant disease. Radiology 137:157–166

Weidner GJ, Mayr N, Saw CB, Zhen W, Wen BC, Hussey DH (1999) Radiation field simulation of gynecologic malignancies: localization of the cervix and vagina with a flexible vaginal localizer contrast tampon. Radiology 211(3):876–881

Weitmann HD, Pötter R, Waldhäusl C, Nechvile E, Kirisits C, Knocke TH (2005) Pilot study in the treatment of endometrial carcinoma with 3D image-based high-dose-rate brachytherapy using modified Heyman packing: clinical experience and dose-volume histogram analysis. Int J Radiat Oncol Biol Phys 62:468–478

Whittaker CS, Coady A, Culver L, Rustin G, Padwick M, Padhani AR (2009) Diffusion-weighted MR imaging of female pelvic tumors: a pictorial review. Radiographics 29:759–774

Williams G, Tobler M, Gaffney D, Moeller J, Leavitt DD (2002) Dose calculation errors due to inaccurate representation of heterogeneity correction obtained from computerized tomography. Med Dosim 27:275–278

Yang WT, Lam W, Yu MY, Cheung TH, Metreweli C (2000) Comparison of dynamic helical CT and dynamic MR imaging in the evaluation of pelvic lymph nodes in cervical carcinoma. AJR Am J Roentgenol 175(3):759–766

Bladder Cancer

16

Ping Jiang and Juergen Dunst

Contents

P. Jiang (✉) • J. Dunst
Department of Radiation Oncology,
University Clinic Schleswig-Holstein,
Christian-Albrechts-University of Kiel,
Feldstr. 21, Kiel D-24105, Germany
e-mail: ping.jiang@uksh.de; Juergen.dunst@uk-sh.de

16.1 Major Clinical Facts About Bladder Cancer

Bladder cancer is the ninth most common cancer diagnosis worldwide. Over 330,000 new cases and more than 130,000 deaths are reported with bladder cancer each year. The ratio between males and females is 3.8:1 (Ploeg et al. 2009). More than 90 % of all bladder cancers are urothelial carcinoma (also called transitional cell neoplasms), while squamous cell carcinoma (SCC) constitutes 5 % of cases and adenocarcinoma constitutes ca. 1–2 % (most often in dome of bladder; urachal remnant). Other tumors in the bladder such as small cell carcinoma, sarcoma, carcinosarcoma, lymphoma, or melanoma are rare and should be treated in accordance with the histopathological entity.

The tumor, node, and metastasis (TNM) classification of malignant tumors is the method most widely used to classify the extent of cancer

A.-L. Grosu, C. Nieder (eds.), *Target Volume Definition in Radiation Oncology*,
DOI 10.1007/978-3-662-45934-8_16, © Springer-Verlag Berlin Heidelberg 2015

Table 16.1 2009 TNM classification of urinary bladder cancer (updated 2012)

T – primary tumor	
TX	Primary tumor cannot be assessed
T0	No evidence of primary tumor
Ta	Noninvasive papillary carcinoma
Tis	Carcinoma in situ: "flat tumor"
T1	Tumor invades subepithelial connective tissue
T2	Tumor invades muscle
T2a	Tumor invades superficial muscle (inner half)
T2b	Tumor invades deep muscle (outer half)
T3	Tumor invades perivesical tissue
T3a	Microscopic
T3b	Macroscopic (extravesical mass)
T4	Tumor invades any of the following: prostate, uterus, vagina, pelvic wall, abdominal wall
T4a	Tumor invades prostate, uterus, or vagina
T4b	Tumor invades pelvic wall or abdominal wall
N – lymph nodes	
NX	Regional lymph nodes cannot be assessed
N0	No regional lymph node metastasis
N1	Metastasis in a single lymph node in the true pelvis (hypogastric, obturator, external iliac, or presacral)
N2	Metastasis in multiple lymph nodes in the true pelvis (hypogastric, obturator, external iliac, or presacral)
N3	Metastasis in common iliac lymph node(s)
M – distant metastasis	
M0	No distant metastasis
M1	Distant metastasis

spread (Table 16.1). Concerning histological grading, the use of the 2004 WHO classification is recommended but still needs to be validated by more clinical trials. Most clinical trials published so far on bladder tumors have been performed using the 1973 WHO classification.

16.2 General Treatment Concepts and Indications for Radiotherapy

16.2.1 Treatment Concepts and Therapy Results in Superficial, Non-Muscle-Invasive Bladder Cancer (NMIBC, Ta, Tis, T1)

Over 80 % of newly diagnosed cases are classified as Ta, Tis, or T1. TUR (transurethral resection) and (in case of risk factors) additional intravesical cytostatic therapy, mainly with bacillus Calmette-Guérin (BCG), are the important cornerstones of initial treatment. The recurrence and progression rate of NMIBC is strongly associated with tumor grade and invasion into the lamina propria. Early cystectomy for high-risk superficial cancers has been recommended because of favorable results in some series, but it is not clear whether the results reflect the efficacy of surgical therapy or are only caused by patient selection. However, patients with failure after TUR and intravesical therapy should be considered for more intense treatment with the decision based on T-category, tumor multiplicity, size, concomitant in situ cancer, and urothelial tumor of the prostatic urethra. Cystectomy is considered as the standard treatment for this subgroup, but concurrent chemoradiotherapy might be an alternative because of good results in some series (Weiss et al. 2006).

16.2.2 Treatment Concepts and Therapy Results in Localized Muscle-Invasive Bladder Cancer (T2–T4 N0/N1 M0)

For localized muscle-invasive bladder cancer, radical cystectomy has been widely considered as the standard treatment. One ancient randomized study showed a nonsignificant advantage of cystectomy over radiotherapy (radiation alone without chemotherapy). However, numerous phase II studies with concurrent chemoradiotherapy have demonstrated survival rates identical to surgical series with 70–80 % bladder preservation in long-term survivors. The most impressive advantage with regard to survival has recently been shown in the British BC 2001 study which demonstrated the superiority of concurrent chemoradiation over radiotherapy alone. The absolute difference in survival was 13 % after 5 years which is higher than the increase in survival with adjuvant or neoadjuvant chemotherapy prior or after radical cystectomy. Thus, chemoradiation is the standard of care for organ preservation and is, with regard to survival, to be considered as equieffective to cystectomy according to the best available evidence at the moment (Fig. 16.1).

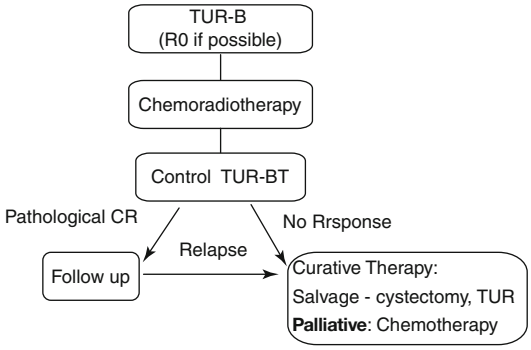

Fig. 16.1 General treatment concept for an organ-preserving treatment approach

16.2.3 Indications for Definitive Curative Radiotherapy

Radiotherapy is an attractive curative option for nearly all patients with muscle-invasive bladder cancer with the additional advantage of bladder preservation in the majority of patients. Standard treatment for patients with curative approach is radiotherapy plus concurrent chemotherapy. The best chemotherapy regimen is not yet clear. The most widely used drug has been cisplatin (Rodel et al. 2002). However, a combination of 5-FU and mitomycin C has also demonstrated significant efficacy in the BC 2001 trial and is surely an evidence-based alternative to cisplatin (James et al. 2012). A further drug for radiosensitization is paclitaxel which has been shown to be safe and efficacious in patients with contraindications to cisplatin (Müller et al. 2007).

All patients should initially undergo a complete transurethral resection of the bladder tumor (TUR-BT). The TUR should be complete, if possible; a macroscopically complete TUR-BT is a major prognostic factor. TUR-BT is followed by chemoradiotherapy. About 6 weeks after chemoradiotherapy, a control cystoscopy is recommended. A pathologically complete remission (pCR) can be achieved in about 70 % of all patients and a pCR is a prognostic factor for survival, long-term tumor control in the bladder, and bladder preservation (Jenkins et al. 1988; Mameghan et al. 1995). Patients with residual invasive tumor on control cystoscopy should undergo salvage cystectomy, if there are no contraindications to major surgery.

Start of radiotherapy is recommended 4–6 weeks after TUR-BT because some time is normally required until local symptoms after TUR (dysuria, urgency) have been solved.

16.2.4 Adjuvant Radiotherapy

The role of adjuvant radiotherapy is not well defined with very limited data. Preoperative radiotherapy has been used in historical studies but is not considered as standard in contemporary guidelines. Preoperative chemoradiation followed by cystectomy is, from a theoretical point of view, an attractive concept but should only be used in clinical trials.

16.2.5 Palliative Radiotherapy

Palliative radiotherapy is useful for the relief of symptoms such as bleeding and reduces the pain for patients with T4 bladder tumors, pelvic nodal disease, and bone and other distant metastases. Short courses of palliative pelvic radiotherapy may be beneficial for elderly patients who have significant comorbidities precluding radical treatment.

16.3 Normal Anatomy and Typical Tumor Spread

16.3.1 Anatomy of the Bladder

The bladder is located on the floor of the pelvic cavity. It is anterior to the rectum, seminal vesicles, and ureters in males. In females it is anterior to the uterus and upper vagina. As the bladder distends, the neck remains fixed and the dome rises into the pelvic cavity. The bladder is a musculomembranous sac. It appears smooth when full and has numerous folds when it is empty.

16.3.2 Spread of Primary Tumor

Tumors may grow papillary or as solid-infiltrative lesions. In papillary tumors, most of the tumor

volume extends into the bladder. The majority of the advanced lesions, however, grow as flat lesions (so-called solid-infiltrative lesions) with most of the tumor in the bladder wall or beyond.

It is obvious from surgical series that all diagnostic modalities bear a large risk of staging error. It is nearly impossible to clearly differentiate between T1 (no muscle invasion), T2a (superficial muscle invasion) and T2b (deep muscle invasion), and extravesical extension (T3). Even if patients are staged by cystoscopy, TUR, and the best available diagnostic modalities (CT, MRI), a significant staging error with regard to T-category remains. In a recent large multicenter trial, even the use of nomograms prior to radical cystectomy underestimated the risk of locally advanced disease in nearly half of all patients. In large surgical series, extravesical disease (T3–T4) is present in more than two-thirds of all patients with proven muscle invasion. Therefore, it is justified and useful to use standard target volumes for the majority of patients and to adapt the standard volumes in cases with large tumor masses.

16.3.3 Spread to Regional Lymph Nodes

In surgical series, about one-third of patients treated with cystectomy for muscle-invasive cancers have nodal involvement (Yafi et al. 2011). Surgical series and sentinel-node series indicate there is no clear step-by-step involvement of regional nodes as, for example, known from axillary involvement in breast cancer. A single involved node may lie more or less randomly in the regional node areas (Leissner et al. 2004; Bruins et al. 2014). However, early nodal involvement is often localized in the paravesical and obturator nodes in direct neighborhood to the bladder (laterally between the bladder and iliac external vessels and behind the bladder). Thus, radical treatment of lymph nodes requires dissection or irradiation of all regional nodes irrespective of tumor volume and stage. On the other hand, a limited nodal treatment with treatment only to the obturator nodes and internal iliac nodes would cover all involved nodes in the majority of node-positive patients.

The optimal extent of lymph node treatment is not well defined. Data from retrospective surgical series suggest that an extended nodal resection might be superior in terms of survival (e.g., Skinner 1982), but this hypothesis is highly controversial in the light of negative results of extended lymph node dissection in all other cancer types where such procedures have failed to demonstrate a survival benefit despite positive data in retrospective series, e.g., in gastric cancer or breast cancer. Moreover, a recent study from a single institution compared different target volumes (whole pelvis versus bladder only) in patients undergoing definitive radiotherapy and found no difference in survival (Tunio et al. 2012).

16.4 Target Volume

16.4.1 Evidence-Based Recommendations for Target Volume of the Primary Tumor

Most of the treatment series have used whole-bladder radiotherapy, either for the complete treatment course or combined with a partial-bladder boost. Arguments in favor of whole-bladder irradiation are the difficulties to clearly define tumor borders in the bladder wall with imaging methods, the risk of multiplicity of tumors in the bladder, and the changes in bladder filling during treatment with subsequent difficulties to exactly locate the tumor. On the other hand, partial-bladder irradiation offers the advantage to reduce acute bladder toxicity and to increase the total dose to the macroscopic tumor. Recently, two randomized studies on this issue have been published. In the BC 2001 study, a subgroup of patients was randomized between whole- and partial-bladder irradiation with no obvious differences in outcome. A second randomized study from Manchester compared whole-bladder irradiation with a standard dose (52.5 Gy in 20 fractions) to dose-escalated partial-bladder irradiation (primary tumor plus

Table 16.2 Randomized study of whole-bladder irradiation with standard doses versus partial-bladder irradiation with escalated dose in patients with unifocal cT2–T3 N0 bladder cancer

	Whole bladder	Partial bladder	
	Standard dose	Dose escalated	
N	60	99	
Fractionation, total dose	20×2.625 Gy 52.5 Gy	20×2.875 Gy 57.5 Gy (*N*=45)	16×3.438 Gy 55.0 Gy (*N*=44)
Median RT volume	815 cm^3	324 cm^3	315 cm^3
CR rate	75 %	80 %	71 %
5-year local control	58 %	59 %	34 %
5-year overall survival	61 %	60 %	51 %
5-year cystectomy-free survival	59 %	50 %	41 %
Late GU tox ≥ grade 2	4 %	18 %	6 %
Late GI tox ≥ grade 2	8 %	8 %	12 %
Surgical intervention due to late toxicity	1 (1.7 %) bowel	1 (2.2 %) bladder	2 (4.5 %) bladder

The median RT volume was significantly lower in patients undergoing partial-bladder radiotherapy. The outcome with regard to CR rate, local control, survival, and cystectomy-free survival was not significantly different; the study failed to demonstrate an increase in local control by using higher than standard doses. However, the absolute figures in terms of bladder preservation were higher with the standard approach. There was also a trend toward increases in complication rate in patients with dose escalation, especially in the accelerated group with 16 fractions (Cowan et al. 2004)

1.5 cm margin, 57.5 Gy in 20 fractions or 55 Gy in 16 fractions) in patients with unifocal T2–T3 N0 M0 cancers and found also no significant difference (Cowan et al. 2004). This second study suggests that, firstly, partial-bladder irradiation with modern imaging and treatment techniques (3D-CRT) does not increase failure rates and, secondly, that the moderate increase in dose did not increase local control or survival. However, the long-term bladder preservation rate in the Manchester study was, in absolute figures, slightly better with whole-bladder as compared to partial-bladder irradiation (Table 16.2), and the patient numbers in both arms were so small that a clinically relevant difference with regard to bladder preservation might not have been detected. Moreover, there was a trend toward increased bladder toxicity in the dose-escalated arms, especially in patients treated with 16 fractions in 3 weeks (Table 16.2).

In summary, whole-bladder irradiation remains the contemporary standard target volume. Partial-bladder irradiation is justified and might be considered as an alternative standard of care in patients in whom reduction of target volume increases the feasibility and tolerability of irradiation.

16.4.2 Evidence-Based Recommendations for Lymph Node Irradiation

Most of the historical series have used large fields including bladder and regional nodes in patients with radical radiotherapy. Smaller treatment fields have been used in patients undergoing palliative radiotherapy.

A recent study compared bladder-only versus whole-pelvis radiotherapy in patients with cN0 status and found no difference, suggesting that omission of regional node irradiation is justified in patients with clinically negative nodes (Tunio et al 2012). Severe acute diarrhea was less frequent in patients with bladder-only radiotherapy (2 % versus 4 % grade 3–4 reactions), but there was no significant difference in late toxicity (Table 16.3).

It should be noted that the majority of potentially involved regional lymph nodes (see Sect. 16.3.2.) are included even in relatively small fields (e.g., CTV = bladder wall plus 2 cm) if standard techniques (e.g., 3D-CRT) are used. Thus, relevant amounts of regional lymph nodes are treated with curative doses even in case of bladder-only irradiation, and the unintended irradiation may have contributed to the clinical efficacy. However,

Table 16.3 Randomized study of whole-pelvis (including regional lymph nodes) and bladder-only irradiation in patients with cT2–T4 N0 bladder cancer treated with radiotherapy plus concurrent chemotherapy (weekly cisplatin)

	Whole-pelvis irradiation	Bladder-only irradiation
N	120	110
Mean age	62 years	62 years
Local recurrence rate	41 %	43 %
Bladder preservation	59 %	57 %
5-year overall survival	53 %	51 %
Acute diarrhea grade 3+	4 %	2 % $p=0.02$

No significant differences with regard to local control, bladder preservation, and overall survival. The frequency of severe diarrhea was low but significantly higher in patients with irradiation of the whole pelvis (Tunio et al. 2012)

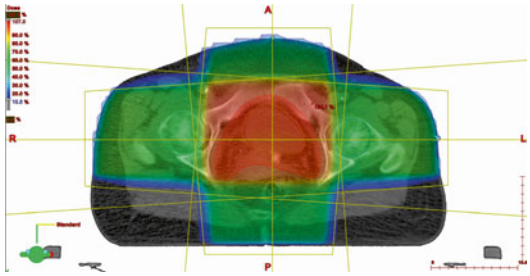

Fig. 16.2 Axial CT slice showing classic conformal plan for bladder irradiation. Relevant amounts of regional lymph nodes are treated with curative doses even in case of bladder-only irradiation

it is not clear whether omission of lymph node irradiation is justified if more precise radiation therapy techniques and reduced volumes (e.g., IMRT or adaptive radiotherapy in combination with bladder-only radiotherapy) are used (Fig. 16.2).

In summary, omission of adjuvant lymph node irradiation is justified in a relevant subset or the majority of cN0 patients, especially in patients in whom reduction of acute toxicity is necessary.

16.4.3 Bladder Filling and Adaptive Radiotherapy

The optimal filling state of the bladder during radiotherapy has been controversially discussed.

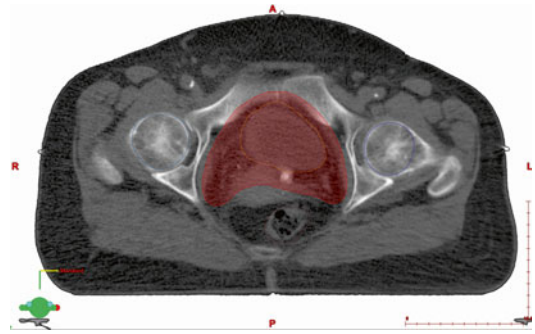

Fig. 16.3 Axial CT slice with CTV: the whole bladder (with a moderate bladder filling) and obturator nodes and OAR: rectum and femoral heads

Increasing bladder volume might decrease the amount of small bowel in the treated volume but surely increases the target volume. A planning study from Poland suggests that the best overall dose distribution to surrounding normal tissue is achieved with a moderate bladder filling, the "partially empty" bladder (Majewski et al. 2009). Moreover, the daily reproducibility is probably better with an average filling state than with extreme situations (bladder empty or full) (Fig. 16.3).

Adaptive radiotherapy with a "plan-of-the-day" treatment concept is an attractive option in bladder cancer due to the daily variability in bladder filling. A recent proof-of-principle study in a small number of patients has demonstrated that this strategy can significantly reduce the dose to the surrounding normal tissues (Tuomikoski et al. 2011). In this study, three to four different treatment plans were calculated with different filling states of the bladder, and the optimal plan was chosen daily on the basis of a cone-beam CT prior to treatment. This study has also demonstrated large interindividual and interfractional variabilities in daily bladder filling.

16.4.4 Preparation of the Patient

Patients are mostly and probably best treated in supine position with ankle supports to stabilize the legs and pelvis and a knee support for comfort. The question of the optimal filling state of the bladder has been controversially discussed in the literature with several arguments in favor of an empty as well as a filled bladder. The bladder

Table 16.4 Standard recommendations for target volume and doses in patients in good general condition and curative treatment approach

Target volume	Description	Fractionation and total dose	Comments
CTV 1	Visible macroscopic bladder tumor (GTV) or tumor area after TUR with 1.5 cm margin. Bladder "partially empty" (e.g., 150 cc)	5 times weekly 1.80 Gy	No evidence for better local control beyond 60 Gy. Slight dose reduction (10 %) seems justified in case of "adjuvant" XRT after R0-TUR
		Total dose 59.6–63.2 Gy (after R2-TUR)	Whole-bladder boost is justified in patients with multiple or large tumors ("Erlangen approach"); total dose should not exceed 60 Gy maximum dose to the whole bladder
		Total dose 54.0 Gy (after R0-TUR)	
CTV 2	Whole bladder (bladder "partially empty," e.g., 150 cc) plus surrounding lymph nodes (internal iliac and obturator nodes)	5 times weekly 1.80 Gy	
		Total dose 50.4 Gy	
CTV 3	All other regional lymph nodes up to aortic bifurcation	5 times weekly 1.80 Gy	Can be omitted in cN0 patients
		Total dose 45.0–50.4 Gy	

should be partially emptied before scanning and treatment, to reduce the radiation volume and dose to the normal tissues. We use a small dose of oral contrast which is given 30 min before the planning CT scan to better visualize the small bowel.

16.4.5 Data Acquisition for CT Planning

A CT scan is performed on the patients in supine in the treatment position with ankle supports and a knee support. The bladder should be partially emptied immediately before scanning and treatment. The scan is performed with 3–5 mm slices from the lower border of L3 to 4 cm until the inferior border of the ischial tuberosities.

16.4.6 Target Volume Definition

The GTV is the primary bladder tumor (macroscopic visible on CT/MRI/ cystoscopy) and any extravesical spread. A typical approach is to define the CTV 1 (boost) as the GTV. The CTV 2 includes the CTV 1 and the whole bladder and lymph nodes (paravesical, obturator, external and internal iliacs, common iliac to L4/L5 (the latter delineated as shown in Chap. 15)) as well as the upper part of the urethra (e.g., the prostatic urethra in men). The PTV is the CTV with a 1–1.5 cm margin. With improved image guidance, these margins can probably be reduced.

According to recent data (see Sects. 16.4.1 and 16.4.2), omission of lymph node irradiation should be considered as an alternative standard in cN0 patients. Moreover, restriction of the target volume to the tumor area only (partial-bladder irradiation) may be considered in selected subgroups with unifocal tumors, especially in elderly patients. Thus, small-volume irradiation with a single CTV (GTV plus surrounding bladder area) is an option in thoroughly selected patients with curative treatment intent (Table 16.4).

In patients undergoing palliative irradiation, the CTV should be restricted to the GTV with a small safety margin (e.g., 1.0–1.5 cm), which is, in most cases of advanced lesions, the whole bladder.

Organs at risks (OAR) should include the rectum, femoral heads, and small bowel. Recommended dose constraints are rectum $V50 < 60$ %, $V60 < 50$ %; femoral heads $V50 < 50$ %; and small bowel $V45 < 250$ cm^3.

For palliation of T4 tumors and pelvic nodal disease, the CTV should encompass only the gross

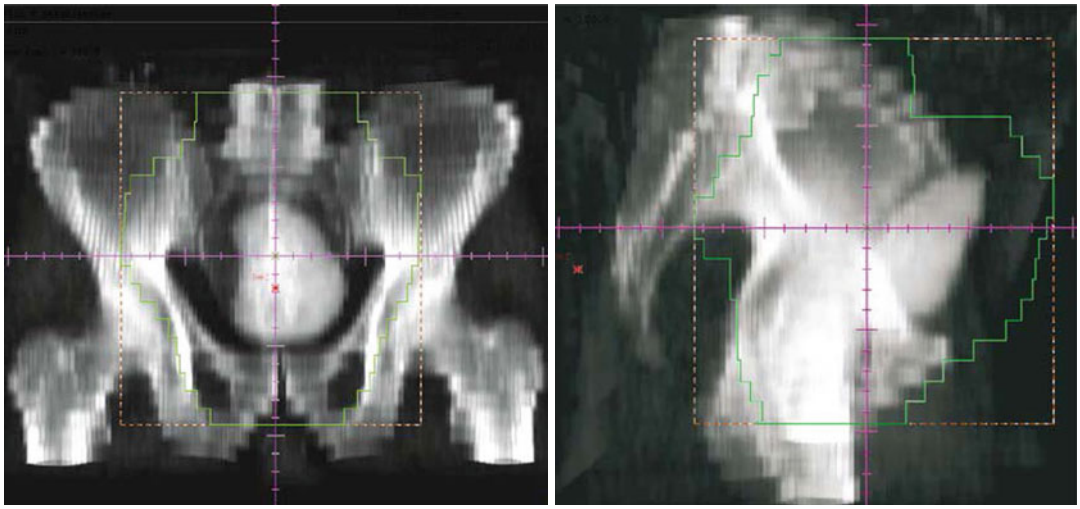

Fig. 16.4 Virtual CT simulation showing DRR with irradiation field

disease. If this volume is too large, it can be reduced to only cover the area causing symptoms.

Where CT planning is not available, the treatment can be simulated conventionally and the bladder visualized with contrast inserted into the bladder via an indwelling urinary catheter (Fig. 16.4).

16.4.7 Dose and Fractionation

Most treatment series and prospective studies have used conventional fractionation with daily doses of 1.8 Gy up to total doses of 56–64 Gy. The optimal total dose is not clearly defined but there is no evidence for an increase in local control beyond 60 Gy. Thus, a total dose of 60–64 Gy (depending on volume) should be considered as standard. Subgroup analyses suggest optimal control in patients treated with "adjuvant" radiotherapy after a complete (R0) TUR; a slightly lower dose of about 56 Gy is probably sufficient in these patients.

One ancient trial found a better outcome with hyperfractionation (three times daily 1 Gy); however, this concept has not gained acceptance despite radiobiological arguments in favor this approach (Edsmyr et al. 1985). On the other hand, the majority of British trials have used radiation regimens with moderate hypofractionation (e.g., about 20 fractions) and have reported identical results as compared to conventional

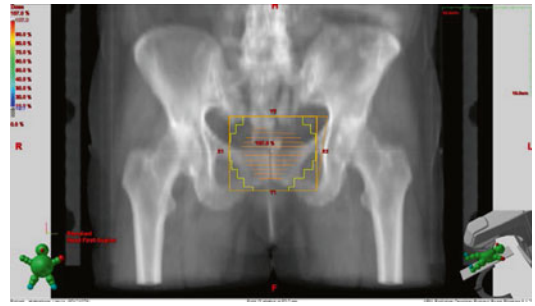

Fig. 16.5 Virtual CT simulation showing DRR with volume for palliative treatment of bladder cancer

fractionation (e.g., James et al. 2012; Cowan et al. 2004); despite the lack of randomized trials, moderate hypofractionation with an overall treatment time of at least 4 weeks should be considered as equieffective.

In case of palliative treatment intent, moderate hypofractionation or strong hypofractionation should be used (Fig. 16.5). An overview over possible fractionation regimens is listed in Table 16.5.

16.5 Side Effects and Supportive Therapy

Anemia has been demonstrated to be a significant poor prognostic factor. Retrospective data and one transfusion study suggest that anemia should be corrected when hemoglobin is below 12 g/dL.

Table 16.5 Alternative recommendations for target volume and doses in patients with poor condition or palliative treatment approach or local relapse

Clinical situation	Target volume (CTV)	Fractionation and total dose	Comments
cT2–T4 N0, poor general condition or advanced age	Standard (see Table 16.4)	5×1.80 Gy or 2.00–60 Gy	
	Or omission of lymph node irradiation	Or moderate hypofractionation (e.g., 20×2.7 Gy)	
	Or partial-bladder irradiation only		
Palliative treatment intent (e.g., M1 with hematuria)	CTV = GTV	Moderate hypofractionation (e.g., 20×2.7 Gy)	Good and fast symptom control with hypofractionated regimens
		Or 5×3.00 Gy to 45 Gy	
		Or 1–2× weekly 5.00–6.00 Gy up to 30–36 Gy	
Local relapse after cystectomy	CTV = GTV	5×1.80 Gy or 2.00–60 Gy	Palliative intent but no data and concerns about severe hypofractionation after surgery
		Or moderate hypofractionation (e.g., 20×2.7 Gy or 12×3 Gy)	

Common acute side effects, which occur in the majority of patients, are acute radiation cystitis and proctitis. In case of urinary symptoms, urinary infection should be excluded and, if present, be treated. There is no evidence for the prophylactic use of antibiotics during radiotherapy. A high fluid intake should be advised. Catheterization should be avoided to minimize the risk of infection. Proctitis can be treated with topical steroids.

Important late side effects in the bladder include urgency and chronic cystitis. Severe late effects (grade 3+) occur in about 5 % of the patients (Rodel et al. 2002). Bladder shrinkage with need for secondary cystectomy has been a problem in older studies but is very rare with contemporary treatment concepts and doses; the risk is surely below 1 %. Late bowel toxicity has been noted in about 5 % of patients. The overall quality of life after a bladder-preserving therapy is good and probably at least as good as or better than after cystectomy although there are no exact data on other symptoms, such as vaginal dryness and stenosis in women, impotence in men, and bladder-specific quality of life.

16.6 Follow-up

Six weeks after the treatment, the response should be evaluated by restaging TUR. In case of complete response (CR), the patient should be observed at regular intervals. In case of persistent or recurrent invasive tumor, salvage cystectomy should be considered. Patients with preserved bladder should undergo lifelong surveillance with regard to new bladder cancers.

References

Bruins HM, Skinner EC, Dorin RP, Ahmadi H, Djadalat H, Miranda G, Cai J, Daneshmand S (2014) Incidence and location of lymph node metastases in patients undergoing radical cystectomy for clinical non-muscle invasive bladder cancer: results from a prospective lymph node mapping study. Urol Oncol 32(1):24.e13–24.e19

Cowan RA, McBain CA, Ryder WD, Wylie JP, Logue JP, Turner SL, Van der Voet J, Collins CD, Khoo VS, Read GR (2004) Radiotherapy for muscle-invasive carcinoma of the bladder: results of a randomized trial comparing conventional whole bladder with dose-escalated partial bladder radiotherapy. Int J Radiat Oncol Biol Phys 59:197–207

Edsmyr F, Andersson L, Esposti PL, Littbrand B, Nilsson B (1985) Irradiation therapy with multiple small fractions per day in urinary bladder cancer. Radiother Oncol 4(3):197–203

James ND, Hussain SA, Hall E, Jenkins P, Tremlett J, Rawlings C, Crundwell M, Sizer B, Sreenivasan T, Hendron C, Lewis R, Waters R, Huddart RA (2012) Radiotherapy with or without chemotherapy in muscle-invasive bladder cancer. N Engl J Med 366: 1477–1488

Jenkins BJ, Caulfield MJ, Fowler CG, Badenoch DF, Tiptaft RC, Paris AM, Hope-Stone HF, Oliver RT, Blandy JP (1988) Reappraisal of the role of radical radiotherapy and salvage cystectomy in the treatment of invasive (T2/T3) bladder cancer. Br J Urol 62(4):343–346

Leissner J, Ghoneim MA, Abol-Enein H, Thüroff JW, Franzaring L, Fisch M, Schulze H, Managadze G, Allhoff EP, el-Baz MA, Kastendieck H, Buhtz P, Kropf S, Hohenfellner R, Wolf HK (2004) Extended radical lymphadenectomy in patients with urothelial bladder cancer: results of a prospective multicenter study. J Urol 171(1):139–144

Majewski M, Wesolowska I, Urbanczyk H, Hawrylewicz L, Schwierczok B, Mizczyk L (2009) Dose distribution in bladder and surrounding normal tissues in relation to bladder volume in conformal radiotherapy for bladder cancer. Int J Radiat Oncol Biol Phys 75(5): 1371–1378

Mameghan H, Fisher R, Mameghan J, Brook S (1995) Analysis of failure following definitive radiotherapy for invasive transitional cell carcinoma of the bladder. Int J Radiat Oncol Biol Phys 31(2):247–254

Müller AC, Diestelhorst A, Kuhnt T, Kühn R, Fornara P, Scholz HJ, Dunst J, Zietman AL (2007) Organ-sparing treatment of advanced bladder cancer: paclitaxel as a radiosensitizer. Strahlenther Onkol 183(4):177–183

Ploeg M, Aben KK, Kiemeney LA (2009) The present and future burden of urinary bladder cancer in the world. World J Urol 27(3):289–293

Rodel C, Grabenbauer GG, Kuhn R, Papadopoulos T, Dunst J, Meyer M, Schrott KM, Sauer R (2002) Combined-modality treatment and selective organ preservation in invasive bladder cancer: long-term results. J Clin Oncol 20(14):3061–3071

Skinner DG (1982) Management of invasive bladder cancer: a meticulous pelvic node dissection can make a difference. J Urol 128(1):34–36

Tunio MA, Hashmi A, Qayyum A, Mohsin R, Zaeem A (2012) Whole-pelvis or bladder-only chemoradiation for lymph node-negative invasive bladder cancer: single-institution experience. Int J Radiat Oncol Biol Phys 82(3):e457–e462

Tuomikoski L, Collan J, Keyriläinen J, Visapää H, Saarilahti K, Tenhunen M (2011) Adaptive radiotherapy in muscle invasive urinary bladder cancer–an effective method to reduce the irradiated bowel volume. Radiother Oncol 99(1):61–66

Weiss C, Wolze C, Engehausen DG, Ott OJ, Krause FS, Schrott KM, Dunst J, Sauer R, Rödel C (2006) Radiochemotherapy after transurethral resection for high-risk T1 bladder cancer: an alternative to intravesical therapy or early cystectomy? J Clin Oncol 24(15):2318–2324

Yafi FA, Aprikian AG, Chin JL, Fradet Y, Izawa J, Estey E, Fairey A, Rendon R, Cagiannos I, Lacombe L, Lattouf JB, Bell D, Drachenberg D, Kassouf W (2011) Contemporary outcomes of 2287 patients with bladder cancer who were treated with radical cystectomy: a Canadian multicentre experience. BJU Int 108(4):539–545

Breast Cancer

17

Marie-Luise Sautter-Bihl, Ute Melcher,
and Felix Sedlmayer

Contents

M.-L. Sautter-Bihl (✉) • U. Melcher
Department of Radiation Oncology,
Städt. Klinikum Karlsruhe, Karlsruhe, Germany
e-mail: Marie-Luise.Sautter-Bihl@klinikum-karlsruhe.de

F. Sedlmayer
Department of Radiation Oncology,
Paracelsus Medical University Hospital,
Salzburg, Austria

17.1 Radiotherapy After Breast-Conserving Surgery (WBI)

17.1.1 Indications for Whole Breast Irradiation (WBI)

Postoperative radiotherapy of the whole breast (WBI) is an essential part of breast cancer treatment and should be offered to all women after breast-conserving surgery (BCS) in the absence of medical contraindications such as severe comorbidities (Belkacémi et al. 2011; NCCN 2014; New Zealand Guidelines Group (NZGG) 2009; S3 2012; Sedlmayer et al. 2013a).

Body of Evidence

The benefit of WBI is illustrated by the latest meta-analysis of the Early Breast Cancer Trialists' Collaborative Group (Darby et al. 2011) (Table 17.1). In 17 randomized studies, results of postoperative radiotherapy vs. none were compared. A total of 10,801 patients with pT1-2 tumors were included, the majority of whom (n=7,287) were node negative (pN0). WBI substantially

A.-L. Grosu, C. Nieder (eds.), *Target Volume Definition in Radiation Oncology*,
DOI 10.1007/978-3-662-45934-8_17, © Springer-Verlag Berlin Heidelberg 2015

Table 17.1 Results of 17 randomized studies comparing postoperative whole breast irradiation vs. none after breast-conserving surgery

–	pN0		pN+	
	RT	No RT	RT	No RT
10-year any recurrence	15.6 %	31.0 %	42.5 %	63.7 %
Absolute gain	**15.4 %**		**21.2 %**	
	$2p < 0.00001$		$2p = 0.00001$	
15-year any death	30.4 %	33.2 %	47.7 %	58.4 %
Absolute gain	**2.8 %**		**10.7 %**	
	n.s.		$2p = 0.005$	
15-year BC mortality	17.2 %	20.5 %	42.8 %	51.3 %
Absolute gain	**3.3 %**		**8.5 %**	
	$2p = 0.005$		$2p = 0.01$	

Darby et al. (2011)

reduced the 10-year rate of any recurrence (local or distant). The 10-year rate of locoregional recurrence (LRR) as first event was threefold higher for non-irradiated women. Moreover, RT provided an absolute reduction of the breast cancer death rate of 3.8 %. In summary, radiotherapy halved the average annual rate of disease recurrence and reduced the annual breast cancer death rate by about one sixth. On average, in all patients about one breast cancer death was avoided by year 15 for every four recurrences avoided by year 10 (Darby et al. 2011).

Elderly Patients

In the above cited meta-analysis, women who were 60–69 years old had an absolute gain in 10-year any recurrence rate of 14.1 % ($2p = 0.00001$) and patients >70 years still 8.9 % ($2p = 0.00002$) (Darby et al. 2011). No subgroup has yet been identified in whom patients did not profit from RT after BCS in terms of improved local tumor control. Hence, omission of RT in patients of advanced age even with favorable prognostic factors (pN0, ER positive, low grade) should only be considered in the presence of comorbidities with a substantial reduction of life expectancy (Belkacémi et al. 2011; Biganzoli et al. 2012; S3 2012; Sautter-Bihl et al. 2012).

17.1.2 Treatment Planning and Technique for WBI

For planning and treatment, patients are usually placed in supine position with elevation of the ipsilateral or both arms in immobilization cradles. Prone position may be an alternative for some patients with regard to sparing normal tissue (Kirby et al. 2011; Leonard et al. 2012). Individual CT-based 3-D planning is mandatory. Several anatomically based instruction guidelines have been published for the definition of the planning target volume (PTV) (Nielsen et al. 2013; RTOG 2014). The PTV includes the mammary gland and the adjacent chest wall. Organs at risk (OAR) like the lung, heart, and contralateral breast are routinely contoured and the esophagus or spinal cord when indicated.

Detailed instructions for contouring of the heart are provided by the atlas of Feng et al. (Feng et al. 2011). Contouring of the whole heart should start directly inferior to the left pulmonary artery. The pericardium should be included as cardiac vessels run within the fatty tissue. Inferiorly, the heart blends with the diaphragm. One of the clinically most relevant structures for late toxicity is the left anterior descending artery (LAD) (Fig. 17.1a, b), as it is the major coronary vessel in the closest vicinity to left-sided tangential RT fields. The LAD originates from the left coronary artery and runs in the interventricular groove between the right and left ventricle and may be difficult to identify without contrast enhancement in the planning CT (Feng et al. 2011).

Homogeneity requirements in dose distribution as described by the ICRU reports 50 and 62 are usually achieved by conformally shaped tangential wedged field techniques, mostly with photons at energies of 4–8 MV. For larger breasts, higher energies and/or intensity modulation (IMRT) within the tangential beams may be appropriate to fulfill the minimum homogeneity criteria (Barnett

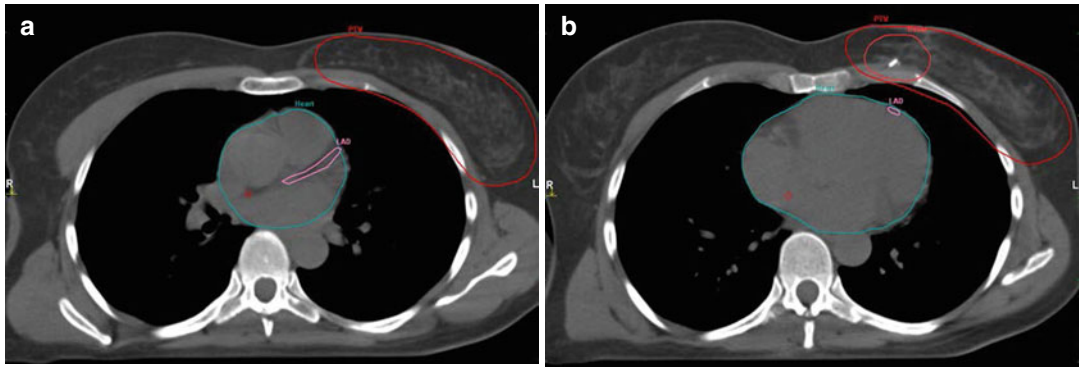

Fig. 17.1 (**a**, **b**) Whole breast irradiation: contouring of the planning target volume (PTV), breast and tumor bed with clip, and the heart and left anterior descending artery (LAD)

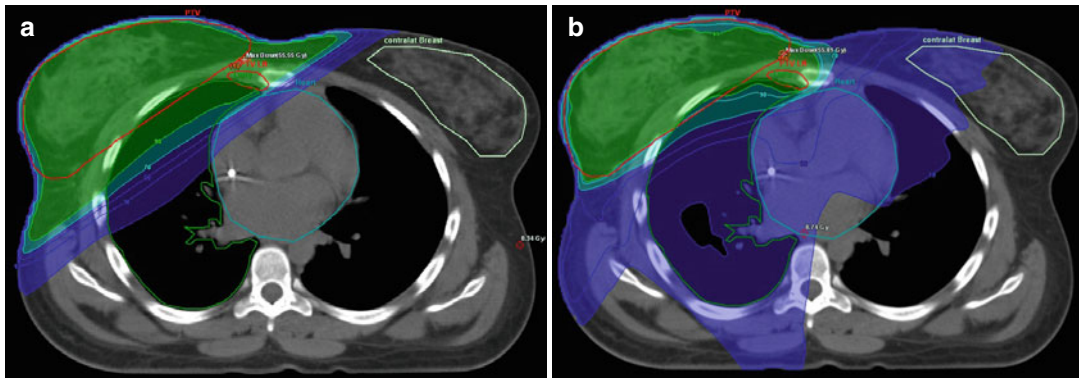

Fig. 17.2 (**a**, **b**) Internal mammary node irradiation (IMN-RT): comparison of the dose distribution with 3-D tangential fields (**a**) versus multiangle IMRT (**b**); reduced lung dose, increased low-dose exposure to a larger volume of normal tissue and contralateral breast

et al. 2012; ICRU 1993, 1999). However, IMRT increases low-dose exposure to a larger volume of normal tissue and contralateral breast (Lohr et al. 2009). Therefore, sparing of OAR must be weighed against a potentially increased risk of secondary tumor induction (Donovan et al. 2012; Hall and Wuu 2003), and the routine use of multi-angle IMRT techniques is critical (Fig. 17.2a, b). However, IMRT may be beneficial for patients with difficult anatomical conditions (i.e., funnel chest) where tangential field arrangements would lead to excessive exposure of OARs. In these cases, WBI in prone position may provide an alternative. For left-sided RT, the use of active breathing control such as computer-assisted breath hold in deep inspiration (Swanson et al. 2013; Zurl et al. 2010) provides another possibility of sparing cardiac dose exposure (Fig. 17.3a–d) as it increases the distance between the target volume and heart (Lin et al. 2008).

The doses for target volume and OAR are documented in dose-volume histograms (DVH). For quality control, repeated imaging (mostly by electronic portal imaging or kV-based scans) should be performed to verify and document correct field setup.

17.1.3 Dose and Fractionation for WBI

Conventional fractionation (CF) with a total dose of 50–50.4 Gy in single fractions of 1.8–2 Gy is still regarded as standard in many current guidelines

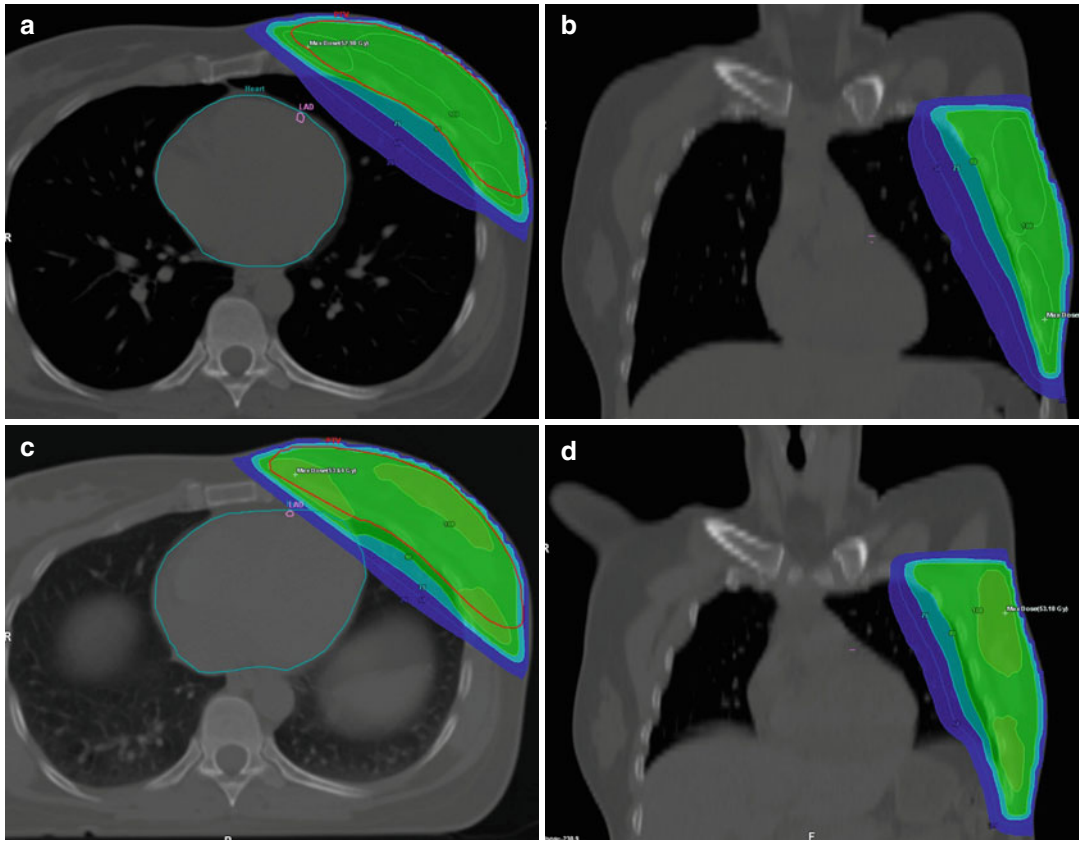

Fig. 17.3 (**a–d**) Whole breast irradiation (WBI): comparison of the dose distribution to the heart, left anterior descending coronary artery (LAD), and lung with (**a**, **b**) and without (**c**, **d**) active breathing control (ABC). ABC increases the distance between the heart and LAD to the treatment volume

(Belkacémi et al. 2011; NCCN 2014; S3 2012; Sedlmayer et al. 2013a). Divergence exists concerning the appraisal of hypofractionation (HF) as a routinely applicable alternative (NCCN 2014; NICE 2009) or as an option restricted to selected patients (S3 2012; Smith et al. 2011). The ASTRO consensus (Smith et al. 2011) and the German S3 guidelines (S3 2012) additionally recommend to refrain from HF when a homogenous dose is not achievable and in patients who need a boost. In the practical guidelines of the DEGRO, hypofractionated WBI with single doses up to 2.7 Gy in 15–16 fractions to total doses of 40–42 Gy is stated as an option for older women with pT1-2 pN0 tumors who need no chemotherapy. The additional use of a sequential boost is possible (Sedlmayer et al. 2013a).

One critical structure for potential late toxicity of RT is the heart. As late cardiac toxicity of HF is not yet been sufficiently evaluated in long-term follow-up and the latency for clinical manifestation of cardiovascular effects may be 15 years or longer (Harris et al. 2006), HF might be critical in cases of relevant dose exposure to the heart, especially in women with a longer life expectancy.

Body of Evidence for Hypofractionation (HF)

Four randomized clinical trials (Bentzen et al. 2008a, b; Haviland et al. 2013; Owen et al. 2006; Whelan et al. 2010) investigated HF schedules (39–42.9 Gy in single fractions of 2.6–3.3 Gy) for iso-effectiveness compared to conventional fractionation (CF) (50 Gy à 2 Gy), three of those in the last decade. In a Cochrane meta-analysis,

published in 2010, these four studies were classified as low to medium quality (James et al. 2010). The authors summarized their findings to provide reassurance that offering HF to carefully selected patients was unlikely to be detrimental in terms of local control, breast appearance, survival, or late radiation breast toxicity for women with small to medium breasts and older than 50 years with small, node-negative tumors.

Longer follow-up was then provided in 2013, when the updated results of the two *START trials* were published (Haviland et al. 2013). Overall, 4,451 women with invasive breast cancer (pT1–3a, pN0–1, M0) were enrolled. Primary endpoints were locoregional recurrence, late normal tissue effects, and quality of life.

For *START A* 2,236 women were randomly assigned for CF with 50 Gy in 25 fractions over 5 weeks compared with 41.6 or 39 Gy in 13 fractions over 5 weeks. Median age was 57 years, 85 % had BCS, 51 % had tumors smaller than 2 cm, 29 % had positive lymph nodes, 70 % had grade 1 or 2 disease, 35 % received adjuvant chemotherapy, 14 % received lymphatic radiotherapy, and 61 % had an additional boost (5 × 2 Gy). The 10-year rates of local-regional relapse did not differ significantly between the 41.6 and 50 Gy regimen groups (6.3 % vs. 7.4 %) or the 39 and 50 Gy regimen groups (8.8 % vs. 7.4 %). Distant relapses, disease-free survival, and overall survival were not significantly different between schedules as compared with 50 Gy (Haviland et al. 2013). *START B:* 2,215 women were recruited, a regimen of 50 Gy in 25 fractions over 5 weeks was compared with 40 Gy in 15 fractions over 3 weeks, and median follow-up was 9.9 years. Median age was 57 years, 92 % had BCS, 64 % had tumors smaller than 2 cm, 23 % had positive lymph nodes, 75 % had grade 1 or 2 disease, 22 % received adjuvant chemotherapy, 7 % received lymphatic radiotherapy, and 43 % patients had an additional boost of 5 × 2 Gy. The proportion of patients with local-regional relapse at 10 years did not differ significantly between the 40 Gy group (4.3 % vs. 5.5 %) and the 50 Gy group. In contrast to START A, the 10-year rate of distant metastases was 12.3 % for HF vs. 16 % for CF ($p = 0.01$); all-cause mortality was 15.9 % for HF vs. 19.2 % for CF ($p = 0.042$). A difference of about 3 % for DFS and OAS had already been described after 5 years in the START B group; according to the authors, it is unexpected and not attributable to differences in local control and remains unexplained in the 10-year update (Haviland et al. 2013).

Cosmesis

Cosmesis was evaluated in about half of the START patients. Photographs were taken before RT and at 2 and 5 years; however an unspecified number had no 5-year photographic assessment. After 5 years, a quality of life study was performed in half of the patients of both studies (2,208 women). Patient-reported symptoms were moderate or marked changes in breast appearance in about 40 %, breast shrinkage in one fourth, and moderate or marked pain in the arm and shoulder in one third of the participants. Change in skin appearance was less in the HF arms (28 % vs. 23 % in START B) (Hopwood et al. 2010). These patient-reported results were not updated in the 10-year analysis; the rate of physician-reported breast shrinkage in the 10-year update was 31.2 % for CF vs. 26.2 % for HF ($p = 0.015$); of breast induration, 17.4 % CF vs. 14.3 % HF (n.s.); and of breast edema, 9.0 % vs. 5.1 % (n.s.) (Haviland et al. 2013).

In the *Canadian study* (Whelan et al. 2010), 1,234 patients with pT1-2 node-negative tumors, a breast size <25 cm (measured as width at the posterior border of the medial and lateral tangential beams), were randomized for CF (50 Gy in fractions of 2 Gy) vs. HF (42.5 Gy in fractions of 2.6 Gy); in both arms, no boost was used, no lymph node irradiation was performed, and chemotherapy was applied in 10.9 %. The majority (76 %) were >50 years. In the whole group, the 10-year LRR was similar (6.2 vs. 6.7 %) with the exception of poorly differentiated tumors where HF provided an inferior tumor control (10-year LRR 15.6 % for HF vs. 4.7 % with CF, $p = 0.01$). No difference in survival was observed.

Cosmesis

It was evaluated by experienced nurses, and the 10-year follow-up revealed fair or poor results in one third, good results in 39 %, and excellent results in 30 % for both groups (Whelan et al. 2010).

Comments and Conclusions

HF appears as a safe treatment concerning oncologic outcome and non-inferior regarding cosmesis. So far, data from the randomized studies refer to women mostly >50 years, predominantly with small- to medium-sized breasts and node-negative tumors. The question remains whether these results are assignable to all women with early breast cancer, especially those of younger age, large breasts, and positive nodes and the large group of women receiving chemotherapy with modern combinations. Changes in breast appearance were reported to be no worse than with CF; however, uncertainty remains whether a rate of about one third fair and poor results is an adequate benchmark nowadays.

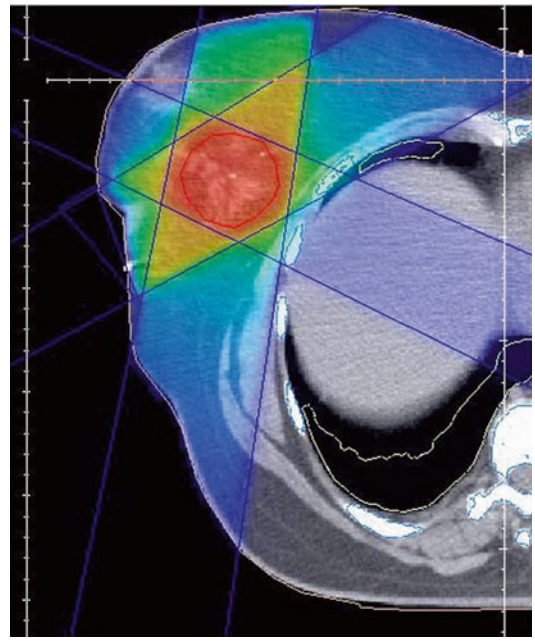

Fig. 17.4 Boost RT: dose distribution 3-D conformal technique, photons. Clip inside the tumor bed for better localization of boost region

17.2 Boost

17.2.1 Indications for Boost RT

An additional boost to the tumor bed improves local control and is therefore generally recommended (Belkacémi et al. 2011; NCCN 2014) with the exception of postmenopausal patients with very low-risk tumors (in particular >60 years of age, small tumors, good prognostic features). The absolute benefit of the boost is smaller in this subgroup; therefore its omission may be considered.

Body of Evidence

Two large randomized studies evaluated local tumor control of WBI alone vs. WBI plus boost. The EORTC trial (Bartelink et al. 2007) comprised 5,318 patients, and the 10-year LRR was 10.2 % for the boost group and 6.2 % for patients with WBI alone (hazard ratio (HR) 0.59, 0.46–0.76). LRR was about halved in all age groups though the absolute reduction was smaller in older patients (Antonini et al. 2007). The boost technique (electrons, external beam photons, or brachytherapy) had no significant impact on the oncologic outcome. The reduction of LRR did not translate into improved survival in this trial. Similar results were achieved in the Lyon Trial (Romestaing et al. 1997); however, no update of these 5-year results has been published.

17.2.2 Treatment Planning and Techniques of Boost RT

The PTV encompasses the tumor bed including seroma and a safety margin (Fig. 17.4). The width of the margin varies from 5 to 30 mm (Nielsen et al. 2013; Poortmans et al. 2009; van der Laan et al. 2010).

The following techniques are used for boost treatment: external beam photons and electrons (Bartelink et al. 2007), interstitial brachytherapy (Polgár and Major 2009), endoluminal brachytherapy (Shah et al. 2010), and intraoperative radiotherapy with electrons (IOERT) (Fastner et al. 2013) or low-energy photons (kV) (Vaidya et al. 2011). Dose distribution is substantially

different for these techniques; therefore, outcome analyses of local control rates have to take account for the limited biological comparability of dose specifications, according to the respective method (Jalali et al. 2007; Nairz et al. 2006).

17.2.3 Dose and Fractionation of Boost RT

For an external beam boost, a dose of 10–16 Gy in 5–8 fractions is commonly recommended (Belkacémi et al. 2011; NCCN 2014; New Zealand Guidelines Group (NZGG) 2009; S3 2012) following WBI.

For the simultaneously integrated boost, single fractions of 2.1–2.25 Gy are applicable (Sedlmayer et al. 2013b).

For brachytherapy and IORT, varying doses are applied according to the respective method (see below).

Body of Evidence

In the EORTC boost trial, a dose of 16 Gy was used either in 8 fractions of 2 Gy EBRT or as low-dose-rate brachytherapy using iridium-192 implants with a dose rate of 0.5 Gy per hour. In the French randomized trial, Romestaing et al. (Romestaing et al. 1997) used 10 Gy in fractions of 2 Gy; updated results have not been published. A subgroup analysis of the EORTC boost trial (Poortmans et al. 2009) assessed the outcome of 251 patients with R1 resection who were randomized to receive either a 10 Gy or a 26 Gy boost. There was no statistically significant difference in local control or survival between the lower and the higher boost dose group. Fibrosis occurred significantly more often after 26 Gy. Extrapolating these results on patients with complete resection, it seems justifiable to use a 10 Gy boost, even though data are less valid than for 16 Gy (S3 2012). In a European survey about current practice in breast RT, one third of the institutions used a 10 Gy boost dose (van der Laan et al. 2010).

Recently, several studies evaluated the technique of a simultaneously integrated boost which is administered by daily zonal dose augmentations (Bantema-Joppe et al. 2012; Hurkmans et al. 2006; Van Parijs et al. 2012). Long-term data are not yet available, but radiobiological considerations suggest that single tumor bed doses of 2.1 Gy for low-risk tumors up to 2.25 Gy for constellations with higher risk for local recurrence seem to be within the acceptable range. Outside clinical trials, SIB technique with HF is discouraged (Sedlmayer et al. 2013b).

17.3 Accelerated Partial Breast Irradiation (APBI)

17.3.1 Indications for APBI

Accelerated partial breast irradiation (APBI) refers to RT of a smaller (partial) breast volume over a shorter treatment time, covering the tumor bed with a limited margin of normal tissue. APBI can be delivered intraoperatively in a single fraction or postoperatively over 1–3 weeks by brachytherapy or external beam radiotherapy.

For patients at a lower risk for local recurrence, APBI has been strongly propagated in the last years as it spares treatment time and costs and allegedly provides less toxicity, however possibly on the expense of deteriorated local control (Valachis et al. 2010).

There is no general consensus regarding the indication for using ABPI as a sole treatment for breast cancer. While the ASTRO and GEC-ESTRO permit APBI for selected patients (Polgár et al. 2010; Smith et al. 2009), the German interdisciplinary guidelines do not recommend APBI outside clinical trials (S3 2012), while the DEGRO practical guidelines (Sedlmayer et al. 2013a) regard ABPI with IORT or brachytherapy as an option for patients >70 years with node-negative T1, luminal A tumors.

Body of Evidence

Four Phase III randomized trials evaluating APBI have been published, three of those have methodological drawbacks concerning failed patient accrual (Dodwell et al. 2005; Polgár et al. 2013) or specification of the technique and target volume (Ribeiro et al. 1993).

A meta-analysis of these trials revealed an increased risk for both local (odds ratio (OR) 2.15; p 0.001) and regional recurrences (OR 3.43; $p<0.001$) for APBI compared to WBI, however, not yet translating in a survival difference (OR 0.91; p 0.55) (Valachis et al. 2010).

TARGIT-A was a randomized, non-inferiority trial (Vaidya et al. 2014). Women aged 45 years and older with invasive ductal carcinoma were enrolled and randomly assigned to receive intraoperative radiotherapy (IORT) ($n=1{,}721$) or WBI with 50 Gy in fractions of 2 Gy.whole breast EBRT ($n=1{,}730$). For IORT, a point source of 50 kV energy x-rays at the center of a spherical applicator is used, delivering a dose of 20 Gy to the surface of the tumor bed that attenuates to 5–7 Gy at 1 cm depth.

Randomization occurred either before lumpectomy (prepathology stratum, i.e., IORT concurrent with lumpectomy) or after lumpectomy (postpathology stratum, i.e., IORT given subsequently by reopening the wound). Of the group randomized for IORT, 15.2 % received supplemental WBRT if unforeseen adverse features were detected on final pathology but counted as APBI according to the intent-to-treat principle. The primary endpoint was the absolute difference in local recurrence in the conserved breast, with a non-inferiority margin of 2.5 % at 5 years. The median follow-up of all patients was 29 months. The 5-year risk for in-breast recurrence was 3.3 % for APBI vs. 1.3 % for EBRT ($p=0.042$). Overall, breast cancer mortality was similar between groups (2.6 % for APBI vs. 1.9 % for WBRT; $p=0.56$). Toxicity was comparable, and grade 3 or 4 skin complications were less frequent with IORT (0.2 %) vs. EBRT (0.7 %, $p=0.029$).

In the ELIOT trial (Veronesi et al. 2013), 1,305 women aged 48–75 years with early breast cancer, a maximum tumor diameter of up to 2.5 cm, were randomly assigned to WBRT ($n=654$) with 50 Gy plus boost or intraoperative radiotherapy with electrons (IOERT) with a single dose of 21 Gy to the tumor bed during surgery ($n=651$). The primary endpoint was occurrence of ipsilateral breast tumor recurrences (IBTR); overall survival was a secondary endpoint; the main analysis was by intention to treat.

After a medium follow-up of 5.8 years, 35 patients in the intraoperative radiotherapy group and four patients in the external radiotherapy group had had an IBTR. The 5-year event rate for IBRT was 4.4 % in the IOERT group and 0.4 % in the WBRT group ($p<0.0001$). The 5-year OAS was identical (96.8 %). The authors state that they observed significantly ($p=0.0002$) fewer skin side effects with IOERT. In patients with data available ($n=876$), acute skin toxicity was 6.9 % with WBI vs. 1.2 % with IOERT; however, chronic skin toxicity was observed in 5 of 464 patients after WBI (1.1 %) and 6 of 412 patients (1.5 %) with IOERT (Veronesi et al. 2013).

Comments and Conclusion

The available data strongly indicate an increased risk of in-breast recurrence for patients treated with APBI alone, while toxicity is comparable. The question remains whether even a small reduction of local control appears justifiable in patients with early breast cancer, who have an excellent prognosis with standard WBI (Moser and Vrieling 2012; Sautter-Bihl et al. 2010). Of note, long-term results of APBI studies are mandatory for final assessment of its effectiveness as true local recurrences are presumed to occur between 40 and 65 months after primary treatment and out-quadrant relapses even later (Brooks et al. 2005; Freedman et al. 2005; Gujral et al. 2011).

17.3.2 Technique and Dose of APBI

The following techniques are used: external beam RT (Lewin et al. 2012; Vicini et al. 2010), interstitial brachytherapy (Arthur et al. 2008; Ott et al. 2007), endoluminal brachytherapy, and intraoperative radiotherapy with electrons (Veronesi et al. 2010) or low-energy photons (Vaidya et al. 2010). Dose distribution is substantially different for these techniques; therefore, outcome analyses of local control rates have to take account for the limited biological comparability of dose specifications, according to the respective method (Sautter-Bihl et al. 2010).

17.4 Postmastectomy Radiotherapy (PMRT)

17.4.1 Indications for Postmastectomy Radiation (PMRT)

While the indication for PMRT is undisputed for women with T4 tumors and ≥4 affected nodes, it has been an issue of debate for those with 1–3 positive nodes. Recent data confirm the benefit of PMRT for pN1 patients (EBCTCG). Moreover, PMRT should be considered in node-negative patients with T3 tumors in case of additional risk factors such as lymphovascular invasion, blood vessel invasion, positive node ratio >20%, resection margins <3 mm, grading 3, young age/premenopausal, extracapsular invasion, negative hormone receptors, invasive lobular cancer, or a tumor size >2 cm.

Body of Evidence

The latest meta-analysis of the Early Breast Cancer Trialists' Collaborative Group (EBCTCG) 2014) confirmed the effectiveness of PMRT for women with 1–3 positive nodes as described by the Danish Breast Group and the British Columbia trial (Overgaard et al. 2007; Ragaz et al. 2005). The EBCTCG analyzed data of 8,135 women in 22 randomized trials (treated before 2000), comparing PMRT to the chest wall and regional lymph nodes after mastectomy and axillary surgery versus the same surgery without radiotherapy. Of those, 3,786 women had axillary lymph node dissection (ALND) to at least level II and/or a median number of at least 10 removed nodes. Less extensive surgery ($n=4{,}065$) was classified as axillary sampling (AS). In 183 patients the extent of surgery was not specified. Analyses were stratified by trial, individual follow-up year, age at entry, and pathological nodal status. Overall, 5,821 patients (72 %) were node positive, of those 54 % had ALND and 44 % had AS, whereas in the 1,594 node-negative women, 44 % had ALND and 55 % underwent AS. After complete axillary dissection, node-negative patients did not profit from PMRT, neither in terms of recurrence nor survival. By contrast, for the 870 women with node-negative disease who underwent axillary sampling only, PMRT provided a fivefold reduction of local recurrence (16.3 vs. 3.3 % $p<0.00001$); moreover, any recurrence was reduced by 12.1 % (34.2 vs. 22.1 %, $p<0.00001$). However, no significant difference in survival was observed (Table 17.2).

Among the 1,314 women who had axillary dissection and only one to three positive nodes, radiotherapy reduced locoregional recurrence ($2p<0.00001$), overall recurrence (RR 0.68, 95 % CI 0.57–0.82, $2p=0.00006$), and breast cancer mortality (RR 0.80, 95 % CI 0.67–0.95, $2p=0.01$).

The absolute gain for irradiated women was comparable between pN1-3 and pN4+ patients: 10-year LC 16.5 % (pN1-3) and 19.1 % (pN4+) in favor of the irradiated group. In terms of overall recurrence, the absolute benefit was 11.5 %

Table 17.2 Results of the EBCTCG 2014 comparing postoperative radiotherapy after mastectomy (PMRT) vs. none

	1–3 LK		4+ LK	
–	RT	No RT	RT	No RT
10-year LRR	3.8 %	20.3 %	13.0 %	32.1 %
Absolute gain	**16.5 %**		**19.1 %**	
	$2p<0.00001$		$2p<0.00001$	
10-year any recurrence	34.2 %	45.7 %	66.3 %	75.1 %
Absolute gain	**11.5 %**		**8.8 %**	
	$2p$ 0.00006		$2p$ 0.0003	
20-year BC mortality	42.3 %	50.2 %	70.7 %	80 %
Absolute gain	**7.9 %**		**9.3 %**	
	$2p=0.01$		$2p=0.04$	

Early Breast Cancer Trialists' Collaborative Group (EBCTCG) (2014)

(pN1-3) and 8.8 % (pN4+). PMRT provided an absolute reduction of 20-year breast cancer mortality of 7.9 % ($2p = 0.01$) for pN1-3 and 9.3 % ($2p = 0.04$) for pN4+ patients. These effects were similar whether patients received systemic treatment or not.

Comments and Conclusion
The available evidence strongly suggests to offer PMRT to all node-positive patients.

17.4.2 Treatment Planning, Technique, and Dose for PMRT of the Chest Wall

Three-dimensional CT planning is mandatory. The PTV comprises the chest wall including the scar and a safety margin. The cranial and caudal field borders are adapted to the size and position of the contralateral breast with the inferior extension about 1.5 cm below the original submammary fold. For sparing of the OAR, the same technical options apply as described for WBI in Sect. 17.1.2. However, the target volume of PMRT differs substantially from WBI as it is usually more flat shaped and includes the chest wall more generously (Fig. 17.5). IMRT may be helpful, especially for left-sided cancer (Rudat et al. 2011).

RT is performed in supine position with abducted arm using breast tilt boards with arm rest. Patients who receive PMRT are often in an advanced stage requiring regional node irradiation (RNI) (Sect. 17.5.3).

17.4.3 Dose and Fractionation

The standard dose is 50–50.4 Gy delivered in 1.8–2 Gy per fraction. In the above cited articles about HF, only a minority of patients (ca.500/7,095) were treated with HF after mastectomy. Data of this subgroup revealed no difference in local control and toxicity (Théberge et al. 2011). As many patients treated with mastectomy have an advanced stage and need RNI or chemotherapy, the same concerns regarding HF should be taken into account as for BCS (Sect. 17.1.3).

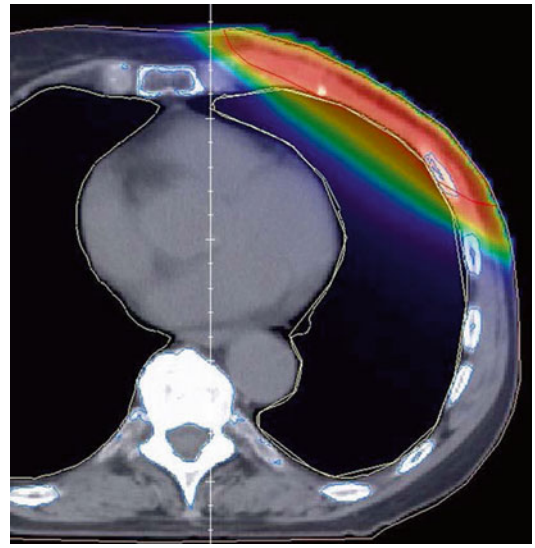

Fig. 17.5 Postmastectomy radiotherapy (PMRT): dose distribution to the heart and lung in deep breath hold

Boost
In areas at high risk of local recurrence, i.e., in case of close margins or R1 resection status, a boost may be considered (Buchholz and Haffty 2008).

17.5 Regional Nodal Irradiation (RNI)

17.5.1 General Indications for Regional Nodal Irradiation

Basically the same indications apply whether BCS or mastectomy has been performed. However, no studies have yet been performed for RNI versus chest wall irradiation alone.

In case of 4 positive axillary nodes, the indication for RNI is undisputed. For patients with 1–3 positive nodes (pN1), recommendations of different international guidelines are conflicting. Indirect evidence for the benefit of RNI for patients with 1–3 positive axillary nodes may be derived from the recent meta-analysis of the Early Breast Cancer Trialists' Collaborative Group (EBCTCG)

that demonstrated an equivalent benefit for patients who received PMRT vs. no radiotherapy in the group of 1–3 positive axillary nodes compared to those who had ≥4 affected nodes. RNI was part of PRMT in almost all of the analyzed trials (EBCTCG) 2014 (see Sect. 17.4.1).

17.5.2 Body of Evidence from Recent Randomized Trials

17.5.2.1 Canadian Trial (NCIC-CTG MA.20) (Whelan et al. 2011)

Beyond retrospective data, the first randomized study providing evidence for the benefit of RNI especially in patients with 1–3 LN was the NCIC-CTG MA.20 trial, to date not yet published as full paper (Whelan et al. 2011). The study comprised 1.832 women with mostly 1–3 positive axillary nodes (85 %) and a minority of women (10 %) with negative nodes in the presence of high risk factors. Patients were randomized after breast-conserving surgery and ALND to either WBI or WBI and additional RNI. The target volume in the RNI group included levels I–III of the axillary nodes and supraclavicular and internal mammary nodes. The 5-year locoregional recurrence-free survival was 96.8 % with and 95.5 % without RNI ($p=0.02$). The 5-year disease-free survival (DFS) was significantly improved in the RNI group: 89.7 % vs. only 84 % patients with WBI alone ($p=0.003$). This difference is twice as high as the absolute benefit in terms of local control and therefore hypothetically attributable to the significant positive impact on distant metastasis-free survival (DMFS) with an absolute 5.4 % reduction at 5 years in the RNI arm ($p=0.002$). There was a trend toward improved OAS (92.3 % vs. 90.7 %), however, just below statistical significance ($p=0.07$). The rate of lymphedema (any grade) was 4 % without vs. 7 % with RNI ($p=0.004$) which is in accordance to recent literature (Shah et al. 2012). The rate of pneumonitis was slightly increased after RNI (1.3 % vs. 0.2 %) but altogether low. Data concerning cardiovascular toxicity were not yet provided. The authors concluded that RNI reduces the risk of locoregional and distant recurrence and improves DFS with a trend in improved OAS (Whelan et al. 2011).

17.5.2.2 European Study EORTC 22922-10925 (Poortmans et al. 2013)

This study, to date not yet published as full paper, included 4.004 women stages I–III with mostly pT1-2 tumors (95 %) and either involved axillary LN (55.6 %) or a medially located primary tumor (44.5 %). Patients were randomized after BCS (76.1 %) or mastectomy (23 %) to receive WBI/PMRT either with or without inclusion of the internal mammary nodes and medial supraclavicular node (IM-MS RT) with 50 Gy in 25 fractions. After mastectomy, chest wall irradiation was applied to 73.2 % of patients in both arms. Dose specifications for WBI or chest wall irradiation were not required; presumably, relevant parts of the axilla were included in these fields. Nearly all LN-positive patients (99.0 %) and 66.3 % of the LN-negative patients received adjuvant systemic treatment. After adjustment for stratification factors, IM-MS RT significantly improved outcome at 10 years: OAS (82.3 vs. 80.7 %, $p=0.049$), DFS (72.1 vs. 69.1 %, $p=0.044$), and metastasis-free survival (78.0 vs. 75.0 %, $p=0.020$). The treatment effect on OAS was similar for pN1 vs. pN2 patients but, interestingly, most pronounced for node-negative patients (HR 0.79, 95 % CI 0.61–1.02). The highest benefit was observed in patients receiving chemo- as well as endocrine therapy (HR 0.72, 95 % CI 0.55–0.94). While the local recurrence rate was similar (5.3 vs. 5.6 %), regional lymph node recurrence was 2.7 % with RNI vs. 4.2 % without. In contrast to the findings in the Canadian study, the rates of any-grade lymphedema at 3 years were identical in both groups (Matzinger et al. 2010). No increase in lethal complications was observed so far, however, without providing details how cardiac toxicity was assessed. Moreover 10 years of follow-up may still be too short for final conclusions.

Nonetheless, the authors conclude that radiotherapy of the IMN and medial SCN should be recommended for patients with involved axillary LN and/or medially located primary tumor.

17.5.2.3 French Study (Hennequin et al. 2013)

In the only trial specifically addressing the contribution of RNI to the internal mammary nodes (IMN), 1,334 patients with either positive axillary nodes (75 %) or central/medial tumors irrespective of nodal status (25 %) were included. All patients were treated with PMRT to the chest wall, including SCN (plus axillary apex, in node-positive cases), and were randomized to receive additional IMN-RT or not. IMN included the first 5 intercostal spaces. Overall, 10-year OAS was 62.57 % with IMN-RT and 59.3 % (n.s.) without. Node-negative patients (25 %) showed a trend toward a worse outcome with IMN-RT (n.s.), whereas node-positive patients seemed to profit from IMN-RT (n.s.). The authors concede that the study may have been underpowered to prove a significant survival benefit for IMN-RT. No increase in cardiac toxicity was observed in the IMN-RT group but may have been incompletely reported; the authors admit that their data do not permit a definite conclusion regarding toxicity and conclude that they cannot reliably recommend for or against IMN-RT (Hennequin et al. 2013).

17.5.2.4 Meta-analysis of These Trials (Budach et al. 2013)

A meta-analysis of these data (Budach et al. 2013) revealed a more distinct benefit of RNI on OAS with a hazard ratio of 0.82 ($p=0.011$). The largest gain was observed for DMFS, possibly supporting the hypothesis of Hellman (Hellman 1997) that radiotherapy is "stopping metastases at their source."

17.5.3 Indications for RNI by Site

17.5.3.1 Indications for RT of the Supraclavicular (or Infraclavicular) Nodes (SCN-RT)

SCN-RT is mandatory for patients with >3 affected axillary nodes, in case of positive nodes in level III of the axilla and when RT of the axillary nodes is indicated (Belkacémi et al. 2011; S3 2012). For women with 1–3 positive nodes, see general indications (Sect. 17.5.1).

17.5.3.2 Indications for RT of the Axilla (ART)

ART is mandatory for patients with residual disease or if axillary nodes are palpably involved and no axillary lymph node dissection (ALND) was performed (NCCN 2014; S3 2012; Sautter-Bihl et al. 2014).

An unresolved question remains on how to treat patients with one or two positive sentinel nodes (SN) who receive no ALND as recently several guidelines (NCCN 2014; S3 2012) have permitted omission of ALND in selected patients with one or two pathologically positive SN after BCS, provided that they receive adjuvant WBI.

Body of Evidence

The American College of Surgeons Oncology Group (Giuliano et al. 2011) performed a non-inferiority trial including 891 women with pT1-2 tumors and clinically negative axilla who underwent SNB, revealing 1–2 pathologically affected nodes. Patients were randomized to either axillary dissection ($n=445$) or no further local treatment ($n=446$). All patients received adjuvant WBI. After a median follow-up of 6.3 years, no difference in LRR, OAS, and disease-free survival (DFS) was observed. The quality of evidence provided by this study has been questioned due to several serious methodological drawbacks (Murthy et al. 2012).

The potential impact of occult SN metastases on prognosis was investigated in a subgroup analysis of the NSABP-B 32 trial (Krag et al. 2010). Immunohistochemical reevaluation of lymph nodes originally classified as pathologically negative revealed occult metastases in 15.9 %. Follow-up showed a significantly worse outcome of these patients compared to those who remained negative. The difference in 5-year OAS was 1.2 % (p 0.03), for 5-year DFS even 2.8 % (p 0.02) (Weaver et al. 2011). Several large retrospective cohort studies show a similar trend (Lupe et al. 2011; Pepels et al. 2012).

A systematic review of the effect of WBI on axillary recurrence after negative sentinel node

biopsy revealed an increased recurrence rate in patients who received no RT (van Wely et al. 2011). This may be explained by the fact that WBI covers at least parts of the axilla (Fig. 17.7d–f) and thus exhibits a preventive effect on LRR.

The effectiveness of axillary radiation (ART) in comparison to ALND was investigated in the EORTC 10981–22023 AMAROS study (Rutgers et al. 2013; Straver et al. 2010). 4,806 patients with clinically negative nodes received SNB, of those, 1,425 revealed a pathologically positive SNB (of whom 60 % contained micrometastases only). These patients were randomized for either ALND or ART. The PTV included levels I–III of the axilla and the medial supraclavicular nodes. The 5-year axillary recurrence rate was 0.54 % after ALND and 1.03 % after ART. The planned non-inferiority test was underpowered because of the unexpectedly low number of events. No difference in OAS and DFS was observed. Lymphedema was found significantly more often after ALND: 5-year rate 28 % compared to ART with 14 % (p 0.0001). These data indicate equivalent effectiveness of ART vs. ALND; however, the question remains whether omission of any local treatment of the axilla would have provided clinically relevant differences. Patients with negative SNB, who had not received any axillary treatment, had a 5-year axillary recurrence rate of 0.8 %. The authors conclude that ART should become standard in SN-positive patients (Rutgers et al. 2013).

A compromise between RT of the complete axilla and total omission of any local treatment was proposed by Haffty et al. accounting for a potentially increased risk of local recurrence for SN-positive patients. He suggested the use of "high tangents" to assure inclusion of the level I of the axillary nodes at risk (Haffty et al. 2011). This was based on several studies investigating the dose delivered to the axillary nodes by conventional tangential fields, and the exploration of a techniques yielding an improved coverage of level I by minor field extensions in cranial direction (Alço et al. 2010; Reznik et al. 2005; Schlembach et al. 2001). To facilitate identification of the region of interest, the SN resection site can be visualized by a clip placed at the hilum of the SN before its removal (Rabinovitch et al. 2008). RT in prone position is not advisable as it may fail adequate coverage of the SN area (Leonard et al. 2012).

17.5.3.3 Indications for RT of the Internal Mammary Nodes (IMN-RT)

IMN-RT is mandatory if these nodes are clinically or pathologically involved.

As IMN-RT increases dose exposure to the heart, it has no longer been recommended as a routine part of RNI in several guidelines (NCCN 2014; S3 2012). Controversy remains about the indication for patients with internal-central tumors and those with >4 positive nodes. In the French guideline, IMN-RT is recommended for all node-positive patients (Belkacémi et al. 2011), and in the American recommendations, IMN-RT should be "strongly considered" for patients with positive axillary nodes, regardless of the number of affected nodes and irrespective of preceding surgery and even "considered" for pN0 patients with tumors >5 cm or close margins after mastectomy (NCCN 2014). In contrast, the interdisciplinary German guideline generally discourages routine use of IMN-RT (S3 2012).

Comments and Conclusions

Recent data strongly suggest the effectiveness of RT for pN1 patients.

Whether or not any local treatment of the axilla (ALND or ART) can be safely omitted in patients with one or two positive sentinel nodes who receive no ALND is a subject of ongoing controversy. ART seems iso-effective compared to ALND in terms of local control.

The perception that IMN-RT should not be performed has to be scrutinized in light of new evidence from recent randomized trials and several population-based studies. Medial tumor location should regain relevance among decision criteria for IMN-RT as part of RNI. No increased cardiovascular disease or lethal complications were observed after a median follow-up period of 10 years, but the limitations discussed above do not yet permit final exclusion of late cardiac toxicity.

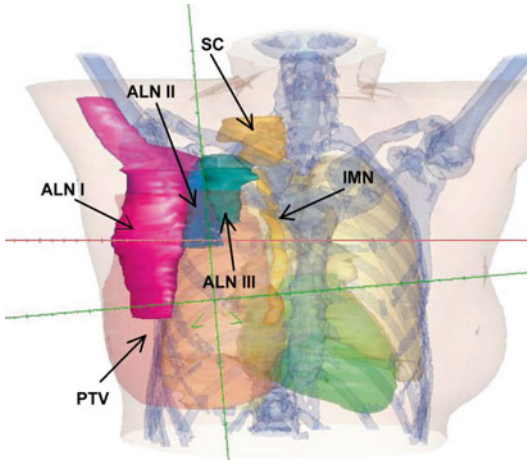

Fig. 17.6 Digital reconstruction of planning CT with depicted lymph node areas: *ALN I–III* axillary lymph nodes, levels I–III; *SC* supraclavicular nodes; *IMN* internal mammary nodes; *PTV* planning target volume (Courtesy Christoph Fussl)

17.5.4 Targeting, Technique, and Dose for RNI

3-D treatment planning is mandatory; the different lymph node areas in planning CTs are shown in Figs. 17.6 and 17.7a–f. Several anatomically based instruction guidelines have been published to define individual contouring of the different lymph node regions (Atean et al. 2013; Dijkema et al. 2004; Kirova et al. 2010; RTOG 2014; Offersen et al. 2015). Substantial variations may be caused by patient positioning, especially the abduction of the arm which plays an important role (Kirova et al. 2010). It is therefore recommended to perform the planning CT with abducted arm (Fig. 17.6).

Isolated RT of the axillary nodes is not performed; usually the SCN and axilla are irradiated simultaneously in one PTV. For IMN-RT, the target volume should be restricted to the homolateral side and not exceed beneath intercostal space 3–4 (Dijkema et al. 2004). Conventional RT is usually performed in mixed beam technique to reduce radiation burden to the heart. IMRT may be useful (Fig. 17.8) – especially in younger women, the benefit has to be balanced against higher exposure to the contralateral breast.

Dose and Fractionation

Generally, 50–50.4 Gy in single fractions of 1.8–2 Gy are recommended (Belkacémi et al. 2011; NCCN 2014; S3 2012; Sautter-Bihl et al. 2014). Hypofractionation is currently not recommended for patients who receive RNI as larger doses per fraction may increase the risk of long-term effects like cardiac toxicity or plexopathy (Andratschke et al. 2011; Galecki et al. 2006).

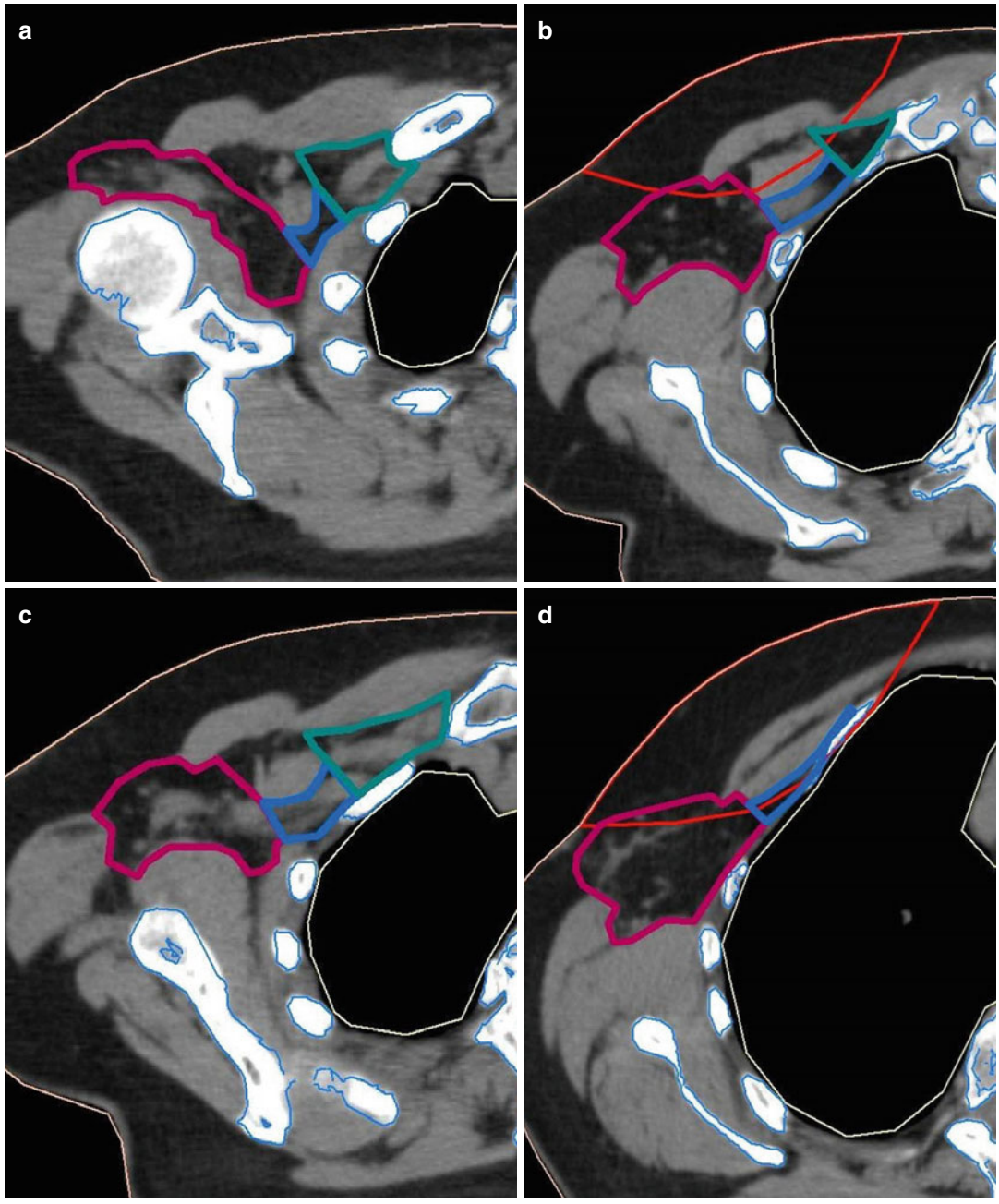

Fig. 17.7 (**a–f**) Axillary nodes: *pink* level I, *blue* level II, and *green* level III. *Red*: target volume for whole breast irradiation. Partial inclusion of level I and a small part of level III by the target volume for whole breast irradiation (Courtesy Christoph Fussl)

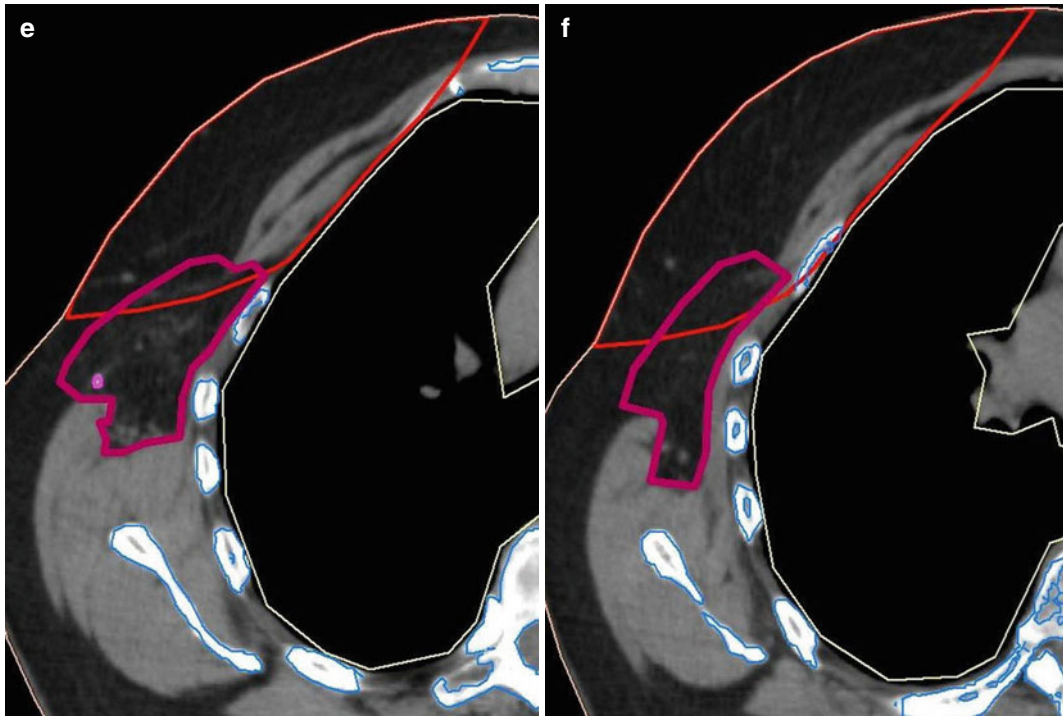

Fig. 17.7 (continued)

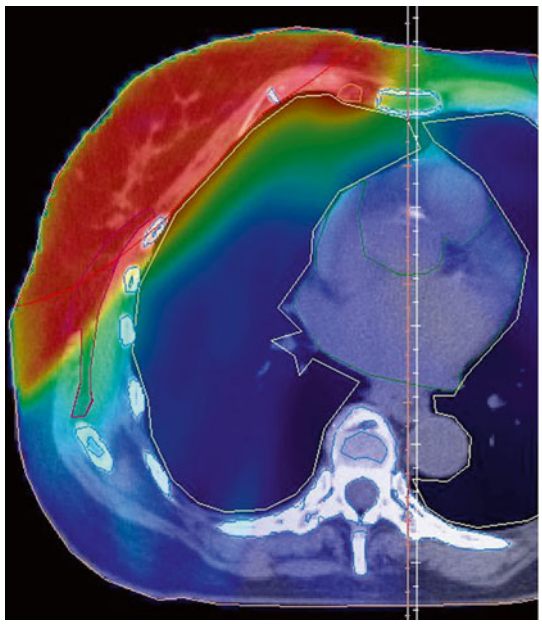

Fig. 17.8 Whole breast irradiation with internal mammary nodes: dose distribution with intensity-modulated radiotherapy (IMRT)

References

Alço G, Iğdem S, Ercan T et al (2010) Coverage of axillary lymph nodes with high tangential fields in breast radiotherapy. Br J Radiol 83:1072–1076

Andratschke N, Maurer J, Molls M et al (2011) Late radiation-induced heart disease after radiotherapy. Clinical importance, radiobiological mechanisms and strategies of prevention. Radiother Oncol 100:160–166

Antonini N, Jones H, Horiot JC et al (2007) Effect of age and radiation dose on local control after breast conserving treatment: EORTC trial 22881–10882. Radiother Oncol 82:265–271

Arthur DW, Winter K, Kuske RR et al (2008) A phase II trial of brachytherapy alone after lumpectomy for select breast cancer: tumor control and survival outcomes of RTOG 95–17. Int J Radiat Oncol Biol Phys 72:467–473

Atean I, Pointreau Y, Ouldamer L et al (2013) A simplified CT-based definition of the supraclavicular and infraclavicular nodal volumes in breast cancer. Cancer Radiother 17:39–43

Bantema-Joppe EJ, Schilstra C, de Bock GH et al (2012) Simultaneous integrated boost irradiation after breast-conserving surgery: physician-rated toxicity and cosmetic outcome at 30 months' follow-up. Int J Radiat Oncol Biol Phys 83:e471–e477

Barnett GC, Wilkinson JS, Moody AM et al (2012) Randomized controlled trial of forward-planned intensity modulated radiotherapy for early breast cancer: interim results at 2 years. Int J Radiat Oncol Biol Phys 82:715–723

Bartelink H, Horiot J-C, Poortmans PM et al (2007) Impact of a higher radiation dose on local control and survival in breast-conserving therapy of early breast cancer: 10-year results of the randomized boost versus no boost EORTC 22881–10882 trial. J Clin Oncol 25:3259–3265

Belkacémi Y, Fourquet A, Cutuli B et al (2011) Radiotherapy for invasive breast cancer: guidelines for clinical practice from the French expert review board of Nice/Saint-Paul de Vence. Crit Rev Oncol Hematol 79:91–102

Bentzen SM, Agrawal RK, Aird EGA et al (2008a) The UK Standardisation of Breast Radiotherapy (START) Trial A of radiotherapy hypofractionation for treatment of early breast cancer: a randomised trial. Lancet Oncol 9:331–341

Bentzen SM, Agrawal RK, Aird EGA et al (2008b) The UK Standardisation of Breast Radiotherapy (START) Trial B of radiotherapy hypofractionation for treatment of early breast cancer: a randomised trial. Lancet 371:1098–1107

Biganzoli L, Wildiers H, Oakman C et al (2012) Management of elderly patients with breast cancer: updated recommendations of the International Society of Geriatric Oncology (SIOG) and European Society of Breast Cancer Specialists (EUSOMA). Lancet Oncol 13:e148–e160

Brooks JP, Danforth DN, Albert P et al (2005) Early ipsilateral breast tumor recurrences after breast conservation affect survival: an analysis of the National Cancer Institute randomized trial. Int J Radiat Oncol Biol Phys 62:785–789

Buchholz T, Haffty B (2008) Breast cancer: locally advanced and recurrent disease, postmastectomy radiation, and systemic therapies. In: Perez and Brady's principles and practice of radiation oncology. Wolters Kluwer/Lippincott Williams & Wilkins, Philadelphia

Budach W, Kammers K, Boelke E et al (2013) Adjuvant radio-therapy of regional lymph nodes in breast cancer – a meta-analysis of randomized trials. Radiat Oncol 8:267

Darby S, McGale P, Correa C et al.; Early Breast Cancer Trialists' Collaborative Group (EBCTCG) (2011) Effect of radiotherapy after breast-conserving surgery on 10-year recurrence and 15-year breast cancer death: meta-analysis of individual patient data for 10,801 women in 17 randomised trials. Lancet 378:1707–1716

Dijkema IM, Hofman P, Raaijmakers CPJ et al (2004) Loco-regional conformal radiotherapy of the breast: delineation of the regional lymph node clinical target volumes in treatment position. Radiother Oncol 71:287–295

Dodwell D, Dyker K, Brown J et al (2005) A randomised study of whole-breast vs tumour-bed irradiation after local excision and axillary dissection for early breast cancer. Clin Oncol 17:618–622

Donovan E, James H, Bonora M et al (2012) Second cancer incidence risk estimates using BEIR VII models for standard and complex external beam radiotherapy for early breast cancer. Med Phys 39:5814

EBCTCG Early Breast Cancer Trialists' Collaborative Group (2014) Effect of radiotherapy after mastectomy and axillary surgery on 10-year recurrence and 20-year breast cancer mortality: meta-analysis of individual patient data for 8135 women in 22 randomised trials. Lancet 383:2127–2135

Fastner G, Sedlmayer F, Merz F et al (2013) IORT with electrons as boost strategy during breast conserving therapy in limited stage breast cancer: long term results of an ISIORT pooled analysis. Radiother Oncol 108:279–286

Feng M, Moran JM, Koelling T et al (2011) Development and validation of a heart atlas to study cardiac exposure to radiation following treatment for breast cancer. Int J Radiat Oncol Biol Phys 79:10–18

Freedman GM, Anderson PR, Hanlon AL et al (2005) Pattern of local recurrence after conservative surgery and whole-breast irradiation. Int J Radiat Oncol Biol Phys 61:1328–1336

Galecki J, Hicer-Grzenkowicz J, Grudzien-Kowalska M et al (2006) Radiation-induced brachial plexopathy and hypofractionated regimens in adjuvant irradiation of patients with breast cancer – a review. Acta Oncol 45:280–284

Giuliano AE, Hunt KK, Ballman KV et al (2011) Axillary dissection vs no axillary dissection in women with invasive breast cancer and sentinel node metastasis: a randomized clinical trial. JAMA 305:569–575

Gujral DM, Sumo G, Owen JR et al (2011) Ipsilateral breast tumor relapse: local recurrence versus new primary tumor and the effect of whole-breast radiotherapy on the rate of new primaries. Int J Radiat Oncol Biol Phys 79:19–25

Haffty BG, Hunt KK, Harris JR et al (2011) Positive sentinel nodes without axillary dissection: implications for the radiation oncologist. J Clin Oncol 29:4479–4481

Hall EJ, Wuu C-S (2003) Radiation-induced second cancers: the impact of 3D-CRT and IMRT. Int J Radiat Oncol Biol Phys 56:83–88

Harris EE, Correa C, Hwang W-T et al (2006) Late cardiac mortality and morbidity in early-stage breast cancer patients after breast-conservation treatment. J Clin Oncol 24:4100–4106

Haviland JS, Owen JR, Dewar JA et al (2013) The UK Standardisation of Breast Radiotherapy (START) trials of radiotherapy hypofractionation for treatment of early breast cancer: 10-year follow-up results of two randomised controlled trials. Lancet Oncol 14:1086–1094

Hellman S (1997) Stopping metastases at their source. N Engl J Med 337:996–997

Hennequin C, Bossard N, Servagi-Vernat S et al (2013) Ten-year survival results of a randomized trial of irradiation of internal mammary nodes after mastectomy. Int J Radiat Oncol Biol Phys 86:860–866

Hopwood P, Haviland JS, Sumo G et al (2010) Comparison of patient-reported breast, arm, and shoulder symptoms and body image after radiotherapy for early breast cancer: 5-year follow-up in the randomised Standardisation of Breast Radiotherapy (START) trials. Lancet Oncol 11:231–240

Hurkmans CW, Meijer GJ, van Vliet-Vroegindeweij C et al (2006) High-dose simultaneously integrated breast boost using intensity-modulated radiotherapy and inverse optimization. Int J Radiat Oncol Biol Phys 66:923–930

ICRU (1993) ICRU report 50; prescribing, recording and reporting photon beam therapy

ICRU (1999) ICRU Report 62. Prescribing, recording and reporting photon beam therapy (Supplement to ICRU Report 50)

Interdisziplinäre S3-Leitlinie für die Diagnostik, Therapie und Nachsorge des Mammakarzinoms, Langversion 3.0, Aktualisierung 2012, AWMF-Register-Nummer: 032–045OL 2012

Jalali R, Singh S, Budrukkar A (2007) Techniques of tumour bed boost irradiation in breast conserving therapy: current evidence and suggested guidelines. Acta Oncol 46:879–892

James ML, Lehman M, Hider PN et al (2010) Fraction size in radiation treatment for breast conservation in early breast cancer. Cochrane Database Syst Rev:CD003860

Kirby AM, Evans PM, Helyer SJ et al (2011) A randomised trial of Supine versus Prone breast radiotherapy (SuPr study): comparing set-up errors and respiratory motion. Radiother Oncol 100:221–226

Kirova YM, Castro Pena P, Dendale R et al (2010) Simplified rules for everyday delineation of lymph node areas for breast cancer radiotherapy. Br J Radiol 83:683–686

Krag DN, Anderson SJ, Julian TB et al (2010) Sentinel-lymph-node resection compared with conventional axillary-lymph-node dissection in clinically node-negative patients with breast cancer: overall survival findings from the NSABP B-32 randomised phase 3 trial. Lancet Oncol 11:927–933

Leonard KL, Solomon D, Hepel JT et al (2012) Axillary lymph node dose with tangential whole breast radiation in the prone versus supine position: a dosimetric study. Radiat Oncol 7:72

Lewin AA, Derhagopian R, Saigal K et al (2012) Accelerated partial breast irradiation is safe and effective using intensity-modulated radiation therapy in selected early-stage breast cancer. Int J Radiat Oncol Biol Phys 82:2104–2110

Lin A, Moran JM, Marsh RB et al (2008) Evaluation of multiple breathing states using a Multiple Instance Geometry Approximation (MIGA) in inverse-planned optimization for locoregional breast treatment. Int J Radiat Oncol Biol Phys 72:610–616

Lohr F, El-Haddad M, Dobler B et al (2009) Potential effect of robust and simple IMRT approach for left-sided breast cancer on cardiac mortality. Int J Radiat Oncol Biol Phys 74:73–80

Lupe K, Truong PT, Alexander C et al (2011) Ten-year locoregional recurrence risks in women with nodal micrometastatic breast cancer staged with axillary dissection. Int J Radiat Oncol Biol Phys 81:e681–e688

Matzinger O, Heimsoth I, Poortmans P et al (2010) Toxicity at three years with and without irradiation of the internal mammary and medial supraclavicular lymph node chain in stage I to III breast cancer (EORTC trial 22922/10925). Acta Oncol 49:24–34

Moser EC, Vrieling C (2012) Accelerated partial breast irradiation: The need for well-defined patient selection criteria, improved volume definitions, close follow-up and discussion of salvage treatment. Breast 21:707–715

Murthy V, Ballehaninna UK, Chamberlain RS (2012) Unanswered questions about the role of axillary dissection in women with invasive breast cancer and sentinel node metastasis. Clin Breast Cancer 12:305–307

Nairz O, Deutschmann H, Kopp M et al (2006) A dosimetric comparison of IORT techniques in limited-stage breast cancer. Strahlenther Onkol 182:342–348

NCCN (2014) Breast cancer version 3.2014. J Natl Compr Canc Netw 12:542–590

NICE (2009) Early and locally advanced breast cancer: diagnosis and treatment. National Institute for Clinical Excellence (NICE), London

Nielsen MH, Berg M, Pedersen AN et al (2013) Delineation of target volumes and organs at risk in adjuvant radiotherapy of early breast cancer: National guidelines and contouring atlas by the Danish Breast Cancer Cooperative Group. Acta Oncol 52:703–710

New Zealand Guidelines Group (NZGG) (2009) Management of early breast cancer – evidence-based best practice guidelines. New Zealand Guidelines Group, Wellington

Offersen BV, Boersma LJ, Kirkove C et al. ESTRO consensus guideline on target volume delineation for elective radiation therapy of early stage breast cancer. Radiother Oncol. 2015;114(1):3–10

Ott OJ, Hildebrandt G, Pötter R et al (2007) Accelerated partial breast irradiation with multi-catheter brachytherapy: local control, side effects and cosmetic outcome for 274 patients. Results of the German–Austrian multi-centre trial. Radiother Oncol 82:281–286

Overgaard M, Nielsen HM, Overgaard J (2007) Is the benefit of postmastectomy irradiation limited to patients with four or more positive nodes, as recommended in international consensus reports? A subgroup analysis of the DBCG 82 b&c randomized trials. Radiother Oncol 82:247–253

Owen JR, Ashton A, Bliss JM et al (2006) Effect of radiotherapy fraction size on tumour control in patients with early-stage breast cancer after local tumour excision: long-term results of a randomised trial. Lancet Oncol 7:467–471

Pepels MJ, de Boer M, Bult P et al (2012) Regional recurrence in breast cancer patients with sentinel node micrometastases and isolated tumor cells. Ann Surg 255:116–121

Polgár C, Major T (2009) Current status and perspectives of brachytherapy for breast cancer. Int J Clin Oncol 14:7–24

Polgár C, Limbergen EV, Pötter R et al (2010) Patient selection for accelerated partial-breast irradiation (APBI) after breast-conserving surgery: recommendations of the Groupe Europeen de Curietherapie-European Society for Therapeutic Radiology and Oncology (GEC-ESTRO) breast cancer working group based on clinical evidence (2009). Radiother Oncol 94:264–273

Polgár C, Fodor J, Major T et al (2013) Breast-conserving therapy with partial or whole breast irradiation: Ten-year results of the Budapest randomized trial. Radiother Oncol 108(2):197–202

Poortmans PM, Collette L, Horiot JC et al (2009) Impact of the boost dose of 10 Gy versus 26 Gy in patients with early stage breast cancer after a microscopically incomplete lumpectomy: 10-year results of the randomised EORTC boost trial. Radiother Oncol 90:80–85

Poortmans P, Kirkove C, Budach V et al (2013) Irradiation of the internal mammary and medial supraclavicular lymph nodes in stage I to III breast cancer: 10 years results of the EORTC Radiation Oncology and Breast Cancer Groups phase III trial 22922/10925. EJC 47(Suppl 2): Abstract

Rabinovitch R, Ballonoff A, Newman F et al (2008) Evaluation of breast sentinel lymph node coverage by standard radiation therapy fields. Int J Radiat Oncol Biol Phys 70:1468–1471

Ragaz J, Olivotto IA, Spinelli JJ et al (2005) Locoregional radiation therapy in patients with high-risk breast cancer receiving adjuvant chemotherapy: 20-year results of the British Columbia Randomized Trial. J Natl Cancer Inst 97:116–126

Reznik J, Cicchetti MG, Degaspe B et al (2005) Analysis of axillary coverage during tangential radiation therapy to the breast. Int J Radiat Oncol Biol Phys 61: 163–168

Ribeiro G, Magee B, Swindell R et al (1993) The Christie Hospital breast conservation trial: an update at 8 years from inception. Clin Oncol 5:278–283

Romestaing P, Lehingue Y, Carrie C et al (1997) Role of a 10-Gy boost in the conservative treatment of early breast cancer: results of a randomized clinical trial in Lyon, France. J Clin Oncol 15:963–968

RTOG. Breast cancer atlas for radiation therapy planning: consensus definitions. http://www.rtog.org/CoreLab/ContouringAtlases/BreastCancerAtlas.aspx. Accessed 30 Apr 2014

Rudat V, Alaradi AA, Mohamed A et al (2011) Tangential beam IMRT versus tangential beam 3D-CRT of the chest wall in postmastectomy breast cancer patients: a dosimetric comparison. Radiat Oncol 6:26

Rutgers EJ, Donker M, Straver ME et al (2013) Radiotherapy or surgery of the axilla after a positive sentinel node in breast cancer patients: final analysis of the EORTC AMAROS trial (10981/22023). J Clin Oncol 31:abstract LBA1001

Sautter-Bihl M-L, Sedlmayer F, Budach W et al (2010) Intraoperative radiotherapy as accelerated partial breast irradiation for early breast cancer: beware of one-stop shops? Strahlenther Onkol 186:651–657

Sautter-Bihl ML, Sedlmayer F, Budach W et al (2012) When are breast cancer patients old enough for the quitclaim of local control? Strahlenther Onkol 188:1069–1073

Sautter-Bihl M-L, Sedlmayer F, Budach W et al (2014) DEGRO practical guidelines: radiotherapy of breast cancer III—radiotherapy of the lymphatic pathways. Strahlenther Onkol 190:342–351

Schlembach PJ, Buchholz TA, Ross MI et al (2001) Relationship of sentinel and axillary level I–II lymph nodes to tangential fields used in breast irradiation. Int J Radiat Oncol Biol Phys 51:671–678

Sedlmayer F, Sautter-Bihl M-L, Budach W et al (2013a) DEGRO practical guidelines: radiotherapy of breast cancer I. Strahlenther Onkol 189:825–833

Sedlmayer F, Sautter-Bihl ML, Budach W et al (2013b) Is the simultaneously integrated boost (SIB) technique for early breast cancer ready to be adopted for routine adjuvant radiotherapy? Strahlenther Onkol 189:193–196

Shah AP, Strauss JB, Kirk MC et al (2010) A dosimetric analysis comparing electron beam with the MammoSite brachytherapy applicator for intact breast boost. Phys Med 26:80–87

Shah C, Wilkinson JB, Baschnagel A et al (2012) Factors associated with the development of breast cancer-related lymphedema after whole-breast irradiation. Int J Radiat Oncol Biol Phys 83:1095–1100

Smith BD, Arthur DW, Buchholz TA et al (2009) Accelerated partial breast irradiation consensus statement from the American Society for Radiation Oncology (ASTRO). Int J Radiat Oncol Biol Phys 74:987–1001

Smith BD, Bentzen SM, Correa CR et al (2011) Fractionation for whole breast irradiation: an American Society for Radiation Oncology (ASTRO) Evidence-Based Guideline. Int J Radiat Oncol Biol Phys 81:59–68

Straver ME, Meijnen P, van Tienhoven G et al (2010) Role of axillary clearance after a tumor-positive sentinel node in the administration of adjuvant therapy in early breast cancer. J Clin Oncol 28:731–737

Swanson T, Grills IS, Ye H et al (2013) Six-year experience routinely using moderate deep inspiration breath-hold for the reduction of cardiac dose in left-sided breast irradiation for patients with early-stage or locally advanced breast cancer. Am J Clin Oncol 36:24–30

Théberge V, Whelan T, Shaitelman SF et al (2011) Altered fractionation: rationale and justification for whole and partial breast hypofractionated radiotherapy. Semin Radiat Oncol 21:55–65

Vaidya JS, Joseph DJ, Tobias JS et al (2010) Targeted intraoperative radiotherapy versus whole breast radiotherapy for breast cancer (TARGIT-A trial): an international, prospective, randomised, non-inferiority phase 3 trial. Lancet 376:91–102

Vaidya JS, Baum M, Tobias JS et al (2011) Long-term results of targeted intraoperative radiotherapy (Targit) boost during breast-conserving surgery. Int J Radiat Oncol Biol Phys 81:1091–1097

Vaidya J, Wenz F, Bulsara M (2014) Risk-adapted targeted intraoperative radiotherapy versus whole-breast radiotherapy for breast cancer: 5-year results for local control and overall survival from the TARGIT-A randomised trial. Lancet 383:602

Valachis A, Mauri D, Polyzos NP et al (2010) Partial breast irradiation or whole breast radiotherapy for early breast cancer: a meta-analysis of randomized controlled trials. Breast J 16:245–251

van der Laan HP, Hurkmans CW, Kuten A et al (2010) Current technological clinical practice in breast radiotherapy; results of a survey in EORTC-Radiation Oncology Group affiliated institutions. Radiother Oncol 94:280–285

Van Parijs H, Miedema G, Vinh-Hung V et al (2012) Short course radiotherapy with simultaneous integrated boost for stage I-II breast cancer, early toxicities of a randomized clinical trial. Radiat Oncol 7:80

van Wely BJ, Teerenstra S, Schinagl DA et al (2011) Systematic review of the effect of external beam radiation therapy to the breast on axillary recurrence after negative sentinel lymph node biopsy. Br J Surg 98: 326–333

Veronesi U, Orecchia R, Luini A et al (2010) Intraoperative radiotherapy during breast conserving surgery: a study on 1,822 cases treated with electrons. Breast Cancer Res Treat 124:141–151

Veronesi U, Orecchia R, Maisonneuve P et al (2013) Intraoperative radiotherapy versus external radiotherapy for early breast cancer (ELIOT): a randomised controlled equivalence trial. Lancet Oncol 14:1269–1277

Vicini F, Winter K, Wong J et al (2010) Initial efficacy results of RTOG 0319: three-dimensional conformal radiation therapy (3D-CRT) confined to the region of the lumpectomy cavity for stage I/II breast carcinoma. Int J Radiat Oncol Biol Phys 77:1120–1127

Weaver DL, Ashikaga T, Krag DN et al (2011) Effect of occult metastases on survival in node-negative breast cancer. N Engl J Med 364:412–421

Whelan TJ, Pignol J-P, Levine MN et al (2010) Long-term results of hypofractionated radiation therapy for breast cancer. N Engl J Med 362:513–520

Whelan T, Olivotto I, Ackerman I et al (2011) NCIC-CTG MA. 20: an intergroup trial of regional nodal irradiation in early breast cancer. J Clin Oncol 29(Suppl): abstract LBA 1003

Zurl B, Stranzl H, Winkler P et al (2010) Quantitative assessment of irradiated lung volume and lung mass in breast cancer patients treated with tangential fields in combination with deep inspiration breath hold (DIBH). Strahlenther Onkol 186:157–162

Erratum to: Chapter 15 Gynecological Cancer

Nina A. Mayr, Larissa Lee, and Catherine Yashar

Erratum to:
Chapter 15 in: A.-L. Grosu, C. Nieder (eds.), *Target Volume Definition in Radiation Oncology*, DOI 10.1007/978-3-662-45934-8_15

The captions of Figures 15.4 and 15.5 were incorrect in Chapter 15. The correct captions are given below:

Fig. 15.4 Contouring of the upper external and internal iliac lymph node target. (**a**) At the level just below the bifurcation of the common iliac arteries and veins, the right and left external and internal iliac arteries, veins and lymph nodes are seen medial to the psoas muscles. (**b**) Vessels and lymph nodes are contoured for reference (*aqua*). The CTV (*green*) adds a 0.7 cm margin to vessels and adjacent lymphatic tissue, excluding small bowel and psoas. (**c**) For the lymph node PTV (*red*) adds an additional margin of 0.7. In addition a 2 cm strip of tissue anterior to the sacrum (*arrow*) is added to include the presacrallymph nodes

Fig. 15.5 Contouring of the mid external and internal iliac lymph node target. (**a**) Below the level in Fig. 4 external iliac vessles and nodes are seen anteriorly, internal iliac posteriorly and con. (**b**) Vessels and lymph nodes and lymph node CTV (*green*) are contoured as in Figs. 3–4. (**c**) For the lymph node PTV (*red*) adds an additional margin of 0.7. and a 2 cm strip of tissue anterior to the sacrum as in Fig. 4

The online version of the original chapter can be found under
DOI 10.1007/978-3-662-45934-8_15

Index

A.-L. Grosu, C. Nieder (eds.), *Target Volume Definition in Radiation Oncology*,
DOI 10.1007/978-3-662-45934-8, © Springer-Verlag Berlin Heidelberg 2015